Vol. 44, No. 3 / 2014

e: ISSN 2068 – 2239
p: ISSN 2068 – 4215

INMATEH – AGRICULTURAL ENGINEERING

SEPTEMBER - DECEMBER

Editorial

The National Institute of Research-Development for Machines and Installations designed to Agriculture and Food Industry - INMA Bucharest has the oldest and most prestigious research activity in the field of agricultural machinery and mechanizing technologies in Romania.

Short History

- In 1927, the first research **Center for Agricultural Machinery** in Agricultural Research Institute of Romania - ICAR (Establishing Law was published in O.D. no. 97/05.05.1927) was established;
- In 1930, was founded **The Testing Department of Agricultural Machinery and Tools** by transforming Agricultural Research Centre of ICAR - that founded the science of methodologies and experimental techniques in the field (Decision no. 2000/1930 of ICAR Manager - GHEORGHE IONESCU ŞIŞEŞTI);
- In 1952, was established the Research Institute for Mechanization and Electrification of Agriculture - ICMA Băneasa, by transforming the Department of Agricultural Machines and Tools Testing;
- In 1979, the Research Institute of Scientific and Technological Engineering for Agricultural Machinery and Tools – ICSITMUA was founded - subordinated to Ministry of Machine Building Industry - MICM, by unifying ICMA subordinated to MAA with ICPMA subordinated to MICM;
- In 1996 the National Institute of Research-Development for Machines and Installations designed to Agriculture and Food Industry – INMA was founded – according to G.D. no.1308/25.11.1996, by reorganizing ICSITMUA, G.D no. 1308/1996 coordinated by the Ministry of Education and Research G.D. no. 823/2004;
- In 2008 INMA has been accredited to carry out research and developing activities financed from public funds under G.D. no. 551/2007, Decision of the National Authority for Scientific Research - ANCS no. 9634/2008.

As a result of widening the spectrum of communication, dissemination and implementation of scientific research results, in 2000 was founded the institute magazine, issued under the name of SCIENTIFIC PAPERS **(INMATEH)**, ISSN 1583 – 1019.

Starting with volume 30, no. 1/2010, the magazine changed its name to **INMATEH - Agricultural Engineering**, appearing both in print format (ISSN 2068 - 4215), and online (ISSN online: 2068 - 2239). The magazine is bilingual, being published in Romanian and English, with a rhythm of three issues / year: January-April, May-August, September-December and is recognized by CNCSIS – with B^+ category. Published articles are from the field of AGRICULTURAL ENGINEERING: technologies and technical equipment for agriculture and food industry, ecological agriculture, renewable energy, machinery testing, environment, transport in agriculture etc. and are evaluated by specialists inside the country and abroad, in mentioned domains.

Technical level and performance processes, technology and machinery for agriculture and food industry increasing, according to national requirements and European and international regulations , as well as exploitation of renewable resources in terms of efficiency, life, health and environment protection represent referential elements for the magazine „**INMATEH - Agricultural Engineering**".

We are thankful to all readers, publishers and assessors.

Editor in chief,
Ph. D. Eng. Pîrnă Ion

Managing Editorial Board - INMA Bucharest

In the present, *INMATEH - Agricultural Engineering* journal is indexed in the next international databases:
ULRICHSWeb: Global Serials Directory, CABI, SCIPIO, ELSEVIER /SciVerse SCOPUS, Index COPERNICUS International, EBSCO Publishing, Elektronische Zeitschriftenbibliothek

INMATEH - Agricultural Engineering
vol. **44**, no. **3** / **2014**
NATIONAL INSTITUTE OF RESEARCH-DEVELOPMENT FOR MACHINES AND INSTALLATIONS DESIGNED TO AGRICULTURE AND FOOD INDUSTRY - INMA Bucharest
6 Ion Ionescu de la Brad Blvd., sector 1, Bucharest
Three issues per year,
e ISSN: 2068 – 2239
p ISSN: 2068 – 4215
Edited by: INMA Bucharest

CUPRINS / *CONTENTS*

INFLUENCE OF TILLAGE TOOLS CUTTING EDGE WEAR OVER TECHNICAL AND ECONOMIC INDICATORS
/
INFLUENŢA UZĂRII MUCHIEI TĂIETOARE ASUPRA INDICATORILOR TEHNICO-ECONOMICI IN PROCESUL DE PRELUCRARE A SOLULUI

Assoc.Prof.Ph.D.Eng. Fechete Tutunaru L. V.[1)], Ph.D. Stud. Eng. Nagy E. M.[2)], Ph.D. Stud. Eng. Coţa C-tin.[2)]
[1)] Technical University of Cluj-Napoca / Romania; [2)] INMA Bucharest / Romania
E-mail: lucian.fechete@auto.utcluj.ro

Abstract: *The geometry of the cutting edge or of the surface contour is of great importance in minimizing the energy required for the mechanical processing operations. The vast majority of the research conducted so far in the soil processing field focuses on macro geometry of the tools without taking into account the geometry of the cutting edge. This paper presents the results of experimental research regarding the influence of the modification by wear of the constructive parameters of the cutting edge corresponding to the tillage tool on the economic indicators in the working process. Thus was established a mathematical model that highlights the correlation between the processed surface and the linear wear of tools, with which the average area that a tool can process until it reaches a wear limit value, can be determined.*

Keywords: *tool, soil, wear*

INTRODUCTION

The studies made [1], [3], [9], [11], show that the resistance force of an agricultural tool, is affected by the wear of the tool, that modifies the geometry of the cutting edge according to the soil type and functional parameters. It was shown that a worn cutting edge increases drag resistance and greatly modifies the value of the vertical component of the resistance force (Inns, 1990 [6]). In 1999, [7], measured the drag resistance for six types of thickness of the cutting edge of the plough blade and showed that the measured force increases exponentially with the thickness of the cutting edge. In 1996 [4], in the research on cutting edge geometry and its effect on tillage performance showed an increase of up to 80% of the drag resistance force for the cultivator arrows and that the direction of the vertical force can change from pushing the tool into the soil to raising it in the case of two tools having the same macro geometry but with the cutting edge in one case sharpened and the other case worn. In the X-ray photos, the level of loosening and the penetration resistance measurements showed that the worn cutting edges often induce the appearance of fissures and cracks in the soil layer below the tool. Among the works consulted, there was no study found on the optimal geometry of the cutting edge in relation to final soil parameters and with the drag resistance force.

MATERIAL AND METHOD

Depending on the soil working tool and its position during operation, the profile of the cutting edge can be symmetrical or asymmetrical. Thus, in general, the tools working in a vertical profile show a symmetrical cutting edge profile whose geometrical parameters are shown in the figures below.

From Figures 1 and 2 is noted that the geometric parameters of the tool's cutting edge and the ones of the tool's contour dependent on two macro geometrical parameters namely: the tool's width *b* and thickness *h* and the functional parameter α – the tool's angle of attack.

Rezumat: *Geometria muchiei tăietoare sau a conturului suprafeţei de lucru prezintă o importanţă deosebită în minimizarea energiei necesare în cadrul operaţiilor de prelucrare mecanică. Marea majoritate a cercetărilor realizate până în prezent in domeniul prelucrării solului se concentrează pe macrogeometria sculelor fără a lua în considerare geometria muchiei tăietoare. În lucrare sunt prezentate rezultatele unor cercetări experimentale privind influenţa modificării prin uzare a parametrilor constructivi ai muchiei tăietoare aferentă sculei de lucrat solul asupra indicatorilor tehnico-economici în procesul de lucru. Astfel a fost stabilit un model matematic care pune în evidenţă corespondenţa între suprafaţa prelucrată şi uzura liniară a sculelor, cu ajutorul căruia se poate stabili suprafaţa medie pe care o poate prelucra o sculă până să ajungă la o valoare limită a uzurii.*

Cuvinte cheie: *sculă, sol, uzură*

INTRODUCERE

Studiile efectuate de [1], [3], [9], [11], au aratat faptul că forţa de rezistenţă a unei scule agricole este afectată de uzura sculei, care modifică geometria muchiei tăietoare în funcţie de tipul solului şi parametrii funcţionali. S-a arătat că o muchie tăietoare uzată măreşte rezistenţa la înaintare şi modifică puternic valoarea componentei verticale a forţei de rezistenţă [6]. În 1999 [7] a măsurat valoarea rezistenţei la înaintare pentru şase grosimi ale muchiei tăietoare a brăzdarului plugului şi a arătat că valoarea forţei măsurate creşte exponenţial cu grosimea muchiei tăietoare. În 1996 [4], în cercetările efectuate asupra geometriei muchiei tăietoare şi efectul ei asupra performanţelor prelucrării solului a arătat o creştere cu până la 80% a forţei de rezistenţă la înaintare pentru săgeţi de cultivator şi că sensul forţei verticale se poate schimba de la a împinge scula în sol la a o ridica în cazul a două scule cu aceeasi macrogeometrie dar cu muchia tăietoare într-un caz ascuţită iar în celălalt caz uzată. În fotografiile cu raze X, gradul de afânare realizat şi determinările rezistenţei la penetrare au arătăt că muchiile tăitoare uzate conduc de cele mai multe ori la apariţia fisurilor şi crăpăturilor în stratul de sol de sub sculă. Printre lucrările consultate nu s-a găsit nici un studiu referitor la geometria optimă a muchiei tăietoare în relaţie cu durabilitatea sculei, uzura sculei în raport cu parametrii finali ai solului şi cu forţa de rezistenţă la înaintare.

MATERIAL ŞI METODĂ

În funcţie de tipul sculei de lucrat solul şi de poziţia ei în timpul funcţionării, profilul muchiei tăietoare poate fi unul simetric sau asimetric. Astfel, în general, sculele ce lucrează în plan vertical prezintă un profil simetric al muchiei tăietoare ai cărei parametri geometrici sunt evidenţiaţi în figurile de mai jos.

Din figurile 1 şi 2 se remarcă că parametrii geometrici ai muchiei tăietoare a sculei şi cei ai conturului sculei sunt dependenţi de doi parametri macrogeometrici respectiv: lăţimea *b* şi grosimea sculei *h* şi de parametrul funcţional α – unghiul de atac al sculei.

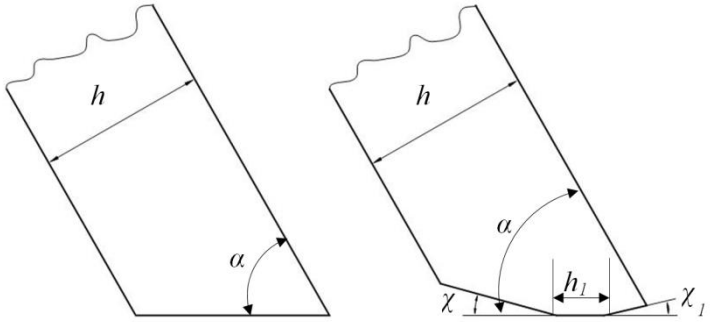

Fig. 1 - Lateral contour of a vertical tillage tool: a) simple; b) complex

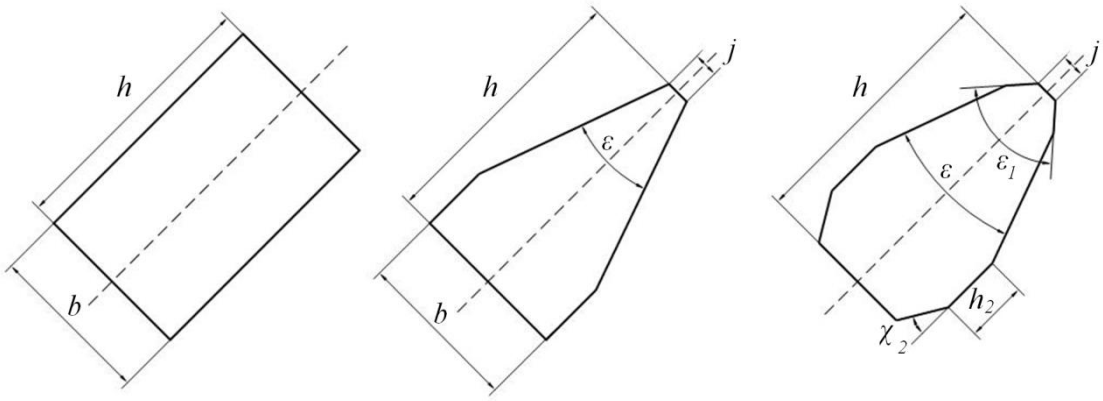

Fig. 2 - Cross section through a vertical tillage tool: a) blunt; b) sharp and chamfered; c) complex profile

For the lateral contour of the tool the following possible geometrical parameters are highlighted:

χ - angle of setting of the lower surface of the tool (it depends on the elasticity of the soil);

h_1 - the friction length of the lower surface of the tool with the soil (furrow bottom) (surface parallel to the ground);

χ_1 – secondary angle of attack (value corresponding to [4] can lead to the compaction of the furrow bottom or on the contrary to the creation of fissures and cracks in the soil beneath the tool).

For the cross section of the tool are outlined the following geometrical parameters of the cutting edge:

ε - the tool sharpening angle (reducing its value leads to lowering the resistance force and mechanical resistance and rigidity of the tool);

j - cutting edge chamfer width (the decrease of j leads to a decrease of the drag resistance force of the tool, depending on the angle ε there is a minimum value for j given by the bending resistance of the tip of the cutting edge related to the type of soil that the tool is working on);

χ_2 – setting angle of the lateral surface of the tool compared to the vertical plane of the soil (furrow wall);

h_2 - the friction length of the lateral surface of the tool with the furrow wall;

ε_1 - secondary sharpening angle (between 180 ° and ε, allows to reduce the value of j and the rapid emergence of a worn cutting profile favorable for cutting soil).

The model for the soil processing tool considered, Fig. 3, starts from a narrow and flat tool and is developed to take into account the effect of the cutting edge on cutting the soil, the maximizing of the amount of broken soil and the determining of the force necessary to overcome the soil resistance.

Starting from the first constructive parameter of the tool, its width b, the model is developed by setting the apex angle ε, the width of the chamfer j and of the radius

Pentru conturul lateral al sculei se evidenţiază ca posibili parametri geometrici:

χ – unghiul de aşezare al suprafeţei inferioare a sculei (depinde de elasticitatea solului);

h_1 – lungimea de frecare a suprafeţei inferioare a sculei cu solul (fundul brazdei) (suprafaţa paralelă cu planul solului);

χ_1 – unghiul de atac secundar (valoarea lui corespunzator cu [4] poate conduce la tasarea fundului brazdei sau dimpotrivă la crearea de fisuri şi crăpături în zona solului de sub sculă).

Pentru secţiunea transversală a sculei se conturează următorii parametri geometrici ai muchiei tăitoare:

ε – unghiul de ascuţire al sculei (micşorarea valorii lui duce la scăderea forţei de rezistenţă şi a rezistenţei mecanice şi a rigidităţii sculei);

j – lăţimea de teşire a tăişului (scăderea lui j duce la micşorarea forţei de rezistenţă la înaintare a sculei; în funcţie de unghiul ε există o valoare minimă a j dată de rezistenţa la încovoiere a vârfului muchiei tăietoare raportată la tipul de sol în care lucrează scula);

χ_2 – unghiul de aşezare al suprafeţei laterale al sculei faţă de planul vertical al solului (peretele brazdei);

h_2 – lungimea de frecare a suprafeţei laterale a sculei cu peretele brazdei;

ε_1 – unghiul de ascuţire secundar (cuprins între 180° şi ε; permite reducerea valorii j şi apariţia mai rapidă a unui profil uzat favorabil tăierii solului).

Modelul sculei de prelucrat solul luat în considerare, fig.3, porneşte de la o sculă îngustă plană şi se dezvoltă pentru a lua în considerare efectul muchiei tăietoare asupra tăierii solului, maximizarea volumului de sol desrămat şi determinarea forţei necesare de învingere a rezistenţei solului.

Pornind de la primul parametru constructiv al sculei, lăţimea acesteia b, se dezvoltă modelul prin impunerea unghiului la vârf ε, a lăţimii teşiturii j şi respectiv a razei

of curvature of the chamfer *r* that occurs as a result of the tool's wear. The functional parameters of the tool that are modeled are imposed by the tool angle *α*, working depth *a,* and working speed *v*.

Thus, in Table 1 are indicated the geometric parameters of tools made from S235JR, SR EN 10025-2:2004/AC:2005 material chosen for its high workability, possibility of electric arc welding and low cost. It is noted the use of a constant width and of seven different apex angles for a set of tools along with the realization of four different chamfers, resulting in a total of 28 tested tools.

de curbură a teşiturii *r* ce apare în urma uzării sculei. Parametrii funcţionali ai sculei ce se modelează sunt impuşi prin unghiul sculei *α*, adâncimea de lucru *a* şi viteza de lucru *v*.

Astfel, în tabelul 1 sunt precizaţi parametrii geometrici ai sculelor fabricate din S235JR, SR EN 10025-2:2004/AC:2005, material ales pentru prelucrabilitatea ridicată, posibilitatea sudării lui cu arc electric şi costul scăzut. Se remarcă utilizarea unei lăţimi constante şi a şapte unghiuri la vârf diferite pentru un set de scule, alături de realizarea a patru teşiri distincte rezultând un total de 28 de scule încercate.

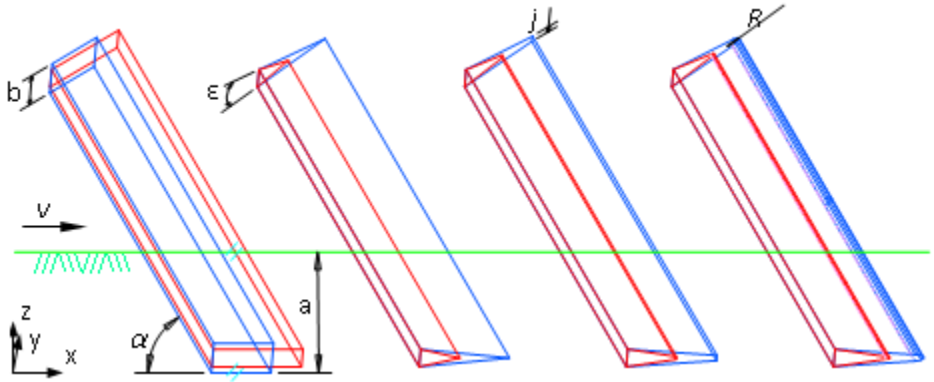

Fig. 3 - Geometrical and functional parameters of the tool

Table 1

Geometrical parameters of the tools used within the experiment

No.	***ε*** [°]	***b*** [mm]	**Chamfer *j*** [mm]			
1	15	20	0	2	4	6
2	30					
3	45					
4	60					
5	90					
6	120					
7	180					

The testing environment is a frictional one, without cohesion and without structure - respectively quartz sand for adhesive dried mortars, washed and mechanically classified with a particle diameter between 0 and 0.3 mm. This corresponds to a conformable maximal wearing effect [12] which states that "the wear is maximum when the percentage of abrasive particles having a 0.25 mm size has a maximum value."

It was also determined the resistance to penetration of the testing environment used with the force gauge (penetrometer), and the results are given in Table 2.

Mediul de încercare este unul fricţional, fără coeziune şi fără structură - respectiv nisip fin cuarţos pentru mortare adezive uscate, spălat şi clasat mecanic cu diametrul particulelor între 0 şi 0,3 mm. Acesta corespunde unui efect de uzare maximă conform [12] în care se precizează că „uzura este maximă când procentul de particule abrazive cu dimensiunea de 0,25 mm are valoare maximă".

A fost de asemenea determinată rezistenţa la penetrare a mediului de încercare utilizat cu ajutorul penetrometrului, iar rezultatele obţinute sunt cele precizate în tabelul 2.

Table 2

Resistance to penetration of the testing environment used

Depth [mm]	50	100	150	200	250
Average [N]	102.4	191.0	258.0	322.2	333.0
Dispersion [%]	8.246	19.3611	15.111	17.9348	12.986
Cone parameters	Cone no. 4; cone base diameter – 25.33 mm; cone base area – 500 mm^2				
Soil resistance [N/cm^2]	20.48	38.20	51.60	64.44	66.60

The tests made under laboratory conditions were carried out on a test stand with a soil channel, by moving the tools in a circular path with a diameter of 1850 mm at a speed of 1.5 m/s. The tool-holder assembly allows changing the depth of processing up to 500 mm with a step of 50 mm and changing the tool's angle of attack between -60° and +60 ° with a step of 15°.

Force measurement was performed with a S2 series force transducers from the HBM company. Data acquisition was performed with the Spider 8

Încercările în condiţii de laborator s-au realizat pe un stand de încercare cu canal de sol, prin deplasarea sculelor pe o traiectorie circulară cu un diametru de 1850 mm cu o viteză de 1,5 m/s. Ansamblul port-sculă realizat permite modificarea adâncimii de prelucrare până la 500 mm cu un pas de 50 mm şi modificarea unghiului de atac al sculei între -60°÷+60° cu un pas de 15°.

Măsurarea forţelor s-a realizat cu traductoare de forţă seria S2 ai companiei HBM. Achiziţia datelor s-a realizat cu sistemul de măsurare Spider 8 produs de aceeaşi

measurement system produced by the same company.

To evaluate the effects of various geometrical and functional parameters of the tillage tool an experiment was designed, which includes four categories of factors. The experiment conception is a standard factorial one that involves all the combinations of the factor levels (3x7x4x3).

Considering the capabilities offered by the experimental stand used, were taken as independent parameters (factors): tool working position (3 positions corresponding to different work depths due to the angle of attack and the tool's constructive parameters - manufacturing errors) given by adjusting the stand; tool sharpening angle, materialized by the 7 tools used; cutting edge chamfering performed to simulate the effect of wear on the cutting edge on the drag resistance, materialized by four discrete values and the tool's angle of attack (3 positions) also given by the stand adjustments.

Briefly, the experiment carried out is shown in table 3.

firmă.

Pentru evaluarea efectelor diferiţilor parametri geometrici şi funcţionali ai sculei de lucrat solul s-a conceput un experiment ce include patru categorii de factori. Concepţia experimentului este una factorială standard ce presupune toate combinaţiile nivelelor factorilor (3x7x4x3).

Luând în considerare capabilităţile oferite de standul experimental utilizat s-au luat ca şi parametri independenţi (factori): poziţia de lucru a sculei (3 poziţii de lucru ce corespund diferitelor adâncimi de lucru datorate unghiului de atac şi parametrilor constructivi ai sculei – erori de fabricare) dată de reglarea standului; unghiul de ascuţire a sculelor, materializate prin cele 7 scule utilizate; teşirea muchiei tăietoare realizată pentru a simula efectul uzării muchiei tăietoare asupra rezistenţei la înaintare, materializată prin patru valori discrete şi unghiul de atac al sculei (3 poziţii) dat de asemenea de reglarea standului.

Sumar, experimentul realizat se prezintă în tabelul 3.

Table 3

Basic data of the experiment carried out

Factors	Levels	Units of measurement	Description
Position	3	mm	Tools working position (vertical)
Tools	7	degrees	Value of the sharpening angle of the tools
Chamfer	4	mm	Value of the cutting edge chamfering of the tools
Angle of attack	3	degrees	Value of the tool's angle of attack
Force		N	Measured value of the drag resistance force of the tools

For each of the 252 tests performed, the measured data were recorded, were further processed by segmenting the appropriate values for starting and stopping the stand. To determine the average value, a low pass Butterworth filter of order 4 was applied with a cutting frequency of 0.1 Hz for all measurements made.

After processing the data from the experimental tests conducted, the average values resulted for the forwarding resistance forces for all (3x7x4x3) combinations of the modeled factor levels.

Pentru fiecare din cele 252 de încercări efectuate, s-au înregistrat datele măsurate care ulterior au fost prelucrate prin segmentarea valorilor corespunzătoare pornirii şi opririi standului. Pentru determinarea valorii medii a fost aplicat un filtru Butterworth trece jos de ordinul 4 cu o frecvenţă de tăiere de 0,1 Hz pentru toate măsurătorile efectuate.

În urma prelucrării datelor încercărilor experimentale efectuate, au rezultat valorile medii ale forţelor de rezistenţă la înaintare pentru toate cele 3x7x4x3 combinaţii ale nivelelor factorilor modelaţi.

Table 4

Tool wear data

Input / Output	New tool					Worn tool							
	F	***i***	***A***	***K***	***L***	F_w	i_w	A_w	K_w	L_w	***S***	***T***	***U***
	[N]	**[mm]**	**[mm²]**	**[mm³]**	**[g]**	**[N]**	**[mm]**	**[mm²]**	**[mm³]**	**[g]**	**[%]**	**[%]**	**[ha]**
a = f(α, ε, *position*); b = 20 [mm]; l_{ug} = 3.24 [g/ha]; j = {2, 4, 6} [mm]; α = {60, 75, 90} [°]; ε = {15, 30, 45, 60, 90, 120} [°]; ρ=7.85 x 10^{-2} [g/mm³]	*measured*	$\frac{b}{2 \cdot \tan\frac{\varepsilon}{2}}$	$\frac{b \cdot i}{2}$	$A \cdot \frac{a}{\sin\alpha}$	$\rho \cdot K$	*measured*	$\frac{j}{2 \cdot \tan\frac{\varepsilon}{2}}$	$\frac{j \cdot i_w}{2}$	$A_w \cdot \frac{a}{\sin\alpha}$	$\rho \cdot K_w$	$\frac{L_w \cdot 100}{L}$	$\frac{F_w \cdot 100}{F}$	$\frac{\rho \cdot K_w}{I_{ug}}$

Data was centralized and processed according to Table 4 where the index *w* refers to the worn volume of the cutting edge: *F* - the drag force; *i* - the height of the triangle corresponding to the cutting edge volume (unworn volume) respectively wasted volume; *A* - triangular sectional area of the cutting edge; *K* - cutting edge volume; *L* - mass of the volume of the cutting edge; *S* – mass of worn volume related to unused volume; *T* - the ratio of the worn tool's drag relative to the unworn one; *U*- the equivalent value of the processed area of agricultural land.

Datele au fost centralizate şi prelucrate conform tabelului 4 în care indicele *w* se referă la volumul uzat al muchiei tăietoare: *F* - forţa de rezistenţă la înaintare; *i* - înălţimea triunghiului corespunzător volumului muchiei tăietoare (volum neuzat) respectiv volumului uzat; *A* - aria secţiunii triunghiulare a muchiei tăietoare; *K* – volumul muchiei tăietoare; *L* – masa volumului muchiei tăietoare; *S* – masa volumului uzat raportată la masa volumului neuzat; *T* – raportul dintre rezistenţa la înaintare a sculei uzate raportată la cea neuzată; *U* – valoarea echivalentă a suprafeţei terenului agricol prelucrat.

RESULTS

Starting from the measured and processed data a statistical model was performed to describe the impact of the influence from the tool's sharpening angle on the size of linear wear of the tools used in the experimental tests performed. Having as a dependent variable (Y) the *linear wear* parameter and as the independent variable (X) the values of the sharpening angles (ε) of the tools used in the experimental tests conducted, the general form of the model selected from the models in the Statgraphics software which shows the maximum correlation and R^2 parameter has the shape (1), where *n* and *m* are the coefficients of the regression equation equivalent to the origin ordinate respectively the slope of a line. The results of the statistical procedure are presented in Table 5.

The regression curve equation obtained is presented in the relation (2).

REZULTATE

Pornind de la datele măsurate şi prelucrate s-a realizat un model statistic care să descrie impactul influenţei unghiului de ascuţire al sculei asupra mărimii uzării liniare a sculelor utilizate în cadrul încercărilor experimentale efectuate. Având ca variabilă dependentă (Y) parametrul *uzare liniară* şi ca variabilă independentă (X) valorile unghiurilor de ascuţire (ε) a sculelor utilizate în cadrul încercărilor experimentale efectuate, forma generală a modelului selectată dintre modelele aplicaţiei Statgraphics ce prezintă valoarea maximă a corelaţiei şi a parametrului R^2 are forma (1), unde *n* şi *m* sunt coeficienţii ecuaţiei de regresie echivalenţi ordonatei la origine respectiv pantei unei drepte. Rezultatele procedurii statistice sunt prezentate in tabelul 5.

Ecuaţia curbei de regresie obţinută este prezentată în relaţia (2).

$$Y = (n+m\cdot\ln(X))^2 \quad (1)$$

Table 5

Results of simple regression procedure

Parameter	*Estimated value (smallest squares)*	*Standard error*	*T*	*P*
n	10.0625	0.428296	23.4943	0.0000
m	-1.87473	0.103318	-18.1452	0.0000

Dispersion error

Source	*Sum of squares*	*Diff.*	*Square average*	*F*	*P*
Model	548.199	1	548.199	329.25	0.0000
Residue	416.25	250	1.665		
Total (Corr.)	964.45	251			
Correlation coefficient= -0.753927 R^2= 56.8407 % Standard estimation error= 1.29035 Absolute error average= 0.935438 d (Durbin-Watson test)= 0.0252341 (P=0.0000) h (D-W test for residue autocorrelation) = 0.970523					

$$Linear\ wear = (10.0625 - 1.87473\cdot\ln(\varepsilon))^2 \quad (2)$$

Having a value on the *P* coefficient from the ANOVA table of less than 0.05 results in a link relation statistically significant between the linear wear and the tool's angle of sharpening. Statistically adjusted R^2 value indicates that the obtained regression curve equation explains 56.8% of the variability for the *linear wear* parameter after the linearization of the model. The value of the correlation coefficient indicates a moderate intensity of the link between variables. The standard error of the estimate shows the standard residue deviation and can be used to define the limits of prediction of the new observations where it is desired to make predictions on the basis of the developed model.

The average absolute error shows the average of the residue values. The Durbin-Watson statistic test tests the residues to determine if there are significant correlations based on the order in which they occur in the data used. Because the value of *P* coefficient is smaller than 0.05, this indicates the possibility of serial correlation to a minimum confidence level of 95%.

Because the R^2 value is only 56.8%, a discrepancy test was applied to determine whether the selected model is appropriate to describe the measured data or if it is necessary to use a different, more complex model. The test is performed by comparing the waste dispersion from the current model with the dispersion between measurements at the iterated values of the independent variable X, and its results are presented in Table 6.

Având valoarea coeficientului *P* din tabelul ANOVA mai mică decât 0.05 rezultă o relaţie de legătură semnificativă din punct de vedere statistic între uzura liniară şi unghiul de ascuţire al sculei. Valoarea R^2 ajustată statistic indică faptul că ecuaţia curbei de regresie obţinută explică 56.8% din variabilitatea parametrului *uzare liniara* după liniarizarea modelului. Valoarea coeficientului de corelare indică o intensitate moderată a legăturii între variabile. Eroarea standard a estimării arată deviaţia standard a reziduurilor şi poate fi folosită pentru a defini limitele de predicţie a noilor observaţii în cazul în care se doreşte a se face predicţii pe baza modelului dezvoltat.

Eroarea absolută medie arată media valorilor reziduurilor. Testul statistic Durbin-Watson testează reziduurile pentru a determina dacă există corelaţii semnificative bazate pe ordinul la care apar în datele utilizate. Pentru că valoarea coeficientului *P* este mai mică de 0.05, aceasta indică posibilitatea unei corelaţii seriale la un nivel minim de încredere de 95 %.

Pentru că valoarea R^2 este de doar 56.8 % s-a aplicat şi un test de neconcordanţă pentru a determina dacă modelul selectat este adecvat pentru a descrie datele măsurate sau dacă este necesară utilizarea unui alt model mai complex. Testul este realizat prin compararea dispersiei reziduurilor modelului curent cu dispersia între măsurători la valorile iterate ale variabilei independente X iar rezultatele acestuia se prezintă în tabelul 6.

Table 6

Dispersion analysis for the discrepancy testSource	Sum of squares	Diff.	Square average	F	P
Model	548.199	1	548.199	329.25	0.0000
Residue	416.25	250	1.665		
Discrepancy	10.027	5	2.0054	1.21	0.3052
Error	406.223	245	1.65805		
Total (correlated)	964.45	251			

The value of P coefficient is higher than 0.05 for the discrepancy value which indicates that the model used is suitable for the measured data at a confidence level of at least 95%.

On the basis of the above, was passed to the graphic representation of the regression equation, the limits of the confidence interval and the prediction limits, together with the measured data (Fig. 4).

Valoarea coeficientului *P* este mai mare decât 0,05 pentru valoarea neconcordanţei ceea ce denotă faptul că modelul utilizat este adecvat pentru datele măsurate la un nivel de încredere de minim 95%.

În baza celor de mai sus, s-a trecut la reprezentarea grafică a ecuaţiei de regresie, a limitelor intervalului de încredere şi a limitelor de predicţie, alături de datele măsurate (fig. 4).

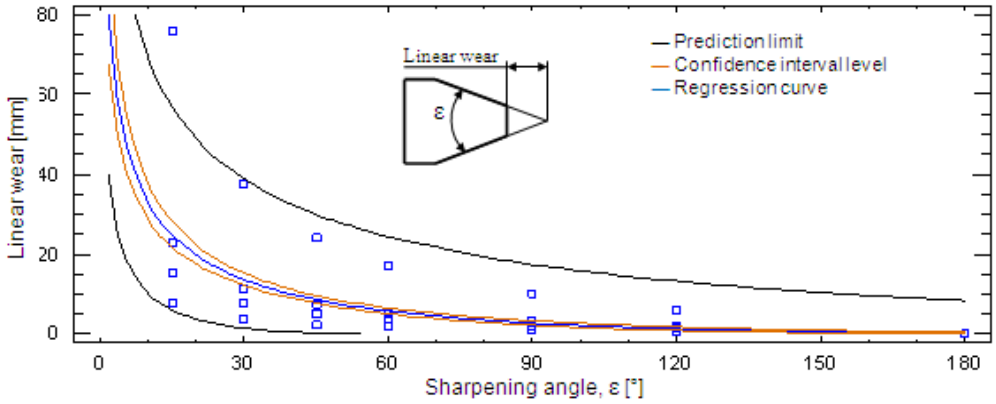

Fig. 4 – The influence of the tool's sharpening angle on their linear wear

From the figure above is easily observed the great influence that the tool's sharpening angle has on the wear, respectively on the linear wear, so that it shows a great importance the choice of this angle in order to achieve a compromise between the tool's drag force (which increases with the increase of wear), and the value of the volume of mobilized soil.

Taking into account the results presented by Tomescu et al. [13] for the witness furrows of the SPC-6 seed drill, respectively the value for the average intensity of wear on the working tool I_{ug} = 3.24 g/ha, results in a set of data in conformity with table X that expresses the used volume mass and the equivalent value of processed agricultural land area. Thus, another model was developed to show the influence of equivalent processed area in relation to the linear wear of the tools used in the experimental tests of this paper.

The general form of the model used that best responds to the measured data, chosen for the maximum values of the correlation coefficient and the R^2 value is given in the relation (3).

Following the introduction of measured data in the Statgraphics application revealed the following in accordance with Table 7.

The equation of the regression curve obtained is shown in the relation (4).

Din figura de mai sus se observă cu uşurinţă influenţa mare pe care o prezintă unghiul de ascuţire al sculelor asupra uzării respectiv asupra uzurii liniare, astfel încât prezintă o mare importanţă alegerea acestui unghi în a realiza un compromis între valoarea rezistenţei la înaintare a sculei (care creşte odată cu creşterea uzurii) şi valoarea volumului de sol mobilizat.

Luând în considerare rezultatele prezentate de Tomescu et al. [13] pentru brăzdarele martor ale semănătorii SPC-6, respectiv valoarea intensităţii medii a uzurii pe scula de lucru de I_{ug} = 3.24 g/ha, rezultă o serie de date în conformitate cu tabelul X ce exprimă valoarea masei volumului uzat şi respectiv valoarea echivalentă a suprafeţei terenului agricol prelucrat. Astfel, s-a realizat un alt model care să arate influenţa ariei prelucrate echivalente în raport cu uzura liniară a sculelor utilizate în cadrul încercărilor experimentale din prezenta lucrare.

Forma generală a modelului utilizat ce răspunde cel mai bine datelor măsurate, ales pentru valorile maxime ale coeficientului de corelare şi a valorii R^2 este dată în relaţia (3).

În urma introducerii datelor măsurate în cadrul aplicaţiei Statgraphics au rezultat următoarele în conformitate cu tabelul 7.

Ecuaţia curbei de regresie obţinută este prezentată în relaţia (4).

$$Y = (a+b \cdot X)^2 \quad (3)$$

Table 7

Result of the simple regression procedure

Parameter	*Estimated value (smaller squares)*	*Standard error*	*T*	*P*
n	0.886856	0.110713	8.01041	0.0000
m	0.224812	0.0060662	37.0598	0.0000

Dispersion analysis

Source	Sum of squares	*Diff.*	Square average	*F*	*P*
Model	3033.37	1	3033.37	1373.43	0.0000
Residue	552.151	250	2.20861		
Total (correlated.)	3585.52	251			
Correlation coefficient = 0.919785 R^2= 84.6005 % R^2(adjusted for d.f.) = 84.5389 % Standard estimation error = 1.48614 Absolute error average = 1.00157 d (Durbin-Watson test)= 0.62325 (P=0.0000) h (D-W test for residue autocorrelation) = 0.645962					

$$\text{Processed area} = (0.886856 + 0.224812 \cdot \text{linear wear})^2 \quad (4)$$

In this model also, the value of the P coefficient from the ANOVA table is less than 0.05 indicating a significant relation form a statistical point of view between the processed area and linear wear. The value of R^2 statistically adjusted shows a rate of 84.6% explaining the variability of the processed area parameter after linearization of the model. The correlation coefficient of 0.919 indicates a strong relation between the variables of the model. The value of the *P* coefficient in the Durbin-Watson test indicates a possible serial correlation at a confidence level of at least 95%, for this being necessary to test the level of discrepancy (Table 8).

Şi în acest model, valoarea coeficientului P din tabelul ANOVA este mai mică decât 0.05 ceea ce indică o relaţie semnificativă din punct de vedere statistic între aria prelucrata şi uzura liniară. Valoarea lui R^2 ajustată statistic arată un procent de 84,6% care explică variabilitatea parametrului aria prelucrata după liniarizarea modelului. Coeficientul de corelare de 0,919 arată o relaţie puternică între variabilele modelului. Valoarea coeficientului *P* în cadrul testului Durbin-Watson arată o posibilă corelare serială la un nivel de încredere de minim 95%, pentru aceasta fiind necesar a se testa şi nivelul de neconcordanţă (tabelul 8).

Table 8

Dispersion analysis for the discrepancy test

Source	*Sum of squares*	*Diff.*	*Square average*	*F*	*P*
Model	3033.37	1	3033.37	1373.43	0.0000
Residue	552.151	250	2.20861		
Discrepancy	395.018	22	17.9553	26.05	0.0000
Error	157.134	228	0.689183		
Total (correlated)	3585.52	251			

The results of the above test show that although the value of R^2 is higher, there is a significant discrepancy from a statistical point of view, by the value of the P coefficient of less than 0.05, which imposes the selection of a different model that describes the influence of the linear wear on the processed area.

Rezultatele testului de mai sus arată faptul că deşi valoarea lui R^2 este mare, apare o neconcordanţă semnificativă din punct de vedere statistic, prin valoarea coeficientului *P* mai mică de 0.05, ceea ce impune selectarea unui alt model care să descrie influenţa uzurii liniare asupra suprafeţei prelucrate.

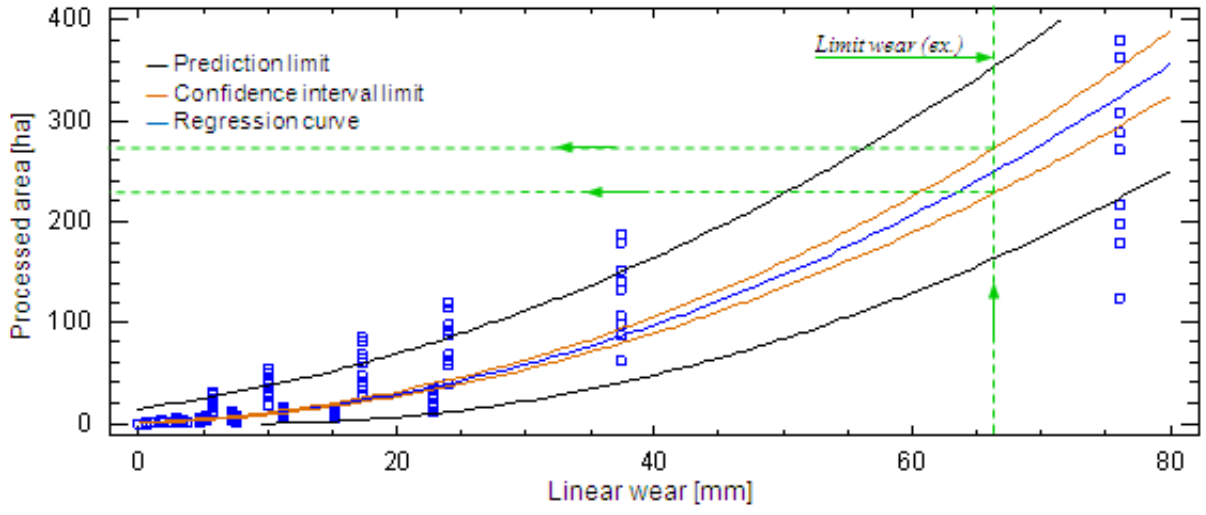

Fig. 5 - Correspondence between the processed area and the tool's linear wear

Figure 5 shows a logarithmic increase of the linear wear according to the processed area, the utility of such chart being that it shows the average area that can be processed by a tool until it reaches a limit value of linear wear.

CONCLUSIONS

The geometry of the cutting edge or of the work surface contour of a tool for processing soil shows a particular importance in minimizing the necessary energy for the working process.

Through wear, during the working process, the constructive parameters of the cutting edge corresponding to the soil processing tools change, having a negative influence on the technical-economic indicators of the process.

Processing the experimental results obtained by mathematical modeling highlights the correlation between the processed surface and the linear wear of tools.

The results obtained and presented can be used to determine the area of the agricultural surface processed by a tool that has reached a certain value of linear wear.

REFERENCES

[1]. Bobobee E.Y.H., Gebresenbet G., (2007) - *Effect of cutting edge thickness and state of wear of ploughshare on draught force and heart rates of Sanga oxen in Ghana*. Soil &Tillage Research, 95, pg.298-307;
[2]. Fechete L.V., (2008) - *Researches regarding optimization of soil tillage process*, Doctoral Thesis, Cluj-Napoca;
[3]. Fielke J.M. et al., (1993) - *Comparisons of tillage forces and wear rates of pressed and cast cultivator shares*. Soil &Tillage Research, 25, pg.317-328;
[4]. Fielke J.M., (1996) - *Interactions of the cutting edge of tillage implements with soil*. JAER, 63, pg.61-72;
[5]. Godwin R.J., (2007) - *A review of the effect of implement geometry on soil failure and implement forces*. Soil & Tillage Research 97, pg.331-340;
[6]. Inns F.M. (1990) - *The mechanics of animal-draught cultivation implements*. Agricultural Engineering, 45 (1) pg.13-17;
[7]. Natsis A., Papadakis G., Pitsilis J., (1999) - *The influence of soil type, soil water and share sharpness of a moldboard plough on energy consumption, rate of the tillage quality*. JAER, 72, pg.171-176;
[8]. Neculăiasa V., Ţenu I., (1996) - *The basis of experimental research on machines and installations in agriculture and food industry* (*tribological research),* Iaşi;
[9]. Nichols M.L., Reed I.F., Reeves C.A., (1958) - *Soil reaction to plough share design*. Agricultural Engineering, 39 (6), pg.336-339;
[10]. Roş V. et al., (1993) - *Analysis of tillage tool geometry*. ASAE Paper No.931091. Spokane, Washington: ASAE;
[11]. Shoji K., (2004) - *Forces on a model 'spot plough'*. Biosyst. Eng., 87 (1), pg.39-45;
[12]. Tenenbaum M.M. et al., (1957) - *Particularities of wear for parts from carboniferous machines*, IDT Bucharest;
[13]. Tomescu D. et al., (1971) - *Reconditioning and increasing the wear resistance of active bodies form agricultural machines*. Ceres Publishing, Bucharest;
[14].*** http://www.hbm.com/
[15].*** http://www.statgraphics.com/

Din figura 5 se observă o creştere logaritmică a uzurii liniare în funcţie de aria prelucrată, utilitatea unui astfel de grafic regăsindu-se în a arăta suprafaţa medie pe care o poate prelucra o sculă până să ajungă la o valoare limită a uzurii liniare.

CONCLUZII

Geometria muchiei tăietoare sau a conturului suprafeţei de lucru a sculelor pentru prelucrarea solului prezintă o importanţă deosebită în minimizarea energieii necesare în cadrul procesului de lucru.

Prin uzare, în timpul procesului de lucru, parametrii constructivi ai muchiei tăietoare aferente sculelor de prelucrat solul se modifică, având influenţă negativă asupra indicatorilor tehnico-economici de proces.

Prelucrarea rezultatelor obţinute experimental prin modelare matematică pune în evidenţă corelarea între suprafaţa prelucrată şi uzura liniară a sculelor.

Rezultatele obţinute şi prezentate pot fi folosite pentru stabilirea ariei suprafeţei agricole prelucrate de către o sculă care a atins o anumită valoare a uzurii liniare.

BIBLIOGRAFIE

[1]. Bobobee E.Y.H., Gebresenbet G., (2007) – *Efectul grosimii muchiei tăietoare şi a gradului de uzură a brăzdarului asupra forţei de înaintare şi a incidenței bolilor cardiace la boii Sanga din Ghana*, Soil &Tillage Research, 95, pag.298-307;
[2]. Fechete L.V., (2008) - *Cercetări privind optimizarea procesului de prelucrare mecanică a solului*, Teză de doctorat, Cluj-Napoca;
[3]. Fielke J.M. et al., (1993) – *Comparaţii între forţele de prelucrare a solului şi gradul de uzură a cuțitelor cultivatoarelor turnate*, Soil&Tillage Research, 25, 317-328;
[4]. Fielke J.M., (1996) – *Interacţiuni ale muchiei tăietoare a utilajului cu solul,* JAER, 63, pag.61-72;
[5]. Godwin R.J., (2007) – *O analiză a efectului geometriei sculei si forţelor aplicate, asupra deformării solului si a fortelor de implementare,* Soil & Tillage Research 97, pag.331-340;
[6]. Inns F.M., (1990) – *Mecanica animalelor – unelte pentru cultivare*, Agricultural Engineering, 45 (1) p:13-17;
[7]. Natsis A., Papadakis, G., Pitsilis, J. (1999) – *Influenţa tipului de sol, a umidităţii solului şi a gradului de ascuţire a cormanei plugului, asupra consumului de energie şi a calităţii lucrării de arat*, JAER, 72, pag.171-176;
[8]. Neculăiasa V., Ţenu I., (1996) - *Bazele cercetării experimentale a maşinilor şi instalaţiilor din agricultura şi industria alimentară (cercetări tribologice)*, Iaşi;
[9]. Nichols M.L., Reed I.F., Reeves C.A., (1958) – *Influența construcției plugului asupra solului*, Inginerie Agricolă, 39 (6), pag.336-339;
[10]. Roş, V. et al., (1993) – *Analiza geometriei sculei de prelucrare a solului,* ASAE Paper No.931091. Spokane, Washington: ASAE;
[11]. Shoji K., (2004) –*Analiza forţelor la un plug cu intoarcerea 'în loc' a brazdei*, Biosyst. Eng.,87(1), pag.39-45;
[12]. Tenenbaum M.M. et al., (1957) - *Particularităţile uzării pieselor de la maşinile carboniere,* IDT Bucureşti;
[13]. Tomescu D. ş.a, (1971) - *Recondiţionarea şi mărirea rezistenţei la uzură a organelor active de la maşinile agricole*. Editura Ceres, Bucureşti;
[14].*** http://www.hbm.com/
[15].*** http://www.statgraphics.com/

DEFINITION OF BASIC PARAMETERS OF SMALL-SIZED FLEXIBLE HARROW / ВИЗНАЧЕННЯ ОСНОВНИХ ПАРАМЕТРІВ МАЛАГАБАРИТНОЇ ГНУЧКОЇ БОРОНИ

PhD. Eng. Usenko M.
Lutsk National Technical University / Ukraine
Tel: +38(0332)74-61-03; Fax: +38(0332)77-48-40; E-mail: rector@lutsk-ntu.com.ua

Abstract: *The advantages and disadvantages of different constructions of flexible harrows are analyzed. A new construction of the flexible chain harrow with tines that rotate in different planes by contact with the soil is presented. The angles of outside links of the harrow and, accordingly, its working width are defined. The power to work of flexible chain harrow is defined.*

Keywords: *motoblock, harrow, chain, link, tine, angle, width, force, power*

INTRODUCTION

Operation of basic soil tillage is prior to all operations for growing crops. Lately gets spread progressive system of minimum tillage which includes reducing of the number of tillages and declining of their depth by combining of various working operations such as ploughing and harrowing. To ensure of this tillage, it is necessary to use combined tillage tools.

Today for the operation of minimum tillage the combined units are used. A lot of constructions among which plows with flexible rotary harrows are developed [1, 2]. These harrows are called modular, flexible, and they are made in the form of chain with tines. Most of these harrows give good work results. But they have disadvantages, namely, their working parts (tines) cannot rotate by the contact with the soil in the longitudinal-vertical and horizontal planes and it is lead to faulty cultivation of different soil texture.

In many scientific papers the parameters of working tools for secondary tillage are substantiated and their constructions are discussed [3, 4, 5, 6, 7]. But many questions are not still clearly understood. Accordingly, the questions of theoretical substantiation of working parts parameters of the new constructions of flexible harrows, particularly for small-sized equipment, are not discussed.

MATERIAL AND METHOD

In works [6, 7] are described the construction of wheel-driven flexible harrow and a perspective of its use on the small-sized equipment. Theoretical researches of these works allowed defining the motion trajectory of characteristic points of flexible harrows tine and the force acting on the tine. But such important parameters as the angles of outside links of the harrow and, accordingly, its operating width and also a draught of flexible chain harrow are not defined. These parameters are particularly important in terms of using of flexible harrow with small-sized tractors and motoblocks. Operating width of small-sized harrow should not be large, since this would lead to an undesirable increase of size of the unit, as well as to increase of its draught. Therefore, the maximum use by the work of the chain harrows length, i.e. using by the work of maximum number of its units or giving it best possible working width by a given number of links are very important for such small-sized harrow.

Резюме: *Проаналізовано переваги та недоліки різних конструкцій гнучких борін. Подана нова конструкція гнучкої ланцюгової борони з зубами, що обертаються в різних площинах при контакті з ґрунтом. Визначені кути нахилу крайніх ланок даної борони і, відповідно, її робоча ширина захвату. Визначена потужність на роботу гнучкої ланцюгової борони.*

Ключові слова: *мотоблок, борона, ланцюг, ланка, зуб, кут, ширина захвату, сила, потужність*

ПЕРЕДУМОВА

Операція основного обробітку ґрунту передує всім операціям з вирощування сільськогосподарських культур. Останнім часом набуває поширення прогресивна система мінімального обробітку ґрунту, яка передбачає скорочення кількості обробітків та зменшення їх глибини за рахунок поєднання різних технологічних операцій, наприклад, оранки і боронування. Для забезпечення такого обробітку ґрунту необхідно застосування комбінованих знарядь.

Сьогодні для виконання операції мінімального обробітку ґрунту використовують комбіновані агрегати. Розроблено багато таких конструкцій, тобто плугів з боронами гнучкими обертальними [1, 2]. Ці борони називають модульними, гнучкими, ланцюговими і вони виконані у вигляді ланцюга з зубами. В основному дані борони дають хороші результати роботи. Але вони мають недоліки, а саме їх робочі органи (зуби) не можуть обертатись при контакті з ґрунтом в поздовжньо-вертикальній та в горизонтальній площинах, що призводить до неякісного обробітку різних за механічними складом ґрунтів.

В багатьох наукових працях обґрунтовані параметри робочих органів для передпосівного обробітку ґрунту та розглянуті їх конструкції [3, 4, 5, 6, 7]. Але багато питань ще повністю не вивчені. Відповідно, не розглянуті питання теоретичного обґрунтування параметрів робочих органів нових конструкцій гнучких борін, зокрема, для малогабаритної техніки.

МАТЕРІАЛ І МЕТОДИКА

В роботах [6, 7] описана конструкція борони гнучкої з приводом від колеса та перспективність її застосування на малогабаритній техніці. Теоретичні дослідження даних робіт дозволили визначити траєкторію руху характерної точки зубу борони гнучкої і силу, що діє на зуб. Але такі важливі параметри як кут нахилу крайніх ланок борони і, відповідно, її ширина захвату, а також тяговий опір гнучкої ланцюгової борони не визначені. Дані параметри особливо важливі з точки зору використання гнучкої борони в агрегаті з малогабаритними тракторами і мотоблоками. Ширина захвату малогабаритної гнучкої борони не повинна бути великою, оскільки це призведе до небажаного збільшення габаритів агрегату, а також до збільшення його тягового опору. Тому максимальне використання при роботі довжини ланцюгової борони, тобто залучення в роботу максимальної кількості її ланок або надання їй найбільш можливої робочої ширини захвату при даній кількості ланок є дуже важливим для такої малогабаритної борони.

For qualitative tillage we proposed the flexible harrow with adjustable tines [8]. Here you can set the desired position (angle) of loosening tines 6, which determines their operation (Fig. 1). The angle of the tines 6 to the longitudinal axis of link is provided by the appropriate position of the bases 3, which are fixed with bolt 2. By turning the support 7 can be achieved the alignment of the supports 7 hole with the shaped sleeves 8 holes and the bases 3 holes for the vertical pin 9 and fix it. Vertical pin 9 can be fixed in position when loosening tine 6 will take perpendicular position to the longitudinal axis of the link, as shown on Fig. 1. To provide of more qualitative cultivation of different types of soils, than discussed above, we need to change the horizontal and vertical angles of location of loosening tines 6 to the longitudinal axis of the link. For this we need to rotate and fix by vertical pin 9 the support 7 in such position in which it is able to achieve the desired tines 6 position in the horizontal plane. To change the angle of the tines 6 in the vertical plane it is necessary to change the location of the bases 3, for the purpose we tighten and release each other bolts 2 as long as the bases 3 do not lie completely by one of the faces of their multifaceted surfaces on the link. In such position of two bases 3, which are attached to the same link, it is provided a stable angle of these bases and, accordingly, of tines 6 in the vertical plane. Optimum angles are selected according to external conditions of work.

Fig. 2 presents a plow with flexible harrow, which is aggregated to motoblock.

Для якісного обробітку ґрунту нами запропонована борона гнучка з регульованим зубами [8]. Тут можливо встановити необхідне положення (кут нахилу) розпушуючих зубів *6*, що визначає їх режим роботи (рис. 1). Кут нахилу зубів *6* до поздовжньої осі ланки забезпечується відповідним положенням основ *3*, яке фіксується за допомогою болтів *2*. Поворотом опори *7* можна досягти співпадання отвору даної опори з отворами фігурної втулки *8* і основи *3* для вертикального пальця *9* і закріпити його. Вертикальний палець *9* можна закріпити в такому положенні, коли розпушуючий зуб *6* займе перпендикулярне положення до поздовжньої осі ланки, як і показано на рис. 1. Для забезпечення більш якісного, ніж у вищерозглянутому випадку, обробітку різних типів ґрунтів необхідно змінити горизонтальні і вертикальні кути розташування розпушуючих зубів *6* до поздовжньої осі ланки. Для цього опору *7* необхідно провернути і зафіксувати вертикальним пальцем *9* в такому положенні, щоб можна було досягти необхідного розташування зубу *6* у горизонтальній площині. Для зміни кута розташування зубів *6* у вертикальній площині необхідно поміняти розташування основ *3*, для чого попеременно відпускають один і затягують іншій болти *2* до тих пір, поки основи *3* не ляжуть повністю однією з граней своїх багатогранних поверхонь на ланку. При такому положенні двох основ *3*, що закріплені на одній ланці, забезпечується стабільний кут розташування цих основ і, відповідно, зубів *6* у вертикальній площині. Оптимальні кути підбираються в залежності від зовнішніх умов роботи.

На рис. 2 поданий плуг з гнучкою борною, яка агрегатується до мотоблоку.

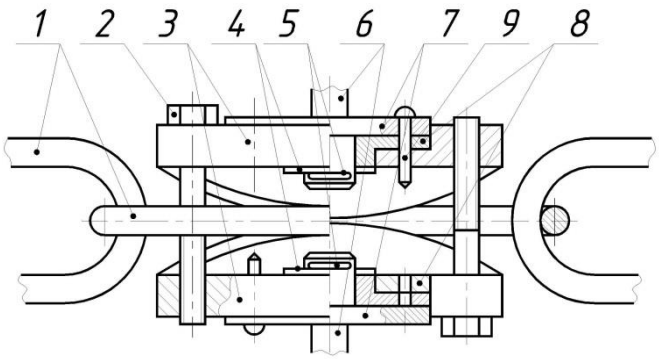

Fig. 1 - Flexible harrow with adjustable tins (excerpt)
1 – chain module with links; 2 – fasteners; 3 – bases ; 4 – washers; 5 – horizontal pins; 6 – loosening tines; 7 – supports; 8 – shaped sleeves; 9 – vertical pin

Fig. 2 – Motoblock with plow with flexible harrow

RESULTS

To characterize the work of the harrow it is necessary to determine the angles of outside links and therefore, the depth of plunging of the tines in the soil and then the power to the work. We consider two outside links of the chain on each side, which do not lie fully on the soil surface. We accept that other central links are fully lying on the soil. An attachment of the outside links to the frame is hinged, and then we take the following fastening scheme of two outside links. At a hinge *O* is fixed homogeneous link (rod) *OA* of the length $2l_1$ and of the weight P_1, at the point *A* with this link is connected by a hinge the second homogeneous link (rod) *AB* of the length $2l_2$ and of the weight P_2, to end *B* of this link is applied a horizontal force P_3. The whole system is in balance in the vertical plane. It is necessary to define the angles φ_1 and φ_2 of links *OA* and *AB* with vertical (Fig.3).

РЕЗУЛЬТАТИ

Для характеристики роботи даної борони необхідно визначити кути нахилу її крайніх ланок і, відповідно, глибину занурення їх зубів в ґрунт і потім потужність на роботу. Будемо розглядати дві крайні ланки ланцюга з кожного боку, які не лежать повністю на поверхні ґрунту. Приймаємо, що інші центральні ланки повністю лежать на ґрунті. Оскільки кріплення крайніх ланок до рами шарнірне, то приймаємо наступну схему кріплення двох крайніх ланок. На шарнірі *O* закріплена однорідна ланка (стрижень) *OA* довжиною $2l_1$ і вагою P_1, в точці *A* з даною ланкою з'єднана за допомогою шарніру друга однорідна ланка (стрижень) *AB* довжиною $2l_2$ і вагою P_2, до кінця *B* даної ланки прикладена горизонтальна сила P_3. Вся система знаходиться в рівновазі у вертикальній площині. Тут необхідно визначити кути φ_1 і φ_2 ланок *OA* і *AB* з вертикаллю (рис. 3).

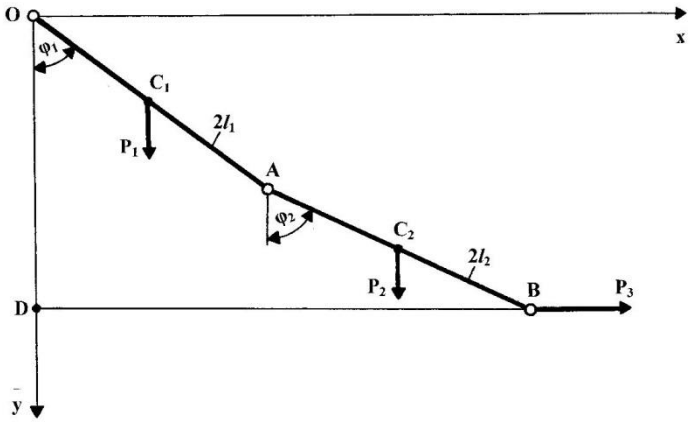

Fig. 3 – Scheme to defining the angles φ_1 and φ_2 of links *OA* and *AB* with vertical

We take the coordinate axes, as shown in Fig. 3. The angles φ_1 and φ_2 we take for generalized coordinates that define the position of the system. From Fig. 3 we find that the coordinates of the points C_1 (x_1, y_1), C_2 (x_2, y_2), B (x_3, y_3), where the forces applied, expressed by φ_1 and φ_2 as follows:

Приймаємо осі координат, як вказано на рис. 3. Кути φ_1 і φ_2 приймаємо за узагальнені координати, які визначають положення даної системи. З рис. 3 знаходимо, що координати точок C_1 (x_1, y_1), C_2 (x_2, y_2), B (x_3, y_3), в яких прикладені задані сили, виражаються через φ_1 і φ_2 наступним чином:

$$\left.\begin{aligned} x_1 &= l_1 \sin\varphi_1, \\ x_2 &= 2l_1 \sin\varphi_1 + l_2 \sin\varphi_2, \\ x_3 &= 2l_1 \sin\varphi_1 + 2l_2 \sin\varphi_2, \\ y_1 &= l_1 \cos\varphi_1, \\ y_2 &= 2l_1 \cos\varphi_1 + l_2 \cos\varphi_2, \\ y_3 &= 2l_1 \cos\varphi_1 + 2l_2 \cos\varphi_2. \end{aligned}\right\} \quad (1)$$

Hence we find the variations of the Cartesian coordinates of points C_1, C_2 and B, which determine the possible movement of these points as full differential functions of x_i and y_i of two independent variables φ_1 and φ_2:

Звідси знаходимо варіації декартових координат точок C_1, C_2 і B, які визначають можливі переміщення даних точок, як повні диференціали функцій x_i та y_i від двох незалежних змінних φ_1 і φ_2:

$$\left.\begin{aligned} \delta x_1 &= l_1 \cos\varphi_1 \delta\varphi_1, \\ \delta x_2 &= 2l_1 \cos\varphi_1 \delta\varphi_1 + l_2 \cos\varphi_2 \delta\varphi_2, \\ \delta x_3 &= 2l_1 \cos\varphi_1 \delta\varphi_1 + 2l_2 \cos\varphi_2 \delta\varphi_2, \\ \delta y_1 &= -l_1 \sin\varphi_1 \delta\varphi_1, \\ \delta y_2 &= -2l_1 \sin\varphi_1 \delta\varphi_1 - l_2 \sin\varphi_2 \delta\varphi_2, \\ \delta y_3 &= -2l_1 \sin\varphi_1 \delta\varphi_1 - 2l_2 \sin\varphi_2 \delta\varphi_2. \end{aligned}\right\} \quad (2)$$

Projections of forces P_1, P_2 and P_3 on the coordinate axes are equal:

Проекції сил P_1, P_2 і P_3 на координатні осі дорівнюють:

$$X_1 = 0,\ Y_1 = P_1,\ X_2 = 0,\ Y_2 = P_2,\ X_3 = P_3,\ Y_3 = 0$$

The sum of the elementary works of all forces acting on the system is defined by the general formulas:

Сума елементарних робіт всіх сил, що діють на систему, визначається за загальними формулами:

$$\left.\begin{aligned}
&\sum_{i=1}^{n}\left(X_i\frac{\partial x_i}{\partial q_1}+Y_i\frac{\partial y_i}{\partial q_1}+Z_i\frac{\partial z_i}{\partial q_1}\right)=Q_1,\\
&\sum_{i=1}^{n}\left(X_i\frac{\partial x_i}{\partial q_2}+Y_i\frac{\partial y_i}{\partial q_2}+Z_i\frac{\partial z_i}{\partial q_2}\right)=Q_2,\\
&\cdots\cdots\cdots\cdots\cdots\cdots\cdots\cdots\cdots\cdots\cdots\cdots\\
&\sum_{i=1}^{n}\left(X_i\frac{\partial x_i}{\partial q_k}+Y_i\frac{\partial y_i}{\partial q_k}+Z_i\frac{\partial z_i}{\partial q_k}\right)=Q_k.
\end{aligned}\right\} \quad (3)$$

Thus, using the general formulas (3) we can find the generalized forces Q_1 and Q_2, corresponding to the generalized coordinates φ_1 and φ_2:

Таким чином, з використанням загальних формул (3) можемо знайти узагальнені сили Q_1 та Q_2, що відповідають узагальненим координатам φ_1 і φ_2:

$$Q_1=\sum_{i=1}^{3}\left(X_i\frac{\partial x_i}{\partial \varphi_1}+Y_i\frac{\partial y_i}{\partial \varphi_1}\right)=P_1\frac{\partial y_1}{\partial \varphi_1}+P_2\frac{\partial y_2}{\partial \varphi_1}+P_3\frac{\partial x_3}{\partial \varphi_1}=$$

$$= -P_1l_1\sin\varphi_1 - 2P_2l_1\sin\varphi_1 + 2P_3l_1\cos\varphi_1 = l_1\,[2P_3\cos\varphi_1 - (P_1 + 2P_2)\sin\varphi_1] \quad (4)$$

$$Q_2=\sum_{i=1}^{3}\left(X_i\frac{\partial x_i}{\partial \varphi_2}+Y_i\frac{\partial y_i}{\partial \varphi_2}\right)=P_1\frac{\partial y_1}{\partial \varphi_2}+P_2\frac{\partial y_2}{\partial \varphi_2}+P_3\frac{\partial x_3}{\partial \varphi_2}=$$

$$= -P_2l_2\sin\varphi_2 + 2P_3l_2\cos\varphi_2 = l_2\,(2P_3\cos\varphi_2 - P_2\sin\varphi_2). \quad (5)$$

Equating to null the generalized forces Q_1 and Q_2 we have the following two equations:

Прирівнюючи до нуля узагальнені сили Q_1 та Q_2, отримаємо наступні два рівняння:

$$2P_3\cos\varphi_1 - (P_1 + 2P_2)\sin\varphi_1 = 0 \quad (6)$$

$$2P_3\cos\varphi_2 - P_2\sin\varphi_2 = 0 \quad (7)$$

After some mathematical transformations from equations (6) and (7) we have found:

Після певних математичних перетворень з рівнянь (6) та (7) знаходимо:

$$tg\varphi_1=\frac{2P_3}{P_1+2P_2}. \quad (8)$$

$$tg\varphi_2=\frac{2P_3}{P_2}. \quad (9)$$

As the links *OA* and *AB* are of the same length, i.e. $2l_1 = 2l_2 = 2l$, we can take that their weights are also the same, i.e. $P_1 = P_2 = P$. Also we take that the power P_3 is equal to the sum of two forces P_1 and P_2, i.e. $P_3 = P_1 + P_2 = 2P$, because the power P_3 is created by two mid-links of chain lying on the ground with all its length. From formulas (8) and (9) we have $\text{tg}\varphi_1 = 4/3$ and $\text{tg}\varphi_2 = 4$, where $\varphi_1 \approx 53°$ and $\varphi_2 \approx 75°$.

Now we can determine the size *OD* - height of the hinge *O* or of the frame above the soil surface. From Fig. 3 we have:

Оскільки ланки *OA* та *AB* однакові за довжиною, тобто $2l_1 = 2l_2 = 2l$, то можемо прийняти, що їх ваги також однакові, тобто $P_1 = P_2 = P$. Також приймаємо, що сила P_3 дорівнює сумі двох сил P_1 та P_2, тобто $P_3 = P_1 + P_2 = 2P$, оскільки сила P_3 створюється двома середніми ланками ланцюга, які лежать на ґрунті всією своє довжиною. З формул (8) і (9) отримуємо $\text{tg}\varphi_1 = 4/3$, а $\text{tg}\varphi_2 = 4$, звідки $\varphi_1 \approx 53°$, а $\varphi_2 \approx 75°$.

Тепер можемо визначити величину *OD* – висоту розташування шарніра *O* або рами над поверхнею ґрунту. З рис. 3 маємо:

$$OD = OA\cos\varphi_1 + AB\cos\varphi_2 = 2l_1\cos\varphi_1 + 2l_2\cos\varphi_2 = 2l\cos\varphi_1 + 2l\cos\varphi_2 = 2l\,(\cos\varphi_1 + \cos\varphi_2) \quad (10)$$

Taking constructive the links length of $2l$ = 10 cm we determine from the formula (10) the value of $OD \approx$ 8.6 cm. This value is acceptable in terms of free passage of frame in the presence of stitches on the soil surface and related to setting of the necessary position of depth wheel.

Working width of harrow is approximately 50 cm in view of the fact that the length of a link is equal to 15 cm (by the outsides points of the tines) and in the work there are involved two central links fully and two outsides (on each side) links in part.

Now we can define the power to work of the harrow. As the angle to the vertical of the link AB is $\varphi_2 \approx 75°$, we have that the tines of this link plunge in the soil, but not fully. In the formula for defining of the power which is supplied on work of harrows, such factors as a section of soil chip c, tillage depth h, the mass of soil that is threw in 1 s Q_s should be taken a little less.

The power which is supplied on work of harrow can be defined from the known formula [4]:

Приймаючи конструктивно довжину ланки $2l$ = 10 см, визначаємо за формулою (10) величину $OD \approx$ 8,6 см. Таке значення є прийнятним з точки зору забезпечення вільного проходу рами при наявності гребенів на поверхні ґрунту та для встановлення необхідного положення опорного колеса.

Робоча ширина захвату борони становить приблизно 50 см з врахуванням того, що довжина однієї ланки дорівнює 15 см (по крайніх точках зубів) і в роботі беруть участь дві центральні ланки повністю і дві крайні (з кожного боку) ланки частково.

Тепер можемо визначити потужність на роботу борони. Оскільки кут нахилу ланки AB до вертикалі становить $\varphi_2 \approx$ 75°, то можемо прийняти, що зуби даної ланки входять в ґрунт, але не повністю. В формулі для визначення потужності, що витрачається на роботу борони, такі коефіцієнти як переріз ґрунтової стружки c, глибина обробітку h, маса ґрунту, що відкидається за 1 с Q_s слід прийняти дещо меншими.

Потужність, що витрачається на роботу борони, можна визначити за відомою формулою [4]:

$$N = 10^{-3} f m g v + 10^{-4} k c h z n /6 + 10^{-3} \delta Q_s v_c^2 \quad (11)$$

Where

f – rolling coefficient (0.2),
m - mass of the harrow (8 kg),
g – gravitational acceleration (9.81 m/s^2),
v – speed of the harrow (0.4 m/s),
k - soil resistivity (0.03 MPa),
c - section of soil chip (50 cm^2),
h - tillage depth (10 cm),
z - number of tillage tools (16 pcs.),
n – rotation frequency of the harrow (17 min^{-1}),
δ - coefficient of throwing, depending on the shape of tillage tool (≈ 1),
Q_s - mass of soil that is thrown in 1 s (≈ 5 kg/s),
v_c - linear speed of the harrow (0.4 m/s).

Substituting these data in the formula (11) we get $N \approx 0.078 \approx 0.1$ kW.

Power of the motoblock for tillage operations (plowing with harrowing) is 5-6 kW. As seen from the calculation this power is sufficient for efficient conduct of this operation.

CONCLUSIONS

Resulted higher analysis of work of the flexible chain harrow allows to defining the angles of outside links of the harrow and, accordingly, its working width and the power to work of this harrow also.

It is established that the angle to the vertical of the outside (on each side) link with tines is 75°, so the tines of this link plunge in the soil, but not fully.

It is established that working width of harrow is approximately 50 cm.

It is established that power which is supplied on work of harrow is approximately 0.1 kW, and as the power of the motoblock for tillage operations (plowing with harrowing) is 5-6 kW, so it is sufficient for efficient conduct of this operation.

We developed a new construction of the flexible chain harrow with tines which are rotated by the contact with the soil in the different planes. This allows providing more intensive tillage cultivation, to increase its quality and reducing the cost of power to work of harrows.

де

f – коефіцієнт перекочування (0,2),
m – маса борони (8 кг),
g – прискорення вільного падіння (9,81 м/с^2),
V – швидкість руху борони (0,4 м/с),
k – питомий опір ґрунту (0,03 МПа),
c – переріз ґрунтової стружки (50 см^2),
h – глибина обробітку ґрунту (10 см),
z–число робочих органів (16 шт.),
n – частота обертання борони (17 хв$^{-1}$),
δ – коефіцієнт відкидання, що залежить від форми робочого органа (≈ 1),
Q_s – маса ґрунту, що відкидається за 1 с (≈ 5 кг/с),
v_c – колова швидкість борони (0,4 м/с).

Підставляючи значення в формулу (11) отримуємо $N \approx 0{,}078 \approx 0{,}1$ кВт.

Потужність мотоблока для виконання операції обробітку ґрунту (оранка з боронуванням) становить 5-6 кВт. Як видно з розрахунків така потужність є достатньою для якісного проведення даної операції.

ВИСНОВКИ

Наведений теоретичний аналіз роботи гнучкої ланцюгової борони дає можливість визначити кути нахилу крайніх ланок даної борони і, відповідно, її робочу ширину захвату, а також потужність на роботу даної борони.

Встановлено, що кут нахилу до вертикалі крайньої (з кожного боку) ланки з зубами становить 75°, і таким чином, зуби даної ланки входять в ґрунт, але не повністю.

Встановлено, що робоча ширина захвату борони становить приблизно 50 см.

Встановлено, що потужність, що витрачається на роботу борони становить приблизно 0,1 кВт і оскільки потужність мотоблока для виконання операції обробітку ґрунту (оранка з боронуванням) становить 5-6 кВт, то вона є достатньою для якісного проведення даної операції.

Розроблена нова конструкція гнучкої ланцюгової борони з зубами, що обертаються в різних площинах при контакті з ґрунтом. Це дозволяє забезпечити більш інтенсивний обробіток ґрунту, підвищити якість обробітку і зменшити витрати потужності на роботу даної борони.

Resulted higher method of calculation is the main for the flexible chain harrows of such construction and, accordingly, for the matching of its optimal parameters for work in various environmental conditions.

REFERENCES

[1]. Bezdolny M.I., (1995) – *Agricultural unit*, Patent №17384 Ukraine, IPC A01B 149/02; appl. 23.02.1995; publ. 29.12.1999; Bul. №8;
[2]. Bezdolny M.I., (1995) – *Device for cultivation*, Patent №17395 Ukraine, IPC A01B 19/02, 49/02; appl. 26.04.1995; publ. 28.02.2000; Bul. №1;
[3]. Kanarev F.M., (1983) – *Rotary tillage machines*, Machine-building, pg.142, Moscow;
[4]. Listopad G.E. (1986) – *Agricultural and reclamation machines*, Agropromizdat, pg.688, Moscow;
[5]. Sysolin P.V., (2001) – *Agricultural machines: theoretical foundations, design*, Harvest, p.384, Kiev;
[6]. Usenko M.V., (2011) – *Study of flexible harrows with driven wheels*, Collection of scientific articles "Agricultural machines", № 21/II, pg.142-149, Lutsk;
[7]. Usenko M.V., Pryshlyak V.M., (2012) – *Experimental studies of the work of flexible harrow with loosening tins*, Scientific collection VSAU, № 11, v. 1 (65), pg.218-223, Vinnitsa;
[8]. Usenko M.V., Ponikarchuk A.M., Bozhydarnik V.V., Mirchuk V.S., (2004) – *Flexible harrow with adjustable tins*, Patent №67581 Ukraine, IPC A01B 49/02; appl. 30.10.2003; publ. 15.06.2004; Bul. №6;
[9]. Usenko M.V., Ponikarchuk A.M., Bozhydarnik V.V., Mirchuk V.S., Kuzhel E.V., Podzizey T.T., (2005) – *Module of flexible rotary harrow with loosening tins*, Patent №74089 Ukraine, IPC A01B 49/02; appl. 17.03.2004; publ. 17.10.2005; Bul. №10;
[10]. Usenko M.V., Bozhydarnik V.V., (2009) – *Flexible harrow with driven wheels,* Patent №42099 Ukraine, IPC A01B 49/02; appl. 05.01.2009; publ. 25.06.2009; Bul. №12.

Наведена методика розрахунку є основною для гнучких ланцюгових борін такої конструкції і, відповідно, для підбору її оптимальних параметрів для роботи в різноманітних зовнішніх умовах.

БІБЛІОГРАФІЯ

[1]. Бездольний М.І., (1995) – *Сільськогосподарський агрегат*. Патент №17384 Україна. МКВ A01B 49/02; заявл. 23.02.1995; опубл. 29.12.1999, Бюл. №8;
[2]. Бездольний М.І., (1995) – *Пристрій для обробітку ґрунту*. Патент №17395 Україна. МКВ A01B 19/02, 49/02; заявл. 26.04.1995; опубл. 28.02.2000, Бюл. №1;
[3]. Канарев Ф.М., (1983) – *Ротационные почвообрабатывающие машины*. – М.: Машиностроение, – 142 с;
[4]. Листопад Г.Е., (1986) – *Сельскохозяйственные и мелиоративные машины*. – М.: Агропромиздат, – 688 с;
[5]. Сисолін П.В., (2001) – *Сільськогосподарські машини: теоретичні основи, конструкція, проектування*. – К.: Урожай, 384 ;
[6]. Усенко М.В., (2011) – *Дослідження роботи борони гнучкої з приводом від колеса,* Збірник наукових статей «Сільськогосподарські машини», №21/II, -с.142-149, Луцьк;
[7]. Усенко М.В., Пришляк В.М., (2012) – *Експериментальні дослідження роботи гнучкої борони з розпушуючими зубами,* Збірник наукових праць ВДАУ, № 11, т. 1 (65), -с. 218-223, -Вінниця;
[8]. Усенко М.В., Понікарчук А.М., Божидарник В.В., Мірчук В.С., (2004) – *Борона гнучка з регульованими зубами*. Патент №67581 Україна. МКВ A01B 49/02; заявл. 30.10.2003; опубл. 15.06.2004, Бюл. №6;
[9]. Усенко М.В., Понікарчук А.М., Божидарник В.В., Мірчук В.С., Кужель Е.В., Подзізей Т.Т., (2005) – *Модуль гнучкої борони обертової з розрихляючими зубами*. Патент №74089 Україна. МКВ A01B 49/02; заявл. 17.03.2004; опубл. 17.10.2005, Бюл. №10;
[10]. Усенко М.В., Божидарник В.В., (2009) – *Борона гнучка з приводом від колеса*. Патент №42099 Україна. МКВ A01B 49/02; заявл. 05.01.2009; опубл. 25.06.2009, Бюл. №12.

EXPERIMENTAL DETERMINATION OF FLOW CONCENTRATION FOR PNEUMATIC CONVEYING SYSTEMS OF AIR-SEEDERS
/
DETERMINATION EXPÉRIMENTALE DE LA CONCENTRATION DE TRANSPORT DANS LES SYSTÈMES DE DISTRIBUTION DES SEMOIRS PNEUMATIQUES

Ph.D. Stud. Yatskul A.I.[1,2], Associate Prof. Ph.D. Lemière JP.[1]
[1] Kuhn SA, 4, Impasse des Fabriques, 67700, Saverne / France ;
[2] National Institute of Higher Education in Agronomy, Food and Environmental Sciences (AgroSup Dijon), 26 Bd Dr. Petitjean, 21079 Dijon cedex / France
E-mail : andr.jat@mail.ru; jean-pierre.lemiere@agrosupdijon.fr

***Abstract**: Taking into account the complexity of wide width air-seeders, they remain less studied. The chief point for air-seeder designers is conception of the pneumatic conveying system. It must be precise in terms of uniformity so that that the agro-technical goals should be achieved. It must also ensure high rates without causing damages to seeds. This paper provides a theoretical analysis of pneumatic conveying designing applied to air-seeders. It shows that the conveying of particles (seeds, fertilizers or their mixture) in a given pipe depends on two interconnected parameters: flow concentration and air velocity. The knowledge of these two parameters is a necessity for the design of conveying systems but they are not defined in the case of agricultural machinery. This paper proposes a method to measure the flow concentration and the air velocity values which must be used to optimize an existing seeder (relatively to machine's outflow) or to design a new pneumatic seeder. In this case choices about pipes' diameters in each part of conveying system can be optimized from an energy point of view and this paper presents how the collected values can be used in a global methodology of design for air-seeders' conveying system.*

***Keywords:** air-seeder, distribution system, pneumatic conveying, flow concentration, stagnation velocity*

INTRODUCTION

Today farmers must have an equipment allowing to cultivate sizeable areas (300 to 500 ha) efficiently and to achieve a controlled seeding during a short period of time. It especially concerns the market economies of emergent countries like Russia, Ukraine and Kazakhstan. So farmers want to have high capacity hoppers for seeds and a wide coulter bar for ensuring a rapid seeding. Consequently, the sowing implements become more sophisticated and heavier. They are called air-seeders and consist of a coulter-bar and a hopper to contain the seeds (and fertilizers if necessary). Seeds are conveyed from the hopper to the coulter-bar by an air-stream. Taking into account the complexity of this type of seed drills, they remain less-studied.

One of the critical points for the design of this kind of machines is the pneumatic conveying system design. Usual approaches of pneumatic conveying design couldn't be applied to air-seeders because of high discrepancy between theoretical calculating and practical measurements. This discrepancy exists because of non-steady-state phenomena during particles' transport (caused by the many bends, changes in pipe diameter, the presence of manifolds, stop and restart of seeding in

***Résumé:** Compte tenu de leur complexité, les semoirs pneumatiques de grande largeur restent peu étudiés. Le point clef pour les concepteurs semoir pneumatique est la conception du système de transport pneumatique. Il doit être précis en termes d'uniformité pour que les objectifs agro-techniques sont atteints. Il doit également permettre des débits élevés sans occasionner de dommages aux semences. Ce document présente une analyse théorique de la conception d'un transport pneumatique appliquée aux semoirs pneumatiques. Il montre que le transport des particules (semences, engrais ou leur mélange) dans une conduite donnée dépend de deux paramètres interdépendants: la concentration de trasport et la vitesse de l'air. La connaissance de ces deux paramètres est nécéssaire à la conception de ces systèmes de transport, mais ils ne sont pas définis dans le cas des machines agricoles. Cet article propose une méthode pour mesurer la concentration de transport et les valeurs de vitesse de l'air qui doivent être utilisées pour optimiser le fonctionnement d'un semoir existant (en fonction du débit de la machine) ou pour concevoir un nouveau semoir pneumatique. Dans ce cas, le choix des diamètres des conduites pour chaque partie du système de transport peut être optimisé d'un point de vue énergétique et cet article présente la manière dont les valeurs collectées peuvent être utilisées dans une méthodologie globale de conception des système de transport des semoirs pneumatiques.*

***Mots-clés:** semoir pneumatique, système de distribution, transport pneumatique, concentration de transport, vitesse de stagnation*

INTRODUCTION

Aujourd'hui les agriculteurs doivent avoir des matériels permettant de cultiver des zones assez importantes (300 à 500 ha) de manière efficace et de réaliser un ensemencement contrôlé pendant un court laps de temps. Ceci concerne en particulier les marchés des pays émergents comme la Russie, l'Ukraine ou le Kazakhstan. Les agriculteurs veulent des trémies grande capacité pour les semences et une large barre de semis pour assurer un ensemencement rapide. Par conséquent, les outils de semis deviennent plus sophistiqués et plus lourd. Ces semoirs pneumatiques se composent d'une barre de semis et une trémie pour contenir les semences et les engrais (si nécessaire). Les graines sont transportées depuis la trémie vers la barre de semis par un flux d'air. Compte tenu de la complexité de ce type de semoirs, ils restent peu étudiés.

L'un des points critiques pour la conception de ce type de machines est la conception du système de transport pneumatique. L'approche habituelle ne peut être appliquée en raison de fortes divergences entre les calculs théoriques et les mesures pratiques. Ces écarts existent en raison de l'existence de régimes non permanents au cours du transport des particules (causés par les nombreux coudes, changements de diamètre, arrêts et redémarrages du semis dans les fourrières.).

headlands...). So, very often, conveying system parameters are chosen intuitively and incorrectly, which leads to a plugging of pipes or to unjustified energy losses (excessive pression loss, the use of oversized turbines).

MATERIALS AND METHODS

Methodology and theoretical approach

When designing a pneumatic transport system, first we define both the transport concentration of particles and the air speed. The velocity of the air which transports the particles must be greater than a limit speed of stagnation of particles. During a vertical transport, air speed is of course greater than the fluidization velocity of the particles. During horizontal transport or in a bend, gravity or inertia movement deport the axis of the flow ducts and can cause deposits of material (Fig.1, b). Once both the air velocity and concentration of transport are set, and knowing the flow-rate of particles to be transported, it is possible to choose a suitable diameter for the pipe.

Moreover, as several transport speeds and several pipe diameters are possible, it is proposed in this paper to choose the most energy efficient solution. The conveying system design involves the definition of a pipe internal diameter, the calculation of pressure drop and the assignation of a fan unit. The power of the fan must be the lowest possible and depends both of the pressure loss and the volumic air-flow rate.

The volumic air-flow rate required from a fan unit is given by:

Ainsi, les paramètres du système de transport sont très souvent choisis de manière intuitive et incorrecte, ce qui conduit à des obturations des conduites ou à des pertes d'énergie non justifiées.

MATERIELS ET METHODES

Méthodologie et approche théorique

Lors de la conception d'un système de transport pneumatique, on définit d'abord la concentration de transport des particules et la vitesse de l'air. La vitesse de l'air véhiculant les particules doit être supérieure à une vitesse limite de stagnation des particules. Au cours d'un transport vertical elle est notamment supérieure à la vitesse de fluidisation des particules. Au cours d'un transport horizontal ou dans un coude, la gravité ou les forces d'inerties déportent la direction des écoulements et peuvent provoquer des dépôts (Fig.1, b). Une fois que la vitesse de l'air et la concentration du transport sont définis, et en connaissant le débit de particules à transporter, il est possible de choisir un diamètre approprié pour les conduites.

Comme plusieurs vitesses de transport et plusieurs diamètres de tuyaux sont possibles, il est proposé ici de choisir la solution la plus économe en énergie. La conception du système de transport implique la définition d'un diamètre interne de conduite, le calcul des pertes de charge et le choix d'un compresseur. La puissance du ventilateur doit être la plus faible possible et dépend à la fois de la perte de charge totale à vaincre et du débit d'air transporté.

Le débit d'air volumique traité par un compresseur est donné par l'équation:

$$Q'_g = \frac{Q_S}{\mu \rho_a}, \text{ [m}^3\text{/s]} \quad (1)$$

The difficulty is in correct interpretation of the machine structure and in detection of all controversial areas causing energy losses and flow perturbations. At this point, it is important to notice that the conveying of particles in air-seeders is assumed to be assimilated to a dilute phase transport. The total system pressure drop is a totality of losses, [6]. We can distinguish horizontal conveying losses $\sum \Delta P_h$, vertical lift losses $\sum \Delta P_v$, losses in bends $\sum \Delta P_c$ and losses in equipment accessory $\sum \Delta P_{ac}$:

La difficulté du calcul est dans l'interprétation correcte de la structure de la machine et dans la détection des zones entraînant des pertes de charges et des perturbations de l'écoulement. À ce stade, il est important de noter que le transport des particules dans un semoir pneumatique est supposé être un transport en phase diluée. La perte de charge totale du système est décomposée en un ensemble de pertes de charges [6]. On distingue les pertes de charges du transport horizontal $\sum \Delta P_h$, les pertes ascentionnelles $\sum \Delta P_v$, les pertes dans les coudes $\sum \Delta P_c$ et les pertes dans les accessoires $\sum \Delta P_{ac}$:

$$\Delta P = \sum_1^n P_i = \sum \Delta P_h + \sum \Delta P_v + \sum \Delta P_c + \sum \Delta P_{ac}, \text{ [Pa]} \quad (2)$$

Horizontal conveying losses can be presented as:

Les pertes de charge liées au transport horizontal seront:

$$\Delta P_h = \Delta P_l + \Delta P_{tr} + \Delta P_a, \text{ [Pa]} \quad (3)$$

Where [8,10,11]:

Avec [8,10,11]:

$$\Delta P_l = \lambda \frac{L}{D} \cdot \frac{\rho v^2}{2} = (0.0056 + \frac{1}{2Re^{0.32}}) \frac{L}{D} \cdot \frac{\rho v^2}{2}, \text{ [Pa]} \quad (4)$$

$$\Delta P_t = \lambda' \frac{L}{D} \cdot \frac{V_m^2 \rho \mu}{2}, \text{ [Pa]} \quad (5)$$

$$\Delta P_a = \lambda_a \mu \frac{\rho_a V_a^2}{2g}, \text{ [Pa]} \quad (6)$$

Vertical conveying is subordinated to the same principles as in horizontal areas, except that in vertical transport we consider an influence of gravity. Pressure drop can be described as [8]:

Le transport vertical est subordonné aux mêmes principes que dans les zones horizontales, sauf que dans le transport vertical on considère une influence de la gravité. La perte de charge peut être décrite comme [8]:

$$\Delta P_v = \mu \frac{V_a \rho}{V_p} g \Delta H, \text{[Pa]} \quad (7)$$

The losses in bends $\sum \Delta P_c$ are generally equated to some equivalent linear losses. In the case of particles transport, losses in accessories $\sum \Delta P_{ac}$ can be determined experimentally.

The classical theories for pressure drops estimations prove the dependence of two interconnected parameters: flow concentration and air velocity having to be accepting in the beginning of each design.

According to [10] the theoretical definitions of flow concentration and of optimal air velocity, relatively to a pipe diameter, are very difficult or are impossible. So, we had to develop a rational method for the experimental definition of flow concentration for various seeds and fertilizers in the case of air-seeders.

It remained to be seen what part of the transportation system should be designed first. To make this choice, observations and field measurements were carried out to find which was the part of the system that suffered the most frequently problems of clogging or flow heterogeneity.

The testing of air-seeders with the granulated fertilizers, testified about numerous stagnations and cloggings between the distribution manifold (called also divider header) and an opener. The “problematic” areas showed inflections of the flexible pipe and low initial air speed. For these reasons we propose to define the maximum flow-concentration and the minimum air-velocity in outlets of distribution manifold for different cultures and pipe diameters. These values must avoid the plugging of the system. Values found will be used as input data for theoretical calculations of the whole pneumatic conveying system.

Experimental setup

Testing was made on a specific experimental setup (Fig.1, a) within the company Kuhn SA in Saverne in France. This setup used for the testing of metering units in the case of small seeds and fertilizers was modified relatively to our purpose. It was reequipped with the metering unit of serial seeder in order to simulate flows equivalent to real flows in the outlet of distribution manifold.

Once seeds are expelled by the metering unit (1) from the pressurized hopper (6), they are picked-up by the air flow provided by the fan (2). They are transported in the flexible pipe (3) toward the plastic box (4) through a cyclone (5). The airflow was controlled using a primary control valve (8) and a fine control valve (7). The material flowrate was controlled by the electronic terminal ISOBUS VT50 of Kuhn, used on the serial machines compatibles with ISOBUS standard.

Air velocity was measured using Venturi tubes (according to [3]) by acquiring the kinetic energy of airflow in the form of pressure difference between the different sections separated by converging area (Fig.1, a). Pressure difference was taken by micro-manometers Testo 512 (11) laterally to air and material flows and in a straight area with a stabilized flow.

Les pertes dans les coudes $\sum \Delta P_c \Sigma$ sont généralement assimilées à des pertes linéaires équivalentes. Dans le cas du transport de particules, les pertes dans les accessoires $\sum \Delta P_{ac}$ peuvent être déterminées expérimentalement.

Les théories élaborées pour estimer les pertes de charge montrent l’interdépendance de deux paramètres: la concentration de transport et la vitesse de l'air qui doivent être posés au début de chaque calcul.

Selon [10] le calcul théorique de la concentration de transport et de la vitesse d'air optimale, par rapport à un diamètre de conduite, est très difficiles voire irréalisable. Ainsi, nous avons dû développer une méthode rationnelle de définition expérimentale de concentration de flux pour diverses semences et engrais dans le cas des semoirs pneumatiques.

Il restait à savoir quelle partie du système de transport devait être conçue en premier. Pour faire ce choix des observations et des mesures sur le terrain ont été réalisées pour chercher quel était l'organe qui subissait le plus fréquemment des problèmes de bouchage ou d'hétérogénéité de débit.

Les essais avec des granulés d’engrais ont montré l’apparition de nombreux dépôts et colmatages entre l’éclateur (également appelé tête de distribution) et un ouvreur. Les zones «problématiques» comportaient des inflexions de la conduite flexible et une faible vitesse initiale de l'air. Pour ces raisons, nous proposons de définir la concentration maximale de transport et la vitesse minimale de l'air après les sorties de la tête de distribution pour différentes semences et différents diamètres de tuyaux. Ces valeurs doivent éviter le colmatage du système et seront utilisées comme données d'entrée pour le dimensionnement de l’ensemble du système de transport pneumatique.

Montage expérimental

Les essais ont été effectués sur un dispositif expérimental spécifique (Fig.1, a) au sein de l'entreprise Kuhn SA à Saverne, en France. Le dispositif initial, qui était utilisé pour le réglage des doseurs dans le cas de petites graines et des engrais, a été modifié en fonction de nos objectifs. Il a été rééquipé avec l'unité de dosage d’un semoir de série afin de simuler des flux équivalents aux flux réels observés à la sortie de la tête de distribution.

Une fois les graines expulsées par le doseur (1) de la trémie sous pression (6), elles sont entraînées par le flux d'air produit par le compresseur (2). Elles sont transportées dans une conduite flexible (3) vers un bac en en plastique (4) à travers un séparateur cyclone (5). Le débit d'air est contrôlé en utilisant une vanne de réglage grossier (8) et une vanne de réglage fin (7). Le débit de matière est contrôlé par un terminal électronique ISOBUS VT50 de Kuhn, utilisé sur les machines de série compatibles avec la norme ISOBUS.

La vitesse de l'air a été mesurée avec des tubes Venturi (conformément à [3]) en captant l'énergie cinétique du flux d'air sous la forme d'une différence de pression entre les différentes sections séparées une zone de convergence (Fig.1, a). La différence de pression a été mesurée à l’aide de micro-manomètres Testo 512 (11) latéralement au flux d'air et de matière et dans une portion droite avec un flux stabilisé.

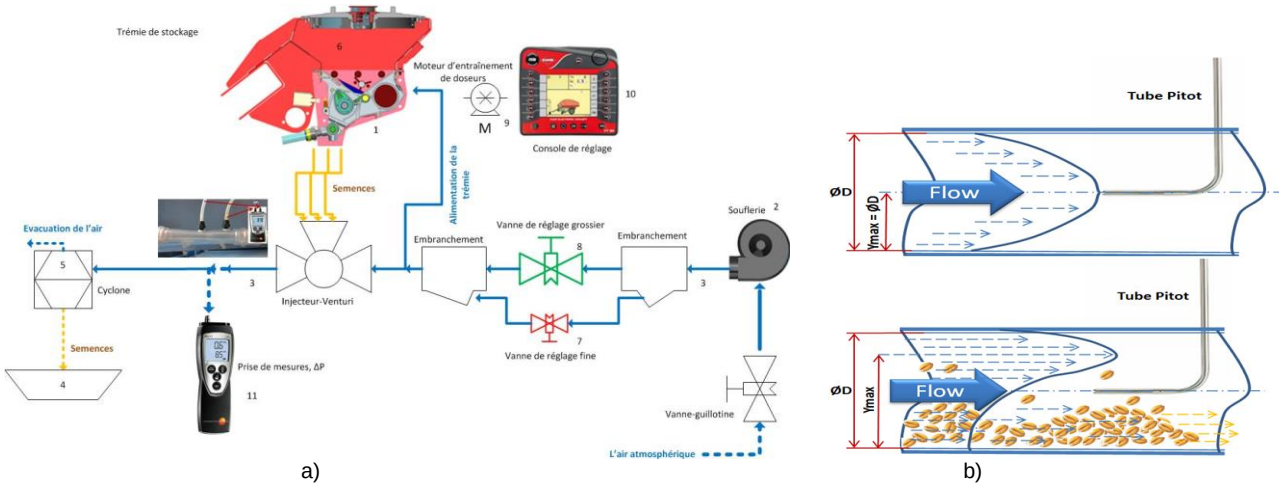

a) b)

Fig.1 - a - The experiment setup configuration scheme
b – Air velocity profils and velocity measurement in a horizontal pipe (air flow alone; loaded flow)

It is important to notice that first measurements of air velocity in the conveying pipe were made with a Pitot-tube but they didn't give good results. The Pitot-tube introduced in the middle of the straight pipe (far from the impermanent-flow area) provided values corresponding to one air velocity value distributed in a core velocity profile (Fig.1, b). Ideally the maximum value is in front of the Pitot-tube but in an horizontal transport this value represents a random and accidental velocity of a flow layer in a point of velocity profile. The value of air velocity reduces towards the walls of the pipe (and in practice it is very problematic to locate the Pitot-tube precisely on the pipe axis). Furthermore when air-flow is loaded with particles, the velocity profile is ousted on the top because of particles concentrated in the bottom of pipe. So the core of velocity profile moves up relatively to the axis of pipe, depending on loading (Fig.1, b). This phenomenon makes impossible a correct utilization of Pitot-tube.

Test procedure and data collection

Three diameters (20, 25, 30mm) of flexible pipes were tested. They were loaded with wheat, barley, starter fertilizers and a barley-fertilizer mixture (with a mass proportion 60/40). The material flow-rate was calculated on the basis of agrotechnical requirements with a seeder ground speed of 10km/h, a coulter-bar width of 12m with 6 manifolds (11 outlets). The established material flow-rate was equal to flow- rate in one outlet of manifold. The flow-rate then was changing from 3 to 30 g/s. Sometimes for the higher rates the metering unit overflowed and material flow-rate could not be respected. It happened typically for smallest diameters.

Each test was realized for horizontal and vertical pipes upon the following sequence: the experimental setup was set to the precise material flow-rate. The fan flow-rate was set to a high and sufficient level to ensure material conveying.

The airflow decreased by progressive closing of the valve increments, waiting at each position that flow

Il est important de noter que les premières mesures de la vitesse de l'air dans le tuyau de transport ont été faites avec un tube Pitot mais ces mesures n'ont pas donné de bons résultats. Le tube Pitot introduit au centre du tuyau rectiligne (loin de toute zone d'écoulement instable) a donné des valeurs de vitesse de l'air variables car distribuées dans une courbe de profils de vitesse (Fig.1, b). Idéalement, la valeur maximale de vitesse est au niveau de la sonde Pitot mais en transport horizontal cette valeur devient aléatoire selon les accidents dans l'écoulement des couches d'air en un point du profil de vitesse. La valeur de la vitesse de l'air diminue lorsqu'on se rapproche des parois (de plus il est très difficile de localiser le tube de Pitot précisément sur l'axe du tube). En outre lorsque l'air est chargé de particules, le profil de vitesse est déformé vers le haut par les particules concentrées dans la partie inférieure du tube. Ainsi, la courbe du profil de la vitesse se déplace vers le haut par rapport à l'axe du tube en fonction de la charge transportée (Fig.1, b). Ce phénomène rend impossible une utilisation correcte des tubes Pitot.

Procédure de test et de collecte de données

Trois diamètres (20, 25, 30mm) de tuyaux flexibles ont été testés. Ils ont été chargés avec du blé, de l'orge, de l'engrais de démarrage et un mélange orge-engrais (selon une proportion massique 60/40). Le débit de matière a été calculé sur la base des exigences agro-techniques pour une vitesse au sol du semoir de 10 km/h, une largeur de barre de semis de 12m avec 6 têtes de distribution (11 sorties). Le débit de particules était égale au débit réel dans une des sorties du collecteur. Le débit a donc varié de 3 à 30 g/s. Il est arrivé que le doseur déborde pour les débits les plus élevés auquel cas le débit souhaité n'a pas pu être respecté. Cela s'est produit typiquement pour des petits diamètres de conduites.

Chaque essai a été réalisé pour des conduites horizontales et verticales selon la séquence suivante: le dispositif expérimental est réglé au débit matière souhaité. Le débit d'air était réglé à un niveau, suffisant pour assurer le transport de la matière.

Le débit d'air était ensuite réduit en fermant progressivement les vannes de réglage, en attendant à

stabilizes, until particles begin to subside and stagnate in the bottom of the pipe. Just as we visually detected material stagnation, the data from micro-manometers were collected. To ensure the most accurate results, a first manipulation was devoted to define the range of air velocities corresponding to particles stagnation. As soon as the velocity range is known and when approaching the stagnation air velocity, we start closing the valve more slowly and precisely, fixing air velocity to a plugging beginning. Each experiment is replicated 5 times.

Particles' flow rate was known. So maximum flow concentration could be calculated for the minimum measured stagnation velocity upon the following equation:

chaque position que l'écoulement se stabilise, jusqu'à ce que les particules commencent à refluer ou à stagner dans la partie inférieure de la conduite. Dès qu'on détecte visuellement une stagnation de matière, les données des micro-manomètres sont recueillies. Pour obtenir des résultats plus précis, une première manipulation est consacrée à définir la gamme de vitesses d'air correspondant au début de stagnation des particules. Dès que la plage de vitesse est connue, et à l'approche de la vitesse de l'air de stagnation, on démarre la fermeture de la soupape plus lente et précise, en fixant la vitesse de l'air à un début de bouchage. Chaque expérience est reproduite 5 fois. Le débit des particules était connu. Ainsi la concentration maximale de transport a pu être calculée pour la vitesse de stagnation minimum observée selon l'équation suivante:

$$\mu = \frac{Q_s}{V_{ast}\pi\frac{D^2}{4}\rho_a}, \text{[kg/kg]} \quad (8)$$

RESULTS AND DISCUSSION

Vertical and horizontal conveying comparing

Stagnation air velocity corresponds to the minimum quantity of energy necessary to the air to move materials and move itself. Stagnation air velocity during vertical transport of wheat is always higher than during horizontal one (Fig.2). Stagnation air velocity during vertical transport is about 25 % higner than during horizontal conveying whatever pipe diameter. It can be explained by the influence of gravity forces which are single forces opposing velocity vector. That's why vertical conveying needs greatest air velocity. This value will be specific for the each type of material according to its physical properties (weight, shape etc.). The vertical stagnation air velocity is then the critical parameter which should be used for the design of air-seeder pneumatic transport systems.

These data about fluidization and pick-up velocities can be compared to literature data taken from [9,10]. Our experimental values of stagnation velocities are in the top of fluidization threshold for a vertical conveying and in the top of pick-up threshold for a horizontal one. Similar results were obtained for wheat, barley and fertilizers.

RÉSULTATS ET DISCUSSION

Comparaison du transport vertical et horizontal

La vitesse de stagnation correspond à la quantité minimale d'énergie nécessaire à l'air pour déplacer les particules et se déplacer lui-même. En transport vertical la vitesse minimale de stagnation pour le blé est toujours plus élevée que lors d'un transport horizontal (Fig.2): La vitesse de stagnation pendant le transport vertical est environ 25% plus élevée qu'en transport horizontal (quel que soit le diamètre de la conduite). Ceci peut s'expliquer par l'influence des forces de gravité qui s'opposent au vecteur vitesse de l'air. Ainsi, un transport ascensionnel nécessite une plus grande vitesse de l'air. Cette valeur sera spécifique à chaque type de matériau transporté en fonction de ses propriétés physiques (poids, forme etc.). La vitesse de l'air limite entraînant une stagnation en transport ascensionnel est donc le paramètre essentiel qui doit être utilisée pour la conception de systèmes de transport des semoirs pneumatiques. Ces données sur la vitesse de fluidisation et la vitesse d'entraînement des particules peuvent être comparées aux données de la littérature tirées de [9, 10]. Nos valeurs expérimentales sont dans la fourchette haute des seuils de fluidisation (transport vertical) cités et dans la fourchette haute des vitesses d'entraînement horizontal citées.

Des résultats similaires ont été obtenus pour le blé, l'orge et l'engrais.

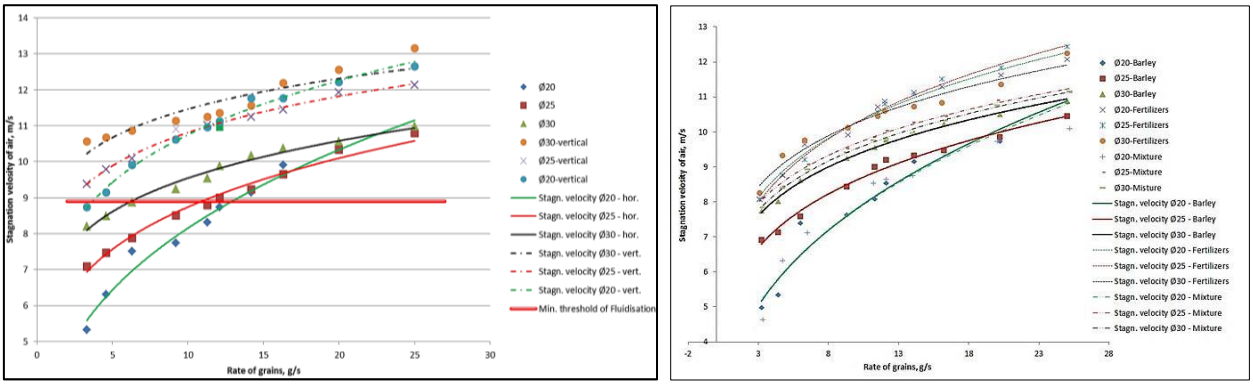

Fig. 2 - Comparing of vertical and horizontal conveying of wheat (on the left) Barley, fertilizers and mixture stagnation velocities (on the right)

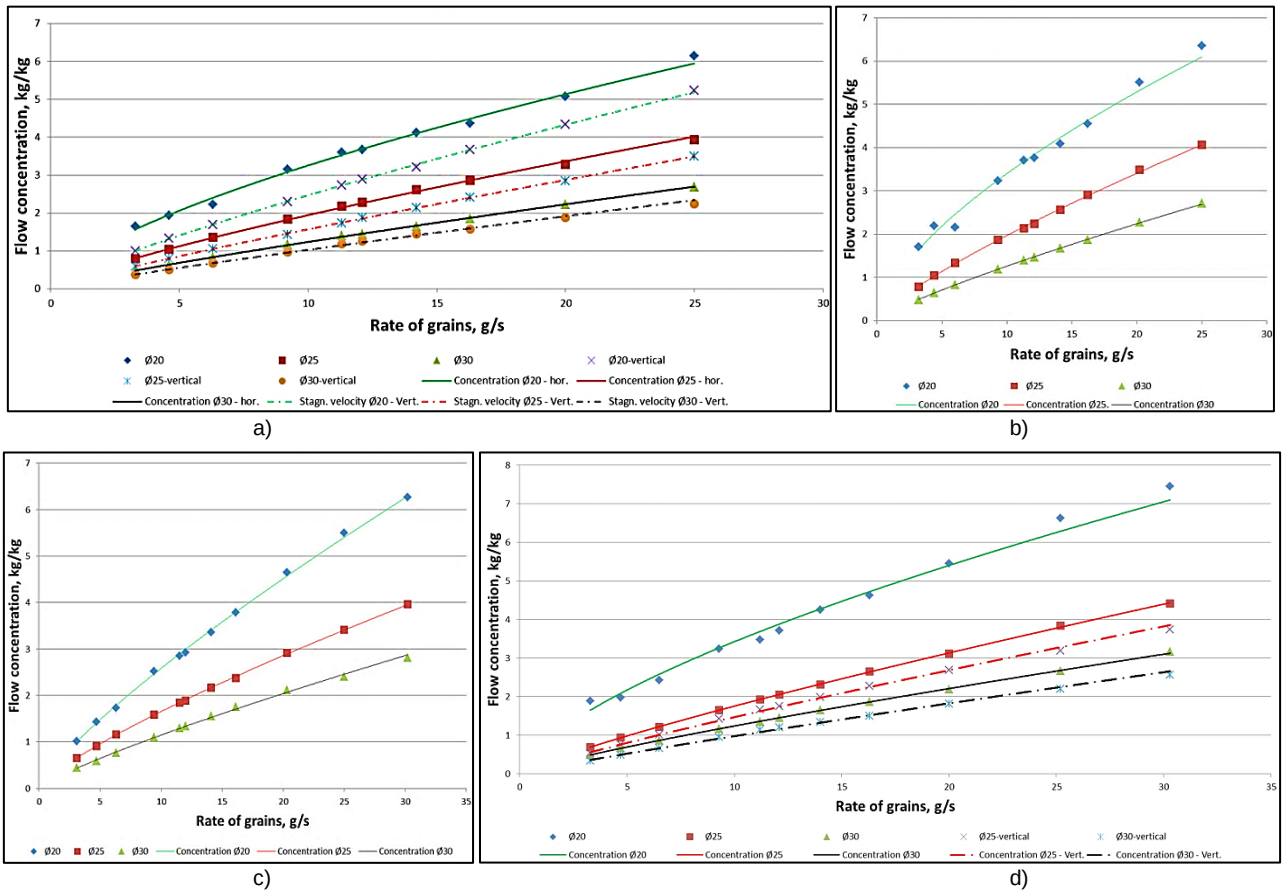

Fig. 3 - a – Maximum flow concentration of wheat; **b -** Maximum flow concentration of barley; **c -** Maximum flow concentration of starter fertilizers; **d –** Maximum flow concentration, barley-fertilizer mixture

Mixture conveying

There are ambiguous observations about barley-fertilizer mixture conveying. The results obtained with barley, fertilizers and their mixture are grouped on the same diagram. In the smallest pipe (diameter 20mm) stagnation velocity of mixture is identical to barley one (green curves, Fig. 2). The ratio 60/40 by weight implicates that barley volume is double than fertilizer's volume in one volume of air. We could suppose the behavior of the fertilizer is masked by the behavior of barley: Barley has a tendency to “carry” fertilizers in the manner of a "broom".

In the pipe of 25 mm the effect of fertilizer presence is more perceptible. The curve of mixture stagnation is just between the barley (green) and fertilizer (red) curves (Fig. 2). We can suppose that as air could circulate freely between the particles, heavier particles (fertilizer and heavier barley seeds) subside easily at the bottom of the pipe. In spite of the superior volume of the barley seeds have a less influence to the fertilizer stagnation because of the wider diameter of the pipe. We can suppose that a bigger content of fertilizer in the mixture will increase the stagnation limit velocity.

However, increasing of pipe diameter to 30 mm (black curves), we observed the same result than for the 20 mm pipe. So further experiments and statistical analysis will be done in order to conclude. In a first approach, we will use the higher stagnation velocity of one part of the mixture (here fertilizer) to design the system of conveying.

Flow concentration and pipe diameter

Transport in a dense phase would be preferable economically [7,10], but it is not possible to provide a

Transport du mélange

Concernant le mélange orge-engrais, on obtient des résultats ambigus. Les résultats obtenus avec l'orge, l’engrais et leur mélange sont regroupés sur un même graphique. Dans le plus petit tuyau (diamètre 20mm), la vitesse de stagnation du mélange est identique à celle de l'orge (courbes vertes, Fig. 2). Le ratio 60/40 en masse implique que le volume de l'orge est le double de celui de l'engrais par volume d'air. Nous pourrions supposer que le comportement de l'engrais est masqué par le comportement de l’orge qui tendrait à "transporter" l’engrais à la manière d'un "balai". Dans le tuyau de 25 mm de diamètre, l'effet de la présence d'engrais est plus perceptible. La courbe de stagnation du mélange (Fig. 2) est entre celle de l'orge (en vert) et de l’engrais courbes (en rouge). On peut supposer que l'air peut circuler librement entre les particules et que les plus lourdes (l’engrais et les grains d’orge les plus lourds) sédimentent plus facilement au fond de la conduite. Malgré le volume supérieur qu’il occupe, l’orge aurait une moindre influence sur le dépot de l'engrais en raison du diamètre plus élevé du tuyau. Nous pouvons supposer qu'une plus grande proportion d'engrais dans le mélange augmenterait la vitesse limite de stagnation. Cependant, quand on augmente le diamètre de tuyau à 30 mm (courbes noires), on observe le même résultat que pour le tube de 20 mm. D'autres expériences et études statistiques seront donc réalisées en vue de conclure. Dans une première approche, nous allons donc utiliser la vitesse de stagnation la plus élevée de celles des éléments d’un mélange (ici l’engrais) pour concevoir le système de transport.

Concentration de transport et diamètre de conduite

Un transport en phase dense serait économiquement préférable [7,10], mais il est impossible d’obtenir un

regular transportation without "seed holes." So dense phase transport cannot be applied in a seeder.

Also, when carrying large seeds (eg. beans), dense phase transport increases the risk of clogging. That's why the conveying of particles in air-seeders is assumed to be assimilated to a dilute phase transport.

The oversizing of pipes' sections is not a solution. Particles present in the bottom part of wide pipes offsets the maximum of air velocity towards the top of the pipe. The subsiding of grains then creates a "brake" for the air (Fig.1, b). The air arriving in this section of pipe has the tendency to "avoid" the pressure loss created by obstacles. So the greatest diameter will always create an "avoidance" of the particles instead of pushing the whole flow of seeds toward the right direction.

Therefore, when the section size decreases, air circulation between the particles will be more homogeneous, so fan energy will be more efficiently used. The oversizing of diameter will also lead to increase airflow rate (for a constant air velocity) and increases the energy consumption (to a power 3). It is necessary to create good conveying conditions, ensuring local velocities are greatest than the critical velocity.

The first parameter to determine is the air velocity in the pipe. It is proposed to set this value from Figure 1 as a function of the flow of seeds (here in the case of wheat). This value may be 10% higher than the limit of stagnation speed in vertical transportation for more safety. This speed value sets the maximum transport concentrations (plotted in Figure 4). In Figure 4 we realize that the diameter of 20 mm would be sufficient to transport the flow concentrations in the case of air seeders. In addition, this pipe diameter reduces the energy cost of the operation. In practice we do not choose smaller diameter because seeder must be versatile and must also sow large seeds.

Previous calculations were made for pipes after the distribution manifold. In an air-seeder, the sum of the sections after the distribution manifold is greater than the section before it. According to the matter conservation law, the airflow velocity before distribution manifold will so be higher and air velocity before head of distribution will be high enough to avoid particles stagnation.

CONCLUSIONS AND PERSPECTIVES

1. Starting point of design must be the optimization of transport after manifold's outlets.
2. An experimental set up was design to obtain experimental values for both the maximum flow concentration and the minimum air velocity suitable for pneumatic conveying.
3. Experimental curves of minimum vertical velocity can be used to define conditions of conveying for a type of seeds.
4. In a first approach, we will use the higher stagnation velocity of one part of the mixture (here fertilizer) to design the system of conveying.

écoulement régulier sans "effet de poquet". Le transport en phase dense ne peut donc appliqué aux semoirs.

En outre, lors du semis de grosses graines (ex. fèves), un transport en phase dense augmenterait le risque de colmatage. C'est pourquoi le transport de particules dans un semoir pneumatique est supposé être assimilé à un transport en phase diluée. Le surdimensionnement des sections des tubes n'est pas une solution. Les particules présentes dans la partie inférieure des tubes larges déportent la vitesse d'air maximale vers le haut du tube. La sédimentation des graines crée alors un "frein" pour l'air (Fig.1, b). L'air arrivant dans cette section de tuyau a tendance à "éviter" la perte de pression créée par les obstacles. Donc, un grand diamètre entrainera un «évitement» des particules au lieu de pousser l'ensemble du flux de graines dans la bonne direction. Utiliser un diamètre élevé accentue ce phénomène comme on peut le voir sur la Fig. 2 (pour de faibles débits de semences). Lorsque la taille de la conduite diminue, la circulation d'air entre les particules est plus homogène, de sorte que l'énergie du compresseur sera utilisée plus efficacement. Le surdimensionnement des conduites accroit aussi le débit d'air nécessaire (à vitesse de transport constante) et augmente la consommation d'énergie (à la puissance 3). Il est nécessaire de créer de bonnes conditions de transport en veillant à ce que les vitesses locales soient plus élevées que la vitesse critique.

Le premier paramètre à déterminer est la vitesse de l'air dans la conduite. Il est proposé de fixer cette valeur d'après la Figure 1 en fonction du débit de graines (ici dans le cas du blé). Cette valeur, par sécurité, peut être supérieure de 10 % à la vitesse limite de stagnation en transport vertical. Cette valeur de vitesse fixe les concentrations maximales de transport (reportées sur la Figure 4). Sur la figure 4 on se rend compte que le diamètre 20 mm serait suffisant pour assurer le transport des concentrations de flux dans le cas des semoirs pneumatiques. De plus, ce diamètre de tuyau réduit le cout énergétique de l'opération. Dans la pratique on ne choisit pas de diamètre plus petit car les semoirs sont polyvalents et doivent aussi semer de grosses graines. Les calculs précédents correspondent aux conduites placées après la tête de distribution. Dans un semoir pneumatique, la somme des sections suivant l'éclateur est plus grande que celle de la section précédente. Selon la loi de conservation de la matière, la vitesse de l'air avant l'éclateur sera plus élevée. La vitesse de l'air avant la tête de distribution sera donc suffisante pour éviter la stagnation des particules.

CONCLUSIONS ET PERSPECTIVES

1. Le point de départ de la conception doit être l'optimisation du transport à la sortie de la tête de distribution.
2. Un dispositif expérimental a été de conçu pour obtenir des valeurs expérimentales de concentration de transport maximale et de vitesse d'air minimum acceptables pour le transport pneumatique.
3. Les courbes expérimentales de vitesses verticales minimum peuvent être utilisées pour définir les conditions de transport pour chaque type de semence.
4. Dans une première approche, on utilisera la vitesse de stagnation la plus élevée de celles des éléments d'un mélange pour concevoir le système de transport.

5. It is recommended to use the pipe sections as lower as possible to favor a homogenous airflow and to reduce the energetic cost of transport.
6. In order to develop knowledge on the transport of mixtures it will be necessary to test several proportions of fertilizers and seeds.

NOMENCLATURE

L, D – is the length and diameter of the conveying pipeline, in m;
N_1, N_2 – the fan shaft horse power, in kW;
Q_s – mass material rate, in kg/s;
Q_a – mass air rate: $Q_a = V_a \pi\ (D^2/4)\rho_a$, in kg/s;
Q'_a - volume air rate, in m^3/s;
Q_{a1}, Q_{a1} – the air rate before and after changing, in m^3/s
Re – Reynolds number: ;
V_a, V_p, V_{ast} – the air, particle and stagnation velocities, in m/s;
ΔH – the lift height, in m;
$\sum \Delta P$ – total pressure drops, in Pa;
$\sum \Delta P_l$ – linear losses, in Pa;
$\sum \Delta P_a$ – acceleration losses, in Pa;
$\sum \Delta P_{tr}$ – material conveying losses, in Pa;
ρ_a - volumetric mass density of air (equal 1.2 kg/m^3 at normal atmospheric pressure and temperature of +10°C)
λ_a – resistance coefficient ;
λ' - resistance coefficient, for agricultural seeds: $\lambda' = 0.0037$ (Zuèv, 1976);
μ – mass flow concentration $\mu = Q_s/Q_a$:, in kg/kg;
ν – kinematic viscosity of the air ($1{,}33 \cdot 10^{-5}\ m^2/s$).

REFERENCES

[1]. Afonso Júnio P.C., Corrêa P.C., Pinto F.A.C.&Queiroz D.M., (2007) - *Aerodynamic properties of coffee grains and beans*. Biosystems Engineering, 98(1), pg.39-46;
[2]. Klinzing G.E., (2003) - *Dilute-Phase Pneumatic Conveying*. Handbook of fluidization;
[3]. Lefebvre J., (1986) – *Measuring the flow rates and velocities of fluids*. Masson;
[4]. Levy A. & Kalman H., (2001) - *Dilute-phase pneumatic conveying problems and solutions*. Handbook of Conveying and Handling of Particulate Solids, 10, p.303;
[5]. Li, H. & Tomita, Y., (2000) - *Particle velocity and concentration characteristics in a horizontal dilute swirling flow pneumatic conveying*. Powder Technology, 107(1), pg.144-152;
[6]. Mills D., (2004) - *Pneumatic Conveying Design Guide*. Second Edition Butterworth-Heinemann;
[7]. Mittal A., Mallick S.S. & Wypych P.W., (2014) - *An investigation into flow mode transition and pressure fluctuations for fluidized dense-phase pneumatic conveying of fine powders*. Particuology;
[8]. Srivastava A.K., Goering C.E., Rohrbach R P., Buckmaster D.R., (2006) - *Conveying of Agricultural Materials. Chapter 14.* Engineering Principles of Agricultural Machines, 2nd ed., pg. 491-524 St. Joseph, Michigan: ASABE. (10.13031/2013.41476);
[9]. Buzenkov G.M., Ma C.A., (1976) - *Crop seeding machines*. Mechanical Engineering, p.270;
[10]. Zuev F.G., (1976) - *Pneumatic conveying on crop processing industries* - M.: Kolos, p.344.

5. Il est recommandé d'utiliser une section de conduite aussi faible que possible pour favoriser l'homogénéité du flux et réduire les coût énergétique du transport.
6. Afin de développer les connaissances sur le transport des mélanges, il sera nécessaire de tester plusieurs proportions d'engrais et de semences.

NOMENCLATURE

L, D – Longueur et diamètre de la conduite, en m;
N_1, N_2 – puissance sur l'arbre du compresseur, en kW;
Q_s – débit massique de la matière, en kg/s;
Q_g – débit massique de l'air: $Q_g = V_a \pi\ (D^2/4)\rho_a$, en kg/s;
Q'_g - débit volumique de l'air, en m^3/s;
Q_{a1}, Q_{a1} – débits de l'air avant et après variation, en m^3/s
Re – nombre de Reynolds: $Re = V_a D/\nu$;
V_a , V_p , V_{ast} – vitesses de l'air, de stagnation et des particules, en m/s;
ΔH – hauteur d'élévation, en m;
$\sum \Delta P$ – pertes de charges totales, en Pa;
$\sum \Delta P_l$ – pertes linéaires, en Pa;
$\sum \Delta P_a$ – pertes d'accélération, en Pa;
$\sum \Delta P_{tr}$ – pertes liées au transport de matière, en Pa;
ρ_a – masse volumique de l'air (égale 1.2 kg/m^3 à la pression atmosphérique et la température de +10°C)
λ_a – coefficient de résistance;
λ' - coefficient de résistance, pour les semences agricoles: $\lambda' = 0.0037$ (Zuèv, 1976);
μ – concentration massique de transport: $\mu = Q_s/Q_g$, en kg/kg;
ν – viscosité cinématique de l'air ($1{,}33 \cdot 10^{-5}\ m^2/s$).

REFERENCES

[1]. Afonso Júnio P.C., Corrêa P.C., Pinto F.A.C.&Queiroz D.M.,(2007)-*Propriétés aérodynamiques de grains de café et des haricots.* Ingénierie des biosystèmes, 98(1), 39-46;
[2]. Klinzing, G. E., (2003) - *Transport pneumatique de la diluer-phase.* Manuel de fluidisation ;
[3]. Lefebvre J., (1986) - *Mesure des débits et des vitesses des fluides*. Masson;
[4]. Levy A., & Kalman H., (2001) - *Problèmes et solutions du transport pneumatique de la diluer-phase.* Manuel de transport et manipulation de particules solides, 10, p.303;
[5]. Li H. & Tomita Y., (2000) - *La vitesse des particules et les caractéristiques de concentration dans une horizontale diluée tourbillonnant pneumatique flux transport.* Technologie des poudres, 107(1), pg.144-152;
[6]. Mills D., (2004) - *Pneumatique Guide de conception de transport.* Second Edition Butterworth-Heinemann;
[7]. Mittal A., Mallick S.S. & Wypych P.W., (2014) - *Une enquête sur le mode d'écoulement et la pression de fluctuations pour fluidisé la phase dense du transport pneumatique de poudres fines. Particuology*;
[8]. Srivastava A.K., Goering C.E., Rohrbach R.P., Buckmaster D.R., (2006) - *Transport des matières. Chapitre 14. Principes d'ordre technique de machines agricoles,* 2-ième Edition, pg.491-524 St. Joseph, Michigan: ASABE. (10.13031/2013.41476) ;
[9]. Buzenkov GM, Ma S.A., (1976) - *Machines et appareils pour le semis de plantes*. Ingénierie mécanique, p.270 ;
[10]. Zuev F.G., (1976)- *Le transport pneumatique dans les industries de transformation des cultures*- Kolos Ed., p.344.

ANALYSIS OF WORK PROCESS OF SEEDING FURROWS EMBEDDING BY A CONICAL ROLLER
/
АНАЛІЗ РОБОЧОГО ПРОЦЕСУ ЗАГОРТАННЯ ПОСІВНИХ БОРОЗЕН КОНІЧНИМ КОТКОМ

Ph.D.Eng. Shvedik M.
Lutsk National Technical University / Ukraine
Tel: +38(0332)74-61-32; Fax: +38(0332)74-61-03; E-mail: lab-amb@ukr.net

Abstract: *In the article the results of analysis of work process of seeding furrows embedding and compaction of soil by the conical roller which is set at the angles α to direction of furrow, and also analytical expressions for definition of resistance force of the roller by moving and lateral force which provides a self-cleaning of soil, which sticks to its surface, are given.*

Keywords: *conical roller, furrow, shift, soil, compaction, force, friction, self-cleaning*

INTRODUCTION

One of the important factors that affect field seed germination and simultaneous emergence of seedlings is a reliable contact with the soil. That end, in soil is formed at the same depth a seeding furrow with compactions bottom to which seeds are sown and immediately embedded by ground. However, it is greatly loosened that does not provide a reliable seed contact with the soil. The use of rollers for packing of crops gives positive results, but in moist soils they are sticking greatly. Herewith the special devices installed to clean the roller surface are ineffective.

Therefore there is a need to develop highly efficient technical means for seed embedding and to improve seeding methods, which would provide herewith a high field seed germination and simultaneous emergence of seedlings.

Analysis of the literature dedicated to development of highly efficient means for seed embedding and for improve seeding methods, for enhance the field seed germination and simultaneous emergence of seedlings shows that they are sufficiently studied [1,2,3,4,5,6,8]. Based on research by the authors developed and proposed to agricultural production an appropriate recommendation, in particular, to provide the required density of stems is proposed to increase the seeding rate by factor of 1.5 ... 2, and to prevent the breakage of the root system after seeding – use the packing of crops.

However, the analysis of work process of seeding furrows embedding by the conical roller and elements of the theory of their self-cleaning of soil, which sticks, in the literature are not given.

MATERIAL AND METHOD

One of the reserves of increase of spiked cereals yield is to create optimal conditions for seed germination and for subsequent plant growth and development and therefore the formation of crop. However, this environment, for many reasons, is not possible to create always. Particularly acute this problem appears after a harvesting of late crops, when it is necessary to conduct the seeding, and the soil after plowing is not yet settled and it cannot sow the seed in fresh tilled soil because of breakage of the root system. So after plowing must be hold the necessary time of full soil self-compaction, which runs for 3 ... 5 weeks and this leads to delaying seeding. To solve this problem, we have developed a new way of seeding of spiked cereals seed in fresh tilled soil with

Резюме: *Наведено результати аналізу робочого процесу засипання посівних борозенок і ущільнення ґрунту конічним котком, установленим під кутом α до напрямку борозенки, а також аналітичні вирази для визначення сили опору котка при переміщенні та бічної сили, яка забезпечує самоочищення від ґрунту, що прилипає до його поверхні.*

Ключові слова: *конічний коток, борозенка, зсув, ґрунт, ущільнення, сила, тертя, самоочищення.*

ПЕРЕДУМОВА

Одним з важливих факторів, що впливає на польову схожість насіння і появу дружніх сходів, є надійний його контакт з ґрунтом. З цією метою в ґрунті формують на однаковій глибині посівну борозну з ущільненим дном, на яке висівають насіння і відразу ж його загортають ґрунтом. Однак він є сильно розпушеним, що не забезпечує надійного контакту насіння з ґрунтом. Застосування котків для прикочування посівів дає позитивний результат, однак на зволожених ґрунтах вони сильно залипають. При цьому спеціальні пристрої, що встановлюються для очищення поверхні котка, малоефективні.

А тому виникає необхідність в розробці високоефективних технічних засобів для загортання насіння та в удосконаленні способів сівби, які забезпечили б при цьому високу польову схожість насіння та появу дружніх сходів.

Аналіз літературних джерел, приурочених питанням розробки високоефективних технічних засобів для загортання насіння та удосконаленню способів сівби, підвищенню польової схожості насіння та появи дружніх сходів показує, що вони є достатньо вивчені [1,2,3,4,5,6,8]. На основі результатів досліджень авторами розроблені і запропоновані сільськогосподарському виробництву відповідні рекомендації, зокрема з метою забезпечення необхідної густоти стеблостою пропонується збільшувати норму висіву в 1,5…2 рази, а щоб не допустити обриву кореневої системи після сівби - застосовувати прикочування посівів.

Однак аналіз робочого процесу загортання посівних борозен конічними котками, а також елементи теорії їх самоочищення від налиплого грунту, в літературних джерелах не наводиться.

МАТЕРІАЛ І МЕТОДИКА

Одним з резервів підвищення врожайності зернових колосових культур є створення оптимальних умов для проростання насіння та наступного росту і розвитку рослин і, відповідно, формування врожаю. Однак такі умови, в силу багатьох причин, не завжди вдається створити. Особлива гостро ця проблеми проявляться після збирання пізніх культур, коли необхідно проводити сівбу, а ґрунт після оранки ще не осів і висівати насіння у свіжозораний ґрунт не можна, оскільки відбувається обрив кореневої системи. Тому після оранки обов'язково витримують необхідний час для повного самоосідання грунту, який проходить протягом 3…5 тижнів, а це призводить до затягування строків сівби. Для вирішення цієї проблеми нами розроблено новий спосіб висіву насіння зернових колосових культур у свіжозораний грунт

stabilization of water-air regime in the topsoil during phase flowing-trough period from seed germination to the tillage and suggest tillage and sowing section with packing of crops [7]. Structural and technological scheme of this section is shown in Fig. 1.

зі стабілізацією водно-повітряного режиму в кореневому шарі на період протікання фази від проростання насіння до настання кущіння, та запропоновано ґрунтообробно-посівну секцію з прикочуванням посівів [7]. Конструктивно-технологічна схема даної секції наведена на рис.1.

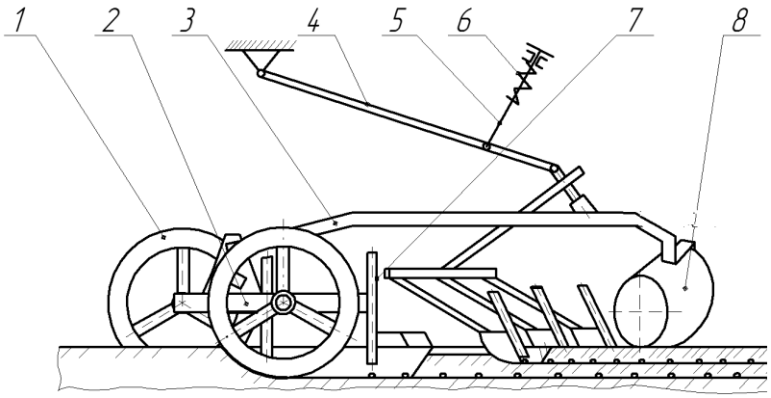

Fig. 1 - Structural and technological scheme of tillage and sowing section for seeding seeds in fresh tilled soil with packing of crops / *1 – ribbed roller ; 2 – frame ; 3 – strip ; 4 – drawbar; 5 – push rod; 6 – spring ; 7 – fertilizer funnel; 8 – conical roller*

Its main working body is annular soil compactor furrow-making device. It consists of a rectangular frame *2*, in which there are three ribbed rollers *1*. Frame *3* is connected to the strip *3*, which by means of radial drawbar *4* and push rod *5* with spring *6* is connected to the frame of sowing unit. Back of frame *2* in the center of each ribbed roller *1* is set a fertilizer funnels *7*, coverers, shoe openers and conical roller *8*, which is set at the angle *α* to the direction of furrow. It provides high-quality seeding furrows embedding and soil compaction.

Основним її робочим органом є кільцевидний ущільнювач-борозноутворювач. Він складається з прямокутної рамки *2*, в якій встановлено три кільчатих котки *1*. Рамка з'єднується з штабою *3*, яка за допомогою радіального повідка *4* і натискної штанги *5* з пружиною *6* з'єднується з рамою посівного агрегату. Ззаду рамки *2* по центру кожного кільчатого котка *1* встановлено тукопроводи *7*, загортачі, килевидні сошники та конічний коток *8*, установлений під кутом *α* до напрямку борозенки. Він забезпечує якісне засипання посівних борозенок і ущільнення ґрунту.

RESULTS

Analysis of work process of such roller shows that it should take the form of a truncated cone and be directed by a smaller base of cone to direction of motion. For interpretation of the interaction of roller with soil and swath we consider the scheme of work of conical roller in the vertical and horizontal planes, Fig.2 a,b.

РЕЗУЛЬТАТИ

Аналіз робочого процесу такого котка показує, що він повинен мати форму зрізаного конуса і бути спрямованим меншою основою до напрямку руху. Для вияснення взаємодії котка з грунтом і валком розглянемо схему роботи конічного котка у вертикальній і горизонтальній площинах, рис.2а,b.

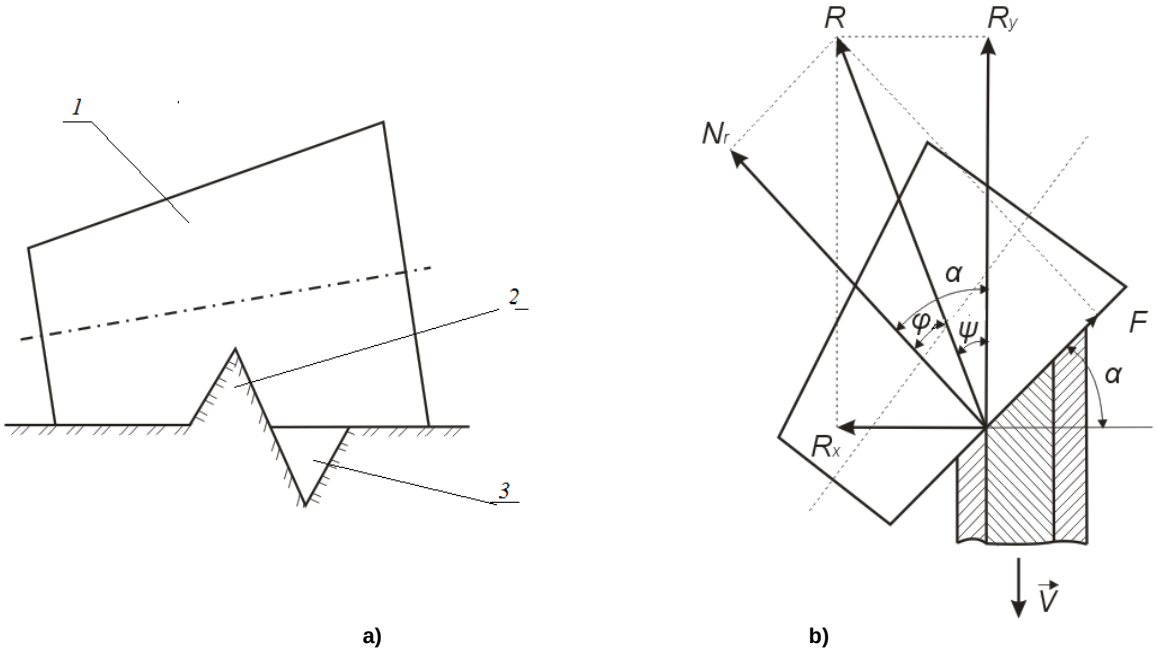

a) **b)**

Fig. 2 - Scheme of the forces acting on the conical roller
1 – roller ; 2 – swath; 3 – furrow

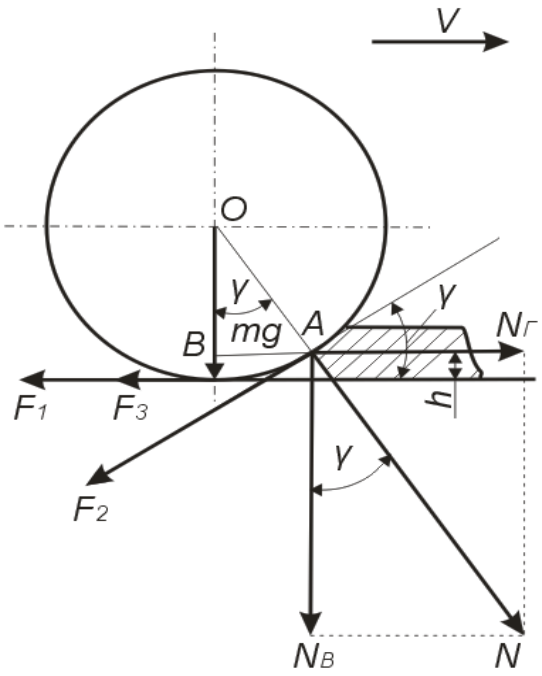

c)

Fig. 2 - Scheme of the forces acting on the conical roller
1 – roller ; 2 – swath; 3 – furrow

From the scheme (Fig.2c) can be seen that gravity force of roller *mg* (here *m* - weight of roller, *g* – gravitational acceleration of the body) cause the frictional force of the roller against the soil:

З наведеної схеми (рис. 2с) видно, що сила ваги котка *mg* (тут *m* – маса котка, *g* – прискорення вільного падіння тіла) викликає силу тертя котка об ґрунт:

$$F_1 = fmg \tag{1}$$

where *f* – coefficient of friction of the roller against the soil.

This force is directed opposite to the direction of rollers rolling.

From the scheme is also seen that at point *A* of contact of rollers rim with swath appears a normal force *N*, which declined from the vertical at the angle *γ* and it cause at this point the frictional force:

де f - коефіцієнт тертя котка об грунт.

Ця сила спрямована протилежно напрямку перекочування котка.

З наведеної схеми також видно, що в точці *A* дотику обода котка з валком виникає нормальна сила *N*, яка відхилена від вертикалі на деякий кут γ і вона викликає в цій точці силу тертя:

$$F_2 = f \cdot N \ . \tag{2}$$

We expand the normal force *N* on the components - horizontal:

Розкладемо нормальну силу *N* на складові – горизонтальну:

$$N_\Gamma = N \cdot sin\gamma \tag{3}$$

and vertical:

і вертикальну:

$$N_B = N \cdot cos\gamma \ . \tag{4}$$

Analysis of the forces components shows that the horizontal force moves the swath in direction of the velocity vector *v*, and the vertical force - compact the swath and cause the friction force:

Аналіз складових сил показує, що горизонтальна сила переміщує валок в напрямку вектора швидкості *v*, а вертикальна – ущільнює валок і викликає силу тертя:

$$F_3 = f_1 \cdot N_B \ , \tag{5}$$

which is directed opposite to direction of the velocity vector *v* (here f_1 – coefficient of friction of the swath against the soil surface).

From the scheme on Fig.2c can be written condition of swath moving by the roller:

яка направлена протилежно напрямку вектора швидкості *v* (тут f_1 - коефіцієнт тертя валка об поверхню грунту).

З наведеної на рис. 2с схеми сил можна записати умову переміщення валка котком:

$$F_1 + F_2 \cdot cos\gamma + F_3 < N_\Gamma .$$

Using expressions (1), (2), (3), (4) and (5) the last inequality can be written in this form:

З урахуванням виразів (1), (2), (3), (4) і (5) останню нерівність можна записати в такому вигляді:

$$fmg + fN \cdot cos\gamma + f_1 N \cdot cos\gamma < N \cdot sin\gamma . \quad (6)$$

But $mg = N_B + F_2 \cdot sin\gamma$ and taking into account the expressions (2) and (4), this expression has the form:

Але $mg = N_B + F_2 \cdot sin\gamma$ і з врахуванням виразів (2) і (4) цей вираз матиме вигляд:

$$mg = N(cos\gamma + f \cdot sin\gamma) \quad (7)$$

where we find that

звідки знайдемо, що

$$N = \frac{mg}{cos\gamma + f \cdot sin\gamma} . \quad (8)$$

In terms of ensuring of swath shift in seeding furrow and of efficient self-cleaning rollers surface from stuck-on soil it is of great interest the projection of the normal force *N* in the horizontal plane N_Γ (Fig. 2b). From the above scheme is seen that this force causes the lateral force *F*, which shifts the swath in the furrow and completely covering the seed with soil. Thus the lateral force provides the rollers self-cleaning from the soil that sticks to the surface. Its value can be determined by the formula $F = f \cdot N_\Gamma$, which with account of expressions (3) and (8) takes on the following form:

З точки зору забезпечення зсування валка в посівну борозенку і ефективного самоочищення поверхні котка від прилиплого грунту, значний інтерес викликає проекція нормальної сили *N* в горизонтальній площині N_Γ (рис. 2b). З наведеної схеми видно, що саме ця сила викликає бічну силу *F*, яка зсуває валок в борозенку і повністю закриває насіння ґрунтом. При цьому бічна сила забезпечує самоочищення котка від ґрунту, що прилипає до його поверхні. Її значення можна визначити за формулою $F = f \cdot N_\Gamma$, яка з врахуванням виразів (3) та (8) набуде наступного виду:

$$F = f \cdot N \cdot sin\gamma = f \cdot sin\gamma \frac{mg}{cos\gamma + f \cdot sin\gamma} . \quad (9)$$

To determine the draught of the roller we turn to the scheme of forces (Fig. 2b), which act from the direction of swath on the roller in a horizontal plane. From the above scheme is seen that the resistance force of the swath is determined by the following formula:

Для визначення тягового опору котка звернемося до схеми сил (рис. 2b), що діють зі сторони валка на коток в горизонтальній площині. З наведеної схеми видно, що сила опору валка визначається за такою формулою:

$$Q = R_Y + F \cdot \sin\alpha , \quad (10)$$

where R_y - projection of the resultant resistance force *R* of the swath along the axis *OY*:

де R_Y – проекція рівнодіючої сили *R* опору валка по осі *OУ*:

$$R_Y = R \cdot \cos\psi = R \cdot \cos(\alpha - \varphi) , \quad (11)$$

here ψ - the angle between the resultant resistance force R of the swath and its constituent R_y;

φ – angle of deflection of resultant resistance force *R* of swath from the normal force N_Γ which is equal to the rollers angle of friction against the swath;

α - angle between the normal force N_Γ and direction of movement of the roller.

тут ψ – кут між рівнодіючою силою опору *R* валка і її складовою R_Y;

φ - кут відхилення рівнодійної сили *R* опору валка від нормальної сили N_Γ, рівний куту тертя котка об валок;

α – кут між нормальною силою N_Γ і напрямком руху котка.

Given that $R = \frac{N_\Gamma}{\cos\varphi}$, and the value of the force N_Γ is defined by the formula (3), expression (11) can be written as $R_Y = \frac{N \cdot sin\gamma}{\cos\varphi} \cdot \cos(\alpha - \varphi)$, which in view of expressions (8) takes the form:

Враховуючи те, що $R = \frac{N_\Gamma}{\cos\varphi}$, а значення сили N_Γ визначається за формулою (3), вираз (11) можемо записати так $R_Y = \frac{N \cdot sin\gamma}{\cos\varphi} \cdot \cos(\alpha - \varphi)$, який з врахуванням виразу (8) набуде виду:

$$R_Y = \frac{mg \cdot sin\gamma}{cos\gamma + f \cdot sin\gamma} \cdot \frac{\cos(\alpha - \varphi)}{\cos\varphi} \quad (12)$$

We substitute the obtained values of R_Y and F in expression (10), and get the draught resistance of the roller

Підставимо отримані значення R_Y і F в вираз (10), і отримаємо тяговий опір котка

$$Q = \frac{mg \cdot \sin\gamma}{cos\gamma + f \cdot sin\gamma} \cdot \frac{\cos(\alpha - \varphi)}{\cos\varphi} + f \cdot \sin\alpha \frac{mg}{cos\gamma + f \cdot sin\gamma}$$

which finally is written as:

який остаточно запишеться так:

$$Q = \frac{mg}{cos\gamma + f \cdot sin\gamma} \cdot \sin\gamma \cdot [\frac{\cos(\alpha - \varphi)}{\cos\varphi} + f] \quad (13)$$

Value of the angle γ of the line of frictional force action F_2 of roller against the swath of soil we define as follows: We substitute in expression (6) instead of mg the expression (7) and obtain the inequality:

Значення кута γ напрямку лінії дії сили тертя F_2 котка об валок грунту визначимо наступним чином. Підставимо в вираз (6) замість mg вираз (7) і отримаємо нерівність:

$$fN(cos\gamma + f \cdot sin\gamma) + fN \cdot cos\gamma + f_1 N \cdot cos\gamma < N \cdot sin\gamma$$

which after reduction on N can be written as follows:

яку після скорочення на N можна записати в такому вигляді:

$$fcos\gamma + f^2 \cdot sin\gamma + fcos\gamma + f_1 \cdot cos\gamma < sin\gamma$$

After the arithmetic operations can be written as:

Після проведення арифметичних дій її можна записати так:

$$cos\gamma(2f + f_1) < sin\gamma(1 - f^2)$$

where we define the angle γ of the line of frictional force action F_2 of roller against the swath

звідки визначимо значення кута γ напрямку лінії дії сили тертя F_2 котка об валок грунту

$$\gamma > arctg \frac{2f + f_1}{1 - f^2}. \quad (14)$$

Calculations show that for light soils by $f=0,5$ and $f_1=1,0$, we have $\gamma > 63^0$, and for heavy soils by $f=0,8$ and $f_1=1,0$, we have $\gamma > 82^0$.

Розрахунки показують, що для легких ґрунтів при $f=0,5$ і $f_1=1,0$, маємо $\gamma > 63^0$, а для важких при $f=0,8$ і $f_1=1,0$, маємо $\gamma > 82^0$.

Knowing the angle γ and the height h of the swath we can determine the minimum allowable rollers diameter. To do this, we consider the triangle AOB (Fig. 1b) from which we can write that $OB = r \cdot \cos\gamma$, $r - OB = h$. Therefore $r - r \cdot \cos\gamma = h$ and $r(1 - \cos\gamma) = h$, or $\frac{D}{2}(1 - \cos\gamma) = h$, whence

Знаючи кут γ і висоту h валка можна визначити мінімально-допустимий діаметр котка. Для цього розглянемо трикутник AOB (рис. 1b), з якого можна записати, що $OB = r \cdot \cos\gamma$, а $r - OB = h$.

Отже $r - r \cdot \cos\gamma = h$ і $r(1 - \cos\gamma) = h$, або $\frac{D}{2}(1 - \cos\gamma) = h$, звідки

$$D = \frac{2h}{1 - \cos\gamma}. \quad (15)$$

Given that by the seeding of spiked cereals seed the shoe openers forming the swath heigt max 6 ... 10 cm, the rollers diameter should be 15 ... 35 cm.

Враховуючи те, що при висіві насіння зернових колосових культур сошники утворюють валок висотою не більше 6…10 см, діаметр котка повинен становити 15-35 см.

CONCLUSIONS

1. During moving a conical roller which is installed at the angle α to the direction of seeding furrow on its surface generator arises a lateral force F, which shifts the swath in the furrow and completely covers the seed with the soil.
2. Efficient self-cleaning of the conical roller of soil that sticks to its surface is provided by the lateral force F.

ВИСНОВКИ

1. Під час переміщення конічного котка, установленого під кутом α до напрямку посівних борозенок, на його твірній поверхні виникає бічна сила F, яка зсуває валок в борозенку і повністю закриває ґрунтом насіння.
2. Ефективне самоочищення конічного котка від ґрунту, що прилипає до його поверхні, забезпечується за рахунок бічної сили F.

REFERENCES

[1]. Basin V.S, Bray V.V., Pogorely L.V. et al., (1987) - *Machines for precise planting of row crops: design and calculation*, Technique, p.151, Kiev;
[2]. Kardashevsky S.V., (1973) - *Seeding device of sowing machines,* Mechanical Engineering, p.176, Moscow;

БІБЛІОГРАФІЯ

[1]. Басин В.С., Брей В.В., Погорелый Л.В. и др, (1987) - *Машины для точного посева пропашных культур: конструирование и расчет*, Техника, - 151с., - Киев;
[2]. Кардашевский С.В., (1973) - *Высевающие устройства посевных машин,* – М.: Машиностроение, – 176 с.;

[3]. Khaylis G.A., Ghelic L.A., (2002) - *Analysis of the process of wheel rolling with the formation of wheel track,* Collection of scientific articles «Agricultural machines», № 10, pg. 225-236, Lutsk;
[4]. Khomenko M.S., Ziryanov V.A., Nasonov V.A., (1989) - *Mechanization of planting crops and grasses*. Handbook, Vintage, p.168, Kiev;
[5]. Kovbasa V.P., Pochka K.I., (2007) – *Kinematics of interaction of compact roller with a layer of medium of finite depth,* Collection of scientific articles «Agricultural machines», № 15, pg.139-147, Lutsk;
[6]. Poletaev A.F., (1971) - *Fundamentals of the theory of rolling resistance and traction of rigid wheel on deformable base,* Mechanical Engineering, p.68., Moscow;
[7]. Shvedyk M.S., (2013) - *Analysis of single-operating working bodies for surface processing of the soil and embedding of seed and their synthesis,* Collection of scientific articles «Agricultural machines», № 24, pg.426-440, Lutsk;
[8]. Zaika P.M., (2001) - *The theory of agricultural machines. Machines and tools for cultivation,* Oko, V. 1 (p.1), p.444, Kharkov.

[3]. Хайлис Г.А., Гелич Л.А., (2002) - *Анализ процесса качения колеса с образованием колеи*, Зб. наук. статей «Сільськогосподарські машини», № 10. –с. 225-236, - Луцьк;
[4]. Хоменко М.С., Зырянов В.А., Насонов В.А., (1989) *Механизация посева зерновых культур и трав.* Справочник, Урожай, -168 с., - Киев;
[5]. Ковбаса В.П., Почка К.І., (2007) - *Кінематика взаємодії ущільнюючого котка з шаром середовища обмеженої глибини,* Зб. наук. статей «Сільськогосподарські машини», № 15. –с. 225-236, - Луцьк;
[6]. Полетаев А.Ф., (1971) - *Основы теории сопротивления качению и тяги жесткого колеса по деформируемому основанию,* – М: Машиностроение, 1971-68 с.;
[7]. Шведик М.С., (2013) - *Аналіз одноопераційних робочих органів для поверхневого обробітку ґрунту заробки насіння та їх синтез,* Зб. наук. статей «Сільськогосподарські машини», № 24. –с. 426-440, Луцьк;
[8]. Заїка П.М., (2001) - *Теорія сільськогосподарських машин. Машини та знаряддя для обробітку ґрунту*, Т. 1 (ч. 1), Око, -444 с., - Харків.

DYNAMICS OF OVERSOWING MACHINE MSPD 2.5 RELATED TO WORKING AND CONSTRUCTIVE PARAMETERS
/
DINAMICA MAŞINII DE SUPRAÎNSĂMÂNŢAT MSPD 2,5 ÎN CORELAŢIE CU PARAMETRII DE LUCRU ŞI CONSTRUCTIVI

Ph.D. Eng. Ene T.A., Ph.D. Eng. Mocanu V.
Research-Development Institute for Grassland Brasov / Romania
E-mail: tudorene@yahoo.com, vasmocanu@yahoo.com

Abstract: *In the paper, the equipment and methodology of experimental research concerning the dynamics of the individual sowing section and the complete machine, are presented. Depending on working conditions (depth: 2 and 4 cm, speed: 5.5 km/h (1.52 m/s) and 7.5 km/h (2.08 m/s)) and constructive solutions (attack angle of share: 25°, 35° and 45°), analyzing the data of experimental trials, there is possibility to find optimal constructive and functional solutions to reduce traction forces and finally fuel consumption of the aggregate.*

Keywords: *grassland, oversowing, traction forces, working depth, aggregate speed*

INTRODUCTION

A new oversowing machine MSPD-2.5 type, which works in unit with 35…50 HP wheeled tractor, at the Research-Development Institute for Grassland Brasov/Romania was designed, manufactured and tested [2]. The main advantages of the new oversowing machine are: the copy of the unevenness of the ground on each row processed and sown, in the limits of ±10 cm; achievement of a good uniformity of distribution on the working width; adjustment and constant maintaining the depth of the share and introducing the seeds into the soil.

Rezumat: *În lucrare sunt prezentate echipamentul şi metodologia cercetării experimentale cu privire la dinamica secţiei individuale de semănat şi a întregii maşini. În funcţie de condiţiile de lucru (adâncime: 2 şi 4 cm, viteză: 5,5 km/h (1,52 m/s) şi 7,5 km/h (2,08 m/s)) şi soluţiile constructive (unghiul de atac al brăzdarului: 25°, 35° şi 45°), analizând datele încercărilor experimentale, este posibilă găsirea soluţiilor constructive şi funcţionale optime pentru a reduce forţa de tracţiune şi ulterior consumul de combustibil al agregatului.*

Cuvinte cheie: *pajişte, supraînsămânţare, forţă de tracţiune, adâncime de lucru, viteza agregatului*

INTRODUCERE

O nouă maşină de supraînsămânţat tip MSPD 2,5, care lucrează în agregat cu tractoare pe roţi de 35 ... 50 CP, a fost proiectată, realizată şi testată la Institutul de Cercetare-Dezvoltare pentru Pajişti Braşov [2]. Principalele avantaje ale maşinii sunt: copierea denivelărilor solului pentru fiecare rând semănat în limita a ± 10 cm; realizează o bună uniformitate de distribuţie pe lăţimea de lucru; reglarea şi menţinerea constantă în lucru a adâncimii brăzdarelor şi introducerea seminţelor în sol.

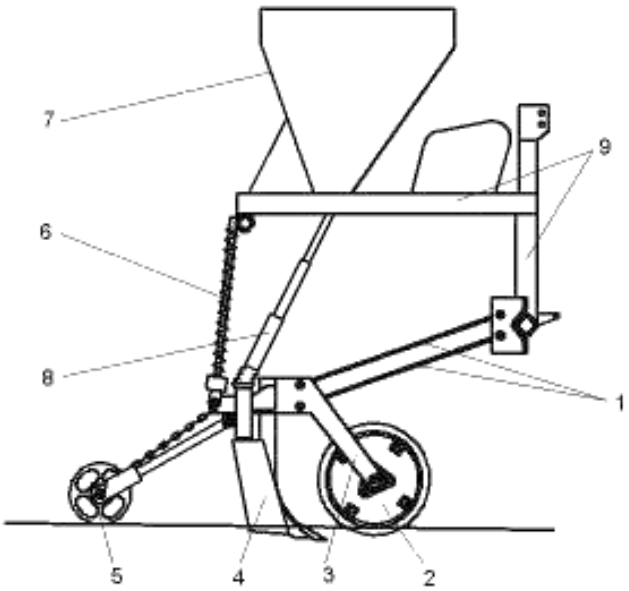

Fig. 1 – Constructive scheme of grassland oversowing machine [1]:
1-deformable parallelogram mechanisms; 2- cutter disc; 3-body of the section;4- share; 5-setting wheel; 6-adjustable springs; 7-seed box; 8-delivery hose; 9-frame of machine

MATERIAL AND METHOD

The constructive and functional optimization of the machine needed an analysis of the dynamics and

MATERIAL ŞI METODĂ

Optimizarea constructivă şi funcţională a maşinii a necesitat analiza dinamică şi energetică prin cercetări

energetics through experimental trials of cinematic, dynamic and energetic parameters of both the sowing sections and the tractor-grassland oversowing machine system [1].

To achieve this objective it was necessary to measure, record and process the following main parameters: the traction forces from coupling bars of the sowing sections (to determine the traction forces of sections), forces acting on cutter disc, forces acting on the soil opener, load forces on section body performed by tensioned springs, the resistance force to traction of the oversowing machine transmitted to tractor by the rear three points hitch, machine working speed and working depth of soil share. To carry out the experimental researches of the mentioned parameters, a series of transducers and sensors were placed on both the tractor and the machine, shown in figure 2.

experimentale ai parametrilor cinematici, dinamici şi energetici ai ambelor secţii de semănat, luate individual, şi a sistemului tractor-maşină de supraînsămânţat [1].

Pentru a îndeplini aceste obiective a fost necesară măsurarea, achiziţia şi procesarea următorilor parametri principali: forţele de tracţiune din mecanismul paralelogram al secţiei de semănat (pentru a determina forţa de tracţiune a secţiilor), forţelor ce acţionează asupra discului, forţelor ce acţionează asupra brăzdarului, forţa de apăsare pe cadrul secţiei prin intermediul arcurilor, forţa de rezistenţă la tracţiune a maşinii de supraînsămanţat transmisă la tractor prin mecanismul de suspendare în trei puncte, viteza de lucru a maşinii şi adâncimea de lucru a brăzdarelor. Pentru realizarea cercetării experimentale a parametrilor menţionaţi, pe tractor şi maşină au fost amplasaţi o serie de traductoare şi senzori, prezentaţi în figura 2.

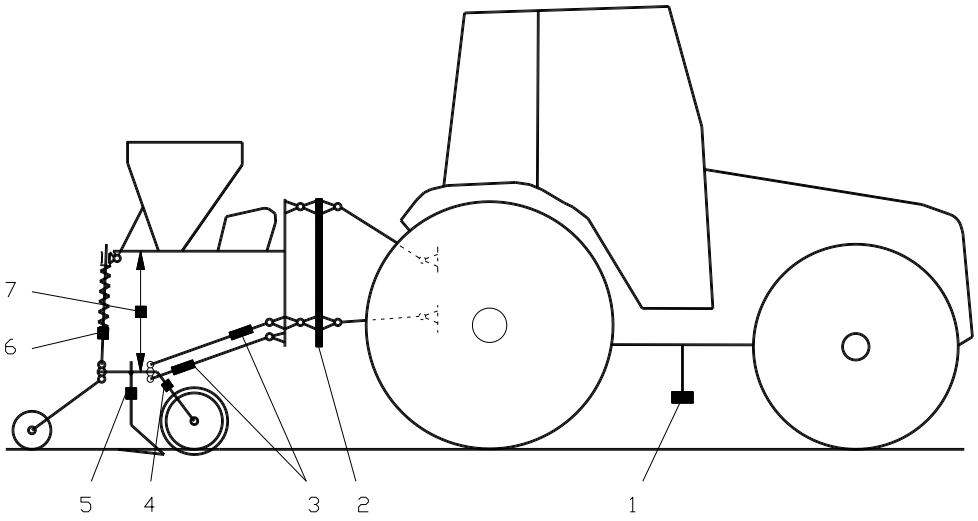

Fig. 2 - Location scheme of transducers and sensors on the tractor-oversowing machine system [1]:

1-optical transducers for measuring the space; 2- frame with tensometric transducers for determining the forces in the three points hitch of the tractor; 3- tensometric transducers for determining the forces in parallelogram mechanisms; 4- tensometric transducers for determining the forces from cutter disc; 5- tensometric transducers for determining the forces from share; 6- tensometric transducers for determining the force from springs of sowing section; 7-inductive transducers for determining the vertical displacements of section related to body of machine.

The experimental trials were carried out on the oversowing machine for degraded grasslands MSPD-2.5 type and the four wheel drive tractor by 100 HP system [1].

In figure 3, the position of sections with tensometric rings (that one red-blue color) relative to body of machine is presented [1].

Cercetările experimentale au fost efectuate pe un sistem format din maşina de supraînsămânţat pajişti degradate tip MSPD 2,5 şi tractor pe roţi 4x4 de 100 CP [1].

În figura 3 este prezentată amplasarea secţiilor cu inele tensometrice (cele de culoare roşu-albastru) relativ la cadrul maşinii [1].

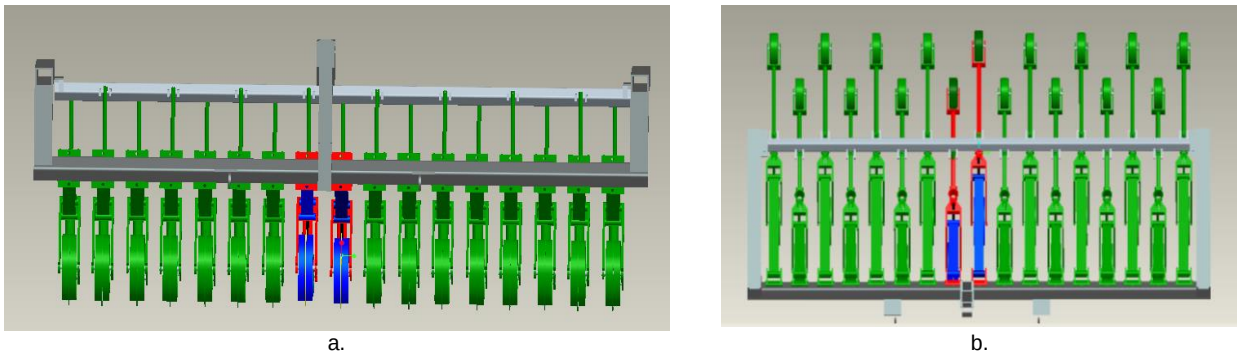

a. b.

Fig. 3 - Position of the section with tensometric rings relative to body of machine [2]:
a-vertical-transversal view; b-horizontal-transversal view

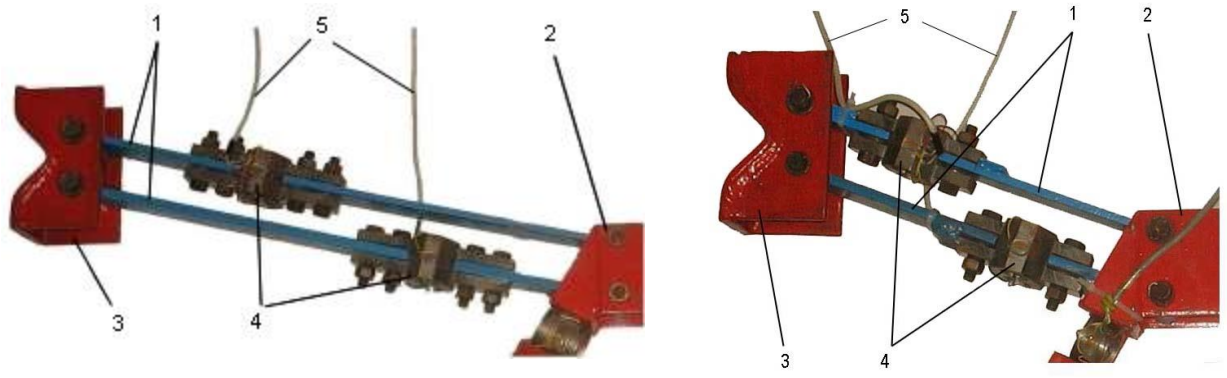

a) b)

Fig. 4 - Mounting of the devices (tensometric rings) from determining the forces from bars for sowing section connected at the body of machine [1]: a) long section; b) short section;
1 - connection bars (parallelogram mechanism); 2 - frame of sowing section; 3 - body of the machine; 4 - tensometric rings; 5 - wires for signal of tensometric rings

The measurement of forces from connection bars 1 (Fig. 4) of the sowing section 2 to the frame of the machine 3 was performed by using devices with tensometric traction rings equipped with electro resistive transducers 4, mounted perpendicularly on the longitudinal axis of the parallelogram bars (Fig. 5,a; 5,c). For each tensometric ring there were used 4 transducers of type 6/120 ZY11 (Hottinger company), with resistance R=120 Ω and constant K=2.07. The resistive transducers were mounted on a strain gauge bridge (Fig. 5, b) [1].

Măsurarea forţelor din barele de legătură 1 (fig. 4) (mecanismul paralelogram) ale secţilor de semănat 2 (scurtă şi lungă) la cadrul maşinii 3 s-a realizat cu ajutorul unor dispozitive cu inele de tracţiune cu traductoare electrorezistive 4, montate perpendicular pe axa longitudinală a barelor paralelogramului (fig. 5,a; 5c). Pentru fiecare inel tensometric s-au folosit patru traductoare de tip 6/120LY11 (firma Hottinger), cu rezistenţa R = 120 Ω şi constanta K=2,07. Montarea rezistenţelor mărcilor tensometrice s-a făcut în punte completă (Fig. 5, b) [1].

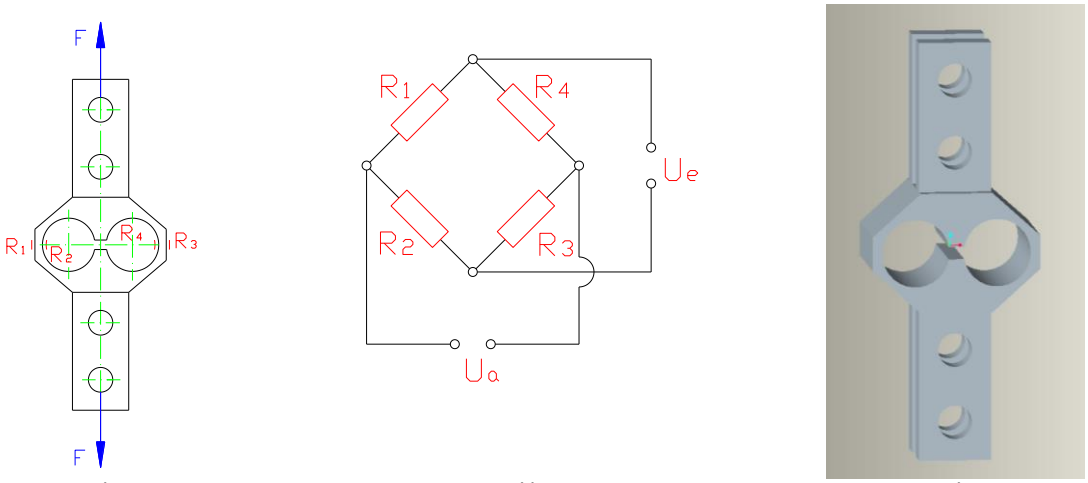

a) b) c)

Fig. 5 - Scheme of tensometric rings for forces measurement from connections bars of parallelogram mechanism [1, 3]:
a – the location of strain gauge marks on the tensometric rings;
b – mounting scheme of trade strain gauge on a strain gauge bridge;c – 3D tensometric ring model.

The measurement of forces from fork 2 of cutter disc 1 (Fig. 6) was performed by using devices with tensometric traction rings 3, mounted on direction of fork 2. On internal and external walls of the rings there are connected resistive tensometric transducers with strain longitudinal axis placed in the same plane with longitudinal axis of the fork of cutter disc (Fig. 7,a; 7,c). There were used 4 trade resistive transducers 10/120 ZY11 type (Hottinger company), with resistance R=120 Ω and constant K=2.07.The trade strain gauges were mounted on a strain gauge bridge as shown in figure 7,b [1].

Măsurarea forţelor din furca 2 a discului de tăiere 1 (forţele de tracţiune a roţii şi de apăsare pe sol) (Fig. 6), s-a realizat un dispozitiv cu inele cu traductoare electrorezistive 3, montate pe direcţia furcii 2. Pe pereţii exteriori şi interiori ai inelului tensometric s-au lipit traductoare tensometrice rezistive cu axa longitudinală de solicitare plasată în acelaşi plan cu axa longitudinală a furcii roţii cu obadă (Fig. 7,a; 7,c). S-au folosit patru traductoare (mărci) tensometrice rezistive de tip 10/120LY11 (firma Hottinger), cu rezistenţa R = 120 Ω şi constanta K=2,07, Montarea rezistenţelor traductoarelor tensometrice s-a făcut în punte completă conform schemei din figura 7, b [1].

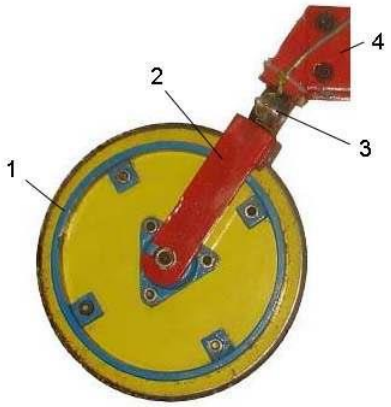

Fig. 6 - The tensometric ring location for determining the resultant force within fork of cutter disc [1]:
1-cutter disc; 2-fork; 3- tensometric ring; 4-body of sowing section.

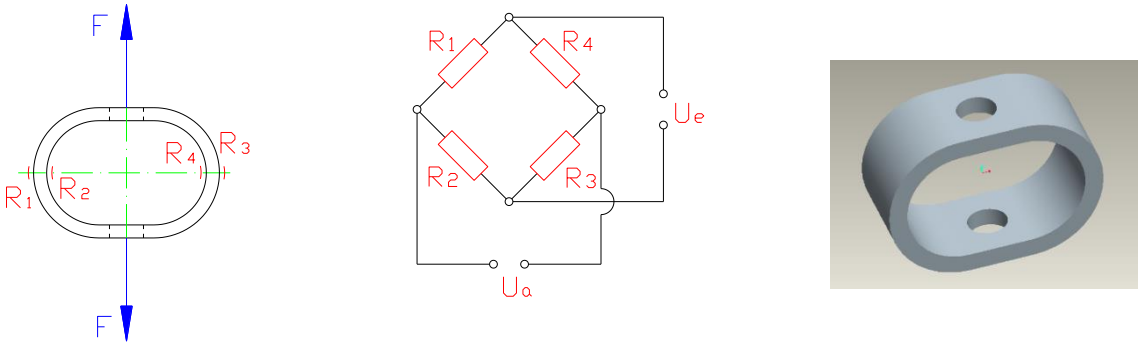

a. b. c.

Fig. 7 - Scheme of tensometric rings for determining the force from fork [1]:
a – the location of strain gauge marks on the tensometric rings; b – mounting scheme; c – 3D design of the tensometric ring.

The measurement of forces at share 1 of the sowing section (Fig. 8) was performed by using devices with tensometric traction rings with electro-resistive transducers 2 mounted on the fixing bar 3 to the frame 4 of the sowing section [1, 3].

Măsurarea forţelor la brăzdarul 1 al secţiei de semănat (Fig. 8) s-a realizat cu un dispozitiv cu inele cu traductoare electrorezistive 2 montat pe braţul de prindere 3 la cadrul 4 al secţiei de semănat [1, 3].

a. b.

Fig. 8 - Tensometric ring device for determining the forces in fixing arm of soil opener (share) [1, 2]:
a- mounting the tensometric ring at the soil opener; b- soil opener mounting on the body of the sowing section;
1-soil opener; 2-tensometric ring; 3-fixing arm devices;4- body of sowing section; 5- cutter disc; 6-spring of section

To design the transducer with tensometric ring (Fig. 9,a; 9,c) there were used 4 strain gauges 6/120 ZY11 type (Hottinger company), with resistance R=120 Ω and constant K=2,07. The strain gauges were mounted on a strain gauge bridge (Fig. 9,b) [1].

Pentru realizarea dispozitivului cu inel tensometric (Fig. 9,a; 9,c) s-au folosit patru traductoare tensometrice rezistive de tip 6/120LY11 (firma Hottinger), cu rezistenţa R = 120 Ω şi constanta K=2,07. Montarea rezistenţelor traductoarelor tensometrice s-a făcut în punte completă (Fig. 9,b) [1].

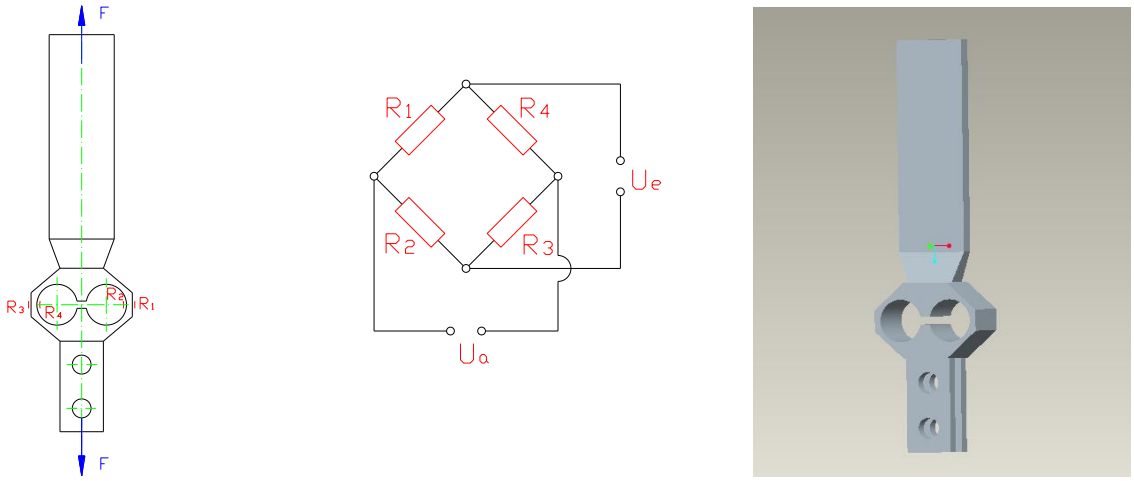

a) b) c)

Fig. 9 - Scheme of tensometric rings for forces measurement from connection bars of parallelogram between sowing section and furrow [1]:
a-the location of trade strain gauges on the tensometric ring;
b-mounting scheme of trade strain gauge on a strain gauge bridge
c-3D design of tensometric ring

The measurement of forces from springs 3 (Fig. 10) that act on the direction of the rod axis 4 of spring and presses the body 1 of the sowing section was performed with tensometric electroresistive transducers ring 2. The electroresistive transducers were mounted on a device with compression rings similar to those shown in figure 10 [1]. During the emplacement of tensometric rings on the spring rod it had in view the rings have no negative influences on the working process.

Măsurarea forţelor din arcurile de apăsare 3 (Fig. 10) care apasă pe cadrul secţiei de semănat 1 pe direcţia axei tijei resortului 4 şi s-a realizat cu inele cu traductoare electrorezistive 2. Mărcile tensometrice au fost montate pe inele tensometrice de comprimare, prezentate în figura 10 [1]. La montarea inelelor tensometrice pe tija de ghidare a arcului de apăsare s-a avut în vedere ca acestea să nu aibă influenţe negative în timpul funcţionării.

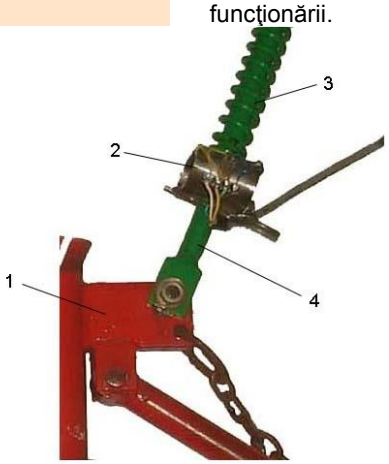

Fig. 10 - Mounting the tensometric ring for determining the force from the spring of the sowing section body [1]:
1-body of sowing section; 2-tensometric ring; 3-spring; 4-rod spring

The measurement of linking forces between the tractor and the oversowing grassland machine (the total traction force for machine operating) was performed with a device with tensometric transducers (tensometric frame) presented in figure 11 [1]. The device is made of 3 frames (central 1 and sides 2, 3) and five strain gauges supports which can be assembled in three positions, making it possible to couple it to the suspension mechanisms at three hitch points and to the coupling devices of the agriculture machine.

The frame is coupled to the rear three points hitch of the tractor by coupling the side and central links of the tractor to the side bolts 4 and central bolts 5.

On side bolts 4 and central bolt 5 are fixed side strain gauges 6 and central strain gauges 7 for coupling the agriculture machine. On side strain gauges supports 6 are connected through bolts 8 the vertical strain gauges supports 9.

Măsurarea forţelor de legătură dintre tractor şi maşina de supraînsămânţat (forţa de rezistenţă la tracţiune a maşinii) s-a realizat cu un dispozitiv cu traductoare tensometrice (ramă tensometrică) prezentat în figura 11 [1]. Rama tensometrică este formată din trei cadre (central 1 şi două laterale 2, 3) şi cinci suporţi tensometrici care se pot asambla prin organe de asamblare în trei poziţii, făcând astfel posibilă cuplarea acesteia atât la mecanismele de suspendare în 3 puncte ale tractoarelor cât şi la dispozitivele de cuplare ale maşinilor agricole.

Cuplarea ramei la mecanismul de suspendare al tractorului se realizează prin cuplarea tiranţilor laterali şi central ai tractorului la bolţurile laterale 4 şi central 5.

La bolţurile laterale 4 şi central 5 de se fixează şi suporţii tensometrici laterali 6 şi central 7, pentru cuplarea maşinii agricole. De suporţii tensometrici laterali 6 sunt articulaţi prin bolţurile 8 suporţii tensometrici verticali 9.

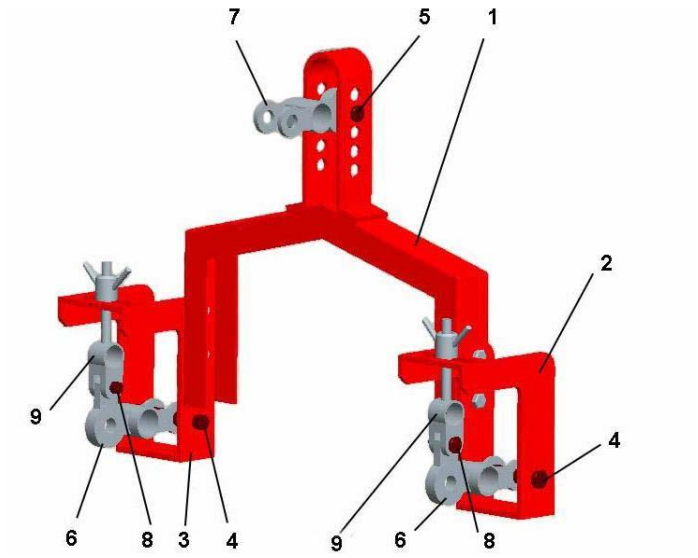

Fig. 11 - Intermediate frame with tensometric rings for measuring the traction force of agricultural machine [1]:
1-central frame; 2,3-lateral frame; 4- lateral pin; 5- central pin; 6-horizontal lateral supports strain gauges; 7- central supports strain gauges; 8-pin; 9- vertical lateral supports strain gauges

The measurement of the working speed of tractor-grassland oversowing machine system was performed with speed transducers, optical type, made by CORRSSYS DATRON Company, of AQUA L 350 type. The transducer is presented in figure 12,a and the mounting solution is presented in figure 12,b [1].

Pentru determinarea vitezei reale de deplasare a agregatului tractor-maşină de supraînsămânţat s-a utilizat un traductor de viteză, de tip optic, tip Aqua L 350, produs de firma CORRSSYS DATRON (SUA). În figura 12.a se prezintă varianta constructivă a traductorul, iar în figura 12.b se prezintă amplasarea acestuia pe tractor [1].

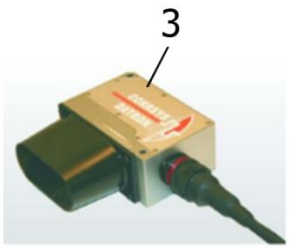

a)

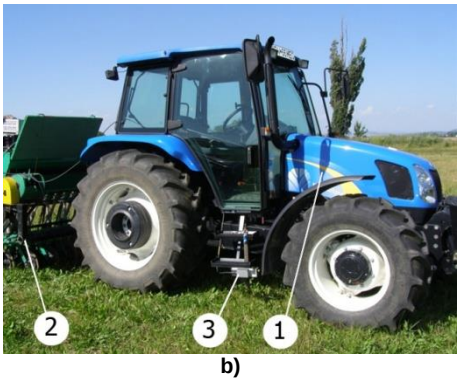

b)

Fig. 12 - Optical speed transducers AQUA L 350 type (a) and transducer location on the tractor (b) [1]:
1-tractor 4 WD (100 HP); 2-oversowing machine (type) MSPD-2,5; 3-optical transducers of speed

The measurement of the vertical displacement of sowing sections in order to determine the vertical position of sowing sections as well as the measurement of the working depth of soil opener, were performed with inductive transducers of linear displacement type WAL 100 (±50 mm) for short section and WAL 200 (±100 mm) for long section (made by Hottinger company). The values of linear displacement and the mathematical formulae were applied in order to calculate the angular position of coupling bars of parallelogram mechanism of sowing sections to correlate the resulting force from parallelogram mechanism bars with resistance traction forces and vertical load forces of sowing sections.

The equipment for measuring and recording the data used for experimental tests of the system compose by the tractor 1 (Fig.13) and oversowing machine 2 has consisted in power supply 4, voltage stabilizer 5 (UPS), booster modular system 6 (MGC plus) and laptop (type P4) 7, all these components being placed on the grassland oversowing machine 2 through frame 3.

Pentru măsurarea deplasărilor liniare faţă de cadrul maşinii de supraînsămânţat a secţiilor de semănat s-au utilizat traductori inductivi de deplasare tip W 200 (± 100 mm) pentru secţia lungă şi tip W 100 (± 50 mm) pentru secţia lungă (produse de firma Hottinger). Cu ajutorul valorilor deplasărilor liniare măsurate şi a formulelor matematice s-au determinat prin calcul poziţiile unghiulare ale barelor mecanismelor paralelogram de cuplare ale secţiilor în vederea corelării forţei rezultante din barele mecanismului paralelogram cu forţele de rezistenţă la tracţiune şi cu forţele de apăsare normală pe sol a secţiilor de semănat.

Echipamentul de măsurare şi achiziţie a datelor folosit la încercările experimentale în câmp agregatului format din tractorul 1 (fig. 13) şi maşina de supraînsămânţat 2, a fost format din: generatorul de curent 4, stabilizatorul de tensiune (UPS) 5, sistemul modular amplificator (MGC-plus) 6 şi un calculator portabil (Laptop P4) 7, toate aceste componente au fost montate pe un cadru de susţinere 3 amplasat pe maşina de supraînsămânţat 2.

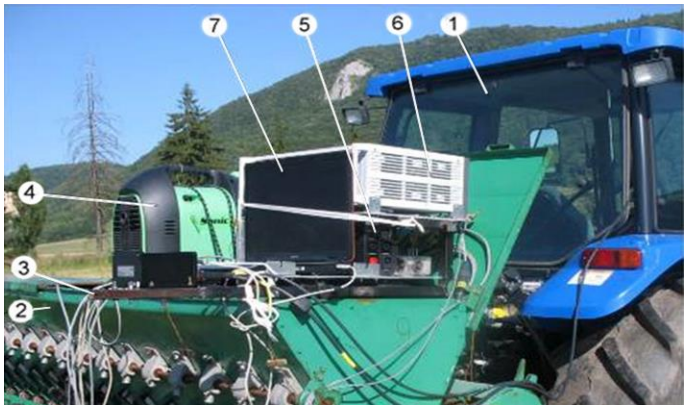

Fig. 13 - Location of measurement and data recording equipment on the tractor-agricultural machine system: *1-tractor; 2-grassland oversowing machine; 3-frame for placement of measurement and data acquisition equipment; 4-power supply; 5- voltage stabilizer; 6- booster modular system (MGCplus); 7-laptop P4*

The characteristics of the soil were determined by measuring the soil humidity, using PT-1 type soil humidity meter, (made by Kapacitiv KKT Budapest Company) and for measuring the degree of soil compaction, using SCT type penetrometer (made by DICKEY-JOHN Company) [4, 5].

The experimental tests were carried out at ICDP Magurele in Brasov, on grassland, on the leaching chemozem soil for different working conditions [3, 4]: two working speeds (v_1=5.5 km/h and v_2=7.5 km/h), two working depths (d_1=2 cm and d_2=4 cm) and three constructive types of soil opener (with inclination angle: α_1=25°, α_2=35° and α_3=45°). Having been determined and recorded simultaneously 18 parameters there was the possibility to quantify the influence of working conditions and constructive parameters on forces variation.

RESULTS

After data processing, have been determined the average values of traction forces for a section, as well as the entire machine (traction force of the tractor) according to the working depth (a_1=2 cm, a_2=4 cm), working speed (v_1=5.5 km/h; v_2=7.5 km/h) and soil opener angle (25°, 35° and 45°). These data are shown in Table 1. Analytically have been determined average values for the traction forces of the stellar wheel for metering apparata and the power consumption of tractor.

Caracteristicile solului au fost determinate prin măsurarea umidităţii solului, utilizând umidometrul portabil de tipul *PT-1 (*model al firmei *Kapacitiv KKT)* şi a rezistenţei la penetrare, utilizând penetrometrul static (model al firmei *DICKEY-JOHN*) [4, 5].

Încercările experimentale s-au desfăşurat la ICDP Braşov – Măgurele, pe pajişte, pe un sol de tip cernoziom levigat pe diferite condiţii de lucru [3, 4]: două viteze de deplasare (v_1=5,5 km/h şi v_2=7,5 km/h), două adâncimi de lucru (d_1=2 cm and d_2=4 cm) şi trei tipuri constructive de brăzdar (α_1=25°, α_2=35° and α_3=45°). S-au determinat simultan 18 parametri care au permis cuantificarea influenţei condiţiilor de lucru şi a parametrilor constructivi asupra variaţiei forţelor.

REZULTATE

După prelucrarea datelor experimentale s-au determinat valorile medii ale forţelor de tracţiune pentru o secţie, precum şi pentru întreaga maşină (forţa de tracţiune a tractorului) în funcţie de adâncimea de lucru (a_1=2 cm; a_2=4 cm), viteza de lucru v_1=5,5 km/h; v_2=7,5 km/h) şi unghiul de atac al brăzdarului (25°, 35° şi 45°). Aceste date sunt redate în tabelul 1. Prin calcule s-au determinat valorile medii ale forţelor de tracţiune pentru roata stelată de antrenare a aparatelor de distribuţie şi puterea consumată de tractor.

Table 1

The values of average traction forces for different trial conditions

Depth [cm]	Speed [km/h]	Angle of soil opener [°]	Traction force of			Consumption of traction power [kW]
			Section [N]	Stellar wheel [N]	Tractor [N]	
a_1=2 cm	v_1=5.5 km/h (v_1=1.52 m/s)	α_1=25	405	280	7.165	10.1
		α_2=35	446	280	7.870	11.9
		α_3=45	518	280	9.091	13.8
	v_2=7.5 km/h (v_2=2.08 m/s)	α_1=25	374	250	6.608	14.8
		α_2=35	429	250	7.547	15.6
		α_3=45	453	250	7.958	16.5
a_2=4 cm	v_1=5.5 km/h (v_1=1.52 m/s)	α_1=25	548	280	9.599	14.5
		α_2=35	654	280	11.403	17.3
		α_3=45	760	280	13.192	20.0
	v_2=7.5 km/h (v_2=2.08 m/s)	α_1=25	505	250	8.838	18.3
		α_2=35	535	250	9.350	19.4
		α_3=45	565	250	9.863	20.5

The following graphs present the variation of traction forces. Figure 14 shows the traction force variation of the sowing section depending on the soil opener attack angle, at different working depths and in the figure 15 is presented the traction force variation of the sowing section depending on the soil opener attack angle, at different working speeds (the signals were filtered).

Graficele următoare prezintă variaţii ale forţelor de tracţiune. Figura 14 redă variaţia forţei de tracţiune a unei secţii în funcţie de unghiul de atac al brăzdarului pentru diferite adâncimi de lucru şi în figura 15 se prezintă variaţia forţei de tracţiune a unei secţii, în funcţie de unghiul de atac al brăzdarului pentru diferite viteze de lucru (semnalele au fost filtrate).

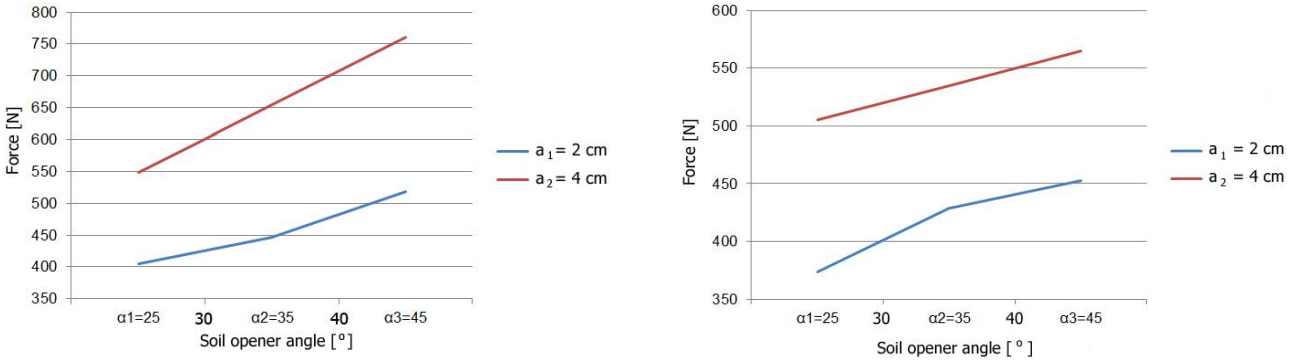

Fig. 14 - Variations of traction force of the sowing section depending on soil opener angle, at different working depths

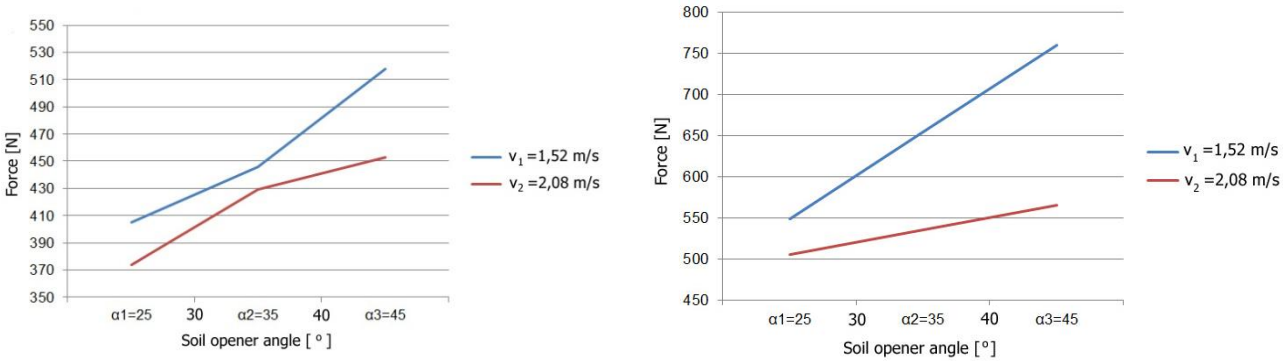

Fig. 15 - Variations of traction force of the sowing section depending on soil opener angle, at different working speeds

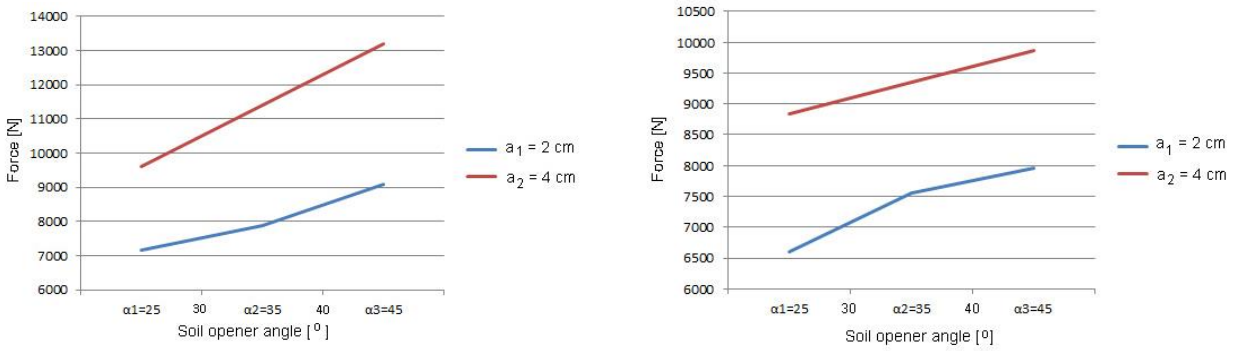

Fig. 16 - Variations of traction force of the oversowing machine depending on soil opener angle, at different working depth

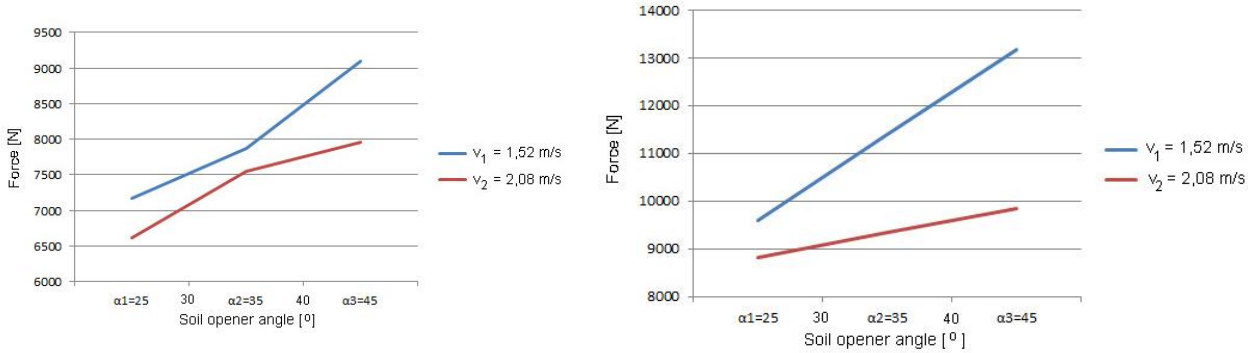

Fig. 17 - Variations of traction force of the oversowing machine depending on soil opener angle, at different working speeds

Figure 16 shows the traction force variation of the oversowing machine depending on the soil opener attack angle, at different working depths and in the figure 17 is presented the traction force variation of the oversowing machine depending on the soil opener attack angle, at different working speeds

Signals recorded and stored in computer memory, ASCII type files, were processed using Microsoft Excel software, and presented in the graphs form, which were processed, eliminating transitory operation (at the beginning and the end of experimental trials).

CONCLUSIONS

After processing the data and analysing the results obtained by trials the following conclusions have resulted

at the same speed and working depth, the traction force of one section increases simultaneously with soil opener angle:

- at working depth a_1=2 cm and working speed v_1=5.5 km/h by increasing the angle of soil opener from α_1= 25° to α_2 = 35° it obtains a 19% increase in traction force of section, and to a larger angle of α_1=25° to α_2=45°, it achieve a 38% increase traction force;
- at working depth a_2=4 cm and working speed v_2=7.5 km/h by increasing the angle of soil opener from α_1=25° to α_2=35° it has achieved a 6% increase in traction force of section and to an angle increase of α_1=25° to α_3=45° it has obtained a higher traction force with 12%.

- by increasing the depth of a_1 =2 cm to a_2 = 4 cm, the traction force of oversowing machine increases with:
  - 34% at section equipped with soil opener angle of α_1 = 25°;
  - 32% at section equipped with soil opener angle of α_2 = 35°;
  - 34% at section equipped with soil opener angle of α_3 = 45°;
- by increasing working depth of a_1 =2 cm to a_2 = 4 cm, the traction force of oversowing machine increases by:
  - approximately 43% at working speed v_1=5.5 km/h;
  - approximately 28% at working speed v_2 = 7.5 km/h;
- at the same speed and working depth, the traction force of oversowing machine increases simultaneously with soil opener angle:
  - at working depth a_1=2 cm and working speed v_1=5.5 km/h by increasing the angle of soil opener from α_1= 25° to α_2 = 35° it obtains a 10% increase in traction force of section, and to a larger angle of α_1=25° to α_3=45°, it achieves a 27% increase traction force;
  - at working depth a_2=4 cm and working speed v_2=7.5 km/h by increasing the angle of soil opener from α_1=25° to α_2=35° it achieves a 6% increase in traction force of section and to an angle increase of α_1=25° to α_2=45° it has obtained a higher traction force with 12%.

REFERENCES

[1]. Ene T.A., (2010) – *Research regarding dinamics and energetics of aggregates used at improving grasslands by sowing and oversowing,* PhD Thesis;
[2]. Hermenean. I., Mocanu V., Popescu S., (2003) *Realizarea şi testarea unei noi maşini de supraînsămânţarea pajiştilor*, Proceedings of the International Congress on Information Technology in Agriculture and Food Industry-ITAFE´ 03-Izmir (Turkey), pg. 670-673;

Figura 16 redă variaţia forţei de tracţiune a maşinii de supraînsămânţat în funcţie de unghiul de atac al brăzdarului pentru diferite adâncimi de lucru şi în figura 17 se prezintă variaţia forţei de tracţiune a maşinii de supraînsămânţat, în funcţie de unghiul de atac al brăzdarului pentru diferite viteze de lucru

Semnalele înregistrate şi salvate în memoria calculatorului, în fişiere tip ASCII, au fost prelucrate cu ajutorul softului Microsoft Excel, şi prezentate sub forma unor grafice, care au fost prelucrate, eliminându-se regimurile tranzitorii de lucru (la începerea şi terminarea probelor experimentale).

CONCLUZII

În urma prelucrării datelor şi analizării rezultatelor obţinute prin încercări rezultă următoarele concluzii:

- la aceeaşi viteză de deplasare şi adâncime de lucru forţa de tracţiune a unei secţii creşte simultan cu unghiul de atac al brăzdarului;
  - la adâncimea de lucru a_1=2 cm şi viteza de lucru v_1=5,5 km/h prin creşterea unghiului de atac al brăzdarului de la α_1=25° la α_2=35° se obţine o creştere de 10% a forţei de tracţiune a unei secţii, iar la o creştere a unghiului de atac al brăzdarului de la α_1=25° la α_2=45° se obţine o creştere de 28% a forţei de tracţiune;
  - la adâncimea de lucru a_2=4 cm şi viteza de lucru v_2=7,5 km/h prin creştere a unghiului de atac al brăzdarului de la α_1=25° la α_2=35° se obţine o creştere de 6% a forţei de tracţiune a unei secţii, iar la o creştere a unghiului de atac al brăzdarului de la α_1=25° la α_3=45° se obţine o creştere de 12% a forţei de tracţiune.
- prin creşterea adâncimii de la a_1=2 cm la a_2=4 cm, forţa de tracţiune a maşinii de supraînsămânţat creşte cu:
  - 34% la secţia echipată cu brăzdar cu unghiul de atac de α_1=25°;
  - 32% la secţia echipată cu brăzdar cu unghiul de atac de α_2=35°;
  - 34% la secţia echipată cu brăzdar cu unghiul de atac de α_3=45°,
- prin creşterea adâncimii de lucru de la a_1=2 cm la a_2=4 cm, forţa de tracţiune a maşinii de supraînsămânţat creşte cu:
  - aproximativ 43 % la deplasarea cu viteza v_1=5,5 km/h;
  - aproximativ 28 % la viteza v_2=7,5 km/h;
- la aceeaşi viteză de deplasare şi adâncime de lucru forţa de tracţiune a maşinii de supraînsămânţat creşte simultan cu unghiul de atac al brăzdarului:
  - la adâncimea de lucru a_1=2 cm şi viteza de lucru v_1=5,5 km/h prin creşterea unghiului de atac al brăzdarului de la α_1=25° la α_2=35° se obţine o creştere de 10% a forţei de tracţiune a unei secţii, iar la o creştere a unghiului de atac al brăzdarului de la α_1=25° la α_3=45° se obţine o creştere de 27% a forţei de tracţiune;
  - la adâncimea de lucru a_2=4 cm şi viteza de lucru v_2=7,5 km/h prin creştere a unghiului de atac al brăzdarului de la α_1=25° la α_2=35° se obţine o creştere de 6% a forţei de tracţiune a unei secţii, iar la o creştere a unghiului de atac al brăzdarului de la α_1=25° la α_2=45° se obţine o creştere de 12% a forţei de tracţiune.

BIBLIOGRAFIE

[1]. Ene T.A., (2010) – *Cercetari privind dinamica şi energetica agregatelor folosite la îmbunătăţirea pajiştilor prin însămânţare şi supraînsămânţare,* Teză de doctorat;
[2]. Hermenean. I., Mocanu V., Popescu S., (2003) *Realizarea şi testarea unei noi maşini de supraînsămânţarea pajiştilor*, Proceedings of the International Congress on Information Technology in Agriculture and Food Industry-ITAFE´ 03-Izmir (Turkey), pag. 670-673;

[3]. Mocanu V., Popescu S., Sperchez Fl., Hermenean I., (1996) – *The method and equipment for experimental investigation of dynamics and energetics of monoaxle tractors at cutting and transport works,* volume II of 8th Conference with international participation VEHICLE AND ENVIRONEMENT, pg.321-326, Transilvania University of Brasov;
[4]. Mocanu V., (1998) – *Dynamic and energetic optimization of monoaxle tractors with agricultural machines for cutting and transport,* PhD Thesis.

[3]. Mocanu V., Popescu S., Sperchez Fl., Hermenean I., (1996) – *Metodă şi echipament pentru investigarea experimentală a dinamicii şi energeticii tractorului monoax în lucru la cosit şi transport,* volumul II al Conferinţei a 8-a cu participare internaţională AUTOVEHICULE ŞI MEDIU, pag.321-326, Universitatea Transilvania din Braşov;
[4]. Mocanu V., (1998) – *Optimizarea dinamică şi energetică a agregatelor formate din tractoare monoax şi maşini agricole de recoltat şi transport,* Teză de doctorat.

INNOVATIVE TECHNOLOGY FOR IRRIGATION AND CLIMATE CONTROL IN VEGETABLE GREENHOUSES
/
TEHNOLOGIE INOVATIVĂ DE IRIGAŢII ŞI CONTROLUL CLIMEI ÎN SERELE LEGUMICOLE

Ph.D. Eng.Marin E., Prof. Ph.D. Eng.Pirnă I., Ph.D. Eng.Manea D., Ph.D. Stud.Matache M., Ph.D.Eng.Popa L.
INMA Bucharest / Romania
Tel: 0749176922; E-mail: marin_43eu@yahoo.com

Abstract: *Irrigation and proper fertilization humidity and climate control are key factors in creating an optimal environment for growing vegetable crops in greenhouses. This paper presents the results of experimental research conducted at INMA Bucharest to determine three of the most important indicators of the health of root area of vegetable crops (water content (%), pore water conductivity (CEp) and temperature (°C), while monitoring of temperature and CO_2 content inside a greenhouse covered with doubled inflated foil . The results and conclusions of this study are useful in identifying optimal parameters for water supply of vegetable crops in greenhouses permanently and of adequate quality in terms of salts and temperature and also in establishing a controlled environment for uniformity of crop conditions*.

Keywords: *irrigation, climate, greenhouse, vegetable growing.*

INTRODUCTION

Essential for life and a vital source of human progress and development, fresh water has become a problem of the contemporary world.

The report submitted in September 2011 in the framework of the XIV-th International Congress of Water (Pernambuco, Brazil) stated that improving water distribution on Terra will have a significant impact on food production for the population as freshwater is distributed to ensure food needs of the planet. It is estimated that water scarcity and its distribution will affect at least half of the world population strating from 2030. [6]

The water crisis could also lead to major conflicts among affected populations. According to the National Report on Water Security Intelligence US, freshwater may become a less common cause of war, which may occur in the Middle East, South Asia and North Africa. According to American experts, the water will become in the future a possible weapon of war or a terrorist threat. [5]

Climate change has led to periods of drought in many years in a row, combined with catastrophic floods and lack of fresh water. All these issues can lead to instability and conflict in the coming decades globally in developing countries, faced with a population explosion, and the serious effects that lead to major climate changes. Water scarcity is obviously one of the key factors that will limit food production. [4]

The need to irrigate vegetable greenhouses efficiently, economically and sustainably is essential for food security. Vegetable plant water consumption varies according to the growing phase, increasing starting with the germination stage to the harvesting stage.

In Romania, the problem of irrigation in protected areas is not resourceful but the distribution and efficient water management.

Rezumat: *Irigarea şi fertilizarea adecvată, reglarea umidităţii şi controlul climatic sunt factori cheie în crearea unui mediu optim de creştere a culturilor în serele legumicole. Lucrarea prezintă rezultatele unor cercetări experimentale desfăşurate la INMA Bucureşti pentru determinarea a trei dintre cei mai importanţi indicatori ai sănătăţii zonei rădăcinii a culturilor legumicole (conţinutul de apă (%), conductivitatea apei din pori (CEp) şi temperatura (°C), concomitent cu monitorizarea temperaturii şi conţinutului în CO_2 din interiorul unei sere acoperită cu folie dublu inflată. Rezultatele şi concluziile acestei lucrări sunt utile în identificarea parametrilor optimi pentru aprovizionarea cu apă a culturilor din serele legumicole permanent şi cu o calitate corespunzătoare din punct de vedere al sărurilor şi a temperaturii şi de asemenea în stabilirea unui microclimat controlat pentru uniformitatea condiţiilor de cultură.*

Cuvinte cheie: *irigaţii, climă, seră, legumicultură*

INTRODUCERE

Element esenţial pentru viaţă şi sursă vitală a progresului şi dezvoltării umane, apa dulce a devenit o problemă a lumii contemporane.

Raportul prezentat în septembrie 2011 în cadrul celui de-al XIV-lea Congres Internaţional al Apei (Pernambuco, Brazilia) precizează faptul că îmbunătăţirea distribuţiei apei la nivelul Terrei va avea un impact semnificativ şi asupra producţiei de hrană pentru populaţie, deoarece apa dulce nu este distribuită astfel încât să asigure necesarul de hrană al planetei. Se estimează că deficitul de apă şi distribuţia ei va afecta cel puţin jumătate din populaţia globului, începând cu anul 2030. [6]

Astfel, criza apei poate determina şi conflicte majore în rândul populaţiilor afectate. Conform Raportului privind Securitatea Apei al National Intelligence din SUA, apa dulce poate deveni un motiv de război mai puţin obişnuit, care poate apărea în Orientul Mijlociu, Asia de Sud şi Africa de Nord. În opinia experţilor americani, apa va deveni în viitor o posibilă armă de război sau o ameninţare teroristă. [5]

Schimbările climatice au condus la perioade de secetă în mai mulţi ani consecutiv, cumulate cu inundaţii catastrofale şi lipsa apei dulce. Toate aceste aspecte pot conduce la instabilităţi şi conflicte la nivel global în următoarele decenii, în ţările în curs de dezvoltare, care se confruntă şi cu o explozie demografică, dar şi cu efecte serioase care duc la schimbări climatice majore. Deficitul de apă este în mod evident unul dintre factorii cheie care vor limita producţia de alimente. [4]

Necesitatea de a iriga serele legumicole eficient, economic şi durabil este esenţială pentru securitatea alimentară. Consumul de apă al plantelor legumicole variază în funcţie de faza de vegetaţie, fiind în creştere de la faza de germinare până la faza de recoltare.

În România, problema irigaţiilor în spaţiile protejate nu este una de resurse, ci modul de distribuţie şi gestionare eficientă a apei.

In this respect, it should find ways to increase food production so that the sustainable management of water and other resources are optimized.

Seeking to meet the above requirements, in the paper were carried out experimental researches to determine the three most important indicators of the health of the root zone of vegetable crops (water content (%), pore water conductivity (ECp) and temperature (°C) while monitoring temperature and CO_2 content in order to promote innovative technologies for irrigation and climate control in vegetable greenhouses that provides a higher recovery of irrigation water.

MATERIAL AND METHOD

The research was conducted inside innovative technology for irrigation and climate control in vegetables greenhouses (fig.1) which is intended to water use efficiency and crop productivity growth in protected areas.

This comprises the following main assemblies:

- Automated installation of extraction of ground water with solar submersible pump (fig.1, item 1) [1];
- Automated installation of irrigation and fertilization (fig.1, item 2) [2];
- An automatic system for controlling the climate in a vegetable greenhouse (fig. 1, item 3).

În acest sens, trebuie găsite metode pentru creşterea producţiei de alimente astfel încât gestionarea durabilă a apei şi a altor resurse să fie optimizată.

Căutând să răspundă cerinţelor de mai sus, în cadrul lucrării au efectuate cercetări experimentale pentru determinarea a trei dintre cei mai importanţi indicatori ai sănătăţii zonei rădăcinii a culturilor legumicole (conţinutul de apă (%), conductivitatea apei din pori (ECp) şi temperatura (°C), concomitent cu monitorizarea temperaturii şi conţinutului în CO_2 în scopul promovării unei tehnologii inovative de irigaţii şi controlul climei în serele legumicole care realizează o valorificare superioară a apei de irigaţie.

MATERIALE ŞI METODĂ

Cercetările au fost efectuate în cadrul tehnologiei inovative pentru irigaţii şi controlul climei în sere legumicole (fig.1) care este destinată eficientizării consumului de apă şi creşterii productivităţii culturilor în spaţii protejate.

Aceasta are în componenţă următoarele ansambluri principale:

- Instalaţie automatizată de extragere a apei din pânza freatică cu pompă submersibilă solară (fig.1, poz.1) [1];
- Instalaţie automatizată de irigare şi fertirigare prin picurare şi microaspersie (fig.1, poz.2) [2];
- Sistem automat pentru controlul climei într-o seră legumicolă (fig. 1, poz. 3).

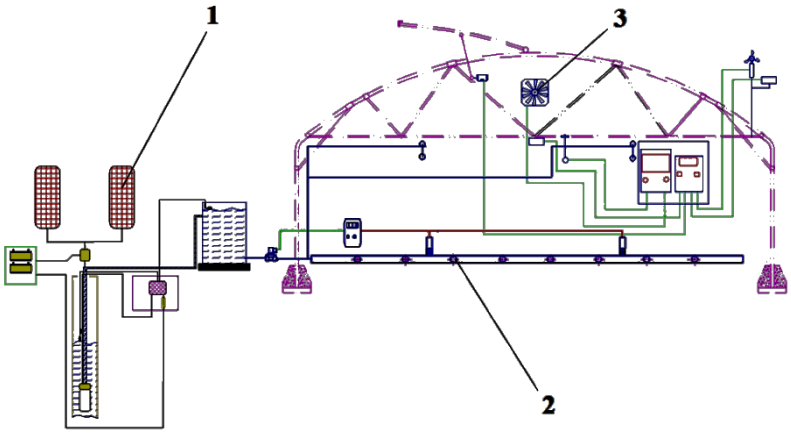

Fig. 1 – Innovative technology for irrigation and climate control in vegetable greenhouses

Installation of groundwater extraction (fig.2) operates under automatic management of a DC powered pumps.

Instalaţia de extragere apă din pânza freatică (fig.2) funcţionează în regim de gestionarea automată a unei pompe alimentată în curent continuu.

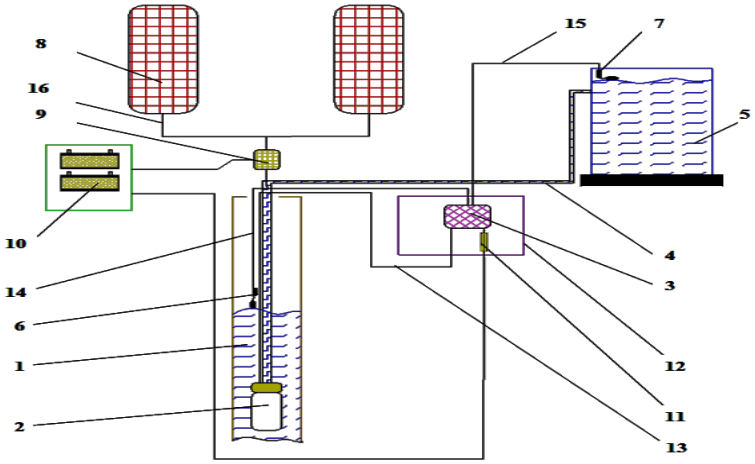

Fig. 2 – Installation of ground water extraction with solar submersible pump

All the necessary energy supply system is obtained by converting solar energy into electrical energy using solar batteries for storing excess. The system consists of a water well drilled PVC tube (Item 1) solar pump (Item 2) a solar pump controller (Item 3), HDPE pipe (Item 4) to contact a reservoir (Item 5) water storage, a water level sensor in the shaft (item 6), a water level sensor in the retention basin (item 7), two solar panels of 240 W (item 8), a current solar charge controller (item 9), two solar batteries (item 10), a fuse (Item 11), an electric panel (item 12), an electrical cable of solar pump(Item 13), an electrical cable-water level sensor in the well (Item 14), an electrical sensor in the water level of the retention basin (pos. 15), a photovoltaic cable (Item 16).

The main technical characteristics of the automated installation of ground water extraction with solar submersible pump are shown in Table 1.

Toată energia necesară sistemului de alimentare se obţine prin convertirea energiei solare în energie electrică, utilizând acumulatori solari pentru stocarea surplusului. Instalaţia se compune dintr-un puţ de apă forat cu tuburi PVC (poz.1), o pompă solară (poz.2), un controller pompă solară (poz.3), o ţeavă HDPE (poz.4) pentru legătura cu un rezervor (poz.5) de stocare a apei, un senzor de nivel a apei în puţ (poz.6), un senzor de nivel a apei în bazin de retenţie (poz.7), două panouri fotovoltaice de 240 W (poz.8), un controller solar încărcare curent (poz.9), două acumulatoare solare (poz.10), o siguranţă fuzibilă (poz.11), un panou electric (poz.12), un cablu electric pompă solară (poz.13), un cablu electric senzor de nivel a apei în puţ (poz.14), un cablu electric senzor de nivel a apei în bazin de retenţie (poz.15) şi un cablu panouri fotovoltaice (poz.16).

Caracteristicile tehnice principale ale instalaţiei automatizată de extragere a apei din pânza freatică cu pompă submersibilă solară sunt prezentate în tabelul 1.

Table 1

Characteristic	UM	Value
Water well drilled:		
- diameter	m	0.150
- depth	m	49
Solar pump		
- electric power	W	150
- rated voltage	Vcc	12
- flow	m^3/s	0.0013
Solar panel		
- maximum electrical power	W	240
- voltage at the maximum power	Vcc	30.8

Automatic installation of drip and sprinkler irrigation and fertigation (fig.3) performed under the direction and control of the irrigation and fertilization process,.

Instalaţia automatizată de irigare şi fertirigare prin picurare şi microaspersie (fig.3) realizează conducerea şi controlul în regim automat a procesului de irigaţie şi fertilizare.

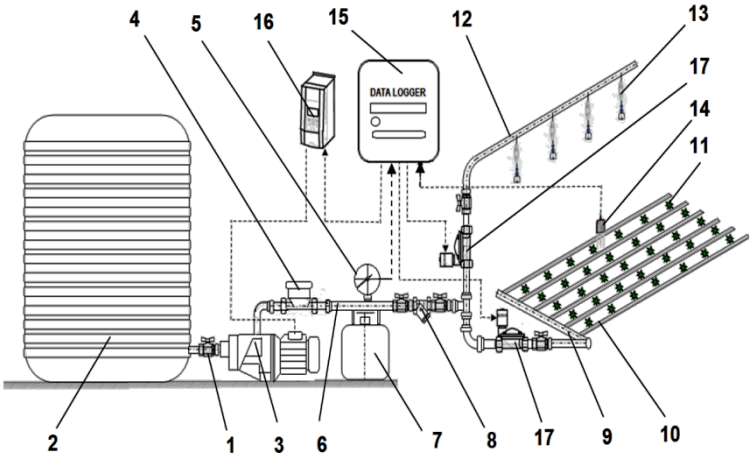

Fig. 3 - Automatic installation of drip and sprinkler irrigation and fertigation [6]

The system consists of a branch (Item 1) for connecting a water storage reservoir (Item 2) and a self-priming electric pump (Item 3), a counter (Item 4), water pressure manometer (item 5), some route items (item 6), head PVC tank control fertilization (Item 7), a filter (Item 8), a pipe (Item 9) with bands (Item 10) equipped with a built-dropping span (Item 11), another pipe (Item 12) with sprinklers (Item 13), a moisture transducer (Item 14), conductivity and temperature WET-2, a Data Logger GP2 (Item 15), a frequency inverter (Item 16) and two water valves (Item 17).

Instalaţia se compune dintr-un branşament (poz.1) pentru legătura între un rezervor (poz.2) de stocare a apei şi o electropompă (poz.3) autoamorsantă, un contor (poz.4) de apă, un manometru (poz.5) de presiune, nişte elemente (poz.6) de traseu, un cap control PVC cu tanc de fertilizare (poz.7), un filtru (poz.8), o conductă (poz.9) cu benzi (poz.10) prevăzute cu picurătoare încorporate într-o travee (poz.11), o altă conductă (poz.12) prevăzută cu microaspersoare (poz.13), un traductor (poz.14) de umiditate, conductivitate şi temperatură WET-2, un Data Logger GP2 (poz. 15), un convertizor (poz.16) de frecvenţă şi două electrovane de apă (poz.17).

Equipment of bands by dropping and sprinklers nozzle (the flow, pressure, mounting equidistance), the number of bays and sprinklers bands nozzle and the distance between rows of plants was performed according to the pedotehnic study and requirements of the crop.

The constituents of the loop of automation are: WET-2 encoder mounted vertically to a certain depth of irrigation / fertigation in the root zone, the GP2 Data Logger for analysis and control parameters monitored WET-2 encoder, frequency converter for command and controlling the speed of rotation of the self-priming solenoid and provided with an inlet and an outlet respectively positioned upstream of the bands and sprinklers dropping nozzle.

Solenoid functions singularly, simultaneously or in a certain order according to the command sent from the Data Logger GP2.

The Data Logger GP2 receives information in the form of electrical signals from the sensor WET-2, and operates with specialized software designed according to the requirements of the water conductivity and temperature specific to crop plant.

Information transmitted by the transducer WET-2 refers to the most important indicators of the health of the root zone: water content (%), electrical conductivity (ECp) and temperature (°C).

The main technical characteristics of automatic installation of drip and sprinkler irrigation and fertigation are shown in Table 2.

Echiparea benzilor cu picurătoare şi microaspersoarelor cu duză (valoarea debitului, presiunii, echidistanţei de montaj), numărul benzilor din travee şi microaspersoarelor cu duză şi distanţa dintre rândurile de plante s-a efectuat în funcţie de studiul pedotehnic şi cerinţele specifice plantei de cultură.

Elementele constituente ale buclei de automatizare sunt: traductorul WET-2 montat în poziţie verticală la o anumită adâncime de irigare/fertirigare în zona rădăcinii, Data Logger-ul GP2 pentru analiza şi controlul parametrilor monitorizaţi de traductorul WET-2, convertizorul de frecvenţă pentru comanda şi controlul vitezei de rotaţie a electropompei autoamorsantă şi electrovanele prevăzute cu o intrare şi respectiv o ieşire poziţionate în amonte de benzile cu picurătoare şi microaspersoarele cu duză.

Electrovanele funcţionează singular, concomitent sau într-o anumită ordine în funcţie de comanda transmisă de la Data Logger GP2.

Data Logger-ul GP2 primeşte informaţii sub formă de semnale electrice de la senzorul WET-2 şi operează cu un software specializat creat în funcţie de cerinţele de apă, conductivitate şi temperatură specifice plantei de cultură.

Informaţiile transmise de traductorul WET-2 se referă la cei mai importanţi indicatori ai sănătăţii zonei rădăcinii: conţinutul de apă (%), conductivitatea electrică (ECp) şi temperatura (°C).

Caracteristicile tehnice principale ale instalaţiei automatizată de irigare şi fertirigare prin picurare şi microaspersie sunt prezentate în tabelul 2.

Table 2

Characteristic	UM	Value
Water storage reservoir*:*		
- volume	m^3	6
- diameter	m	1.83
Self-priming electric pump		
- electric power	W	370
- rated voltage	Vca	220
- flow	m^3/s	$83…8.3·10^{-6}$
Head PVC tank control fertilization		
- fertilizer tank capacity	m^3	0.06
- filter size	m	0.0508

The automatic climate control system (fig.4) provides ventilation and forced air ventilation, air-conditioned greenhouse - temperature, CO_2 and optimum air humidity.

Sistemul automat pentru controlul climei (fig.4) asigură aerisirea şi ventilaţia forţată a aerului în seră cu aer condiţionat – temperatură, CO_2 şi umiditate atmosferică optime.

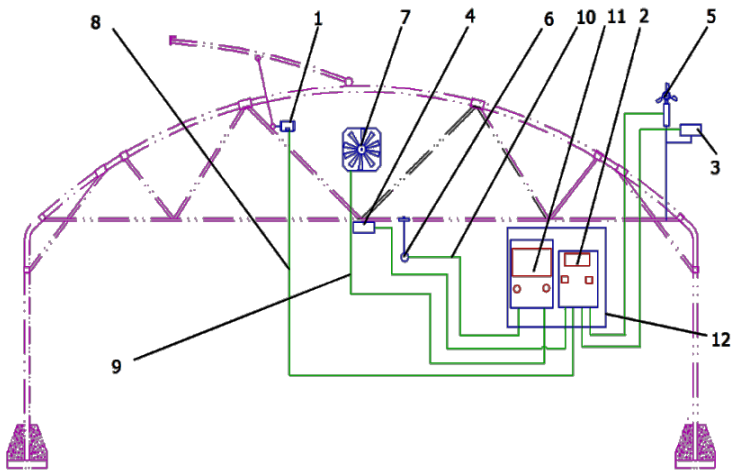

Fig. 4 - Automatic climate control system

Automatic climate control system consists of an engine with greenhouse openings (Item 1), a control panel for greenhouse openings (Item 2), a rain sensor (Item 3), a temperature sensor (Item 4), a wind sensor (Item 5), a CO_2 sensor (item 6), an axial fan (item 7), an electric cable openings engine emissions (item 8), cable of axial fans (item 9), sensor cable (item 10), a Data Logger GP 2 (item 11) and an electrical panel (item 12).

The main technical characteristics of the automatic climate control system are presented in Table 3.

Sistemul automat pentru controlul climei se compune dintr-un motor deschideri seră (poz.1), un panou de control pentru deschideri seră (poz.2), un senzor de ploaie (poz.3), un senzor de temperatură (poz.4), un senzor de vânt (poz.5), un senzor de CO_2 (poz.6), un ventilator axial (poz.7), cablu electric motor deschideri seră (poz.8), cablu ventilatoare axiale (poz.9), cablu pentru senzori (poz.10), un Data Logger GP 2 (poz.11) şi un panou electric (poz.12).

Caracteristicile tehnice principale ale sistemului automat pentru controlul climei sunt prezentate în tabelul 3.

Table 3

Characteristic	UM	Value
Engine greenhouse openings		
- speed	$rot \cdot s^{-1}$	0.033…0.150
- power	W	370
Axial fan		
-electric power	W	300
- rated voltage	Vca	220
- flow	m^3/s	1.591

Data Logger receives information in the form of electrical signals from the CO_2 sensor and operates with another specialized software created by the content of carbon dioxide (CO_2) which is an essential component of photosynthesis. According to information received Data Logger commands the start of a recirculating fan which creates a constant airflow around the plants to provide an optimal climate for culture.

To perform experimental research of innovative technology for irrigation and climate control in real conditions, has been organized an experimental group (Fig. 5) in a greenhouse covered with double inflated foil inside INMA Bucharest.

The experimental group was prepared for drip irrigation and climate control of a *Cornichon Cucumbers of Paris* culture - *Cucumis Sativus* cycle II.

To establish a culture of cucumbers was performed a starting irrigation for determining the field capacity, by excessively wetting a portion of the experimental plot and setting the amount of water remaining after gravitationally losing the excess.

Knowledge of field capacity is of great importance because it represents the upper limit of water useful for plants. Soil found at field capacity is the optimum moisture, plants finding the best conditions for development.

Data Logger-ul primeşte informaţii sub formă de semnale electrice de la senzorul de CO_2 şi operează cu un alt software specializat creat în funcţie de conţinutul în dioxid de carbon (CO_2) care este o componentă esenţială a fotosintezei. În funcţie de informaţia primită Data Logger-ul comandă pornirea unui ventilator de recirculare care creează un curent de aer constant reciclat în jurul plantelor pentru a oferi un climat optim de cultură.

Pentru efectuarea cercetărilor experimentale ale tehnologiei inovative pentru irigaţii şi controlul climei în condiţii reale a fost organizat un lot experimental (fig. 5) într-o seră acoperită cu folie dublu inflată din incinta INMA Bucureşti.

Lotul experimental a fost pregătit pentru irigaţie prin picurare şi controlul climei a unei culturii de *Castraveţi cornichon de Paris - Cucumis Sativus* din ciclul II.

În vederea înfiinţării culturii de castraveţi s-a practicat o irigare de start pentru a determina capacitatea de câmp, umezind în exces o porţiune din parcela experimentală şi stabilind cantitatea de apă rămasă după ce s-a pierdut gravitaţional excesul.

Cunoaşterea capacităţii de câmp are o mare importanţă, deoarece reprezintă limita superioară a apei utile pentru plante. Solul aflat la capacitatea de câmp se găseşte în condiţii optime de umiditate, plantele găsind cele mai bune condiţii de dezvoltare.

Fig. 5 - Experimental group in a greenhouse covered with double inflated foil

RESULTS

The diagram in Figure 6 is the variation of soil moisture from start irrigation.

REZULTATE

În diagrama din figura 6 este reprezentată variaţia umidităţii solului la irigarea de start.

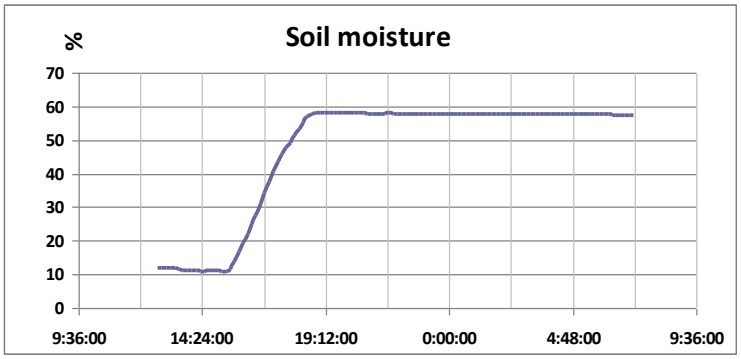

Fig. 6 - Graphical representation of the variation of soil moisture from start irrigation

From the analysis of data obtained from start irrigation has been noticed the moisture capping at a rate of 58% water in the soil, reaching saturation.

The diagram in Figure 7 is the variation of the electrical conductivity ECp of soil at start irrigation.

Din analiza datelor obţinute la irigarea de start se observă stabilirea plafonului de umiditate la un procent de 58 % apă în sol, acesta atingând saturaţia.

În diagrama din figura 7 este reprezentată variaţia conductivităţii electrice ECp a solului la irigarea de start.

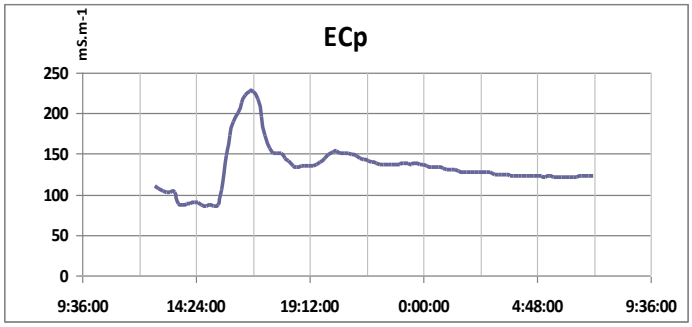

Fig. 7 - Graphical representation of the variation of electrical conductivity ECp at soil start irrigation

According to the results, the start irrigation is an increase in the electrical conductivity of ECp, which reflects the total amount of total dissolved salts or ions dissolved in water up to 225 mS·m-1 at the same time with increment of soil moisture to 58% or a decrease by 120 $mS \cdot m^{-1}$ while soil moisture remained the same. Some ions such as those of sodium or chloride contribute more than others in the ECP, e.g., the phosphorus and potassium. Some high level of ions, the chloride ions, for example, are undesirable and in large quantities may even endanger the plant.

The diagram in Figure 8 is the variation of soil temperature at start irrigation.

Conform datelor rezultate la irigarea de start se observă o creştere a conductivităţii electrice ECp, care reflectă cantitatea totală de săruri dizolvate sau totalul ionilor dizolvaţi în apă, până la 225 $mS \cdot m^{-1}$ concomitent cu mărirea umidităţii solului la 58 % şi o scădere până la 120 $mS \cdot m^{-1}$ în timp ce umiditatea solului a rămas aceeaşi. Unii ioni, ca de exemplu, cei de sodiu sau cei de clorură, contribuie mai mult la ECp decât alţii, de exemplu, cei de fosfor sau de potasiu. Unele niveluri ridicate de ioni, cei de clorură, de exemplu, sunt nedoriţi, iar în cantităţi mari pot chiar periclita dezvoltarea plantelor.

În diagrama din figura 8 este reprezentată variaţia temperaturii solului la irigarea de start.

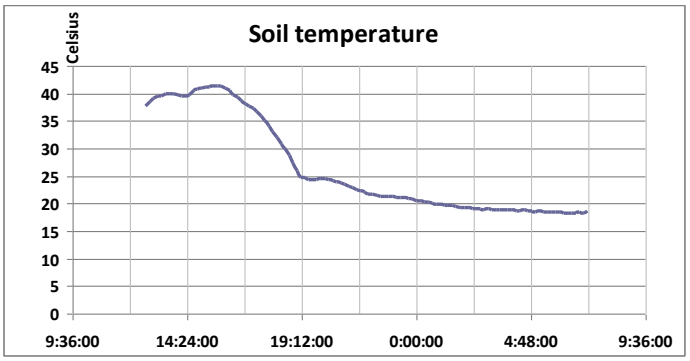

Fig. 8 - Graphical representation of variation of soil temperature at start irrigation

Analyzing the data shown above has been noticed a decrease from 40 °C to 19°C of soil temperature throughout the start irrigation. Soil temperature regime in protected areas is critical in growing vegetables. It is therefore necessary to maintain soil temperature control (optimum conditions are 20...22°C) through proper ventilation and irrigation.

Before carrying out research on the experimental plot cultivated with *Cornichon Cucumbers of Paris* in software of control of Data Logger GP2 were introduced:
- Minimum of 20% and maximum 30% value of soil moisture for control of Automatic Drip irrigation system;
- The minimum concentration of 400 ppm CO_2 in the air to control the automatic control greenhouse microclimate.

Figure 9 is the START window of the software control of drip irrigation.

Analizând datele reprezentate mai sus se observă o scădere de la 40°C la 19°C a temperaturii solului pe toată perioada irigării de start. Regimul de temperatură a solului în spaţiile protejate este factorul decisiv în cultura legumelor. De aceea este necesar să se menţină sub control temperatura solului (condiţiile optime sunt 20…22°C) printr-o aerisire şi irigare corectă.

Înainte de efectuarea cercetărilor pe lotul experimental cultivat cu *Castraveţi cornichon de Paris*, în softurile de comandă ale Data Logger-lor GP2 au fost introduse:
- valoarea minimă de 20 % şi maximă a umidităţii solului de 30 % pentru comanda instalaţiei automată de irigat prin picurare;
- valoarea minimă a concentraţiei de CO_2 în aer de 400 ppm pentru comanda sistemului automat de control al microclimatului în seră.

În figura 9 este reprezentată fereastra de START a softului de comandă a irigării prin picurare.

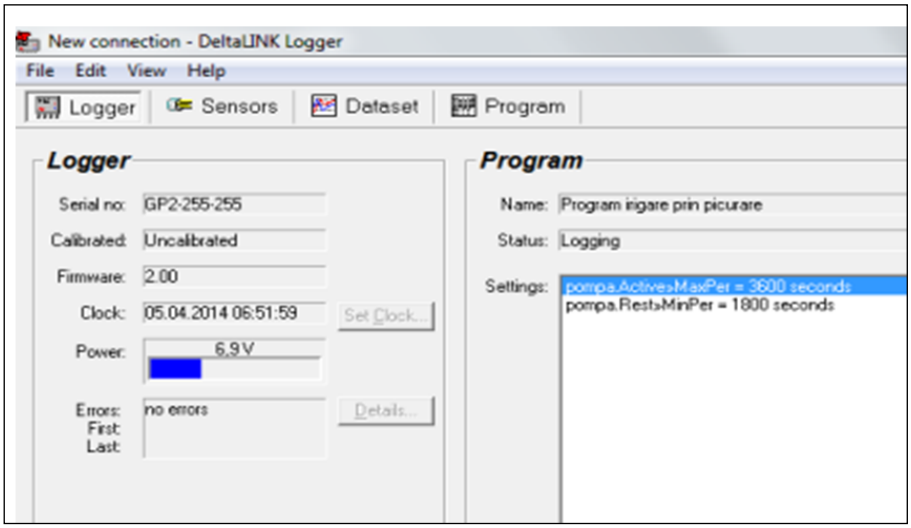

Fig. 9 - Program drip irrigation - START window

The measured values of sensors can be viewed in real time using a software based control, as in Figure 10.

Valorile măsurate de senzori pot fi vizualizate în timp real folosind o funcţie a softului de comandă, ca în figura 10.

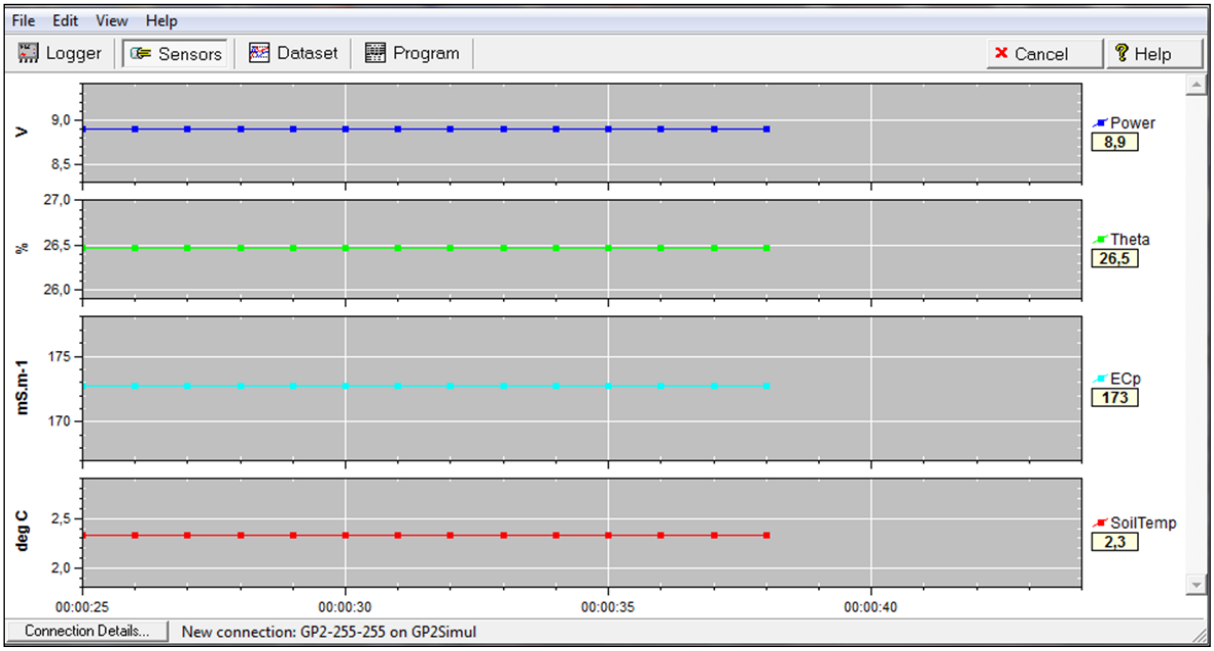

Fig. 10 - Window viewing parameters measured by the sensor in real time

Data recorded and stored in the internal Data Logger memory GP2 were imported into a laptop and using an

Datele înregistrate şi stocate în memoria internă a Data Logger-lor GP2 au fost importate pe un Laptop şi cu

Excel spreadsheet software were processed resulting in variation diagrams parameters over time.

The diagram in Figure 11 is the variation of soil moisture in a given period of time.

ajutorul unui soft de calcul tabelar Excel au fost prelucrate rezultând diagramele de variaţie a parametrilor în timp.

În diagrama din figura 11 este reprezentată variaţia umidităţii solului pe un anumit interval de timp.

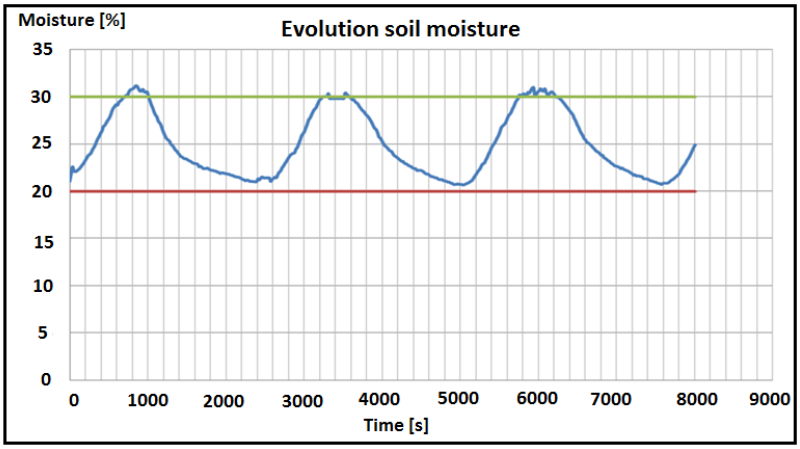

Fig.11 - Graphical representation of variation of soil moisture in a given period of time

From the analysis of the data shown in Figure 8, there has been noticed the inclusion of moisture values within the limits imposed by the control software, such as between 20% and 30%. Exceeding maximum value is caused by process inertia.

CONCLUSIONS

From the results obtained from the experimentation of innovative technology it results that technology provides:

- Irrigation water required with fully automated installation and energy independent installation by using a combination of photovoltaic panel - submersible pump;
- Monitor and control the process of irrigation / fertigation by dripping and / or sprinkler depending on health indicators of root zone of vegetable crops in greenhouses and solariums (water content (%), pore water conductivity (CEp) and temperature (°C));
- Maintaining a controlled environment inside a greenhouse covered with double inflated foil by monitoring and controlling in automatic mode the microclimate parameters (CO_2 content).

REFERENCES

[1]. Dukes M. et al., (2010) *"Use of Irrigation Technologies for Vegetable Crops in Florida",* Hort Technology, vol.20, no.1, pg.133-142;
[2] Marin E., Pirnă I, Manea D., Matache M., Sorică C., (2014) - *Automatic installation of drip and / or sprinkler irrigation and fertigation,* Patent Application no. A00567 / 28.07.2014, OSIM Bucharest;
[3]. West A.G. et al., (2006), *"Water extraction times for plant and soil materials used in stable isotope analysis"*, Rapid Communications in Mass Spectrometry. 20(8):1317-21;
[4]. *** European Institute of Romania (EIR) (2013) - Conference "*Food security and water resources: from European perspective and national realities*", Bucharest, http://www.ier.ro/webfm_send/5181;
[5]. *** Intelligence Community Assessment on Global Water Security**,** http://www.state.gov/e/oes/water/ica/index.htm;
[6]. *** http://www.futura-sciences.com/fr/news/t/developpement- durable-1/d/dans-le-monde-les-ressources-en-eausont-suffisantes-mais-mal-distribuees_33641/.

Din analiza datelor reprezentate în figura 8, se observă încadrarea valorilor umidităţii în limitele impuse prin softul de comandă, respectiv între 20 % şi 30 %.

Depăşirea valorii maxime se datorează inerţiei procesului.

CONCLUZII

Din analiza rezultatelor obţinute în urma experimentării tehnologiei inovative rezultă că tehnologia asigură:

- apa necesară irigaţiei în seră cu un instalaţie automatizată complet şi independentă energetic prin utilizarea combinaţiei panou fotovoltaic - pompă sumersibilă;
- monitorizarea şi controlul în regim automat a procesului de irigare/fertirigare prin picurare şi/sau microaspersie în funcţie de cei mai importanţi indicatori ai sănătăţii zonei rădăcinii a culturilor legumicole din sere şi solarii (conţinutul de apă (%), conductivitatea apei din pori (CEp) şi temperatura (°C);
- menţinerea unui microclimat controlat în interiorul unei sere acoperită cu folie dublu inflată prin monitorizarea şi controlul în regim automat a parametrilor de microclimat (conţinutul în CO_2) programaţi.

BIBLIOGRAFIE

[1]. Dukes M. ş.a., (2010) *"Utilizarea tehnologiilor de irigare pentru culturile vegetale in Florida",* Tehnologia Horticolă, vol.20, no.1, pg.133-142;
[2]. Marin E., Pirnă I, Manea D., Matache M., Sorică C., (2014) - *Instalaţia automatizată de irigare şi fertirigare prin picurare şi/sau microaspersie,* Cerere brevet de invenţie nr. A00567/28.07.2014, OSIM Bucureşti;
[3]. West A.G. ş.a., (2006), "*Timpul de extracție a apei pentru materiale vegetale și elementele solului utilizat în analiza cu izotopi stabil*", Comunicații rapide în spectrometria de masă 20(8):1317-21;
[4]. *** Institutul European din România (IER) (2013) - Conferinţa „*Securitatea alimentară si a resurselor de apă: între perspective europene si realităţi naţionale*" Bucureşti, http://www.ier.ro/webfm_send/5181;
[5]. *** Intelligence Community Assessment on Global Water Security**,** http://www.state.gov/e/oes/water/ica/index.htm;
[6]. *** http://www.futura-sciences.com/fr/news/t/developpement- durable-1/d/dans-le-monde-les-ressources-en-eausont-suffisantes-mais-mal-distribuees_33641/

SIMULATION OF SALINITY STRESS ON GROWTH OF WINTER WHEAT BY SOIL WATER ATMOSPHERE PLANT MODEL IN LOESS PLATEAU

/

用 SWAP 模拟盐分胁迫对黄土高原冬小麦生长的影响

Ph.D. Quan Quan[1, 2)], Prof. Ph.D. Bing Shen[2)], Prof. Ph.D. Runxun Jin [3)], Ph.D. Changxing Jin[4)]

[1)]State Key Laboratory of Hydrology-Water Resources and Hydraulic Engineering, Nanjing Hydraulic Research Institute, Nanjing/ China, [2)] Xi'an University of Technology, Xi'an / China; [3)]Anglia Ruskin University, Cambridge CB1 1PT, Cambridge / United Kingdom, [4)] Environmental Consulting & Technology, inc. Florida / U.S.A.

Tel: +8613772431776; Email: qq@xaut.edu.com

Abstract: *The sustainable development of efficient water-saving agricultural irrigation in Loess Plateau requires reasonable and quantitative planning, design, management, and strategies based on crop-water-salt response relationship. In the present paper, data were measured by using the soil-water-salt sensor CS655 to modify the simulation of root uptake in the original Soil Water Atmosphere Plant (SWAP) model. Spring wheat field experiment data in the salinized irrigation district of Fuping County, Shaanxi Province, China were used to test the feasibility of using the SWAP model in irrigation districts of Loess Plateau. The comparison of soil moisture and salt concentration in the root system, along with simulated and measured values of partial above-ground biomass showed the following results: the average relative error and root-square error of soil moisture in the root layer were close to 0; model R^2 tended to be 1; simulation accuracy of water module was high; salt concentration in the simulation varied, but the overall simulation consistency was good; crop growth parameters matched well; and simulated yield was close to the actual value with a relative error of 3.6%. The SWAP model can be well applied to simulate soil, water and salt transfer at field scale in salinized districts of Loess Plateau.*

Keywords: *SWAP; soil moisture; soil salt; agricultural crops*

摘要: *黄土高原农业可持续发展的高效节水灌溉需要依据作物-水-盐响应关系来合理定量规划设计和管理决策。本文以 SWAP（soil water atmosphere plant）模型为工具，通过土壤水盐传感器 CS655 实测数据以修正原 SWAP 模型对根系吸水的模拟。采用陕西省富平县盐渍化灌区春小麦田间试验数据，对 SWAP 模型在黄土高原灌区适用性进行了检验。对比分析植物根系层土壤水分与盐分浓度、作物地上部分生物量的模拟值与实测值，结果表明，根系层土壤水分的平均相对误差 MRE 和均方根误差 RMSE 均接近于 0 且模型 R^2 值趋于 1，水分模块模拟精度较高，盐分浓度模拟存在差异但总体模拟一致性较好，且作物生长指标匹配良好，模拟产量较接近实际值相对误差为 3.6%。综上所述，该模型可良好地应用于黄土高原盐渍化区田间尺度土壤水盐运移的模拟。*

关键词: *SWAP; 土壤含水量; 土壤含盐量;农作物*

INTRODUCTION

Because of poor soil, sparse vegetation, great surface evaporation, severe water and soil loss, and frequent drought, the Fuping district of Loess Plateau in Shaanxi Province is under severe soil salinization. This district is known for agriculture; hence, the salinity stress on crop growth has attracted the attention of local and foreign researchers [10]. Salinity stress is a growth adversity for crops and most commonly exists under field conditions. The reasonable adjustment of crops and agricultural management initially requires an understanding of crops' responses to such adversity [12]. Salinity stress affects crops' internal and external responses physiologically, biochemically, and morphologically. Many studies have investigated salinity stress, and Hsiao described salinity stress in detail [7]. Famous agro-ecological models around the world that could simulate crop growth include Dutch World Food Study (WOFOST), Crop and Environmental Research Synthesis (CERES) series developed by United States Department of Agriculture, Root Zone Water Quality, Daisy developed by Denmark and other countries, and Semiarid Prairie Agricultural Research Center (SPARC)-Wheat and PARC-Barley developed by SPARC, which localized CERES [3].

Dutch Soil Water Atmosphere Plant (SWAP) model simulates water amount and provides many options relating to field moisture [2]. This model has definite

引言

陕西富平黄土高原区由于土壤贫瘠、植被稀疏、地表蒸发量大、水土流失严重，加之气候特征十年九旱，从而导致土壤盐渍化严重，而作为以农业生产为主要产业的地区，盐分胁迫对作物生长的影响已经成为目前国内外同行研究的热点[10]。盐渍化胁迫是田间条件下存在最广泛的一种作物生长逆境，了解作物对该逆境的响应，是对作物进行合理调控、实现农业管理的前提[12]。盐渍化胁迫使作物从内到外发生一系列生理、生化及形态上的响应，这方面已有大量研究，Hsiao 曾对此做过详细综述[7]。目前国际上比较著名的农业生态模型都能够模拟作物的生长状况。例如荷兰的 WOFOST（World Food Study）模型，美国农业部研究开发的 CERES（Crop and Environmental Research Synthesis）系列模型，RZWQ（Root Zone Water Quality）模型，丹麦等国共同研制的 DAISY 模型，加拿大农业部半干旱草原农业研究中心（Semiarid Prairie Agricultural Research Center，SPARC）对 CERES 模型进行本地化形成的 SPARC-Wheat 和 SPARC-Barley 模型[3]。

荷兰的 SWAP（Soil Water Atmosphere Plant）模型将

physical mechanisms for different districts and conditions and can predict the changes of soil moisture content. SWAP can simulate the transfer of field moisture, solute, and heat quantity between saturated and unsaturated soils during the entire growth period of crops; with SWAP, irrigation can be planned according to various standards [4]. SWAP can be used to solve problems in the study of agriculture, water resource management, and environmental protection. After considering the above mentioned applications of this model, we used SWAP to study winter wheat growth under salinity stress.

模拟重点放在水量过程上，提供了多种和田间水分相关的模拟选项[2]。另外该模型有明确的物理机制，适合在不同地区、不同条件下移植应用，同时还有预测土壤含水量变化过程的功能。SWAP 模型可以模拟作物整个生长期内田间水分、溶质和热量在饱和/非饱和土壤中的移动，还可根据各种标准制定出灌溉计划[4]。该模型可用以解决农业、水资源管理和环境保护等几个领域的研究与实践问题。所以本研究采用该模型来对盐分胁迫下的冬小麦生长问题进行研究。

Fig. 1 - Channel networks arrangement plan of ditch for water storage

MATERIAL AND METHOD

Study area

Experiments were performed at the Shaanxi Estate Development Service Corporation and Xi'an University of Technology, China. The study area is located in Shaanxi Province, China, as shown in figure 1 (101°21′ to 101°26′E, 34°47′ to 34°49′N). The regional climate is semiarid, with a mean annual precipitation of approximately 437 mm and evaporation of 1,000 mm to 1,300 mm; these values for precipitation and evaporation mostly result in intense storms from June to September [5]. The mean annual air temperature is approximately 13.4 °C, with a pH of 8.3 to 8.6. A salinity level in the range 2.8 g/L to 3.2 g/L was found in the semiarid zone. Corn, wheat, and cotton are the main crops cultivated in fields in this area. Fields are irrigated by using ditch systems. The study area consisted of a number of fields covering a piece of land 40 m long and 10 m wide, with a total area of 400 m^2. The salinity of groundwater affected the distribution and variability of salinity in the topsoil and was also the main limiting factor for crops because high salinity resulted in high mineral concentration in the groundwater.

Model introduction

In salinized farmlands, dissolved salt moved with the water. The core of SWAP is related to the simulation of water movement, thereby defining the water source, destination, and changes in soils. Water mostly came from rain and artificial irrigation. After canopy interception, rain reaches the ground. Part of the rain water becomes runoff, and the rest infiltrates the soil. Some of the rain water in the soil evaporated and disappeared, but most of it went back to the air via plant transpiration; thus, salt is left on the soil surface [8]. Water in soil moved according to the description of the Richards equation, and key factors influencing the process include soil property and moisture content. Water infiltrating downward turned into deep phreatic water, and water that moved to the lateral sides would flow into drainage systems (rivers and drain pipes) [6].

材料与方法

研究区域

本试验的研究是在陕西地产开发服务公司和西安理工大学共同努力下进行的。研究区位于中国的陕西省如图 1 所示位置（101°21′101°26′E，34°47′34°49′n）。陕西气候干旱年平均降水量约 437 毫米，蒸发量 1000-1300 毫米，降雨大多集中在六月到九月[5]。年平均气温约为 13.4ºC，研究区土壤 pH 值为 8.3～8.6，含盐量 2.8-3.2 g／L。在这个区域主要种植玉米，小麦，棉花采取渠系灌溉方式。研究区由一个长 40 米，宽 10 米的田块组成，用地面积 400 平方米。高盐分的地下水影响着表层土壤含盐度的分布与变化。高矿化度的地下水也是限制了作物生长的主要因素 。

模型介绍

在盐渍化的农田中，溶解在水分中的盐分会随着水分运移。SWAP 模型的核心部分是对水分运动的模拟，即确定水的来源、去向以及在土壤中的变化过程。水的来源主要是降雨以及人工灌溉。降雨经过冠层截留后到达地面，一部分形成径流，其余则渗入土层。土壤中较少部分的水通过蒸发散失，大多数则是通过植物的蒸腾作用返回大气，盐分就被留在了土壤表层[8]。土壤中的水分按 Richards 方程的描述运动，影响这一过程的关键因素是土壤性质和土壤含水量。水分向下入渗会成为深层地下水，向侧向运动则会从排水系统（河道、排水管网等）流走[6]。溶质的

The movement of solute depended on soil property, whereas crop growth can be considered as dry matter accumulation determined by radiation and transpiration; solute was then allocated into different crop tissues in proportion [11]. Crops consisted of canopy and roots, which function differently. For winter wheat, development revolved around canopy growth in general; thus, canopy dry matter accumulation is an in decreasing function of time [9]. Root system growth determined the water uptake of the crops, and gradually reached the maximum with crop development. In this period, crop growth was an increasing function of time. Afterward, matter accumulation decreased because of fading and the output of dry matter to canopy. Thus, growth became a decreasing function of time. Therefore, studying the dynamic changes of crops' above-ground biomass and root uptake under water and salinity stress is important [1].

Root water uptake module under water and salinity stress

To calculate water stress in SWAP, the sectional linear water stress function proposed by Feddes et al. was used; calculating salinity stress required the corresponding linear function suggested by Maas and Hoffman. The function was constructed based on the relationship between soil saturation extract conductivity (EC_e) and root uptake. Actual root uptake rate S_{act} (h, EC, z) (cm/d) can then be expressed as follow:

运动取决于土壤特性，而作物生长则可认为是由辐射和蒸腾作用决定干物质积累，再按一定比例分配到不同组织[11]。作物整体由冠和根两种功能不同的器官组成。就冬小麦而言，大部分时间是以冠生长为中心，因此冠部干物质积累是时间的单调不减函数[9]。根系生长决定着作物对水分的吸收，并随作物不断发育而快速生长并达到最大值，此期间其生长是时间的递增函数，此后由于衰老和干物质向冠部输出，物质积累量开始下降，生长为时间的递减函数。那么研究在水盐胁迫下作物地上部分生物量的动态变化，以及水盐胁迫下作物根部对水分的吸收状况具有十分重要的意义 [1]。

水盐胁迫下根系吸水模块

SWAP 中水分胁迫的计算采用了 Feddes 等提出的分段线性水分胁迫函数。盐分胁迫则采用 Maas 和 Hoffman 建议的线性相应函数，该函数是基于土壤饱和浸提液电导率（EC_e）与根系吸水关系构建的。故 Actual root uptake rate S_{act} (h, EC, z) (cm/d)可表示为：

$$S_{act}(h, EC, z) = a_{rw}(h) a_{rs}(EC) S_{pot}(z) \quad (1)$$

Where,

a_{rw} (h) - the water stress reduction factor (fig.2);
a_{rs} (ECe) - the salinity stress reduction factor, as shown in figure 3;
S_{pot} (z) - the potential root uptake rate, cm/d;
EC - the electrical conductivity (smcm-1);
H - the soil water pressure head (cm).

式中，

a_{rw}(h) - 水胁迫折减系数，见图 2；
a_{rs}(EC_e) - 盐胁迫折减系数，见图 3；
S_{pot}(z) - 根系实际吸水 速率；
EC - 电导率 $smcm^{-1}$；
H - 土壤压力水头；

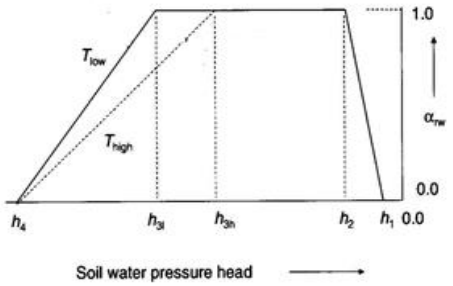

Fig. 2 - Water stress reduction factor

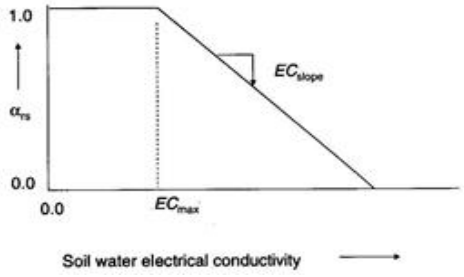

Fig. 3 - Salinity stress reduction factor

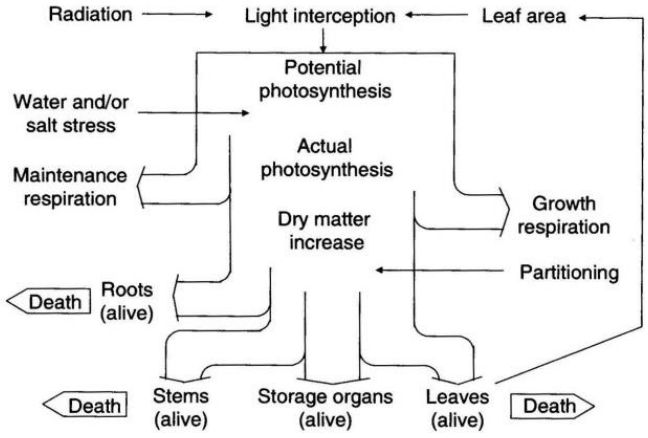

Fig. 4 - Crop growth processes

Crop growth module

The module used in SWAP to simulate crop growth was WOFOST 6.0, as shown in Fig.4. WOFOST was used to determine the radiation absorbed by crop canopy as a function of incident radiation and leaf area and to calculate potential photosynthesis with the feature of photosynthesis in leaves. Potential photosynthesis would be reduced due to water and salinity stress, and some of the radiation was used for maintaining respiration. Thus, the actual photosynthesis is achieved. Furthermore, the amount of CO_2 that was assimilated into carbohydrates CH_2O was obtained. After obtaining the amount of respiration required for growth, the increased amount of dry matter was determined. The dry matter was allocated to different tissues in proper proportions, and the amount that reached the leaves determined leaf growth. The crop growth model at simplified field scale refers to formula (2), simple model (field scale), as follows:

作物生长模块

SWAP 模拟作物生长模块所用的是 WOFOST 6.0 程序见图 4。WOFOST 将作物冠层吸收的辐射能看成入射辐射和作物叶面面积的函数，并考虑叶片发生光合作用的特性，计算得出潜在光合作用。潜在光合作用会因水分和盐分压力有所消减，而且还有一部分要用于维持呼吸作用，由此得到实际光合作用，进而得出 CO_2 同化为碳水化合物 CH_2O 的量。这一部分扣除用于生长的呼吸作用后就可得出干物质的增加量，产生的干物质再按一定的因子分配到作物的各个组织。划分到叶片的那部分干物质又会决定叶片生长。可以将其简化田间尺度的作物生长模型见公式（2），简化模型（田间尺度）：

$$\frac{Y_a}{Y_p} = \prod_{k=1}^{N} \frac{T_{a,k}}{T_{p,k}} \tag{2}$$

Where: Y_a - actual crop yield;
Y_p - potential crop yield;
$T_{a,k}$ - actual transpiration at stage k;
$T_{p,k}$ - potential transpiration at stage k;
N - number of growth stages.

式中：Y_a - 实际产量；
Y_p - 潜在产量；
$T_{a,k}$ - 在 k 田块的实际蒸发；
$T_{p,k}$ - 在 k 田块的潜在蒸发；
N - 田块总数.

RESULTS

Model verification and discussion

In the present paper, the field experimental data of winter wheat irrigated with Yellow River water were obtained in the salinized irrigation district of Fuping County, Shaanxi Province in 2014. The field plot area was 40 m × 10 m = 400 m^2, and the soil was mostly loess. The typical local field irrigation and fertilization systems were used. Soil moisture content and conductivity were detected daily by real-time forecast using the soil-water-salt sensor CS655. During harvest, a variety study and a yield test were conducted. Inspection wells were available around experimental plots for detecting ground water level, and an automatic water level detector was used to measured groundwater level once daily. The initial conditions of the model were determined by measuring groundwater level and salt concentration. The upper boundary was the flux formed by rain, interception, evaporation, and transpiration, or variable waterhead boundary, and the lower boundary was the variable waterhead boundary defined by measuring ground water level.

结果

模型验证与讨论

本文分别采用在陕西富平盐渍化灌区开展的 2014 年冬小麦引黄渠灌田间试验数据。试验田间小区面积为个 40m×10m=400m^2，土壤质地以黄土为主，采用当地典型田间灌溉及施肥制度，通过土壤水盐传感器 CS655 实时测报的方法每天测定土壤含水率和土壤电导率。收获时进行考种测产。试验小区附近布设有地下水位观测井，自动水位计每天进行 1 次地下水位监测。模型的初始条件根据实测地下水位与盐分浓度确定，上边界由降雨、截留、蒸散发组成的通量或变水头边界，下边界条件采用由实测地下水位确定的变水头边界。

Table 1

Calibrated values of primary crop biological parameters in SWAP crop growth module

Parameters	2014 winter wheat
Light use efficiency of crops RUE ([kg hm^{-2}].[$MJm^{-2)-1}$]	36
Curve shape parameter ab1	13.15
Curve shape parameter ab2	62.27
Controlling value of root uptake weakening curve because of the water condition	-15
Controlling value of root uptake weakening curve because of the salt condition	6.0
crop resistance r_{crop}	70
Canopy's rainfall interception coefficient cm	0.25

Winter wheat was sown and harvested on 20 December 2013 and 30 May 2014, respectively. In Fuping, Shaanxi, soil is usually thawed by middle January and melted by

冬小麦播种和收获日期分别为 2013 年 12 月 20 日和 2014 年 5 月 30 日，陕西富平自 1 月中旬开始解冻，至 2

late February or early March. Accordingly, the simulation of winter wheat's growth period considered the soil thawing process. Table 1 lists the corresponding definite values of parameters of winter wheat modules. The comparison of simulated and observed values of soil moisture in different layers indicated that these values matched well. The overall the average relative error (MRE) and root-square error (RMSE) tended to be 0, whereas R^2 was close to 1, as shown in Fig. 5, thereby proving that the simulated and measured values of soil moisture matched well. Meanwhile, the sudden increase of water in the upper soil layer was closely linked with concentrated rainfall. The lower soil layer had high moisture content and underwent relatively little changes because of the effect of shallow groundwater level. Fig. 6 shows the simulated and measured values of water-salt concentration in root soil, and these values differed slightly with consistent overall tendency. The statistics of overall simulated and measured salt concentrations were MRE = -0.037, RMSE = 0.227, and R^2 = 0.806, which indicated good consistency. The low simulated value R^2 of salt concentration may be due to a system error in the soil water model generalization. For instance, average values of irrigation and rainfall were obtained in one day. After irrigation or concentrated rainfall, water salt concentration in root soil significantly declined, which enhanced crop growth. Increased water consumption by crops led to the gradual rise of salinity accumulation and concentration in the root zone.

Fig. 7 shows that the simulated value was close to the measured value of above-ground biomass, thereby indicating the accuracy of simulation results. Nash-Sutcliffe efficiency was approximately 0.96, but MRE and RMSE values were large, which may be related to the small size of measured data. In existing studies, above-ground biomass of wheat tended to follow a mono-linear growth trend in the middle and late growth periods. The measured values of biomass in this research, however, covered only one growth cycle of wheat. Therefore, we still adopted SWAP biomass calculation and allocation formulas, and we will focus on simulation of above-ground biomass in future studies to further improve the model. The simulated yield was 0.86 kg/m^2, which was slightly smaller than the observed value of 1 kg/m^2. As the actual field conditions were complex, crops might be affected by other factors during growth. For this reason, differences in simulation of growth parameters were acceptable. The comparison of soil moisture, soil salinity, simulated values, and measured values of growth parameters indicated that SWAP simulated the dynamic changes of field water and salinity and growth coupling process of spring wheat in Loess Plateau.

月底或 3 月初融通。因此，冬小麦生育期模拟需考虑土壤融化过程，冬小麦所对应的作物模块参数率定值列于表 1. 比较各层土壤水分的模拟值与观测值，二者吻合结果较好。总体的 MRE 和 RMSE 趋于 0，R^2 则接近于 1 如图 5，进一步表明了土壤水分模拟值与实测值匹配良好。同时，上层土壤水分的突增与灌溉和集中降雨密切相关，而下层土壤又同时受到浅地下水位的影响，其维持着较高的含水率且变化相对较小。根系层土壤水盐分浓度的模拟值与实测值，如图 6 所示，二者差异较小，且总体趋势一致。总体的模拟与实测盐分浓度统计值 MRE=-0.037、RMSE=0.227、R^2=0.806，表明二者具有较好的一致性。但土壤盐分浓度模拟统计值 R^2 值较小。可能是由于土壤水模型概化中的系统误差所致，如对采用了灌溉、降雨的日内平均化处理。同时，根系在灌溉或集中降雨后，根区土壤水盐分浓度呈现明显下降趋势，这有利于作物生长；其后随着作物耗水的增加又引起根区盐分积累和浓度逐步上升。

如图 7 所示，地上部生物量的模拟值与实测值较为接近，模拟效果基本可以接受， NSE 值约为 0.96，但 MRE 和 RMSE 值则相对较大，这可能与实测数据的数量过少有关。考虑到已有研究中小麦地上部生物量在生长中后期多呈现单一的近似线性增长趋势，且本研究中生物量观测值仅为小麦一个生长周期，因此，本文仍采用 SWAP 生物量计算及分配公式，并将在后续研究中关注与地上部生物量的模拟，以求进一步改进模型。产量模拟值为 0.86kg/m^2，略小于观测值 1 kg/m^2。考虑到田间实际状况复杂，作物生长可能还会受到其他因素影响，因此，上述作物生长指标的模拟差异是可以接受的。综合以上土壤水分、土壤盐分、作物生长指标模拟值与实测值的对比结果，表明 SWAP 模型可以良好的模拟黄土高原春小麦田间土壤水盐动态及作物生长耦合过程。

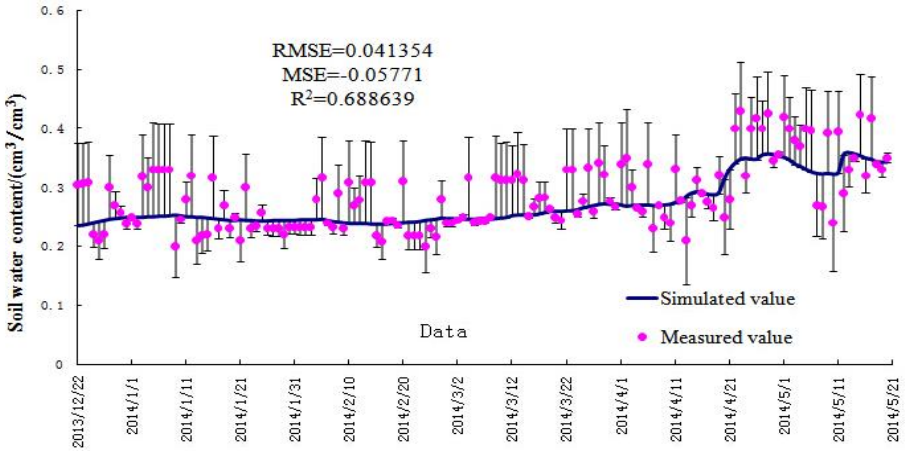

Fig. 5 - Soil water content of root layer

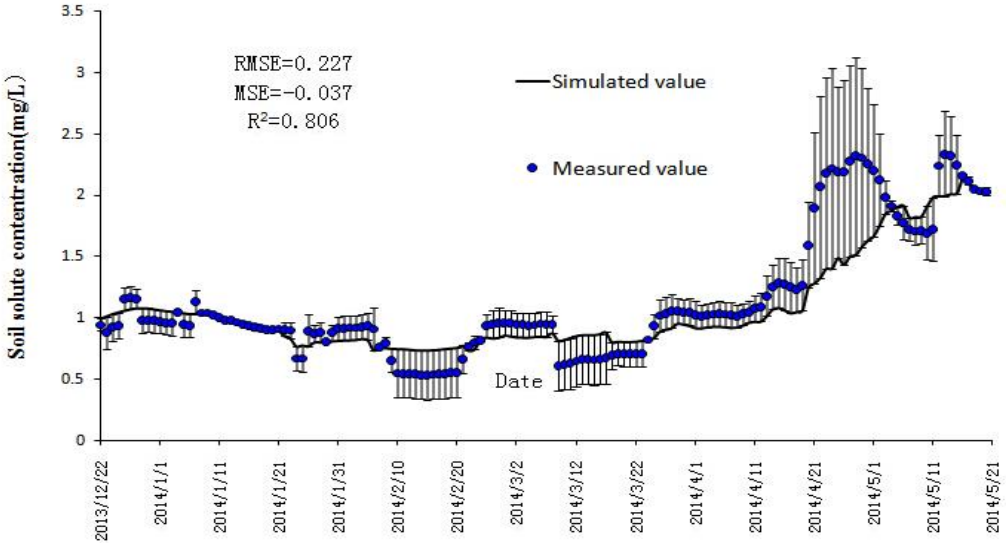

Fig. 6 - Soil salinity content of root layer

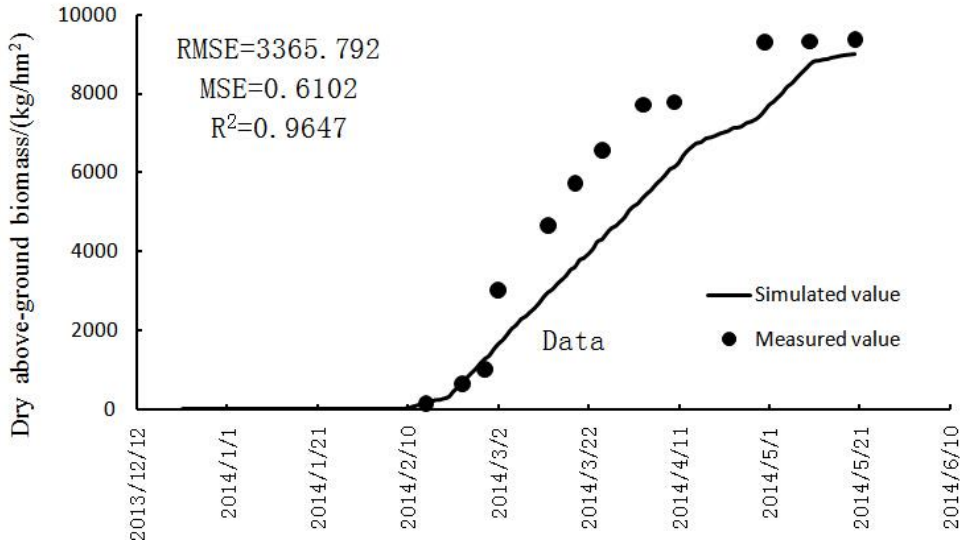

Fig. 7 - Above-ground biomass

CONCLUSIONS

Based on SWAP, we used the field data of winter wheat in the salinized irrigation district of Fuping, Shaanxi to test field applicability and to compare soil water, soil salinity, and the simulated and measured values of above-ground biomass. We also analyzed the parameters based on SWAP. The simulation results demonstrated the following:

1) Crop growth module of SWAP described the details of crops' physiological process and morphology in a simple manner. Simulation of the growth and distribution of the root system and the increase of plant height or group leaf distribution was not achieved using the model. However, the model was able to simulate the process of crop growth and yield. Thus, the simulation of the dynamic changes of soil water salinity and daily crop growth was still achieved.

2) SWAP required detailed physical processes and many rare formulas, which resulted in the unreasonable generalization of the initial growth period of crops. Thus, distorted simulation was achieved.

结论

本研究以 SWAP 模型为基础，采用陕西富平盐渍化灌区冬小麦田间试验数据进行了田间适用性检验，分别对土壤水分、盐分浓度、作物地上部生物量的模拟值与观测值进行了对比与指标统计分析。模拟结果表明：

1）SWAP 模型的作物生长模块，对作物生理过程与形态特征的细节描述仍较为简单，尚不能模拟作物根系生长动态及分布、株高的增长动态及群体叶片分布等，其主要适用于模拟作物生长与产量形成的主要过程。但实现了以日为时间步长的土壤水盐动态及作物生长的模拟。

2）由于 SWAP 考虑的物理过程十分详细，用到了很多公式，而且其中很多都是不常见的，使得作物生长初期概化不合理而导致的模拟失真。

3) MRE and RMSE of soil moisture in winter wheat experiment were close to 0, and model R^2 value was close to 1. Thus, the water module showed high simulation accuracy. The simulation of salinity concentration differed slightly, but was generally consistent.

ACKNOWLEDGEMENT

This work was supported by Open Foundation of State Key Laboratory of Hydrology-Water Resources and Hydraulic Engineering (Grant No. 2013490511), the Hydraulic Science and Technology Plan Foundation of Shaanxi Province (Grant No. 2013slkj-08) and Natural Science Foundation of Shaanxi Province (Grant No. 2014JQ5188).

REFERENCES

[1]. Hirekhan M., Gupta S.K., Mishra K.L., (2007) - *Application of WaSim to assess performance of a subsurface drainage system under semi-arid monsoon climate.* Agricultural Water Management, vol. 88, no. 1-3, pg. 224-234;

[2]. Jia Z., Luo W., Xie J., Pan Y., Chen Y., Tang S., Liu W., (2011) - *Salinity dynamics of wetland ditches receiving drainage from irrigated agricultural land in arid and semi-arid regions,* Agricultural Water Management, vol. 100, no. 1, pg. 9-17.

[3]. Mathias S., Butler A. and Wheater H., (2008) - *Modelling radioiodine transport across a capillary fringe,* Journal of Environmental Radioactivity, vol. 99, no. 4, pg. 716-729;

[4]. Noory H., van der Zee S.E.A.T., Liaghat A.M. et al., (2011) - *Distributed agro-hydrological modeling with SWAP to improve water and salt management of the Voshmgir Irrigation and Drainage Network in Northern Iran.* Agricultural Water Management, vol. 98, no.6, pg. 1062-1070;

[5]. Quan Q., Shen B., Xie J.C., Luo W., Wang WY., (2013) - *Assessing soil salinity in the fields of western China using spatial modeling and remote sensing.* Acta Agriculturae Scandinavica, Section B - Soil & Plant Science, vol. 63, no.4, pg. 289-296;

[6]. Roose T. and Fowler A.C., (2004) - *A mathematical model for water and nutrient uptake by plantroot systems,* Journal of Theoretical Biology, no.228, pg. 173-184;

[7]. Tang J.W., Bolstad P.V., Desai A.R. et al., (2008) - *Ecosystem respiration and its components in an old-growth forest in the Great Lakes region of the United States.* Agricultural and Forest Meteorology, no.148, pg. 171-185;

[8]. Van Dam J.C., Groenendijk P., Hendriks R.F.A. et al., (2008) - *Advances of modeling water flow in variably saturated soils with SWAP*. Vadose Zone Journal, vol. 7, no.2, pg. 640-653.

[9]. Wang Shijing, Huang Guanhua, Yang Jianguo et al., (2010) - *Effect of irrigation with saline water on water-saltdynamic and spring wheat yield* . Transactions of the Chinese Society of Agricultural Engineering, vol. 26, no.5, pg. 27-33.

[10]. Xie T., Liu X.H., Sun T. et al., (2011) - *The effects of groundwater table and flood irrigation strategies on soil water and salt dynamics and reed water use in the Yellow River Delta, China* . Ecological Modelling. Vol. 222, no.2, pg. 241-252;

3）冬小麦试验中土壤水分的平均相对误差 MRE 和均方根误差 RMSE 均接近于 0，且模型 R^2 值趋近于 1，水分模块模拟精度较高，盐分浓度模拟存在略微差异但总体上一致性较好。

致谢

本课题受到水文水资源与水利工程科学国家重点实验室开放基金的资助（项目号：No. 2013490511），陕西省水利厅科技项目的资助（2013slkj-08），陕西省科技厅科技项目资助（2014JQ5188）。

参考文献

[1]. Hirekhan M., Gupta S.K., Mishra K.L. (2007) - *半干旱季风气候下 Wasim 方法在地下排水系统性能评估中的应用研究,* 农业水资源管理, 第 88 卷, 第 1-3 期, 224-234.

[2]. Jia Z., Luo W., Xie J., Pan Y., Chen Y., Tang S., Liu W. (2011) - *干旱和半干旱地区湿地沟渠接受灌溉农用地排水盐碱动态分析,* 农业水资源管理, 第100卷, 第1期, 9-17.

[3]. Mathias S., Butler A. and Wheater H. (2008) - *放射碘穿越毛细边缘的运输模型研究,* 环境辐射杂志, 第99卷, 第4期, 716-729;

[4]. Noory H., van der Zee S.E.A.T., Liaghat A.M. et al. (2011) – *基于 SWAP 方法的分散型农业水资源模拟改善伊朗北部 voshmgir 地区灌排网络中的水盐管理,* 农业水资源管理, 第 98 卷, 第 6 期, 1062-1070;

[5] .权全, 沈冰, 解建仓, 罗纨, 王文焰. (2013) – *利用空间模型和遥感对中国西部土壤盐分的评定分析,* 农业科学学报 B-土壤和植物, 第 63 卷, 第 4 期, 289-296;

[6]. Roose T. and Fowler A.C. (2004) -*植物根系对水和营养吸收的数学模型研究,* 计算生物学杂志, 第228期, 173-184;

[7]. Tang J.W., Bolstad P.V., Desai A.R. et al. (2008) - *美国大湖区古森林的生态系统呼吸及其构成要素分析，*农业与林业气象学, 第148期, 171-185;

[8]. Van Dam J.C., Groenendijk P., Hendriks R.F.A. et al. (2008) - 利用*swap*方法对饱和土中水流模型研究的进展, 包气带学报, 第7卷, 第2期, 640-653;

[9]. 王诗景, 黄冠华, 杨建国, 等.(2010) -*微咸水灌溉对土壤水盐动态与春小麦产量的影响,*中国农业工程学报, 第26卷, 第5期, 27-33.

[10]. Xie T., Liu X.H., Sun T. et al. (2011) - *大水漫灌对中国黄河流域地下水、地下水位及盐分迁移的影响,* 生态模型, 第222卷, 第2期, 241-252;

[11]. Xu Xu, Huang Guanhua, Qu Zhongyi et al., (2011) - *Regional scale model for simulating soil water flow and solute transport processes-GSWAP,* Transactions of the Chinese Society of Agricultural Engineering (Transactions of the CSAE), vol. 2, no.7, pg. 58-63;
[12]. Yan L.M., Chen S.P., Huang J.H. et al., (2010) - *Differential responses of auto- and heterotrophic soil respiration to water and nitrogen addition in a semiarid temperate steppe,* Global Change Biology, vol. 16, pg. 2345-2357.

[11]. 徐旭, 黄冠华, 屈忠义, 等. (2011) -*区域尺度农田水盐动态模拟模型—GSWAP*, 中国农业工程学报, 第27卷, 第7期, 58-63;

[12]. Yan L.M., Chen S.P., Huang J.H. et al. (2010) - *半干旱温带草原地区自养和异养生物土壤呼吸对不同水和氮增量反应研究*, 世界生物进展, 第 16 卷, 2345-2357.

KINEMATIC STUDY OF THRESHING PROCESS CONDUCTED BY TANGENTIAL THRESHING SYSTEM OF CONVENTIONAL CEREAL HARVESTING COMBINES

/

STUDIUL CINEMATIC AL PROCESULUI DE TREIER REALIZAT DE APARATUL DE TREIER TANGENŢIAL AL COMBINELOR CONVENŢIONALE DE RECOLTAT CEREALE

PhD. Eng. Ivan Gh., PhD. Eng. Vlăduț V.N.
INMA Bucharest / Romania
Tel: 021.269.32.55; Fax: 021.269.32.73; E-mail: geoivan2006@yahoo.com

Abstract: *The working capacity of conventional cereal harvesting combines is mainly determined by the working capacity of tangential threshing system. This depends on the technical and functional characteristics of the threshing system itself and the biological characteristics of the harvested vegetal mass.Portion of material driven by one bar of threshing cylinder is laminated in to the threshing space and under the action of the friction and centrifugal forces it is produced the combing of material and the seeds separation. The paper presents the kinematic study of threshing process along threshing space and the conditions for optimization of process.*

Keywords: *cereal harvesting combine, tangential threshing system*

Rezumat: *Capacitatea de lucru a combinelor convenţionale de recoltat cereale este in principal determinată de capacitatea de lucru a aparatului de treier tangenţial. Capacitatea de lucru a acestuia depinde de caracteristicile tehnice şi functionale ale aparatului de treier tangenţial propriu-zis şi de caracteristicile biologice ale masei vegetale recoltată. Tranşa de material antrenată de o şina a batatorului este laminată in spaţiul de treier şi sub actiunea forţelor de frecare şi centrifuge se produce pieptănarea materialului şi separarea seminţelor. Articolul prezintă studiul cinematic al procesului de treier de-a lungul spaţiului de treier şi condiţiile de optimizare a procesului.*

Cuvinte cheie: *combina de recoltat cereale, aparat de treier tangenţial*

INTRODUCTION

The threshing system of the conventional cereal harvesting combines is of tangential type. This is the main working part of these harvesting combines in terms of the separation of the seeds and the energy consumption [4].

The tangential threshing system is positioned in the technological flow of a conventional cereal harvesting combine between the feederhouse and the straw walker.

The main components of tangential threshing system with bars are: threshing cylinder with bars, concave, beater and concave extension (Figure 1). [2]

INTRODUCERE

Aparatul de treier al combinelor convenţionale de recoltat cereale este de tip tangenţial. Acesta este principalul organ de lucru al acestor combine din punct de vedere al separararii seminţelor şi consumului energetic [4].

Aparatul de treier tangenţial este poziţionat în fluxul tehnologic al combinei convenţionale de recoltat cereale între elevatorul central şi scuturator.

Componentele principale ale aparatului de treier tangenţial cu şine sunt: bătătorul cu şine, contrabătătorul, postbătătorul şi prelungirea contrabătător (figura 1). [2]

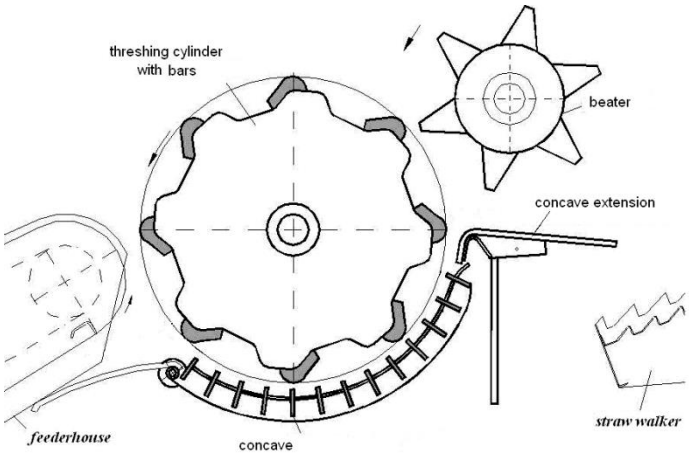

Fig.1 - The main components of tangential threshing system

In the tangential threshing system takes place the threshing process, which consists in the separating of the seeds from vegetal mass through a concave. Separated seeds get to cleaning system and the straw get to the straw walker.

The threshing cylinder is the component which drives and transports the vegetal mass in the threshing space (between the cylinder and concave), to achieve the separation of the seeds from the rest of plants. The threshing cylinder with bars comprises a shaft, a number of moulded or stamped rosettes, in which are screwed 6...10 bars, made of forged steel profile (Fig.2).

In aparatul de treier tangenţial are loc procesul de treier, care constă în separarea prin contrabătător a seminţelor din masa vegetală. Seminţele separate ajung la sistemul de curăţire şi paiele ajung pe scuturător.

Bătătorul este componentul care antrenează şi transportă masa vegetală în spaţiul de treier (între bătător şi contrabătător), pentru realizarea separării seminţelor de restul plantelor. Bătătorul cu şine este format dintr-un ax, un număr de rozete turnate sau ambutisate, pe care sunt prinse în şuruburi 6…10 şine, făcute dintr-un profil forjat de oţel (fig.2).

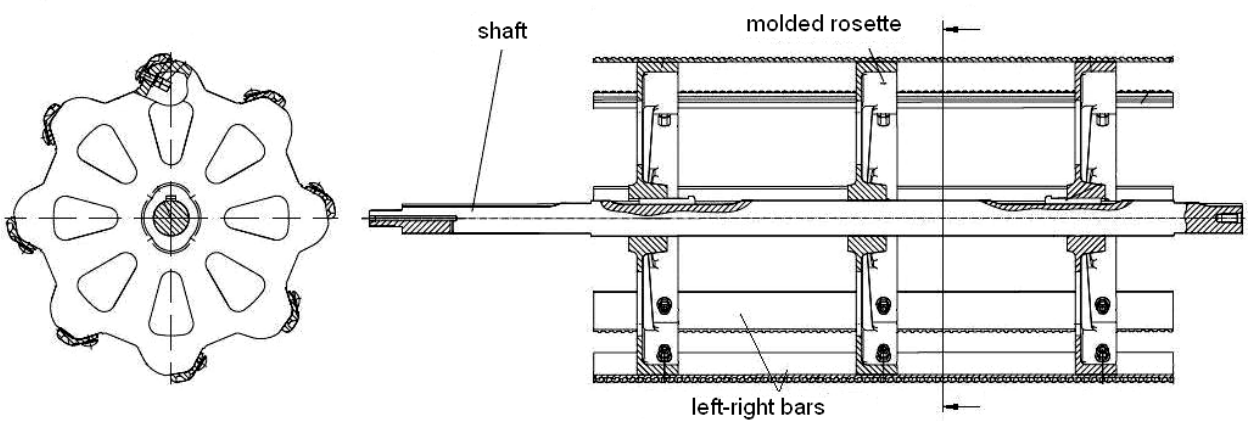

Fig.2 - The threshing cylinder with bars of Romanian cereal harvesting combine C110

Threshing cylinder bars of Romanian harvesting combines C110 and C140 are provided with a flat area and a dimpled area. Flat area makes first contact with vegetal mass brought by the conveyor with chains and slats of feederhouse, providing a good taking and reducing the percentage of seeds damaged.

Flat area produces a fan effect, an effect that determines the increases of speed of the vegetal mass which enters the threshing space (Fig.3).

Şinele bătătoarelor combinelor româneşti C110 şi C140 sunt prevăzute cu o zona netedă şi o zona riflată. Zona netedă face primul contact cu masa vegetală adusă de transportorul cu lanţuri si racleţi al elevatorului central, asigurând o buna preluare a acesteia şi reducând procentul seminţelor vătămate.

Zona neteda produce si un efect de ventilator, efect ce determină creşterea vitezei masei vegetale la intrarea în spaţiul de treier (fig.3).

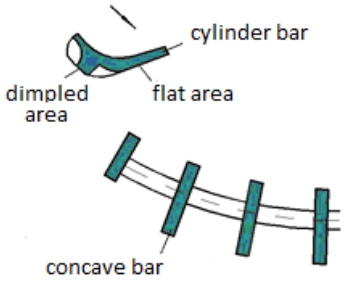

Fig. 3 – Cylinder bar configuration of cereal harvesting combines C110, C140

MATERIALS AND METHOD

The material part driven by one cylinder bar is laminated in the area of the plate articulated to concave, diagram of forces being shown in Figure 4.

MATERIALE ŞI METODĂ

Tranşa de material antrenată de şina bătătorului este laminată în zona plăcii articulată la contrabătător, diagrama forţelor fiind prezentată în figura 4.

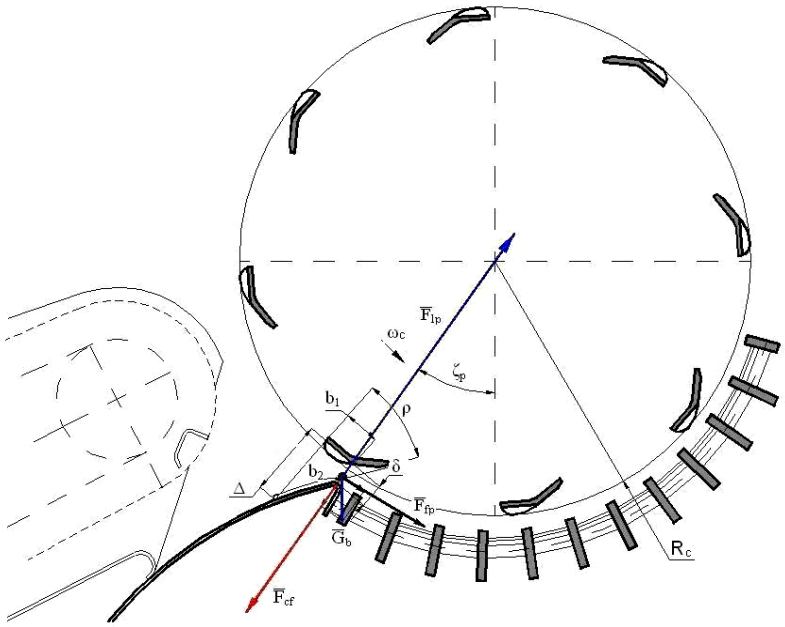

Fig. 4 – Forces diagram acting on the portion of material in the area of the plate articulated at concave

The centrifugal force which acts on a material point of material driven by one cylinder bar is according to relation 1:

Forţa centrifugă care acţionează asupra unui punct material al tranşei antrenată de o şina bătătorului este conform relaţiei 1:

$$F_{cf} = m_b \omega_c^2 R_c \quad (1)$$

where:

F_{cf} is centrifugal force acting on a material point of material part driven by cylinder bar, in N;

m_b – material portion mass driven by cylinder bar, in kg;

ω_c – angular speed of the cylinder, in rad^{-1};

R_c – cylinder radius, in m.

The material portion weight driven by cylinder bar is according to relation 2:

unde:

F_{cf} este forţa centrifugă care acţionează asupra unui punct material al tranşei de material antrenată de şina bătătorului, în N;

m_b – masa tranşei de material antrenată de şina bătătorului, în kg;

ω_c – viteza unghiulară a bătătorului, în rad^{-1};

R_c – raza bătătorului, în m.

Greutatea tranşei de material antrenată de şina bătătorului este conform relaţiei 2:

$$G_b = m_b g \quad (2)$$

where:

G_b is material portion weight driven by cylinder bar, in N;

g - gravity acceleration, in m/s^2.

The lamination pressure of material portion driven by cylinder bar in the area of plate articulate at concave, is given by relation 3 [3]:

unde:

G_s este greutatea tranşei de material antrenată de şina bătătorului, în N;

g – acceleraţia gravitaţională, în m/s^2.

Presiunea de laminare a tranşei de material antrenată de şina bătătorului, în zona plăcii articulată la contrabătător, este dată de relaţia 3 [3]:

$$p_{lp} = Ae^{C\left(1-\frac{\delta}{\Delta}\right)} \quad (3)$$

where:

p_{lp} - lamination pressure of material portion driven by cylinder bar in the area of plate articulate at concave, in N/m^2;

δ – portion of material thickness laminated in area of the articulate plate at concave, in m;

Δ – material portion thickness driven by cylinder bar in the area of plate articulate at concave, before lamination, in m;

A,C – experimental coefficients with constant value depending on the crop harvested (for wheat is $A=10$ N/m^2 and $C=12$).

The lamination force of material portion in the area of articulate plate at concave is given by relation 4 [3]:

unde:

p_{lp} este presiunea de laminare a tranşei de material antrenată de şina bătătorului, în zona placii articulată la contrabătător, în N/m^2;

δ – grosimea tranşei de material laminată în zona plăcii articulată la contrabătător, în m;

Δ – grosimea tranşei de material antrenată de şina bătătorului în zona plăcii articulată, înaintea laminării, în m;

A,C – coeficienţi experimentali cu valoare constanta în funcţie de cultura recoltată (pentru grâu fiind $A=10$ N/m^2 şi $C=12$).

Forţa de laminare a tranşei de material în zona plăcii articulată la contrabătător este conform relaţiei 4 [3]:

$$F_{lp} = p_{lp}\left(S_b - S_p\right) \quad (4)$$

where:

F_{lp} is lamination force of material portion in the area of plate articulate at concave, in N;

S_b – material surface contact with the dimpled area of cylinder bar, in m^2;

S_p – material surface contact with the plate articulate at concave, in m^2.

The contact surface of the material with cylinder bar increases with the number and size of the dimples. The ratio of dimpled surface with the bar surface, if it had not been dimpled, it is called the dimpled coefficient.

The contact surface of the material with cylinder bar is given by relation 5:

unde:

F_{lp} este forţa de laminare a tranşei de material în zona plăcii articulată la contrabătător, în N;

S_b – suprafaţa de contact a materialului cu zona riflată a şinei bătătorului, în m^2;

S_p – suprafaţa de contact a materialului cu placa articulată la contrabătător, în m^2.

Suprafaţa de contact a materialului cu şina bătătorului creşte proporţional cu numărul şi marimea riflurilor. Raportul suprafeţei riflate cu suprafaţa şinei, dacă n-ar fi fost riflată, poarta numele de coeficient de riflare.

Suprafaţa de contact a materialului cu şina bătătorului este conform relaţiei 5:

$$S_b = C_d b_1 L_S \quad (5)$$

where:

S_b is material surface contact with the dimpled area of cylinder bar, in m^2;

C_b – dimple coefficient;

b_1 – dimple area width of cylinder bar, in m;

L_s – cylinder bars length, in m;

Contact surface of the material with plate articulate at concave is the projection of dimple area of cylinder bar on articulate plate at concave, at a laminating angle,

unde:

S_b este suprafaţa de contact a materialului cu zona riflată a şinei bătătorului, în m^2;

C_b – coeficientul de riflare;

b_1 – laţimea zonei riflată a şinei bătătorului, în m;

L_s – lungimea şinelor bătătorului, în m.

Suprafaţa de contact a materialului cu placa articulată la contrabătător este proiecţia suprafeţei riflate a şinei bătătorului pe placa articulată la contrabătător, sub un

denoted by ρ, multiplied with the cylinder bars length. At the Romanian combines C110 and C140 this lamination angle has an average value of ρ=32°.

The material surface contact with the plate articulate at concave is given by relation 6:

unghi de laminare, notat cu ρ, înmulţită cu lungimea şinei bătătorului. La combinele româneşti C110 şi C140, acest unghi de laminare are valoarea medie de ρ=32°.

Suprafaţa de contact a materialului cu placa articulată la contrabătător este dată de relaţia 6:

$$S_p = \frac{b_1 L_S}{\sin\rho} \quad (6)$$

where ρ is the lamination angle.

The lamination force of material portion in the area of plate articulate at concave is given by relation 7:

unde ρ este unghiul de laminare.

Forţa de laminare a tranşei de material în zona plăcii articulată la contrabătator este dată de relaţia 7:

$$F_{lp} = Ae^{C\left(1-\frac{\delta}{\Delta}\right)} b_1 L_s \left(C_r - \frac{1}{\sin\rho}\right) \quad (7)$$

Frictional force acting on the portion of material, in the area of plate articulate at concave, is given by relation 8:

Forţa de frecare care acţionează asupra tranşei de material, în zona plăcii articulată la contrabătător, este dată de relaţia 8:

$$F_{fp} = f\left(F_{lp} - G_s\cos\zeta_p - F_{cf}\right) - G_s\sin\zeta_p \quad (8)$$

where:

F_{fp} is frictional force acting on the portion of material, in the area of plate articulate at concave, in N;

f - friction coefficient of the material with plate articulate at concave and cylinder bar;

ζ_p – angle made by the radius that defines the vertical position of the cylinder bar.

In Figure 5 it is shown the diagram of forces acting on a material point under the action of first bar of concave.

unde:

F_{fp} este forţa de frecare care acţionează asupra tranşei de material, în zona plăcii articulată la contrabătător, în N;

f - coeficientul de frecare al materialului cu placa articulată şi şina bătătorului;

ζ_p – unghiul facut de raza care defineşte poziţia şinei bătătorului cu verticala.

În figura 5 este prezentată diagrama forţelor care acţionează asupra unui punct material aflat sub acţiunea primei şine a contrabătătorului.

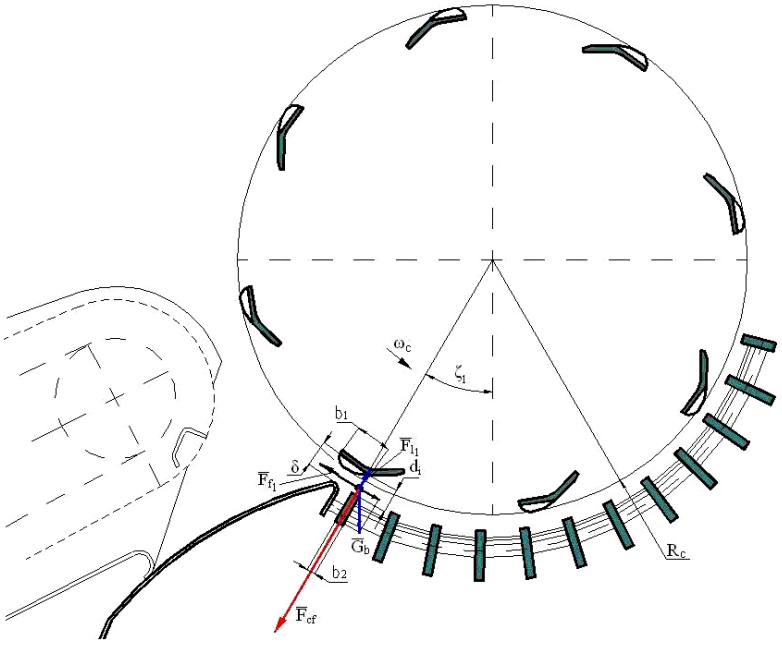

Fig. 5 – Forces diagram acting on material point of the material under the action of first bar of concave

Centrifugal force and weight of the material are defined by the relations 1 and 2. The lamination pressure produced by the first concave bar is given by rel.9 [3]:

Forţa centrifugă şi greutatea materialului sunt definite de relaţiile 1 şi 2. Presiunea de laminare produsă de prima şina a contrabătătorului este dată de relaţia 9 [3]:

$$p_{l_1} = Ae^{C\left(1-\frac{d_1}{\delta}\right)} \quad (9)$$

where:

p_{l1} is lamination pressure produced by the first concave bar, in N/m^2;

d_1 - portion of material thickness laminated in area of the first concave bar, in m;

δ – portion of material thickness laminated in area of the articulate plate at concave, in m;

unde:

p_{l1} este presiunea de laminare produsă de prima şina a contrabătătorului, în N/m^2;

d_1 - grosimea tranşei de material laminat în zona primei şine a contrabătătorului, în m;

δ – grosimea tranşei de material laminată în zona plăcii articulată la contrabătător, în m;

A,C – experimental coefficients with constant value depending on the crop harvested (for wheat is *A=10 N/m²* and *C=12*).

The lamination force of material portion in the area of the first concave bar is given by relation 10:

A,C – coeficienţi experimentali cu valoare constanta în funcţie de cultura recoltata (pentru grâu fiind *A=10 N/m²* şi *C=12*).

Forţa de laminare realizată de prima şină a contrabătătorului este data de relaţia 10:

$$F_{l_1} = Ae^{C\left(1-\frac{d_1}{\delta}\right)} L_s \left(C_r b_1 - b_2\right) \quad (10)$$

where:

F_{l1} is lamination force of material portion in the area of the first concave bar, in N;
L_s – cylinder bars length, in m;
b_1 – dimple area width of cylinder bar, in m;
b_2 – concave bar width, in m;

The frictional force which acts on the material portion, in the area of the first concave bar, is given by relation 11:

unde:

F_{l1} este forţa de laminare realizată de prima şina a contrabătătorului, în N;
L_s – lungimea şinelor bătătorului, în m.
b_1 – laţimea zonei riflată a şinei bătătorului, în m;
b_2 – grosimea şinei contrabătătorului, în m.

Forţa de frecare care acţionează asupra tranşei de material, în zona primei şine a contrabătătorului, este dată de relaţia 11:

$$F_{f_1} = f\left(F_{cf} + G_b \cos\zeta_1 - F_{l_1}\right) - G_b \sin\zeta_1 \quad (11)$$

where:

F_{f1} is frictional force acting on the material portion, in the area of the first concave bar, in N;
f – friction coefficient of the material with plate articulate at concave and cylinder bar;
ζ_1 – angle made with the vertical by position of the cylinder bar, corresponding to material lamination in area of the first concave bar.

The frictional force, in this case, represents the action of concave bar over the material, unlike the area of plate articulated at concave, when friction force represents the action of cylinder bar over the material for entraining it into the threshing space.

In the Figure 6 is shown the forces diagram acting on a material point located on the direction of the first interval between the concave bars.

unde:

F_{f1} este forţa de frecare care acţionează asupra tranşei de material, în zona primei şine a contrabătătorului, în N;
f – coeficientul de frecare al materialului cu şina contrabătătorului şi şina bătătorului;
ζ_1 – unghiul facut cu verticala de poziţia şinei bătătorului corespunzatoare laminării materialului, în zona primei şine a contrabătătorului.

Forţa de frecare, în acest caz, reprezintă acţiunea şinei contrabătătorului asupra tranşei de material, spre deosebire de zona plăcii articulată la contrabătător, când forţa de frecare reprezentă acţiunea şinei bătătorului asupra materialului pentru antrenarea acestuia în spaţiul de treier.

În figura 6 este prezentată diagrama forţelor care acţionează asupra unui punct material aflat pe direcţia primului interval dintre şinele contrabătătorului.

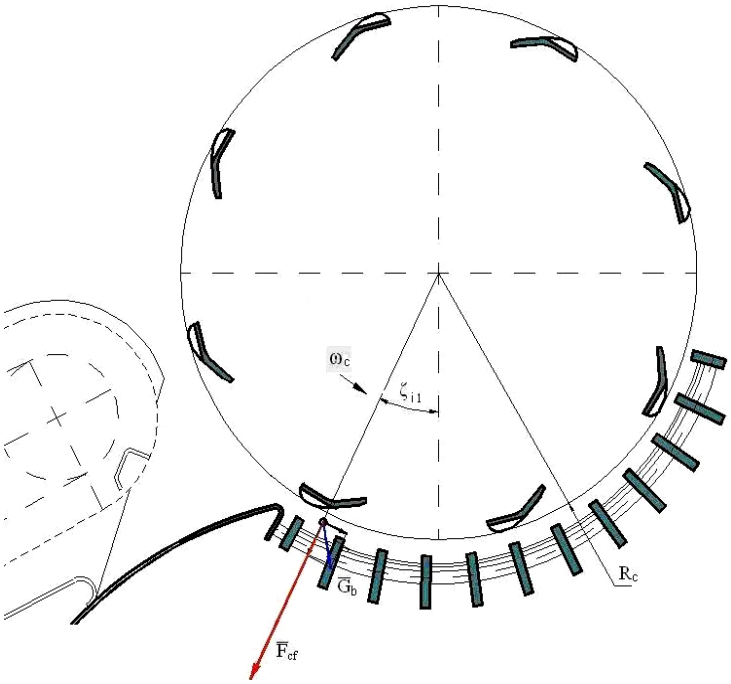

Fig. 6 – Forces diagram acting on a material point located on the direction of the first interval between the concave bars

The forces acting on the material point located on the direction of the first interval of concave bars are centrifugal force and weight of the material, defined by relations 1 and 2, which will cause separation of the free seeds from threshing space through the concave.

Forţele care acţionează asupra punctului material aflat pe direcţia primului interval dintre şinele contrabătătorului sunt forţa centrifugă şi greutatea materialului, definite de relaţiile 1 şi 2, care vor produce separarea seminţelor libere din spaţiul de treier prin contrabătător.

In Figure 7 it is shown the forces diagram acting on a material point under the action of the second concave bar.

În figura 7 este prezentată diagrama forţelor care acţionează asupra unui punct material aflat sub acţiunea şinei a doua a contrabătătorului.

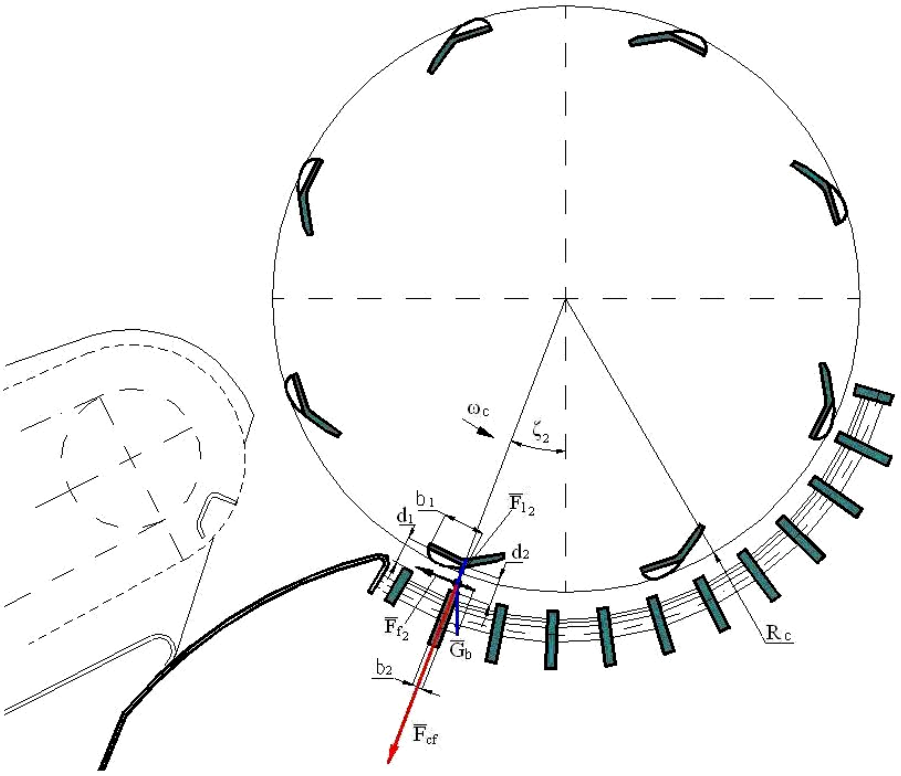

Fig. 7 – Forces diagram acting on a material point under the action of the second concave bar

The centrifugal force and weight of the material, defined by relations 1 and 2.

The lamination pressure of material portion in the area of the second concave bar, is given by relation 12:

Forţa centrifugă şi greutatea materialului sunt definite de relaţiile 1 si 2.

Presiunea de laminare a materialului în zona şinei a doua a contrabătătorului este dată de relaţia 12:

$$p_{l2} = Ae^{C\left(1-\frac{d_2}{d_1}\right)} \quad (12)$$

where:

p_{l2} is lamination pressure produced by the second concave bar, in N/m^2;

d_1 -material portion thickness laminated in area of the first concave bar, in m;

d_2 - material portion thickness laminated in area of the second concave bar, in m.

unde:

p_{l2} este presiunea de laminare produsă de şina a doua a contrabătătorului, în N/m^2;

d_1 - grosimea materialului laminat în zona primei şine a contrabătătorului, în m;

d_2 - grosimea materialului laminat în zona şinei a doua a contrabătătorului, în m.

The lamination force of material in the area of the second concave bar is given by relation 13

Forţa de laminare a tranşei de material în zona şinei a doua a contrabătătorului este dată de relaţia 13:

$$F_{l2} = Ae^{C\left(1-\frac{d_2}{d_1}\right)} L_s \left(C_r b_1 - b_2\right) \quad (13)$$

where:

F_{l2} is lamination force of material portion in the area of the second concave bar, in N;

unde:

F_{l2} este forţa de laminare realizată de şina a doua a contrabătătorului, în N;

The friction force acting on the material portion, in the area of the second concave bar, is given by relation 14:

Forţa de frecare care acţionează asupra tranşei de material în zona şinei a doua a contrabătătorului este dată de relaţia 14:

$$F_{f2} = f\left(F_{cf} + G_b \cos\zeta_2 - F_{l2}\right) - G_b \sin\zeta_2 \quad (14)$$

where:

F_{f2} is friction force acting on the material portion with the second concave bar, in N;

unde F_{f2} este forţa de frecare care acţionează asupra tranşei de material cu şina a doua a contrabătătorului, în N;

f - friction coefficient of the material with plate articulate at concave and cylinder bar;
ζ_2 – angle made with the vertical by position of the cylinder bar, corresponding to lamination of material, in area of the second concave bar.

Further on, the material entrained by cylinder bar will be laminated by following concave bars, and friction forces will pull the material, causing the combing of the ears, under the action of dimpled area of cylinder bar and liberation of the seeds.

Free seeds, located in threshing space, will be separated through concave when cylinder bars will be positioned in the concave bars intervals, when the centrifugal force and weight force act on free seeds (the threshing of wheat, centrifugal force is about 300 times greater than the weight force).

It should be noted that, if the size intervals between the concave bars is constant, the other two bars of the threshing cylinder acting on the material entrained by the first cylinder bar, should not be in the same position on concave bars.

In other words, when the first cylinder bar is positioned on the concave bar, the material being pulled by the friction force, the other two following cylinder bars will be positioned at intervals of concave bars, the material is free to move and because of multiple contacts with concave bars producing the separation of seeds (effect of "Beating the carpet").

In Figure 8 it is shown the forces diagram acting on a material portion entrained by cylinder bar, under the action of the last concave bar.

f – coeficientul de frecare al materialului cu şina contrabătătorului şi şina bătătorului;
ζ_2 – unghiul facut cu verticala de poziţia şinei corespunzatoare laminării materialului, în zona şinei a doua a contrabătătorului.

În continuare, materialul antrenat de şina bătătorului va fi laminat de urmatoarele şine ale contrabătătorului, iar forţele de frânare vor trage de material, producând-se pieptanarea spicelor sub acţiunea riflurilor şinei bătătorului şi eliberarea seminţelor.

Seminţele libere, aflate în spaţiul de treier, se vor separa prin contrabătător în momentele în care şinele bătătorului se vor afla poziţionate în intervalele dintre şinele contrabătătorului, când forţa centrifugă şi forţa de greutate acţionează asupra seminţelor libere (la treieratul grâului, forţa centrifugă este de circa 300 de ori mai mare decât forţa de greutate).

Mai trebuie remarcat că, în cazul în care marimea intervalelor dintre şinele contrabătătorului este constantă, celelalte doua şine ale bătătorului care acţionează asupra materialului antrenat de prima şina, nu trebuie să se afle în aceeaşi poziţie faţă de şinele contabătătorului.

Altfel spus, cand prima şina se află poziţionată pe o şina a contrabătătorului, materialul fiind tras de forţa de frecare, celelalte doua şine urmatoare ale bătătorului se vor afla poziţionate pe intervale ale şinelor contrabătătorului, materialul fiind liber să se deplaseze şi datorită contactelor multiple cu şinele contrabătătorului producându-se separarea seminţelor (efectul “batutul covorului”).

În figura 8 este prezentată diagrama forţelor de frecare care acţionază asupra tranşei de material antrenată de şina bătătorului, aflată în zona ultimei şine a contrabătătorului.

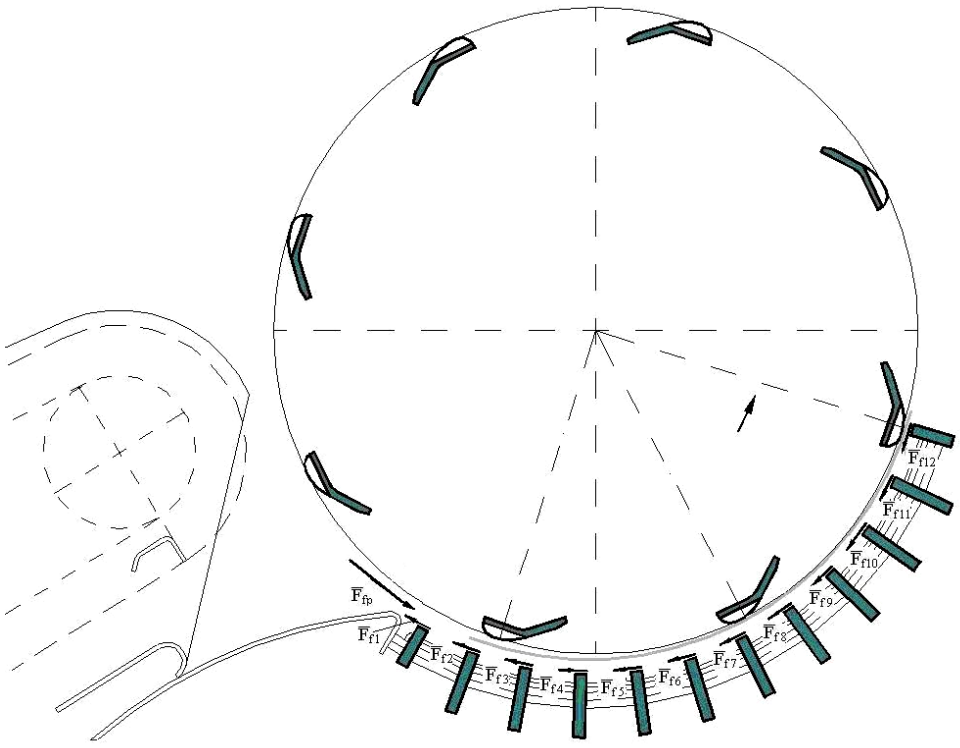

Fig. 8 – Forces diagram acting on the material tranche entrains by cylinder bar

The friction forces sum acting on a material portion under the action of the three cylinder bars and *n* concave bars is given by the relation 15:

Suma forţelor de frecare care acţionează asupra unei tranşe de material aflată sub acţiunea celor trei şine ale bătătorului şi şinele contrabătătorului este dată de relaţia 15:

$$F_{ft} = 3\left(F_{fp} - F_{fi}\right);\ i = 1...n \quad (15)$$

where:
F_{ft} is friction total force acting on the material portion
entrained by one cylinder bar, in N;
F_{fp} – frictional force acting on the material, in the area of plate articulate at concave, in N;
F_{fi} – frictional force acting concave bars on the material portion, in N;
n – number of concave bars.

Because the weight force has a little action on the material and the lamination forces produced by concave bars are approximately equal, it is resulting relation 16:

unde:
F_{ft} este forţa de frecare totală care acţionează asupra materialului antrenat de o şina a bătătorului, în N;
F_{fp} – forţa de frecare care acţionează asupra tranşei de material, în zona plăcii articulată la contrabătător, în N;
F_{fi} – forţa de frecare care acţionează şinele contrabătătorului asupra tranşei de material, în N;
n – numarul de şine ale contrabătătorului.

Pentru ca forţa de greutate are o acţiune mică asupra materialului, iar forţele de laminare a materialului produse de şinele contrabătătorului sunt aproximativ egale, rezultă relaţia 16:

$$F_{ft} = 3f\left[\left(F_{lp} - F_{cf}\right) - n\left(F_{cf} - F_{ls}\right)\right] \quad (16)$$

where:
F_{ft} is friction total force acting on the material portion entrained by one cylinder bar, in N;
F_{lp} – lamination force of material portion in the area of plate articulate at concave, in N;
F_{cf} – centrifugal force acting on the material portion entrained by cylinder bar, in N;
n – number of concave bars;
F_{lc} – lamination force of material portion achieved by one concave bar, in N.

The moving of material in the threshing space under the action of friction forces caused by concave bars, is according to relation 17:

unde:
F_{ft} este forţa de frecare totală care acţionează asupra materialului antrenat de o şina a bătătorului, în N;
F_{lp} – forţa de laminare a tranşei de material în zona plăcii articulată la contrabătător, în N;
F_{cf} – forţa centrifugă care acţionează asupra tranşei de material antrenată de şina bătătorului, în N;
n – numărul de şine al contrabătătorului;
F_{lc} – forţa de laminare realizată de o şină a contrabătătorului, în N.

Deplasarea materialului în spaţiul de treier sub acţiunea forţelor de frecare produse de şinele contrabătătorului, este conform relaţiei 17:

$$S_f = \frac{F_{ft} T_t^2}{2m_b} \cos\alpha_r \quad (17)$$

where:
S_f is moving of material in the threshing space under the action of friction forces caused by the plate articulate at concave and concave bars, in m;
T_t – duration of all the bangs, in seconds;
m_b – material portion mass entrained by cylinder bar, in kg;
α_r – dimples inclination angle of cylinder bars.

The duration of all the bangs is given by relation 18[5]:

unde:
S_f este deplasarea materialului în spaţiul de treier sub acţiunea forţelor de frecare produse de placa articulată la contrabătător şi şinele contrabătătorului, în m;
T_t – durata tuturor loviturilor, în secunde;
m_b – masa tranşei de material antrenată de şina bătătorului, în kg;
α_r – unghiul de înclinare al riflurilor şinei bătătorului.

Durata tuturor loviturilor este dată de relaţia 18 [5]:

$$T_t = \frac{3nb_2}{\omega_c R_c} \quad (18)$$

where:
T_t is duration of all the bangs, in seconds;
b_1 – dimple area width of cylinder bar, in m;
ω_c – angular speed of the cylinder, in rad^{-1};
R_c – cylinder radius, in m.

unde:
T_t este durata tuturor loviturilor, în secunde;
b_1 – laţimea riflată a şinei bătătorului, în m;
ω_c – viteza unghiulară a bătătorului, în rad^{-1};
R_c – raza bătătorului, în m.

RESULTS

For calculation of parameters used in study, the following values characteristic to harvesting combine *C110* are being used [1,6]:
- cylinder radius: R_c=*0.3 m*;
- cylinder bars number: z=*8*;
- material portion mass entrained by cylinder bar: m_b=*0.162 kg*;
- threshing cylinder speed n_c=*950 min*$^{-1}$;
- portion of material thickness laminated in area of the articulate plate at concave: δ= *0.018 m*;
- material portion thickness driven by cylinder bar in area of plate articulate at concave, before lamination: Δ=*0.070 m*;

REZULTATE

Pentru calculul marimilor prezentate în studiu, se folosesc urmatoarele valori caracteristice combinei *C110* [1,6]:
- raza bătătorului: R_c=*0,3 m*;
- numarul de şine ale bătătorului: z=*8*;
- masa materialului antrenată de şina bătătorului: m_b=*0,162 kg*;
- turaţia bătătorului la recoltarea grâului: n_c=*950 min*$^{-1}$;
- grosimea tranşei de material laminată în zona plăcii articulatală la contrabătător: δ= *0,018 m*;
- grosimea tranşei de material antrenat de şina bătătorului în zona plăcii articulată la contrabătător, înaintea laminării: Δ=*0,070 m*;

- cylinder bars length: L_s =1.08 m;
- dimple area width of cylinder bar: b_1=0.043 m;
- friction coefficient of the material with the components of threshing system: f =0.4;
- angle made by the radius that defines the vertical position of the cylinder bar: ζ_p = 35º;
- material portion thickness laminated in area of the first concave bar: d_1= 0.022 m;
- material portion thickness laminated in area of the second concave bar: d_2=0.021 m;
- concave bar width: b_2=0.010 m;
- angle made with the vertical by position of the cylinder bar, in area of the first concave bar: ζ_1 = 30º;
- number of concave bars: n=12;
- dimples inclination angle of cylinder bars: α_r = 30 º.

According to kinematic study presented, the results are:

- centrifugal force acting on a material point of material portion entrained by cylinder bar: F_{cf}=481 N;
- material portion weight entrained by cylinder bar: G_b=1.59 N;
- lamination force of material portion in the area of plate articulate at concave: F_{lp} = 8.681.1 N;
- frictional force acting on the portion of material, in the area of plate articulate at concave: F_{fp}= 3,253.5 N;
- lamination force of material portion in the area of the first concave bar: F_{l1} =F_{ls}=4.98 N;
- frictional force acting on the material portion, in the area of the first concave bar: F_{f1}=191.04 N;
- friction total force acting on the material portion entrained by one cylinder bar: F_{ft} =2.909.8 N;
- duration of all the bangs: T_t = 0.012 s;
- moving of material in the threshing space under the action of friction forces caused by the plate articulate at concave and concave bars: S_f =0.039 m.

CONCLUSION

- The material portion entrained by one cylinder bar is laminated in the area of the plate articulated at concave, friction force resulted entraining the portion in threshing space.
- The material portion entrained will be laminated by concave bars, and friction forces resulted will pull the material, causing the combing of the ears under the action of dimpled area of cylinder bar and liberation of the seeds.
- Free seeds, located in threshing space, will be separated through concave when cylinder bars will be positioned in the concave bars intervals, when the centrifugal force and weight force act on free seeds.
- Under the friction forces, the material portion moves according to cylinder bars, and displacement can be calculated. In the study conducted on the threshing system of combine *C110*, material portion moves relatively to cylinder bars with distance L_f=39 mm, this movement not affecting entrainment and transport of next material tranche.

REFERENCES

[1]. INMA Bucharest, (1995) - *Results of tests for homologating the self-propelled cereal harvesting combine C110,* Testing Report;
[2]. Ivan Gh., (2009) - *Researches regarding the influence of constructive and functional parameters of shaking-separating system on seed losses of cereal harvesting combines*, PhD thesis, University Transilvania from Brasov, Romania;

- lungimea şinelor bătătorului: L_s =1.08 m;
- laţimea riflată a şinei bătătorului: b_1=0.043 m;
- coeficientul de frecare al materialului cu componentele aparatului de treier: f =0,4;
- unghiul făcut de raza care defineşte poziţia şinei bătătorului cu verticala: ζ_p = 35º;
- grosimea tranşei de material în zona primei şine a contrabătătorului: d_1= 0,022 m;
- grosimea materialului laminat în zona şinei a 2-a a contrabătătorului: d_2=0,021 m;
- grosimea şinei contrabătătorului: b_2=0,010 m;
- unghiul facut de poziţia şinei bătătorului aflată în zona primei şine a contrabătătorului cu verticala: ζ_1=30º;
- numarul de şine al contrabătătorului: n=12;
- unghiul de înclinare al riflurilor şinei bătătorului: α_r=30º.

Conform studiului cinematic prezentat, rezultatele sunt:

- forţa centrifugă care acţionează asupra tranşei de material antrenată de şina bătătorului: F_{cf}=481 N;
- greutatea tranşei de material antrenată de şina bătătorului: G_b=1,59 N;
- forţa de laminare a tranşei de material în zona plăcii articulată la contrabătător: F_{lp}=8.681,1 N;
- forţa de frecare care actionează asupra tranşei de material, în zona plăcii articulată la contrabătător: F_{fp}=3.253,5 N;
- forţa de laminare realizată de prima şina a contrabătătorului: F_{l1}=F_{ls}=4,98 N;
- forţa de frecare care acţionează asupra tranşei de material, în zona primei şine a contrabătătorului: F_{f1}=191,04 N;
- forţa de frecare totală care acţionează asupra materialului antrenat de o şina a bătătorului: F_{ft}=2909,8 N;
- durata tuturor loviturilor: T_t=0,012 s;
- deplasarea materialului în spaţiul de treier sub acţiunea forţelor de frecare cauzate de placa articulată la contrabătător şi şinele contrabătătorului S_f=0,039 m.

CONCLUZII

- Tranşa de material antrenată de şina bătătorului este laminată în zona plăcii articulată la contrabătător, forţa de frecare rezultată antrenand tranşa în spaţiul de treier.
- Tranşa de material antrenată va fi laminată de şinele contrabătătorului, iar forţele de frânare rezultante vor trage de material, producându-se pieptănarea spicelor sub acţiunea riflurilor şinei bătătorului şi eliberarea seminţelor.
- Seminţele libere, aflate în spaţiul de treier, se vor separa prin contrabătător când şinele bătătorului se vor afla poziţionate în intervalele şinelor contrabătătorului, când forţa centrifugă şi forţa de greutate acţionează asupra seminţelor libere.
- Sub acţiunea forţele de frecare, tranşa de material se deplasează în raport cu şinele bătătorului, deplasarea putând fi calculată. În studiul realizat pe aparatul de treier al combinei *C110*, tranşa de material se deplasează în raport cu şinele bătătorului pe distanţa de S_f=39 mm, această deplasare neafectând antrenarea şi transportul urmatoarei tranşe de material.

BIBLIOGRAFIE

[1]. INMA Bucureşti, (1995) - *Rezultatele incercărilor în vederea omologării a combinei autopropulsate de recoltat cereale C110*, Referat de încercări;
[2]. Ivan Gh., (2009) – *Cercetări privind influenţa parametrilor constructivi şi funcţionali ai sistemelor de scuturare-separare asupra pierderilor de seminţe la combinele de recoltat cereale*, Teza de doctorat, Universitatea Transilvania Braşov, România;

[3]. Krasnicenko A.V., (1962-1964) - *Handbook of Agricultural Machinery Builder – vol.2*, Technical Publishing House Bucharest, Romania, pg. 403-430;
[4]. Kutzbach H.D., (2003) – *Grain Harvesting, Combine Harvesting*, Hohenheim Germany, pg.129-136;
[5]. Miu P., (2005) – *Modeling the threshing process at ceral harvesting combines*, PhD thesis, Polytechnic Institute of Bucharest, pg. 23-25;
[6]. S.C. Semanatoarea S.A., (2001) - *Technical Book for combine harvester C110.*

[3]. Krasnicenko A.V., (1962-1964) - *Manualul constructorului de maşini agricole – vol. 2*, Ed. Tehnică, Bucureşti, România, 1964, pag. 403-430;
[4]. Kutzbach H.D., (2003) – *Recoltarea grâului, Combine de recoltat,* Hohenheim Germania, pag.129-136;
[5]. Miu P., (2005) – *Modelarea procesului de treier la combinele de recoltat cereale*, Teză de doctorat, Institutul Politehnic Bucureşti, pag. 23-25;
[6]. S.C. Semănătoarea S.A., (2001) - *Carte Tehnică pentru combina C110*.

THEORETICAL ARGUMENTATION ON THE CHOICE OF VALUES FOR THE PARAMETERS OF THE PRESS DESIGNED TO SQUEEZE OUT THE JUICE FROM PLANTS STEMS

/

MOTIVAREA TEORETICĂ A ALEGERII VALORILOR PARAMETRILOR PRESEI PENTRU STOARCEREA SUCULUI DIN TULPINILE PLANTELOR

PhD. Eng. Cerempei V.
Institute of Agricultural Machinery „Mecagro", Chişinău / Moldova
Tel: (37322) 49-21-31, 44-00-87. E-mail: institut@mecagro.md, www.mecagro.md

Abstract: *In order to ensure the optimum conditions of process of squeezing the juice from plants stems (sweet sorghum, sugar cane, etc.) the choice of the value for parameters of the press are argued.*

Keywords**:** plants stems, press, rollers, driving, squeezing, juice, constructive and kinematic parameters.

INTRODUCTION

Analyses of technologies which capitalize the sugar cane and sweet sorghum energetic potential have demonstrated the importance of stems juice squeezing process [3, 8, 9]. Squeezing influences the quality and cost price of the end product-ethanol. At the same time, the efficiency of the process above depends on constructive scheme and parameters of the squeezing installation. Within the existing information sources [1, 3, 6, 8, 9, 10] scheme and parameters argumentation is fragmentary presented, the plants morphological features (particularly of sweet sorghum) are not always taken into account.

Therefore, the aim of this paper is the theoretical argumentation on the choice of the values for the parameters of the roller press (roller diameter *D*, the clearance *s* between rollers, the pressing force *P*, roller RPM *n*) in dependence with the rate of extraction of juice, the productivity of the technological process of pressing green matter, the energy consumed.

MATERIAL AND METHOD

Only after studying and taking into consideration the morphological particularities of sorghum stems and their related deformation theories, it will be possible to choose a successful pressing principle. As recently mentioned [1,3], the sorghum stem consists in short nodes and long internodes (l = 100...200mm), externally protected by a solid cellulose, relatively thin, tegument. Internodes are full of developed medullar tissue inside, the saccharides are dissolved into water and stored in medullar tissue. So, sorghum stem consists in two basic elements:

a) Solid tegument with a reduced humidity degree (10...15%);
b) Medullar tissue with a humidity degree up to 90%.

At their turn, each of mentioned elements has a carcass with elastic and plastic features, mainly of cellulose and a filling substance with viscosity properties, particularly made of watery solutions of carbon hydrates.

It is obvious that during the juice extraction from sorghum stems, the tegument should be first crushed and afterwards the medullar tissue deformed for the juice could let out.

Specialists from VISHOM Institute [11] have studied the influence of load applied on maize stems relative deformation, which have a similar morphology with sweet sorghum stems. In the first stage (OA) when the force is applied, the stem deformation raises proportionally (up to 16%) along with force increased up to 0.26 kN (fig. 1).

Rezumat: *Cu scopul asigurării condiţiilor optime ale procesului de stoarcere a sucului din tulpinile plantelor (sorgului zaharat, trestiei de zahăr etc.) se motivează teoretic alegerea valorilor parametrilor presei.*

Cuvinte cheie: *tulpinile plantelor, presa, tăvălugi, antrenare, stoarcere, suc, parametrii constructivi şi cinematici*

INTRODUCERE

Analiza tehnologiilor de valorificare a potenţialului energetic al trestiei de zahăr şi sorgului zaharat demonstrează importanţa procesului de stoarcere a sucului din tulpinile acestora [3 ,8, 9]. Procesul de stoarcere influenţează calitatea şi preţul de cost al produsului final - etanolul. La rândul său, eficienţa procesului menţionat depinde de schema constructivă şi parametrii utilajului de stoarcere. În sursele de informaţie existente [1,3,6,8,9,10] argumentarea schemelor şi a parametrilor este prezentată fragmentar, nu totdeauna sunt luate în consideraţie proprietăţile morfologice ale plantelor (îndeosebi, ale sorgului zaharat).

Prin urmare, scopul prezentei lucrări este motivarea teoretică a alegerii valorilor parametrilor presei cu tăvălugi (diametrului tăvălugilor *D*, jocul *s* dintre tăvălugi, forţei de presare *P*, turaţiilor tăvălugilor *n*) în dependenţă de gradul extragerii a sucului, productivitatea procesului tehnologic de presare a masei verzi, puterea consumată.

MATERIAL ŞI METODĂ

Alegerea unui principiu reuşit de presare este posibilă în baza studierii şi respectării particularităţilor morfologice ale tulpinilor de sorg şi teoriilor existente de deformare a acestora. După cum s-a menţionat recent [1,3], tulpina sorgului constă din noduri scurte şi internoduri lungi (l = 100...200mm), protejate din exterior de un tegument solid din celuloză, relativ subţire. Internodurile sunt pline în interior de ţesut medular dezvoltat, zaharurile sunt dizolvate în apă şi depozitate în ţesutul medular. Aşadar, tulpina sorgului constă din două elemente de bază:

a) tegument solid cu grad mic de umiditate (10...15%);
b) ţesut medular cu grad de umiditate de până la 90%.

La rândul său, fiecare din elementele menţionate are o carcasă cu proprietăţi elastice şi plastice, preponderent din celuloză, şi o substanţă de umplere cu proprietăţi de viscozitate, preponderent din soluţii apoase ale hidraţilor de carbon.

Este evident că, în procesul extragerii sucului din tulpinile sorgului trebuie mai întâi să fie zdrobit tegumentul şi apoi deformat ţesutul medular, pentru a se scurge sucul.

Specialiştii Institutului VISHOM [11] au studiat influenţa sarcinii aplicate asupra deformaţiei relative a tulpinilor de porumb, care au morfologia similară cu cea a tulpinilor de sorg zaharat. La prima etapă (OA) de aplicare a forţei, deformaţia tulpinii creşte proporţional (până la 16%) cu majorarea forţei până la 0,26 kN (fig. 1).

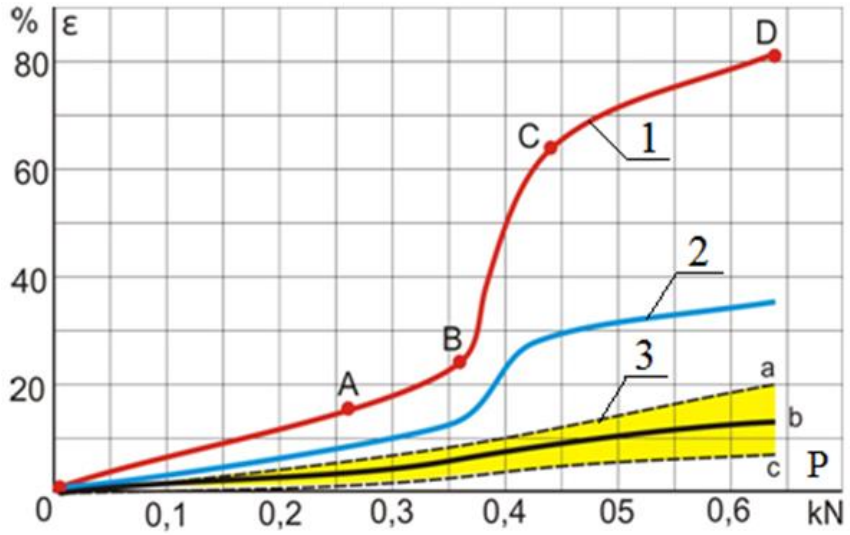

Fig. 1 – Dependence of relative deformation of maize stems $\mathcal{E}$ on applied load F:

1 – accoding to data [11]; 2,3 - according to hypothesis of subsequent deformations [4], 3a, 3b, 3c - ε = f(P)at different speed Of force applyin $(\frac{dP_a}{d\tau} < \frac{dP_b}{d\tau} < \frac{dP_c}{d\tau})$

In this stage, the variation of relative deformation is ($\mathcal{E}_{OA}$=*0.62%* / 0.01 kN). Force growth can probably lead to relaxation of internal tensions in tegument body and its deterioration along fibers. This is proved by increased variation of deformation ($\mathcal{E}_{AB}$=*0.8%* / 0.01 kN) up to 24%, along with a rather small growth of force (up to 0.36kN). Deterioration of tegument is, in fact, determined by force applying on medullar tissue, which is deforming at a variation of 5% / 0.01 kN speed. Thus, by a small growth of compressing force (up to 0.44 kN) results a stem deformation up to 64% (BC). When it keeps on increasing the force up to 0.64 kN the stem can deform from 64% up to 80% ($\mathcal{E}_{CD}$=*0.8%* / 0,01 kN). Research conducted on the press of the wine press type [5] on sweet sorghum stems have shown the same character in the variation of the relative deformation depending on the force applied. For the last, in the fourth stage (CD), the actual juice extraction is highlighted.

According to acad. F. Beleankin's theory, under the action of external forces *P*, elements of carcass begin to deform, and the filling substance presents a viscous resistance against the movement of carcass elements, thus increasing the resistance and rigidity of whole body. The limit of resistance of the carcass R_{carc} does not depend on length of action of static load, viscous resistance of filling substance R_{visc} changes in time, approaching zero when force *P.is* is driven for a long time. In this case, the body resistance will be determined only by the carcass resistance, so that for the deterioration of the body in the purpose of extracting the juice it is necessary to apply a load bigger than carcass resistance limit ($P>R_{carc}$). When rapidly acted to deteriorate the body, the load applied should surpass the carcass resistance and viscous resistance of the filling substance ($P>R_{carc}+R_{visc}$).

La această etapă variaţia deformaţiei relative ($\mathcal{E}_{OA}$=*0,62%* / 0.01 kN). Creşterea în continuare a forţei duce, probabil, la relaxarea tensiunilor interne în carcasa tegumentului şi deteriorarea lui de-a lungul fibrelor. Acest lucru este relevat de variaţia sporită ($\mathcal{E}_{AB}$=*0,8%* / 0,01 kN) a deformării, până la 24%, de creşterea relativ mică a forţei (până la 0,36kN). Aplicarea forţei asupra ţesutului medular determină deteriorarea tegumentului, care se deformează cu variaţia de 5% / 0,01 kN. Prin urmare, o creştere mică a forţei de comprimare (până la 0,44 kN) detemină ca deformaţia tulpinii să ajungă până la 64% (BC). Continuarea majorării forţei până la 0,64 kN are drept consecinţă deformarea tulpinii de la 64% până la 80% ($\mathcal{E}_{CD}$=*0,8%* / 0,01 kN). Cercetările efectuate pe presa de tip teasc [5] cu tulpinile de sorg zaharat au demonstrat acelaşi caracter al variaţiei deformaţiei relative funcţie de sarcina aplicată. La ultima, a patra etapă (CD), s-a evidenţiat extragerea propriu-zisă a sucului.

Conform teoriei acad. F. Beleankin, sub acţiunea forţelor exterioare *P*, elementele carcasei se deformează, iar substanţa de umplere manifestă rezistenţă vâscoasă contra mişcărilor elementelor carcasei, sporind rezistenţa şi rigiditatea corpului întreg. Limita rezistenţei carcasei R_{carc} nu depinde de durata acţionării sarcinii statice, rezistenţa vâscoasă a substanţei de umplere R_{visc} se schimbă în timp, apropiindu-se de zero la acţionarea îndelungată a forţei *P*. În acest caz, rezistenţa corpului va fi determinată numai de rezistenţa carcasei, astfel încât pentru deteriorarea corpului în scopul extragerii sucului este necesară aplicarea unei sarcini mai mari decât limita rezistenţei carcasei ($P>R_{carc}$). La acţionarea rapidă pentru deteriorarea corpului, sarcina aplicată trebuie să depăşească rezistenţa carcasei şi rezistenţa vâscoasă a substanţei de umplere ($P>R_{carc}+R_{visc}$).

Within the context of those above said, it can be supposed that the force applied on sweet sorghum stems first deforms (sector OA, fig.1) and deteriorates (sector AB) the solid tegument, which, having reduced humidity, puts resistance to carcass R_{carc}. Therefore, for deteriorate the tegument it is important not only the period of applying external force *P*, but also its value, respecting the condition: $P>R_{carc}$. When the medullar tissue containing up to 90% juice is deteriorated, the viscous resistance R_{visc} becomes decisive. After deteriorating the tegument by the influence of an external force, the medullar tissue carcass is deformed and deteriorated by removing the air between tissue elements (sector BC, fig.1). Further on (sector CD), in order to squeeze the juice, force P should surpass resistance $R_{visc}+R_{carc}$.

It results that the juice extraction degree GE depends not only on the force applied *F*, but also on application length of time *τ*, namely *GE =f (P;τ).* Respectively, for squeezing the juice from the press with rollers *GE = f (P,1/n, n- roller speed)* (fig.1). Previous experiments have demonstrated that the juice extraction degree *GE* when applying the force *P* during the same period τ is higher, when force *P* does not apply continuously, but periodically, several times. This application method reduces the value of force necessary for deteriorating the carcasses of tegument and medullar tissue, as well as for squeezing the juice from green matter by improving the draining conditions.

According to the theory of academics A. Ioffe, P. Rebinder, I. Frenkeli, resistance to deterioration of solid bodies mostly depends on micro and macro defects, in body structure. Because of these shortcomings the deterioration resistance diminishes by 100...1000 times comparing to ideal body without any defects. In the process of solid body deformation, the number and dimensions of defects, which at a certain density joint by relaxing internal strains increase, forming cracks. Formation of cracks, with stem structure deterioration is the main condition for extracting the juice. Applying cyclically loads on solid body gets more numerous and bigger the defects, thus reducing the body resistance.

At wine press type presses (fig.2.a) the viscous resistance may be excluded R_{visc} from the great acting duration of load applied P, assuring evacuation conditions for juice. Surpassing this load upon stem carcass resistance ($P>R_{visc}$) is theoretically possible, first, by diminishing the area of cross section of the press. But, practically, it is impossible, because it importantly reduces the press productivity, which is discreetly driven.

Comparing to press house, the helical press (screw) (fig.2.b) has a steady driving system, enabling to obtain high productivity. In this case, the duration of applying load *P* will be relatively small and determined by the period spent by raw matter in press chamber. As a result, the load applied should surpass the sum of carcass resistance of stems fragments and viscous substance: $P>R_{carc}+R_{visc}$.

În contextul celor expuse, se poate presupune că aplicarea forţei la tulpinile sorgului zaharat la început deformează (sector OA, fig.1) şi deteriorează (sector AB) tegumentul solid, care, având umiditatea mică, manifestă prioritar rezistenţă carcasei R_{carc}. De aceea, pentru deteriorarea tegumentului contează nu atât perioada acţionării forţei exterioare *P*, cât valoarea ei, respectându-se condiţia: $P>R_{carc}$. La deteriorarea ţesutului medular cu conţinut de suc de până la 90%, factor determinant devine rezistenţa vâscoasă R_{visc}. După deteriorarea tegumentului sub influenţa forţei exterioare, se produce deformarea şi deteriorarea carcasei ţesutului medular cu înlăturarea aerului dintre elementele ţesutului (sectorul BC, fig.1). Mai departe (sectorul CD), pentru stoarcerea sucului, forţa P trebuie să depăşească rezistenţa $R_{visc}+R_{carc}$.

De aici rezultă că gradul extragerii sucului GE depinde nu numai de forţa aplicată *P*, dar şi de durata aplicării *τ*, adică *GE =f (P;τ).* Respectiv, pentru stoarcerea sucului în presa cu tăvălugi *GE = f(P,1/n, n- turaţiile tăvălugilor)* (fig.1). Experimentele prealabile au demonstrat că gradul de extragere *GE* a sucului la aplicarea forţei *P* cu una şi aceeaşi durată τ este mai ridicat, când forţa *P* nu se aplică în continuu, ci periodic, de mai multe ori. Acest mod de aplicare reduce valoarea forţei necesare pentru deteriorarea carcaselor tegumentului şi ţesutului medular, precum şi pentru stoarcerea sucului din masă verde prin îmbunătăţirea, în stratul tulpinilor, a condiţiilor de scurgere.

Conform teoriei academicienilor A. Ioffe, P. Rebinder, I. Frenkeli, rezistenţa deteriorării corpurilor solide depinde în mare măsură de micro şi macrodefecte, amplasate în structura corpului. Datorită acestor defecte, rezistenţa la deteriorare scade de 100...1000 de ori în raport cu corpul ideal fără defecte. În procesul deformării corpului solid, sporesc numărul şi dimensiunile defectelor, care, la o anumită densitate, se unesc prin relaxarea tensiunilor interne, formându-se crăpături. Formarea crăpăturilor, cu deteriorarea structurii tulpinilor, este principala condiţie pentru extragerea sucului. Aplicarea ciclică a sarcinilor asupra corpului solid majorează, cu fiecare ciclu următor, numărul şi dimensiunile defectelor, reducând prin urmare, rezistenţa acestui corp.

La prese de tip teasc (fig.2.a) se poate exclude rezistenţa vâscoasă R_{visc} din contul duratei mari de acţionare a sarcinii aplicate *P*, asigurându-se condiţii de evacuare a sucului. Depăşirea acestei sarcini asupra rezistenţei carcasei tulpinii ($P>R_{visc}$) teoretic este posibilă, în primul rând, prin micşorarea ariei secţiunii transversale a presei. Însă, practic, este imposibilă, deoarece reduce esenţial productivitatea presei, care este cu acţionare discretă.

Spre deosebire de teasc, presa elicoidală (şnec) (fig.2.b) este cu acţionare continuă, ceea ce avantajează obţinerea unei înalte productivităţi. În acest caz, însă durata acţionării sarcinii *P* va fi relativ mică şi determinată de perioada aflării materiei prime în camera presei. Prin urmare, sarcina aplicată trebuie să depăşească suma rezistenţelor carcaselor fragmentelor tulpinilor şi substanţei vâscoase: $P>R_{carc}+R_{visc}$.

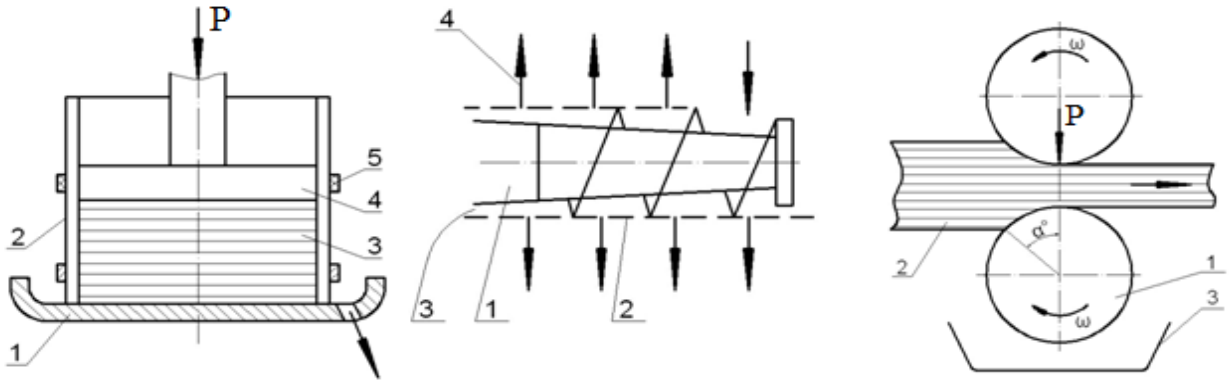

a) .... .b) c)

Fig. 2 – Main schemes of press operating:
a) of house press type (*1–support plate; 2–bowl; 3–matter pressed; 4–piston; 5–band*);
b) helical (*1–screw; 2–cylinder; 3–cane trash; 4–juice*); c) with rollers (*1–roller; 2–pressed matter; 3–vessel recipient*)

An important drawback of helical press is the necessity to mince the stems fragments, including the tegument fibers: non compliance to these conditions might determine the press clogging. The work necessary for shredding is determined according to [6] from equation: $A = kD^q$, where: *D*–dimension characteristic of fragments (particles) obtained; *m, q* – coefficients (*q*=2 – Rittinger law, *q* =3 – Kirpiciov-Chik, *q*=2,5 – Bond).

From the formula above, it results that for shredding the raw material, much more energy than for pressing might be consumed.

The roller press (fig. 2.c), as well as the helical press operates continuously, but comparing to the latter it is simpler and more reliable in exploitation. As the raw material contact to rollers lasts little time, the condition $P>R_{carc}+R_{visc}$. has to be respected. Rollers specificity is given by the fact that, in area of contact with processed matter, the load first applied is rather small, mostly increasing to its highest point in area where the distance between rollers is minimal. Therefore, if one respects certain requirements (green matter compression when entering the rollers, conducting the pressing process according to the scientific recommendations), can be obtained suitable loads to extract the juice, with less energy consumption than helical press. Moreover, the roller press does not need to mince the stems, unless when necessary to mechanization process of stems loading and, respectively separating the leaves from the stems.

Dependence of the relative deformations of stems on the applied load $\varepsilon = f(P)$ (fig.1) is mostly respected in case of roller presses, where when entering the passages (fig.2.c) with rather reduced forces, determines tegument deformation and deterioration, and in area of minimum distance between rollers (maximum load) – juice squeezing, draining through the layer of stems deformed when entering the passage. Dependence $\varepsilon = f(P)$ when stems move through the subsequent passages has, probably, less deformations (fig.1, curves 2, 3). After choosing the optimum relations between passages gaps, the most part of energy in the last passage will be consumed for pressing the matter and extracting the juice.

Un neajuns important al presei elicoidale este necesitatea mărunţirii fine a fragmentelor tulpinilor, inclusiv a fibrelor tegumentului: nerespectarea acestei condiţii duce la înfundarea presei. Lucrul mecanic necesar la mărunţire se determină conform [6] din ecuaţia: $A = mD^q$, unde: *D*– dimensiunea caracteristică a fragmentelor (particulelor) obţinute; *m, q* – coeficienţi (*q*=2 – legea lui Rittinger, *q*=3 – Kirpiciov-Chik, *q*=2,5 – Bond).

Din formula mai sus menţionată, rezultă că pentru mărunţirea materiei prime poate fi consumată mai multă energie decât la presare.

Presa cu tăvălugi (fig.2.c), ca şi cea elicoidală, are funcţionare continuă, însă, spre deosebire de ultima este mai simplă şi mai sigură în exploatare. Deoarece durata contactului materiei prime cu suprafaţa activă a tăvălugilor este mică, este necesară respectarea condiţiei $P>R_{carc}+R_{visc}$. Specificul tăvălugilor constă în faptul că, în zona contactului cu materia prelucrată, sarcina aplicată iniţial este relativ mică, crescând la maximum în zona distanţei minime dintre tăvălugi. Prin urmare, respectând unele condiţii (tasarea masei verzi la intrarea în tăvălugi, executarea procesului de presare conform recomandărilor ştiinţifice), se pot obţine sarcini necesare pentru extragerea sucului, cu consum de energie mai mic decât la presa elicoidală. Cu atât mai mult, presa cu tăvălugi nu necesită mărunţirea tulpinilor, ultima fiind executată numai în măsura necesară mecanizării procesului de încărcare în utilaj şi separării aerodinamice a frunzelor de tulpini.

Dependenţa deformaţiilor relative ale tulpinilor de sarcina aplicată $\varepsilon = f(P)$ (fig.1) se respectă în cea mai mare măsură la prese cu tăvălugi, unde la intrarea în pasaje (fig.2.c) cu forţe relativ mici, se produce deformarea şi deteriorarea tegumentului, iar în zona distanţei minime dintre tăvălugi (sarcina maximă) – stoarcerea sucului, care se scurge prin stratul tulpinilor deformate. Dependenţa $\varepsilon = f(P)$ la trecerea tulpinilor prin următoarele pasaje are, probabil, deformaţii în scădere (fig.1, curbele 2, 3). După alegerea raporturilor optime dintre jocurile pasajelor, cea mai mare parte a energiei în ultimul pasaj va fi consumată pentru presarea masei şi extragerea sucului.

RESULTS

After analyzing the existing technologies and equipment for extracting the juice from saccharate plant stems, was argued the necessity of using roller presses to squeeze the juice from the sweet sorghum stems.

To motivate the values of the basic parameters of a press, which, having a reasonable price ensures the necessities of modern production in high quantities of raw juice from sweet sorghum, the work conditions of the pressing process were analyzed.

The initial and compulsory phase of the pressing process is the engaging (laminating) the stems between the rollers. Laminating the solid substances is well reflected theoretically and largely used in the functioning of the corn harvesters [11], aggregates for laminating fodder crops [6], equipment in the food industry [9, 10], metallurgical rolling mills [4]. The next stage of the pressing process is the mechanical squeezing of juice by applying the necessary load. Further, a theoretical analysis will be conducted for the pressing process as a whole (the stages of engaging the stems and squeezing the juice), which is insufficiently reflected in the specialty literature.

REZULTATE

În baza analizei tehnologiilor şi utilajelor existente pentru extragerea sucului din tulpinile plantelor zaharoase, a fost argumentată necesitatea utilizării preselor cu tăvălugi pentru stoarcerea sucului din tulpinile sorgului zaharat.

Pentru motivarea valorilor parametrilor de bază ai unei prese, care, având un preţ rezonabil, să asigure necesităţile producţiei moderne în cantităţi mari de suc brut din sorg zaharat, destinat obţinerii etanolului şi altor produse, au fost analizate condiţiile de lucru ale procesului de presare.

Faza iniţială şi obligatorie a procesului de presare este antrenarea (laminarea) tulpinilor între tăvălugi. Laminarea substanţelor solide este bine reflectată teoretic şi utilizată pe larg în funcţionarea combinelor de recoltat porumb [11], agregatelor de laminat culturi furajere [6], utilajelor din industria alimentară [9,10], laminoarelor metalurgice [4]. Următoarea fază a procesului de presare este stoarcerea mecanică a sucului prin aplicarea sarcinilor necesare. În continuare va fi efectuată analiza teoretică a procesului de presare în ansamblu (faze de antrenare a tulpinilor şi stoarcere mecanică a sucului), care este insuficient reflectat în literatura de specialitate.

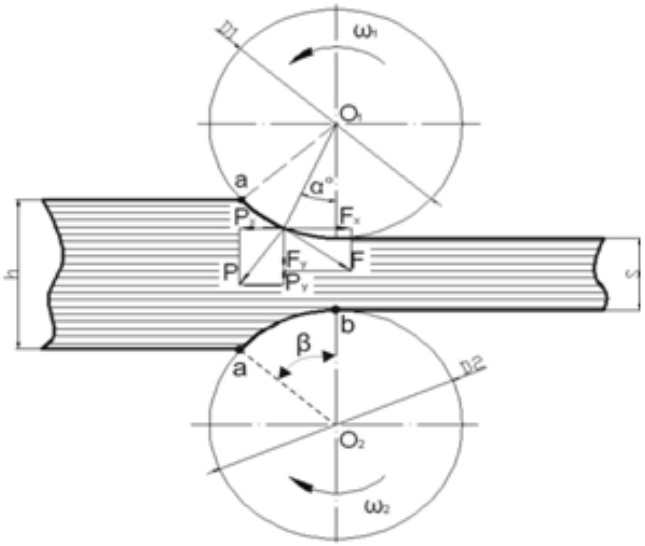

Fig. 3 – Scheme of force applying on material pressed

Stems driving between rollers

When extracting the juice from saccharate plants stems, the most frequent operation is matter pressing between two rollers with equal diameters and rotation speed. Layer of raw material with initial thickness *h* (fig.3) is pressed up to its thickness *s*, equal to gap between rollers. According to [4, 6, 10], rollers load on stem layer for each area are perpendicular on contact surface and can be reduced at a resulting force *P.* Decomposing this force in two perpendicular directions, that of material compression and respectively, its displacement, we receive the components P_y (material is compressed) and P_x (material is pushed from the passage). Except this, the friction forces act tangentially to rollers surface on material, forces shown by resultant *F*. Decomposing this force on the same directions as *P,* we obtain the components F_x, which drive the material between rollers and F_y which contributes to material pressing. A detailed study of pressing process has demonstrated that, when rollers approach and gap *s* in passage

Antrenarea tulpinilor între tăvălugi

La extragerea sucului din tulpinile plantelor zaharoase, cea mai frecventă este presarea materialului între doi tăvălugi cu valori egale ale diametrelor şi vitezelor de rotaţie. Stratul de materie primă cu grosimea iniţială *h* (fig.3) se presează până la grosimea *s*, egală cu jocul pasajului dintre tăvălugi. Conform [4,6,10], forţele tăvălugilor asupra stratului de tulpini pentru fiecare zonă sunt îndreptate perpendicular pe suprafaţa de contact şi pot fi reduse la o forţă rezultantă *P.* Descompunând această forţă în două direcţii perpendiculare, a comprimării materialului şi respectiv, a deplasării lui, primim componentele P_y (comprimă materialul) şi P_x (împinge materialul din pasaj). În afară de aceasta, tangenţial suprafeţei tăvălugilor asupra materialului acţionează forţele de frecare, care pot fi prezentate prin rezultanta *F*. Descompunând această forţă pe aceleaşi direcţii ca şi *P,* obţinem componentele F_x, care antrenează materialul între tăvălugi şi F_y, care contribuie la presarea materialului. Din studiul mai detaliat al procesului de presare este evident că, la apropierea tăvălugilor cu micşorarea jocului *s* în pasaj, unghiul de contact α creşte

diminishes, the contact angle α increases (if thickness *h=const*.) and force applying point *P* moves away from line of centre O_1O_2, which makes component P_x grow on the account of P_y. When force P_x surpasses the component of friction force F_x the roller begins to skid and material displacement stops.

RESULTS

As it results from those said above, the condition of material driving between rollers is:

(dacă grosimea *h=const*.) şi punctul de aplicare a forţei *P* se îndepărtează de linia centrului O_1O_2 , ceea ce duce la majorarea componentei P_x din contul P_y. În momentul în care forţa P_x depăşeşte componenta forţei de frecare F_x începe patinarea tăvălugului şi deplasarea materialului se stopează.

REZULTATE

După cum rezultă din cele expuse, condiţia antrenării materialului între tăvălugi este:

$$F_x \geq P_x, \quad (1)$$

or

sau

$$F \cdot \cos\alpha \geq P \cdot \sin\alpha \rightarrow P\,tg\,\varphi\cos\alpha \geq P\sin\alpha \quad (2)$$

where:

φ is the material friction angle to the roller suface.

From here result:

unde:

φ este unghiul de frecare a materialului pe suprafaţa tăvălugului.

De aici rezultă:

$$\text{tg}\ \varphi \geq \text{tg}\ \alpha \quad \text{sau} \quad \varphi \geq \alpha \quad (3)$$

In the limit case, when material is stopped when entering the passage, the application point of force *P* moves to point *a* ($tg\ \varphi \geq tg\ \beta$ *şi* $\varphi \geq \beta$). In this case, the distance between centers O_1 *and* O_2 will be equal to $D+s = D\cos\beta + h$ (fig.4), maximum thickness of layer between rollers can be determined by relation:

În cazul limită, când începe stoparea materialului la intrarea în pasaj, punctul de aplicare a forţei *P* se deplasează în punctul *a* ($tg\ \varphi \geq tg\ \beta$ *şi* $\varphi \geq \beta$). În acest caz, distanţa dintre centrele O_1 şi O_2 va fi egală cu $D+s = D\cos\beta + h$ (fig.4), iar grosimea maximă a stratului antrenat între tăvălugi poate fi determinată din relaţia:

$$h = D\,(1-\cos\beta) + s \quad (4)$$

Where *D* – roller diameter, m.

Allowable decrease (thinning) of material layer thickness, pressed between rollers, is determined:

unde *D* - diametrul tăvălugilor, m.

Micşorarea (subţierea) admisibilă a grosimii stratului de material, presat între tăvălugi, se determină:

$$\Delta h = h - s = D\,(1-\cos\beta) \quad (5)$$

Taking into consideration the condition of material driving between rollers ($tg\ \varphi \geq tg\ \beta$) and trigonometric relation $\cos\beta = 1/\sqrt{1+tg^2\beta}$, we will obtain $\Delta h \leq D(1-1/\sqrt{1+tg^2\varphi})$. In previous researches, it was established that the friction coefficient *f* of sorghum stems against the metallic surface (steel) depends on their physical state: for whole stems *f=0.4÷0.5*, for crushed stems *f=0.5÷0.55*. Hence it results that for increasing stems driving in the first passage, they have to be previously crushed, compaction and leveling the layer when entering the passage.

It results that the thickness *h* and the compression degree *Δh* of driven layer, for pressing, between two rollers, depend on diameter of rollers *D* and coefficient of friction *(f=tg φ)* of material on roller surface. Therefore, increasing diameter *D* and friction coefficient *tg φ* increase the values of thickness of layer *h* and its thinness Δh, which not only that improves the engaging conditions of the stems layer, but also increases the productivity of the pressing process *Q* and the juice squeezing degree *GE.*

Productivity and liquid extraction degree when material is pressed between rollers

The volume of material passing within a period of time through a passage formed by two rollers, which peripheral speed is equal and only when there is no skidding, is determined by the relation:

Luând în consideraţie condiţia antrenării materialului între tăvălugi ($tg\ \varphi \geq tg\ \beta$) şi relaţia trigonometrică $\cos\beta = 1/\sqrt{1+tg^2\beta}$, obţinem $\Delta h \leq D(1-1/\sqrt{1+tg^2\varphi})$. În cercetările prealabile este stabilit că coeficientul de frecare *f* al tulpinilor sorgului pe suprafaţa metalică (oţel) depinde de starea fizică a acestora: la tulpini întregi f=0,4÷0,5, la cele strivite f=0,5 ÷0,55. De aici rezultă că pentru majorarea probabilităţii antrenării tulpinilor în primul pasaj este necesar de efectuat strivirea prealabilă a acestora, tasarea şi nivelarea grosimii a stratului la intrare în pasaj.

Din cele expuse rezultă că grosimea *h* şi gradul de comprimare *Δh* a stratului antrenat, pentru presare, între doi tăvălugi, depind de diametrul tăvălugilor *D* şi coeficientul de frecare *(f=tg φ)* a materialului de suprafaţa tăvălugului. Prin urmare, majorarea diametrului *D* şi a coeficientului de frecare *tg φ* măreşte valorile grosimii stratului *h* şi subţierii acestuia Δh, ceea ce nu numai îmbunătăţeşte condiţiile de antrenare a stratului de tulpini, dar şi sporeşte, la rândul său, productivitatea procesului de presare *Q*, gradul de stoarcere a sucului *GE.*

Productivitatea şi gradul de extragere a lichidului la presarea materialului între tăvălugi

Volumul materialului care trece, într-o unitate de timp, printr-un pasaj format de doi tăvălugi, a căror viteză periferică este egală, şi cu condiţia lipsei patinării se determină din relaţia:

$$V = b \cdot h \cdot v \quad (6)$$

where:
b – roller length (the width of the pressing area), m;
h – thickness of the layer driven between rollers, m;
v – rollers peripheral speed, m/s.

The mass of material processed within a time unit (productivity) can be determined, knowing the bulk mass (volume mass) γ of the material (kg/m$^{3)}$.

unde:
b - lungimea tăvălugului (lăţimea zonei de presare), m;
h – grosimea stratului antrenat între tăvălugi, m;
v – viteza periferică a tăvălugilor, m/s.

Masa materialului prelucrat într-o unitate de timp (productivitatea) poate fi determinată, ştiind masa în vrac (masa volumetrică) γ a materialului (kg/m³):

$$Q_{M.V.} = V\gamma = bhv\gamma \quad (7)$$

When material passes through rollers, the layer compresses from *h* thickness up to *s* (value of passage). As a result of compressing process, the liquid is released and the volume mass of squeezed material γs raises.

The liquid extraction degree can be determined by the relation:

La trecerea materialului printre tăvălugi, stratul se comprimă de la grosimea *h* până la *s* (valoarea pasajului). Ca rezultat al procesului de comprimare, are loc eliberarea lichidului din material şi creşterea masei volumetrice a materialului stors γs .

Gradul de extragere a lichidului poate fi determinat din relaţia:

$$GE = \frac{Q_{M.V.} - Q_{M.S.}}{Q_{M.V.}} = \frac{Q_s}{Q_{M.V.}}, \quad (8)$$

where $Q_{M.S.}$, Q_s - mass of sqeezed material (cane trash) and juice extracted, within a time unit, kg/s:

unde $Q_{M.S.}$, Q_s - masa materialului stors (bagasei) şi a sucului extras, într-o unitate de timp, kg/s:

$$Q_{M.S.} = V_s \gamma_s = b \cdot s \cdot v \cdot \gamma_s. \quad (9)$$

By replacing $Q_{M.V.}$ and $Q_{M.S.}$ from expressions (7) and (9) in expression (8) we obtain:

Prin substituirea lui $Q_{M.V.}$ şi $Q_{M.S.}$ din expresiile (7) şi (9) în expresia (8) obţinem:

$$GE = 1 - \frac{\gamma_s \cdot s}{\gamma \cdot h} = 1 - k\frac{s}{h} = 1 - k\frac{h - \Delta h}{h}, \quad (10)$$

where $k = \frac{\gamma_s}{\gamma}$ - coefficient of compressing the vegetal mass.

In formula (10) the denominator $(\gamma \cdot h)$ reflects the raw material state, and numerator $(\gamma_s \cdot s)$ – reflects the squeezed material (cane trash). Maximum theoretical value of extraction degree GE_{max} is determined by fraction of juice in stems f_s, from here:

unde $k = \frac{\gamma_s}{\gamma}$ - coeficientul de comprimare a masei vegetale.

În formula (10) numitorul $(\gamma \cdot h)$ reflectă starea materiei prime, iar numărătorul $(\gamma_s \cdot s)$ starea materiei stoarse (bagasei). Valoarea teoretică maximă a gradului de extragere GE_{max} este determinată de fracţia sucului în tulpini f_s, de aici:

$$GE_{\max} = f_s = 1 - \frac{\gamma_s \cdot s}{\gamma \cdot h} = 1 - \frac{\gamma_s}{\gamma} \cdot \frac{h - \Delta h}{h}. \quad (11)$$

As a result, $\frac{\gamma_s \cdot s}{\gamma \cdot h} = 1 - f_s = f_{su}$ and respectively:

Prin urmare $\frac{\gamma_s \cdot s}{\gamma \cdot h} = 1 - f_s = f_{su}$ şi respectiv:

$$\frac{s}{h} = f_{su}\frac{\gamma}{\gamma_s} = \frac{f_{su}}{k}, \quad (12)$$

where f_s, f_{su} – mass fractions of juice and respectively, dry substance in pressed stems, %. In each concrete case, values f_s, f_{su} are determined in laboratory conditions, afterwards using the formula (12), the ratio $\frac{s}{h}$ is calculated.

Based on formulae (5) and (11) we are calculating the thickness of layer Δh, allowing to drive the stems and extract the juice with $GE \rightarrow f_s$, *namely* $\Delta h = D(1 - \cos\varphi) = h(1 - f_{su}\frac{\gamma}{\gamma_s})$, from where:

unde f_s, f_{su} –fracţiile masice ale sucului şi respectiv substanţei uscate în tulpinile presate, %. În fiecare caz concret valorile f_s, f_{su} se determină în condiţii de laborator, după aceasta, utilizând formula (12), se calculează raportul $\frac{s}{h}$.

În baza formulelor (5) şi (11) calculăm subţierea grosimii stratului Δh, care permite antrenarea tulpinilor şi extragerea sucului cu $GE \rightarrow f_s$, adică $\Delta h = D(1 - \cos\varphi) = h(1 - f_{su}\frac{\gamma}{\gamma_s})$, de unde:

$$D = h\frac{1 - f_{su} \cdot \gamma / \gamma_s}{1 - \cos\varphi} = h\frac{1 - f_{su}/k}{1 - \cos\varphi} \quad (13)$$

Thus, calculating *h* by formula (7) and measuring values of physical properties of pressed material (f_s, f_{su}, γ, γ_s, φ), we can determine the diameter of rollers *D* and gap *s*. For obtaining high values of extraction degree ($GE \rightarrow f_s$) and conditions of press efficient operating, the material pressing should be performed by passing through several passages along with decreasing step by step the gap *s* up to the necessary value ($s \rightarrow 0$, $\Delta h \rightarrow h$), using the constructive parameters (rollers diameter *D*), kinematic parameters (rollers speed ω) and force (*P*) with reasonable values.

Rollers diameter *D* increases along with length of white sector of driving-pressing ($l = R\beta$, fig.3) and respectively, duration of pressing, improving the conditions for letting dry the juice (sector CD, fig.1). Concomitantly with this, it is necessary to increase the load applied on the driving-pressing sector ($P = p_m l B$ where p_m is the average pressure in the pressing are, N/m^2) and assure the uniformity of green matter layer thickness *h*.

For increasing the extraction degree *GE*, it is necessary to reduce the gap *s* of passage, namely $\Delta h \rightarrow h$. But, from the relations (4, 7) it is obvious that value *s* is limited by Δh for a given value *h*, which corresponds, at its turn to necessary productivity Q_{mv}. Taking this into consideration, obtaining the extraction degree *GE* aimed, may be achieved by making the material pass through several squeezing sectors.

When pressing the material, it is necessary to obtain not only the press functionality with secure driving of stems, but also high values for productivity and extraction degree, and minimum energy consumption.

Power consumed when pressing the material between rollers

As we recently mentioned, for ensuring the stems driving and pressing by the rollers, it is necessary to apply a force *P* on material, which is perpendicularly headed on the contact surface (fig.4). In order to act the rollers with speed ω, according to [4], a torsion moment is necessary:

Aşadar, calculând *h* după formula (7) şi măsurând valorile proprietăţilor fizice ale materialului presat (f_s, f_{su}, γ, γ_s, φ), se determină diametrul tăvălugilor *D* şi jocul *s*. Pentru obţinerea valorilor înalte ale gradului de extragere ($GE \rightarrow f_s$) şi condiţiile de funcţionare eficientă a presei, este necesar ca presarea materialului să fie realizată în baza trecerii lui prin mai multe pasaje cu scăderea treptată a jocului *s* până la valoarea necesară ($s \rightarrow 0$, $\Delta h \rightarrow h$), utilizând parametrii constructivi (diametrul tăvălugilor *D*), cinematici (viteza tăvălugilor ω) şi de forţă (*P*) cu valori rezonabile.

Majorarea diametrului tăvălugilor *D* sporeşte concomitent lungimea sectorului *ab* de antrenare-presare ($l = R\beta$, fig.3) şi respectiv, durata presării, îmbunătăţind condiţiile pentru scurgerea sucului. Concomitent, în aceste condiţii, este necesară mărirea sarcinii aplicată asupra sectorului de antrenare-presare ($P = p_m l b$, unde p_m este presiunea medie în zona de presare, N/m²) şi asigurarea uniformităţii grosimii stratului de masă verde *h*.

Pentru majorarea gradului de extragere *GE*, este necesară micşorarea jocului *s* al pasajului, adică $\Delta h \rightarrow h$. Însă din relaţiile (4, 7) este evident că valoarea *s* este limitată de Δh pentru o valoare dată *h*, care corespunde, la rândul său, productivităţii necesare Q_{mv}. Luând în consideraţie acest fapt, obţinerea gradului dorit de extragere *GE*, poate fi realizată prin trecerea materialului prin mai multe pasaje de stoarcere.

La presarea materialului este necesar să se obţină nu numai funcţionalitatea presei cu antrenarea sigură a tulpinilor, valori înalte ale productivităţii şi gradului de extragere (stoarcere) a sucului, dar şi un consum minim de energie.

Puterea consumată la presarea materialului între tăvălugi

După cum a fost recent menţionat, pentru asigurarea procesului antrenării şi presării tulpinilor din partea tăvălugilor este necesar de aplicat asupra materialului forţa *P*, care este îndreptată perpendicular suprafeţei de contact (fig.4). Pentru acţionarea tăvălugilor cu viteza ω, conform [4], este necesar moment de torsiune:

$$M_t = 2P\psi l \quad (14)$$

where ψ - coefficient of arm, $\psi = \frac{\alpha}{\beta} = \frac{l_p}{l}$,

$-\alpha, \beta$ - angles of applying the force *P* and respectively the driving-pressing sector ;

- l_p, l – length of arm of applying the force *P* and respectively the driving-pressing sector .

From formula (5) it comes out that, $\Delta h = D(1-\cos\beta)$, and from trigonometry, it is known that $1-\cos\beta = 2\sin^2\frac{\beta}{2}$, then:

unde ψ - coeficientul braţului, $\psi = \frac{\alpha}{\beta} = \frac{l_p}{l}$,

$-\alpha, \beta$ - unghiuri de aplicare a forţei *P* şi respectiv a sectorului de antrenare - presare;

- l_p, l – lungimile braţului de aplicare a forţei *P* şi respectiv a sectorului de antrenare-presare.

Din formula (5) reiese, că $\Delta h = D(1-\cos\beta)$, totodată din trigonometrie se cunoaşte că $1-\cos\beta = 2\sin^2\frac{\beta}{2}$, atunci:

$$\Delta h = 2D\sin^2\frac{\beta}{2} \quad (15)$$

For smaller values of angle β: $\sin\beta = \beta$, from where

Pentru valori mici ale unghiului β: $\sin\beta = \beta$, de unde:

$$\Delta h = 2D\frac{\beta^2}{4} = R\beta^2. \quad (16)$$

Length of driving – pressing sector is equal:
$l = \beta R$, where *R*- pressing roller radius.

Lungimea sectorului de antrenare-presare este egală:
$l = \beta R$, unde *R*- raza tăvălugului de presare.

It results, $\beta = \frac{l}{R}$, from where $\Delta h = R\frac{l^2}{R^2} = \frac{l^2}{R}$ şi $l = \sqrt{R \cdot \Delta h}$. Then:

Prin urmare, $\beta = \frac{l}{R}$, de unde $\Delta h = R\frac{l^2}{R^2} = \frac{l^2}{R}$ şi $l = \sqrt{R \cdot \Delta h}$. Atunci:

$$M_t = 2P\psi\, l = 2P\psi\sqrt{R\Delta h} = 2p_m\psi\, BR\,\Delta h \quad (17)$$

where
p_m – average pressure in driving-pressing sector ($p_m = \frac{P}{Bl} = \frac{P}{B\sqrt{R \cdot \Delta h}}$);
B – width of driving-pressing sector .

According to author's experimental data [1,5], values of arm coefficient are within the limit of ψ = 0,33÷0,67, the average value being ψ = 0,5, then the torsion moment is $M_t = P\sqrt{R\Delta h} = p_m BR\,\Delta h$.

Power consumed for achieving the process of driving-pressing the green matter will be equal to:

unde
p_m - presiunea medie în sectorul de antrenare - presare ($p_m = \frac{P}{Bl} = \frac{P}{B\sqrt{R \cdot \Delta h}}$);
B – lăţimea sectorului de antrenare – presare.

Conform datelor experimentale ale autorilor [1,5], valorile coeficientului braţului se află în limita ψ = 0,33÷0,67, valoarea medie fiind ψ = 0,5, atunci momentul de torsiune $M_t = P\sqrt{R\Delta h} = p_m BR\,\Delta h$.

Puterea consumată pentru realizarea procesului de antrenare-procesare a masei verzi va fi egală:

$$N = M_t\,\omega = P\sqrt{R\Delta h}\;\omega = p_m BR\cdot\Delta h\,\omega\,. \quad (18)$$

Thus, the secure driving conditions of green matter impose the rollers diameter D, the friction coefficient f to be as high as possible (formula 5). At the same time, values of productivity Q_{mv} and extraction degree GE are directly proportional with the layer thickness h and respectively the thinness Δh (formulae 7, 10), these ones being proportional with the rollers diameter D, namely, h_{max}, Q_{mv}, $GE=f(D)$. At the same time, increasing the rollers diameter determines the growth of torsion moment and consumed power M_t, $N = f(D)$ at the same pressure and angular speed $(p_m, \omega=const)$.

Value of rollers diameter D is imposed by press productivity Q_{mv} and secure driving requirements of vegetal matter. This value is initially calculated and then experimentally checked. Real maximum values of diameter D are limited by energetic capacities of press users and technological possibilities of machinery building enterprises. More complex is the determination of force parameters values (P, p_m), speed (ω, V), rollers placement (s).

Aşadar, condiţiile de antrenare sigură a masei vegetale impun, ca valorile diametrului tăvălugilor D, coeficientului de frecare f să fie maxim posibile (formula 5). Totodată, valorile productivităţii Q_{mv} şi gradului de extragere GE depind direct proporţional de grosimea stratului h şi respectiv de subţierea stratului Δh (formulele 7, 10), acestea, la rândul său, fiind dependenţi direct proporţional de diametrul tăvălugilor D, adică, h_{max}, Q_{mv}, $GE=f(D)$. Simultan majorarea diametrului tăvălugilor are drept consecinţă creşterea momentului de torsiune şi a puterii consumate M_t, $N = f(D)$ la aceeaşi presiune şi viteza unghiulară $(p_m, \omega=const)$.

Valoarea diametrului tăvălugilor D este impusă de productivitatea presei Q_{mv} şi cerinţele de antrenare sigură a masei vegetale. Aceasta valoare iniţial se calculează şi apoi se verifică experimental. Real valorile maxime ale diametrului D sunt limitate de capacităţi energetice ale utilizatorilor preselor şi de posibilităţi tehnologice ale întreprinderilor constructoare de maşini. Mai complexă este determinarea valorilor parametrilor de forţe (P, p_m), viteză (ω, V), poziţionare a tăvălugilor (s).

CONCLUSIONS

1. Based on equipment analysis and existing theories, for extracting the juice from sweet sorghum the roller press is recommended, which ensures a high degree of juice extraction and high productivity with reduced consumption of energy, because this press ensures a better extraction of juice than other presses (hand press, screw press).

2. It is argued the dependency of the juice extraction degree GE to the K coefficient of increasing the density of pressed material, the clearance s between the rollers and the initial thickness h of the pressed material. It was argued that a desired degree of extraction can be achieved by passing the material through various squeezing passages, gradually decreasing the clearance s until it reaches the necessary value.

CONCLUZII

1. În baza analizei utilajelor şi teoriilor existente, pentru extragerea sucului din tulpinile sorgului zaharat este recomandată presa cu tăvălugi, care asigură un grad ridicat de extragere a sucului şi productivitatea înaltă cu consum redus de energie datorită faptului că în aşa tip de prese se pot asigura condiţii mai bune de stoarcere a sucului din tulpinile sorgului decât în alte prese (cu teasc, melc).

2. Este argumentată dependenţa gradului de extragere a sucului GE de coeficientul K de majorare a densităţii materialului presat, jocul s dintre tăvălugi şi grosimea iniţială h a materialului presat. S-a argumentat că obţinerea gradului dorit de extragere poate fi realizată datorită trecerii materialului prin mai multe pasaje de stoarcere, cu scăderea treptată a jocului s până la valoarea necesară.

REFERENCES

[1]. Antohe I., (2006) – *Culture of saccharate sorghum and its total industrialization. Perspective Romanian agriculture sustainable development prospects*, Bucharest, Chiminform Data, p.302, ISBN 973-88183-1-1; 978-973-88183-1-6;
[2]. Grassi G., Pietro Moncada P.C., Zibetta H., (1992) - *Promising industrial energy crop: Sweet Sorghum.*

BIBLIOGRAFIE

[1]. Antohe I., (2006) - *Cultura sorgului zaharat şi industrializarea lui totală. Perspective pentru dezvoltarea durabilă a agriculturii româneşti*, Bucureşti, Chiminform Data, pag.302, ISBN 973-88183-1-1; 978-973-88183-1-6;
[2]. Grassi G., Pietro Moncada P.C., Zibetta H., (1992) – *Culturile energetice promițătoare: Sorgul zaharat.*

Recent developments in Europe, Commission of the European Communities, p.73;
[3]. Hăbăşescu I., Cerempei V. et al., (2009)- *Energy from biomass, technologies and technical methods,* Editura Bons Offices Publishing, Chişinău, p.368;
[4]. Korolev A.A., (1969) – *Construction and calculation of machines and mechanisms for rolls,* Metallurgia Publishing, Moscow, p.277;
[5]. Hăbăşescu I., Cerempei V., Molotcov Iu., Raicov V., (2013) – *Installation for researching the pressing processes of sweet sorghum,* in Materials of the International Scientific Symposium "Modern Agriculture – Achievement and Perspectives", vol.38, pg.39-43, ISSN 978-9975;
[6].Melnikov S.V.,(1978) – *Mechanization and automation of animal farms*, Spic Publishing, Leningrad, p.560;
[7]. Sapronov A.R., (1983)- *Technology of sugar*. Food and Consumer Industry Publishing, Moscow, p.292;
[8]. Smith ş.a., (1987) - *Evolution of Sweet Sorghum for fermentable Sugar production Potential. In: Crop Science*, vol. 27, nr. 4, 1, pg. 788-790;
[9]. Sokolov A., (1969) – *Bases of calculus and design of machines and automated installations in food production*, Publishing: Machinery Manufacturing Industry, Moscow, p.640;
[10]. Stabnicov V.N., (1976) – *Processes and apparata in food production,* Food Industry Publishing House, Moscow, p.664;
[11]. Şatilov K.V. ş.a., (1981) – *Maize harvesting machines*, Machinery Manufacturing Industry Publishing, Moscow, p.224.

Evoluțiile recente din Europa, Comisia Comunităților Europene, pag.73;
[3]. Hăbăşescu I., Cerempei V. şi alţii, (2009)- *Energie din biomasă: tehnologii şi mijloace tehnice,* Editura Bons Offices, Chişinău, pag.368;
[4]. Korolev A.A., (1969) - *Construcţia şi calculul maşinilor şi mecanismelor pentru laminoare,* Editura Metallurgia, Moscova, pag.277;
[5]. Hăbăşescu I., Cerempei V., Molotcov Iu., Raicov V., (2013) - *Instalaţia pentru cercetarea proceselor de presare a tulpinilor de sorg zaharat*, Materialele simpozionului Ştiinţific Internaţional „Agricultura Modernă – Realizări şi Perspective", vol.38, pag.39-43, ISSN 978-9975;
[6]. Melnikov S.V.,(1978) – *Mecanizarea şi automatizarea fermelor zootehnice,* Editura Spic, Leningrad, pag.560;
[7]. Sapronov A.R.,(1983) – *Tehnologia zahărului*. Editura Industria Alimentară şi Uşoară, Moscova, pag.292.
[8]. Smith ş.a., (1987) – *Evoluția sorgului zaharat pentru potențialul de producție a zahărului fermentabil.* Știința Recoltării, vol. 27, nr.4,1, pag.788-790;
[9]. Sokolov A., (1969) – *Bazele calculului şi proiectării maşinilor şi automatelor în producţia alimentară*, Editura: Industria Construcţiilor de Maşini, Moscova, pag.640;
[10]. Stabnicov V.N., (1976) – *Procese şi aparate în producţia alimentară*, Editura Industria Alimentară, Moscova, pag.664;
[11]. Şatilov K.V. ş.a., (1981) – *Maşini de recoltat porumb*, Editura: Industria Construcțiilor de Maşini, Moscova, pag.224.

EXPERIMENTAL ARGUMENTATION OF PRESS PARAMETERS FOR SQUEEZING JUICE FROM PLANT STEMS
/
ARGUMENTAREA EXPERIMENTALĂ A PARAMETRILOR PRESEI PENTRU STOARCEREA SUCULUI DIN TULPINILE PLANTELOR

Assoc.Coresp. Mem. of MSA, PhD.Eng. Hăbăşescu I., PhD.Eng. Cerempei V., Eng. Balaban N.
Institute of Agricultural Machinery „Mecagro", Chisinau / Moldova
Tel: (37322) 49-21-31, 44-00-87 E-mail: institut@mecagro.md, www.mecagro.md

Abstract: This paper presents the obtained results of experimental research from the squeezing juice process from sweet sorghum stems. Mathematical models have allowed to obtain optimized values of functional press with rollers parameters: in the original game from the squeezing force passage of pressing speed rollers.

Keywords: *plant steams, press rollers, squeezing, juice, parameters, mathematical models, optimization*

INTRODUCTION

The theoretical argument veracity of the squeezing juice parameters from the press plant stems can be confirmed by experimental research. However, existing sources of information [2, 4, 6, 7, 8, 9] do not contain virtually experimental data on the effective values of the press parameters for squeezing juice. The aim of this paper is argumentation of the experimental parameters for optimization press resulted as mechanical juice extraction from sweet sorghum stems.

MATERIAL AND METHOD

In paper [1] are being described the design scheme and general technical parameters of the mills with rollers, but there are missing the calculation method and argumentation technological parameter process of mechanical squeezing the juice. Therefore, were calculated, taking into account, the theoretical and constructive technological parameter recommendations.

Subsequently, to obtain optimal values of the ***s*** game in the squeezing passage, pressing force ***P*** and ***n*** speeds of rollers were measured the degree of juicing GE, Q_{mv} productivity and power consumption N. Preliminary research results have allowed to assume the existence of nonlinearity response function and the existence of reciprocity factor interaction.

For this reason it was used a plan B_3 (Box-Benkin) [3].

Varying levels of factors are shown in Table 1, where X_1 - initial game in spin passage, mm; X_2 - Pressing force, P, kN; X_3 - Speeds rollers n, min^{-1} .

For researches were used and chopped whole stems of sorghum, defoliated without panicles, with humidity of 71% and mass fraction of 12% sugar juice. The press was uniform fed with strains, providing the required values of the factors.

Rezumat: *În lucrare sunt prezentate rezultatele cercetărilor experimentale ale procesului de stoarcere a sucului din tulpinile sorgului zaharat. Modelele matematice obţinute au permis optimizarea valorilor ale parametrilor funcţionali ai presei cu tăvălugi: jocului iniţial în pasajul de stoarcere, forţei de presare, turaţiilor tăvălugilor.*

Cuvinte cheie: *tulpinile plantelor, presa cu tăvălugi, stoarcere, suc, parametrii, modele matematice, optimizare*

INTRODUCERE

Veridicitatea argumentării teoretice a parametrilor presei pentru stoarcerea sucului din tulpinile plantelor poate fi confirmată prin cercetări experimentale. Însă sursele existente de informaţie [2, 4, 6, 7, 8, 9] practic nu conţin date experimentale privind valorile eficiente ale parametrilor presei pentru stoarcerea sucului. Prin urmare, scopul prezentei lucrări este argumentarea experimentală şi optimizarea parametrilor presei, destinate stoarcerii mecanice a sucului din tulpinile de sorg zaharat.

MATERIAL ŞI METODĂ

În lucrarea [1] sunt descrise schema constructivă şi parametrii tehnici cu caracter general ale preselor cu tăvălugi, însă lipsesc metodica calculării şi argumentarea parametrilor tehnologici ai procesului de stoarcere mecanică a sucului. De aceea, ţinând cont de recomandări teoretice, au fost calculaţi parametrii tehnologici şi constructivi. Ulterior pentru obţinerea valorilor optime ale jocului ***S*** în pasajul de stoarcere, forţei de presare P, turaţiilor n ale tăvălugilor au fost măsuraţi gradul de extragere a sucului GE, productivitatea Q_{mv}, puterea consumată N. Rezultatele cercetărilor prealabile permit a presupune existenţa nelinearităţii a funcţiei de replică şi existenta acţiunilor reciproce ale factorilor.

Din această cauză a fost folosit plan B_3 (Box-Benkin) [3].

Niveluri de variere ai factorilor sunt prezentaţi în tabel 1, unde X_1 - jocul iniţial în pasajul de stoarcere, mm; X_2 – forţa de presare, P, kN; X_3 – turaţiile tăvălugilor n, min^{-1}

Pentru cercetări au fost utilizate tulpinile întregi şi tocate ale sorgului zaharat, defoliate şi fără panicule, cu umiditatea 71% şi fracţia masică a zahărului în suc 12%. Presa a fost alimentată uniform cu tulpini, asigurând valorile necesare ale factorilor.

Table 1

Levels of factor variation (plan B_3)

Levels	Code	Factor values		
		X_1 [mm]	X_2, [kN]	X_2 [min^{-1}]
Base	0	6.5	120	11
Superior	+1	10.0	150	15
Inferior	-1	3	90	7
Interval	-	3.5	30	4

The research have been performed on the press model with 3 rollers (Figure 1 a), the exploitation tests - on the technological line for processing sorghum, which comprises 3 blocks for compression (figure 1, b, c).

The model machine for squeezing juice (Figure 1 a) includes hopper container 1, block 2 with two power rollers and crushing strains, transporter 3, block 4 with three pressed rollers, operating mechanism 5 and guidance system 6.

Cercetările au fost efectuate pe macheta presei cu 3 tăvălugi (fig.1, a), încercările de exploatare – pe linia tehnologică pentru procesarea sorgului zaharat, care include 3 blocuri de presare (fig.1, b,c).

Macheta utilajului pentru stoarcerea sucului (fig.1, a) include buncărul recipient 1, blocul 2 cu doi tăvălugi de alimentare şi strivire a tulpinilor, transportorul 3, blocul de presare 4 cu trei tăvălugi, mecanismul de acţionare 5, sistemul de dirijare 6.

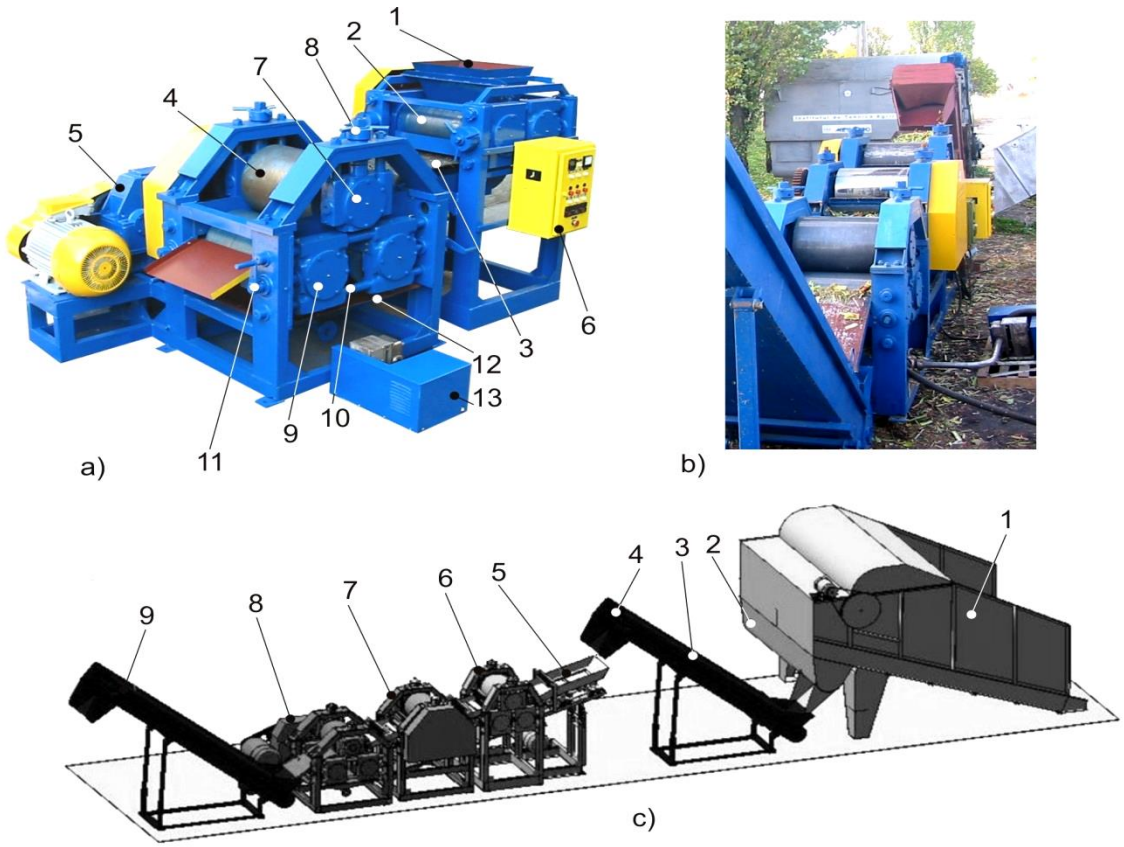

Fig.1 - Equipment ITA „Mecagro" for pressing sweet sorghum
a - model press *(1 – hopper container, 2 – the power supply, 3 – transporter, 4 – pressing block, 5 – mechanism of action, 6 – routing system, 7, 9 – bearings, 8 - nuts, 10 - the guide rods, 11 – screw, 12 - container, 13 – pump);*
b,c – technological line *(1 – receiving aggregate, 2 – conveyer -slug, 3 – feed conveyor, 4 – aerodynamics separator, 5 – dispenser vibrant, 6,7,8, - presses rollers, 9 – scraper conveyor)*

In the pressing block 4 of the upper pressure roller is being placed on two bearings 7, each one of those being installed on two vertical guide rods. On the superior side 7 of the bearings operate arc-disc collection camps which are being adjusted with nuts 8. Each of the following rollers is installed on two bearings 9, mobile mounted horizontally with guide rods 10.

Adjusting the clearance between rollers is obtained by moving the lower rollers on the guide lines with the help of screw mechanisms 11. The speed control is performed by changing the gear ratio and electric frequency current with the help of an inverter. Squeezed juice accumulates in the vessel 12, where it is discharged with pump 13.

The technology line for squeezing juice from sweet sorghum is composed by (Figure 1, b, c) the aggregate 1 (Volum-15 m^3) for the reception and distribution of raw materials, worm - conveyor 2, power scraper system conveyor 3, aerodynamic separator 4, vibrant dispenser 5, press 6, 7, 8 with three rollers each for squeezing juice, discharge conveyor 9 for evacuating and putting in transport vehicles.

În blocul de presare 4 tăvălugul superior este amplasat pe două lagăre 7, fiecare din acestea fiind instalat pe două tije verticale de ghidare. Pe partea superioară a lagărelor 7 acţionează arc-discuri, strângerea cărora este reglată cu piuliţe 8. Fiecare din tăvălugii de jos este instalat pe două lagăre 9, montate mobil pe tije orizontale de ghidare 10.

Reglarea jocului dintre tăvălugi se obţine prin deplasarea tăvălugilor inferiori pe ghidaje cu ajutorul mecanismelor cu şurub 11. Reglarea turaţiilor tăvălugilor de presare se efectuează prin schimbarea raportului de transmisie şi a frecvenţei curentului electric cu ajutorul invertorului. Sucul stors se acumulează în recipientul 12, de unde este evacuat cu pompa 13.

Linia tehnologică pentru stoarcerea sucului din sorg zaharat are în componenţa sa (fig.1, b,c) agregat 1 (Volum-15 m^3) pentru recepţia şi distribuirea materiei prime,transportor-melc 2, transportor de alimentare cu raclete 3, separator aerodinamic 4, dozator vibrant 5, prese 6, 7, 8 cu trei tăvălugi fiecare pentru stoarcerea sucului, transportor 9 pentru evacuarea bagasei în mijloace de transport.

During the experiments, there have been determined the squeezing degree (extraction) of juice *GE*, productivity Q_{mv}, specific energy consumption C_e depending on the pressure force *P*, the clearance between rollers *s* and rollers rotation speed *n*, various laden conditions of G_i press, how fragmented passages strains go forward into spin (longitudinal, transverse, mixed).

The squeezing juice was determined using the formula:

În cadrul experimentelor au fost determinate gradul de stoarcere (extragere) a sucului *GE*, productivitatea Q_{mv}, consumul specific de energie C_e în dependenţă de forţa de presare *P*, jocul dintre tăvălugi *s*, viteza de rotaţie a tăvălugilor *n*, gradul de încărcare a presei G_i modalitatea de înaintare a tulpinilor fragmentate în pasajele de stoarcere (longitudinal, transversal, mixt).

Gradul de stoarcere a sucului a fost determinat după formula:

$$GE = \frac{m_s}{m_v} \cdot 100\% = \frac{m_v - m_b}{m_v} \cdot 100\%, \quad (1)$$

where: m_v - the amount of green mass, kg;
m_s - mass of juice, kg;
m_b - bagasse mass (squeezed stems), kg.

Press productivity was calculated using the formula:

unde: m_v - cantitatea de masă verde, kg;
m_s - masa sucului, kg;
m_b - masa bagasei (tulpinilor stoarse), kg.

Productivitatea presei a fost calculată după formula:

$$Q = \frac{m_v}{\tau}(kg/s) = 3{,}6\frac{m_v}{\tau}(t/h), \quad (2)$$

where: τ - pressing duration, s.

The specific energy consumption:

unde: τ – durata presării, s.

Consumul specific de energie:

$$C_e = \frac{E}{m_v}(kWh/kg) = \frac{E \cdot 1000}{m_v}(kWh/t), \quad (3)$$

where E - energy consumption, kWh.

Press force *P* was determined by the size of deformation arc - disc standard (calibrated) above. The clearance between the rollers was spy measured by feeler gauge. In order to determine the mass of samples were used electronic balance scales Alex, Kern with ±1% error. Power and energy consumption were determined with inverter (model EI–S9001) and K505 measuring block, length of time - with timer (model SOP type pr-2a-2-010).

The pressing force *P* depends on the arc-deflection degree of the discs, which are located in the lateral supports of the upper roller (fig. 1) and can be assembled one by one (fig. 2, a) or in package couples (fig. 2, b). Compressive modulus of each arc disc *E* = 57.5 kN / mm. Researches were performed with three different arc-disc assembly (in packages of 2,3,4 couples), which ensures the maximum values of technological parameters: a) s_{max} = 19 mm, P_{max} = 180kN; b) s_{max} = 14 mm, P_{max} = 270 kN; c) s_{max} = 9mm, P_{max} = 360kN.

unde E – consum de energie, kW·h.

Forţa de presare *P* a fost determinată după mărimea deformării arc – discurilor etalonate (calibrate) anterior. Jocul dintre tăvălugi s-a măsurat cu lere spioni. Pentru determinarea masei probelor s-au utilizat balanţe electronice Alex, Kern cu incertitudinea de măsurare ±1%. Puterea şi energia consumate au fost determinate cu invertor (model EI–S9001) şi blocul de măsurare K505, durata de timp - cu cronometru (model SOP pr-2a-2-010).

Forţa de presare *P* depinde de gradul deformării arc-discurilor, care sunt amplasaţi în suporturi laterali ai tăvălugului superior (fig. 1) şi pot fi asamblaţi câte unul (fig. 2,a) sau mai multe cupluri în pachet (fig. 2,b). Modulul de elasticitate la compresiune al fiecărui arc-disc *E* = 57,5 kN/mm. Cercetările au fost efectuate cu trei variante de asamblare a arc-discurilor (în pachete câte 2,3,4 cupluri), care asigură respectiv valorile maxime ale parametrilor tehnologici: a) s_{max} = 19 mm, P_{max} =180kN; b) s_{max} =14 mm, P_{max} = 270 kN; c) s_{max} = 9mm, P_{max} = 360kN.

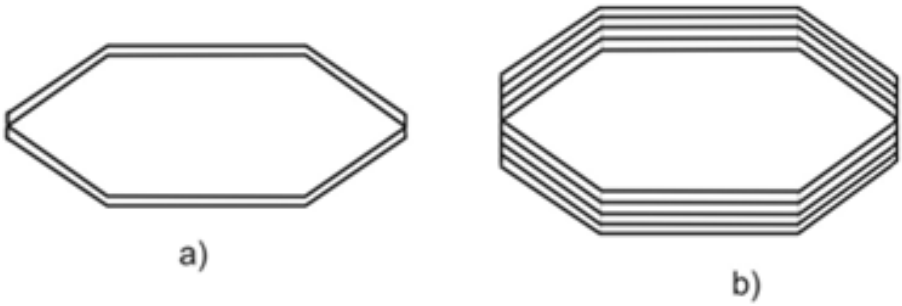

Fig. 2 - Placement scheme of arc-disc package:
a) as 1 couple; b) as 4 couples

In the process research diameter of rollers, took constant value (D=470 mm), which provides preliminary calculations and research training in the passage strains of sorghum and expected work productivity (Q_{MV} = 10t / h).

For mathematical relationships was used Statgraphics Centurion XVI software, Version 1.16.17 (32-bit).

În procesul cercetărilor diametrul tăvălugilor a avut valoare constantă (D=470 mm), care conform calculelor şi cercetărilor prealabile asigură antrenarea tulpinilor de sorg zaharat în pasaj şi productivitatea de lucru scontată (Q_{mv} =10t/h).

Pentru stabilirea relaţiilor matematice a fost utilizat soft-ul STATGRAPHICS Centurion XVI, Version 16.01.17 (32-bit).

RESULTS

After mathematical processing of the experimental results, is obtained the regression equation that adequately expresses the degree of mechanical development of the juice extraction *GE* based on pressing technological regimes:

REZULTATE

După procesarea matematică a rezultatelor experimentelor este obţinută ecuaţia de regresie, care adecvat exprimă evoluţia gradului de extragere mecanică a sucului *GE* funcţie de regimurile tehnologice de presare:

$$GE = -57.4 + 6.86x_1 + 0.43x_2 + 6.5x_3 - 0.477x_1^2 - 0.0012x_2^2 - 0.34x_3^2 \quad (4)$$

From the analysis of the mathematical model (4), graphically shown in Figure 3, results the correctness of theoretical argumentation, which demonstrates that the extraction degree *GE* increases with report decreasing ***s/h*** (the passage game / initial layer thickness). This may be possible due to the increased labor force pressing P. Increasing force P in the range of 90 ÷ 130 kN results in faster growth of GE degree than in the range of P = 130÷150 kN.

This can be explained by the fact that in the range P = 130 ÷ 150 kN P occurs the intense increase compression plant mass coefficient, $K = \gamma_s / \gamma$. (volumetric mass of the raw material and mass squeezed respectively, kg / m³)

Same phenomenon occurs in the situation of increased loading application on corn strains [9].

The low initial game between rollers (s≈3 mm) can create conditions for pressing irregular coating raw materials: stems with increased diameters are pressed to a greater extent. Increasing the pressing force P reduces the non-uniformity of strains (fig. 3). Initially game range values of Sin = 5 ÷ 7 mm ensures the highest degree of extraction. Increasing game up to 10 mm again will reduce application of pressing uniformity forces.

Din analiza modelului matematic (4), prezentat grafic în figura 3, rezultă corectitudinea argumentărilor teoretice, care demonstrează că gradul de extragere GE creşte concomitent cu diminuarea raportului ***s/h*** (jocul în pasaj/grosimea iniţială a stratului). Aceasta este posibil datorită majorării forţei de presare *P*. Majorarea forţei *P* în diapazonul 90 ÷130 kN are drept consecinţă creşterea mai rapidă a gradului GE, decât în diapazonul P = 130 ÷ 150 kN.

Aceasta se poate de explicat prin faptul că în diapazonul P=130 ÷ 150 kN are loc majorarea intensă a coeficientului de comprimare a masei vegetale $K = \gamma_s / \gamma$. masa volumetrică a materiei prime şi respectiv masei stoarse, kg/m³).

Fenomenul identic are loc şi în cazul aplicării sarcinii majorate asupra tulpinilor de porumb [9].

Valoarea mică a jocului iniţial dintre tăvălugi (s≈3 mm) creează condiţii pentru presarea neuniformă a stratului de materia primă: tulpinile cu diametrele majorate sunt presate în măsura mai mare. Mărirea forţei P reduce neuniformitatea presării tulpinilor (fig. 3). Jocul iniţial cu intervalul valorilor Sin =5÷7 mm asigură cel mai înalt grad de extragere. Majorarea jocului până la 10 mm din nou reduce uniformitatea aplicării forţelor de presare.

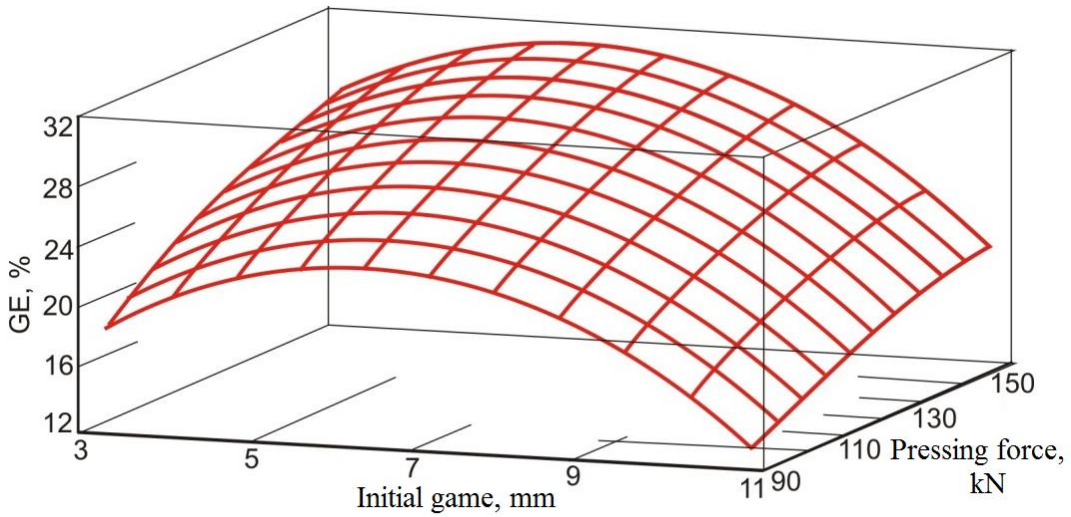

Fig. 3 - The degree of juice extraction from stems of sorghum based on technological press regimes (roller speeds n = 11 min^{-1})

The second power of independent variables (equation 1) forms the surface response curve (Figure 3) having the reverse influence, which is the strongest in the original game (x_1^2) and roller speeds (x_3^2). Following the dominant influence effects on the extraction degree (fig.4) allows to be determined the character of technological regimes (S_{in}, *P, n*) influence on *GE* and critical points coordinates.

Variabilele independente la puterea a doua (ecuaţia 1) formează curbura suprafeţei de replică (fig.3), având influenţă inversă, care este cea mai puternică din partea jocului iniţial (x_1^2) şi turaţiilor tăvălugilor (x_3^2).

Urmărirea influenţei efectelor dominante asupra gradului de extragere (fig.4) permite să fie determinate caracterul influenţei regimurilor tehnologice (S_{in}, *P, n*) asupra *GE* şi coordonatele punctelor critice.

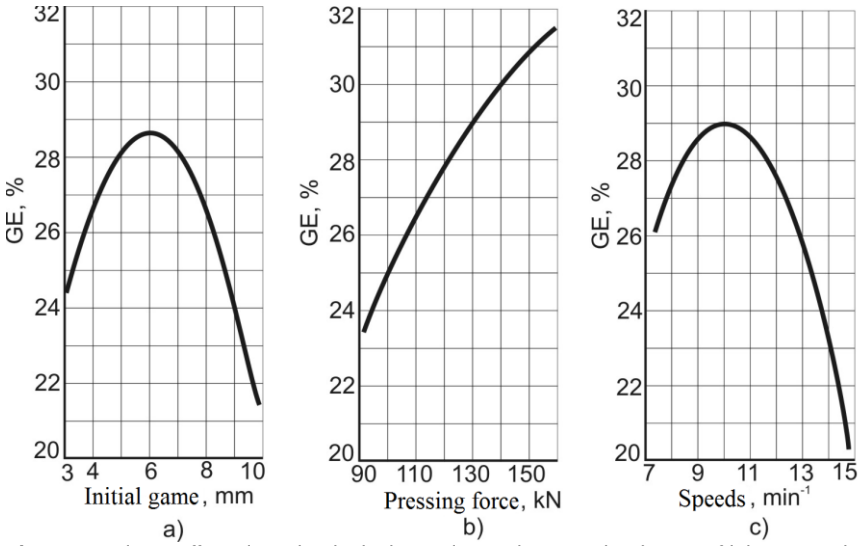

Fig. 4 - Dominant effects in technological pressing regimes on the degree of juice extraction

Using higher engine speed values by 10 ÷ 11 min^{-1} to reduce the extraction degree from 28 ÷ 29% to 20% of the decrease in the weight proportion of the influence period concerning the force of pressing plant. This phenomenon increases also the hydraulic resistance to the flow of juice.

Therefore, maximum values of extraction level are obtained with the initial game between rollers Sin = 5÷7 mm, speeds rollers n = 10 ÷ 11 *min*$^{-1}$, with the pressing force P ≤ 150 kN.

The dependence of the pressing productivity process Q_{mv}, by the three factors (initial game, roller pressing force and speed) is reflected in the next regression equation (5):

Utilizarea turaţiilor cu valori mai mari de 10 ÷ 11 min^{-1} reduce gradul de extragere de la 28÷29% până la 20% din cauza scăderii proporţionale a perioadei de influenţă asupra masei vegetale a forţei de presare. Acest fenomen majorează şi rezistenţa hidraulică la curgerea sucului. Aşadar, valori maxime ale gradului de extragere se obţin cu jocul iniţial între tăvălugi s_{in} = 5÷7 mm, turaţiile tăvălugilor *n*=10÷11 min^{-1}, forţa de presare *P* ≤ 150 kN.

Dependenţa productivităţii procesului de presare Q_{mv} de cei trei factori (jocul iniţial, forţa de presare şi turaţia valţurilor) este reflectată în ecuaţia de regresie (5):

$$Q_{mv} = 0.3 + 0.946x_1 - 0.086x_2 + 0.49x_3 - 0.0659x_1^2 + 0.032x_1x_3 + 0.0004x_2^2 + 0.0038x_2x_3 - 0.028x_3^2 \quad (5)$$

Analysis of the model (5), as shown in Figure 5, demonstrates, as it was expected, from a theoretical analysis, a dependence of productivity Q_{mv} productivity on technological regimes. The strongest influence on Q_{mv} have speeds rollers: increasing n from 7 min^{-1} to 15 min^{-1} increases almost proportionately the productivity (from 4.8 t / h to 9.0 t / h) (Figure 6). A small decrease of the gradient of growth of productivity at high speeds is probably due to strains on the surface of the slip rollers. Productivity dependence on the initial game is more complex, as increasing (S_{in}, P) enables growth of h thickness with raw material and only afterwards - increasing the productivity.

By changing the initial slack within 3 ÷ 10 mm productivity is increased from 5.4 up to 7.9 t / h (Fig.6a). The force P applied to press-drive sector of the length L is determined from the formula:

Analiza modelului (5), prezentat în figura 5, demonstrează, precum a şi fost de aşteptat din analiza teoretică, dependenţa productivităţii Q_{mv} de regimurile tehnologice. Cea mai puternică influenţă asupra Q_{mv} au turaţiile tăvălugilor: majorarea turaţiei *n* de la 7 min^{-1} până la 15 min^{-1} sporeşte productivitatea aproape proporţional (de la 4,8 t/h până 9,0 t/h) (fig.6). O scădere mică a dinamicii de creştere a productivităţii la turaţii mari se datorează, probabil, patinării tulpinilor pe suprafaţa tăvălugilor. Mai complexă este dependenţa productivităţii de jocul iniţial, deoarece majorarea (S_{in}, *P)* permite creşterea grosimii stratului *h* al materiei prime, numai după aceasta – mărirea productivităţii.

Cu schimbarea jocului iniţial în limita 3÷10 mm productivitatea creşte de la 5,4 pînă la 7,9 t/h (fig.6a). Forţa P aplicată asupra sectorului de antrenare-presare cu lungimea *l* se determină din formula*:*

$$P = p_m \cdot l \cdot b \quad (6)$$

where :

p_m - average pressure rollers on the material, N / m²;

b - width of compression zone, m.

Since the experiments *b* width had a constant value, increasing force *P* (for each specific value of the game *s* of the rollers) was possible by adding specific quantity (Q_{MV} productivity) of the raw material, which influenced the increasing of the raw thickness *h*, increasing the

unde:

p_m – presiunea medie a tăvălugilor asupra materialului, N/m²;

b – lăţimea zonei de presare, m.

Deoarece în experimentele efectuate lăţimea *b* a avut valori constante, majorarea forţei *P* (pentru fiecare valoare concretă a jocului *s* dintre tăvălugi) a fost posibilă prin adăugarea cantităţii specifice (productivităţii Q_{mv}) a materiei prime, care a influenţat creşterea valorilor grosimii stratului *h*, lungimii sectorului de antrenare-

drive-pressing length sector, *l*, and mean pressure p_m.

Therefore, the increase of the pressing force P of 90 to 150 kN results in increased productivity within 6.5÷9.2 t/h (Fig. 6b), and at the same time the degree of extraction *GE* - 23.5 ÷ 31.5 % (fig. 4b).

Independent variables at the second power cause surface curvature of the response, being the highest in changing the original game. This is probably due to reduced mass bulk layer strains for S_{in} = 9 ÷ 10 mm.

presare, *l,* şi presiunii medii p_m.

Prin urmare, majorarea forţei de presare *P* de la 90 până 150 kN are drept consecinţă creşterea productivităţii în limita 6,5÷9,2 t/h (fig. 6b) şi concomitent gradului de extragere *GE* – 23,5÷31,5 % (fig. 4b).

Variabilele independente la puterea a doua determină curbura suprafeţei de răspuns, ea fiind mai înaltă la schimbarea jocului iniţial. Aceasta se întâmplă, probabil, din cauza scăderii masei în vrac a stratului de tulpini pentru S_{in} = 9÷10 mm.

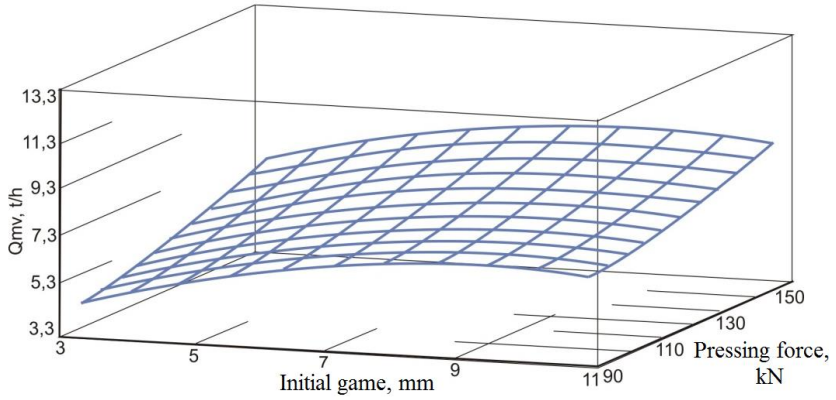

Fig. 5 - Productivity process of the juice extraction according to the technological regimes (roller speeds n = 11 min^{-1})

Following the influence of dominant effects (Figure 6) makes the determination possible to establish the coordinates of the critical points and character of the technological influence on productivity pressing process.

Under the investigated conditions, for the maximum productivity (Q_{mv} ≈ 9.3 t / h) can be obtained with the original game Sin = 9 ÷ 10 mm, the pressing force - P ≤ 150 kN, speed - n = 15 min^{-1}. Final recommendations regarding the optimal values of the technological regimes can be done on the basis for joint analysis of all technical and economic parameters, including power consumption.

Power required to drive the torque rollers depends on technological regimes studied conforming to the model.

Urmărirea influenţei efectelor dominante (fig.6) face posibilă determinarea coordonatelor punctelor critice şi caracterului influenţei regimurilor tehnologice asupra productivităţii procesului de presare.

În condiţiile cercetate valorile maxime ale productivităţii (Q_{mv} ≈ 9,3 t/h) pot fi obţinute cu jocul iniţial Sin = 9÷10 mm, forţa de presare - P ≤ 150 kN, turaţii – n = 15 min^{-1}. Recomandări finale privind valorile optime ale regimurilor tehnologice se poate de făcut în baza analizei comune a tuturor parametrilor tehnico-economici, inclusiv puterii consumate.

Puterea necesară pentru acţionarea cuplului de tăvălugi depinde de regimuri tehnologice în condiţii cercetate conform modelului.

$$N = 3.83 - 0.53x_1 - 0.047x_2 - 0.043x_3 + 0.05x_1^2 + 0.0003x_2^2 + 0.004x_2x_3 + 0.013x_3^2 \quad (6)$$

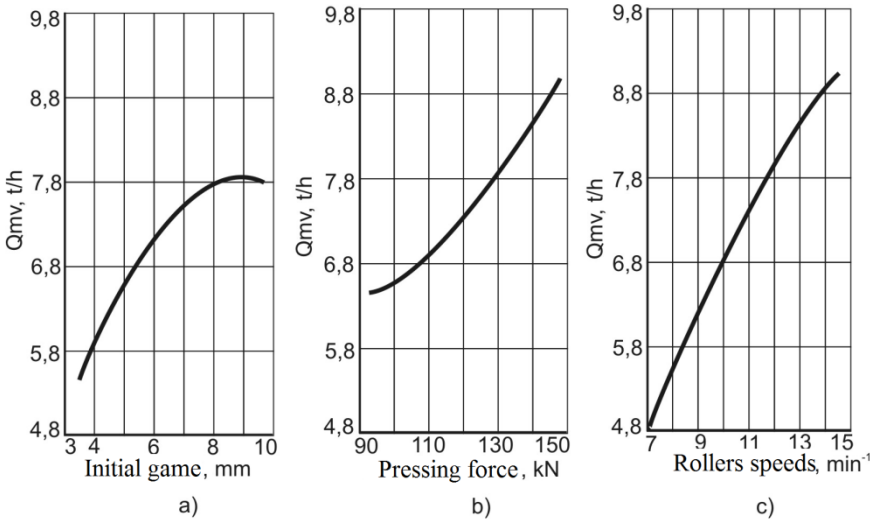

Fig. 6 - Dominant effects of technological regimes on productivity of the pressing process

The results obtained show the minimal impact on the power consumption of the S_{in} initial game (fig.7) and the more significant influence N of the pressing force P and the engine speed n rollers, which corresponds to the theoretical calculations, that the power consumption depends proportionally by the average pressure in the rollers contact area, raw material thickness degree, angular velocity $N = f(p_m, \Delta h, \omega)$. That is, in our case, the power N depends preponderantly by force P and speeds n.

Rezultatele obţinute demonstrează influenţa minimă a jocului iniţial S_{in} asupra puterii consumate (fig.7) şi influenţa mult mai însemnată asupra N a forţei de presare P, precum şi a turaţiilor tăvălugilor n, ceea ce corespunde calculelor teoretice, conform cărora puterea consumată la presare depinde proporţional de presiunea medie în zona de contact cu tăvălugii, gradul subţierii stratului de materie primă, viteza unghiulară: $N = f(p_m, \Delta h, \omega)$. Adică, în cazul nostru puterea N depinde prepoderent de forţa P şi turaţii n.

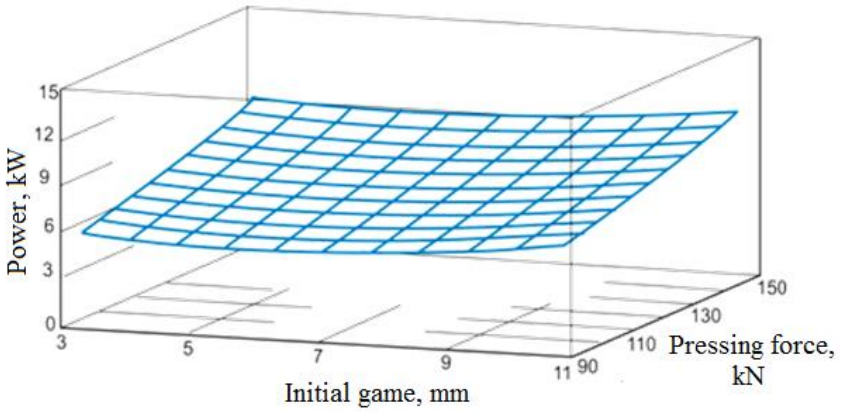

Fig. 7 - Power consumption in the process of pressing sorghum strains depending on technological regimes (n speed rollers = 11 min^{-1})

The dynamics of dominant effects influence demonstrates that changing the original game within S_{in} = 3 ÷ 10 mm limits of power consumption, N, remains at 7.4 ± 0.4 kW (fig.8) and increase pressure force from 90 to 150 kN enhances power consumption in the range of 5.4 ÷ 9.4 kW. The greatest influence has the speed rollers: they are increasing from 7 to 15 min^{-1} is due to increased consumption from 4.4 to 10.2 kW.

The conducted researches have allowed optimal technological argumentation parameters by mechanical squeezing juice from sorghum stems. Under the conditions studied the optimal initial game S_{in} = 5.5 ÷ 7.5 mm ensure the maximum degree extraction of GE and productivity Q_{mv}, little influence on the power N. Pressing force P value ≤ 150 kN allows to achieve the maximum possible values of GE and Q_{mv} requiring maximum power consumption.

Dinamica influenţei efectelor dominante demonstrează că, cu schimbarea jocului iniţial în limita S_{in} =3÷10 mm puterea consumată N se menţine la nivel de 7,4 ± 0,4 kW (fig. 8.), iar majorarea forţei de presare de la 90 până 150 kN sporeşte consumul puterii în diapazonul 5,4 ÷ 9,4 kW. Cea mai mare influenţă au turaţiile tăvălugilor: mărirea acestora de la 7 până 15 min^{-1} este cauza creşterii consumului de la 4,4 până 10,2 kW.

Cercetările efectuate permit argumentarea valorilor optime ale parametrilor tehnologici de stoarcere mecanică a sucului din tulpinile sorgului. În condiţiile studiate valoarea optimă a jocului iniţial S_{in} = 5,5 ÷ 7,5 mm asigură valorile maxime ale gradului de extragere GE şi productivităţii Q_{mv}, puţin influenţând asupra puterii N. Valoarea forţei de presare P ≤ 150 kN permite a obţine valorile maxim posibile ale GE şi Q_{mv}, necesitând şi consumul maxim al puterii.

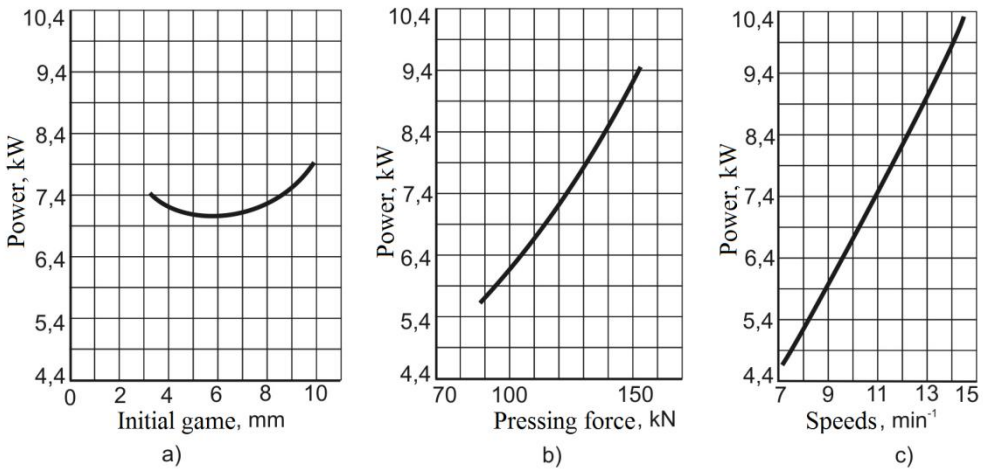

Fig. 8 - Dominant effects of technological regimes regarding the power consumption

The recommended amount of speed rollers is n = 10 ÷ 11min^{-1}, providing, in first place, the maximum degree of extraction.

CONCLUSIONS

1. Experimental research results show the correctness of the theoretical argumentation of the basic constructive scheme and functional parameters of the press for squeezing juice.
2. Mathematical models obtained under experimental research for determining the optimal values of process parameters for squeezing juice from sweet sorghum stems, using press rollers: first game between the first passage by squeezing rollers: 5.5 ÷ 7.5 mm, the pressing force: 140 ÷ 150 kN roller speeds: 10 ÷ 11 min^{-1} (linear speed: 0.246 ÷ 0.27 m/s).

REFERENCES

[1]. Antohe I., (2006) - *Sorghum culture and total industrialization. Perspectives for sustainable development of Romanian agriculture,* Chiminform, p.302, Bucharest, ISBN 973-88183-1-1; 978-973-88183-1-6.
[2]. Grassi G, Pietro Moncada P.C., Henri Z., (1992) - *Promising industrial energy crop: Sweet Sorghum. Recent developments in Europe*, Commission of the European Communities, p.73;
[3]. Hailis G.A., Kovalev M.M., (1994) - *Agricultural technology research and experimental data.* Spic Publishing House Moscow, p.170;
[4]. Korolev A.A., (1969) - *Construction and calculating the laminate machines and mechanisms.* Publisher Metallurg, Moscova, p.277;
[5]. Sapronov A.R., (1983) - *Sugar technology*. Publisher Food and Consumer Industry Publishing, Moscova, 292;
[6]. Smith et al., (1987) - *Evolution of Sweet Sorghum for fermentable Sugar production Potential.* In: Crop Science, vol. 27, nr. 4, 1, pg.788-790;
[7]. Sokolov A., (1969) - *Basis of calculation and design for vending machines and food production,* Publishing: Machinery Manufacturing Industry, Moscova, p.640;
[8]. Stabnicov V.N., (1976) - *Food production equipment and processes.* Food Industry Publishing House, Moscova, p.664;
[9]. Şatilov K.V. et al., (1981) - *Corn harvesting machineries.* Publishing: Machinery Manufacturing Industry, Moscova, p.224.

Valoarea recomandată a turaţiilor tăvălugilor este n = 10 ÷ 11min^{-1}, asigurând, în primul rând, valoarea maximă a gradului de extragere.

CONCLUZII

1. Rezultatele cercetărilor experimentale demonstrează corectitudinea argumentărilor teoretice ale schemei constructive şi parametrilor funcţionali de bază ai presei pentru stoarcerea sucului.
2. Modelele matematice obţinute în baza cercetărilor experimentale permit determinarea valorilor optime ale parametrilor procesului de stoarcere a sucului din tulpinile sorgului zaharat, utilizând presa cu tăvălugi: jocul iniţial dintre tăvălugi în primul pasaj de stoarcere: 5,5 ÷ 7,5 mm, forţa de presare: 140 ÷ 150 kN, turaţiile tăvălugilor: 10 ÷ 11 min^{-1} (viteza liniară: 0,246 ÷ 0,27 m/s).

BIBLIOGRAFIE

[1]. Antohe I., (2006) - *Cultura sorgului zaharat şi industrializarea lui totală. Perspective pentru dezvoltarea durabilă a agriculturii româneşti,* Chiminform, 302 p., Bucureşti, ISBN 973-88183-1-1; 978-973-88183-1-6.
[2]. Grassi G, Pietro Moncada P.C., Henri Z., (1992) - *Promițător pentru culturile energetice, industriale: Sorghum dulce. Evoluțiile recente din Europa*, Comisia Comunităților Europene, 73p.;
[3]. Hailis G.A., Kovalev M.M., (1994) - *Cercetarea tehnicii agricole şi prelucrarea datelor experimentale*. Editura Spic Moscova, 170 p.;
[4]. Korolev A.A., (1969) - *Construcţia şi calculul maşinilor şi mecanismelor pentru laminoare.* Editura Metallurgia, Moscova, 277 p.;
[5]. Sapronov A.R., (1983) - *Tehnologia zahărului.* Editura Industria Alimentară şi Uşoară, Moscova, 292 p;
[6]. Smith ş.a. (1987)- *Evolutia sorgului dulce pentru potențialul de fermentație a zahărului.* In: Stiința Recoltării, vol. 27, nr. 4, 1, p. 788-790;
[7]. Sokolov A., (1969) - *Bazele calculului şi proiectării maşinilor şi automatelor în producţia alimentară*, Editura Industria Construcţiilor de Maşini, Moscova, 640 p.;
[8]. Stabnicov V.N., (1976) - *Procese şi aparate în producţia alimentară*. Editura Industria Alimentară, Moscova, p.664;
[9]. Şatilov K.V. şi alţii, (1981) - *Maşini de recoltat porumb.* , Editura Industria Construcţiilor de Maşini, Moscova, 224 p.

DEVELOPMENT OF A NEW METHOD FOR VOLUME MEASUREMENT BASED ON *MOIRÉ* TECHNIQUES
/
DESENVOLVIMENTO DE UM NOVO MÉTODO PARA MEDIDA DE VOLUME BASEADO EM TÉCNICAS DE MOIRÉ

Ph.D. Stud. Eng. Marcos V. G. Silva[1)], Prof. Ph.D. Eng. Adilson Enes[2)], Prof. Ph.D. Eng. Inácio M. D. Fabbro[1)], Ph.D. Eng. Celina de Almeida

[1)] Faculty of Agricultural Engineering, UNICAMP, Campinas, SP / Brazil [2)]Department of Agricultural Engineering, UFS, Aracaju, SE / Brazil

Tel: +55 19 3521-1059; E-mail: inacio@feagri.unicamp.br

Abstract: *This research work reports a shadow moiré method applied in generating spatial dimensions of solid figures. The focus of this work is to study as well as to turn feasible a new method of measuring object shape as plant organs. Selected experimental setup included four Ronchi optical grids out of phase by ¼ of period, a conventional white light source and a digital camera. The samples were hold by a support, following by data acquisition process generating four elevation digital models (EDM). EDM were employed to create the tridimensional Model (TM) which, in turn, was also applied to generate the object volume. The method of water volume displacement has been used for data comparison in which the change of liquid volume is equal to the object volume. The results allowed to state that moiré techniques can be used for volumetric determination of irregular objects as fruits and others vegetable organs. The work includes error determination.*

Keywords: *fruit shape determination, shadow moiré technique, fruit classification*

INTRODUCTION

Nowadays the techniques devoted in measuring volume, shape and surface profile of irregular objects are supported by optical phenomena and no longer on instruments requiring physical contact. .The pertinent literature discloses a group of methods named *moiré*, in which the authors emphasize the simplicity, low cost and short time demand. Shape measuring techniques are close associated to the medical science, reverse engineering process, stress-strain analysis, quality control, mathematical modeling, thermal science, soil – tire contact area determination, plant-machine mechanical relationship, vegetable shape determination, etc. The geometric representation of an object shape in a X_i coordinate system within an acceptable tolerance limit is of unquestionable application in many subjects associated to research and technology developments, including within the agricultural process, since seedling up to harvesting, transportation and storage, as emphasized by the literature, [9], [5]; and [8] present a comprehensive study on *moiré* techniques applications in agriculture. [6] reported the application of a *moiré* technique in studying the mechanical interactions of sugarcane stalks with cutting disks. [5] presented a study on fruit packing by means of a *moiré* method. [2] presented a *moiré* model to describe plant architecture. Three dimensional shape surveys of fruits became a thematic subject, as reported by [8], [5], [17]. The pertinent literature also discloses applications of *moiré* techniques associated to mechanical properties of vegetative materials, bamboo, composites, etc, as [5], [11], [2], [17]. *Moiré* technique applied to strain as well as stress distributions in a diversity of systems, as

Resumo: Este trabalho relata o uso do método de Moiré de Projeção *com Deslocamento de Fase aplicado na geração de dimensões espaciais de figuras sólidas. O foco deste trabalho é estudar e tornar viável um novo método de medir a forma de objetos tais como órgãos de plantas. A configuração experimental selecionada consistiu em quatro grades ópticas Ronchi fora de fase por ¼ do período, uma fonte de luz branca convencional e uma câmera digital. As amostras foram detidas por um suporte, seguido pela aquisição de dados e gerar quatro modelos digitais de elevação (EDM). EDM foram utilizados para criar o modelo tridimensional (TM) que, por sua vez, também foi aplicado para gerar o volume do objeto. O método de deslocamento de volume de água foi utilizado para a comparação de dados, tendo em conta que a variação do volume de líquido é igual ao volume do corpo de prova. Os resultados permitiram afirmar que as técnicas de moiré podem ser empregadas para determinar o volume de objetos irregulares como frutas e outros órgãos vegetais. O trabalho inclui a determinação de erro.*

Palavras-chave: *frutas determinação forma, técnica de moiré de sombra, classificação de frutas*

INTRODUÇÃO

Hoje em dia as técnicas consagradas na medição de volume, forma e perfil de superfície de objetos irregulares são auxiliadas por fenômenos ópticos e não tanto por instrumentos baseados em contato físico. A literatura revela um grupo de métodos denominados *moiré*, em que os autores enfatizam a simplicidade, baixo custo e baixa demanda de tempo. As técnicas medição de superfícies estão normalmente associadas à ciência médica, nos processos de engenharia reversa, análise de tensão-deformação, controle de qualidade, modelagem matemática, ciências térmicas, determinação da área de contato de pneu -solo, relação mecânica máquina-planta, determinação da forma vegetal, etc. A representação geométrica da forma do objeto em um sistema de coordenadas X_i dentro de um limite de tolerância aceitável é de aplicação inquestionável em muitos assuntos relacionados com a pesquisa e desenvolvimentos tecnológicos, inclusive dentro do processo agrícola, desde o plantio até a colheita, transporte e armazenamento, conforme enfatiza a literatura, [9], [5] e [8] apresentam um estudo abrangente sobre as aplicações técnicas de *moiré* em engenharia agrícola. [6] relataram a utilização de uma técnica de *moiré* no estudo das interações mecânicas dos caules de cana com discos de corte. [5] apresentam um estudo sobre embalagens de frutas por meio de um método de *moiré*. [2] apresentou um modelo *moiré* para descrever a arquitetura da planta. O levantamento tridimensional da forma de frutas tornou-se um assunto temático, conforme relatado por [8], [5], [17]. A literatura pertinente também revela aplicações das técnicas de *moiré* associadas às propriedades mecânicas dos materiais vegetais, bambu, compósitos etc. [5]; [11]; [17] e [2]. A técnica de *moiré* aplicada a deformações, bem como a distribuição de tensões em uma diversidade de sistemas,

wood structure, soil-tire, soil mechanical test, etc, has been reported by [2] and [7]. Applications of *moiré* methods in animal material have reported by [5]. [13] reported the application of *moiré* methods in thermal analysis. A recent research work reported by [9] emphasizes the association of the ANSYS software with phase translation moiré technique in generating the three dimensional coordinates of solid bodies.

The name *moiré* has its origin in the French language, referring to *wave like pattern.* When screens of same mesh density are superposed, fringes are generated which move when their relative positions are displaced [16]. Lord Rayleigh, 1874 [12] proposed the application of a *moiré* technique in testing diffraction grids. Mulot (1925) [12] applied that technique in studying deformations of mica layers. Later on, Tollenar (1945) [12] reported that *moiré* fringes could be used to magnify displacements, being also suitable as a photoelastic method.

Recent reports present comprehensive classifications of the methods termed as *moiré. Moiré* methods include a large number of techniques as *shadow moiré*, *projection moiré* and others as reported by Meadows et al and Takasaki [4]. Projection *moiré* consists in positioning a pair of grids in front of a light source and by moving the reference grid to modulate the light beam amplitude will generate interference pattern fringes on the object surface. Projection *moiré* with phase shift is a high precision technique, consisting in shifting the camera grid phase against the projecting grid [4]. [8] reports a successful application of a projection *moiré* technique in surveying plant organs shape. A digital projection *moiré* would employ a direct grid projection and superimposition onto the object surface by means of multimedia equipment following by image capturing and demodulation.

[4] states that two images are necessary, being one on the reference plane and the second one on the object surface, however when a spatial parallel phase shift is used only one interferogram is required for image analysis. If a grid is positioned between the object and the light source, its shade will be observed onto the object surface, in which the interference between grid lines and the shade grid will generate the moiré fringes, which reproduces the object contour.

A phase shift is generated by changing the distance between the object and the grid or by the translation of the grid on its own plane. A useful tool consists in generating a grid with varying gray level [4].

Grid modulation intensity is given by:

como estrutura de madeira, solo-pneu, testes em mecânica de solo, etc, tem sido relatada por [2] e [7]. Aplicações de métodos de *moiré* em material animal já foi relatado por [5]. [13] relataram a utilização de *moiré* em métodos de análise térmica. Um trabalho de investigação recente relatada por [9] enfatiza a associação do programa ANSYS utilizando a técnica *moiré* com variação de fase para gerar as coordenadas tridimensionais de corpos sólidos.

O nome *moiré* tem sua origem na língua francesa, referindo-se a onda como padrão. Quando grades de mesma densidade de malha são sobrepostas, franjas são geradas que se movem quando suas posições relativas são deslocadas [16]. Lord Rayleigh, 1874 [12] propuseram a aplicação de uma técnica de *moiré* em grades de difração. Mulot (1925) [12] aplicou essa técnica para estudar as deformações de camadas de mica. Mais tarde, Tollenar (1945) [12] relatou que a defasagem da franja pode ser utilizada para ampliar os deslocamentos, sendo também apropriado como um método fotoelástico.

Relatórios recentes apresentam classificações completas dos métodos denominados como *moiré*. Métodos de *moiré* incluem um grande número de técnicas como *moiré* sombra, projeção moiré e outros, conforme relatado por Meadows et al e Takasaki [4]. *Moiré* de projeção consiste em projetar uma grade utilizando uma fonte de luz em um plano de referencia e posteriormente no objeto, a sobreposição das duas grades gera padrão de franjas na superfície do objeto. *Moiré* Projeção com deslocamento de fase é uma técnica de alta precisão, que consiste no deslocamento da fase de alimentação da câmara em relação à grade que se projeta [4]. [8] relata uma aplicação bem-sucedida de uma técnica de *moiré* de projeção no levantamento da topográfica da planta. No *moiré* de projeção digital emprega-se uma projeção de grade direta e sobreposição na superfície do objeto por meio de equipamentos de multimídia seguidos por captura de imagens e demodulação.

[4] afirma que duas imagens são necessárias, sendo uma no plano de referência e a segunda na superfície do objeto, no entanto, quando uma mudança de fase em paralelo espacial apenas um interferograma é necessário para a análise das imagens. Se uma grade é posicionada entre o objeto e a fonte de luz, a sua sombra vai ser observada na superfície do objeto, em que a interferência entre as linhas da grade e a grade sombra irá gerar as franjas de *moiré*, que reproduz o contorno do objeto sendo essa técnica denominada *moiré de sombra*.

Uma mudança de fase é gerada alterando a distância entre o objeto e a grade ou a translação da grade no seu próprio plano. Uma ferramenta útil consiste na geração de uma grade com diferentes níveis de tons de cinza [4].

A intensidade de modulação da grade é dada por:

$$T(x) = \frac{1}{2} + \frac{1}{2} * \text{sen}\left(\frac{2 * \pi * x}{p}\right) \quad (1)$$

Where *T(x)* the modulation intensity and p is the grid period. Meadows et al (Degrieck, 2001) present the following equation for light intensity distribution in (x, y, z) point considering a sinusoidal grid.

Onde *T (x)* é a intensidade da frequência e p é o período de grade. Meadows et al (Degrieck, 2001) apresentam a seguinte equação para a distribuição da intensidade de luz em (x, y, z), considerando uma grade senoidal.

$$I(x,y) = \frac{I}{r^2} * \cos(\phi(x,y,z(x,y))) * \left(\left[\frac{1}{2} + \frac{1}{2} * \text{sen}\left(\frac{(2 * \pi * h1 * x)}{(p * (h1 + z))}\right)\right] * \left[\frac{1}{2} + \frac{1}{2} * \text{sen}\left(\frac{(2 * \pi)}{p} * \left(\frac{(dz + h2x)}{(h2 + z)}\right)\right]\right) \quad .....(2)$$

Where *I* is light intensity, *r* is the distance between the light source and the surface being illuminated, ϕ is the angle between the incident light beam and the normal to the surface, p is the reference grid period, *hl* is the distance between light source and the reverence

Onde *I* é a intensidade da luz, *r* é a distância entre a fonte de luz e a superfície a ser iluminada, ϕ é o ângulo entre o feixe de luz incidente e a normal à superfície, p é o período de grade de referência, *hl* é a distância entre a fonte de luz e a grade de referência, *h2* é a distância do

grid, *h2* is the distance between the observer and the reference grid. [15] reports that system non-linearity and noise occurrence might generate edge errors due to surface discontinuity in relation to the plane. The same author also reports that three or four images with different and continuous grids and sinusoidaly spaced fringes are needed to obtain object surface and contour. For three-dimensional contour determination it is generally necessary four sinusoidal grids projected onto the object surface with fringes phase varying as *0, π/2, π e 3π/2*, [15]. Image light intensity distribution for these phases is:

observador e da grade de referência. [15] relata que o sistema de não linearidade e a ocorrência de ruído podem gerar erros nas bordas devido a descontinuidade da superfície em relação ao plano. O mesmo autor também relata que três ou quatro imagens com grades diferentes e contínuas e franjas espaçadas senoidalmente são necessários para obter o contorno e a superfície do objeto. Para a determinação tridimensional do contorno são geralmente necessárias quatro grades senoidais projetadas sobre a superfície do objeto com a fase variando de *0, π/2, π e 3π/2*, [15]. As equações de distribuição de intensidade de luz para estas fases são:

$$I_1(x,y) = a(x,y) + b(x,y)\cos(\varphi(x,y)) \quad (3)$$

$$I_2(x,y) = a(x,y) + b(x,y)\cos(\pi/2 + \varphi(x,y)) \quad (4)$$

$$I_3(x,y) = a(x,y) + b(x,y)\cos(\pi + \varphi(x,y)) \quad (5)$$

$$I_4(x,y) = a(x,y) + b(x,y)\cos(3\pi/2 + \varphi(x,y)) \quad (6)$$

Where a (x, y) is the average light intensity, or background, b (x, y) is the modulation intensity and φ(x,y) the phase to be determined. Phase can be obtained from the following equation:

Onde a (x, y) é a intensidade média da luz, ou fundo, b (x, y) é a intensidade da demodulação e φ(x, y) da fase a determinar. A demodulação pode ser obtida a partir da seguinte equação:

$$\varphi(x,y) = \arctan\left(\frac{I_4(x,y) - I_2(x,y)}{I_1(x,y) - I_3(x,y)}\right) \quad (7)$$

Fringes of same period can be adjusted by changing pixel number of a projector with liquid crystal display (LCD). This fringe projection method makes easier the object contour determination [15]. Uncertainties in phase-depth conversion can generate errors on the final measurement, which limits the application of that method for some cases. Digital camera distortion also generates significant errors (Liu, 2003) cited [8]. By using a unique sinusoidal grid instead of a full grid and by translating only 1/4 of the wave period keeps the light intensity variation tendency in the same sense, minimizing the errors due to surface discontinuity in relation to the reference plane [2]. Based on what it has been explained above the objective of this work is to apply the Phase Translation Method in obtaining the three dimensional coordinates of fresh fruits.

Franjas de igual período podem ser obtidas ajustando o número de pixels de um projetor com a tela de cristal líquido (LCD). Esse método de projeção de grades torna mais fácil a determinação do contorno objeto [15]. Incertezas na conversão da fase empacotada pode gerar erros na medição final, o que limita a aplicação desse método para alguns casos. Distorção da câmera digital também gera erros significativos (Liu, 2003) apud [8]. Usando uma única grade senoidal no objeto em vez de um conjunto de quatro grades sendo as grades defasadas em um quarto do período de onda no plano de referência, minimizam os erros devidos a descontinuidade da superfície em relação ao plano de referência [2]. Baseado no que foi explicado acima o objetivo deste trabalho é aplicar o método de deslocamento de fase na obtenção das coordenadas tridimensionais de frutos

MATERIAL AND METHODS

The experimental phase of this research work was carried in the Laboratory of Optics at Faculty of Agricultural Engineering of UNICAMP, Campinas, as well as at the Laboratory of Optics at the IAC, Jundiaí, SP, Brazil. As is displayed on Figure 1, the experimental setup included a PC with Windows XP and GNU/Linux systems, a LCD NEC VT560 projector, a SAMSUNG SDC312 CCD digital camera with 640 columns and 480 lines, a digital calibrator with 0.001 mm of precision and 04 Ronchi grids, out of phase by π/2 one from each other, including the software Scilab, IMAGEJ, Rising Sun Moiré, Sisvar and AUTO CAD 2000.

Volume determination by submersion

Five testing fruits were selected for shape and volume determination. The fruits were firstly submerged in a graded testing tub of 25 ml with 2 ml of of unit scale filled with 99,3º INP alcohol, holding a replication number of five.

MATERIAL E MÉTODOS

A fase experimental deste trabalho de pesquisa foi levada a cabo no Instituto Agronômico de Campinas, em Jundiaí, como também na Faculdade de Engenharia Agrícola da UNICAMP, Campinas, SP, Brasil. O aparato experimental selecionado, como mostrado em Figura 1, incluiu um PC com Windows XP associado ao sistema GNU/Linux, um projetor LCD NEC VT560, uma câmera SAMSUNG SDC312 CCD com 640 colunas e 480 linhas, um calibrador digital com 0,001 mm de precisão e quatro grades Ronchi fora de fase π/2 um de um ao outro. Software empregado incluiu Scilab, IMAGEJ, Rising Sun Moiré, Sisvar e AUTO CAD 2000.

Determinação do volume por imersão

Foram feitas várias repetições na medição volumétrica através de imersão das sementes de mamonas em solução de Álcool Anidro Hidratado de 99,3º INP em uma Proveta de 25ml cuja graduação variava de dois em 2ml.

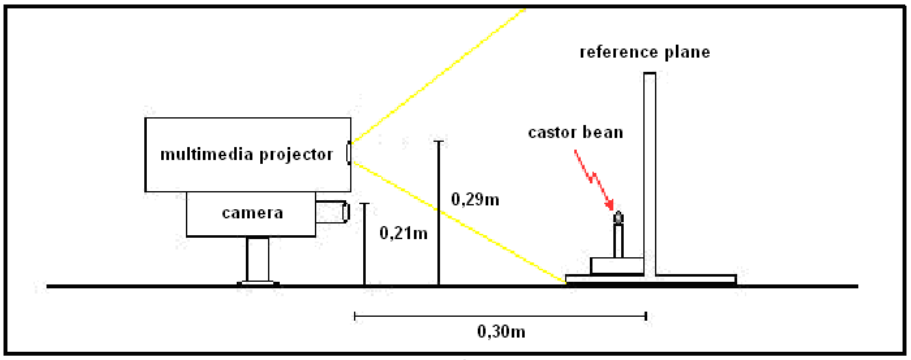

Fig. 1 - Adopted moiré experimental setup

Moiré tests

Out phase grids were denoted as G_i (i =1, 2, 3, 4), fig. 2 were projected onto a white opaque panel, generating the images P_i. However, the objected was divided into four faces, named F_i, on which the grid G_i was projected, generating the image O_i. Those images P_i and images O_i were converted to gray gradient by means of the software ImageJ. The subtraction of images O_i from P_i will generate a set of sixteen images M_i which was forwarded for filtering process by means of the ImageJ software, yielding images presented in gray gradient as well as with *moiré* fringes. The ImageJ software filtration process applies the Gaussian Blur method to eliminate the original grid, preventing, that way, undesirable interferences. The set of images M_i were then forwarded to the SCILAB software to generate the final matrix form expressed in X_i coordinates, refereeing to a unique origin *O,* expressed in millimeters.

Ensaios com *moiré*

Grades defasadas nomeadas como *Gi* (i = 1, 2, 3, 4), fig. 2 foram projetadas em um painel branco opaco, gerando as imagens *Pi*. No entanto, foi dividida em quatro faces, nomeado *Fi*, em que a grade *Gi* foi projetada, gerando a imagem *Oi*. Aquelas imagens *Pi* e imagens *Oi* foram convertidas em gradiente cinza por meio do software ImageJ. A subtração das imagens O_i de P_i gerou um conjunto de imagens M_i, que foram encaminhados para o processo de filtragem por meio do software ImageJ, produzindo imagens apresentadas no gradiente cinza, sendo essas as franjas de *moiré*. O processo de filtragem utilizando o software ImageJ aplicando o método de Gaussian Blur para eliminar a grade original, evitando, dessa forma, as interferências indesejáveis. As imagens do M_i foram então encaminhadas para o software SCILAB para gerar a forma matricial final expresso em coordenadas X_i, arbitragem para uma única origem *O*, expressa em milímetros.

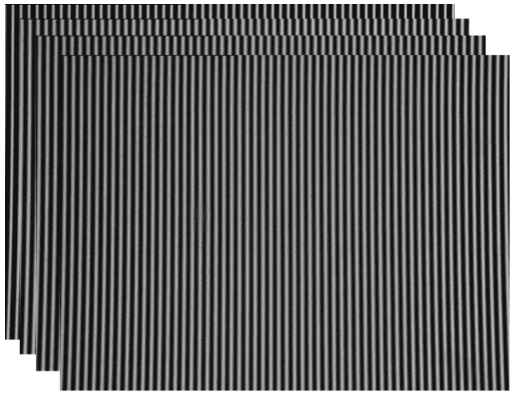

Fig. 2 - Ronchi grids named G_1, G_2, G_3 and G_4, out of phase by π/2 and referred as G_i (i= 1,2,3,4)

RESULTS

RESULTADOS

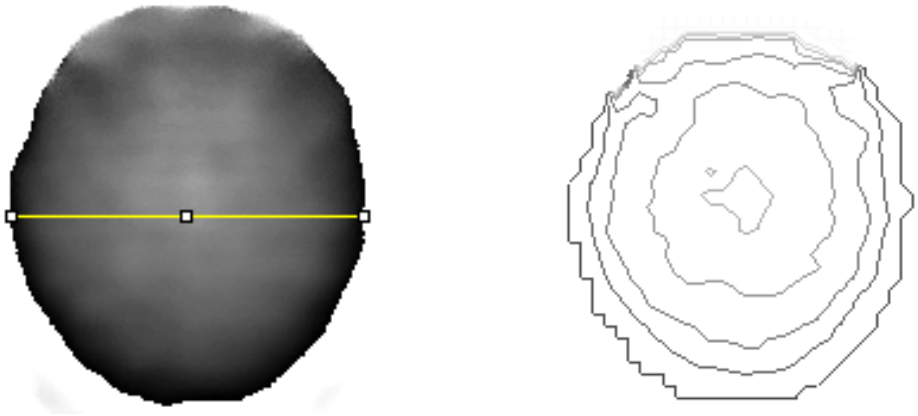

(A) (B)

Fig. 3 - Wrapped phase map, having the phase varying from -π to π. (A) Face 1 of castor bean 2. (B) Top view with contour lines

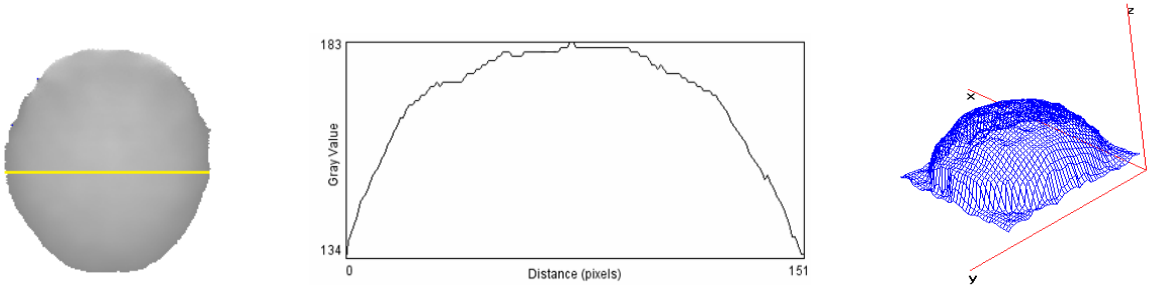

(A) (B) (C)

Fig. 4 - (A) Mde of The Castor Bean Fruit in Gray Gradient. (B) Profile Line at The Middle Point and (C) Topographic Representation

Table 1

Fruit volume values obtained from liquid displacement

Calibrator					
Seed1	**weight**	**Seed 2**	**weight**	**Seed 3**	**weight**
4.5 ml	0.689	5ml	0.778	5	0.9334
4.5ml	0.688	5ml	0.778	5	0.9323
4.5ml	0.688	5ml	0.777	5	0.9310

Table 1 indicates that the volume determination shows high precision keeping the human subjectivity at a minimum level, as indicated by the coefficient of variation with three repetitions. Figure 2 exhibits an image of the castor bean fruit generate from the unwrapped moiré fringes as processed by the Rising Sun Moiré software presented in gray scale, which vary from zero for dark color and 255 for white color to represent the body topography. Moiré results can be further generating the three-dimensional view of the fruit, as it is shown on Figure 4. Those data can lead to the volume calculation and compared with the submersion technique.

A Tabela 1 mostra os valores obtidos volumetricamente através de ensaios envolvendo comparação de deslocamento de liquido, onde a influencia da subjetividade humana, foi mínima como indicado pelo coeficiente de variação efetuadas pelas três repetições. A Figure 2 exibe uma imagem da semente de mamona, onde foi gerada a franja de *moiré* que desempacotam por meio do programa Rising Sun Moiré, que é representado em gradiente cinza. Intensidades cinza variam do zero (cor escura) para 255 (cor branca) que inclui um plano de gradiente cinza representando a topografia de objeto. Resultado do fruto gerado por *moiré* pode ser visto tridimensionalmente, na Figura 4. Esses dados podem levar ao cálculo do volume e comparado com a técnica de imersão.

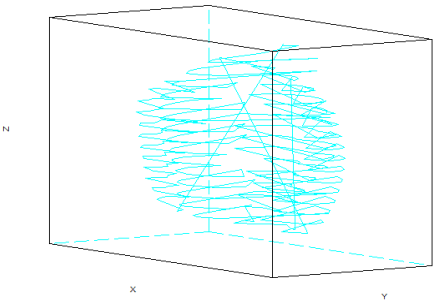

Fig. 5 - Volume representation as generated by the moiré method

CONCLUSION

Based on what it was explained before, it can be concluded that the moiré techniques are highly precise in measuring object topography, however some human factors can be inserted in the process during setup preparation as well as during the experimental data surveying.

REFERENCES

[1]. Abràmoff M.D., Magalhães P.J., Ram Sunanda J., (2004) – *Image processing with ImageJ,* Berkshire Common, Laurin Publishing, Biophotonics International, vol.11, no.7;
[2]. Albiero D., Maciel, A.J.S., Dal Fabbro I.M., Rodrigues S., Mazzeti Filho V., (2005) - *Moiré assisted deformation distribution study on soil-tire system,* Proceedings of the International Congress on Information Technology in Agriculture, Food and Environment, ITAFE05. (CD ROM) vol.II, Balcali Campus, Çukurova University, Adana, Turkey, October 12-14, 2005, pg. 681-683;
[3]. Amidror I., (2000) - *The theory of the moiré phenomenon*, Kluwer Academics Publishers. Dordrecht, p.474;

CONCLUSÕES

Com base no que foi explicado anteriormente, pode se concluir que as técnicas de *moiré* são altamente precisas na medição topográfica de objetos, no entanto, alguns fatores humanos podem ser inseridos no processo durante a preparação do setup, bem como durante o levantamento dos dados experimentais.

REFERÊNCIAS

[1]. Abràmoff M.D., Magalhães P.J., Ram Sunanda J. (2004) – *Processamento de Imagens por ImageJ*, Berkshire Common, Laurin Publishing, Biophotonics International, vol.11, n.7;
[2]. Albiero D., Maciel A.J.S., Dal Fabbro I.M., Rodrigues S., Mazzeti Filho V., (2005) - *Aplicação da Tecnica de Moiré no Estudo da Distribuição de Deformação num Sistema Associado a Pneu e Solo,* Proceedings of the International Congress on Information Technology in Agriculture, Food and Environment, ITAFE05. (CD ROM) vol.II, Balcali Campus, Çukurova University, Adana, Turkey, October 12-14, 2005, pg. 681-683;
[3]. Amidror I., (2000) - *A Teoria do Fenômeno de Moiré*, Kluwer Academics Publishers, Dordrecht, 474 p.;

[4]. Hu Y., Xi J., Chicharo J., Yang Z., (2006) - *Improved Three-step Phase Shifting Profilometry Using Digital Fringe Pattern Projection*, Proceedings of the International Conference on Computer Graphics, Imaging and Visualisation (CGIV'06). IEEE Computer Society. Sydney, Australia;
[5].Dal Fabbro I.M., Albiero D., Gazzola J., Rodrigues, S., Rabelo G.F., Fujii A. K., (2005) - *Moiré assisted mechanical behavior of sugarcane stalks under axial compression*, Proceedings of the International Congress on Information Technology in Agriculture, Food and Environment, ITAFE05. (CD ROM) vol. I, (ISBN 975-487-125-6). Balcali Campus, Çukurova University, Adana, Turkey, October 12-14, 2005, pg.242-245;
[6]. Degrieck Joris, Van Paepegem W., Boone P., (2001) - *Application of Digital Phase-shift shadow moiré to micro deformation measurements of curved surfaces,* Optics and Lasers in Engineering, v.36, pg.29-40;
[7]. Demarzo M.A., Affonso E.A., Dal Fabbro I.M., (2003) - *Application of a moiré interferometric technique in studying wooden structural elastic connections,* Proceedings of the International Congress - Information Technology in Agriculture, Food and Environment, ITAFE 2003, vol. 1, (ISBN 975-483-598-5). Ege University, Bornova, Izmir, Turkey, October, 07 -10 2003, pg.689-692;
[8]. Lino A.C.L., (2002) - *Moiré Optical Technique Applied to the Study of Irregular Surfaces,* Maters Thesis. Faculty of Agricultural Engineering, State University of Campinas, SP, p.86, Brazil;
[9]. Marotti D., Dal Fabbro I.M.D., Lino A.C.L., (2008) - *Computational Implementation of Moiré Methods Applied to Three Dimensional Image Reproductions.* Umpublished Paper. State University of Campinas, SP, Brazil;
[10]. Mazzeti Filho V., (2004) - *Use of moiré interferometry to study the dynamic stresses on floppy disks*, p.136, Dissertation (MSc in Agricultural Engineering), State University of Campinas, Campinas, SP, Brazil;
[11]. Minamisawa R.A., Gazolla J., Albiero D., Dal Fabbro I.M., Beraldo A.L., (2005) - *Shadow moiré technique applied in testing composite material,* Proceedings of the International Congress on Information Technology in Agriculture, Food and Environment, ITAFE05. (CD ROM) vol.I, (ISSN 975-487-125-6). Balcali Campus, Çukurova University, Adana, Turkey, October 12-14, 2005, pg. 237-241;
[12]. Oster G., Nishijima Y., (1964) - *Moiré patterns.* Scientific American Resource Library: Readings in the Physics Sciences and Technology. Washington. v.3. Offprints 291-326. pg.54-63;
[13]. Oliveira S.A.G., (1988) - *Development of materials for reflection photoelasticity*, p.93. Dissertation in Mechanical Engineering - Faculty of Mechanical Engineering, Federal University of Uberlândia, MG, Brazil;
[14]. Post D., Han B., Ifju P., (1994) - *High sensivity moiré: Experimental analysis for mechanics and materials*, New York: Spring-Verlag;
[15]. Quan C., He X.Y., Wang C.F., Tay C.J., Shang H. M., (2001) - *Shape measurement of small objects using LCD fringe projection with phase shifiting*, Optics Communication, vol.189, pg.21-29.
[16]. Sciammarella C.A., (1982) - *The moiré method – A review.* Experimental Mechanics. v.44, no.8, pg.418-433;
[17]. Vieira M.A.P., Dal Fabbro I.M., Laurenti R., (2003) - *Application of a moiré interferometric technique in a simple structural member vibration analysis.* in Proceedings of the International Congress - Information Technology in Agriculture, Food and Environment, ITAFE 2003, vol. 1, (ISBN 975-483-598-5). Ege University, Bornova, Izmir, Turkey, October, 07 -10, 2003, pg.599-603.

[4]. Hu Y., Xi J., Chicharo J., Yang Z., (2006) - *Perfilometria Melhorada com Mudança de Fases em Tres Degraus com Applicação de Projeção de Padões de Franjas Digitais*, Anais da Conferencia Internacional de Computação Gráfica, Imagem e Visualização. IV'06). IEEE Computer Society. Sydney, Australia;
[5]. Dal Fabbro I.M., Albiero D., Gazzola J.; Rodrigues S., Rabelo G.F., Fujii A. K., (2005) - *Aplicação da Técnica de Moiré no Estudo do Comportamento Mecânico de Colmos de Cana-de-Açucar sob Tensão Axial*, Proceedings of the International Congress on Information Technology in Agriculture, Food and Environment, ITAFE05. (CD ROM) vol. I, (ISBN 975-487-125-6). Balcali Campus, Çukurova University, Adana, Turkey, October 12-14, 2005, pg.242-245;
[6]. Degrieck Joris, Van Paepegem W., Boone P., (2001) - *Aplicação da Técnica de Moiré Sombra Digital na Medição de Microdeformações em Superficies Curvas,* Optics and Lasers in Engineering, v.36, pg.29-40;
[7]. Demarzo M.A., Affonso E.A., Dal Fabbro I.M., (2003) - *Aplicação da Técnica Interferométriica de Moiré no Estudo de Conecções Elásticas em Estrututa de Madeira,* Proceedings of the International Congress - Information Technology in Agriculture, Food and Environment, ITAFE 2003, vol. 1, (ISBN 975-483-598-5). Ege University, Bornova, Izmir, Turquia, october, 07 -10 2003, pg.689-692;
[8]. Lino A.C.L., (2002) - *Técnica óptica de moiré visando a aplicação no estudo de superfícies irregulares*, Dissertação (Mestrado em Engenharia Agrícola), Universidade estadual de Campinas. Campinas, p.86;
[9]. Marotti D., Dal Fabbro I.M.D., Lino A.C.L. (2008) - *Implentação Computacional dos Métodos de Moiré Aplicada a Reprodução Tridimensional de Imagens.,* Trabalho não publicado. Universidade Estadual de Campinas, SP, Brasil;
[10]. Mazzeti Filho V., (2004) - *Utilização da interferometria de moiré no estudo de tensões dinâmicas em discos flexíveis,* 136 p. Dissertação (Mestrado em Engenharia Agrícola), Universidade estadual de Campinas. Campinas, SP, Brazil;
[11]. Minamisawa R.A, Gazolla J., Albiero D., Dal Fabbro I.M., Beraldo A.L., (2005) - *Aplicação da Técnica òptica de Moiré em Ensaios Mecânicos de Compósitos.* in Proceedings of the International Congress on Information Technology in Agriculture, Food and Environment, ITAFE05. (CD ROM) vol. I, (ISSN 975-487-125-6). Balcali Campus, Çukurova University, Adana, Turkey, October 12-14, 2005, pg. 237-241;
[12]. Oster G., Nishijima Y., (1964) - *Padrões de Moiré.* Scientific American Resource Library: Readings in the Physics Sciences and Technology. Washington. v.3. Offprints 291-326. pg.54-63;
[13]. Oliveira S.A.G., (1988) - *Desenvolvimento de materiais para fotoelasticidade de reflexão,* 93 p. Dissertação de Mestrado em Engenharia Mecânica – Faculdade de Engenharia Mecânica, Universidade Federal de Uberlândia,MG, Brazil;
[14]. Post D., Han B., Ifju P., (1994) - *Moiré de Alta Sensibilidade: Analise Experimental para Mecânica de Materiais*, New York: Spring-Verlag;
[15]. Quan C., He X.Y., Wang C.F., Tay C.J., Shang H. M., (2001) - *Medida de Formato de Pequenos Objetos com Projeção de Franjas com Mudança de Fase por LCD,* Optics Communication, v. 189, pg.21-29;
[16]. Sciammarella C.A.,(1982) - *O Método de Moiré. Uma Revisão.* Experimental Mechanics. v.44, n.8, pg.418-433;
[17]. Vieira M.A.P., Dal Fabbro I.M., Laurenti R., (2003) - *Aplicação da Técnica Interferomátrica de Moiré na Análise Vibracional de um Membro Estrutural Simples..* in Proceedings of the International Congress - Information Technology in Agriculture, Food and Environment, ITAFE 2003, vol. 1, (ISBN 975-483-598-5). Ege University, Bornova, Izmir, Turquia, october, 07 -10, 2003, pg. 599-603.

RESEARCH INTO THE GRADING METHOD OF KIWI FRUIT BASED ON VOLUME ESTIMATION AND SURFACE DEFECT
/
基于体积估计和表面缺陷的猕猴桃分级方法

Prof. Ph.D. Lijia Xu [1)], Stud. Yu Feng [1)], Stud. Zhangkun Fan [1)], Ph.D. Dingchun Yun [2)]
[1)] College of Mechanical and Electrical Engineering, Sichuan Agriculture University, Ya'an / China,
[2)] University of Applied Sciences Upper Austria, Softwarepark 11, Hagenberg / Austria
Tel: 0835-2882035; E-mail: lijiaxu13@163.com

Abstract: *Kiwi fruit grading is a key link of fruit treatment after picking. In respect that low sorting rate and grading rate of kiwi fruits affect commodity value in China, the paper acquires the volumetric characteristic of kiwi fruit through the 3D reconstruction of its three views, and fits volumetric pixel P with actual weight W to get a mathematical model between the two parameters, and identifies the area characteristic of the surface defect of kiwi fruit by iterative method. Volumetric characteristic and the characteristic of the surface defect are inputted into Support Vector Machine (SVM), and then suitable kernel function and kernel parameters are selected, finally the kiwi fruit grading accuracy of 97.73% is gotten. Compared with the grading accuracy of BP network with 92.11%, it can be seen that the grading effect of SVM is better than that of BP network and its grading performance is stable. The experimental results show that the SVM grading method based on kiwi fruit volume and its surface defect is feasible and can be used for online inspection of appearance quality of kiwi fruits.*

Keywords: *Kiwi fruit grading; SVM; BP neural network; Image processing; Agricultural technology extension*

INTRODUCTION

At present, the kiwi fruit grading of China mainly depends on artificial way to complete it, so both the grading efficiency and the grading accuracy are low. China has the largest production of kiwi fruits. With the increasing import and export volume of kiwi fruit year by year, the low price of kiwi fruits needs to be changed in a short time. So it is very important to improve the grading technical for kiwi fruits, which can produce more economic benefits and significantly improve its market competitiveness.

With the development of machine vision in recent years, many scholars at home and broad have developed a number of methods for quality inspection of kiwi fruit, e.g., Lü Q [3] developed detection of hidden bruise on kiwi fruit using hyperspectral imaging and parallelepiped classification, and the experimental result showed the error with 14.5% for internal damage detection by high spectrum. Wijithunga et al. [5] studied kiwi fruit detection based on generalized color picture segmentation. Yongjie [1] advanced a surface detection method for kiwi fruit grading. Wu Tao et al. [7] studied the object extraction of kiwifruit based on machine vision. While there are rare studies on external inspection and grading methods for kiwi fruits. Hence the paper developed a grading method for kiwi fruits, which used SVM as the classifier. The method can achieve the accuracy grading results for kiwi fruits according to volume estimation and surface defect.

MATERIAL AND METHOD

Feature Extraction of Kiwi Fruit

Usually a picture shot by the camera is noisy, so it needs pre-processing [10]. Picture of Kiwi fruit snapped

摘要: *猕猴桃分级是水果产后处理的重要环节，针对中国猕猴桃分选率和分级率低而影响商品价值现状，本文通过对猕猴桃三视图进行三维重建得到猕猴桃体积特征，拟合体积像素 P 和实际重量 W，得到两者之间的数学模型；根据迭代法切割得到猕猴桃表面缺陷面积特征。将体积特征和表面缺陷特征输入支持向量机 SVM，通过选择合适的核函数和核参数，得到猕猴桃的分级正确率为 97.73%。对比 BP 网络分级的正确率 92.11%，可知 SVM 比 BP 网络的分级效果好且 SVM 的分级性能稳定。实验结果表明基于猕猴桃体积和表面缺陷的 SVM 分级方法可行，可用于猕猴桃外部品质在线检测。*

关键词: *猕猴桃分级；SVM；BP 神经网络；图像处理；农业技术推广*

引言

目前，猕猴桃分级的中国主要依靠人工的方式来完成，分类效率和分类精度都比较低。中国拥有最大生产的猕猴桃生产基地。每年随着越来越多的猕猴桃进口和出口量，猕猴桃价格偏低的现象急需在较短的一段时间内改变。所以提高猕猴桃分级的技术非常重要，它能够产生很好的经济效益，提高其市场竞争力。

近年来，随着机器视觉的发展，国内外学者做了许多关于猕猴桃品质检测的方法，如吕强等[3] 利用高光谱图像检测猕猴桃内部损伤，其实验结果表明高光谱检测内部损伤的误差为 14.5%；P. Wijithunga 等[5]研究了基于广义彩色图像分割的猕猴桃检测方法；崔永杰等[1]提出了猕猴桃分级果实表面缺陷的检测方法；武涛等[7]做了基于机器视觉的猕猴桃果实目标提取研究。综上所述可知对猕猴桃外部检测并进行分级的研究较少，对此，本文研制了一种基于猕猴桃体积估计和表面缺陷的分级方法，以 SVM 作为分类器，并根据猕猴桃等级规格，实现了基于体积估计和表面缺陷的猕猴桃准确分级。

材料与方法

猕猴桃的特征提取

通常摄像头拍摄的图像存在噪声，故需要对图像进行预

by camera is shown in Fig. 1(a), and the original picture is transferred from RGB space into the second channel (saturation) in HSV space, as shown in Fig. 1(b). Picture with median filtering for Fig. 1(b) is shown in Fig. 1(c), from which it can be seen that the picture has strong contrast, less fuzziness and complete edge information. Edge extracting is conducted by canny operator for Fig. 1(c), and the result is shown in Fig. 1(d). Fig. 1(e) is obtained through the expansion of Fig. 1(d), and then Fig. 1(f) is gotten through the fill in Fig. 1(e). Later the region picture of kiwi fruit is acquired through corrosion, open operation, redundant pixel deletion and other operations for Fig. 1(f), as shown in Fig. 1(g). Then Fig. 1(g) is viewed as formwork and inverted, finally logical product is conducted for R, G and B components of the picture shown in Fig. 1(a) to get kiwi fruit picture divided from the background, as shown in Fig. 1(h).

处理 [10]。摄像头拍摄的猕猴桃图像如图 1(a) 所示，将原始图像从 RGB 空间转换为 HSV 空间的第二通道(饱和度)如图 1(b)所示。对图 1(b)进行中值滤波处理的图像如图 1(c), 可知图 1(c)的对比度强，模糊少，边缘信息保存较完整。对图 1(c) 用 canny 算子进行边缘提取，结果如图 1(d)。对图 1(d)进行膨胀处理得图 1(e)，再对图 1(e)进行填充得图 1(f)，继而对图 1(f)进行腐蚀、开运算和删除冗余像素等操作后，获得猕猴桃的区域图像如图 1(g)。将图 1(g) 作为模板并取反，与图 1(a)所示图像的 R、G、B 分量进行与运算，得到从背景中分割出来的猕猴桃图像如图 1(h)。

(a) (b) (c) (d) (e) (f) (g) (h)

Fig. 1 - Picture pre-processing process
(a) Kiwi fruit picture (b) Saturation picture (c) Median filtering picture (d) Canny edge extracting picture (e) Expansion picture (f) Fill picture (g) Region picture of Kiwi fruit (h) Division picture of Kiwi fruit

Extraction of volumetric feature

Volume is a key indicator in many fields, and a very important feature for fruit grading. Normally, the larger a fruit is, the heavier it will be. The paper designs a volume measuring method of the kiwi fruit based on computer vision.

After the pre-processing of 3 views of the kiwi fruit picture, all of its front view, side view and top view are in 100×100 pixels, as shown in Fig. 2(a-c). Front view is read in to calculate its edge, as shown in Fig. 2(d), and the coordinates of 4 orientation points locating at the easternmost, the westernmost, the northernmost and the southernmost areas respectively among the edge contour points of the front view are found out. Side view is read in to calculate its edge, and the coordinates of 4 orientation points in the easternmost, the westernmost, the northernmost and the southernmost respectively among the edge contour points of side view are found out. Taking the edge of the front view as the benchmark, the edge position of the side view is adjusted to align the horizontal coordinate of the northernmost orientation point among the edge contour points of the side view with that of the northernmost orientation point among the edge contour points of the front view, and the result is shown in Fig. 2(e). Top view is read in to calculate its edge, and then its edge position is adjusted as per the coordinates of 4 orientation points on the edge of the front view and those of 4 orientation points on the edge of the adjusted side view, so that the horizontal coordinate of the northernmost orientation point among the edge contour points of the top view is corresponding to the ordinate of the easternmost orientation point among the edge contour points of the side view. Similarly, the edge of the top view is adjusted so that the ordinate of the westernmost orientation point among its edge contour points is corresponding to that of the westernmost orientation point among the edge contour points of the front view, and the result is shown in Fig. 2(f). The coordinates of the 4 orientation points in the easternmost, the westernmost, the northernmost and the southernmost among the edge contour points of the adjusted top view are achieved to find out the center point of the top view's edge further.

体积特征的提取

在许多领域中体积是一个重要的指标，在水果分级中它更是一个非常重要的特征，一般而言，体积越大则重量越大。本文设计了基于计算机视觉的猕猴桃体积测量方法。

对猕猴桃的三视图进行预处理后，使其正视图、侧视图和俯视图都为100×100像素，如图 2(a-c)所示。读入正视图，求取正视图边缘，如图 2(d)，找到正视图边缘轮廓点中的最东面、最西面、最北面和最南面的 4 个方位点的坐标；读入侧视图，求取侧视图边缘，找到侧视图边缘轮廓点中的最东面、最西面、最北面和最南面的 4 个方位点的坐标。以正视图边缘为标准，调整侧视图边缘的位置，使其边缘轮廓点中的最北面方位点的横坐标与正视图边缘轮廓点中的最北面方位点的横坐标相对准，结果如图 2(e)所示。读入俯视图，求取俯视图边缘，以正视图边缘 4 个方位点坐标和调整后的侧视图边缘 4 个方位点坐标为参照，调整俯视图边缘的位置，使其边缘轮廓点中的最北面方位点的横坐标对应侧视图边缘轮廓点中的最东面方位点的纵坐标；同理，调整俯视图边缘使其边缘轮廓点中的最西面方位点的纵坐标与正视图边缘轮廓点中的最西面方位点的纵坐标相对应，结果如图 2(f)。获得调整后俯视图边缘轮廓点中的最东面、最西面、最北面和最南面的 4 个方位点的坐标，利用此 4 个方位点的坐标找到俯视图边缘的中心点。

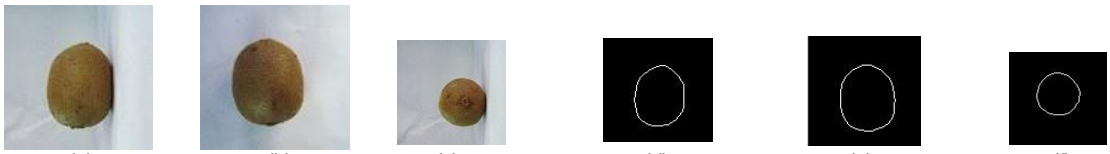

(a) (b) (c) (d) (e) (f)

Fig. 2 - Three views and edges of all adjusted views of kiwi fruit
(a) Front view (b) Side view (c) Top view (d) Edge of adjusted front view (e) Edge of adjusted side view (f) Edge of adjusted top view

Creating $100 \times 100 \times 100$ cube zero matrix named as $KJ1$. Edges of the front view, edges of the side view and edges of the top view are adjusted to correspond to the front, side and top of $KJ1$, respectively. Taking the ordinate i_1 of the westernmost orientation point among the edge contour points of the side view as the initial point and the ordinate i_n of the easternmost one as the end point, the edge of the front view is copied to Layer i_x of $KJ1$ to get $KJ1(:, i_x, :)$, $i_x \in (i_1, i_2, \cdots, i_x, \cdots, i_{n-1}, i_n)$. Taking the ordinate j_1 of the easternmost orientation point among the edge contour points of front view as the initial point and the ordinate j_n of the westernmost one as the end point, $KJ1(j_x, :, :)$, $j_x \in (j_1, j_2, \cdots, j_x, \cdots, j_{n-1}, j_n)$ are transposed and further assigned to 100×100 square zero matrix named as QP. Aligning QP with the center point of the side view's edge and then conducting overlap, the results are shown in Fig. 3(a-c). Then the coordinate (x_z, y_z), $z \in (1 \cdots \omega)$ of the edge contour points of their intersection can be found out, where ω is number of edge contour points. Clearing the j_x Layer of $KJ1$, i.e., $KJ1(j_x, :, :)$ and assigning $KJ1(j_x, x_z, y_z)$ to 1, the slice set of edge of side view can be obtained through traversing all j_x values, as shown in Fig. 3(d-f).

创建$100 \times 100 \times 100$的正方体零矩阵$KJ1$。将正视图边缘对应$KJ1$的正面，侧视图边缘对应$KJ1$的侧面，俯视图边缘对应$KJ1$的上面。以侧视图边缘轮廓点中的最西面方位点的纵坐标i_1为起点，最东面方位点的纵坐标i_n为终点，将正视图边缘复制在$KJ1$的第i_x层上得到$KJ1(:, i_x, :)$，$i_x \in (i_1, i_2, \cdots, i_x, \cdots, i_{n-1}, i_n)$。以正视图边缘轮廓点中的最东面方位点的纵坐标$j_1$为起点，最西面方位点的纵坐标$j_n$为终点，将$KJ1(j_x, :, :)$，$j_x \in (j_1, j_2, \cdots, j_x, \cdots, j_{n-1}, j_n)$转置后赋给$100 \times 100$的正方形零矩阵$QP$。将$QP$和侧视图边缘的中心点对准后进行叠加，叠加图如图 3(a-c)所示。从而可以找到两者交集部分的边缘轮廓点的坐标(x_z, y_z)，$z \in (1 \cdots \omega)$，ω为边缘轮廓点数。将上述$KJ1$的第j_x层$KJ1(j_x, :, :)$清零，再将$KJ1(j_x, x_z, y_z)$赋值为 1，遍历完所有j_x值得到侧视边缘切片集，如图 3(d-f)所示。

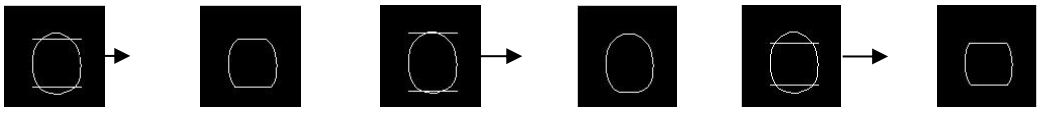

(a) (d) (b) (e) (c) (f)

Fig. 3 - Edge cutting effect graph of side view
(a) Overlap picture 1 (b) Overlap picture 2 (c) Overlap picture 3
(d) Slice 1 of side view (e) Slice 2 of side View (f) Slice 3 of side view

In $KJ1(:, :, k_x)$, different k_x values correspond to different rectangular slices, thereof, $k_x \in (k_1, k_2, \cdots, k_x, \cdots, k_{n-1}, k_n)$. k_1 is the horizontal coordinate of the northernmost orientation point among the edge contour points of the front view, and k_n is that of the southernmost one. Schematic graphs of different rectangular slices are shown in Fig. 4(a-c).

在$KJ1(:, :, k_x)$中不同k_x对应不同的矩形切片，其中，$k_x \in (k_1, k_2, \cdots, k_x, \cdots, k_{n-1}, k_n)$。$k_1$为正视图边缘轮廓点中的最北面方位点的横坐标，$k_n$为正视图边缘轮廓点中的最南面方位点的横坐标。不同矩形切片示意图如图 4(a-c)所示。

(a) (b) (c)

Fig. 4 - Schematic graphs of rectangular slices

After traversing all rectangular slices, the minimum ordinates of contour points of each layer of rectangular slices are saved in array named as *M*. Then the maximum and minimum in *M* are found out, and the absolute value of their difference is viewed as the minification base number. Taking k_1 and k_n as the initial and end point respectively, the rectangular slice of k_x Layer， i.e., $KJ1(:,:,k_v)$，is transposed and further exchanged vertically, and then assigned to matrix named as *N*. Subtracting the minimum ordinate value of rectangular slice contour points in *N* by the minimum in *M*, and the quotient of dividing the absolute value of their difference by the minification base number is viewed as minification λ of the k_x layer edge of top view, i.e.

遍历完所有矩形切片，将各层矩形切片轮廓点中的最小纵坐标存放在数组 M 中。找到 M 中的最大值和最小值，将两者相减的绝对值作为缩小倍数基数。以 k_1、k_n 分别作为起点和终点，将第 k_x 层的矩形切片 $KJ1(:,:,k_x)$ 转置并上下交换后赋给矩阵 *N*。将 *N* 所述矩形切片轮廓点中的最小纵坐标值与 M 中的最小值相减，相减后的差值的绝对值和缩小倍数基数相除的结果作为第 k_x 层俯视图边缘缩小的倍数 λ，即：

$$\lambda = \frac{\left|\min(N) - \min(M)\right|}{\left|\max(M) - \min(M)\right|} \tag{1}$$

Edges of the top view are contracted by double interpolation algorithm [2] according to minification number λ, and the contracted picture matrix is further expanded into 100×100 matrix. During the expansion process, the coordinates of each point of the original picture matrix remain, and all new expanded points are filled by 0. Center point of the contracted picture is aligned with that of edge of the top view to get matrix named as *L*. The center points of *L* and *N* are aligned and overlapped to get matrix named as *S*, as shown in Fig. 5(a) and 5(c). In *S*, the intersection between *L* and *N* is defined as boundary. The center point of *S* is found out by the coordinates of the easternmost, the westernmost, the southernmost and the northernmost orientation points in *S*. Such center point will be rounded into an integer if it isn't an integer, and viewed as the initial growing coordinate [6]. Starting from these initial growing points, the growth spreads to all directions in *S* till the coordinates of all growing initial points and the points (x_m, y_m) within it and the boundary whose values are equal to 0 are found out, where, $m = 1 \cdots \psi$, ψ is number of all points equaling to 0 therein. $100 \times 100 \times 100$ cube zero matrix $KJ2$ is created, and all elements of $KJ2(y_m, x_m, k_v)$ are assigned with 1. Regional growing slice sequence graph can be achieved after all $k_v \in (k_1, k_2, \cdots, k_v, \cdots, k_{n-1}, k_n)$ values are traversed, where different k_x values correspond to different regional growing slices, as shown in Fig. 5(b) and Fig.5(d).

利用双插值算法[2]对俯视图边缘按照倍数 λ 进行缩小，将缩小后的图像矩阵进一步扩展为 100×100 的矩阵。在扩展过程中，原图像矩阵各点的坐标不变，新扩展的点则全部用 0 来填充。将缩小后的图像的中心点和俯视图边缘的中心点对准得到矩阵 *L*。将 *L* 和 *N* 的中心点对准后进行叠加得到矩阵 *S*，*S* 如图 5(a)和图 5(c)。在 *S* 中将 *L* 和 *N* 的交集部分定义为边界.利用 *S* 中的最东面、最西面、最南面和最北面方位点的坐标找到 *S* 的中心点，若该中心点不为整数则将其化为整数，以此中心点作为生长起始坐标 [6]。从该生长起始点开始，在 *S* 中向四面生长，直到找完包括生长起始点在内的生长起始点和边界之间所有值为 0 的点的坐标 (x_m, y_m)，$m = 1 \cdots \psi$，ψ 为生长起始点和边界之间所有值为 0 的点的个数。创建 $100 \times 100 \times 100$ 的正方体零矩阵 $KJ2$，将所有 $KJ2(y_m, x_m, k_x)$ 赋值为 1，遍历完所有 $k_x \in (k_1, k_2, \cdots, k_x, \cdots, k_{n-1}, k_n)$ 值即得到区域生长切片序列图，不同 k_x 对应不同区域生长切片如图 5(b)和图 5(d)。

(a) (b) (c) (d)

Fig. 5 - Schematic graphs of *S* and region growing slice
(a) Schematic graph 1 of *S;* (b) Schematic graph 1 of region growing slice; (c) Schematic graph 2 of *S;* (d) Schematic graph 2 of region growing slice

All points equaling to 1 in $KJ2$ are drawn by MATLAB to get the 3D scatter graph of kiwi fruit, and statistics is made for the number of 1 in $KJ2$ to get the pixel numbers of 3D scatter graph of kiwi fruit named as P, which is also used as volumetric feature of kiwi fruit. The 3D scatter graph of kiwi fruit is shown in Fig. 6.

利用 MATLAB 绘制出 $KJ2$ 中所有值为 1 的点即得到猕猴桃的立体三维散点图，统计 $KJ2$ 中 1 的个数即可得到猕猴桃立体三维散点图的像素个数 P，P 即作为猕猴桃的体积特征。猕猴桃的三维散点图如图 6 所示。

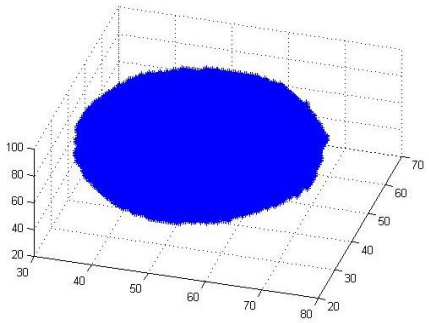

Fig. 6 - 3D Scatter graph of kiwi fruit

Abstraction of surface defect characteristic

Surface defects of kiwi fruit mainly include scrape, bruise, press, sunburn [8]. First, kiwi fruit is transferred from RGB space to HSV space, and then kiwi fruit picture is abstracted from the background of original picture in the saturation channel. The abstracted picture is cut to get Fig. 7(a), and then the gray scale chart of the cut picture is obtained, as shown in Fig. 7(b). Gray scale transformation is made for the gray scale chart, and the contrast of such chart is intensified to get Fig. 7(c). Fig.7(c) is divided by optimal threshold T_2 to get Fig. 7(d), and the threshold is calculated by iterative method. Defect detection is conducted for Fig.7(d) by canny operator with the threshold of 0.79 to get canny division graph shown in Fig. 7(e). Edge in Fig. 7(e) is removed to get Fig. 7(f), and defect in Fig. 7(f) is filled to get Fig. 7(g). Finally, Fig.7(g) is restored to get defect color graph shown in Fig. 7(h). Defect area of kiwi fruit in Fig. 7(g) is calculated as the surface defect feature of kiwi fruit.

表面缺陷特征的提取

猕猴桃表面缺陷主要有划伤、碰压伤和日灼缺陷等[8]。首先，将猕猴桃由 RGB 空间转换为 HSV 空间，在 HSV 空间的饱和度通道中将对猕猴桃图像从原始图像的背景中提取出来。对提取出来的猕猴桃裁剪得到图 7(a)，求取裁剪图的灰度图如图 7(b)；对灰度图进行灰度变换，增强灰度图的对比度得到图 7(c)；将灰度变换图 7(c)用最佳阀值 T_2 分割得到图 7(d)，最佳阀值采用迭代法求取；利用 canny 算子对图 7(d)进行缺陷检测，其中 canny 算子的参数阀值设置为 0.79，得到图 7(e)所示的 canny 分割图；对图 7(e)去除边缘得到图 7(f)；对图 7(f)填充其缺陷得到图 7(g)；最后对图 7(g)进行复原得到缺陷彩色图 7(h)；计算图 7(g)中猕猴桃的缺陷面积并作为猕猴桃表面缺陷特征。

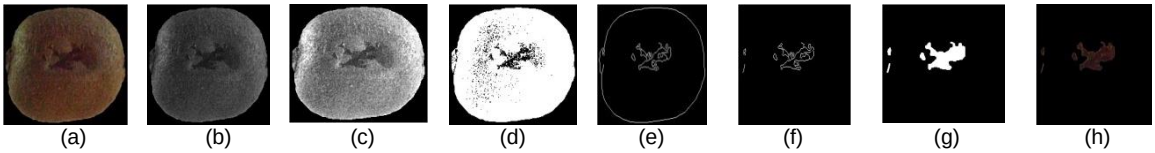

Fig. 7 - Defect characteristic abstraction graph of iterative method
(a) Tailed graph; (b) Gray scale chart; (c) Gray scale transformation graph; (d) Iterative effect graph; (e) Canny division graph; (f) Edge removal graph; (g) Defect fill graph; (h) Defect color graph

RESULTS AND ANALYSIS

Weight Estimation

Total 40 kiwi fruits in different sizes, regular shape, the same variety and the same batch are randomly selected as sample. The volumetric pixel with $P/1000$ is fitted with actual weight W by least square method, and the result is shown in Figure. 8.

实验结果和分析

重量估计

随机选取 40 个大小不一且形状规则的同品种同批次的猕猴桃作为样本，用最小二乘法拟合猕猴桃的体积像素 $P/1000$ 与重量 W 的关系，拟合结果如图 8 所示。

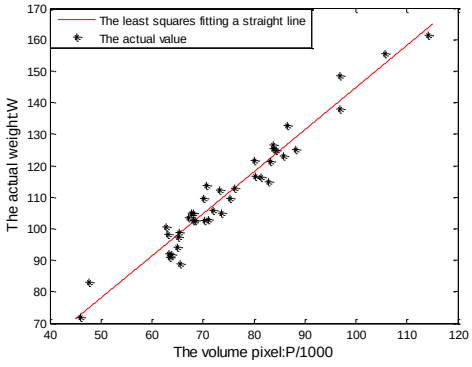

Fig.8 - Graph of relation for fitting of volumetric pixel with weight

According to experimental data, the relation between volumetric pixel $P/1000$ (unit: piece) and weight W (unit: g) of kiwi fruit is shown as follow:

经实验数据得出猕猴桃的体积像素值 $P/1000$ (单位：个)与其重量 W (单位： g)之间的关系为：

$$W = \frac{1.3350 \times p + 11.2655}{1000} \quad (2)$$

Analysis of variance for weight W and volumetric pixel P is shown in Table 1, in which the testing value $F > (F_\alpha = F_{0.01}(1, n-2))$. The value of F shows that the influence is highly significant. The coefficient of determination r is shown as follow:

重量 W 与体积像素 P 的方差分析如表 1 所示，其中，检验值 $F > (F_\alpha = F_{0.01}(1, n-2))$ 故为高度显著，可决系数 r 为：

$$r^2 = \frac{SSR}{SST} = 0.9501 \quad (3)$$

In the formula, the sum of squared residuals (SSR) is the sum of squares of residuals, and the total sum of squares (SST) is defined as being the sum, over all observations, of the squared differences of each observation from the overall mean.

The result that the value of r is approximate to 1 shows good regression effect when using volumetric pixel P of kiwi fruit to estimate its weight W. Moreover, weight of kiwi fruit W is in positive correlation with its volumetric pixel P. The more volumetric pixel P is, then the larger weight W will be. Standard error S_y is shown as follow:

式中， SSR 代表回归值与均值的总离差平方和， SST 代表观测值与均值的总离差平方和。

可决系数 r 接近 1，表明用猕猴桃的体积像素 P 估计其重量 W 的回归效果良好。猕猴桃的重量 W 和体积像素 P 成正相关性，体积像素越大，实际重量越大。标准误差 S_y 为：

$$S_y = \sqrt{\frac{SSE}{n-2}} = 4.2490 \quad (4)$$

In the formula, $SSE = SST - SSR$, and n means the number of kiwi fruits. The value of S_y shows small error and validates the effectiveness of the model, i.e., formula. (2).

式中， $SSE = SST - SSR$, n 代表猕猴桃个数。 S_y 的计算结果表明误差偏小，验证了本模型即式（2）的可行性。

Table 1

Analysis of variance for actual weight and volumetric pixel

Source of variance	*Ssd*	*Df*	*Va*	*F*	*Fa*	*Significance*
Regression	13052	1	13052	722.93	4.098	Highly Significant
Residual	686.06	8	18.054		7.352	
Total	13738	9	•		•	

Total 20 kiwi fruits in different sizes, regular shape, the same variety and the same batch are randomly selected as sample, and their volumetric pixels are inputted into the model to get the fitted value of kiwi fruit weight. The result of comparison between the fitted values and actual weights of kiwi fruits is shown in Fig. 9.

随机选取待测猕猴桃中的 20 个大小不一且形状较规则的、同品种同批次的猕猴桃，将其体积像素输入该模型得到猕猴桃重量的拟合值，该拟合值和猕猴桃的实际重量值的比较结果如图 9 所示。

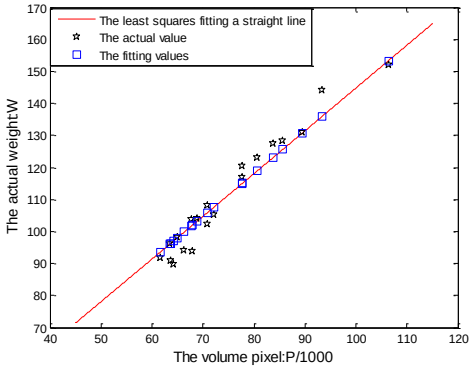

Fig.9 - Comparison graph for fitted value and actual value of kiwi fruit weight

From Fig.9, it can be seen that the fitted values of kiwi fruits weight are approximate to their actual weights, thus the model shown in formula.(2) has good regression

由图 9 可知，猕猴桃重量的拟合值接近其实际重量值，表明此模型回归拟合效果良好，可用于猕猴桃的实际重量

fitting result and can be used for estimating the actual weights of kiwi fruits .

估计。

Empirical classification of kiwi fruits and data preprocessing

Kiwi fruits are empirically graded into 4 grades [9]. The same variety and batch of kiwi fruits are classified into large type (marked as L), medium type (marked as m), small type (marked as S) and very small type (marked as VS) by size, and they are also classified into defect type (marked as D) and no defect type (marked as ND) by surface defect. Different classes of kiwi fruits are shown in Table 2.

猕猴桃的经验分类与数据预处理

将猕猴桃按照经验分为 4 类[9]，同品种同批次的猕猴桃按外观大小分为大(L)、中(M)、小(S)、很小（SS），按表面缺陷面积分为缺陷（D）和无缺陷(ND)，分类标准如表 2 所示。

Table 2

Grading of kiwi fruits

Grade	*Size*	*Defect*
First-class	L	ND
Second-class	M	ND
Third-class	S	ND
Fourth class	L	D
	M	D
	S	D
	VS	ND
	VS	D

Volumetric pixels and surface defect areas of total 88 kiwi fruits are selected and normalized. Different standardization methods generate different grading results. Through repetitive experiments, z-score standardization method is selected, i.e.

选择 88 个猕猴桃的体积像素和缺陷面积并将其归一化处理。不同标准化方法对分级结果有不同影响，经过反复实验选择 z-score 标准化方法，即：

$$z_{ij} = \frac{x_{ij} - \overline{x}_i}{s_i} \tag{5}$$

In the formula, z_{ii} means converted real variable value, and x_{ii} means actual variable value. $\overline{x}_i$ and s_i are arithmetic mean and standard deviation of variable, respectively.

式中，z_{ij} 为转化后的实变量值，x_{ij} 为实际变量值，$\overline{x}_i$ 和 s_i 分别是变量的算术平均值和标准差。

Grading effect of SVM

The 2 kinds of features, i.e., standardized volumetric pixel and surface defect area, are inputted into SVM with v-SVC type and SVM with c-SVC type. Different kernel functions are selected for experiment. Sample number of training set and that of testing set are 44, respectively, and the grading results are shown in Table 3.

SVM 的分级效果

将上述标准化后的体积像素和表面缺陷面积 2 类特征输入 v-SVC 型 SVM 和 c-SVC 型 SVM。选择不同核函数进行实验，训练集和测试集样本数各 44 个，分级结果如表 3 所示。

Table 3

Results of grading by different kernel functions

SVM type	Kernel function type	Grading accuracy
c-SVC	Linear kernel function	84.09%(37/44)
	Polynomial kernel function	88.64%(39/44)
	RBF kernel function	97.73%(43/44)
	Sigmoid kernel function	70.45%(31/44)
v-SVC	Linear kernel function	86.36%(38/44)
	Polynomial kernel function	88.64%(39/44)
	RBF kernel function	97.73%(43/44)
	Sigmoid kernel function	81.82%(36/44)

From Table 3, it can be seen that the highest grading accuracy of the 2 kinds of SVMs adopting RBF kernel function is 97.73%, but the SVM with v-SVC type adopting other kernel functions has a little better grading result, so all subsequent grading experiments use such SVM as the classifier and RBF as the kernel function.

由表 3 可知，两类 SVM 均在选择 RBF 核函数时获得最高的分级准确率 97.73%，但选择其他核函数时 v-SVC 型 SVM 的分级效果稍高些，故后续的分级实验均是以此类 SVM 作为分类器，且选择 RBF 作为核函数。

SVM training is attributed to the solution of convex quadratic programming problems under linear constraint [11], and SVM will occupy large storage space when training set is large. Different training sets are inputted into SVM, and the grading results are shown in Table 4.

SVM 的训练归结为求解线性约束下的凸二次规划问题[11]，当训练集较大时，SVM 将会占据较大的存储空间。将不同训练集输入 SVM，结果如表 4 所示。

Table 4

Grading results of different training sets

Training set number	*Testing set number*	*Grading accuracy*
25	44	97.73%
30	44	97.73%
36	44	97.73%
44	44	97.73%

From Table 4, it can be seen that different numbers of training sets inputted into SVM with v-SVC type bring the same grading accuracy of 97.73%, so this type of SVM has stable grading performance and can always realize very high grading accuracy for different sample inputs.

In order to investigate the influence of kernel parameter σ of SVM on kiwi fruit grading accuracy [4], 44 training sets and 44 testing sets are selected respectively, and the grading results of SVM using different σ values are shown in Table 5.

由表 4 可知，不同训练集输入 v-SVC 型 SVM 得到相同的分级正确率 97.73%，由此可知该型 SVM 分级性能稳定，在不同样本输入的情况下均能得到很高的分级准确率。

为了考察 SVM 的核参数 σ 对猕猴桃分级正确率的影响[4]，分别选择训练集和测试集各 44 个，在 σ 取不同值时 SVM 的猕猴桃分级结果如表 5 所示。

Table 5

Grading results at different σ values

Nuclear parameters(σ)	*Grading accuracy*
0.5	93.18%
1.0	95.45%
1.5	97.73%
2.0	97.73%
3.0	97.73%
5.0	95.45%
10.0	90.91%

From Table 5, it can be seen that different σ values influence grading results greatly. SVM has optimal grading accuracy for σ distributed in the interval [1.5, 3.0]. SVM is in a state of over learning for σ <1.5 and in a state of under learning for σ >3.0.

由表 5 可知，σ 值在[1.5, 3.0]时 SVM 的分级精度达到最佳。当 σ <1.5 时，SVM 过度学习；当 σ >3.0 时，SVM 学习不足。

Grading effect of BP network

BP network is the most widely applied back propagation network. The next kiwi fruit grading experiment based on BP network will be conducted with sample numbers of training set and testing set are 50 and 38, respectively. Training times is 50 and learning velocity is 0.1. The volumetric and defect area features are inputted into BP network, so the number of input layer neurons is set to 2. Kiwi fruits have 4 grades, so BP network has 4 output layer neurons, and the grading results for different numbers of hidden layers are shown in Table 6. From Table 6, it can be seen that BP network has the grading accuracy with 92.11% for 8 hidden neurons.

BP 网络的分级效果

BP 网络是目前应用最广泛的反向传播网络。下面进行基于 BP 网络的猕猴桃分级实验，训练集、测试集样本数分别为 50 个和 38 个，训练次数为 50，学习速率为 0.1，输入层神经元个数为 2，体积特征和缺陷面积特征作为 BP 网络的输入，故其输入层神经元个数为 2，猕猴桃有 4 个等级故 BP 网络的输出层神经元个数为 4，选择不同的隐含层个数获得分类结果如表 6 所示。由表 6 可知，当隐含层神经元个数为 8 时，BP 网络的分级正确率为 92.11%。

Table 6

Grading results based of different numbers of hidden neurons

Number of hidden layer neurons	5	6	7	8	9	10
Grading accuracy	86.84%	86.84%	86.84%	92.11%	76.32 %	84.21%

Comparison of SVM and BP network in grading results

Grading experiments by SVM with v-SVC at different sample numbers of training set and that by BP network with 8 hidden neurons are conducted, and their grading results are shown in Table 7.

SVM 与 BP 网络的分级结果比较

选择在不同训练集样本数的情况下进行 v-SVC 型 SVM 和隐含层神经元个数为 8 的 BP 网络的分级实验，分级结果如表 7 所示。

Table 7

Comparison of SVM and BP network in grading results

Training set number	Test set number	SVM Grading accuracy	BP Grading accuracy
25	40	97.50%	82.50%
30	40	97.50%	87.50%
36	40	97.50%	90.00%
44	40	97.50%	92.50%

From Table 7, it can be seen that the grading accuracy of SVM is always 97.50% for different sample numbers of training set, while that of BP network is greatly influenced by the training sample number. Moreover, the grading accuracy of SVM is always higher than that of BP network, so SVM can also obtain higher grading accuracy for small training samples while BP network needs more training samples.

CONCLUSIONS

The paper develops a grading method of kiwi fruit based on volume estimation and surface defect. Mathematical model for the weight and volumetric pixel of kiwi fruit is fitted. The coefficient of determination is 0.9501, and the standard error is 4.2490, so the model has a good fitting effect and can be used for actual weight estimation of kiwi fruits. The SVM with v-SVC type adopting RBF kernel function can obtain the grading accuracy with 97.73% under the optimal kernel parameter σ ; The grading accuracy of BP network is rising along with the increase of numbers of training sets when the optimal number of hidden layers is 8. The grading performance of SVM is superior to that of BP neural network under different numbers of training set, and the grading accuracy of SVM is always higher than that of BP neural network.

ACKNOWLEDGEMENT

This paper was funded by the Natural Science Project of Sichuan Education Department under Grant 12ZA277.

REFERENCES

[1]. Cui Yongjie, Li Pingping, Ding Xian, et al., (2012) - *Kiwi fruit grading methods used for the detection of surface defects*, Agricultural Mechanization Research, Vol.34, No.10, pg.139-142;
[2]. Li Zhen,Hong Tiansheng,Wu Weibin, et al., (2006)- *Bilinear interpolation algorithm in the numerical simulation of litchi tree photosynthetic leaves the application of the image rotation*, Transactions of the CSAE, Vol.22, No.11, pg.179-182;
[3]. Lü Q, Tang M J., (2012) - *Detection of hidden bruise on kiwi fruit using hyperspectral imaging and parallelepiped classification*, Procedia Environmental Sciences,Vol.12, Part B, pg.1172-1179.
[4]. Lin Shengliang, Liu Zhi., (2007)- *Parameter selection in SVM with RBF kernel function*, Journal of Zhejiang University of Technology, Vol. 35, No.2, pg.163-167.
[5]. P. Wijethunga, S. Samarasinghe, D. Kulasiri., (2009)- *Towards a generalized color image segmentation for kiwifruit detection*, 24th International Conference Image and Vision Computing, Wellington , New Zealand , Nov. 23-25, pg.62-66.
[6]. Shao Hehong, Zheng Wanting, et al. (2009)- *Chinese gooseberry stage division based on computer vision*, Beijing Biomedical Engineering,Vol.28,No.5, pg.531-533;

由表 7 可知，在训练集样本数不同的情况下，SVM 的分级正确率均为 97.50%，BP 网络的分级正确率则受训练样本数的影响较大，且 SVM 的分级正确率高于 BP 网络的分级准确率，这说明 SVM 在训练样本数较小时也可获得很高的分级正确率， BP 网络则需要较多的训练样本数。

结论

本文研究了一种基于猕猴桃体积估计和表面缺陷的分级方法。本方法拟合出猕猴桃的重量和体积像素之间的数学模型，计算出可决系数为 0.9501，标准误差为 4.2490，表明该模型的拟合效果良好，可用于猕猴桃的实际重量估计。核函数为 RBF 的 v-SVC 型 SVM 在最佳核参数 σ 时其分级正确率可达 97.73%；BP 网络的最佳隐含层个数为 8，分级正确率随着训练集个数的增加而增加。在不同训练样本数下 SVM 的分级性能优于 BP 神经网络的分级性能，且其分级正确率高于 BP 网络的分级正确率。

致谢

本文受到四川省教育厅自然科学重点项目（项目号：12ZA277）。

参考文献

[1]. 崔永杰, 李平平, 丁宪, 等., (2012)- *猕猴桃分级果实表面缺陷的检测方法*，农业机械化研究，第 34 卷，第 10 期, 139-142;
[2]. 李震, 洪添胜, 吴伟斌, 等., (2006) - *双线性差值算法在荔枝树光合模拟中叶片图像旋转中的应用*, 农业工程学报, 第 22 卷, 第 11 期, 179-182;
[3]. 吕强, 唐明杰., (2012)- *利用高光谱成像和平行分类检测隐藏挫伤猕猴桃*. Procedia 环境科学，第 12 卷, B 部，1172-1179;
[4]. 林升梁. 刘志., (2007)- *基于RBF 核函数的支持向量机参数选择*, 浙江工业大学学报,第 35 卷,第 2 期,163-167;
[5]. P. Wijethunga, S. Samarasinghe, D. Kulasiri 等., (2009) - *基于广义彩色图像分割的猕猴桃检测*，第 24 届图像与视觉计算国际会议，新西兰惠灵顿，2009 年 11 月 23-25 日，62-66;
[6]. 邵和鸿. 郑万挺. 彭加寅.,(2009)- *基于计算机视觉技术的猕猴桃分级方法*, 北京生物医学工程, 第 28 卷, 第 5 期, 531-533;

[7]. Wu Tao, Yuan Chi, Chen Jun. (2012) - *Research on the object extraction of kiwifruit based on machine vision*, Agricultural Mechanization Research, Vol.34, No.12, pg. 21-26;
[8]. Wang Junhao, Yang Wenhui. (2011) - *Common pests and Integrated Prevention of kiwifruit*, Plant Doctor, Vol.24, No.3, pg.16-17;
[9]. Xu L., You Z., Wu S. et al., (2013) - *Development and experiment on automatic grading equipment for kiwi*, INMATEH-Agricultural Engineering, Vol.41, No.3, pg. 55-64;
[10]. Yang Jie, Huang Chaobing., (2010) - *Digital image processing and MATLAB*, Beijing: Electronic Industry Press;
[11]. Ying Wei, Wang Zhengou, An Jinglong., (2006) - *Study on Multiclass Text Categorization Method Based on Improved Support Vector Machine*, Computer Engineering, Vol.32, No.16, pg.74-76.

[7]. 武涛, 袁池, 陈军., (2012) - *基于机器视觉的猕猴桃果实目标提取研究*, 农机化研究, 第 34 卷,第 12 期, 21-26;
[8]. 王筠皓. 杨文辉., (2011) - *猕猴桃常见病虫害种类及综合防治*,植物医生, 第 24 卷, 第 3 期,16-17;
[9]. 许丽佳, 游志昆, 邬盛, 等. (2013) - *猕猴桃自动分级设备的研究与应用*,农业工程,第 41 卷,第 3 期, 55-64;
[10]. 杨杰, 黄朝兵., (2010) - *数字图像处理及 MATLAB 实现*, 北京: 电子工业出版社;
[11]. 应伟, 王正欧, 安金龙., (2006) - *一种基于改进的支持向量机的多类文本分类方法*, 计算机工程, 第 32 卷,第 16 期, 74-76.

MATHEMATICAL MODEL OF THE PNEUMATIC-SCREW CONVEYOR MECHANISM OPERATION
/
МАТЕМАТИЧНА МОДЕЛЬ ФУНКЦІОНУВАННЯ ШНЕКОВОГО МЕХАНІЗМУ ПНЕВМОШНЕКОВОГО ТРАНСПОРТЕРА

Ph.D. Hevko R.B. [1)], Assoc.Prof. Ph.D. Stud. Dzyura V.O.[2)], Romanovsky R.M.[2)]
[1)]Ternopil National Economical University, Lvivska str., 11, Ternopil / Ukraine
[2)]Ternopil Ivan Pul'uj National Technical University, Ruska str., 56, Ternopil / Ukraine
E-mail: volodymyr-dzyura@rambler.ru

Abstract: *The paper comprises a mathematical model of technological process of dry material transporting by the screw conveyor. The mathematical model developed in the article, presents the movement of material particle of the dry medium in the screw feeder, mounted cantilever with the gap relatively casing. Initial data for building the mathematical model were: screw rotation angle speed, feeder screw diameter, helical line pitch of the feeder screw turn, material part parameters. This model can be used for interpreting the design-kinematic parameters of the pneumatic-mechanic transporter. Graphs of dependence of the angle change deflection and the screw angle speed on the time of the screw turn rotation under vibration processes have been built.*

Keywords: *technological process, mathematic model, dry material, transporting, transporter*

Анотація. *Розроблено математичну модель роботи пнемо шнекового транспортера для транспортування сипких матеріалів з шнеком, який встановлено консольно з зазором відносно кожуха. Вихідними даними для побудови математичної моделі були: кутова швидкість обертання шнека, діаметр шнека живильника, крок гвинтової лінії витків шнека живильника, параметри матеріальної частинки. Дана може бути використана для обґрунтування конструктивно-кінематичних параметрів пнемо шнекового транспортера. Побудовані графіки залежності зміни кута відхилення та кутової швидкості шнека від часу повороту витка шнека при вібраційних процесах та без них.*

Ключові слова: *технологічний процес, математична модель, сипкий матеріал, транспортування, транспортер*

INTRODUCTION

Screw spiral conveyors as the individual technical part of transporting mechanisms have been widely applied in the component schemes of machines used for loading or transporting of small dry materials owing to their simple design, easy technical maintenance and possibility to load and unload at any stage of technological process of the transporting device operation [1].

General disadvantage of the screw mechanisms operation is not only the fact, that the spiral screw conveyor turns the material along the axis longitudinally, but can rotate and cause the damage of material, which results in the decrease of the mechanisms efficiency [2,3] The highest economic efficiency or the maximum productivity is obtained by the pneumatic-screw conveyor (PSC).

MATERIAL AND METHOD

While optimizing the parameters of transporting-technical systems, the operating elements of which are screw mechanisms, at the stage of their design it is worthy building the mathematical model of the technological process of the PSC screw feeder in order to obtain the regularities of operating screw feeder mechanism, which is mounted cantilevered on its support, depending on its main design-kinematic parameters [4].

To analyze and to build the mathematical model of the technological process of the screw feeder operation, let us study the movement of the material particle of the dry medium, which can be treated as the combined material body of mass m_c, which is on the surface of the spiral turns 1 of the screw 2, which is mounted cantilevered with the gap relatively casing 3, the particle moving along the axis of rotation Ox with the longitudinal speed V_0 towards the pneumatic system PSC.

ПЕРЕДУМОВА

Шнекові гвинтові конвеєри, як окремий технічний елемент транспортних механізмів, знайшли широке використання в компонувальних схемах машин для перенавантаження, або переміщення дрібносипких матеріалів у зв'язку з їх простотою конструкції, нескладністю технічного обслуговування та можливістю завантаження й розвантаження матеріалу в будь якому місці технологічного процесу роботи транспортного пристрою [1].

Загальним недоліком роботи шнекових механізмів є надання спіральними витками гвинтового конвеєра не тільки поступального осьового переміщення матеріалу, але й обертового руху, що призводить не тільки до пошкодження матеріалу, але і зменшення продуктивності механізмів [2,3] і, як наслідок досягнення найвищої економічної ефективності, або максимальної продуктивності пнемо шнекового транспортера (ПШТ) в цілому.

МАТЕРІАЛ І МЕТОДИКА

В процесі оптимізації параметрів транспортно-технічних систем, які мають робочі органи гвинтових механізмів і на стадії їх проектування доцільно спочатку побудувати математичну модель технологічного процесу роботи шнекового живильника ПШТ з метою отримання закономірностей процесу функціонування механізму шнекового живильника, який встановлено консольно на своїй опорі, залежно від його основних конструктивно-кінематичних параметрів [4].

Для аналізу та побудови математичної моделі технологічного процесу роботи шнекового живильника розглянемо рух матеріальної частинки сипкого середовища, яку уявимо як зв'язане матеріальне тіло приведеною масою m_c, яка знаходиться на поверхні спіральних витків 1 шнека 2, який встановлено консольно з зазором відносно кожуха 3, при цьому частинка рухається вздовж його осі обертання Ox з поступальною швидкістю V_o до пневмосистеми ПШТ.

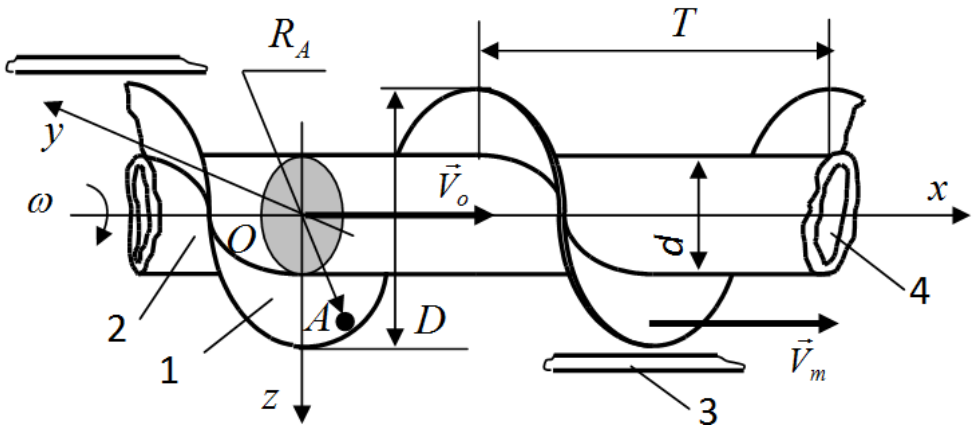

Fig. 1 – Sheme of calculation movement of the dry material particle of mass mc:
1 – screw turn; 2 – screw; 3 – screw casing ; 4 – screw tube

When the particle of the body with mass m_c starts contacting the surface of the spiral turns of the screw, it slides along the surface of the screw turn and casing, travelling simultaneously along the vector direction of the axis displacement of the conveyor turns $\vec{V}_m$ towards the vector of longitudinal speed $\vec{V}_o$, owing to the rotation of the spiral turns of the screw feeder with the angular speed ω during some time. (Fig.1).

In this case we have a complicated movement of the physical body, when the particle takes part in: relative displacement – along the surface of the screw feeder turns with speed V_{1c}; transporting displacement together with the turn with the speed V_{2c} and simultaneously in the horizontal displacement towards the vector $\vec{V}_m$.

RESULTS

The material body, that is, the particle of the material with mass m_k, which is on the surface of the screw conveyor turn at the moment $t=0$ is subject to gravitation m_cg , reaction force of the turn surface N_1 and casing N_2, and, correspondingly, to functional drag force F_{1m} and F_{2m}, when the material moves along these surfaces. Let us introduce the stable three-dimensional coordinate system *Oxyz* (Fig.1), in which the axis *Ox* coincides with the rotation axis of the screw feeder, and the axis *Oy* is parallel to the horizontal surface.

During the period of time *t*, or at the moment of time *t* the screw turn will be in the angular rotation $\varphi(t)$, the screw angular rotation being expressed in terms of the dependence [5]:

З початком контакту частинки тіла масою m_c з поверхнею спіральних витків шнека, вона за рахунок обертання спіральних витків шнекового живильника з кутовою швидкістю ω за проміжок часу ковзає по поверхні витка шнека і кожуха та одночасно переміщується вздовж напрямку вектора осьового переміщення витків конвеєра $\vec{V}_m$ у напрямку вектора поступальної швидкості $\vec{V}_o$ (рис.1).

У цьому випадку маємо складний рух фізичного тіла, коли частинка приймає участь: у відносному – вздовж поверхні витків шнекового живильника з швидкістю V_{1c}; у переносному – разом з витком з швидкістю V_{2c} та одночасно у горизонтальному переміщенні у напрямку вектора $\vec{V}_m$.

РЕЗУЛЬТАТИ

На матеріальне тіло, тобто частинку матеріалу приведеною масою m_k,, яка знаходиться на поверхні витка шнекового конвеєра у момент часу $t=0$, діє сила тяжіння m_cg, сили реакції поверхні витка N_1 і кожуха N_2 та, відповідно, сили тертя ковзання F_{1m} і F_{2m} при русі коренеплоду по даним поверхням.

Введемо нерухому просторову систему координат *Oxyz* (рис.1) у якій вісь *Ox* співпадає з віссю обертання шнекового живильника, а вісь *Oy* розташована паралельно горизонтальній площині.

За проміжок часу t , або в момент часу t виток шнека повернеться на кут повороту $\varphi(t)$, при цьому кут повороту шнека виразимо залежністю [5]:

$$\varphi(t) = 2\pi\omega t + \varphi_1 = 2\pi\frac{d\varphi}{dt} + \varphi_1, \quad (1)$$

Where: ω - screw angular rotation speed, rad/sec;

$\varphi_1 = const$ – initial screw angular rotation at $t=0$, rad.

According to [6], simultaneously with the rotation movement the screw is under the two-dimensional parallel movement in the plane *zOy*, which is perpendicular to the rotation axis of the tube 4 of the screw 3, that is, to the screw shaft axis.

When $x=0$, this displacement of the screw can be expressed by the canonical equation of the axis 0 center movement of the screw feeder shaft:

Де: ω – кутова швидкість обертання шнека, рад/с;

$\varphi_1 = const$ – початковий кут повороту шнека при $t=0$, рад.

Згідно з [6], поряд з обертальним рухом шнек здійснює плоскопаралельний рух в площині *zOy* яка перпендикулярна осі обертання труби 4 шнека 3, тобто осі вала шнека.

При $x=0$ дане переміщення шнека можливо задати канонічним рівняння руху центру осі O вала шнекового живильника:

$$[z_0(t); y_0(t); x_0(t)] = [z_0(t); y_0(t); 0], t \geq 0, \quad (2)$$

where z_0 and y_0 according to [5] can be expressed as:

де z_0 і y_0 згідно з [5] можна задати у вигляді:

$$\left.\begin{aligned} z_0(t) &= -f\left[\varphi_o(t)\cos\varphi_A(t)\right] + g\left[\varphi_o(t)\sin\varphi_o(t)\right]; \\ y_0(t) &= -f\left[\varphi_A(t)\sin\varphi_A(t)\right] - g\left[\varphi_A(t)\cos\varphi_o(t)\right] \end{aligned}\right\}. \quad (3)$$

The equation of the movement of the particle of the material with the mass m_c in the stable system of coordinates Oxy, according to the classic laws of mechanics [7], in the vector form can be expressed as:

Рівняння руху частинки матеріалу приведеною масою m_c у нерухомі системі координат Oxy згідно з класичними законами механіки [7] у векторній формі запишеться у наступному вигляді:

$$m_c\ddot{\vec{x}}_i = m_c\vec{a}_c = m_c\frac{d^2\vec{R}_A}{dt^2} = \vec{G}_{m_c} + \sum_{i=1}^{2}\vec{N}_{n_i} + \sum_{i=1}^{2}\vec{F}_{m_i},\ t > 0. \quad (4)$$

In this case the dependence components (4), that is, angular-momentum radius-vector $\vec{R}_A$, particle $\vec{G}_{m_c}$ force vector, vector value of the total reaction of surfaces $\sum_{i=1}^{2}\vec{N}_i$ and the total frictional drag force $\sum_{i=1}^{2}\vec{F}_{m_i}$ of the particle along the surfaces is determined by:

– momentum vector $\vec{R}_A$ of the particle location in the plane zOy, or the combination of the vector and coordinate manner of the particle movement:

При цьому складові залежності (4), тобто біжучий радіус-вектор $\vec{R}_A$, векторний запис сили ваги частинки $\vec{G}_{m_c}$, векторне значення сумарної реакція поверхонь $\sum_{i=1}^{2}\vec{N}_i$ і сумарної сили тертя ковзання $\sum_{i=1}^{2}\vec{F}_{m_i}$ частинки по поверхнях визначаються:

- біжучий вектор $\vec{R}_A$ положення частинки в площині zOy, або зв'язок векторного и координатного способу руху частинки:

$$\vec{R}_A(t) = \left[x_A(t); y_A(t); z_A(t)\right] = ix(t) + jy(t) + kz(t) \quad (6)$$

Where: i, j, k - the cross-cuts of corresponding axis of the coordinate system;

– vector of the particle mass force $\vec{G}_{m_c}$:

де i, j, k – орти відповідних осей системи координат;

- векторний запис сили ваги $\vec{G}_{m_c}$ частинки:

$$\vec{G}_{m_c} = \left(m_c g; 0; -m_c g\right); \quad (7)$$

- vector value of the force reaction $\vec{N}_i$ of the contacting surface P_i, of the feeder according to [5]:

- векторне значення сили реакції $\vec{N}_i$ контактуючої поверхні P_i живильника згідно з [5]:

$$\vec{N}_i = \vec{n}_i\mu_i, \quad (8)$$

where $\vec{n}_i$ - unit vector, perpendicular to the plane of the corresponding surface P_i, or unit normal to the surface P_i, i = 1,2;

μ_i - corresponding plane sticking reaction:

– vector value of the particle frictional drag force on the P_i surface

де $\vec{n}_i$ – одиничний вектор, перпендикулярний до площини відповідної поверхні P_i, або одинична нормаль до поверхні P_i, i = 1,2;

μ_i – реакція в'язі відповідної площини:

– векторне значення сили тертя ковзання частинки по P_i поверхні

$$\vec{F}_{m_i} = -f_i m_c\vec{a}_{c_i} = -f_i\left|\vec{N}_i\right|\left(\dot{\vec{R}}_A - \vec{V}_i\right)/\left|\dot{\vec{R}}_A - \vec{V}_i\right| = -f_1\left|\vec{N}_i\right|\left(\frac{d\vec{R}_A}{dt} - \vec{V}_i\right)/\left|\frac{d\vec{R}_A}{dt} - \vec{V}_i\right|, \quad (9)$$

Where: f_i - frictional drag coefficient P_i of the surface; V_i - movement speed P_i of the surface in the point $\vec{R}_A(t)$ at the moment of time t.

If the screw feeder is mounted under angle α to the horizon, then the projection of the vector of the particle gravitation of the mass m_c of the dry medium on the coordinate axis will look like:

Де: f_i – коефіцієнт тертя ковзання P_i поверхні;

V_i – швидкість руху P_i поверхні в точці $\vec{R}_A(t)$ і момент часу t.

Якщо шнековий живильник встановлено під кутом α до горизонту, тоді проекції вектора сили тяжіння частинки приведеної маси m_c сипкого середовища на координатні осі матимуть вигляд:

$$\vec{G}_{m_c} = \left(m_k g\cos\alpha; 0; -m_k g\sin\alpha\right) \quad (10)$$

Solution of the task is reduced to finding the sticking reaction μ_i of the corresponding plane P_i of the surface, or in our case for finding μ_1 and μ_2 - correspondingly, sticking reaction of the screw turn surface and the feeder casing surface.

Рішення задачі зводиться до знаходження реакцій в'язі μ_i відповідної площини P_i поверхні, або в нашому випадку для знаходження μ_1 та μ_2 – відповідно, реакції в'язі поверхні витка шнека та поверхні кожуха живильника.

With this purpose let us write the location of unit vectors $\vec{n}_1$ and $\vec{n}_2$, which are perpendicular to the planes of corresponding surfaces of contact of the material particle, having written at first the equation, by which the screw surface and the PSC screw feeder casing surface are presented.

According to [7,8] canonical appearance of the equation of the screw surface P_1, and casing surface P_2 are presented as relations:

Для цього запишемо положення одиничних векторів $\vec{n}_1$ і $\vec{n}_2$, які перпендикулярні до площин відповідних поверхонь контакту частинки матеріалу, записавши спочатку рівняння якими задані поверхні шнека та кожуха шнекового живильника ПШТ.

Згідно з [7, 8] канонічний вигляд рівняння поверхні шнека P_1 та кожуха P_2 задані відношеннями:

$$\left.\begin{aligned} P_1(0{,}5D;R;\varphi;x) &\equiv x+\frac{T}{2\pi}(\varphi-\varphi_0)=0;\\ P_2(x;y;z) &\equiv z^2+y^2-0{,}25D^2=0 \end{aligned}\right\}, \tag{11}$$

Where:

D – feeder screw diameter, m;

T – turns spiral pitch of the screw feeder, m.

Then the location of unit vectors $\vec{n}_1$ and $\vec{n}_2$ will be found:

Де:

D – діаметр шнека живильника, м;

T – крок гвинтової лінії витків шнека живильника, м.

Тоді положення одиничних векторів $\vec{n}_1$ і $\vec{n}_2$ будуть визначатися:

$$\left.\begin{aligned} \vec{n}_1 &= \left(-T\sin\varphi;T\cos\varphi;\frac{\pi D}{c(0{,}5D)}\right);\\ \vec{n}_2 &= (-\cos\varphi;\sin\varphi;0) \end{aligned}\right\}, \tag{12}$$

Where: C screw parameter is:

де параметр шнека:

$$c(0{,}5D)=\sqrt{T^2+\pi^2D^2}=\pi D\sqrt{tg^2\beta+1}$$

$$T=\pi D tg\beta$$

β -angle of pitch of the screw turns, (degree):

Taking into account the canonic equation of the screw rotation (2) and its longitudinal movement we obtained:

β – кут підйому гвинтової лінії витків шнека, град.

З врахуванням канонічного рівняння обертання шнека (2) та його поступального руху одержано:

$$\vec{V}_1=\frac{d}{dt}[0{,}5D\cos\varphi_o(t);0{,}5D\sin\varphi_o(t);0]+\frac{d}{dt}[z_o(t);y_o(t);0], \tag{13}$$

or

або

$$\vec{V}_1=\left(-\pi D\frac{d\varphi}{dt}\cdot y+z_o'(t);y_o'\left(+\pi D\frac{d\varphi}{dt}\cdot z;0\right)\right) \tag{14}$$

Then in order to find the sticking reaction of the screw turn surface μ_1 and the sticking reaction of the feeder casing μ_2, let us multiply the written scalar values of corresponding components of the equation (4) by the corresponding values of unit vectors $\vec{n}_1$ and $\vec{n}_2$ from the equation (12).

As a result we will obtain:

- provided $i=1$:

Тоді для знаходження реакції в'язі поверхні витка шнека μ_1 та реакції в'язі поверхні кожуха живильника μ_2 помножимо записані скалярні значення відповідних складових рівняння (4) на відповідні значення одиничних векторів $\vec{n}_1$ і $\vec{n}_2$ з рівняння (12).

В результаті одержимо:

- при умові $i=1$:

$$\begin{aligned} 0=&-\frac{T}{c(0{,}5D)}m_c g\cos\alpha\sin\varphi-\frac{\pi D}{c(0{,}5D)}m_c g\sin\alpha+\mu_1-\\ &-f_2\mu_2\frac{\pi DT}{c(0{,}5D)\left|0{,}5\dot{\vec{D}}\right|}\left(\frac{d\varphi}{dt}\right)+f_1\mu_1 T\frac{[-z_o'(t)\sin\varphi+y_o'(t)\cos\varphi]}{c(0{,}5D)\left|0{,}5\dot{\vec{D}}-\vec{V}_1\right|} \end{aligned} \tag{15}$$

or taking into account (14) and the fact, that

або з врахуванням (14) і того, що

$$\dot{\vec{D}}=\frac{d\vec{D}}{dt},\ c(0{,}5D)=\pi D\sqrt{tg^2\beta+1}=\frac{\pi D}{\cos\beta}$$

$$0 = -m_c g(\cos\alpha \sin\varphi \sin\beta + \sin\alpha \cos\beta) + \mu_1 - f_2\mu_2 \frac{\pi D \sin\beta}{\left|\frac{d\vec{D}}{dt}\right|}\left(\frac{d\varphi}{dt}\right) + \tag{16}$$

$$+ f_1\mu_1 \sin\beta \frac{[-z_o'(t)\sin\varphi + y_o'(t)\cos\varphi]}{\left|0{,}5\frac{d\vec{D}}{dt} - \frac{d}{dt}[0{,}5\cos\varphi_o(t); 0{,}5\sin\varphi_o(t)] - \frac{d}{dt}[z_o]\right|}$$

– provided $i = 2$:

- при умові $i = 2$:

$$m_c a_c = 0{,}5 m_c D(\dot{\varphi})^2 = 0{,}5 D m_c \left(\frac{d\varphi}{dt}\right)^2 = \tag{17}$$

$$= -m_c g \cos\alpha \cos\varphi + \mu_2 - \frac{f_1\mu_1[z_o'(t)\cos\varphi + y_o'(t)\sin\varphi]}{\left|0{,}5\dot{\vec{D}} - \vec{V}_1\right|}$$

or taking into account (14) and the fact, that

або з врахуванням (14) і того, що

$$\dot{\vec{D}} = \frac{d\vec{D}}{dt}$$

$$0{,}5 D m_c \left(\frac{d\varphi}{dt}\right)^2 = -m_c g \cos\alpha \cos\varphi + \mu_1 - \tag{18}$$

$$- \frac{f_1\mu_2[z_o'(t)\cos\varphi + y_o'(t)\sin\varphi]}{\left|0{,}5\frac{d\vec{D}}{dt} - \frac{d}{dt}[0{,}5\cos\varphi_o(t); 0{,}5\sin\varphi_0(t)] - \frac{d}{dt}[z_o(t); y_o(t); 0]\right|}$$

Dependencies (17), (18) are the system of equations, solution of which relatively the unknown reactions of sticking of the screw turn surface μ_1 and the screw feeder casing surface μ_2 can be expressed as:

Залежності (17), (18) є системою рівнянь, розв'язок якої відносно невідомих реакцій в'язі поверхні витка шнека μ_1 та поверхні кожуха μ_2 шнекового живильника має вигляд:

$$\mu_1 = \frac{m_c g \sin\beta(\cos\alpha \sin\varphi + m_c g \sin\alpha) - f_2\mu_2 \frac{\pi D \sin\beta}{\left|0{,}5\frac{dD}{dt}\right|}\left(\frac{d\varphi}{dt}\right)}{1 + f_1 \sin\beta \frac{[-z_o'(t)\sin\varphi + y_o'(t)\cos\varphi]}{\left|0{,}5\frac{d\vec{D}}{dt} - \frac{d}{dt}[0{,}5\cos\varphi_o(t); 0{,}5\sin\varphi_o(t)] - \frac{d}{dt}[z_o]\right|}} \tag{19}$$

$$\mu_2 = m_c\left[0{,}5D\left(\frac{d\varphi}{dt}\right)^2 + g\cos\alpha\cos\varphi\right] + \tag{20}$$

$$+ f_1\mu_1 \frac{[z_o'(t)\cos\varphi + y_o'(t)\sin\varphi]}{\left|0{,}5\left(\frac{d\vec{D}}{dt}\right) - \frac{d}{dt}[0{,}5\cos\varphi_o(t); 0{,}5\sin\varphi_o(t)] - \frac{d}{dt}[z_o(t); y_o(t); 0]\right|}$$

or, having substituted the value of the sticking reaction of the casing surface μ_2 from the dependence (2) in the equation (19), we will obtain the dependence for finding the sticking reaction μ_2 of the screw-feeder turn surface

або підставивши значення реакцій в'язі поверхні кожуха μ_2 із залежності (20) у рівняння (19) одержимо залежність для визначення реакції в'язі μ_1 поверхні витка шнека-живильника

$$\mu_1 = m_c\left\{0{,}5D\left(\frac{d\varphi}{dt}\right)^2 f_2 + g\left[\cos\alpha \sin\varphi \sin\beta + \sin\alpha \cos\beta + f_2 \cos\alpha \cos\varphi\right]\right\}$$

$$\Big/ \frac{\left(\frac{d\vec{D}}{dt}\right)}{2\pi D \sin\beta\left(\frac{d\varphi}{dt}\right)} + \left[\frac{1}{\left|0{,}5\left(\frac{d\vec{D}}{dt}\right) - \frac{d}{dt}\left[0{,}5\cos\varphi_o(t); 0{,}5\sin\varphi_o(t)\right] - \frac{d}{dt}\left[z_o(t); y_o(t); 0\right]\right|}\right] \times \tag{21}$$

$$\times f_1\left\{\sin\beta\left[-z_o'(t)\sin\varphi + y_o'(t)\cos\varphi\right]\right\} - f_1 f_2\left[z_o'(t)\sin\varphi + y_o'(t)\cos\varphi\right]$$

Finally, from the equation of the material particle movement of the mass m_c (4) we will find:

У кінцевому випадку з рівняння руху частинки матеріалу приведеною масою m_c (4) знаходимо:

$$m_c T\ddot{\varphi} = 2\pi m_c g \sin\alpha - \frac{\mu_1}{c(0,5D)}(2\pi)^2\, 0,5D - f_2\mu_2 \frac{T(\dot{\varphi}-2\pi\omega)}{\left|0,5\ddot{\vec{D}}\right|} - f_1\mu_1 \frac{T(\dot{\varphi}-2\pi\omega)}{\left|0,5\ddot{\vec{D}}-\vec{V}_1\right|}, \quad (22)$$

or

або

$$m_c \pi D tg\beta\left(\frac{d^2\varphi}{dt^2}\right) = 2\pi\left(m_c g\sin\alpha - \mu_1 cos\,\beta\right) - 2\pi D\left(tg\beta - 1\right)\left(\frac{d\varphi}{dt}\right)\times$$
$$\times\left[f_2\mu_2\left|\frac{d\vec{D}}{dt}\right|^{-1} - f_1\mu_1\left|\left(\frac{d\vec{D}}{dt} - 2\frac{d}{dt}\left[0,5cos\,\varphi_o(t);0,5sin\,\varphi_o(t)\right] - 2\frac{d}{dt}\left[z_o(t);y_o(t);0\right]\right)\right|^{-1}\right] \quad (23)$$

If the vibration of the cantilever screw-feeder does not occur, then dependencies (20) and (21) are sufficiently simplified. Then we will obtain:

Якщо вібрація консольного шнека-живильника відсутня, тоді залежності (20) і (21) значно спрощуються. При цьому одержимо:

$$\mu_1 = 0,5m_c f_2 D(\dot{\varphi})^2 \frac{2\pi 0,5D\left(\frac{d\varphi}{dt}\right)T}{c(0,5D)\left|0,5\ddot{\vec{D}}\right|} + m_c g\frac{T}{c(0,5D)}cos\alpha\, sin\varphi + \Bigg\}$$
$$+ m_c g\frac{2\pi 0,5D}{c(0,5D)}sin\alpha + m_c f_2 g\frac{2\pi 0,5D\left(\frac{d\varphi}{dt}\right)}{c(0,5D)\left|0,5\ddot{\vec{D}}\right|}cos\alpha\, cos\varphi \quad (24)$$

$$\mu_2 = 0,5m_c D(\dot{\varphi})^2 + m_c g\, cos\alpha\, cos\varphi, \quad (25)$$

or, after the transformation and simplification of (24), (25), we will obtain:

або після перетворення та спрощення (24), (25) одержимо:

$$\mu_1 = \frac{2\pi m_c f_2 D\, sin\beta\left(\frac{d\varphi}{dt}\right)}{\left|\frac{d\vec{D}}{dt}\right|}\left[0,5D\left(\frac{d\varphi}{dt}\right)^2 + g\, cos\alpha\, cos\varphi\right] + \Bigg\};$$
$$+ m_c g\left(cos\alpha\, sin\varphi\, sin\beta + sin\alpha\, cos\beta\right) \quad (26)$$

$$\mu_2 = 0,5m_c D\left(\frac{d\varphi}{dt}\right)^2 + m_c g\, cos\alpha\, cos\varphi \quad (27)$$

Thus, the obtained differential dependencies (20-23), (26), (27) are the mathematical model, which specifies the technological process of the screw feeder operation and can be used for the further interpreting of the construction-kinematic parameters of PSC.

To provide more complete description of the technological process of the PSC screw feeder operation differential dependencies (20), (21), (23) must be supplemented by the given initial conditions:

Таким чином одержані диференціальні залежності (20-23), (26), (27) є математичною моделлю, яка характеризує технологічний процес роботи шнекового живильника та може бути використана для подальшого обґрунтування конструктивно-кінематичних параметрів ПШТ.

Для більш повного опису технологічного процесу роботи шнекового живильника ПШТ диференціальні залежності (20), (21), (23) необхідно доповнити заданими початковими умовами:

$$\varphi(0) = \varphi_o;\ \dot{\varphi}(0) = d\varphi/dt = \varphi_1, \quad (28)$$

But it must be noted, that the mathematical model (20-23) is correct only if $\mu_i > 0$. If this condition is not provided and $\mu_i < 0$, then the material particle breaks the contact with the surface and equation (4) does not describe correctly the real process of the screw feeder movement.

It should be noted, that dependencies (23), (26) and (27) can have fixed solutions as to the reaction of the corresponding planes sticking μ_{iP_i} and the angular rotation φ_{P_i}, which correspond to the points of rest:

при цьому, необхідно зауважити, що математична модель (20-23) адекватна тільки при умові $\mu_i > 0$. Якщо дана умова не виконується і $\mu_i < 0$, тоді частинка матеріалу втрачає контакт з поверхнею і рівняння (4) вже не адекватно описує реальний процес руху шнекового живильника.

Необхідно також додати, що залежності (23), (26) і (27) можуть мати стаціонарні рішення відносно реакцій в'язі відповідних площин μ_{iP_i} і кута повороту φ_{P_i}, які відповідають точкам спокою:

$$\mu_{1P_i} = \frac{T}{c(0{,}5D)} m_c g \cos\alpha \sin\varphi_{P_i} + \frac{2\pi 0{,}5D}{c(0{,}5D)} m_c g \sin\alpha + \\ + 2\pi m_c f_2 g \cos\alpha \cos\varphi_{P_i} 0{,}5D / c(0{,}5D) \quad (29)$$

$$\mu_{2P_i} = m_c g \cos\alpha \cos\varphi_{P_i} \quad (30)$$

$$0 = 2\pi m_c g \sin\alpha - \frac{\mu_{1P_i}}{c(0{,}5D)} (2\pi)^2 0{,}5D + 2\pi f_2 \mu_{2P_i} + 2\pi f_2 \mu_{2P_i} T / c(0{,}5D) \quad (31)$$

or after the transformation and simplification (24), (25) we will obtain:

або після перетворення та спрощення (24), (25) одержимо:

$$\left.\begin{aligned} \mu_{1P_i} &= m_c g\left(\cos\alpha \sin\varphi_{P_i} \sin\beta + \sin\alpha \cos\beta + f_2 \cos\alpha \cos\varphi_{P_i} \cos\beta\right); \\ \mu_{2P_i} &= m_c g \cos\alpha \cos\varphi_{P_i}; \\ m_c g - \mu_{1P_i} &\cos\beta + f_2 \mu_{2P_i} \sin\beta = 0 \end{aligned}\right\} \quad (29)$$

To find φ_{P_i} from the system of equations (29) μ_{iP_1} will be excluded.

Для визначення φ_{P_i} із системи рівнянь (29) виключимо μ_{iP_1}.

$$\cos\varphi_{p_i}\left(1 + ctg\varphi_{p_i}\left\{ctg\beta + [\pi D \sin\beta(f_2 \sin\beta - \cos\beta)]^{-1}\right\}\right) = . \\ = \left\{ctg\beta - [\pi D \sin\beta(f_2 \sin\beta - \cos\beta)]^{-1}\right\} \quad (30)$$

In this case, when $\mu_{P_i} > 0$ the set of the acceptable parameters of the model can be defined, because of its correctness and stability of the fixed solutions of the vibration-free process of the screw feeder operation.

Numerical investigation of the mathematic model (20), (21), (23), (28) was carried out in the mathematic package of the applied software for PC, as the result of change $\dot{\varphi}(t) = \psi(t)$ the dependence (23) being reduced to the system of differential equations of the first degree.

In Fig.2 and Fig.3 typical graphs of the equation system solution behavior (20), (21), (23), (28) or the dependence of the change of the deflection $\varphi(t)$ and the angular speed of the screw $\omega(t)$ on the time of the screw turn rotation, taking into account the vibration processes, which appear during the PSC screw feeder operation, are presented.

У цьому випадку при умові $\mu_{P_i} > 0$ можна виділити множину допустимих параметрів моделі, виходячи з точки зору її адекватності і стійкості стаціонарних рішень безвібраційного процесу роботи шнекового живильника.

Числове дослідження математичної моделі (20), (21), (23), (28) проводили в математичному пакеті прикладної програми для ПК, при цьому в результаті заміни $\dot{\varphi}(t) = \psi(t)$ залежність (23) приводилася до системи диференціальних рівнянь першого порядку.

На рис. 2 і рис. 3 наведено типові графіки поведінки рішення системи рівнянь (20), (21), (23), (28), або залежність зміни кута відхилення $\varphi(t)$ та кутової швидкості шнека $\omega(t)$ від часу повороту витка шнека з врахуванням вібраційний процесів, які виникають під час роботи шнекового живильника ПШТ.

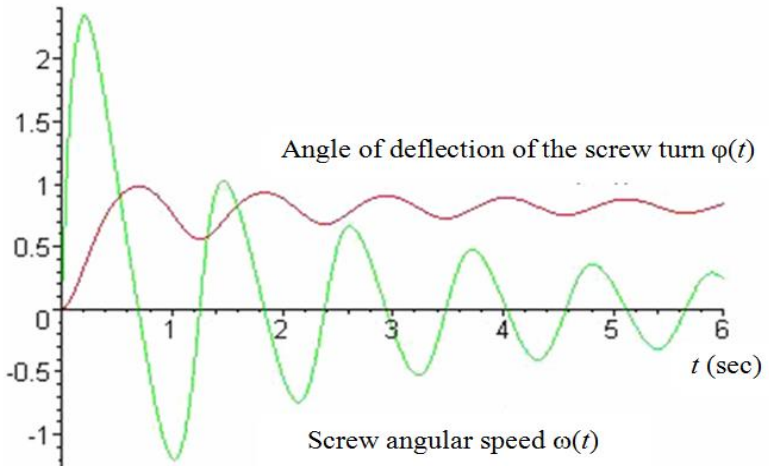

Fig. 2 - Dependence of the angle of deflection and the screw angular speed change on the time of the screw turn rotation

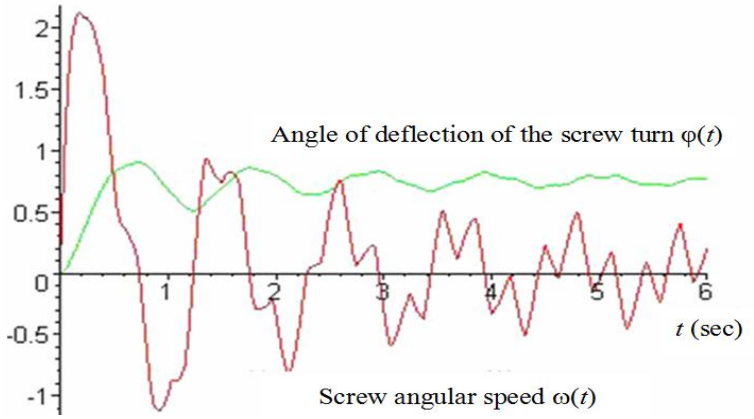

Fig. 3 - Dependence of the angle of deflection and the screw angular speed change on the time of the screw turn rotation under vibration.

Analysis of the graphic dependencies testifies the effect of the increased vibration amplitudes on the system solutions, which are presented in Fig.3 compared with those in Fig.2.

In Fig.4 some integrated results of numerical calculations of possible options of the system behavior are presented.

Аналіз графічних залежностей показує вплив на рішення системи збільшених амплітуд вібрацій коливного процесу, які наведено на рис. 3 в порівняння з рис. 2.

На рис. 4 приведені деякі інтегровані висновки числових розрахунків можливих варіантів поведінки системи.

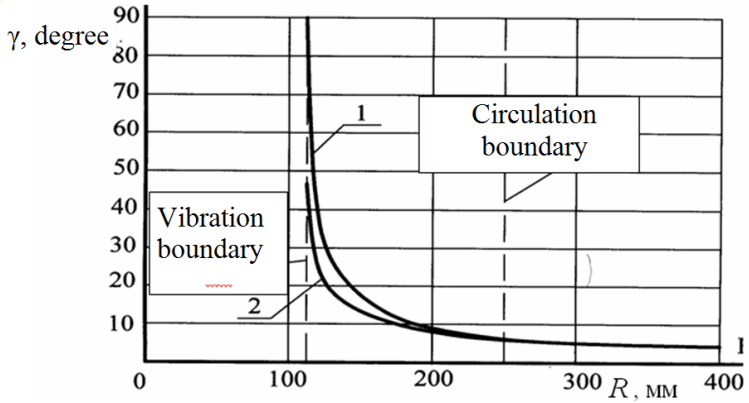

Fig. 4 - Dependence of the angle of deflection of the material particle on the screw radius at T= 0,66 м; $\alpha = \pi/36$; $\omega = 0.68$; $f_1 = f_2 = 0.3$
1 – amplitude value; 2 – fixed value

CONCLUSIONS

The obtained differential dependencies (20-23), (26), (27) can be treated as the mathematical model, which specifies the technological process of the screw feeder operation and can be used for the further interpreting of the construction-kinematic parameters of the pneumatic-screw conveyer.

REFERENCES

[1]. Gevko B.M., Danil'chenko M.G., Rogatins'kij R.M., (1993) - *Mechanisms of helical devices,* L'viv: Svit, p. 208;
[2]. Gevko R.B., Vitrovij A.O., (2012) - *Improving the technical level of flexible screw conveyors*, Ternopil: Aston, pg. 209;
[3]. Rogatins'kij R., Gevko I., Rogatins'ka L., (2013) - *Optimization of parameters screw transport and technological systems*, Visnik TNTU, Tom 69. No.1. pg. 116–125;
[4]. Hevko R., Dzyura V., Romanovsky R., (2006) - *Screw pneumo-mechanic transporter,* Patent №44544, IPC-G65B 53/00, Applicant and owner of the patent: Ternopil National Economical University.- № u200903515; Applied 13.04.2009; published 12.10.2009, Bulletin № 19, p.3.

ВИСНОВКИ

Одержані диференціальні залежності (20-23), (26), (27) є математичною моделлю, яка характеризує технологічний процес роботи шнекового живильника та може бути використана для подальшого обґрунтування конструктивно-кінематичних параметрів пнемо шнекового транспортера.

БІБЛІОГРАФІЯ

[1]. Гевко Б.М., Данильченко М.Г., Рогатинський Р.М., (1993) - *Механізми з гвинтовими пристроями*, Львів : Світ, 208 с;
[2]. Гевко Р.Б., Вітровий А.О., (2012) - *Підвищення технічного рівня гнучких гвинтових конвеєрів,* Тернопіль: Астон, 209 с;
[3]. Рогатинський Р., Гевко І., Рогатинська Л., (2013) - *Оптимізація параметрів гвинтових транспортно–технологічних систем*, Вісник ТНТУ, № 1 (69), С. 116–125;
[4]. Гевко Р.Б., Дзюра В.О., Романовський Р.М., (2006) - *Шнековий пневмомеханічний транспортер,* Пат. №44544, МПК G65B 53/00, Заявник і власник патенту Тернопільський національний економічний університет. - № u200903515; заявл. 13.04.2009р., Опубл. 12.10.2009. Бюл. №19, 3с.

THE VISION SYSTEM USAGE AS DATA SOURCE FOR STATISTICAL PROCESS CONTROL IN THE FOOD EXTRUSION
/
WYKORZYSTANIE SYSTEMU WIZYJNEGO DO STATYSTYCZNEJ KONTROLI PRZEBIEGU PROCESU EKSTRUZJI PRODUKTÓW ŻYWNOŚCIOWYCH

PhD. Eng. Żelaziński T., PhD. Eng. Ekielski A., PhD. Stud. Eng. Florczak I.
Warsaw University of Life Sciences**,** Faculty of Production Engineering,
Department of Production Management and Engineering, Warsaw / Poland
Tel: +48 22 59 345 00; e-mail: tomasz_zelazinski@sggw.pl

Abstract: *The aim of this study was to use a vision system for statistical quality control of the course of extruded products quality changes described by the expansion coefficient of the product and the color distribution. The expansion coefficient was measured directly at the extruder nozzle and referred to the resulting changes in the electric current values recorded during the extrusion process. Tests were carried out on a single screw extruder with a screw length to its diameter ratio L2/D2 = 6.5 and nozzle diameter D = 10 mm.*

Material intended for the extrusion process was a mixture of crushed maize (80%) and buckwheat (20%) humidified to a moisture content of 17%. The results suggest that the direct observation and analysis of the extrusion process using vision systems can be a sensitive instrument supporting the process control. This is indicated by the changes of the radial expansion coefficient and color (Lab) of products measured directly at the extruder nozzle and simultaneously recorded changes in the intensity of electric current drawn by the extruder's motor.

Keywords: *extrusion, stability, expansion, color*

INTRODUCTION

Extrusion of raw plant materials is a very complex process, which consists of a number of factors such as geometry of working elements, screw and feeder rotation speed and process temperature [7; 11; 12]. On the other hand, for the proper course of the process extremely important factors are also material properties of the input, i.e. type and chemical composition of feedstock, blend composition, fragmentation degree and humidity [3;9;13;18]. The combination of both one and the second parameters contributes further to the 'output' changes of extrusion, which are process pressure and energy consumption [1;14;19]. Collation of all these variables gives a very large number of input data and, consequently, many significant factors and their interaction during the process. This makes difficult, in some cases, the accurate and stable maintenance of the extrusion process [6; 14; 20].

For a stable process flow follows parallel the quality of the product, which can be a sensitive factor that reflects the continuity of the process. To test the quality of extruded products, a wide range of physical and chemical methods are used, included determination of density, expansion coefficients, strength parameters, water absorption index and water solubility index, testing of gelatinisation degree, water activity, micro and macroelements content etc. [14; 15]. With many qualitative methods, parameters that initially and quickly

Abstrakt: *Celem niniejszej pracy było zastosowanie systemu wizyjnego do statystycznej kontroli przebiegu zmian jakościowych wyrobów ekstrudowanych opisanej współczynnikiem ekspansji produktu oraz rozkładu barwy. Wartości współczynnika ekspansji mierzono bezpośrednio przy dyszy wylotowej ekstrudera, a następnie odniesiono do uzyskanych zmian wartości natężenia prądu elektrycznego rejestrowanych podczas przebiegu procesu ekstruzji. Badania przeprowadzono na jednoślimakowym ekstruderze o stosunku długości ślimaka do jego średnicy L2/D2=6,5 i średnicy dyszy wylotowej D=10 mm. Materiałem przeznaczonym do procesu ekstruzji była mieszanka rozdrobnionej kukurydzy (80%) i gryki (20%) nawilżonej do wilgotności 17%. Uzyskane wyniki badań powalają stwierdzić, że obserwacja i bezpośrednia analiza przebiegu procesu ekstruzji za pomocą systemów wizyjnych może stanowić czuły przyrząd wspomagający sterowanie procesem ekstruzji. Wskazują na to uzyskane zmiany wskaźnika ekspansji radialnej i barwy (Lab) produktów mierzonych bezpośrednio przy dyszy wylotowej ekstrudera oraz równolegle rejestrowane zmiany natężenia prądu elektrycznego pobieranego przez silnik ekstrudera.*

Słowa kluczowe: *ekstruzja, stabilność, ekspansja, barwa*

WSTĘP

Ekstruzja surowców roślinnych to bardzo złożony proces, na który składa się wiele czynników takich, jak geometria elementów roboczych ekstrudera, prędkość obrotowa ślimaków i podajnika oraz temperatura procesu [7; 11; 12]. Z drugiej strony, dla prawidłowego przebiegu procesu niezwykle istotnymi czynnikami są też własności materiału wejściowego, czyli rodzaj i skład chemiczny stosowanego surowca, skład mieszanki oraz jej stopień rozdrobnienia i wilgotność [3;9;13;18]. Połączenie zarówno jednych, jak i drugich parametrów przyczynia się dalej do zmian „wynikowych" ekstruzji, jakimi są ciśnienie procesu oraz pobór energii elektrycznej [1;14;19]. Zestawienie tych wszystkich zmiennych daje bardzo dużą liczbę danych wejściowych, a w konsekwencji wiele czynników istotnych oraz ich interakcji zachodzących podczas procesu. Sprawia to, że prawidłowe i stabilne utrzymanie procesu ekstruzji w niektórych przypadkach może być trudne [6; 14; 20].

Oczywiście za stabilnym przebiegiem procesu podąża równolegle jakość produktu, która może być wrażliwym czynnikiem odzwierciedlającym ciągłość przebiegu procesu. Powszechnie do badań jakości wyrobów ekstrudowanych wykorzystuje się szereg metod fizycznych i chemicznych, do których można zaliczyć wyznaczanie gęstości, wskaźników ekspansji, parametrów wytrzymałościowych, wskaźników wodochłonności i wodorozpuszczalności, badania stopnia żelifikacji, aktywności wody, zawartości mikro i makroelementów itp.

allow to describe the quality of extruded products are mainly expansion coefficients and parameters of color and shape [4;5;17]. The values of these quantities can be measured relatively easily during the process, for example, directly at the extruder nozzle. Performed in this manner, measurements increase the possibility of observation and process control, contributing to a more precise control of the extrusion, especially during the processing of raw plant materials that are difficult to convert, such as heterogeneous or with high humidity materials.

Considering the above, the aim of this study was to investigate the course of qualitative changes of extruded products, which were measured directly at the nozzle of the extruder, and then reference the results to changes in electric current recorded during the extrusion process.

MATERIAL AND METHOD

Research material

The research material intended for extrusion was a blend of crushed Credo varieties of maize (80%) and Luba varieties of buckwheat (20%). Table 1 shows an example of the size distribution of grit. The individual raw materials were mixed and moistened with water to a moisture content of 17% using a laboratory mixer (type Agrometr Inofama). Before the extrusion, blend was conditioned for a period of about 20 min.

[14; 15]. Z wielu metod jakościowych, parametrami, które wstępnie i szybko pozwalają opisać jakość wyrobów ekstrudowanych są głównie wskaźniki ekspansji oraz parametry barwy i kształtu [4;5;17]. Wartości tych wielkości można w stosunkowo prosty sposób mierzyć w trakcie trwania procesu np. bezpośrednio przy dyszy wylotowej ekstrudera. Wykonywane w ten sposób pomiary zwiększają możliwości obserwacji i kontroli przebiegu procesu, przyczyniając się do bardziej precyzyjnego sterowania procesem ekstruzji, szczególnie podczas ekstruzji surowców roślinnych trudnych do przetworzenia np. niejednorodnych lub o wysokiej wilgotności.

Biorąc pod uwagę powyższe, celem niniejszej pracy było zbadanie przebiegu zmian jakościowych wyrobów ekstrudowanych, które mierzono bezpośrednio przy dyszy wylotowej ekstrudera, a następnie odniesienie wyników do zmian natężenia prądu elektrycznego rejestrowanych podczas przebiegu procesu ekstruzji.

MATERIAŁ I METODYKA

Materiał badawczy

Materiałem badawczym przeznaczonym do procesu ekstruzji była mieszanka rozdrobnionej kukurydzy odmiany Credo (80%) i gryki odmiany Luba (20%). W tabeli 1 przedstawiono przykładowy skład granulometryczny grysu. Poszczególne surowce mieszano i nawilżano wodą do wilgotności 17% za pomocą mieszalnika laboratoryjnego (typ Agrometr Inofama). Mieszanka przed poddaniem procesowi ekstruzji była kondycjonowana przez czas około 20 min.

Table 1

Granulometric size distribution of raw materials subjected to extrusion process [%]

Fraction [mm]	Corn	Buckwheat
>2	3.5	2.7
2-1.5	3.4	4.3
1.5-1.2	0.2	0.2
1.2-1.02	3.3	4.1
1.02-0.75	31.7	21.5
0.75-0.6	7.8	4.6
0.6-0.43	17.9	14.8
0.43-0.25	19.7	15.4
<0.25	12.5	32.4

Extrusion process

To perform the research, it was used a modified single screw extruder KZM-2 with a screw length to diameter ratio L2/D2 = 6.5 and 10 mm nozzle diameter. Screw speed of the extruder was 170 rpm·min^{-1} with an efficiency of 100 kg·h^{-1}. Power of extruder's engine was 22 kW. The extruder was equipped with a system to maintain the temperature in the extruder barrel (heater with a power of 2000 watts and a thermostat) that allowed to control the extrusion temperature of about 150-160°C in the last section of the extruder. In addition, the extruder was equipped with a thermocouple positioned in the machine head, clamp (type Z202A, METRAWAT, AC 0..20/200) to measure the electric current drawn by the extruder's engine, the temperature sensor (thermocouple) TP-371J and adjustable single screw material feeder.

In order to obtain an image of the extrudate, CCD color camera KP-FD30 HITACHI was placed at the extruder's nozzle, mounted on a tripod, and a fan to blow off steam. The whole was illuminated by fluorescent daylight D65 Philips TL-D De Luxe Pro 18W/965.

Sensors and a camera were combined with a set for data acquisition (National Instrument) and a PC. Then both figures and images were recorded at intervals of 1 second.

Proces ekstruzji

Do badań zastosowano zmodyfikowany jednoślimakowy ekstruder KZM-2 o stosunku długości ślimaka do jego średnicy L2/D2=6,5 i dyszy wylotowej 10 mm. Prędkość obrotowa ślimaka ekstrudera wynosiła 170 obr·min^{-1}, przy wydajności 100 kg·h^{-1}. Moc silnika ekstrudera wynosiła 22 kW. Ekstruder wyposażony był w układ do podtrzymywania temperatury w cylindrze ekstrudera (grzałka o mocy 2000 wat i termostat) pozwalający na kontrolowanie temperatury ekstruzji wynoszącej około 150-160ºC w ostatniej sekcji ekstrudera. Dodatkowo ekstruder wyposażony był w termoparę umiejscowioną w głowicy maszyny, cęgi (typu Z202A firmy METRAWAT, AC 0..20/200) do pomiaru natężenia prądu pobieranego przez silnik ekstrudera, czujnik temperatury (termopary) typu TP-371J oraz regulowany jednoślimakowy podajnik surowca.

W celu uzyskania obrazu ekstrudatu, przy dyszy wylotowej ekstrudera umieszczono kolorową kamerę CCD KP-FD30 firmy HITACHI zamontowaną na statywie oraz wentylator do zdmuchiwania pary wodnej. Całość oświetlano świetlówkami światła dziennego D65 firmy Philips TL-D De Luxe Pro 18W/965.

Czujniki oraz kamerę połączono z zestawem do akwizycji danych firmy National Instrument i komputerem PC. Następnie zarówno dane liczbowe oraz zdjęcia

Numerical files were recorded in Excel 2003. Photographs were saved in TIF format.

Data were recorded from the start of the extrusion process to its completion, but for the purposes of the study a section of the extrusion process with a length of 305 measurement points (305 seconds) was analyzed.

Methods of qualitative research

To measure the degree of radial expansion LabView program, Vision Assistance. 7.1 for image analysis was used. The program enabled the precise measurement of the extrudate diameter, which was measured at a distance of about 10 cm from the extruder's nozzle.

Expansion coefficient was calculated according to the formula below [2]:

$$SEI = \frac{S_e}{S_d} \quad (1)$$

where: S_e - extrudate diameter, S_d - nozzle diameter.

The study of the color was performed using Adobe Photoshop 6.0. CE, in which, using the "histogram" function, values of the parameters L*, a*, b* for each field were obtained, which had to be calculated by the following equations [10]:

$$L^* = \frac{L}{255} \cdot 100\% \quad (2)$$

$$a^* = \frac{240a}{255} - 120 \quad (3)$$

$$b^* = \frac{240b}{255} - 120 \quad (4)$$

where: L – brightness, a - color indicator changing from green to red, b - color indicator changing from yellow to blue, L*, a*, b* - the correct values of the color after standardization.

Statistical analysis

For statistical analysis it was used a module of statistical quality control (SPC) of STATISTCA 10 program. For presentation and preliminary analysis of the recorded data there were used control charts (individual observations and moving gap) available in the module DOE, industry statistics. In a further step ANOVA analysis was performed, followed by the presentation of individual variables on the graphs in the form of three-dimensional approximated surface responses.

In order to present and provide accurate experimental data analysis, obtained results were recorded using the so-called control charts, on which the boundary conditions of process stability were marked as: lower control limit, LCL, and upper control limit, UCL determined for the central line (actual mean value of n samples). The limits LCL and UCL were set at (±)3 of calculated sigma value (standard deviation of individual points), [16].

RESULTS

The results show that extrusion is a complex process. Even during the stabilized course using single screw extruder there may be significant variations in power consumption and related changes in the quality of the resulting products. Especially it can be seen clearly by on-

rejestrowano w odstępach 1 sekundowych. Pliki liczbowe zapisywano w programie Excel 2003. Zdjęcia były zapisywane w formacie TIF.

Dane rejestrowano od rozpoczęcia procesu ekstruzji do jego zakończenia, jednak dla potrzeb badań analizowano odcinek przebiegu procesu ekstruzji o długości 305 punktów pomiarowych (305 sekund).

Metodyka badań jakościowych

Do pomiaru stopnia ekspansji radialnej wykorzystano program do analizy obrazu LabViev, Vision Assistance. 7.1. Program umożliwiał precyzyjne zmierzenie średnicy ekstrudatu, którą mierzono w odległości około 10 cm od dyszy wylotowej ekstrudera.

Wskaźnik ekspansji obliczano według wzoru [2]:

gdzie: S_e - średnica ekstrudatu, S_d - średnica dyszy.

Badania barwy wykonano wykorzystując program Adobe Photoshop 6.0. CE, w którym za pomocą funkcji „histogram" uzyskiwano wartości parametrów L*, a*, b* dla każdego pola, które należało wyliczyć według poniższych zależności [10]:

gdzie: L – jasność, a - wskaźnik barwy zmieniający się od koloru zielonego do czerwonego, b - wskaźnik barwy zmieniający się od koloru żółtego do niebieskiego, L*, a*, b* - prawidłowe wartości parametrów barwy po standaryzacji.

Analiza statystyczna

Do analizy statystycznej wykorzystano moduł statystycznej kontroli jakości (SPC) programu STATISTCA 10. Do przedstawienia oraz wstępnej analizy zarejestrowanych danych zastosowano karty kontrolne (obserwacje pojedyncze i ruchomy rozstęp) dostępne w module DOE, statystyki przemysłowe. W kolejnym etapie badań przeprowadzono analizę ANOVA, a następnie poszczególne zmienne zaprezentowano na wykresach trójwymiarowych w postaci aproksymowanych powierzchni odpowiedzi.

W celu przedstawienia oraz dokładniejszej analizy danych doświadczalnych uzyskane wyniki rejestrowano za pomocą tzw. kart kontrolnych, na których warunki brzegowe stabilności procesu zostały oznaczone jako: dolna granica kontrolna - lower control limit, LCL oraz górna granica kontrolna - upper control limit, UCL wyznaczonych dla linii centralnej (średnia rzeczywista z n próbek). Granice LCL i UCL ustalono na poziomie (±)3 wielkości obliczonej sigmy (odchylenie standardowe pojedynczych punktów), [16].

WYNIKI BADAŃ

Uzyskane wyniki badań pokazują, że ekstruzja to proces złożony, Nawet podczas ustabilizowanego przebiegu z wykorzystaniem ekstrudera jednoślimakowego mogą występować znaczne odchylenia w poborze prądu elektrycznego i związane z tym zmiany jakościowe uzyskiwanych produktów. Szczególnie wyraźnie można to

line recording of the basic parameters of the resulting products, such as radial expansion and the color indices L*, a*, b*, and monitoring of the electric current drawn by the extruder's engine.

Figure 1 below shows the control chart recording process of power consumption by the extruder's engine. On the graph it can be clearly seen that part of the points go beyond the established boundary lines, which may indicate some deregulation of the process. Locally, between 130 and 250 second occurrence of the shift of the operating point can be observed, superimposed on the growth of the instability of its course. It is worthing to note that the cyclical nature of work point changes is manifested by periodic crossing of the lower or upper control line.

zaobserwować rejestrując on-line podstawowe parametry uzyskiwanych produktów takie, jak ekspansja radialna i wskaźniki barwy L*, a*, b* oraz monitorując przebieg natężenia prądu pobieranego przez silnik ekstrudera.

Poniżej na rysunku 1 przedstawiono kartę kontrolną rejestrującą przebieg poboru prądu przez silnik ekstrudera. Na wykresie można wyraźnie zaobserwować, że część punktów wychodzi poza ustalone linie graniczne, co może świadczyć o pewnym rozregulowaniu procesu. Lokalnie pomiędzy 130 a 250 sekundą można zaobserwować wystąpienie przesunięcia się punktu pracy, nakładające się na wzrost niestabilności jego przebiegu. Warto zwrócić uwagę na cykliczność zmiany punktu pracy przejawiającą się okresowym przekraczaniem dolnej lub górnej linii kontrolnej.

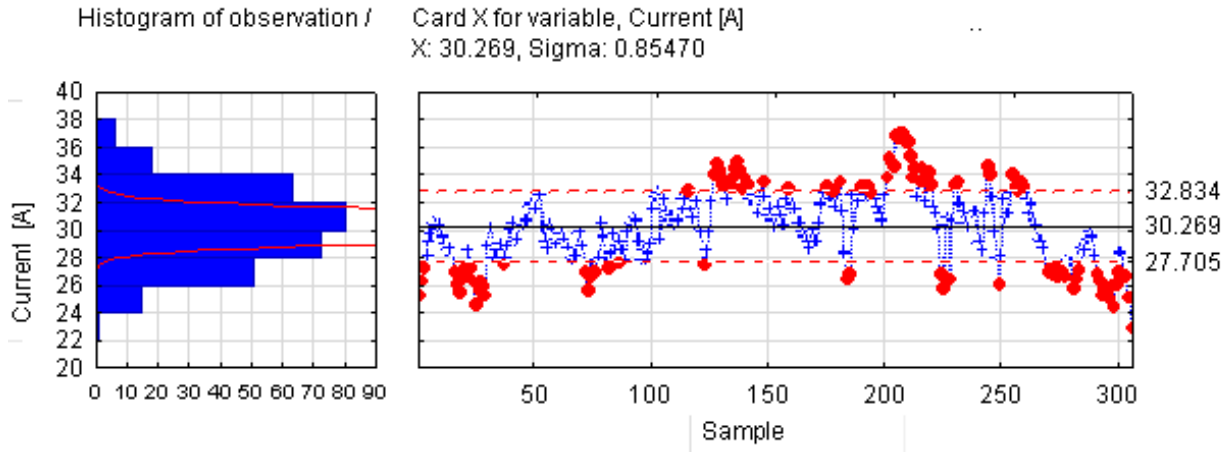

Fig. 1 - Record of the course of the changes in the intensity of electric current drawn by the extruder's engine

The variation of the radial expansion is also characterized by a similar course, where part of the values exceeds the limits established by UCL and LCL too (Fig. 2). This behavior may indicate that some correlation may occur between these two parameters. However, the rate of expansion shows no drift in value over time, but only increased dispersion of the measured results. It can therefore be assumed that stabilizing the electrical current draw will largely contribute to a more stable quality of extruded products.

Podobnym przebiegiem charakteryzuje się również zmienność wskaźnika ekspansji radialnej, której część wartości także przekracza granice ustalonych UCL i LCL (rys. 2). Takie zachowanie może świadczyć, że pomiędzy tymi dwoma parametrami może występować pewna korelacja. Niemniej wskaźnik ekspansji wykazuje brak dryftu wartości w czasie, a jedynie zwiększony rozrzut wyników pomiarowych. Można zatem przypuszczać, że ustabilizowanie wartości poboru prądu elektrycznego w dużej mierze przyczyni się do bardziej ustabilizowanych jakościowo wyrobów ekstrudowanych.

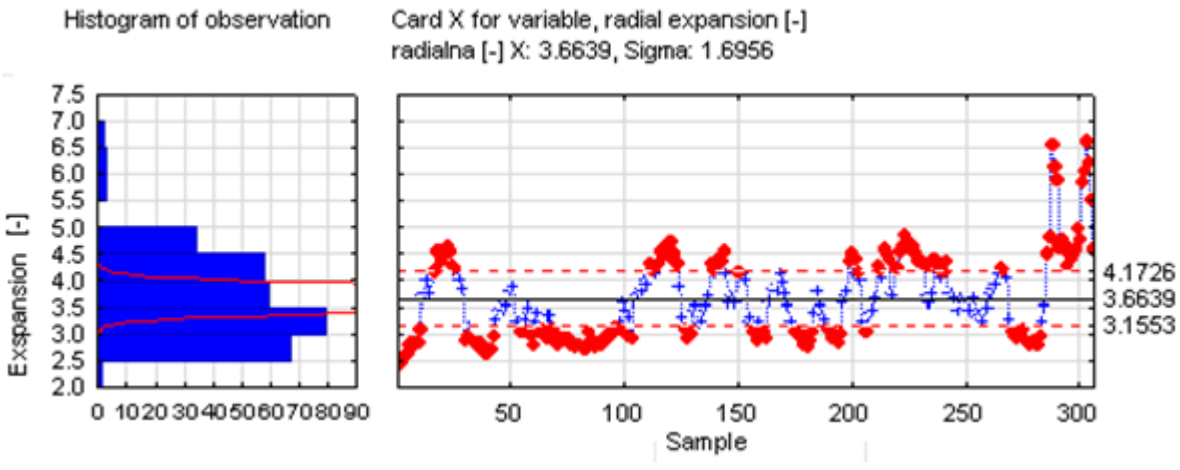

Fig. 2 - Record of changes in the course of the radial expansion index

Based on tests performed it was found that the change of the radial expansion and the electric current drawn by the extruder followed extrudates color change. That is why on the following courses (Fig.3, 4, 5) there can be observed the changes in color parameters L*, a*, b* measured in parallel to the expansion values. Analyzing the results it can be concluded that the color change is also very sensitive indicator of the quality of the resulting products, however, from the standpoint of extrusion process stability control seems to be less sensitive indicator than the radial expansion values. This is indicated by a small number of variables passing through the established boundaries of stability.

Na podstawie wykonanej próby stwierdzono, że za zmianą ekspansji radialnej oraz natężeniem prądu elektrycznego pobieranego przez ekstruder podążały również zmiany barwy ekstrudatów. Dlatego też na poniższych przebiegach (rys.3, 4, 5) można zaobserwować zmiany parametrów barwy L*, a*, b* mierzonych równolegle z wartościami ekspansji. Analizując wyniki można stwierdzić, że zmiany barwy są również bardzo czułym wskaźnikiem jakościowym uzyskiwanych produktów, jednak z punktu widzenia kontroli stabilności procesu ekstruzji wydają się być mniej wrażliwym wskaźnikiem niż wartości ekspansji radialnej. Wskazuje na to niewielka liczba zmiennych przechodzących przez ustalone granice stabilności.

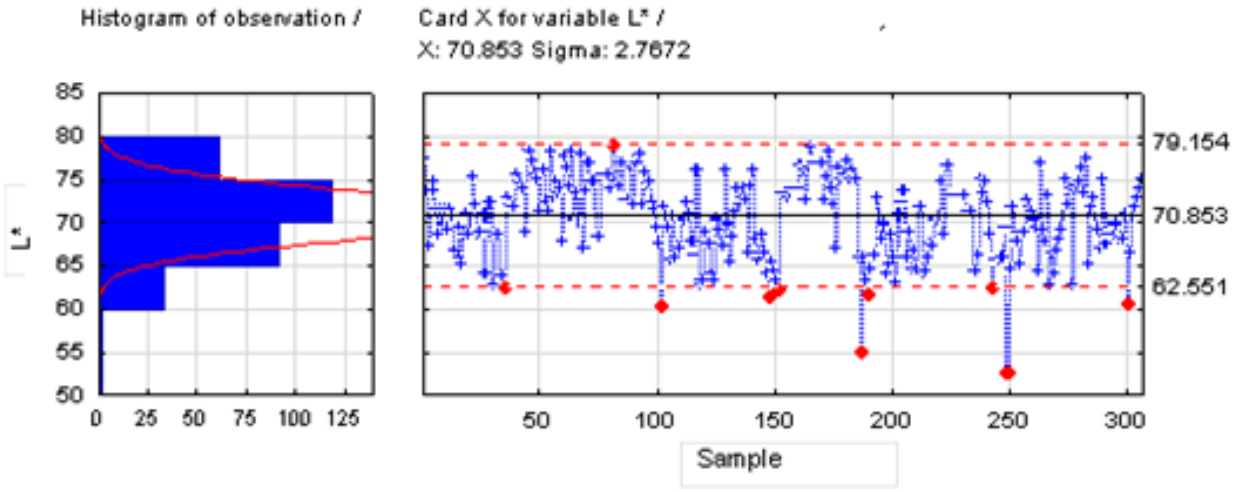

Fig. 3 - Record of changes in the course of color indicator L*

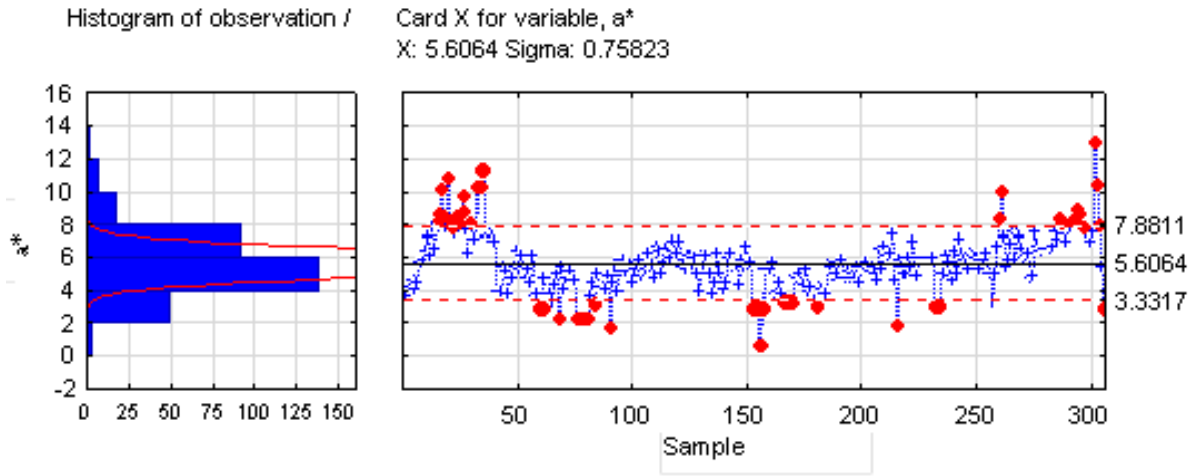

Fig. 4 - Record of changes in the course of color indicator a*

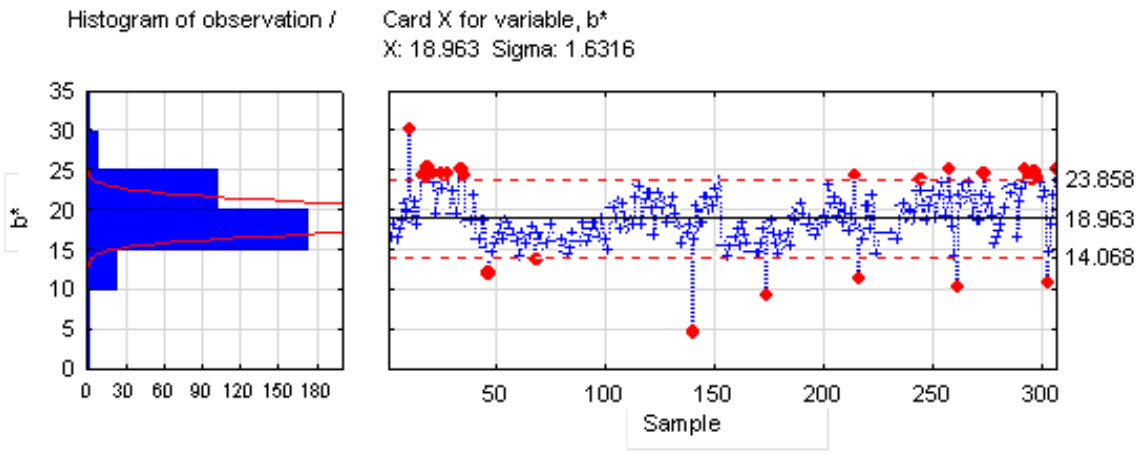

Fig. 5 - Record of changes in the course of color indicator b*

The resulting courses allow to conclude that direct observation and analysis of the process of extrusion using vision systems can be a sensitive instrument supporting the extrusion process control. This is indicated by the research results of changes of all qualitative indicators and parallel recorded courses of electric current drawn by the extruder's engine. Given the above, it seems appropriate to examine correlations between changes in current consumption and quality parameters of extruded products. Therefore, in order to confirm this thesis a statistical analysis of the results obtained was conducted.

The following table 2 presents the results of ANOVA analysis, which show that the variation of all the parameters analyzed, that is the rate of radial expansion and the color indices L*, a*, b*, was statistically significant ($p<0.05$). While in the case of radial expansion and the color index b* it was found that the effect of current intensity has a linear course, and in the case of color indices a* and b* the course found was linear and quadratic.

Uzyskane przebiegi powalają stwierdzić, że obserwacja i bezpośrednia analiza przebiegu procesu ekstruzji za pomocą systemów wizyjnych może stanowić czuły przyrząd wspomagający sterowanie procesem ekstruzji. Wskazują na to uzyskane wyniki badań zmian wszystkich wskaźników jakościowych oraz równolegle rejestrowane przebiegi natężenia prądu elektrycznego pobieranego przez silnik ekstrudera. Biorąc pod uwagę powyższe, wydaje się słuszne poszukiwanie zależności pomiędzy zmianami poboru prądu a parametrami jakościowymi wyrobów ekstrudowanych. Dlatego w celu potwierdzenia powyższej tezy przeprowadzono analizę statystyczną uzyskanych wyników badań.

W poniższej tabeli 2 zamieszczono wyniki analizy ANOVA, które pokazują, że zmienność wszystkich analizowanych parametrów, czyli wskaźnika ekspansji radialnej oraz wskaźników barwy L*, a*, b*, była istotne statystycznie ($p<0,05$). Przy tym w przypadku ekspansji radialnej i wskaźnika barwy b* stwierdzono, że wpływ natężenia prądu miał przebieg liniowy, natomiast w przypadku wskaźników barwy a* i b* stwierdzono przebieg liniowy i kwadratowy.

Table 2

Anova table with important factors for p<0.05

Factor	Radial exspansion [-]				(R^2-0.2965)
	SS	df	MS	F	p
Current	1.6598	1	1.6598	3.0893	0.07982
Current^2	3.9824	1	3.9824	7.4121	0.00685*
Error	162.7945	303	0.5373		
Całk. SS	167.7604	305			
			L*		**(R^2-0.2384)**
Current	75.207	1	75.207	3.8342	0.05114
Current^2	81.484	1	81.4844	4.1542	0.0424*
Error	5943.312	303	19.6149		
Całk. SS	6128.638	305			
			a*		**(R^2-0.2834)**
Current	71.785	1	71.7853	23.0469	0.000002*
Current^2	34.048	1	34.0481	10.9313	0.00106*
Error	943.769	303	3.1148		
Całk. SS	1036.534	305			
			b*		**(R^2-0.2879)**
Current	123.883	1	123.8833	13.4455	0.00029*
Current^2	208.241	1	208.2406	22.6011	0.000003*
Error	2791.762	303	9.2137		
Całk. SS	3081.140	305			

- Significant difference at the level of p < 0,05

The results of above analysis are shown on a three-dimensional graphs presenting the changes in electric current as a function of radial expansion [ER] and the color indices L*, a*, b*. The graph in Figure 6 shows electric current changes as a function of index L* and the ER. In the figure it can be seen that ER index increases with increasing current reaching a maximum value of ER amounting 5-6 [-]. At the same time it can be observed that with the ER increase, product brightness L* increases too. Moreover, there can also be noticed a sudden downward inflection in the graph (a decrease of electric current), where the product reached the highest rate of ER = 6.5 [-] and the sudden reduction in the brightness L*, which was probably associated with the local overheating of the material in the extruder.

Wyniki powyższej analizy przedstawiono za pomocą trójwymiarowych wykresów przedstawiających zmiany natężenia prądu w funkcji ekspansji radialnej [ER] oraz wskaźników barwy L*, a*, b*. Na wykresie rys. 6 pokazano zmiany natężenia prądu elektrycznego w funkcji wskaźnika barwy L* oraz ER. Na rysunku można zaobserwować, że wskaźnik ER zwiększa się wraz ze wzrostem natężenia prądu, osiągając maksymalne wartości ER wynoszące ok. 5-6 [-]. Jednocześnie można zaobserwować, że wraz ze wzrostem ER zwiększa się również jasność produktu L*. Na wykresie można również zaobserwować nagłe przegięcie wykresu ku dołowi (spadek natężenia prądu elektrycznego), gdzie produkt osiągał najwyższy wskaźnik ER = 6,5 [-] oraz nagłe zmniejszenie jasności L*, które związane było prawdopodobnie z lokalnym przegrzewaniem się materiału w ekstruderze.

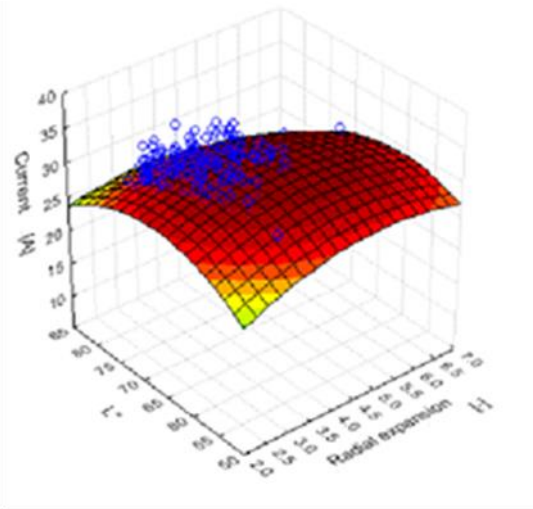

Fig. 6 - Changes in the current as a function of changes in L* and the radial expansion coefficient

Although the color values of a* and b* were in most cases within UCL and LCL lines, on the approximated graphs some course trends can be observed. It was found that in the case of graph on Figure 7, the value of the parameter a* slightly increased with the decrease in current. Simultaneously with the increase in the ER, no significant changes were noticed in this parameter.

Pomimo, że wartości parametrów barwy a* i b* mieściły się w większości przypadków granicach linii UCL i LCL, na aproksymowanych wykresach można zaobserwować pewne trendy przebiegu. Stwierdzono, że w przypadku wykresu na rys. 7, wartość parametru a* nieznacznie zwiększała się wraz ze zmniejszeniem natężenia prądu. Jednocześnie wraz ze wzrostem ER nie zaobserwowano znaczących zmian tego parametru.

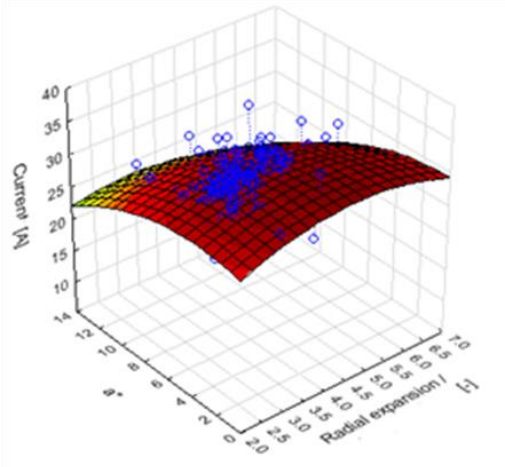

Fig. 7 - Changes in the current as a function of changes in the color index a* and radial expansion

Analyzing the changes in the parameter b* (Fig. 8), it could be concluded that the parameter has been changing along with changes in current drawn by the extruder. Most significantly, however, the changes were observed at small values of the parameter b* from about 0-10, and for the products whose ER was about 2-3.5.

Analizując zmiany parametru b* (rys. 8), można było z kolei stwierdzić, że wskaźnik zmieniał się wraz z zmianami natężenia prądu pobieranego przez ekstruder. Najbardziej wyraźnie zmiany obserwowano jednak przy małych wartościach parametru b* od około 0-10 oraz dla produktów, których ER wynosiła około 2-3,5.

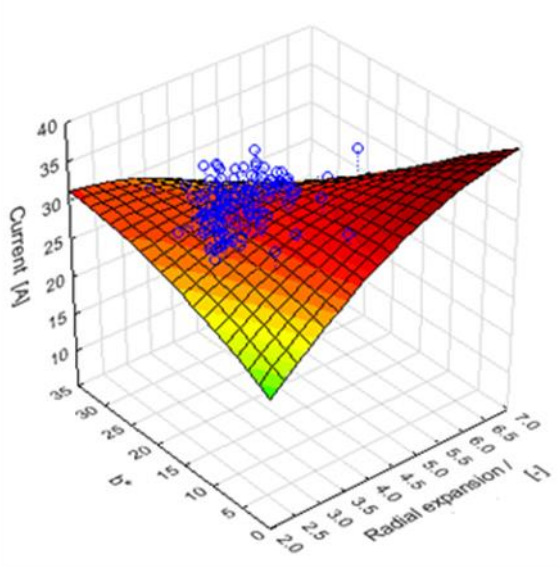

Fig. 8 - Changes in current intensity as a function of color changes b* and the rate of radial expansion

CONCLUSIONS

1. The results achieved allowed to conclude that observation and direct analysis of the extrusion process using vision systems can be a sensitive instrument supporting the extrusion process control. This is shown by changes in the obtained results, the radial expansion coefficient and the color coefficients (Lab) of products measured directly at the outlet extruder's nozzle and simultaneously recorded changes in the intensity of electric current drawn by the extruder's engine.

2. The initial use of control charts to present and analyze the results of changes in electric current and the quality parameters of the extrudate (corn - buckwheat) looks very promising. It should be noted, however, that setting the appropriate value of the UCL and LCL for the extrusion process may require probably carrying out a series of preliminary studies.

3. The results presented in the approximated surface responses graphs suggest that even in a stable process it can be traced to certain trends. Estimation of process variables describing its correct course may allow the determination of the optimal threshold values describing the quality of the obtained products.

REFERENCES

[1]. Akdogan H., Rui L., Oliveira T. J. C., (1997) - *Rheological properties of rice starch at high moisture contents during twin-screw extrusion.* Food Science and Technology, 30 (5), 488-496;

[2]. Alvarez-Martinez L., Kondury K. P., Harper J. M., (1988) - *A general model for expansion of extruded products.* Journal of Food Science, 53, 609-615;

[3]. Ding Q.-B., Ainsworth P., Plunkett A., Tucker G., Marson H., (2006) - *The effect of extrusion conditions on the functional and physical properties of wheat-based*

WNIOSKI

1. Uzyskane wyniki badań powalają stwierdzić, że obserwacja i bezpośrednia analiza przebiegu procesu ekstruzji za pomocą systemów wizyjnych może stanowić czuły przyrząd wspomagający sterowanie procesem ekstruzji. Wskazują na to uzyskane wyniki badań zmian wskaźnika ekspansji radialnej i barwy (Lab) produktów mierzonej bezpośrednio przy dyszy wylotowej ekstrudera oraz równolegle rejestrowane zmiany natężenia prądu elektrycznego pobieranego przez silnik ekstrudera.

2. Wstępne zastosowanie kart kontrolnych do przedstawienia i analizy uzyskanych wyników zmian natężenia prądu elektrycznego oraz parametrów jakościowych ekstrudatu (kukurydziano – gryczanego) wygląda bardzo obiecująco. Należy jednak zaznaczyć, że ustawienie odpowiednich wartości UCL i LCL w przypadku procesu ekstruzji może wymagać prawdopodobnie przeprowadzenia szeregu badań przedwstępnych.

3. Uzyskane wyniki przedstawione na wykresach aproksymowanych powierzchni odpowiedzi sugerują, że w nawet w ustabilizowanym procesie można doszukiwać się pewnych trendów. Oszacowanie wartości wielkości procesowych opisujących prawidłowy jego przebieg może pozwolić na optymalne ustalenie wartości progowych opisujących jakość uzyskiwanych wyrobów.

LITERATURA

[1]. Akdogan H., Rui L., Oliveira T. J. C., (1997) - *Właściwości reologiczne skrobi ryżowej o wysokich zawartościach wilgoci podczas ekstruzji dwuślimakowej.* Lebensmittel Wissenschaft und Technologie, 30 (5), 488-496;

[2]. Alvarez-Martinez L., Kondury K. P., Harper J. M., (1988) - *Ogólny model ekspansji wyrobów ekstrudowanych.* Journal of Food Science, 53, 609-615;

[3]. Ding Q.-B., Ainsworth P., Plunkett A., Tucker G., Marson H., (2006) - *Wpływ warunków wytłaczania na funkcjonalne i fizyczne właściwości ekspandowanych*

expanded snacks. Journal of Food Engineering, 73 (2), 142-148;
[4]. Ekielski A., (2013) - *The use of image analysis for assessment of selected parameters describing the porous structures on the example of cereal extrudates.*Viilage of tomorrow Publishing House, ISBN 978-83-62815-21-0;
[5]. Ekielski A., Biller E., Żelaziński T. (2005) - *Effect of extrusion process parameters on the color changes of the extrudate.* Agricultural Engineering, 10 (70), 65-73;
[6]. Ekielski A., Majewski Z., Żelaziński T. (2007) – *Effect of extrusion conditions on physical properties of buckwheat –maize blend extrudate*. Polish Journal of Food and Nutrition Sciences, 57, 2(A), 57-61;
[7]. Girish M., Ganjyal G. M., Milford A., Hanna M. A., (2004) – *Effect of extruder die nozzle dimension on expansion and micrographic characterization during extrusion of acetylated starch*. Starch, 56, 108-117;
[8]. Girish M., Ganjyal G. M., Milford A., Hanna M. A., (2006) – *Digital image processing for measurement of residence time distribution in a laboratory extruder*. Journal of Food Engineering, 75 (2), 237–244;
[9]. Gondek E, Jakubczyk E, Wieczorek B., (2013) - *The physical properties of gluten-free crispbread.* Progress Problem Notebooks of Agricultural Sciences, 574, 29-38;
[10]. Kit L. Y., Spyrydion E., Papadakis E., (2004) - *A simple digital imaging method for measuring and analyzing color of food surfaces.* Journal of Food Engineering, 61 (1), 137-142;
[11]. Mezreb K., Goullieu A., Ralainirina R., Queneudec M. (2003) - *Application of image analysis to measure screw speed influence on physical properties of corn and wheat extrudates.* Journal of Food Engineering, 57, 145-152;
[12]. Mitrus M., (2005) - *Changes of specific mechanical energy during extrusion cooking of thermoplastic starch.* Teka Automotive and Energy Commission of Agriculture Sciences, 5,152-157;
[13]. Moraru C. I., Kokini J. L., (2003) - *Nucleation and expansion during extrusion and microwave heating of cereal foods.* Comprehensive Reviews in Food Science and food Safety, 2, 120-138.
[14]. Mościcki L., Mitrus M., Wójtowicz A., (2007) - *Extrusion technique in food industry.* PWRiL, Warszawa;
[15]. Perez A. A., Drago S. R., Carrara C. R., De Greef D. M., (2008) - *Extrusion cooking of a maize/soybean mixture: Factors affecting expanded product characteristics and flour dispersion viscosity.* Journal of Food Engineering, 87 (3), 323-332;
[16]. Statsoft Handbook, http://www.statsoft.pl/textbook/stathome.html
[17]. Sacchetti G., Pinnavaia G. G., Guidolin E., Dalla Rosa M., (2004) - *Effects of extrusion temperature and feed composition on the functional, physical and sensory properties of chestnut and rice flour-based snack-like products.* Food Research International, 37 (5), pp.527-534;
[18]. Shankar T. J., Bndyopadhyay S., (2005) - *Process variables during single-screw extrusion of fish and rice-flour blends.* Journal of Food Processing and Preservation, 29 (2), 151-164;
[19]. Wójtowicz A., Mościcki L, (2008)-*Energy consumption during extrusion-cooking of precooked pasta.* Teka Automotive and Energy Commission of Agriculture Sciences, 2, 311-318;

przekąsek na bazie pszenicy. Journal of Food Engineering, 73 (2), 142-148;
[4]. Ekielski A., (2013) - *Wykorzystanie analizy obrazu do oceny wybranych parametrów opisujących struktury porowate na przykładzie ekstrudatów zbożowych.* Wyd. Wieś Jutra. ISBN 978-83-62815-21-0;
[5]. Ekielski A., Biller E., Żelaziński T., (2005) - *Wpływ wybranych parametrów procesu ekstruzji na zmiany barwy ekstrudatu.* Inżynieria Rolnicza, 10 (70), 65-73;
[6]. Ekielski A., Majewski Z., Żelaziński T., (2007) - *Wpływ warunków ekstruzji na właściwości fizyczne ekstrudatów gryczano-kukurydzianych.* Polish Journal of Food and Nutrition Sciences, 57, 2(A), 57-61;
[7]. Girish M., Ganjyal G. M., Milford A., Hanna M. A., (2004) - *Wpływ wymiaru dyszy wylotowej wytłaczarki na ekspansję i mikrograficzną charakterystykę podczas ekstruzji skrobi acetylowanej.* Starch, 56, 108-117;
[8]. Girish M., Ganjyal G. M., Milford A., Hanna M. A., (2006) - *Cyfrowe przetwarzanie obrazu do pomiarów rozkładu czasu przebywania w laboratoryjnym ekstruderze.* Journal of Food Engineering, 75 (2), 237-244;
[9]. Gondek E, Jakubczyk E, Wieczorek B., (2013) - *Właściwości fizyczne bezglutenowego pieczywa chrupkiego.* Zeszyty Problemowe Postępów Nauk Rolniczych, 574, 29-38;
[10]. Kit L. Y., Spyrydion E., Papadakis E., (2004) - *Prosta metoda obrazowania cyfrowego dla pomiaru i analizy koloru powierzchni żywności.* Journal of Food Engineering, 61 (1), 137-142;
[11]. Mezreb K., Goullieu A., Ralainirina R., Queneudec M., (2003) - *Zastosowanie analizy obrazu do pomiaru wpływu prędkości ślimaka na właściwości fizyczne kukurydzianych i pszenicznych ekstrudatów.* Journal of Food Engineering, 57, 145-152;
[12]. Mitrus M., (2005) - *Zmiany jednostkowej energii mechanicznej podczas ekstruzji termoplastycznej skrobi.* Teka Komisji Motoryzacji i Energetyki Rolnictwa PAN, 5, 152-157;
[13]. Moraru C. I., Kokini J. L., (2003) - *Zarodkowanie i ekspansja podczas ekstruzji i mikrofalowego ogrzewania produktów zbożowych.* Comprehensive Reviews in Food Science and food Safety, 2, 120-138.
[14]. Mościcki L., Mitrus M., Wójtowicz A., (2007) - *Technika ekstruzji w przemyśle rolno-spożywczym.* PWRiL, Warszawa;
[15]. Perez A. A., Drago S. R., Carrara C. R., De Greef D. M., (2008) - *Ekstruzja mieszaniny kukurydzy i soi: Czynniki wpływające na właściwości produktu oraz lepkość dyspersji mąki.* Journal of Food Engineering, 87 (3), 323-332;
[16]. Podręcznik Statsoft, http://www.statsoft.pl/textbook/stathome.html
[17]. Sacchetti G., Pinnavaia G. G., Guidolin E., Dalla Rosa M., (2004) - *Wpływ temperatury ekstruzji i składu wsadu na funkcjonalne, fizyczne i sensoryczne właściwości jak przekąsek na bazie kasztanów i mąki ryżowej.* Food Research International, 37 (5), 527-534;
[18]. Shankar T. J., Bndyopadhyay S., (2005) - *Zmienne procesowe podczas jednoślimakowej ekstruzji mieszanek mąki rybnej i ryżowej.* Journal of Food Processing and Preservation, 29 (2), 151-164;
[19]. Wójtowicz A., Mościcki L., (2008) - *Zużycie energii podczas ekstruzji preparowanego makaronu.* Teka Komisji Motoryzacji i Energetyki Rolnictwa PAN, 2, 311-318;

[20]. Żelaziński T., (2014) - *Effect of selected working parameters of single screw extruder on energy consumption in the extrusion process*. Annals of Warsaw University of Life Sciences, 63.

[20]. Żelaziński T., (2014) - *Wpływ wybranych parametrów pracy wytłaczarki jednoślimakowej na zużycie energii w procesie ekstruzji.* Annals of Warsaw University of Life Sciences, 63.

MODELING FOR USE OF WATER IN AGRICULTURE
/
MODELLAZIONE PER L'USO DELLE ACQUE IN AGRICOLTURA

Prof. Eng. Trulli E.[1)], Prof. Eng. Ph.D. Torretta V.[2)], Dr. Eng. Ph.D. Rada E.C.[3)], Lect. Eng. Ph.D. Istrate I.A.[4)], Prof. Eng. Papa E.A.[2)]
[1)]University of Basilicata, Potenza / Italy; [2)] University of Insubria / Italy, [3)] University of Trento / Italy,
[4)] University POLITEHNICA Bucharest/Romania
Tel: +39-0971205153; E-mail: ettore.trulli@unibas.it

Abstract: *The present paper examines and evaluates the results of a survey carried out to define the criteria for restoring the surface water of the karstic stream "Gravina" (Southern-Italy). The stream runs through a watershed including several agricultural areas. The stream shows an environmental heterogeneity which is of great value to the conservation of biodiversity. The analysis supports a more general water pollution control strategy aimed at safeguarding natural water quality in the urbanized watershed with the aim, also, to reuse partially the water in agriculture. The methodology was based on the surface water sampling, quality parameter analysis and simulation by modelling. The variation and compatibility of wastewater discharge and water stream quality were verified by using a model available in literature in function of biodegradable pollutant load and dissolved oxygen. Several scenarios based on the fixed yield of treatment plants were examined.*

Keywords: *modelling, water quality, wastewater treatment, planning, agriculture*

INTRODUCTION

The issues related to the quality of surface water bodies and the strategies to adopt for limiting the impact from the discharge of the effluents of urban, agricultural and industrial origin are extremely interesting and topical, not only because of an increasing environmental sensitivity but also and mainly in order to meet the legal requirements, both on the Community and on the national scale [6]. In this respect, several studies analysed the anthropic influences on the quality of surface waters crossing urbanized basins and the analysis of the main pressure components suited to the study of the quality of the waters themselves and consequently, the whole environment [5]. Among the several pressure sources, the impacts due to the input of civil and industrial wastewaters are particularly important to the flow of the receiving body and its diluting capacity. In order to protect the quality of surface water it is crucial to prevent and reduce pollution and implement the restoration of water bodies by controlling all the anthropic factors, among which the correct management and functioning of wastewater treatment plants is very important. In a methodological approach of applied research, the development of monitoring networks as well as modelling constitute fundamental tools to analyse and assessing actions for the protection of water [1,4].

The present study examines the results of a survey aimed at examining the basic elements of an action to safeguard the quality of the stream "Gravina", in the urban area of the town of Matera. The stream network is located inside an important natural area, important under the touristic and agriculture point of view.

MATERIAL AND METHOD

The study area

The watershed of the stream "Gravina" in the urbanized area of Matera is the object of the present

Sommario*: Il presente lavoro esamina e valuta i risultati di un'indagine effettuata per definire i criteri per ripristinare l'acqua superficiale del torrente carsico "Gravina" (Sud-Italia). Il ruscello scorre attraverso uno spartiacque tra cui diverse aree agricole. Il flusso mostra una eterogeneità ambientale che è di grande valore per la conservazione della biodiversità.*
L'analisi supporta una strategia di controllo dell'inquinamento delle acque più generale volta a salvaguardare la qualità dell'acqua naturale spartiacque urbanizzata, con l'obiettivo, inoltre, di riutilizzare parzialmente l'acqua in agricoltura. La metodologia si è basata sul campionamento superficie dell'acqua, l'analisi dei parametri di qualità e di simulazione modellistica.
La variazione e la compatibilità delle acque reflue sono state verificate utilizzando un modello disponibile in letteratura in funzione del carico inquinante biodegradabile e ossigeno disciolto. Diversi scenari basati sul rendimento fisso di impianti di trattamento sono stati esaminati.

Parole chiave*: modellazione, qualità delle acque, trattamento delle acque reflue, pianificazione, agricoltura*

INTRODUZIONE

Le questioni relative alla qualità dei corpi idrici superficiali e le strategie da adottare per limitare l'impatto degli effluenti di origine urbana, agricola e industriale, sono estremamente interessanti e di attualità, non solo a causa di una crescente sensibilità ambientale, ma anche e soprattutto al fine di soddisfare i requisiti di legge, sia a livello comunitario che nazionale [6]. A questo proposito, diversi studi hanno analizzato le influenze antropiche sulla qualità delle acque superficiali che attraversano bacini urbanizzati e l'analisi dei componenti principali di pressione adatte per lo studio della qualità delle acque stesse [5]. Tra le varie fonti di pressione, gli impatti dovuti alla immissione dei reflui civili ed industriali sono particolarmente importanti per il flusso del ricevente e la sua capacità di diluizione. Al fine di tutelare la qualità delle acque superficiali è fondamentale per prevenire e ridurre l'inquinamento e attuare il ripristino dei corpi idrici controllando tutti i fattori antropici, tra cui risultano fondamentali la corretta gestione e il funzionamento degli impianti di trattamento delle acque reflue.

In un approccio metodologico di ricerca applicata, lo sviluppo di reti di monitoraggio e modellazione costituiscono strumenti fondamentali per l'analisi e valutazione delle azioni per la tutela delle acque [1,4]. Il presente studio esamina i risultati di un monitoraggio volto a esaminare le azioni da intraprendere per salvaguardare la qualità del torrente "Gravina", nell'area urbana della città di Matera. La rete di flusso si trova all'interno di una importante area naturale, importante dal punto di vista turistico e dell'agricoltura.

MATERIALI E METODI

L'area di studio

Lo spartiacque del torrente "Gravina" nell'area urbanizzata di Matera è l'oggetto della presente indagine;

survey; it is schematically represented in Figure 1.

The stream “Gravina” develops in the north-east area of the main watershed of the river Bradano, and crosses the border area between Apulia and Basilicata. The area of study is mainly located in the territories of the town of Matera in Basilicata and the towns of Altamura and Santeramo in Apulia. All along the urbanized part of the stream, its river-bed is extremely narrow and deep.

Downstream from the town of Matera, the hydraulic section is greatly variable; in dry periods, hydraulic heights vary between 0.1 and 1.5 metres, with flows between 0.1 and 0.6 m^3/sec.

The stream “Jesce”, fed by the waters of the Murgia, flows into this area; it is the main tributary of the stream “Gravina”. The catchment basin above the town of Matera is mainly made up of clay materials, which favour the surface flow of waters that, successively, collect in the ravines of the “Gravina”. The watershed surface can be assessed here in about 490 km2 with a length of the main line of 27 kilometres. The river-bed sections of the streams are adjusted and standardized with reinforced concrete slabs to form a typical trapezoidal section.

The surface water bodies object of present study, which cross a semi-dry climate area, show a stream-like regime, characterised by sudden floods due to short and intense rainfalls. In the long dry periods, the flow is mainly made up of the point sources produced in the urban and industrial areas. The drainages of urban wastewaters originate in the treatment plants serving the town of Matera, which dump the treated effluents directly into the river-bed of the stream “Gravina”, and the urban plant serving the town of Altamura, which dumps into the stream “Jesce”.

Overall, a population of around 150,000 inhabitants is served. Only some of the commercial and industrial areas operating in the area are served by treatment plants.

Survey

The main activities of the survey are summarized as follows.

- field measurements
- surface water quality analyses

Water quality was determined on several samples collected at 20 stations located along the rivers. The survey was carried out in a period of about 150 days. The main physical and chemical parameters were: temperature, pH, electrical conductivity, dissolved oxygen, suspended solids, COD, total nitrogen, ammonia, nitrates, and orthophosphate.

Hydraulic flow measurement

The hydraulic flow was defined by using the data available at the territory’s management bodies and the data collected on the streams examined through a turbine flow-meter. The hydraulic flow was directly measured at two different times, at two sections located downstream of the main municipal wastewater treatment plant operating in the towns of Matera and Altamura. In figure 1 the study area: the watershed of the stream *“Gravina”* in the town of Matera is presented.

QUAL2K software-based modelling

The main aim of modelling was the representation of the current conditions of water quality observed during the measurement period. The simulation was useful in assessing the state of qualitative parameters for a stretch of the river-bed of the stream “Gravina”, not easily accessible, for which it was not possible to acquire measurements.

è schematicamente rappresentato in figura 1. Il torrente "Gravina" si sviluppa nella zona nord-est dello spartiacque principale del fiume Bradano, e attraversa la zona di confine tra Puglia e Basilicata. L'area di studio si trova principalmente nei territori del comune di Matera, in Basilicata e le città di Altamura e Santeramo in Puglia. Lungo tutta la parte urbanizzata del torrente, il suo letto fluviale risulta estremamente stretto e profondo. A valle della città di Matera, la sezione idraulica è molto variabile; in periodi di siccità, le altezze idrauliche variano tra 0,1 e 1,5 metri, con flussi tra 0,1 e 0,6 m^3/s. Il torrente "Jesce", alimentato dalle acque della Murgia, sfocia in questo tratto; è il principale affluente del torrente "Gravina". Il bacino idrografico a monte della città di Matera è costituito principalmente da materiali argillosi, che favoriscono il flusso superficie delle acque che, successivamente, raccolgono negli anfratti della "Gravina". La superficie spartiacque può essere valutata in circa 490 km2 con una lunghezza dell’asta principale di 27 chilometri. Le sezioni dell’alveo dei torrenti sono adeguati e standardizzati con lastre di cemento armato per formare una tipica sezione trapezoidale.

I corpi idrici oggetto del presente studio, che attraversano una zona di clima semi-secco, mostrano un regime di flusso simile, caratterizzato da improvvise inondazioni dovute a piogge brevi e intense.

Nei lunghi periodi di siccità, il flusso è principalmente costituito delle sorgenti puntiformi prodotte nelle aree urbane e industriali. Gli scarichi di acque reflue urbane sono originari di impianti di trattamento che servono la città di Matera, che iscarica effluenti trattati direttamente nel letto del torrente "Gravina", e l'impianto urbano che serve la città di Altamura, che scarica nel torrente "Jesce".

Nel complesso gli impianti di trattamento in questione sono al servizio di una popolazione di circa 150.000 abitanti. Solo alcune delle aree commerciali e industriali che operano nell'area sono serviti da specifici impianti di trattamento.

Il monitoraggio

Le principali attività di monitoraggio ambientale che sono state svolte nel’ambito del presente lavoro sono:

- misure di campo
- analisi della qualità delle acque superficiali

La qualità dell'acqua è stata determinata su diversi campioni prelevati in 20 stazioni situate lungo i fiumi. L'indagine è stata effettuata in un periodo di circa 150 giorni. I principali parametri fisici e chimici sono stati: temperatura, pH, conducibilità elettrica, ossigeno disciolto, solidi sospesi, COD, azoto totale, ammoniaca, nitrati, e ortofosfato.

Flusso idraulico

Il flusso idraulico è stato definito utilizzando i dati disponibili presso gli organi di gestione del territorio e raccogliendo i dati raccolti sui flussi esaminati attraverso una turbina flussometro. Il flusso idraulico è stato direttamente misurato in due momenti diversi, in due sezioni che si trovano a valle del principale impianto di trattamento delle acque reflue municipali che operano nei comuni di Matera e Altamura. Nella figura 1 è presentata l'area di studio: lo spartiacque del torrente "Gravina", nel comune di Matera.

Modellazione basata su software QUAL2K

L'obiettivo principale della modellazione era la rappresentazione delle attuali condizioni di qualità dell'acqua osservati durante il periodo di misurazione. La simulazione è stata utile per valutare lo stato di parametri qualitativi per un tratto di alveo del torrente "Gravina", non facilmente accessibili, per i quali non è stato possibile effettuare misurazioni.

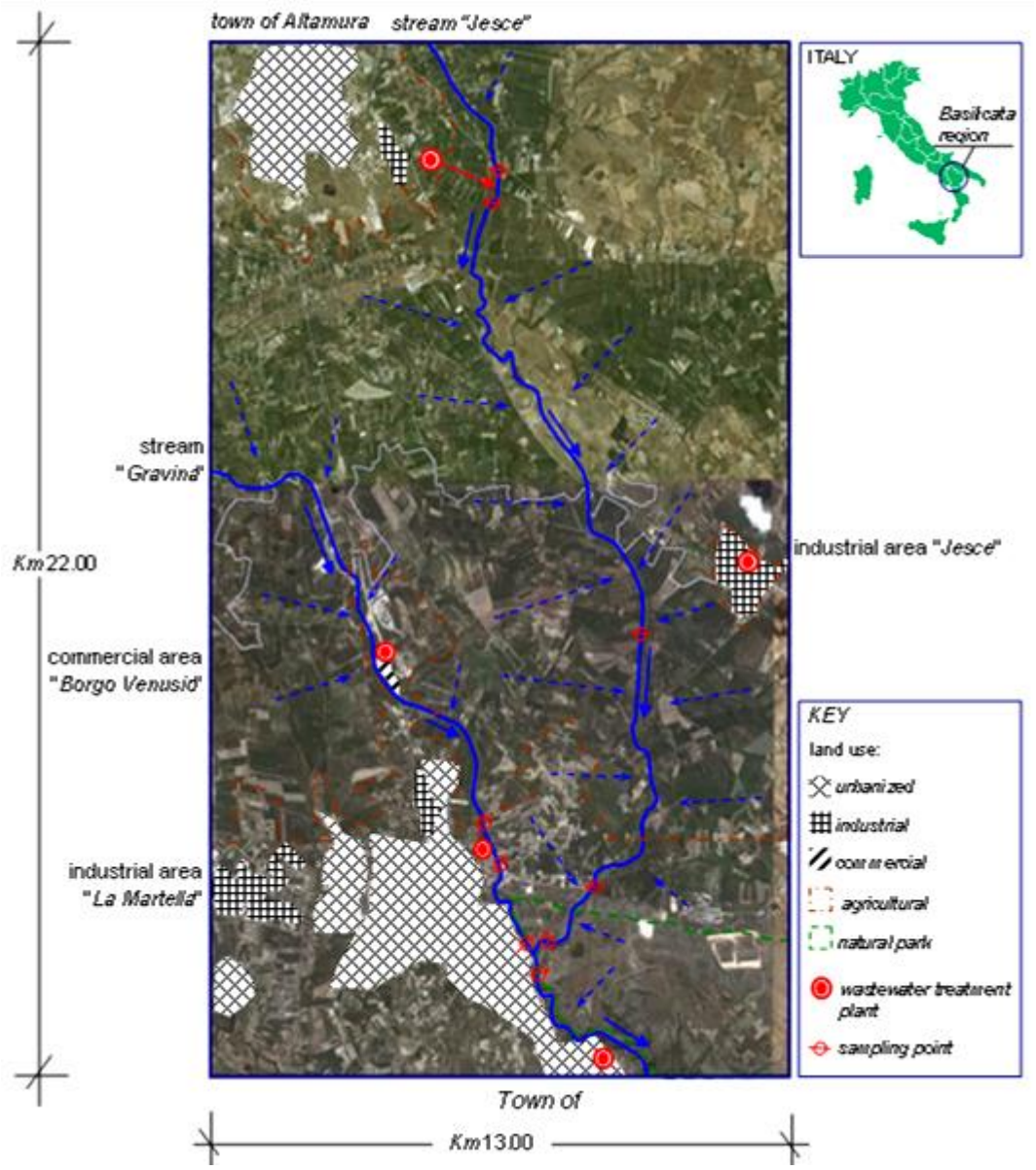

Fig. 1 - The study area: the watershed of the stream *"Gravina"* in the town of Matera.

Simulations were carried out for the following parameters: temperature, dissolved oxygen, biodegradable organic matter (as COD), ammonia and nitrate nitrogen. In order to carry out the modelling, the QUAL2K software, version 2.07, was used [2].

Representation of the hydraulic scheme

The hydraulic system taken into account is made up of the stream "Gravina" and its tributary, the stream "Jesce", for a river-bed length of about 3 km and 22 km respectively. The modelling representation involved the splitting up of the two river branches into 75 reaches, which represent stretches of river that have constant hydraulic characteristics (e.g., slope, bottom width, etc.). The hydraulic sections were considered with regular trapezoidal shapes.

The model calibration was carried out on the basis of the data related to the geometry of the river, the headwater characteristics, the discharges and with reference to the measures collected in the campaign phases.

Table 1 reports the values adopted for the main coefficients ruling the chemical variables of the model. In

Le simulazioni sono state effettuate per i seguenti parametri: temperatura, ossigeno disciolto, materia organica biodegradabile (come COD), ammoniaca e azoto nitrico. Al fine di effettuare la modellazione, il software QUAL2K, versione 2.07, è stato utilizzato [2].

Rappresentazione del sistema idraulico

Il sistema idraulico preso in considerazione è costituito dal torrente "Gravina" e il suo affluente, il flusso "Jesce", per una lunghezza dell'alveo rispettivamente di circa 3 km e 22 km. La rappresentazione modellistica ha comportato il frazionamento dei due rami del fiume in 75 tratti, che rappresentano porzioni di fiume che hanno caratteristiche idrauliche costanti (ad esempio, pendenza, larghezza fondo, ecc). Le sezioni idrauliche sono state considerate con forme trapezoidali regolari.

La calibrazione del modello è stata effettuata sulla base dei dati relativi alla geometria del fiume, le caratteristiche dei punti sorgente, degli scarichi e con riferimento alle misure raccolte nelle fasi campagna.

La tabella 1 riporta i valori adottati per le principali coefficienti che regolano le variabili chimiche del modello. Per calcolare il processo di riaerazione, è stato utilizzato

order to calculate the re-aeration process, the O'Connor-Dobbins model was used [6]. Assumed the morphology of stream, which is constituted by concrete trapezoidal channel with low water height and natural small hydraulic section with high water velocity, application of model does not take in account an increase of biological activity promoted by algal growth.

il modello O'Connor-Dobbins [6]. Assunta la morfologia del torrente, che è costituito dal canale trapezoidale in calcestruzzo con altezza ridotta di acqua e modesta sezione idraulica naturale con alta velocità di acqua, l'applicazione del modello non ha tenuto in conto dell'aumento di attività biologica promossa dalla crescita delle alghe.

Table 1

Applied values of the kinetic parameters of the model

Parameters	unit	Value
Slow CBOD hydrolysis rate	d^{-1}	0.4
Fast CBOD oxidation rate	d^{-1}	3.2
Organic nitrogen hydrolysis rate	d^{-1}	0.2
Nitrification rate for ammonia nitrogen	d^{-1}	1.2

Stream water quality

The stream "Gravina" downstream of the urban discharge of the town of Matera

Downstream of the treatment plant serving the town of Matera, the concentrations of the pollutant parameters usually show substantial increases with respect to the concentrations measured in the samples upstream from the same discharge.

Values vary from 16,7÷20,7 to 51,5÷73,6 mgO_2/l for the COD, from 0,50÷0,52 to 14,5÷30,8 mgN/l, for ammonia nitrogen. Electrical conductivity shows a sensible reduction, with values included between 733 and 967 µs/cm.

The processes of dilution and concentration of pollutants are strongly affected by the amount of hydraulic flows of the treatment plant discharges, which, in the measurement period, constitute most of the water outflow along the river-bed.

Further downstream, we observed a restoration of qualitative conditions, the concentrations of pollutants tend to decrease, clearly because of diffusion and re-aeration processes.

Immediately downstream of the discharge, we observed a nearly instantaneous decrease in the concentration of dissolved oxygen ascribable to the mixing of waters with greater flows characterised by lower concentration values. Immediately upstream of the confluence with the stream "Jesce", the concentration of the dissolved oxygen further tends towards a decrease, evidently because of the process of degradation of the biodegradable organic matter present in the secondary effluents, both in particulate and in dissolved forms. The average rates of oxygen consumption are about 0.02 mg/l*m.

The COD rises downstream of the discharge from the treatment plant and then decreases.

The concomitant reduction of ammonia concentrations with the increase of nitrate nitrogen highlights the development of nitrification processes.

The stream "Jesce"

Downstream of the discharge of the treatment plant serving the town of Altamura, the waters show a worse quality. The COD values reach 95,6 mgO_2/l, ammonia nitrogen stabilizes at 57,7 mgN/l. Electrical conductivity shows values between 1123÷1182 µs/cm.

Dissolved oxygen shows a remarkable decrease downstream of the plant serving the town of Altamura; low levels of dissolved oxygen are also recorded downstream of the industrial area of "Jesce", with concentrations next to 1÷2 mg/l. The average rates of oxygen consumption are between 0.01÷0.02 mgO_2/l*m.

We noticed a re-oxygenation of the waters further downstream and near the confluence with the stream "Gravina"; this was due to the adjustment of the large-section river-bed and of the hydraulic falls realised through water withdrawals works. The average rates of

Qualità dell'acqua

Il torrente "Gravina" a valle dello scarico urbano della città di Matera

A valle del depuratore che serve la città di Matera, le concentrazioni dei parametri inquinanti mostrano solitamente aumenti sostanziali rispetto alle concentrazioni misurate nei campioni a monte dello stesso scarico.

I valori variano da 16,7÷20,7 a 51,5÷73,6 mgO_2/l per il COD, da 0,50÷0,52 a 14,5÷30,8 mgN/l, per l'azoto ammoniacale. La conducibilità elettrica mostra una sensibile riduzione, con valori compresi tra 733 e 967 ms/cm.

I processi di diluizione e la concentrazione degli inquinanti sono fortemente influenzati dalla quantità di flussi idraulici degli scarichi dell'impianto di trattamento, che, nel periodo di misurazione, costituiscono la maggior parte del deflusso dell'acqua lungo il letto del fiume.

Più a valle, abbiamo osservato un ripristino delle condizioni qualitative, le concentrazioni di inquinanti tendono a diminuire, chiaramente a causa di processi di diffusione e riaerazione.

Immediatamente a valle dello scarico, abbiamo osservato una riduzione quasi istantanea della concentrazione di ossigeno disciolto ascrivibile alla miscelazione di acque con maggiori flussi caratterizzati da valori di concentrazione inferiori.

Immediatamente a monte della confluenza con il torrente "Jesce", la concentrazione dell'ossigeno disciolto tende verso una ulteriore diminuzione, evidentemente a causa del processo di degradazione della sostanza organica biodegradabile presente negli effluenti secondari, sia nel particolato e in forme disciolte. I tassi medi di consumo di ossigeno sono circa 0,02 mg/l*m.

Il COD si rivela a valle dello scarico del depuratore e poi diminuisce.

La concomitante riduzione delle concentrazioni di ammoniaca con l'aumento di azoto nitrico evidenzia lo sviluppo di processi di nitrificazione.

Il torrente "Jesce"

A valle dello scarico dell'impianto di depurazione che serve la città di Altamura, le acque mostrano una qualità peggiore. I valori di COD raggiungono 95,6 mgO_2/l, l'azoto ammoniacale si stabilizza attorno a 57,7mgN/l. La conducibilità elettrica mostra valori compresi tra 1123÷1182 ms/cm.

L'ossigeno disciolto mostra una notevole diminuzione a valle dell'impianto che serve la città di Altamura; bassi livelli di ossigeno disciolto vengono registrati anche a valle della zona industriale di "Jesce", con concentrazioni prossime a 1÷2 mg/l. I tassi medi di consumo di ossigeno sono compresi tra 0,01÷0,02 mgO_2/l*m.

Abbiamo notato una riossigenazione delle acque più a valle e in prossimità della confluenza con il torrente "Gravina".

Questa situazione era dovuta alla regolarizzazione della sezione dell'alveo che risultava più larga e alla presenza di cascate idrauliche realizzate attraverso opere di derivazione e prelievo idrico. I tassi medi di

oxygenation are between 0.001÷0.003 mgO_2/l*m.

In other sections downstream, the COD stays almost constant, except for a reduction in the stretches of river-bed where hydraulic falls are present.

Downstream of the treatment plant, ammonia nitrogen remains substantially constant, as well as the values of nitrate nitrogen; in the following stretches we observed a slight reduction in ammonia and an increase in nitrate nitrogen.

Electrical conductivity, in the central and final fluvial branches, remains steady with values between 1152 and 1156 μs/cm.

The stream “Gravina” downstream of the confluence with the stream “Jesce”

Downstream of the confluence with the stream “Jesce”, we found remarkable increases in the values of pollutant parameters: COD concentrations vary from 25.8÷29.9 to 43.8÷47.4 mgO_2/l, those of ammonia nitrogen from 13.4÷13.5 to 26.7÷38.5 mgN/l. Electrical conductivity increased weakly.

As far as dissolved oxygen is concerned, we observed an effect of re-oxygenation, favoured by the mixing with the waters of the stream “Jesce”, characterised by a higher concentration of dissolved oxygen since, before the confluence, they cross natural falls. The consumption rates of oxygen are included the stretches where it is required, between 0.02 ÷ 0.12 mg/l*m and for the stretches where there is re-oxygenation between 0.001÷0.006 mg/l*m.

RESULTS

The diagrams in Figure 2 represent the results. The diagram related to the flow reports the values assumed as the basis of the calculation: two increases are evident, one in correspondence with the discharge of the treatment plant serving the town of Matera, the other in correspondence with the confluence of the stream “Jesce”.

Both the effects of the inflow of the wastewater treatment plant serving the town of Matera and the inflow of the stream “Jesce” are clear.

More specifically, the waters of the stream “Gravina”, downstream from the discharge of the plant of Matera, show decreases in the values of dissolved oxygen and increases in the concentrations of COD and ammonia nitrogen. Oxygen is consumed by the processes of self purification of the water body.

After the confluence of the stream “Jesce”, the analysis on the stream “Gravina” makes evidence an increases in the concentrations of oxygen, COD and ammonia.

Increase of oxygen is due to the aeration from the morphology of the confluence area, the increase in polluting parameters is caused by the bad quality of drainage waters in the stream “Jesce” from urban effluents which are not sufficiently treated and from wastewaters from illegal point sources.

In general, the simulated values of the analysed water quality parameters represent the observed data well. In particular, the simulated results satisfactorily represent the variations in biodegradable organic matter and dissolved oxygen. Nitrification processes are well traced when there are no sensible variations in ammonia concentration. Main problems of modelling process can be summarize as follows:

- applied values of oxidation rate do not allow to

ossigenazione sono tra 0,001÷0,003 mgO_2/l*m.

In altre sezioni a valle, il COD rimane quasi costante, eccetto per una riduzione nei tratti di alveo in cui sono presenti alcuni salti idraulici.

A valle del depuratore, l’azoto ammoniacale rimane sostanzialmente costante, così come i valori di azoto nitrico; nei seguenti tratti abbiamo osservato una lieve riduzione di ammoniaca e un aumento dell’azoto nitrico.

La conducibilità elettrica, nei tratti fluviali centrale e finale, rimane stabile con valori compresi tra 1152 e 1156 ms/cm.

Il torrente "Gravina" a valle della confluenza con il torrente "Jesce"

A valle della confluenza con il torrente "Jesce", abbiamo riscontrato notevoli aumenti nei valori dei parametri inquinanti: le concentrazioni di COD variano dal 25,8÷29,9 a 43,8÷47,4 mgO_2/l, quelli di azoto ammoniacale da 13,4÷13,5 fino a 26,7÷38,5 mgN/l. La conducibilità elettrica è aumentata debolmente.

Per quanto riguarda l'ossigeno disciolto, per questo parametro abbiamo osservato un effetto di riossigenazione, favorito dalla miscelazione con le acque del torrente "Jesce", caratterizzata da una maggiore concentrazione di ossigeno disciolto in quanto, prima della confluenza, il torrente affluente è caratterizzato dalla presenza di alcune piccole cascate naturali. I tassi di consumo di ossigeno sono compresi i tratti in cui è richiesto, tra 0,02÷0,12 mg/l*m e per i tratti in cui vi è la riossigenazione tra 0,001÷0,006 mg/l*m.

RISULTATI

I diagrammi di Figura 2 rappresentano i risultati. Il diagramma relativo al flusso riporta i valori assunti come base del calcolo: due aumenti sono evidenti, uno in corrispondenza dello scarico del depuratore che serve la città di Matera, l'altro in corrispondenza della confluenza del torrente "Jesce".

Entrambi gli effetti del flusso dell'impianto di trattamento delle acque di scarico che serve la città di Matera e l'afflusso del torrente "Jesce" sono molto evidenti.

Più in particolare, le acque del torrente "Gravina", a valle dello scarico dell'impianto di Matera, evidenziano una diminuzione nei valori di ossigeno e aumenti delle concentrazioni di COD e azoto ammoniacale disciolto. L'ossigeno viene consumato dai processi di auto purificazione del corpo idrico.

Dopo la confluenza del torrente "Jesce", l'analisi sul torrente "Gravina" rende testimonianza di un aumento delle concentrazioni di ossigeno, COD e ammoniaca.

L’aumento di ossigeno è dovuto alla aerazione legata alla morfologia della zona di confluenza; l'aumento dei parametri inquinanti è causato invece dalla cattiva qualità delle acque di scarico ricevuto dalle correnti del fiume "Jesce" e costituite da effluenti urbani non sufficientemente trattati e da reflui non trattati e, con tutta probabilità, illegali.

In generale, i valori simulati dei parametri di qualità dell'acqua analizzati rappresentano bene i dati osservati. In particolare, i risultati simulati rappresentano soddisfacentemente le variazioni di materia organica biodegradabile e ossigeno disciolto.

I processi di nitrificazione sono ben tracciate quando non ci sono sensibili variazioni nella concentrazione di ammoniaca. I principali problemi di processo di modellazione possono riassumere come segue:

- i valori del tasso di ossidazione utilizzato nella

represent the more strong path of stabilization of organic matter; values higher than those described in literature (lower 3÷4) could be more suitable to represent the process of readily biodegradable compounds;

- use of higher values of nitrification rate does not permit a good interpretation of more intensive observed process, associated to an increase of nitrate; we observe that oxygen concentration presents observed value up to 60÷70 % of saturation.

simulazione non consentono di rappresentare il sensibile processo di stabilizzazione della sostanza organica; valori superiori a quelli descritti in letteratura (inferiori di 3÷4) potrebbero essere più adatti a rappresentare il processo di composti facilmente biodegradabili;

- l'uso di valori elevati del tasso di nitrificazione non consente una buona interpretazione del processo osservato nelle fasi in cui il processo è più accentuato, associato ad un aumento di nitrato; osserviamo valori osservati di concentrazione di ossigeno fino al 60 ÷ 70% di saturazione.

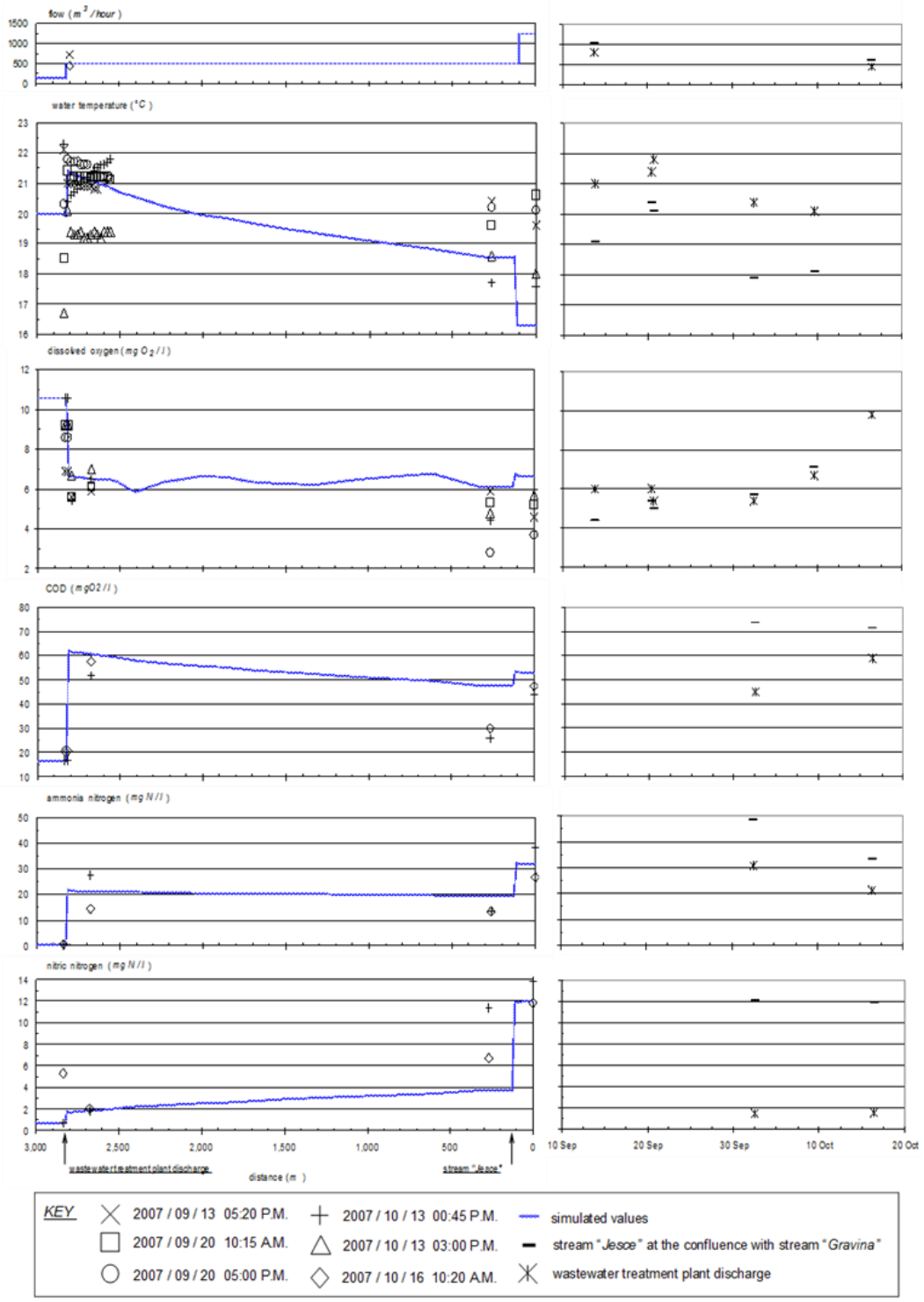

Fig. 2 - Observed and simulated water quality data of the stream *"Gravina"*, during the months of September and October 2007; diagrams at the right side report the observed data of the Matera treatment plant discharge and the stream "*Jesce*" upstream the confluence with stream "*Gravina*"

Water restoration and use

In order to manage the quality of surface waters in the watershed studied, an analysis of a series of peculiar aspects is required.

Control pollution from point and non-point sources

The first actions concern the control of pollution of urban wastewater and in particular:

- the assessment of how the treatment plants serving the urban areas of the towns of Matera and Altamura are functioning; as far as the plant of Altamura is concerned, it is important to consider that the discharge occurs in the territory of a nearby region with negative effects on the Lucanian territory;
- management control of treatment plants, with special reference to the discharge of effluents that were not depurated as envisaged by the rules and the discharge into river-beds of sludge in excess by the effluent.

Further specific aspects are:

- the collection of point discharges presently not collected;
- the control of pollution from diffused sources draining off from the urban areas and from the areas used for agricultural and farming activities; during rainy periods, these waters bring organic and inorganic pollutants, also through fertilizers and pesticides.

The remedial actions that mainly must be undertaken on the watershed scale are:

- the determination of the polluting loads produced by urban areas and collected by the sewage systems;
- the determination of polluting loads produced by industrial areas;
- the adjustment of sewage networks, for their correct functioning during rainfall events.
- action for wastewater treatment: in order to obtain a better treatment of wastewaters, it is worth:
- verifying the depurative capacity of the existing plants serving the urban areas;
- checking the management activities of the existing treatment plants;
- building new plants and upgrade the existing ones in the industrial and commercial areas;
- assessing the solution to refine treated municipal secondary effluents in order to protect the quality of surface waters and restore natural habitats; in this respect we should consider that the existing treatment plant of the secondary effluents is not yet used.

A second aspect concerns the treatment of discharges produced by industrial and commercial areas. In this respect we observe that the existing plants are not running.

An operational approach could envisage the refining of the secondary effluents of the treatment plants with techniques of phyto-treatment and lagoons, to be carried out either in or outside the river-bed. The interventions in the river-bed could involve actions of re-oxygenation in river-bed based on hydraulic techniques. As for the feasibility of a constructed wetland plant, the main problems concern the localization of the treatment area (in and outside the river-bed) and the need to modify the hydraulic flow.

Recupero e uso dell'acqua

Al fine di gestire la qualità delle acque di superficie nel bacino studiato, è necessaria l'analisi di una serie di aspetti peculiari.

Controllo inquinamento da fonti puntuali e non puntuali

Le prime azioni riguardano il controllo dell'inquinamento delle acque reflue urbane e in particolare:

- la valutazione di come gli impianti di trattamento che servono le aree urbane delle città di Matera e Altamura funzionano; per quanto riguarda l'impianto di Altamura è interessante e importante considerare che lo scarico avviene nel territorio di una regione vicina con effetti negativi sul territorio lucano;
- il controllo di gestione degli impianti di trattamento, con particolare riferimento allo scarico di effluenti che non sono stati depurati come previsto dalle norme e allo scarico in alvei di fanghi di supero.

Ulteriori aspetti specifici sono:

- l'intercettazione e la raccolta degli scarichi puntuali attualmente non trattati;
- il controllo dell'inquinamento da fonti diffuse drenanti fuori dalle aree urbane e dalle aree utilizzate per le attività agricole e di allevamento; durante i periodi piovosi, queste acque portano inquinanti organici e inorganici, anche per l'uso estensivo di fertilizzanti e pesticidi.

Le azioni correttive che devono essere intraprese prevalentemente su scala di bacino sono:

- la determinazione dei carichi inquinanti prodotti da aree urbane e raccolti dai sistemi fognari;
- la determinazione dei carichi prodotti da aree industriali inquinanti;
- l'adeguamento delle reti fognarie, per il loro corretto funzionamento soprattutto durante eventi piovosi.
- azioni per il trattamento delle acque reflue: per ottenere un miglior trattamento dei reflui, risulta consigliabile;
- verificare la capacità depurativa degli impianti esistenti destinati alle aree urbane;
- il controllo delle attività di gestione degli impianti di depurazione esistenti;
- costruzione di nuovi impianti e aggiornare quelli esistenti nelle aree industriali e commerciali;
- valutare la soluzione per affinare il trattamento di effluenti secondari comunali al fine di tutelare la qualità delle acque superficiali e ripristinare gli habitat naturali; a questo proposito si deve considerare che l'impianto di trattamento esistente degli effluenti secondari non viene ancora utilizzato.

Un secondo aspetto riguarda il trattamento degli scarichi prodotti dalle aree industriali e commerciali. A questo proposito si osserva che gli impianti esistenti spesso non sono in esercizio.

Un approccio operativo potrebbe prevedere il trattamento degli effluenti secondari degli impianti di trattamento con tecniche di fito-trattamento e lagune, da effettuare all'interno o al di fuori del letto del fiume. Gli interventi in alveo potrebbero comportare azioni di riossigenazione in alveo basati su tecniche idrauliche. Per quanto riguarda la fattibilità di un impianto di fitodepurazione, i principali problemi riguardano la localizzazione della zona da trattare (dentro e/o fuori il letto del fiume) e la necessità di modificare artificialmente il deflusso idraulico.

CONCLUSIONS

In order to safeguard surface water quality in the urbanized area of Matera (Basilicata region, Southern Italy) a survey was carried out to evaluate the basic elements of planning action.

The negative effects of water pollution originating in the anthropic pressure are widely evident in the watershed of the stream “Gravina”. During the summer and early autumn season, the effluent flows from municipal wastewater treatment plant constitute the largest part of the stream water. Furthermore, the polluted water of the influent stream “Jesce” increases the load to be controlled.

Most of the measured parameters are characterized by a value higher than the limits envisaged by law. The conditions occurring in waters, above all the low concentrations of dissolved oxygen, nullify the presence of most aquatic species.

Simulation carried out by using the model QUAL2K allowed a good representation of water quality observed in field measures.

The described conditions clarify the necessity to safeguard the natural environment by understanding the causes and eliminating the effects. An improvement of the water quality could mainly be obtained through the control of the discharged polluted flow from urbanized watershed and agricultural and industrial areas, during both the dry and the rainy period. Phyto-treatment and lagoons of municipal secondary effluents could be an effective solution. When properly realized, such a system allows a reduction in the environmental impact and an improvement in the quality of the stream waters to be used in safe way, also in agriculture.

REFERENCES

[1]. Boyacioglu H., Boyacioglu H., (2007) - *Surface Water Quality Assessment by Environmetric Methods*. Environ Monit Assess 131, 371–376;
[2]. Chapra S.C., (1997) - *Surface Water-Quality Modeling*. WCB/McGraw-Hill, Boston, USA;
[3]. O'Connor, D.J., W.E. Dobbins, (1958). *Mechanism of Reaeration in Natural Streams*. ASCE Transactions. Paper N. 2934;
[4]. Ouyang Y., (2005) - *Evaluation of river water quality monitoring stations by principal component analysis*. Water Research, 39, 2621–2635;
[5]. Simeonov V., Stratis J.A., Samara C., Zachariadis G., Voutsa D., Anthemidis A., Sofoniou M., Kouimtzis T., (2003) - *Assessment of the surface water quality in Northern Greece Water Research*, 37, 4119-4124;
[6]. *** EU (2000) - EEC Directive 2000/60, *Single Text on Environment*, Legislative Decree n.152/2006, n.4/2008, Bruxelles, Belgium.

CONCLUSIONI

Al fine di salvaguardare la qualità delle acque superficiali nella zona urbanizzata di Matera (Basilicata, Italia meridionale) un monitoraggio è stato condotto per valutare gli elementi di base per la pianificazione degli interventi.

Gli effetti negativi dell’inquinamento delle acque provenienti dalle aree urbanizzate sono ampiamente evidenti nel bacino del torrente "Gravina". Durante l'estate e inizio autunno, i flussi di effluenti dall’impianto municipale di trattamento delle acque reflue costituiscono la maggior parte del flusso del corso d’acqua. Inoltre, l'acqua inquinata del torrente affluente "Jesce", aumenta ulteriormente il carico di contaminanti da tenere sotto controllo.

La maggior parte dei parametri misurati sono caratterizzati da un valore superiore ai limiti previsti dalla legge. Le condizioni che si verificano nelle acque, soprattutto le basse concentrazioni di ossigeno disciolto, annullano la presenza della maggior parte delle specie acquatiche.

La simulazione effettuata utilizzando il modello QUAL2K ha permesso una buona rappresentazione della qualità dell'acqua, con una buona corrispondenza fra valori calcolati e misurati in campo.

Le condizioni descritte chiariscono la necessità di salvaguardare l'ambiente naturale attraverso la comprensione delle cause e di eliminare gli effetti. Un miglioramento della qualità dell'acqua può principalmente essere ottenuto attraverso il controllo del flusso inquinato scaricato dal bacino urbanizzato con il contributo di aree agricole e industriali, sia durante il periodo secco che nel periodo delle piogge. I trattamenti di fitodepurazione o l’uso di lagune per depurare gli effluenti degli impianti di depurazione municipali, potrebbero costituire una soluzione efficace. Se correttamente realizzato, tale sistema consente una riduzione dell'impatto ambientale e un miglioramento della qualità delle acque del torrente, per poter essere utilizzate in sicurezza, anche per usi agricoli.

BIBLIOGRAFIA

[1]. Boyacioglu H., Boyacioglu H., (2007) – *La Valutazione della qualità dell'acqua superficiali da metodi Environmetric*. Environ Monit Assess. 131, 371–376;
[2]. Chapra S.C., (1997) - *Modellazione di qualità dell'acqua superficiali.* WCB/McGraw-Hill, Boston, USA.
[3]. O'Connor, D.J., W.E. Dobbins (1958). *Meccanismo di Reaeration in corsi d'acqua naturali.* ASCE Transactions. N. 2934;
[4]. Ouyang Y., (2005) - *Valutazione delle stazioni di monitoraggio della qualità delle acque del fiume per analisi delle componenti principali*. Ricerca sulle Acque, 39, 2621–2635;
[5]. Simeonov V., Stratis J.A., Samara C., Zachariadis G., Voutsa D., Anthemidis A., Sofoniou M., Kouimtzis T. (2003) - *La valutazione della qualità delle acque superficiali nel nord della Grecia.* Ricerca sulle Acque, 37, 4119-4124;
[6]. *** EU (2000) - Direttiva CEE 2000/60, *Testo Unico sull'Ambiente*, Decreto Legislativo n.152/2006, n.4/2008, Bruxelles, Belgio.

OPTIMIZATION OF THE DOSING PUMP FUNCTIONAL PARAMETERS USED FOR AGRICULTURAL CROPS FERTIGATION
/
OPTIMIZAREA PARAMETRILOR FUNCŢIONALI AI POMPEI DE DOZARE UTILIZATĂ LA FERTIRIGAREA CULTURILOR AGRICOLE

PhD. Eng. Biolan I.[1)], PhD. Eng. Vişan A.L.[2)], Eng. Vulpe G.[1)], Eng. Biolan C.[1)]
[1)] I.N.C.D.I.F."ISPIF" Bucharest / Romania; [2)] INMA Bucharest / Romania
E-mail: iliebiolan@gmail.com.

Abstract: *The paper presents the mathematical model that was used to optimize the performances of an hydraulic dosing pump used to agricultural crop fertigation. These research activities have been conducted during the 1986-2010, period during which the hydraulic dosing pump operated in conjunction with an irrigation installation.*

Keywords: *dosing pump, fertigation, membranes, performances.*

INTRODUCTION

Fertigation is a modern concept and represents the newest technology used in intensive agriculture field, that combines the irrigation technique with fertilization systems. Using this method, the fertilizing substances are dosed and distributed simultaneously with the irrigation water, so the plants receive the nutrients along with water, in accordance with the vegetation state. This technology can control and improve the crop productivity in accordance with crop agronomical requirements and the meteorological conditions. More than that, these systems can be easily adapted to the type of crop, to the vegetation state and the type of fertilizer (chemical or biological liquids). From this reason, the dosing pump must meet the international market requirements and to be easily adapted to the technologic systems that are already used in this area.

The latest tendency in the intensive agriculture technological systems is the bio-fertigation, trend that is widely spread in the developed countries (France, Italy, England etc.), due to people concern to have a healthy body and a long life expectancy by using only natural products (products without genetic mutation or chemical fertilizers).

Also this type of agriculture is applied to a small scale (local and private farms) and the biological products placed on the market are very expensive.

Previous researches obtained lead to the conclusion that it is necessary to optimize the working parameters of the dosing pump, in order to adapt it to the classical systems, that are used in intensive agriculture in most arable areas, but also to the bio-farming [3, 4].

MATERIALS AND METHOD

The research activity was made in order to highlight of the advantages of the combined usage of irrigation techniques were performed with fertilization systems using different types of dosing pumps manufactured abroad or in Romania - dosing pump type PD1-2 made within the National Institute of Research-Development for Land Improvements (INCDIF-ISPIF Bucharest), which was tested in Research Development Institute for Capitalization of Horticultural Products Bucharest (ICDIMPH–HORTING Bucharest).

Fertilization of crops in greenhouses, by classical method, is done in stages: before plating and during the vegetation. The organic and chemical fertilizing solutions

Rezumat: *În acest articol este prezentat modelul matematic utilizat pentru optimizarea performanţelor unei pompe hidraulice de dozare, folosită la fertirigarea culturilor agricole. Această activitate de cercetare a fost desfăşurată în perioada 1986-2010, perioadă în care pompa hidraulică de dozare a funcționat în cadrul unei instalaţii de irigare.*

Cuvinte cheie: *pompa de dozare, fertirigare, membrane, performante.*

INTRODUCERE

Fertirigarea este un concept modern şi reprezintă cea mai nouă tehnologie utilizată în domeniul agriculturii intensive, care combină tehnica de irigare cu sistemele de fertilizare. Utilizând această metodă, substanţele de fertilizare sunt dozate şi sunt distribuite în acelaşi timp cu apa de irigare, astfel plantele asimilează substanţele hrănitoare o dată cu apa, în conformitate cu stadiul vegetativ. Această tehnologie poate controla şi îmbunătăţi productivitatea agricolă în conformitate cu cerinţele agronomice ale culturii şi cu condiţiile meteorologice. Mai mult decât atât, aceste sisteme pot fi cu uşurinţă adaptate la diverse tipuri de culturi, în funcţie de stadiul de vegetaţie şi de tipul fertilizatorului (substanţe chimice sau biologice). Din acest motiv, pompa de dozare trebuie să respecte cerinţele pieţei şi să poată fi adaptată cu uşurinţă la sistemele tehnologice care sunt deja utilizate în acest domeniu.

Printre cele mai noi tendinţe în cadrul sistemelor tehnologice destinate agriculturii intensive este bio-fertirigarea, trend care este foarte des întâlnit în ţările dezvoltate (Franţa, Italia, Anglia etc.), datorită faptului că populaţia este preocupată pentru a avea un corp sănătos şi o durată de viaţă lungă, utilizând numai produse naturale (produse fără modificări genetice şi fertilizatori chimici).

De asemenea, acest gen de agricultură este practicată în prezent la scară mică (în ferme locale şi particulare) iar produsele biologice comercializate au preţuri ridicate.Cercetările anterioare au condus la concluzia că, este indicat să se optimizeze parametrii funcţionali ai pompei de dozare, pentru a putea fi adaptată la sistemele clasice utilizate în agricultura intensivă, sisteme care au o mare răspândire pe suprafetele arabile dar şi la fermele bio [3, 4].

MATERIALE ŞI METODĂ

Activitatea de cercetare a fost realizată pentru a evidenţia avantajele utilizării combinate a tehnicilor de irigare cu sistemele de fertilizare, utilizând diverse tipuri de pompe de dozare, produse în străinătate, respectiv în Romania - pompa de dozare tip PD1-2, realizată în cadrul Institutului Naţional de Cercetare - Dezvoltare pentru Îmbunătăţiri Funciare (INCDIF - ISPIF Bucureşti) care a fost testată în cadrul Institutului de Cercetare - Dezvoltare pentru Valorificarea Produselor Horticole-Bucureşti (ICDIMPH – HORTING Bucureşti).

Fertilizarea culturilor în sere prin metoda clasică se face în etape: înainte de plantare şi în vegetaţie. Soluţiile de îngrăşăminte organice şi chimice se administrează numai

are applied only by spraying as fertilizing irrigation – fertigation, comparing to solid fertilizers that are generally applied by manual distribution, requiring an intensive labor and the plant injury risk is not eliminated as a result of increased concentration etc. [3].

The fertigation can be applied in greenhouses using micro spraying or dripping irrigation installations, because they are equipped with liquid fertilizer injection devices in irrigation water - dosing pump.

Consulting the scientific literature, it has concluded that "The most efficient system for applying fertigation is the drip irrigation with nutrient solution, which creates the most favorable soil air-thermo-hydric and plant nutrition regime" [3].

The greenhouse conditions in which were made the research on fertirigation are:

- Fertilizer dose applied must be constant and evenly distributed;
- The amount of fertilizer to be injected has to be in accordance with the vegetation period of the plant;
- Source of water used in the greenhouse should be well determined (network, rain etc.).

The research activity was conducted in greenhouses on tomato crops through IUP/ NETAFIN drip watering system which was connected to the PD 1-2 dosing pump, which has also the role to inject the liquid fertilizer into irrigation water [3].

The tests used liquid fertilizer on nitrogen and potassium base.

The IUP - low pressure dripping watering system has the next components: one filtering system (gravimetric or screen filter), watering pipe with length of 100 m, distance between dropping is 0.6 m, the supply pressure is maximum 2.5 bar, the dripping flow 2 l/h and the maximum water quantity is 150 $m^{3/}$ha.

The 1-2 PD dosing pump which comprises two membranes that inject fertilizers into irrigation system, using the irrigation water from the system as power source. This type of pump is the latest prototype made in Romania designed to increase the crops productivity on Romanian soil and to reduce the water consumption [1,4].

The PD 1-2 pump (Fig.1), is mounted in parallel with the main irrigation circuit AMF from which is drawing the hydraulic power due to supply line AM in order to drive the mechano-hydraulic system which has: an opening valve R1 to main pipe, supply valve R1', a rapid coupling system C1 and manometer M1. The pressurized water reaches the hydraulic directional vale controller 1 and from here flows towards the pomp 2. Water evacuation is made by EM circuit, in this pipe line the water is either free flowing or at low pressure in order to allow its recycling and its reintroduction in the installation's circuit [1].

The manometer M3 measures the water pressure form the installation supply line, Q1 determines the IUP water flow from the installation supply line and is positioned after the filter F. During the experimental activity was also used an chronometer in order to establish the operating period of fertigation installation.

At this stage, the piston shaft is achieving a movement of translation C, thus driving the two membranes and triggering absorption of the fertilizing into the chamber of the central body AP, where the membrane is decompressed and creates a pressure drop that is needed for adsorption. Meanwhile, inside the other chamber where the membrane is being compressed, the fertilizer absorbed during the previous stage of this process is injected into the IP circuit.

After the piston stroke C is done, lever commands the directional valve controller reversing the water circuit inside and implicitly changing the fertilizer's circuit.

prin aspersiune sub formă de irigare fertilizantă – fertirigatie, în comparație cu îngrășămintele solide, care se aplică in general prin distribuție manuala, necesitând un consum mare de forță de muncă, iar riscul vătămării plantelor nu este eliminat ca urmare a concentrației mărite etc. [3]

Fertirigatia se poate aplica in sere prin intermediul instalației de udare prin microaspersiune prin picurare, deoarece acestea sunt dotate cu dispozitive de injecție îngrășământ lichid în apa de irigat – pompa de dozare.

Consultând literatura de specialitate s-a ajuns la concluzia că „cel mai eficient sistem de realizare a fertirigației îl constituie irigarea prin picurare cu soluție nutritivă, care creează cel mai favorabil regim aerotermohidric al solului şi de nutriţie a plantelor" [3].

Condițiile din sera în care s-au efectuat cercetările pentru fertirigatie, sunt:

- Doza de îngrășământ administrată trebuie să fie constantă şi uniform distribuită;
- Cantitatea de îngrășământ injectată să fie in conformitate cu perioada de vegetație a plantei;
- Sursa de apă folosită in seră trebuie sa fie bine determinată (rețea, ploaie etc.).

Activitatea de experimentare s-a desfăşurat în sere, asupra culturilor de tomate, prin intermediul instalaţiei de udare prin picurare IUP/NETAFIN care a fost conectata la pompa de dozare, PD1-2, şi care mai are şi rolul de injecţie a îngrăşământului lichid în apa de irigat [3].

Încercările s-au realizat cu îngrășământ lichid pe baza de azot şi potasiu.

Instalaţia de udare prin picurare de joasă presiune – IUP, prezintă următoarele componente: sistem de filtrare (filtru gravimetric sau filtru cu sită), conducte de udare cu lungimea de 100 m, distanța dintre picurătoare fiind de 0,6 m, presiunea de alimentare maximă de 2,5 bar, debitul picurătoarelor 2 l/h si norma de udare 150 m^3/ha.

Pompa de dozare PD1-2, are în componenţa ei două membrane care injectează fertilizant în sistemul de irigare, folosind apa de irigare din sistem ca sursă de putere. Această pompa este cel mai nou prototip realizat în Romania, proiectat pentru a mări productivitatea culturilor agricole de pe solul autohton şi pentru a reduce consumul de apă [1, 4].

Pompa PD 1-2 (Fig.1) este montată în paralel cu circuitul principal de irigare AMF din care îşi trage agentul de lucru, apa, prin conducta de alimentare AM, pentru a acţiona sistemul mecano-hidraulic, care este prevăzut cu: un robinet de cupare la reţeaua principală R1, robinet de alimentare R1', cuplă rapidă C1 şi un manometru M1. Apa sub presiune ajunge la distribuitorul hidraulic 1 şi de acolo la pompa 2. Evacuarea apei se realizează prin circuitul EM, circuit în care apa are fie o curgere liberă, sau la presiune scăzută, pentru a fi recuperată şi reintrodusă în circuitul instalaţiei [1].

Manometru M3, are rolul de a măsura presiunea apei din circuitul de alimentare a instalației, Q1 măsoară debitul de apă introdus în IUP şi este montat după filtrul F. In timpul experimentărilor a fost utilizat de asemenea un cronometru pentru a determina intervalul de timp de funcționare a instalației de fertirigat.

În această poziţie, axul şi pistonul realizează o mişcare de translație C, antrenând cele două membrane şi declanşând absorbţia fertilizantului în camera corpului central AP, unde membrana se destinde, creând depresiunea necesară absorbţiei.

Între timp în camera cealaltă unde membrana este comprimată, fertilizatorul absorbit din faza anterioară este injectat în circuitul IP.

După ce pistonul realizează cursa C, levierul acţionează asupra distribuitorului inversând circuitul apei în distribuitor şi implicit circuitul îngrăşământului.

The movement of the dosing pump's rod is cyclic and it inject a constant quantity of fertilizer in the system assuring a constant fertilizer concentration; however, in order to modify this concentration one has to change the operating pump frequency and also the AM valve positioned on water supply circuit or valve from the pump's injection circuit IP [3].

Mişcarea tijei pompei dozatoare este ciclică, injectând un debit constant de fertilizant în sistem, la o concentraţie constantă; însă, pentru a regla concentrația trebuie să se modifice frecvenţa de lucru a pompei şi a debitului prin robinetul de pe circuitul de alimentare sau prin valva de pe circuitul de injecție a pompei IP [3].

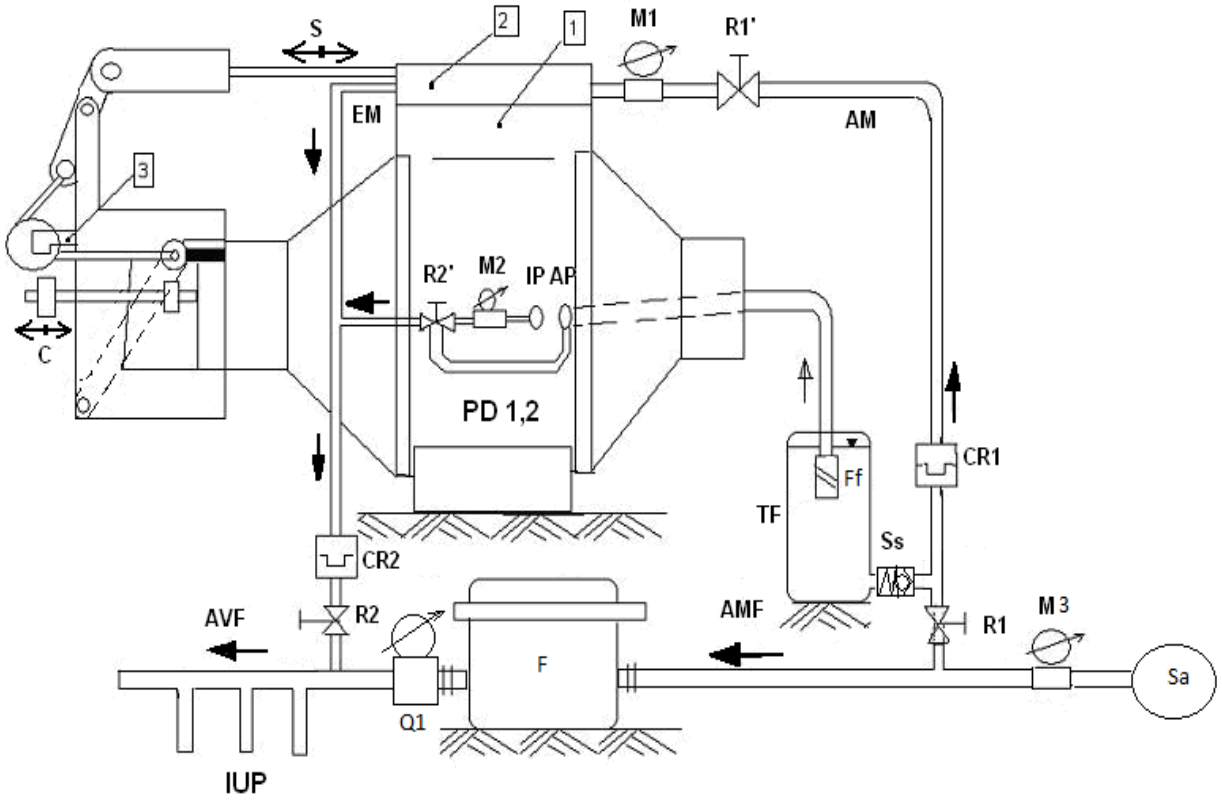

Fig. 1 – Functional scheme of IUP drip irrigation installation and the PD 1-2 dosing pump
1-hydraulic pomp; 2-directional control valve; 3-directional control valve command lever; R1, R1', R2, R2'- opening valve; CR1, CR2 –rapid coupling systems; Ss – directional valve; TF- fertilizer tank;M1, M2, M3 –manometer; Ff –fertilize filter; Sa – water supplay source; Q1 – water flow meter; F- water filter.

Technical characteristics of P1-2 pump are: the working pressure: 1.4 - 6 bar; the water volume consumed by the pump is between 1.4 - 2 times the injected fertilizer volume.

The measurement devices used are:

- Pressure gauge with glycerin Φ 60, anti-vibration, measurement field 0 - 600 kPa, with 1.6 precision class;
- Water flowmeter for supply line Φ 50 with 3% accuracy class.

The water flow consumed by the pump was estimated volumetric and reported to the working period. By the same method was estimated injected fertilizer quantity.

MATHEMATICAL MODEL

The PD 1-2 dosing pump transforms the irrigation water energy in mechanical power in order to inject the liquid fertiliser into the irrigation system that is directly distributed to the crops. This pump has the advantage, that operates with low and medium pressures (170 ÷ 400 kPa) and various flow rates. The optimum operating regime can be achieved by choosing a dosing pump's stroke that is correlated to the service pressure at which the irrigation system operates, that also leads to reduced water consumption.

It is already common knowledge that the ratio between the volume of fertilizer injected by the pump and the volume of water consumed by the motor establishes the pump

Caracteristicile tehnice ale pompei P1-2 sunt: presiunea de lucru a pompei: 1,4…6 bar, volumul de apă consumat de pompă variază între 1,4…2 ori volumul de îngrăşământ injectat.

Aparatele de măsură utilizate sunt:

- Manometru cu glicerina Φ 60, antivibrator, câmp de măsură 0…600 kPa, clasa de precizie 1,6;
- Apometru pentru circuitul de alimentare Φ 50, clasa de precizie 3%.

Debitul de apă consumat de pompă s-a determinat volumetric şi raportat la intervalul de lucru, 15 min. Prin aceeaşi metodă se determină şi cantitatea de îngrăşământ injectat.

MODEL MATEMATIC

PD 1-2 transformă energia apei de irigat în putere mecanică, pentru a injecta soluţia de fertilizare în sistemul de irigat, care apoi este distribuit direct asupra culturilor. Această pompă prezintă avantajul că funcționează la presiuni joase şi medii (170…400 kPa) şi debite variabile. Regimul de funcţionare optim este realizat numai atunci când cursa pompei de dozare este corelată cu presiunea de alimentare a instalației de irigare, fapt care va conduce la reducerea consumului de apă.

Este cunoscut că, raportul dintre cantitatea de fertilizator injectată de pompă şi cantitatea de apă consumată, influenţează eficienţa pompei. De aceea,

efficiency. It is therefore very important to know the pump stroke and its frequency in order to operate efficiently and to achieve an accurate injection of the fertilizing substance. For this purpose has been created a mathematical model that will allow to optimize the PD 1-2 performances, Fig. 2.

este foarte important să cunoaştem caracteristicile pompei (cursa si frecvenţa de lucru) pentru a stabili un regim de lucru eficient şi de a realiza o injecţie precisă de substanţe fertilizante. În acest scop, a fost creat un model matematic care să ne permită să optimizăm performanţele pompei de dozare PD 1-2, Fig.2.

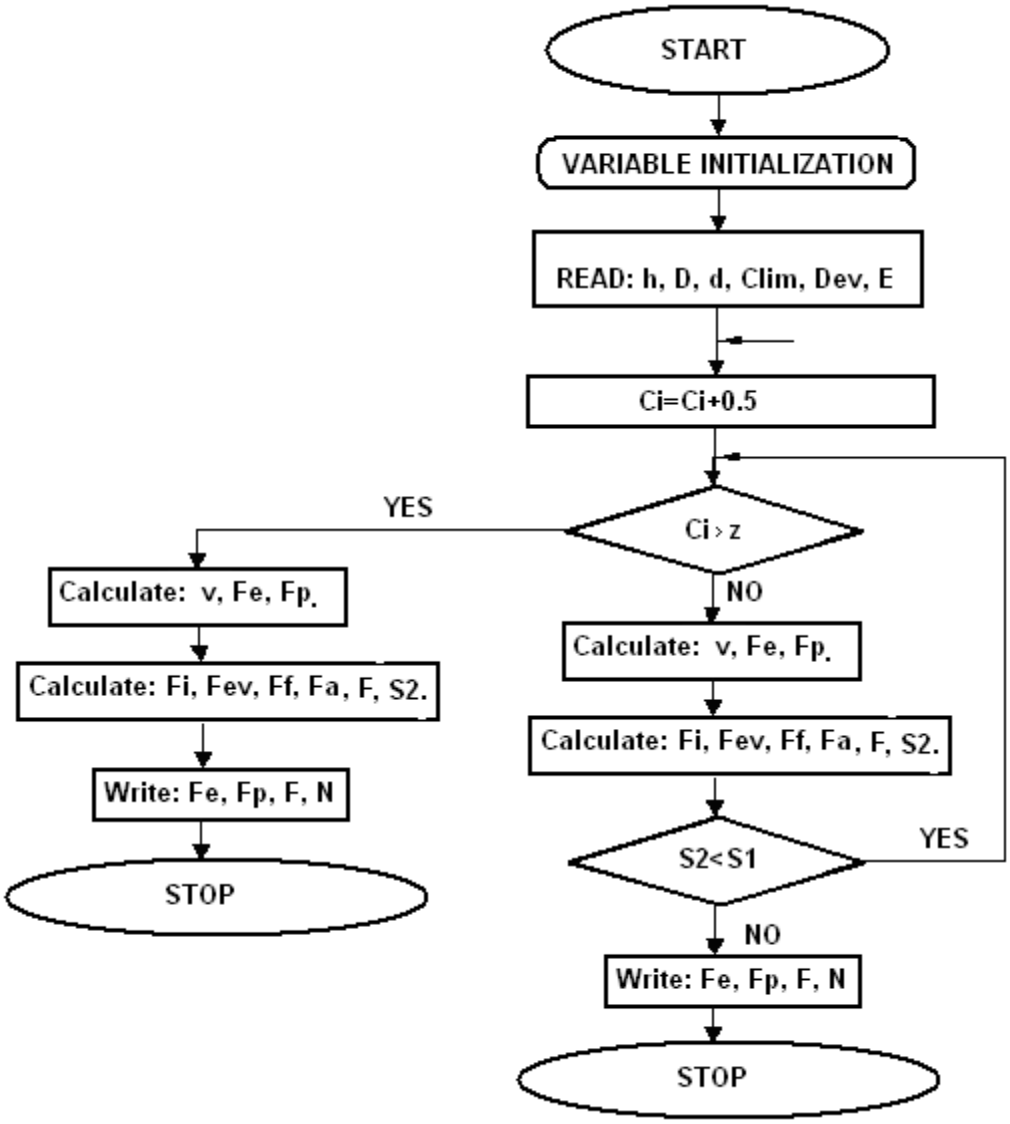

Fig. 2 - Mathematical algorithm applied to determine the hydraulic pump technical parameters

As the mathematical model of the dosing pump to be right, it is necessary to contain the following input data: the dimensional membrane characteristics, the pump operating model and the working conditions.

The membrane utilized has the same dimensional parameters with the one used inside the manual pump for spraying vegetables, fig.3, which has the next characteristics: h – diaphragm thickness; D - external diameter; d - internal diameter; S_1 - admissible effort per length unit; E - elasticity module; g - specific water mass; K - rod friction coefficient; H_{ev} - medium membrane pressure when the water is evacuated; F_a - maximum spring force of the directional control valve (DCV); H_1 - medium pressure in the active chamber; C - active rod stroke; D_{ev} - effective working surface, (D_{ev}=(D+d)/2); C_{lim} - minimal displacement (C_{lim} = 1.00 [cm]), g - gravitational acceleration and z – is the safety coefficient that depends on the membrane type [2].

Ca modelul matematic al pompei de dozare să fie corect, acesta trebuie să conţină următoarele date de intrare: caracteristicile dimensionale ale membranei, modelul funcţional al pompei şi condiţiile de lucru.

Membrana utilizată are aceleaşi caracteristici dimensionale ca cele care sunt utilizate la pompele manuale de spreiat legumele, fig.3, care este caracterizată de următorii parametrii: h – grosimea membranei; D – diametrul exterior; d – diametrul intern; S_1 – efortul admisibil pe unitatea de lungime; E – modulul de elasticitate; g – masa specifică de apă; K – coeficientul de frecare a tijei; H_{ev} – presiunea medie a membranei la evacuarea apei; F_a – forţa maximă a arcului din distribuitor (DCV); H_1 – presiunea medie din camera activă; C- cursa activă a axului; D_{ev} – suprafaţa efectivă de lucru, (D_{ev} = (D+d)/2); C_{lim} – deplasarea minimă; g - acceleraţia gravitaţională şi z – coeficientul de siguranţă, care depinde de tipul membranei [2].

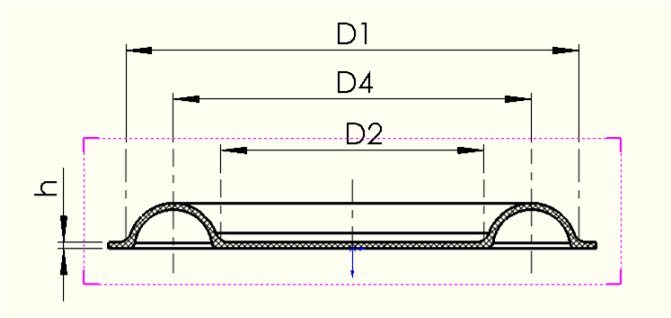

Fig. 3 – Characteristics of the hydraulic dosing pomp diaphragm, PD 1-2

As it was mentioned above, the mathematical model of the dosing pomp depends also by the pump working parameters, like: Q– installation flow rate, l/s; q_p- pump flow rate, l/min; f_v- rod frequency, strokes/min; F_e- elastic force exerted, N; F- active working force, N; P_R– mechanical power, W; P_H- hydraulic power, W; N– efficiency, % and S_2- maximum admissible membrane effort, daN/cm^2.

Once they were established the input data, it can be created a mathematical algorithm to optimize its performances.

This mathematical algorithm consists in next steps:

1) To determine the pump's operating pressure H and working frequencies f_v by the flow rate q_p, from experimental characteristics. In this way can be obtain eq. (1) and (2).

Aşa cum s-a menţionat mai sus, modelul matematic al pompei de dozare depinde şi de parametrii funcţionali, cum ar fi: Q– debitul instalaţiei, l/s; q_p– debitul pompei, l/min; f_v– frecvenţa de lucru a axului, cursa/min; F_e– forţa elastică exercitată, N; F– forţa activă dezvoltată, N; P_R– puterea mecanică, W; P_H- puterea hidraulică consumată, W; N– eficienţă, % şi S_2– efortul maxim admisibil al membranei, daN/cm^2.

O dată ce au fost stabilite datele de intrare, poate fi creat un algoritm matematic pentru a-i optimiza performanţele.

Acest algoritm este compus din 7 etape:

1) Determinarea presiunii de lucru H şi a frecvenţei f_v a pompei, în funcţie de debitul q_p, din caracteristicile experimentale. Astfel se obţin ecuaţiile (1) şi (2).

$$H_1 = f(q_p) \tag{1}$$

$$f_v = f(q_p) \tag{2}$$

2) The active and passive forces of elastic membrane are calculated by the eq. (3) and (4).

2) Forţele active şi pasive ale membranei elastice se pot determina cu ajutorul ecuaţilor (3) şi (4).

$$F_{11} = \frac{\pi \cdot E \cdot H}{\ln \frac{D_1}{D_2}} \frac{12 - C}{\sqrt{1 + \left(\frac{2 \cdot (12 - C)}{D_1 - D_2}\right)^2}} \cdot \ln \frac{\sqrt{1 + \left(\frac{2 \cdot (12 - C)}{D_1 - D_2}\right)^2}}{\sqrt{1 + \left(\frac{2 \cdot C_{\lim}}{D_1 - D_2}\right)^2}} \tag{3}$$

$$F_{12} = \frac{\pi \cdot E \cdot H}{\ln \frac{D_1}{D_2}} \frac{C}{\sqrt{1 + \left(\frac{2C}{D_1 - D_2}\right)^2}} \cdot \ln \frac{\sqrt{1 + \left(\frac{2C}{D_1 - D_2}\right)^2}}{\sqrt{1 + \left(\frac{2C_{\lim} \cdot}{D_1 - D_2}\right)^2}} \tag{4}$$

3) The total elastic force is established by eq.(5).

3) Calcularea forţei elastice totale cu ecuaţia (5).

$$F_e = F_{12} - F_{11} \tag{5}$$

4) The pressure force developed by the active membrane, eq. (6):

4) Forţa de presiune dezvoltată de membrana activă cu ecuaţia (6):

$$F_p = \frac{\pi \cdot H_1 \cdot (D+d)^2}{16} \quad (6)$$

5) Fluid evacuation force developed by the second membrane has the expression from eq. (7).

5) Forţa de evacuare a fluidului dezvoltată de cea de-a doua membrană, are expresia din ecuaţia (7).

$$F_{ev} = \frac{\pi \cdot \left(D^2 + 2 \cdot d \cdot D + d^2\right) \cdot H_{ev}}{16} \quad (7)$$

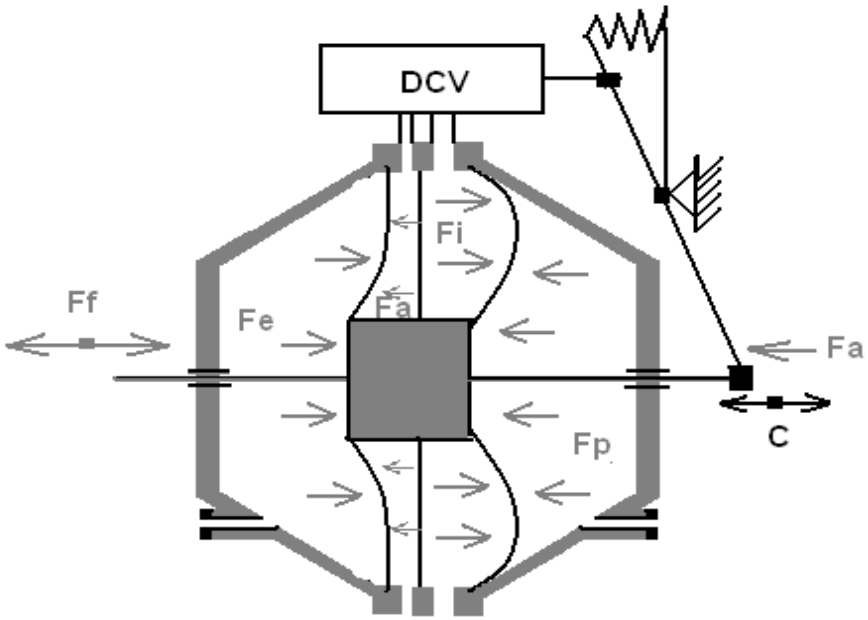

Fig. 4 - Force diagram developed in the hydraulic dosing pomp, PD 1-2

6) From the force diagram, fig.4, it was established the effective working force F, eq. (7), where F_f is bearings friction force and F_i is the injection force, that can be determined by Eq.(8).

6) Din diagrama de forţe, fig.4, a fost stabilită expresia forţei de lucru efective F, ec.(7), unde F_f este forţa de frecare din rulmenţi şi F_i este forţa de injecţie, a cărei valoare poate fi calculată cu ecuaţia (8).

$$F = F_p - F_i - F_{ev} - F_e - F_a - F_f \,,\; F \geq 0 \quad (7)$$

$$F_i = \frac{\pi \cdot \left(D^2 + 2 \cdot d \cdot D + d^2\right) \cdot H_i}{16} \quad (8)$$

7) And finally, is established the admissible effort S2 using Eq.(9).

7) În final, este determinat efortul unitar admisibil, S_2, cu ajutorul ecuaţiei (9).

$$S_2 = \frac{E \cdot (D-d) \cdot H_i}{d \cdot \ln \frac{D}{d}} \cdot \ln \frac{\sqrt{1+\left(\frac{2 \cdot x}{D-d}\right)^2}}{\sqrt{1+\left(\frac{2 \cdot x_1}{D-d}\right)^2}} \quad (9)$$

Knowing the pomp stroke C which depends on the membrane features and the experimental dependency between the H_1 and q_p, and also between f_v and q_p, it can be obtained the values from the parameters: F_i, F_{ev}, P_H, N and S_2.

This algorithm stops when the membrane maxim effort is bigger then the admissible effort (S_2<S_1) and the safety coefficient is exceeded.

If the first condition is satisfied, it can be determine the mechanical and hydraulic power developed by the dosing pump and in this way can be estimate the fertigation system's efficiency.

Cunoscând cursa pompei C, care depinde caracteristicile membranei şi de caracteristicile experimentale dintre H_1 si q_p, precum şi de f_v si q_p, pot fi obţinuţi parametrii: F_i, F_{ev}, P_H, N şi S_2.

Acest algoritm se opreşte atunci când efortul maxim al membranei este mai mare decât efortul admisibil (S_2<S_1) şi când coeficientul de siguranţă este depăşit.

Dacă prima condiţie este satisfăcută, atunci se pot determina puterile mecanice şi hidraulice dezvoltate de pompa de dozare şi de asemenea şi eficienţa sistemului de fertirigatie.

RESULTS

From the experimental research activity, it was determined the pump's hydraulic power, P_{Hmax}=50 W. Thus, the efficiency of the ferigation hydraulic system was estimated to 0.4… 0.5 %. In spite of pumps low efficiency that is influenced by the friction forces from mechanical transmission (bearings, levers etc.) and the resistance force of the elastic elements (springs and membrane) the obtained value is good.

The membrane type was EP DM - STAS 7277-73, from ethylene propylene rubber - STAS 10635-76 without textile insertion and good resistance to: water, flammable hydraulic fluids, acids and bases. Temperature range is from -40 until +130 ^{0}C, [2].

The operational parameters of fertigation installation are:

- average working pressure of hydraulic pomp, H_1= 200÷400 [kPa];
- required pump water flow rate, qp= 1÷3.6 [l/min];
- working frequency, f_v = 5÷40 [strokes/min];
- loss at maximum load, D_H = 2÷4 [kPa] and depends on the pump's flow rate;
- hydraulic pomp power, P_H= 50 [W].

REZULTATE

Din activitatea de cercetare experimentală, a fost determinată puterea maximă a pompei hidraulice, P_{Hmax}=50 W. De aceea, eficienţa sistemului hidraulic de fertirigare este estimată la 0,4… 0,5 %. Deşi pompa are o eficienţă scăzută, deoarece este influenţată de forţele de frecare din transmisiile mecanice (rulmenţi, pârghii etc.) precum şi de forţele de rezistenţă din elementele elastice (arcuri şi membrane), valoarea obţinută este bună.

Membrana utilizată este de tip EP DM - STAS 1063-76, din cauciuc etilen propilen – STAS 10635-76, fără inserţie textilă precum şi o bună rezistenţă la: apă, fluide hidraulice inflamabile, acizi şi baze. Domeniu de lucru, din punct de vedere termic, este de la -40 la +130 ^{0}C, [2].

Parametrii de lucru ai instalației de fertirigare sunt:

- presiunea medie de lucru a pompei hidraulice, H_1= 200…400 [kPa];
- debitul de apă necesar pompei, q_p=1…3,6 [l/min];
- frecvenţa de lucru, f_v = 5…40 [curse/min];
- pierderile înregistrate la sarcină maximă, D_H=2…4 [kPa] şi variază în funcţie de debitul pompei;
- puterea hidraulică a pompei, P_H= 50 [W].

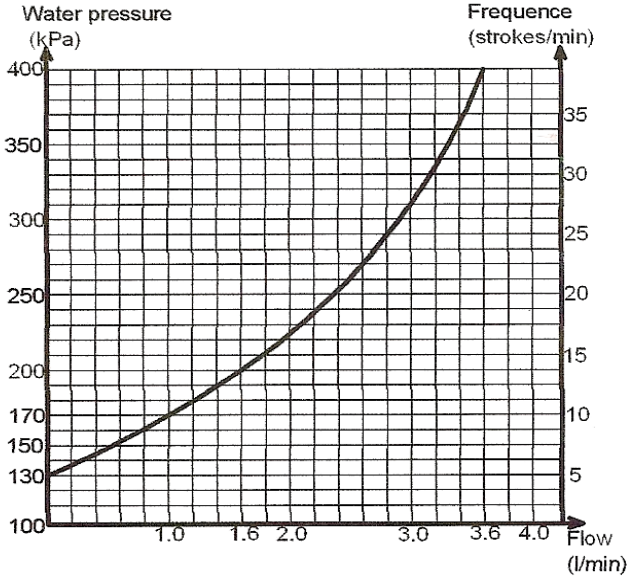

Fig. 5 - Variation of the fertiliser's flow depending on the supplay pumps pressure and working frequency

CONCLUSIONS

The fertigation system can work also with water of lower quality because of the directional valve's construction and the water discharege from the motor is introduced in the irigation system and distribute to crop field. Taking into account that the optimum pressure in the dripping irrigation system is 50 to 250 [kPa] and in sprinkler irrigation from 300 to 500 [kPa], this dosing pump can work in both situations, but the operating mode is changed.

For micro-spray irrigation systems, which operate at low pressure, requires the implementation of a filter which prevent nozzle clogging, in this way the water from the pump's actuation system is distributed and sprayed on the crops, fact that will eliminate the sprinkler irrigation systems and will optimize the nutrient absobtion rate.

A very important advantage of this dosing pump is that is maintains a constant concentration of fertilizer in the plant throughout its working field.

During the experimental research was noticed that, if the power fluid exceeds the pressure of 400 [kPa], the supply fertiliser rate is low and it is recommended to replace the supply fertilizer valve.

CONCLUZII

Sistemul de feritirigare poate utiliza şi ape reziduale, construcţia acestuia permiţând o funcţionare optimă. Dacă se ia în considerare faptul că presiunea optimă a sistemului de irigare prin picurare este 50…250 [kPa], respectiv 300…500 [kPa] pentru sistemul cu aspersoare, această pompă de dozare poate fi utilizată în ambele situaţii, regimul de funcţionare schimbându-se.

În ceea ce priveşte sistemele de irigare prin micro-pulverizare, care funcţionează la presiuni scăzute, este necesară implementarea unui filtru care previne colmatarea duzelor, astfel încât apa din sistemul de acţionare a pompei să fie distribuită şi pulverizată pe culturi, eliminând astfel sistemul de irigaţii prin aspersiune şi va optimiza rata de absorbţie a nutrienţilor.

Un avantaj foarte important al acestei pompe este acela că menţine o concentraţie constantă a nutrienţilor pe tot intervalul de funcţionare.

În timpul cercetărilor experimentale s-a observat că, dacă presiunea de lucru depăşeşte 400 [kPa], alimentarea cu substanţe nutritive este scăzută şi se recomandă a se înlocui supapa de alimentare.

Production growth when was applied separately watering and fertilization is between 9-17% to tomato crops, and for fertirigation records higher values, about 40-50%.

Further research will be made, so the dosing pump to be implemented into automated control system, which will control the fertilizer concentration in irrigation water from a main control panel, in accordance with: crop type, stage of development and climatic conditions.

REFERENCES

[1]. Biolan I., et al., (1991) – *Dosing pump*, Romanian Patent no. 102887;
[2]. Demian T., Banu V., (1984) – *Linear and rotative pneumatic micromotors*, Ed.Tehnică Publishing, Bucharest;
[3]. Serbu I., Biolan I., Sovaiala Gh., Mardare F., (2010) - *Crops fertigation techniques and technologies*, AGIR Publishing house, Bucharest, ISBN 978-973-720-344-1;
[4]. Sovaiala Gh., Biolan I., Visan A., Nicolae N., (2007) – *Fertirigation installation with double pump,* Hidraulica Publishing Journal, no.1-2 (20), pg.47-51, ISSN 2343 – 7707.

Sporul de producţie atunci când s-a aplicat separat udarea şi fertilizarea este între 9–17 % la culturile de tomate, iar atunci când este aplicat fertirigația acesta înregistrează valori superioare, de circa 40–50%.

Se vor face cercetări viitoare pentru ca pompa de dozare să aibă implementat un sistemul de control automat, care va monitoriza concentraţia de îngrăşământ în apa de irigare şi va permite comandarea acesteia printr-un panou de control, în conformitate cu: tipul de cultură, stadiul de dezvoltare şi de condiţiile climatice.

BIBLIOGRAFIE

[1]. Biolan I., ş.a., (1991) - *Pompa dozatoare*, Brevet nr. 102887;
[2]. Demian T., Banu V., (1984) - *Micromotoare pneumatic lineare şi rotative*, Ed. Tehnică, Bucureşti;
[3]. Serbu I., Biolan I., Sovaiala Gh., Mardare F., (2010) - *Tehnici si tehnologii de feririgare a culturilor agricole*, editura AGIR, Bucureşti 2010, ISBN 978-973-720-344-1;
[4]. Sovaiala Gh., Biolan I., Visan A., Nicolae N., (2007) - *Instalatie de fertirigat cu pompa dubla*, Revista Hidraulica, nr.1-2 (20), pag. 47-51, ISSN 2343 – 7707.

QUADRATIC REGRESSION - BASED ORTHOGONAL DESIGN AND NUMERICAL SIMULATION OF A NEW-TYPE AGRICULTURAL WELL PUMP
/
一种新型农用井泵的二次回归正交设计与数值模拟

Ph.D. Stud. Wang Hongliang [1)], Prof. Ph.D. Shi Weidong [1)], Ph.D. Stud. Wang Chuan [2)]
[1)] Research Center of Fluid Machinery Engineering and Technology, Zhenjiang / China;
[2)] Nangyang Technological University, 50 Nanyang Avenue, 639798 Singapore / Singapore
Tel: +8615961196329; E-mail: wnghongliang@163.com

Abstract:*Currently,the Greenhouse Effect has caused great influence on the development of industry and agriculture. Considering the research development request of new-type agricultural deep well pump, the test research was taken to increase the efficiency of well pump using hydraulic design of impeller, the modern numerical CFD technology and the orthogonal test method based on quadratic regression. The experiment was carried out with two geometric factors including outlet angle and outlet width. Then ten impellers were designed as per the orthogonal testing schemes based on quadratic regression. The full flow field of the two-stage agricultural well pump including impellers and guide vanes under the design condition was simulated by CFD, finally obtaining the rated efficiency of each scheme. The influence mechanism of outlet angle and outlet width on efficiency was investigated through the orthogonal testing method. According to the calculation results, constrained quadratic regression equation of the efficiency was put forward. The result showed that it would be instructive to increase the hydraulic efficiency of the new-type deep well centrifugal pump for agriculture engineering by using the impeller maximum - diameter approach.*

Keywords: *Agricultural well pump; Hydraulic design; Quadratic regression; Orthogonal experiment; CFD*

INTRODUCTION

Due to the strict working conditions, the diameter of the submersible pump for agricultural well is limited by the well diameter when it works in the motor-pumped well, and the single-stage head of the pump can't be efficiently increased due to the limited space using the traditional design methods, especially regarding the performance of centrifugal pump[6]. Therefore, the maximum diameter design method of impeller was proposed for the first time [4, 8], this method was successfully applied to the 100SJ8 centrifugal pump for deep well. The theoretical analysis, numerical simulation as well as the experimental investigation showed that the single-stage head of the centrifugal pump for deep well had been improved dramatically and the efficiency was also higher than before. This method is highly superior to the traditional design method in the hydraulic design of the agricultural well pump.

According to the requirements of orthogonal test based on quadratic regression, 10 impellers of the 150QJ20 new-type agricultural well submersible pump were optimized using the maximum diameter method. After conducting two-stage full flow field CFD simulation using 10 groups of impeller with twisted return guide vane of the new-type agricultural deep well pump, and comparing the test results with the simulation results, the influence of two main geometric parameters including outlet width and outlet angle on the efficiency of the pump was found. The efficiency constrained quadratic regression equation of this type well pump was also obtained [9].

摘要：*目前，温室效应已经对工业、农业造成了很深的影响。鉴于新型井泵的研究发展需要，通过运用现代数值CFD技术和二次回归正交试验方法及叶轮水力设计来增加新型农用井泵的效率。试验选取叶轮出口安放角和出口宽度两个几何因素，按二次回归正交试验方案，设计了10副叶轮。通过计算流体动力学技术对包含叶轮、导叶在内的两级新型农用井泵的全流场进行了设计工况下的三维流场数值模拟，得到了10组设计方案额定点的效率值。通过二次回归正交试验法研究了叶轮出口安放角、出口宽度对效率的影响规律，根据计算结果对新型农用井泵效率提出了二次回归约束方程。结果表明，采用叶轮极大直径设计法对提高新型深井离心泵的水力效率具有一定的参考价值。*

关键词：*农用井泵；水力设计；二次回归；正交试验；计算流体动力学*

引言

泵一般在机井内工作，因外径受井径的限制，运用传统的设计方法，单级扬程不能有效的提高[6]。文献[4,8]第一次提出了一种深井离心泵叶轮极大直径设计法。采用叶轮极大直径设计法，对某典型的 100QJ8 型深井离心泵进行水力设计, 数值模拟和试验研究结果表明，该设计方法对提高深井离心泵单级扬程取得了明显的效果，同时其效率较原有设计又不降低。这种方法相比较传统设计方法尤其适用于农用井泵。

文中采用叶轮极大直径设计法，对某典型的 150QJ20 型农用井泵进行水力设计，并进行二次回归正交试验，设计出 10 副叶轮。通过 CFD 对 10 组叶轮配合扭曲反导叶的方案分别对两级全流场进行数值模拟，分析模拟结果，以研究叶轮的两个主要几何参数即出口宽度、出口安放角对深井离心泵效率的影响规律，从而得到该类型农用井泵效率的回归约束方程 [9]。

MATERIALS AND METHODS

Hydraulic Design

Q_d - Flow rate (m^3/s);

H - Head (m);

n - Rotation speed (r/min) ;

Q - Flow (m^3/s);

n_s - Specific speed= $\frac{3.65n\sqrt{Q}}{H^{3/4}} = \frac{3.65.r/\min\sqrt{m^3/s}}{m^{3/4}}$.

P_i - Total pressure at inlet (Pa);

P_0 - Total pressure at outlet (Pa)

M - Moment of force ($N\cdot m$);

η - Efficiency (%);

β_2 - Vane outlet angle (°);

b_2 - Outlet width(mm);

x_j - Natural variables(Dimensionless);

z_j - Canonical variable (Dimensionless);

r - Asterisks arm (Dimensionless);

m – Factor.

The design parameters

The basic design parameters of the 150QJ20 agricultural well submersible pump is that, Q_d=20 m^3/h, single-stage head H=11m, speed n=2850r/min, n_s=128. 10 impellers were optimized according to orthogonal experiment.

The maximum diameter design method of impeller

According to the relevant national standard, the allowable outer diameter and inner diameter of the 150QJ-type agricultural well pump are 143mm and 121mm respectively. Supposing the diameter of the impeller front shroud to be 119mm, the impeller diameter could achieve maximum, which was shown in Fig.1. Once the diameter of impeller's front cover was determined, then other parameters of the impeller can be determined. Seeing Tab.1 for the specific information, other parameters of this design could be found in [5].

(1) The diameter of the shaft and wheel hub

Matching power with *P*=11kW, minimum shaft diameter was calculated using the following formula:

材料与方法

水力设计

Q_d – 额定流量（m^3/s）；

n – 转速（r/min）；

Q – 流量（m^3/s）；

n_s – 比转速= $\frac{3.65n\sqrt{Q}}{H^{3/4}} = \frac{3.65.r/\min\sqrt{m^3/s}}{m^{3/4}}$；

P_i – 进口总压（Pa）；

P_0 – 出口总压（Pa）；

M – 力矩（$N\cdot m$）；

η – 效率（%）；

β_2 – 出口安放角（°）；

b_2 – 出口宽度（mm）；

x_j – 自然变量（Dimensionless）；

z_j – 规范变量（Dimensionless）；

r – 星号臂长度（Dimensionless）；

m – 因素数；

H – 扬程（m）.

设计参数

150QJ20 型深井离心泵的基本设计参数为额定流量 20 m^3/h，单级扬程 11 m，转速 2850 r/min。经计算，比转速 n_s=128，10 组叶轮通过正交试验要求来设计。

极大扬程设计法

依据国家相关标准，150QJ 型农用井泵的外径及内径要求分别为 143mm 和 121mm。叶轮的前盖板设计为 119mm，叶轮的直径达到最大，如图 1 所示。一旦叶轮的前盖板尺寸确定，叶轮的其他尺寸也就确定了。表格 1 中表示了各个设计参数值 [5]。

（1）确定轴径和轮毂直径

配套功率 $P=11$kW 计算，最小轴径为：

$$d_{\min} = \sqrt[3]{\frac{M_n}{0.2[\tau]}} = 16 \quad \text{mm} \tag{1}$$

Φ16mm stainless steel shaft was selected, the wheel hub diameter was selected as follow:

$D_h = 22$ mm

(2) Impeller inlet diameter

$D_{j,k} = 3.75$

选用Φ16mm 的不锈钢轴，则轮毂直径 Dh=22mm

（2）叶轮进口直径

$D_{j,k} = 3.75$

$$D_0 = 1000 \times k \times \sqrt[3]{\frac{Q}{3600 \times n}} = 46.84 \text{ mm} \tag{2}$$

$$D_j = \sqrt{D_0^2 + D_h^2} = 47.82 \text{ mm} \tag{3}$$

$D_j = 48$ mm was determined

(3) Impeller outlet width

According to the structure and experience, take b_2=(9～13) mm.

(4) Vane outlet angle

According to the structure and engineering experience, take β_2=(10°～25°).

Blade number z, wrap angle and hydraulic fillet radius of front and back cover plate was selected based on experience and graphing.

取 $D_j = 48$ mm

（3）叶轮出口宽度

根据结构和经验，取 b_2=（9～13 ）mm

（4）叶轮出口安放角 β_2

根据经验初选，由基本方程和全扬程公式验算，取 β_2=（10°～25°）.

叶片数 Z、包角及盖板水力圆角半径根据经验及作图选择。

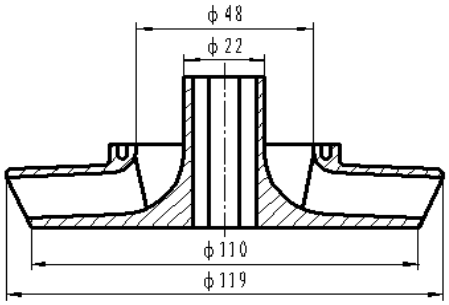

Fig. 1 - Cross-section of impeller

Table 1

Main structural parameters of the impeller

Structural parameters of impeller	Parameter selection
Blade number Z	6
Inlet vane angle β_1（°）	39
Wrap angle ϕ（°）	125
Impeller front covering plate D_{2max}（mm）	119
Impeller front covering plate D_{2min}（mm）	108
Impeller inlet diameter D_j（mm）	48
Wheel hub diameter d_h（mm）	22
Hydraulic fillet radius of front cover plate R_1（mm）	5
Hydraulic fillet radius of back cover plate R_2（mm）	18
Shaft diameter d（mm）	16

In order to reduce the production costs of the well pump, a new type of twisted return guide vane was selected to replace the common guide blades. Compared with the old space guide vane, the axial length of twisted return guide vane is shorter, and it is easier to be manufactured. The conventional return guide vane is pure cylindrical blades, its hydraulic loss is larger than common guide blades. The main innovations are as follows:

(1) The inlet of guide vane within φ100mm and φ121mm was twisted, its blades angle was selected basing on flow directions. This is the main differences between new twisted return guide vane and conventional return guide vane, which is also the main measure to reduce the hydraulic loss.

(2) The outlet diameter of the guide vane is φ48mm as shown in Fig.2.

(3) The middle part of guide vane's convex surface, which 2D cylindrical surface. The concave surface 3D surface and connected with vane inlet and outlet smoothly.

为降低深井离心泵的生产成本，设计了一种新型反导叶导流壳代替常用的空间导叶式导流壳。与传统的空间导叶的比较，它的轴向长度最短，且制造较容易。空间导叶容易其轴向长度的扭曲反导叶是短越来，而且很容易容易制作比旧的空间导叶。传统的反导叶是纯圆柱形叶片，其水力损失大于普通的导向叶片。主要创新点如下：

（1）导叶在 φ100mm 和 φ121mm 的入口处叶片是扭曲的，叶片的安放角根据流动方向选择。这是新的扭曲反导叶与常规反导叶之间的主要差异。也是减少水力损失的主要措施；

（2）导叶出口直径是 φ48mm 如图 2 所示；

（3）导叶的中间部分均为二维圆柱面。进口一段叶片是三维曲面。

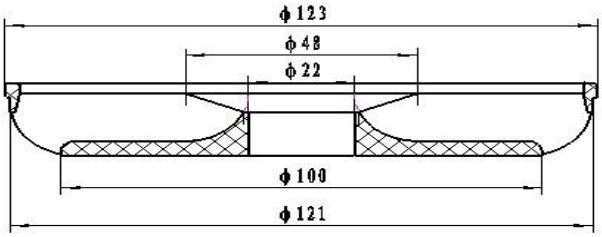

Fig. 2 - Cross-section of guide vane

Orthogonal testing method based on Quadratic regression

Using the point of mathematical statistics and principle of orthogonality, orthogonal testing method based on quadratic regression is a scientific method which is used to examine a number of factors simultaneously when these factors are under changing, For various factors in the changing circumstances; we use a normalized orthogonal table to arrange the test rationally. Orthogonal testing method based on quadratic regression uses combination design, which has the feature of less times of experiment, higher precision, simpler testing results treatment; meanwhile it could be optimized and analyzed [9].

The factors which affect the efficiency and head are Z, β_2, D_2, b_2, u_2 and so on. Based on professional knowledge and special design requirements of the new-type agricultural well, the following geometric parameters were taken into consideration: β_2 (vane outlet angle), b_2 (outlet width).

This study applied the orthogonal testing method based on quadratic regression to analyze the relationship among these factors such as β_2 (10°～25°), b_2 (9mm～13 mm) with the head and efficiency.

As the factor (m=2), if the frequency of zero level testing m_0=2, according to the formula of asterisk arm length r [3] (r =1.078).

According to the factor x_{1r}, for which the upper limit is 25°, the lower limit is 10 degrees, so the zero level (x_{10} =17.50), change interval (Δ_1 =6.96), upper level (x_{12} =24.46), lower level (x_{22} =10.54). The code of exit width b_2 (x_2) can be calculated similarly, shown in Table 2.

Considering the factor number ($m = 2$), using orthogonal table L_4 (23) for transforming, two level test number ($m_c = 2^2 = 4$), test scheme is shown in Tab.3. Other geometric factors were set according to the calculated values. 10 groups of hydraulic model were obtained.

二次回归正交试验

二次回归正交试验设计是一种处理多因素试验的科学方法，它采用数理统计学观点，应用正交性原理，对多个因素同时进行考查，在各个因素都处于变动的情况下，用一套规格化的正交表来合理地安排试验。二次回归正交试验采用组合设计，具有试验次数少，精确度高，试验结果处理简便，并可进行优化分析的特点 [9]。

影响效率与扬程的因素为 Z、β_2、D_2、b_2、u_2 等。在专业知识和设计的特殊需要的基础上，选取影响深井离心泵效率、扬程最重要的因素为叶轮出口安放角 β_2，出口宽度 b_2。

本研究应用二次回归正交试验分析这两个因素 β_2（10°～25°），b_2（9～13 mm）和效率、扬程之间的关系。

由于因素数 m =2，如果取零水平试验次数 m_0=2，根据星号臂长 r 的计算公式[3]，得到 r =1.078。

根据两个因素（x_1）的上限 x_{1r} 为 25°，下限 x_{2r} 为 10°，所以零水平为 x_{10} =17.50，变化间距 Δ_1=6.96，上水平 x_{12} =24.46，下水平 x_{22} =10.54。同理，可以计算出因素出口宽度 b_2（x_2）的编码，见表 2。

由于因素数 $m = 2$，选用正交表 L_4（23）进行变换，二水平试验次数 $m_c = 2^2 = 4$，试验方案见表 3。其他几何因素按之前计算所得值设计，得到 10 组水力模型。

Table 2

Factors and levels

Canonical variable (z_j)	Natural variables (x_j)	
	x_1	x_2
Asterisks arm (r)	25.00	13.00
Upper level (1)	24.46	12.86
Zero level (1)	17.50	11.00
Lower level (-1)	10.54	9.15
Under asterisks arm (-r)	10.00	9.00
Changes in pitch (Δ_j)	6.96	1.86

Table 3

Experiment program

Test number	z_1	z_2	Vane outlet angle β_2 / (°)	Outlet width b_2 / mm
1	1	1	12.86	24.46
2	1	-1	12.86	10.54
3	-1	1	9.15	24.46
4	-1	-1	9.15	10.54
5	1.078	0	13.00	17.50
6	-1.078	0	9.00	17.50
7	0	1.078	11.00	25.00
8	0	-1.078	11.00	10.00
9	0	0	11.00	17.50
10	0	0	11.00	17.50

Numerical simulations

Governing equations

The over-current components of agricultural well pump consist of the inlet, several stages impeller and guide vane. The relative reference system fixed to the rotor with speed 2850r/min was adopted. The whole flow field was assumed to be 3-D incompressible steady viscous turbulent flow field. The calculation model was created based on the real machine; the whole flow domain of two stages consists of 5 components: inlet section, seal ring, impeller, guide vane, and outlet section, as shown in Fig.4. The outlet section extended to 2 times the impeller diameter length, so that the flow could be fully developed at the outlet. After modeled in Pro/E, the assembly model was imported to Gambit for further processing.

数值计算

控制方程组

深井离心泵的过流部件由进水节、 若干级叶轮和导叶体组成。采用固系于旋转叶轮上的相对参考系，转速为 2 850 r/min。设整个流道内部流场为三维不可压稳态粘性湍流场。整个计算模型建立在真实的流场中，整个流场如图 4，其包括 5 个部分：进口、密封环、叶轮、涡轮、出口，出口长度是进口长度的 2 倍以便于流体能够在出口处完全扩散。经过 Pro/E 建模后，整个模型导入 Gambit 中进行后续的运算。

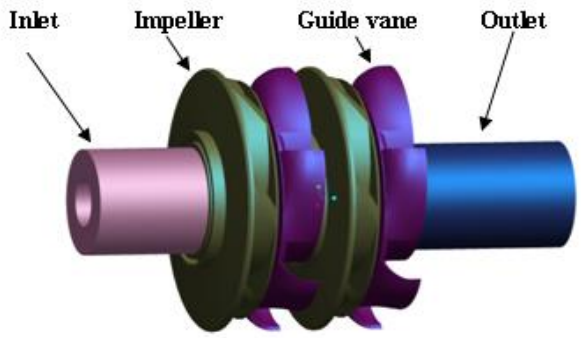

Fig.4 - Sketch of flow domain

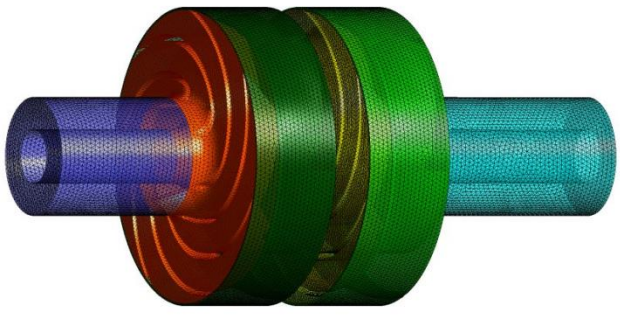

Fig.5 - Mesh mode

The properties of working media

The medium is water at room temperature and pressure with fixed density (ρ=998.2 kg/m^3) and dynamic viscosity (μ = 0.001003 kg / m·s).

Meshing of calculation region and the selection of calculation model

After modeled by Pro/E, the import section, impeller and guide vane were imported to the Gambit for further processing. The two stages full-flow field was meshed with structured and unstructured grids, shown in Fig.5. After comparing the five groups model grids between(1～2.5)million, the results showed that the efficiency

工作介质属性

在常温常压下介质为清水，密度为 998.2 kg/m3，动力粘度为 0.001 003 kg /m·s）。

计算区域网格划分及计算模型选取

在 Pro/E 中分别对进口段、叶轮、导叶筒体建模，导入 Gambit 中作进一步处理。完成两级全流场的计算区域构建后，进行网格划分，采用结构化网格和非结构化网格相结合的方法，如图 5 所示。比较 100 万到 250 万网格数

fluctuates within 0.5% when the grid number surpass 1.75 million. Considering the performance of the computer, grid number of 1.75 million was selected.

The two stages flow channel of agricultural deep well pumps was taken as the computing area. At the same time, the whole calculation area was divided into two parts. The first is the import section of the pump and the rotating part of the impeller chamber. The second is the distorted-reversed guide vane static area. The connection surface between the two sub-regions is the interface. The coupling between the rotator and stator was simulated using Multiple Reference Frame (MRF).

Boundary condition

Supposing that the impeller inlet is irrotational flow [5], inlet surface center as the pressure reference point [1, 2, 3, 7, 10, 11], and the relative pressure is zero. The boundary condition of outlet is set to be outflow [4]. Solid-wall is supposed to be no slip. The turbulent flow of near-wall was handled by standard wall function [7].

Numerical algorithm and solution control parameters

The SIMPLEC algorithm and discrete difference equation of second-order upwind were applied. The factor coefficients of sub-relaxation for algebraic equations are as follows, pressure coefficient of Asian Relaxation is 0.3, momentum sub-relaxation factor 0.7, turbulent kinetic energy sub-relaxation factor 0.8, turbulent kinetic energy dissipation rate 0.8. The convergence precision is set to be 10^{-5}.

RESULTS ANALYSIS

Orthogonal combination design based on binary quadratic regression

Using numerical simulation of 10 sets of programs at rated conditions the efficiency value of deep well centrifugal pump, the table and results of orthogonal combination design based on dual quadratic regression were shown in Tab.4. According to the requirements of orthogonal combination design based on dual quadratic regression, centralization of the quadratic term of z_1^2, z_2^2, z_1', z_2' is shown in Tab .5.

之间的 5 组模型，发现在网格总量达到 175 万后，效率波动稳定在 0.5%以内，考虑计算机性能，选取 175 万网格数。

以深井离心泵的两级泵壳内流道为计算区域，采用全流道方式，同时将整个计算区域分为泵的进口段与叶轮室的旋转部分和包括反导叶区的静止部分，两个子区域之间联接的平面作为分界面。对于旋转部分和静止部分之间的耦合，通过计算比较，采用多参考坐标系模型的定常计算结果进行泵的数值模拟。

边界条件

设叶轮进口为无旋流动[5]，进口面中心处为压力参考点 [1,2,3,7,10,11]，其相对压力为零；出口流动设为充分发展状态，即出流（outflow）形式[4]；固壁面无滑移，即壁面上各向速度均为零，对近壁面的湍流流动按标准壁面函数法处理[7]。

数值算法及求解控制参数

应用 SIMPLEC 算法，采用二阶迎风格式离散差分方程。代数方程迭代计算采取亚松弛，各项系数分别为压力亚松弛系数 0.3，动量亚松弛系数 0.7，湍动能亚松弛系数 0.8，湍动能耗散率 0.8 。设定收敛精度为 10^{-5}。

结果分析

二元二次回归正交组合设计

运用数值模拟得到 10 组方案在额定工况下深井离心泵的效率值，二元二次回归正交组合设计表及试验结果见表 4。根据二元二次回归正交组合设计的要求，将二次项 z_1^2 和 z_2^2 分别进行中心化，得到 Z_1' 和 Z_2'，二次项中心化结果见表 5。

Table 4

Design and test result of binary quadratic regression combination

Test number	Z_1	z_2	z_1z_2	z_1	z_2	z_1	z_2	y
1	1	1	1	1	1	0.368	0.368	64.46
2	1	-1	-1	1	1	0.368	0.368	66.74
3	-1	1	-1	1	1	0.368	0.368	66.54
4	-1	-1	1	1	1	0.368	0.368	67.44
5	1.078	0	0	1.162	0	0.530	-0.632	63.31
6	-1.078	0	0	1.162	0	0.530	-0.632	67.34
7	0	1.078	0	0	1.612	-0.632	0.531	65.29
8	0	-1.078	0	0	1.612	-0.632	0.531	67.25
9	0	0	0	0	0	-0.632	-0.632	66.46
10	0	0	0	0	0	-0.632	-0.632	66.46

Table 5

Binary quadratic regression combination design calculations (Part A)

i	z_1	z_2	z_1z_2	z_1'	z_2'	y	y^2	z_1y	z_2y
1	1	1	1	0.368	0.368	64.46	4 155.092	64.46	64.46
2	1	-1	-1	0.368	0.368	66.74	4 454.228	66.74	-66.74
3	-1	1	-1	0.368	0.368	66.54	4 427.572	-66.54	66.54
4	-1	-1	1	0.368	0.368	67.44	4 548.154	-67.44	-67.44
5	1.078	0	0	0.530	-0.63	63.31	4 008.156	68.25	0
6	-1.078	0	0	0.530	-0.632	67.34	4 534.676	-72.60	0
7	0	1.078	0	-0.632	0.530	65.29	4 262.784	0	70.38
8	0	-1.078	0	-0.632	0.530	67.25	4 522.563	0	-72.50
9	0	0	0	-0.632	-0.632	66.46	4 416.932	0	0
10	0	0	0	-0.632	-0.632	66.46	4 416.932	0	0
∑						661.29	43 747.09	-7.12	-5.29

Binary quadratic regression combination design calculations (Part B)

i	$(z_1z_2)y$	$z_1'y$	$z_2'y$	$(z_1z_2)^2$	$z_1'^2$	$z_2'^2$	z_1^2	z_2^2
1	64.46	23.721	23.721	1	0.135	0.135	1	1
2	-66.74	24.560	24.560	1	0.135	0.135	1	1
3	-66.54	24.486	24.486	1	0.135	0.135	1	1
4	67.44	24.817	24.817	1	0.135	0.135	1	1
5	0	33.554	-40.011	0	0.281	0.399	1.162	0
6	0	35.690	-42.558	0	0.281	0.399	1.162	0
7	0	-41.263	34.603	0	0.399	0.281	0	1.162
8	0	-42.502	35.642	0	0.399	0.281	0	1.162
9	0	-42.003	-42.002	0	0.399	0.399	0	0
10	0	-42.003	-42.002	0	0.399	0.399	0	0
∑	-1.38	-0.939	1.256	4	2.701	2.701	6.324	6.324

Notes: Owing to the limited space, Table 5 was divided into Part A and Part B.

According to Tab.4, each regression coefficient is listed below:

根据表 4 可知，各个回归系数分别为：

$$a = \frac{1}{n}\sum_{i=1}^{n} y_i = 66.129 \tag{4}$$

$$b_1 = \sum_{i=1}^{n} y_i z_{1i} \Big/ \sum_{i=1}^{n} z_{1i}^2 = -1.12653 \tag{5}$$

$$b_2 = \sum_{i=1}^{n} y_i z_{2i} \Big/ \sum_{i=1}^{n} z_{2i}^2 = -0.83693 \tag{6}$$

$$b_{12} = \sum_{i=1}^{n} y_i (z_1 z_2)_i \Big/ \sum_{i=1}^{n} (z_1 z_2)_i^2 = 0.345 \tag{7}$$

$$b_{22} = \sum_{i=1}^{n} y_i (z'_{2i})_i \Big/ \sum_{i=1}^{n} (z'_{2i})^2 = -0.465 \tag{8}$$

Therefore, the regression relationship (regression equation) between the standardized variables and test index is shown as follow:

因此，规范变量与试验指标 y 之间的回归关系式（回归方程）为：

$$y = 66.129 - 1.12653z_1 - 0.83693z_2 - 0.345z_1z_2 - 0.34799z_1' + 0.46505395z_2' \tag{9}$$

Variance analysis of orthogonal test based on quadratic regression

二次回归正交试验的方差分析

From Tab. 4, we know:

由表 4 可知：

$$\sum_{i=1}^{n} y^2_i = 43747.09 \tag{10}$$

So the total variation can be expressed as:

所以有总变差为：

$$SS_T = \sum_{i=1}^{n} y_i^2 - \frac{1}{n}\left(\sum_{i=1}^{n} y_i\right)^2 = 16.6395 \tag{11}$$

The variation of quadratic regression can be expressed respectively as follow:

二次型的回归变差分别为：

$$SS_1 = b_1^2 \sum_{i=1}^{n} z_{1i}^2 = 8.025755 \tag{12}$$

$$SS_2 = b_2^2 \sum_{i=1}^{n} z_{2i}^2 = 4.4297651 \tag{13}$$

$$SS_{12} = b_{12}^2 \sum_{i=1}^{n} (z_1 z_2)^2 = 0.4761 \tag{14}$$

$$SS_{11} = b_{11}^2 \sum_{i=1}^{n} z'^2_{1i} = 0.327101 \tag{15}$$

$$SS_{22} = b_{22}^2 \sum_{i=1}^{n} z'^2_{2i} = 0.584207 \tag{16}$$

Total regression variance could be expressed as follow:

总回归变差为：

$$SS_R = SS_1 + SS_2 + SS_{12} + SS_{11} + S_{22} = 13.84292 \tag{17}$$

Experimental error could be expressed as follow:

实验误差为：

$$SS_e = SS_T - SS_R = 16.63949 - 13.84292 = 2.796569 \tag{18}$$

Variance analysis is shown in Tab.6, the results show that, two partial regression coefficient reached significant level, in which $F_{0.1}(1,4) = 4.54$

方差分析见表 6，结果表明，两个偏回归系数达到了显著水平，其中：$F_{0.1}(1,4) = 4.54$。

Table 6

Variance analysis

Difference stems	Deviation quadratic sum (SS)	Free degree (d_f)	Estimate of variance (MS)	Statistical quantity F	Conspicuousness
z_1	8.025	1	8.026	11.479	**
z_2	4.429	1	4.429	6.336	**
z_1z_2	0.476	1	0.476	0.681	
z_1'	0.327	1	0.327	0.467	
z_2'	0.584	1	0.584	0.835	
Recurrence	13.842	5	2.768	3.959	
Residual	2.796	4	0.699		
Sum	16.639	9	1.848		

Quadratic regression equation of the efficiency

效率的二次回归约束方程

From the centralization formula of quadratic term, we know:

由二次项中心化公式，我们可得：

$$z_1' = z_1^2 - \frac{1}{n}\sum_{i=1}^{n} z_{1i}^2 = z_1^2 - 0.6324 \tag{19}$$

$$z_2' = z_2^2 - \frac{1}{n}\sum_{i=1}^{n} z_{2i}^2 = z_2^2 - 0.6324 \tag{20}$$

These formulas were substituted into the following equation, then we obtain:

代入回归方程，则有：

$$y = 66.129 - 1.12653z_1 - 0.83693z_2 - 0.345z_1z_2 - 0.34799(z_1^2 - 6.324/10) + 0.46505395(z_2 - 6.324/10) \quad (21)$$

According to the coding formula:

又根据编码公式：

$$z_1 = \frac{x_1 - 11}{3.71},\ z_2 = \frac{x_2 - 17.5}{13.91} \quad (22)$$

The quadratic regression-based constrained equation of the efficiency of the new-type deep well centrifugal pump for agricultural engineering could be expressed as follow:

代入上式，整理后可得新型深井离心泵效率的二次回归约束方程（回归公式）为：

$$y = 66.835 + 0.373x_1 - 0.0699x_2 - 0.0068x_1x_2 - 0.025x_1^2 + 0.0024x_2^2 \quad (23)$$

So η can also be expressed as follow:

故，η 也可表示为：

$$\eta = 66.835 + 0.373\beta_2 - 0.0699b_2 - 0.0068\beta_2b_2 - 0.025\beta_2^2 + 0.0024b_2^2 \quad (24)$$

CONCLUSIONS

Based on the orthogonal testing method of quadratic regression and numerical calculation, the hydraulic model of the new-type deep well centrifugal pump was conducted using the numerical simulation of two-stage full flow field. The influence mechanism of impeller outlet angle, outlet width on the pump for agriculture was obtained, the conclusions are shown as follows:

(1) The single-stage head of the deep well centrifugal pump which was designed using the maximum-diameter method is improved greatly and the efficiency is also higher than before. And combining the numerical simulation and orthogonal test based on binary regression could optimize the design of the centrifugal pump while complying with the design requirements.

(2) Using the two levels of the whole flow field for numerical simulation on the multistage deep well centrifugal pump for agriculture could optimize the design more accurately.

(3) Through the 10 groups of design schemes obtained from orthogonal testing method based on quadratic regression, we find the influence mechanism of two main geometric parameters of impeller with outlet width and outlet angle on the efficiency of the pump, meanwhile the optimal regression equation of this type well pump was also obtained, which can provide references for the optimization target design of new-type deep well pump for agricultural engineering.

结论

在二次回归正交试验设计、数值计算的基础上，采用数值计算和样机试验验证相结合的方法，对新型深井离心泵的水力模型进行两级全流场数值模拟，得到叶轮出口安放角、出口宽度对深井离心泵性能的影响规律，结论如下：

（1）采用极大直径设计法设计的深井离心泵单级扬程高，效率也不降低，采用数值模拟与二次回归正交试验相结合，能够指导深井离心泵的设计，找到符合设计要求的优选方案；

（2）针对多级深井离心泵，采用两级全流场作数值模拟能够较为准确的指导设计；

（3）通过二次回归正交试验设计出10组设计方案，得出了叶轮两个主要设计参数出口安放角和出口宽度对深井离心泵效率的影响规律，并优选出回归方程，从而为实现对新型深井离心泵的优化设计目标提供了设计依据。

AKNOWLEGEMENT

This research was supported by the National Scientific and Technological Personnel Service Enterprise Actions of China (Grant No.2009GJC30002), the Natural Science Foundation Project of Jiangsu Province (No.BK2011505).

致谢

本文受到国家科技人员服务企业项目（2009GJC30002）和江苏省自然基金项目（BK2011505）资金资助。

REFERENCES

[1]. Chen K.W., Lee T.S., Winoto S.H. et al., (2007) – *Numerical flow simulation in a centrifugal pump at design and off-design conditions*. International Journal of Rotating Machinery, vol. 2007, pg.1-8;

[2]. Dupont P., Cugal M., (2006) – *CFD in pump design expertise improves products*. Sulzer Technical Review, vol.88, no.2, pg.22-25;

参考文献

[1]. Chen K W, Lee T S, Winoto S H, et al., (2007) –*工况与非工况条件下离心泵数值模拟计算*, 旋转机械学报,第2007 卷, 1-8;

[2]. Dupont P,Cugal M., (2006) –*泵设计实践中运用CFD提高产品品质, 苏尔寿技术回顾*, 第 88 卷, 第 2 期, 22-25;

[3]. Kitano Majidi, (2005) – *Numerical study of unsteady flow in a centrifugal pump*. Journal of Turbo machniery,vol.127, no.2, pg.363-371;
[4]. Lu Weigang, Zhang Qihua, Shi Weidong, (2006) – *Impeller diameter maximum approach on deep well pump*. Drainage and Irrigation Machinery, vol.24, no5, pg.1-7;
[5]. Li Yuyan, Hu Chuanrong, (2008) – *Experiment Design and Data Processing*. Beijing: Chemical Industry Press;
[6] Mihalic T., Medic S., Kondic Z., (2013) – *Improving centrifugal pump by adding vortex rotor,* Tehnicki Vjesnik, vol.20, no.2, pg.305-309;
[7]. Rouhollah Torabi, Ahmad Nourbakhsh S., (2011) – *Hydrodynamic design of the volute of centrifugal Pump using CFD,* Proceedings of ASME-JSME-KSME Joint Fluids Engineering Conference 2011/AJK2011-06077, Hamamatsu, Japan;
[8]. Shi Weidong, Lu Weigang, Zhang Qihua, et al., (2008) – *Flow calculation of new-type deep well pump*, Fluid Machinery, vol.36, no.5, pg.21-24;
[9]. Shi Wei-dong, Wang Hong-liang, Yu Xue-jun., (2009) – *Development and prospect of deep well pump in China*. Drainage and Irrigation Machinery, vol.27, no.5, pg.64-68;
[10]. Shi Wei Dong, Lu Wei Gang, Wang Hong Liang et al., (2009) – *Research on the theory and design methods of the new type submersible pump for deep well*. Proceedings of the ASME 2009 Fluids Engineering Division Summer Meeting (FEDSM2009). Vail, Colorado USA, pg.1-7;
[11]. Voorde J.V., Dick E, Vierendeels J., et al., (2002) – *Performance prediction of centrifugal pumps with steady and unsteady CFD-methods.* The 4th International on Advances in Fluid Mechanics, Ghent, Belgium, pg.559-568.

[3]. Kitano Majidi, (2005) – *离心泵非定常流动研究*, 透平机械,第 127 卷,第 2 期, 363-371;
[4]. 陆伟刚, 张启华, 施卫东.(2006)– *深井离心泵叶轮极大直径设计法*, 排灌机械, 第 24 卷, 第 5 期, 1-7;
[5]. 李云雁, 胡传荣. (2008) –*试验设计与数据处理*. 北京: 化学工业出版社;
[6]. Mihalic T., Medic S., Kondic Z. (2013) –*通过增加涡流旋翼改善离心泵性能*, 技术工程, 第 20 卷, 第 2 期, 305-309;
[7]. Rouhollah Torabi，Ahmad Nourbakhsh S .(2009) – *离心泵蜗壳的 CFD 设计*, ASME-JSME-KSME 流体工程联合会议 2011/AJK2011-06077, 滨松, 日本;
[8]. 施卫东, 陆伟刚, 张启华 等. (2008) – *新型深井离心泵叶轮内部流动的研究,流体机械*, 第 36 卷, 第 5 期, 21-24;
[9]. 施卫东, 王洪亮, 余学军. (2009) – *深井泵的研究现状与发展趋势*, 排灌机械, 第 27 卷, 第 5 期, 64-68;
[10]. 施卫东, 陆伟刚, 王洪亮.（2009）– *一种新型深井泵的理论设计方法研究*, 美国机械工程协会流体机械 2009 年夏季会议(FEDSM 2009), ASME 出版社, 1-7;
[11]. Voorde J.V., Dick E., Vierendeels J. 等.(2002) – *用稳态与非稳态 CFD 对离心泵性能的预测研究*, 第四届流体机械前沿国际会议,根特, 比利时, 559-568.

BLADE TYPE CAVITATION PREDICTION ON THE TWICE DEFORMATION OF AGRICULTURAL AUTOMOBILE ENGINE COOLING WATER PUMPS BASED ON CFD
/
基于 CFD 的农用汽车发动机冷却水泵二次变曲率叶型空化特性预测

Lect. Ph.D. Xue Dangqin[1, 2)], Lect. Ph.D. Ma Shibang[3)], Lect. Ph.D. Eng. Shi Huojie [4)] , Prof. Ph.D. Hou Shulin[1)]
[1)] College of Engineering ,China Agricultural University, Beijing / China; [2)] School of Mechanical ＆Automotive Engineering, Nanyang Institute of Technology, Henan / China; [3)] Nangyang Normal University, Henan / China,
[4)]Department of Biological Systems Engineering, Washington State University, Pullman / U.S.A.
Tel: +8613782173858; Email: xdq5599@163.com

Abstract: *Based on the CFD imitation of the three-dimensional flow field of the agricultural automobile engine cooling water pump, the thesis analyzes the energy characteristics and cavitation performance of the farm vehicle using two variable curvature blade type cooling water pump without cavitation, forecasts the cavitation distribution in the impeller and the stream line load distribution under different cavitation conditions and compares with the test results. The results showed that: in the design flow of 25 ℃, the simulated head was13.49m and the error between numerical simulation and the test results was within 2%. The head of the pump engine cooling model of agricultural vehicles of the design operating point under 85℃ is 9.6m, much lower than the head value of the design flow under 25 ℃. This shows that there is serious cavitation in the actual operation of pump, the cavitation performance curve and the numerical change trend converge, numerical value is less than the full cavitation range measured values and as the flow increases, the critical cavitation allowance also increases accordingly. The research provides a theoretical basis for the improvement of the cavitation performance of agricultural machinery engine cooling water pumps and the prevention and mitigation of cavitation.*

Keywords: *The two curvature blade; Cooling water pump of agricultural automobile engine; Cavitation performance; Leaf blade load; Performance prediction*

INTRODUCTION

Cooling water pump of agricultural automobile engines is the key component to ensure the normal work of the engine cooling system and influences more of the performance of the engine. While cavitation has also influenced the performance of the cooling pump. The production and development of cavitation accompanied by the vibration, noise and even corrosion damage of flow parts, which will degrade the pump performance and shorten its service period [10]. Compared with common pumps, the cooling water pump, with high work temperature, large speed change range and limited size, is more prone to cavitation [7, 8]. The cavitation leads to the degradation of the performance and causes instability of the engine cooling system.

In view of the seriousness of the cavitation damage, both domestic and foreign scholars have conducted in-depth studies on cavitation of the inner mechanical flow field. R.F.Kunz and some researchers [4] predicted the occurrence and development of cavitation by applying two-phase flow model based on Navier-Stokes equation and obtained good effect; Luo Xianwu and some other researchers [10], based on VOF cavitation model numerical simulation on the whole flow field, conducted a systematical

摘要： *基于 CFD 模拟农用汽车发动机冷却水泵内部的三维湍流流场，分析了某一农用汽车采用二次变曲率叶型冷却水泵无空化时的能量特性和空化性能，预测了不同空化状态下叶轮内的空泡分布和叶片中间流线上载荷分布，并与实验结果进行对比。结果表明：在 25℃设计流量下，模拟得到的扬程为 13.49m，数值模拟及试验的扬程和效率误差在 2%以内。在 85℃下农用汽车发动机冷却模型水泵在设计工况点的扬程为 9.6m，大大低于 25℃下设计流量下的扬程值。说明在实际运行时泵内已发生严重汽蚀，设计工况下的空化性能曲线与数值计算变化趋势一致，全空化范围内实测值小于数值计算值，而随着流量增大，临界汽蚀余量也相应增大。研究结果对于改善农用机械发动机冷却水泵的汽蚀性能、防止和减轻空化现象的产生提供了理论依据。*

关键词: *两段变曲率叶型; 农用汽车发动机冷却水泵; 空化性能; 叶片载荷; 性能预测*

引言

农用汽车发动机冷却水泵是保障发动机冷却系统正常工作的关键部件，对发动机的性能影响日益显著。而空化现象对发动机冷却水泵的性能具有重要的影响，空化的产生、发展往往会伴随着产生振动、噪声甚至是过流部件的腐蚀破坏，降低泵的性能并缩短其服役期[10]。而在农用汽车发动机冷却系统中，由于冷却水泵具有工作温度高，转速变化范围大和结构尺寸总体受限等特殊性，其与普通水泵相比更容易发生空化现象[7,8]。空化现象造成的性能急降和空化破坏严重影响发动机冷却系统的稳定性。

鉴于空化破坏的严重性，国内外学者对机械内部流场的空化现象进行了深入研究。R.F.Kunz 等[4]对运用基于 Navier-Stokes 方程的两相流模型对空化的发生和发展进行了预测，获得了良好的效果；罗先武等[10]基于 VOF 空化模型对锅炉给水泵全流场进行数值模拟，系统地对叶轮进

study on the influence of the impeller inlet parameter on cavitation and found that the low specific speed centrifugal pump in the direction of the wheel hub properly extending blade inlet edge and the use of blade placing angle can improve the cavitation performance of the pump; Wang Yong and some researchers [3,7,13], based on CFD technology numerical simulation of centrifugal pump, found that the cavitation performance under design conditions has no significant difference in different angles and analyses the cavitation distribution in the impeller and the stream line load distribution under different cavitation conditions.

The thesis studies a specific two curvature blade agricultural automobile engine cooling water pump which has appeared severe cavitation damage in the actual operation. By using CFD numerical simulation on the unsteady flow cavitation, it forecasts the location and the degree of cavitation damage and provides reference for the prediction of the impeller cavitation performance optimization and cavitation performance.

MATERIAL AND METHOD

The engine cooling water pump works under（85±2）°C in clear water, whose performance parameters and basic geometric parameters are shown in Table 1. Due to the special requirements of cylinder structure and agricultural vehicle engine, the design method of engine cooling water pump is different from the ordinary one, impeller width wide and impeller semi-open, the structure shown in figure 1, and the suction chamber section is annular. Use Creo 2 to generate the model pump whole field three-dimensional map, the computational domain shown in figure 2.

口参数对空化的影响进行了研究，发现对低比转速离心泵朝轮毂方向适当延伸叶片进口边，并采用较大的叶片安放角可以改善泵的空化性能；王勇等[3,7,13]基于 CFD 技术对离心泵进行数值模拟，发现不同叶片包角对设计工况下空化性能无明显影响，并分析了不同空化状态下叶轮中间截面内的空泡分布和叶片中间流向的载荷特性。

本文针对某一采用两段变曲率叶型的农用汽车发动机冷却水泵进行研究，其在实际运行中出现了较为严重的汽蚀破坏。利用 CFD 软件对其全流场的定常空化流动进行数值模拟，预测流道内空化发生的部位和程度，为叶轮空化性能的优化和空化性能的预测提供参考。

材料与方法

发动机冷却水泵工作条件为（85±2）℃温度条件下的清水介质，性能参数和基本几何参数如表 1 所示，由于缸体结构及农用汽车发动机的特殊要求，发动机冷却水泵的设计方法与普通的离心泵设计方法不一样，叶轮宽度较宽，叶轮为半开式，其结构型式如图 1，吸水室截面为环形。采用 Creo 2.0 生成了模型泵全流场三维立体图，计算域如图 2。

Table 1

Design and structure parameters of pump

parameters	values
flow/(kg·h-1)	8
head/m	14
rotation rate/(r·min-1)	3700
impellerouterdiameter/mm	53
impeller output width/mm	7
the number of blades	6

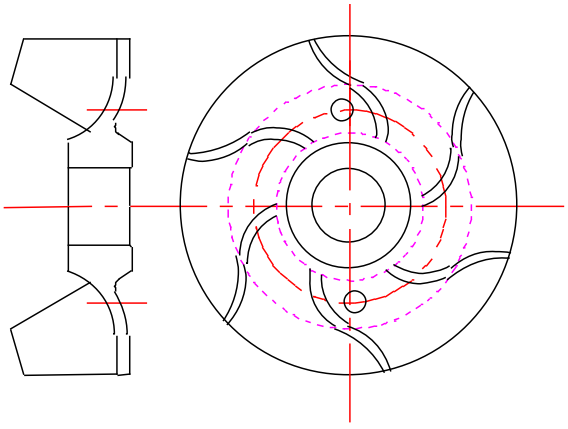

Fig.1 - The impeller's structure

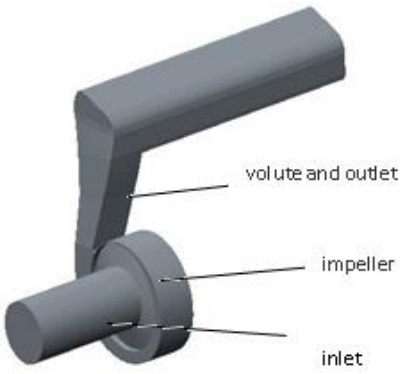

Fig.2 - The computational domain three-dimensional map

The choice of numerical model

In single phase calculation, take N-S equations as governing equations and Standard *k-ε* turbulence model as 3D turbulent numerical calculation. The turbulent kinetic energy *k* and the dissipation rate of turbulent kinetic energy *ε* of turbulent transport equation model is:

数值模型的选择

单相计算以时均 N-S 方程作为基本控制方程，利用 Standard k-ε 湍流模型进行三维湍流数值计算。该湍流模型湍动能 k 和湍动能耗散率 ε 的输送方程为:

$$\mu_t = \rho C_\mu \frac{k^2}{e} \tag{1}$$

$$\frac{\partial(\rho k)}{\partial t} + \frac{\partial(\rho k u_i)}{\partial x_i} = \frac{\partial}{\partial x_j}\left[\left(\mu + \frac{\mu_t}{\sigma_k}\right)\frac{\partial e}{\partial x_j}\right] + G_k - \rho e \tag{2}$$

$$\frac{\partial(\rho e)}{\partial t} + \frac{\partial(\rho e u_i)}{\partial x_i} = \frac{\partial}{\partial x_j}\left[\left(\mu_\varepsilon + \frac{\mu}{\sigma_\varepsilon}\right)\frac{\partial e}{\partial x_j}\right] + \frac{C_{1\varepsilon}}{k} G_k - C_{2\varepsilon}\frac{\rho e^2}{k} \tag{3}$$

Where: μ_t - the turbulent kinematic viscosity;
G_k - the generation item of mean velocity gradient caused by the turbulent kinetic energy *k;*
σ_k - the prandtl number corresponding to turbulent kinetic energy *k*; σ_k =1.0;
σ_ε - the prandtl number corresponding to dissipation rate epsilon; σ_ε =1.3;
C_μ, $C_{1\varepsilon}$ and $C_{2\varepsilon}$ are empirical constant, C_μ =0.09; $C_{1\varepsilon}$ =1.44; $C_{2\varepsilon}$ =1.92.

In this thesis, multi-phase simulation uses flow field and velocity field of same Homogeneous Model and vapor - liquid two - phase. Cavitation is calculated by Rayleigh-Plesset model which provides rate equations and condensing vacuoles produced. The development process of the bubble in the fluid is as below:

式中：μ_t - 湍流运动粘度
G_k - 平均速度梯度引起的湍动能 k 的产生项
σ_k - 湍动能 k 对应的 Prandtl 数；σ_k =1.0
σ_ε - 耗散率 ε 对应的 Prandtl 数；σ_ε =1.3
C_μ，$C_{1\varepsilon}$ 和 $C_{2\varepsilon}$ 为经验常数，C_μ =0.09；$C_{1\varepsilon}$ =1.44；$C_{2\varepsilon}$ =1.92.

本文的多相模拟采用 Homogeneous Model 及汽液两相具有相同的流场和速度场。空化计算采用 Rayleigh-Plesset 模型，该模型给出了空泡产生和凝结的速率方程，汽泡在流体中的发展过程如下式:

$$R_B \frac{d^2 R_B}{dt^2} + \frac{3}{2}\left(\frac{dR_B}{dt}\right)^2 + \frac{2\sigma}{\rho_f R_B} = \frac{p_v - p}{\rho_f} \tag{4}$$

Where, R_B—the bubble radius
p_v—the inside cavity pressure
p—the around bubble pressure of fluid
ρ_f—fluid density
σ —the coefficient of surface tension and bubble

Note that the equation (4) does not consider the influence of thermal effects on the development of cavitation. Ignoring the order condition and surface tension, equation (4) is simplified as:

式中：R_B——汽泡半径
p_v——空泡内的压力
p——空泡周围流体的压力
ρ_f——流体密度
σ ——流体与空泡交界面的表面张力系数

要注意的是方程（4）未考虑热效应对空泡发展的影响。在忽略二阶条件和表面张力的条件下，方程（4）简化为:

$$\frac{dR_B}{dt} = \sqrt{\frac{2}{3}\frac{p_v - p}{\rho_f}} \tag{5}$$

The change rate of the vacuole volume:

则空泡体积的变化速率：

$$\frac{dR_B}{dt} = \frac{d}{dt}\left(\frac{4}{3}\pi R_B^3\right) = 4\pi R_B^3 \sqrt{\frac{2}{3}\frac{p_v - p}{\rho_f}} \tag{6}$$

the quality change rate of the vacuole:

空泡的质量变化速率：

$$\frac{dm_B}{dt} = \rho_g \frac{dV_B}{dt} = 4\pi R_B^2 \rho_g \sqrt{\frac{2}{3}\frac{p_v - p}{\rho_f}} \tag{7}$$

If there are N_B vacuoles per unit volume, the volume fraction of r_g can be expressed as:

如果在每单位体积内有 N_B 个空泡，则其体积分数 r_g 可以表示为:

$$r_g = V_B N_B = \frac{4}{3}\pi R_B^3 N_B \tag{8}$$

The transfer rate of overall mass of unit volume:

单位体积内总体相间质量传输速率为：

$$\dot{m}_{fg} = N_B \frac{dm_B}{dt} = \frac{3r_g\rho_g}{R_B}\sqrt{\frac{2}{3}\frac{p_v - p}{\rho_f}} \tag{9}$$

The equation is derived by the development of the vacuoles (vaporization). When taking the bubble condensation into consideration:

上式由空泡的发展（汽化作用）推导得到。

在考虑空泡凝结作用时，得到：

$$\dot{m}_{fg} = F\frac{3r_g\rho_g}{R_B}\sqrt{\frac{2}{3}\frac{|p_v - p|}{\rho_f}}\,\mathrm{sgn}(p_v - p) \tag{10}$$

Although the equation can be commonly used in the vaporization and condensation process, it should be further optimized in vaporization. Vaporization starts at nucleation. With the increase of vacuole volume fraction, the nucleation density must decreases accordingly. r_{nuc} (1-r_g) taking place of r_g:

尽管上式普遍使用与汽化和凝结过程，在汽化情况下仍需要进一步的优化。汽化作用起始于成核位置，随着空泡体积分数的增长，成核中心密度必然相应下降。用 r_{nuc}（1-r_g）代替上式中的 r_g:

$$\dot{m}_{fg} = F\frac{3r_{nuc}(1-r_g)\rho_g}{R_B}\sqrt{\frac{2}{3}\frac{|p_v - p|}{\rho_f}}\,\mathrm{sgn}(p_v - p) \tag{11}$$

Where, F - empirical coefficient

r_{nuc} - nucleation position volume fraction

R_B - The nucleation semi-diameter is gained through documents. 85 ℃ saturated main steam parameters is shown in table 2.

式中:F - 经验系数

r_{nuc} - 成核位置体积分数

R_B - 此式中指成核位置的半经由文献得到 85℃下饱和水蒸汽的主要物性参数，如表 2。

Table 2

85°C saturated main steam parameters

Material Properties	Value
Thermodynamic state	Gas
Molar Mass/kg·kmol^{-1}	18
Density/kg·m^{-3}	0.35735
Specific heat capacity/J·g^{-1}·K^{-1}	1.88
Specific heat type	Constant pressure
Dynamic viscosity/Pa·s	346.8
Thermal conductivity/W·m^{-1}·K^{-1}	695.6
Saturation pressure/kPa	57.815

Mesh generation and boundary condition

ICEM hexahedral mesh generation is applied to the model pump full flow field and 10-15 layer to the big part of the impeller radius of curvature to ensure the block accord with the internal flow of the agricultural machinery engine cooling pumps while ensuring the calculation accuracy of the impeller near wall [6]. In order to obtain the most economical grid number and calculation step, the independent mesh study on numerical simulation under the design condition is conducted. It shows that when the number of the mesh reaches above 1,500,000, the change range of the head is within 2%, which can think as mesh having no influence on the calculation results. Impeller block and the computational domain mesh are shown in Figure 3.

网格划分和边界条件

对模型泵全流场采用 ICEM 进行六面体网格划分，对叶轮曲率半径较大的地方设置 10-15 层的边界层网格，在保证分块较好符合农用机械发动机冷却泵内的流动状态的同时保证叶轮近壁面的计算精度[6]。为了获得最经济的网格数和计算步长，对设计工况下的数值模拟进行了网格无关性的研究，发现当网格数达到 150 万以上时，扬程的变化幅度在 2%之内，可以认为网格对计算结果没有影响。叶轮的分块及计算域网格如图 3。

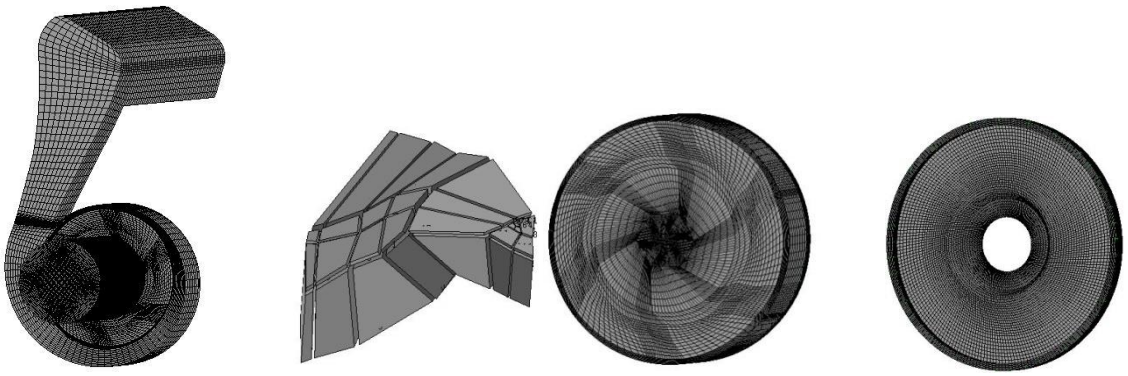

Fig. 3 - The computational domain mesh
a) Full flow field mesh model; b) Impeller block and mesh model; c) The impeller back cavity mesh model

The cavitation allowance (NPSH) is closely related to the inlet pressure of the pump, and therefore the boundary conditions of the pressure inlet and mass flow outlet are applied to the model pump. Inlet bubble phase volume fraction is set to 0, the volume fraction of liquid phase 1 and the surface roughness 0.02mm; the near wall uses standard wall function, the wall boundary condition is set to no slip insulation wall [2].

Cavitation simulation takes the no-cavitation calculation results as the initial results. By changing the inlet pressure, the centrifugal pump cavitation occurs and then obtains better calculation convergence effect, so as to shorten the time of calculation [12].

RESULTS

Validation and comparison between the external characteristics numerical simulation results and the experimental results

For the cavitation free single-phase flow, the flow – head and flow - efficiency curve under 25℃ is calculated under the five conditions of 0.7 Q_d, 0.85 Q_d, 1.0 Q_d, 1.15 Q_d and 1.3 Q_d. From figure 4, the numerical simulation results agree well with the experimental results. In the 1.0 Q_d, the numerical simulation head is 13.49m and efficiency of 56.9%. As seen from the graph, under the five conditions selected, the efficiency has a high degree of goodness of fit. While the efficiency values obtained from the numerical calculation are higher than that of the experimental results, the error value within about 2% due to the ignoring of the mechanical loss caused by caused by the bearing and friction in numerical simulation process [1].

由于空化余量（NPSH）与泵的进口压力密切相关，因此对模型泵采用压力进口和质量流量出口的边界条件。设置进口空泡相体积分数为 0，液相体积分数设为 1。壁面粗糙度设为 0.02mm；近壁面处选用标准壁面函数，壁面边界条件设为绝热无滑移壁面[2]。

空化模拟计算以无空化计算结果作为计算的初始结果。通过改变进口压力使离心泵发生空化，这样能获得较好的计算收敛效果，从而缩短计算时间[12]。

结果

外特性数值模拟结果与实验结果的对比验证

对于无空化单相流动时，在 25℃下分别在 0.7Q_d、0.85Q_d、1.0Q_d、1.15Q_d、1.3Q_d 五种工况下模拟计算出其流量-扬程和流量-效率曲线，从图 4 可以看出数值模拟得到的结果与实验结果吻合较好。此时在 1.0Q_d 数值模拟得到扬程为 13.49m，效率为 56.9%。从图中可以看出，所选取的五个工况中，效率吻合度较高，而数值计算得到的效率值均高于试验结果，误差值约在 2%左右，这是由于在数值模拟中忽略了轴承、摩擦副等引起的机械损失[1]。

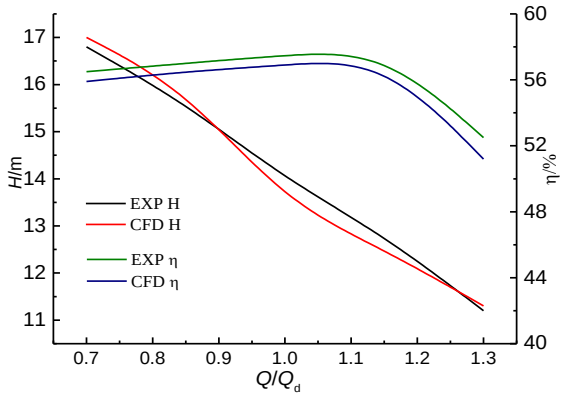

Fig. 4 - 25°C model pump numerical simulation and experimental

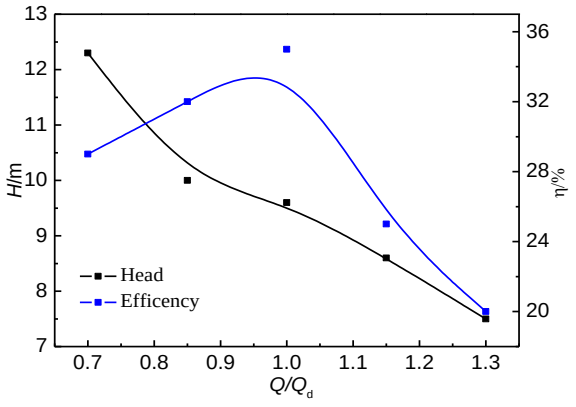

Fig. 5 - 85°C performance curve of the model pump

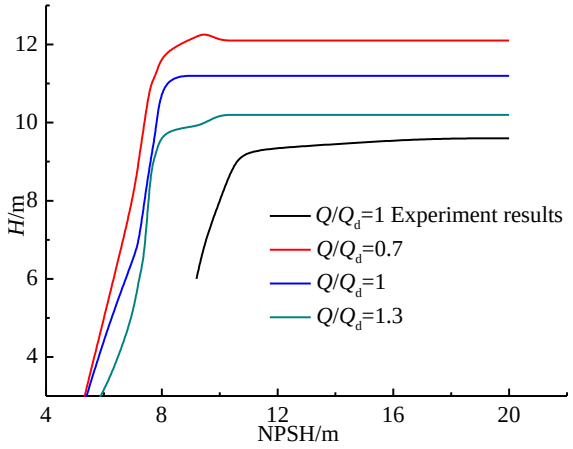

Fig. 6 - Comparison of calculated value and cavitation test

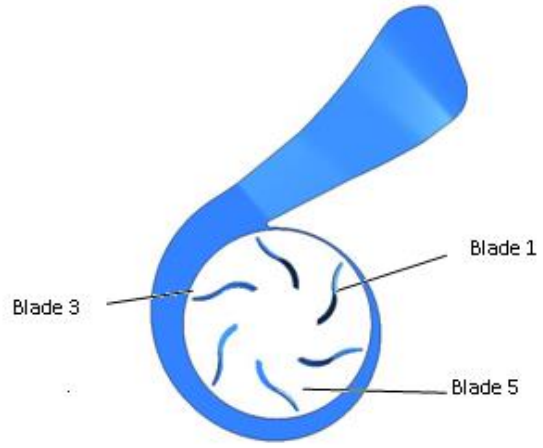

Fig. 7 - The blade numbers

In the outer characteristic test, when heated to about 85℃, the head is 9.6m of the model pump under the design flow head. At the same time, the gradual change of the net energy absorbing head [5] occurs when keeping a constant flow, changing the inlet opening and reducing the pump inlet pressure by increasing the inlet resistance. When the head drops 3%, the NPSH (NPSH) is 11m. Test characteristic curve obtained under 85℃ is shown in figure 5, and the cavitation performance curve of the model pump under the design condition and the simulation results of 0.7Q_d, 1.0 Q_d and 1.3 Q_d under the condition are shown in figure 6.

Seen from the figure, the overall decline in the performance of the model pump at the temperature of 85℃ is greater than that under the temperature of 25℃. From figure 6, the cavitation performance curve and numerical calculation change are prone to be the same under the design condition, the measured numerical value within the full cavitation range is less than the calculated value; when the flow rate increases, the critical cavitation allowance also increases accordingly; in each case, when NPSH>11.5m, the increasing of NPSH has little effect on the head.

The load distribution on the blade surface

The blade surface load is the difference between the pressure surface and the suction surface of a same blade, which is an important parameter affecting the cavitation performance. If the pressure difference defined, it is:

在外特性试验中，当加温至 85℃左右，模型泵在设计流量扬程下扬程为 9.6m，同时进行汽蚀性能试验，保持流量不变，改变进口阀门的开度，通过增加进口阻力来降低模型泵进口压力，从而逐渐改变净吸能头[5]。当扬程下降 3%时，得到汽蚀余量（NPSH）为 11m。在 85℃温度下得到的试验外特性曲线如图 5，而模型泵在设计工况的空化性能曲线与 0.7Q_d、1.0Q_d 及 1.3Q_d 工况下模拟结果如图 6。

可以发现，85℃下模型泵的整体性能比在 25℃下有极大的下降。由图 6 中可以看出，设计工况下的空化性能曲线与数值计算的变化趋势一致，全空化范围内实测值小于数值计算值，而随着流量增大，临界汽蚀余量也相应增大；在各工况下，当 NPSH>11.5m 时，汽蚀余量的增大对扬程几乎没有影响。

叶片表面载荷分布

叶片表面载荷是同一叶片和相同半径处压力面和吸力面压力之差。而叶片两面的压力差是影响空化性能的重要参数。将这一压力差量纲化，即：

$$\Delta p=\frac{p_{ps}-p_{ss}}{\frac{1}{2}\rho U^2} \tag{12}$$

Where: p_{ps} - the middle streamline pressure of the pressure surface

p_{ss} - the middle streamline pressure of the suction surface

U - The circular velocity blade numbers used at the intersection of the impeller blade inlet edge and the front cover plate are shown in figure 7. Figure 8 is about the load distribution curve of the blade surface and the middle streamline of the pump model under the design flow, the abscissa shows the relative position of a point on the streamline.

式中：p_{ps} - 压力面表面中间流线压强

p_{ss} - 吸力面表面中间流线压强

U - 模型泵中采用叶轮叶片进口边与前盖板交点处的圆周速度叶片序号如图 7，图 8 为模型泵在设计流量下各叶片表面的叶片中间流线上载荷分布曲线，其中横坐标表示某点在流线方向上的相对位置。

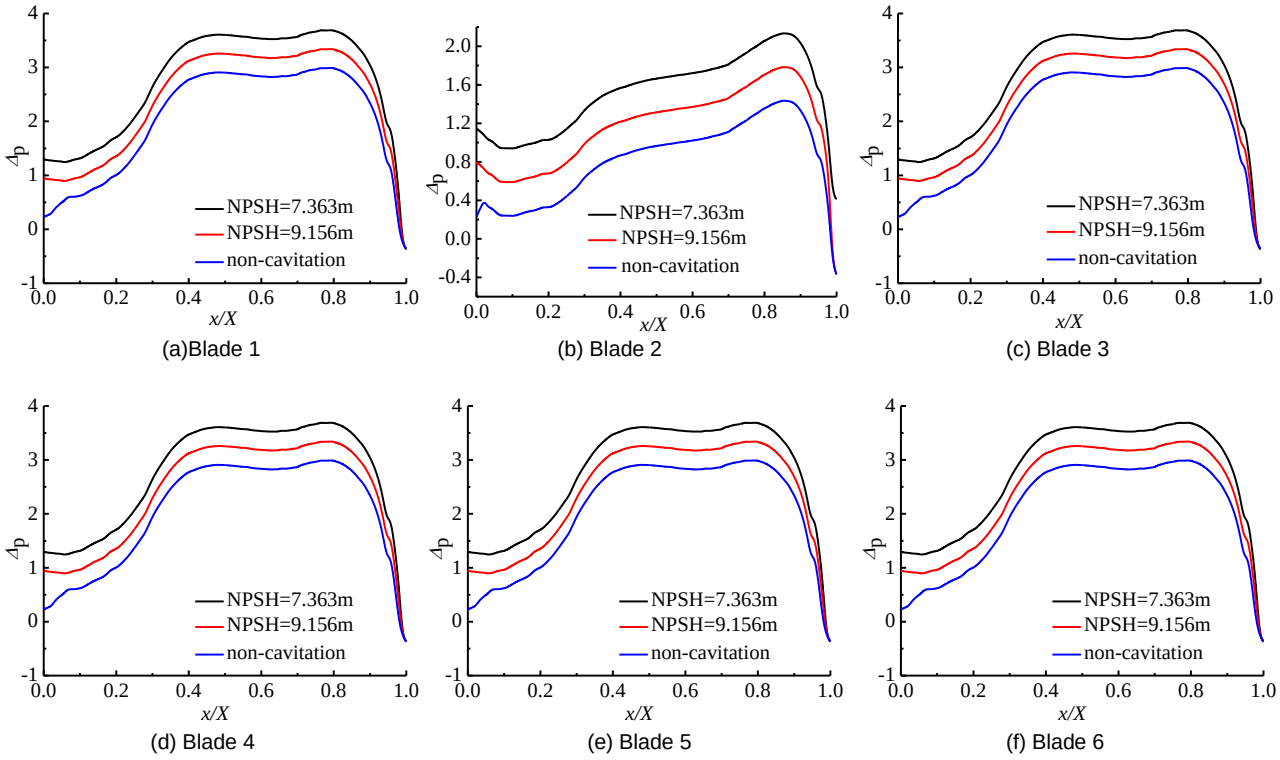

Fig. 8 - The load distribution curve of the blade middle streamlines

It can be seen from the figure 8 that from the blade inlet to outlet, except for blade 2, the curve appears an parabolic increasing; when x/X=0.5~0.8, the pressure difference coefficient appears a stable trend and the fluid enters the bended part of the two curvature blade impeller; when x/X > 0.8, the nearer impeller outlet, its pressure difference steeply drops, which may even lead to the pressure of the suction surface exceeding that of the pressure surface. This is because near the outlet, the fluid flows into the suction surface from the working surface, during which leakage happens and results in decreased pressure difference coefficient. While at the inlet of the blade 2, the pressure coefficient is higher than that of the other 5 blades, but the overall pressure difference coefficient is small so that the load on blade 2 is minimum. Comparing the different NPSH coefficient of the pressure difference, it find that as the NPSH decreases, the pressure difference coefficient rise of all the blades, which shows that cavitation has great influence on blade loading and the blade pressure difference coefficient is in direct proportion to cavitation.

Inner impeller cavitation bubbles distribution

According to the saturated vapor pressure hypothesis, when the inner pressure of the pump is lower than the medium corresponding operating pressure, cavitation bubble will happens to the fluid medium. Figure 9 shows the void distribution under different NPSH in the impeller. We can see from Figure 4, as the NPSH decreases, the inside pump cavitation volume distribution increases. Vacuoles appear first at the blade inlet edge near the back flow passage and near the baffle tongue with an asymmetric distribution. Inside the pump the vacuole volume increases as the NPSH decreases, along the blade impeller back to drain diffusion, and extends to the pressure surface. When NPSH=7.363m, it can be found that the cavitation bubbles have occupied much of the channel, greatly influencing the performance of the pump. In the same NPSH, the cavitation becomes

由图 8 可以看出从叶片进口到出口，除叶片 2 外基本呈抛物线形趋势增加；当 x/X=0.5~0.8 时，压差系数出现平稳趋势，此时流体进入二段变曲率叶型叶轮的后弯部分；当 x/X 大于 0.8 时，及靠近叶轮出口处，压差陡降，甚至吸力面的压力会超过压力面，这是由于在出口边处，流体由工作面流入吸力面，产生泄漏流，造成压差系数的下降。而叶片 2 在叶片入口处，压力系数高于其他 5 个叶片，但是总体上压差系数较小，叶片 2 上所受载荷也就最小。对比不同 NPSH 时的压差系数，发现随着 NPSH 的减小，在各叶片上的压差系数都呈明显的上升，说明空化对于叶片载荷有较大的影响。同时也说明叶片压差系数越高，空化越严重。

叶轮内部空泡分布

根据饱和蒸汽压的假说，当泵内的压力小于介质相应工况的饱和蒸汽压时，流体介质将发生汽化产生空泡。图 9 为不同 NPSH 下叶轮内的空泡分布。由图 4 可知，随着 NPSH 的减小，泵内部的空泡体积分布增大，空泡首先在叶片背面进口边附近出现，并且首先出现在靠近隔舌的流道内，且在全流量内空泡的分布成不对称分布。泵内部的空泡体积随着 NPSH 的减小而增大，沿叶片背面向叶轮处漏扩散，并同时向压力面方向扩展。在 NPSH=7.363m 时，可以发现，空泡已经占据了很大部分的流道，极大地影响了泵的性能。在同一 NPSH 下， 空化程度随着流量

serious as the flow rate increases. Figure10 shows the vacuole distribution of the 1.0Q_d impeller intermediate flow and reflects the distribution rule. When NPSH=10.541m, there's no void distribution in the intermediate flow, cavitation is mainly distributed at the inlet near the front pump cavity edge; as the decline of NPSH to 7.363m, the flow near the baffle tongue is almost blocked by the vacuoles, where there appears obvious fault in the external characteristics.

Figure 11 shows the static pressure distribution the middle section of the impeller 1.0Q_d cases. As seen from the graph, when the NPSH=10.541m, at the cavitation inception stage, there's no void distribution in the middle section but obviously appears in the low pressure area. With the decline of HPSH, near the septal area of low pressure in the flow channel near the tongue first appear the attachment holes which make the water flow channel separated from the solid boundary. When HPSH=9.156m, we can see that the vacuoles cross the channels and cavitation bubbles appear in each channel. Except for the channel near the separation tongue, the static pressure in the flow passage appears a symmetrical distribution.

增大而变得严重。图 10 为 1.0Qd 叶轮中间流面内空泡分布,也体现了上述的分布规律。NPSH=10.541m 时，在中间流面内无空泡分布，空泡主要分布在靠近前泵腔的进口边处，随着 NPSH 的下降，到 NPSH=7.363m 时，靠近隔舌的流道几乎被空泡堵塞，此时在外特性上出现明显的断裂。

图 11 为 1.0Q_d 工况下叶轮中间截面上的静压分布，从图中可以看出，在 NPSH=10.541m 时，空化初生阶段，虽然在中间截面上无空泡分布，但是已存在明显的低压区，随着 HPSH 的下降，在靠近隔舌附近的流道内的低压区域首先发展为附着空穴，使水流从过流通道的固体边界脱离。在 HPSH=9.156m 时，可以看出空泡跨流道延伸，在各流道内均出现空泡，除靠近隔舌位置的流道，其他流道内的静压基本成对称分布。

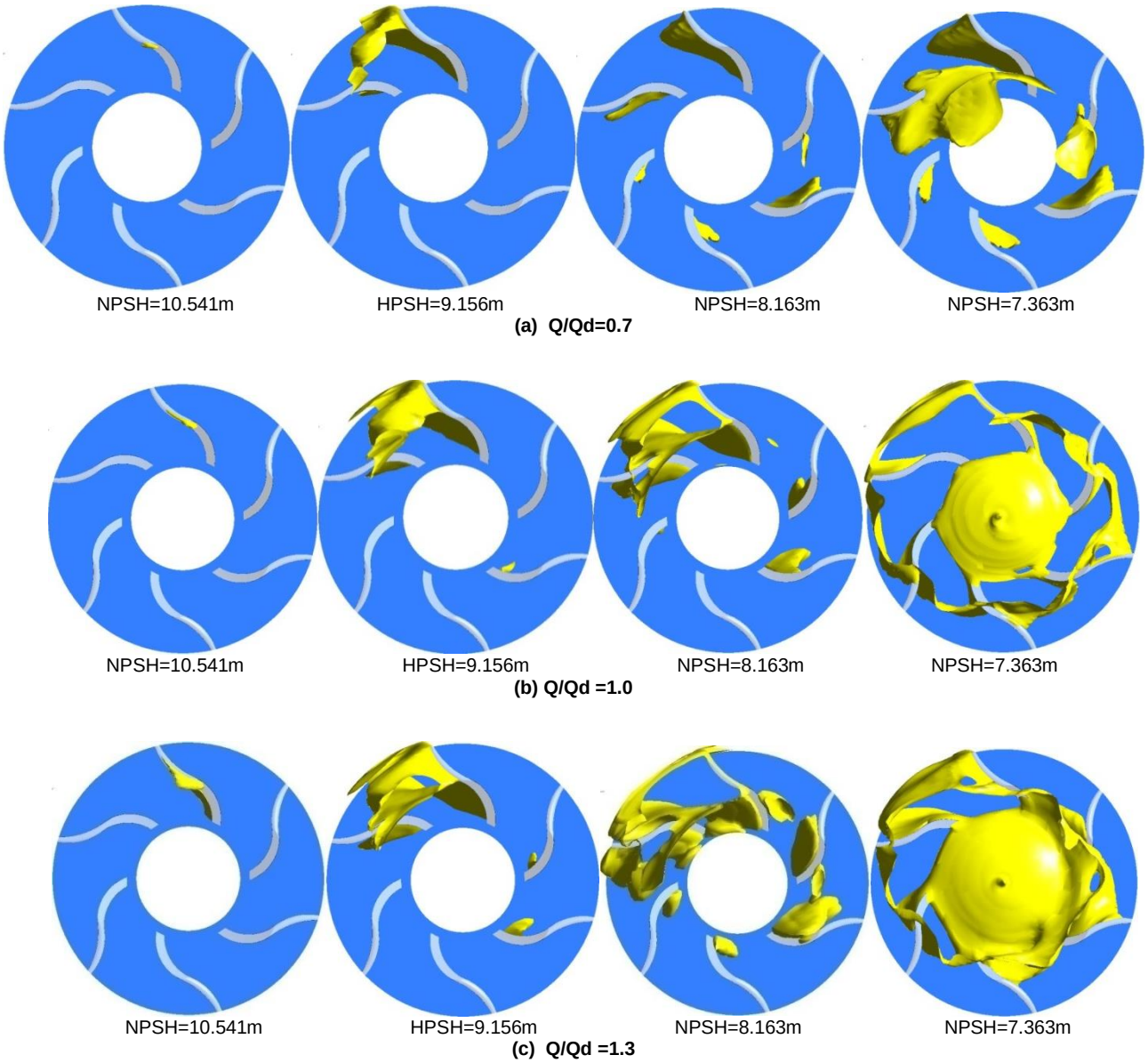

Fig. 9 - Inner impeller cavitation bubbles distribution

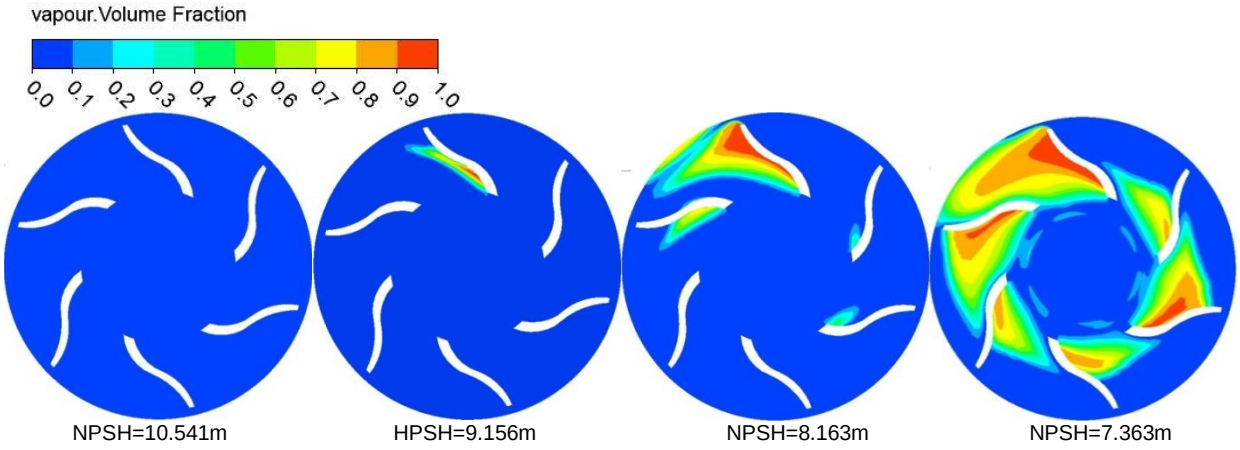

Fig. 10 - The void distribution in the intermediate flow surface of the impeller

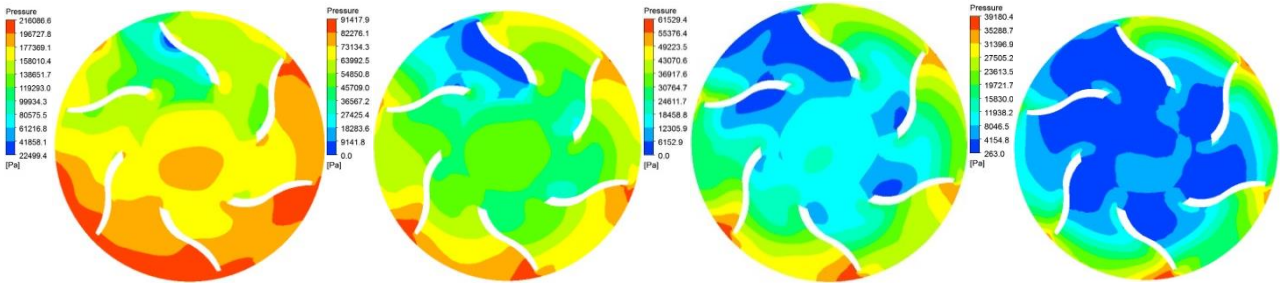

Fig.11- The static pressure distribution in the impeller intermediate section

CONCLUSIONS

(1) This thesis, adopting numerical calculating method, studies that the cavitation performance curve and the calculation values are prone to be same, the numerical calculation value is lower than the measured value in the full cavitation range, and will provide a good guiding for the agricultural and fluid pump application.

(2) For the blades near the baffle tongue, regardless of pump cavitation or not, the pressure difference coefficient on the streamlines is minimum. With the development of cavitation, the pressure difference coefficient on the middle streamline increases obviously, which proves that the cavitation has a significant influence on the load of the blades.

(3) For the two curvature blade type centrifugal pump, as the inlet pressure decreases, cavitation bubbles occur firstly at the blade inlet and then extend to the impeller outlet along the streamline, until there appear a large number of cavitation bubbles on the pressure surface of blade curved part.

ACKNOWLEDGEMENT

The study was supported by the National High technology and Development Program of china (2012AA10A503), Science and Technology Research Project of Henan Province (142102210555).

REFERENCES

[1]. Fan Yang, Chao Liu, (2013) - *Numerical and Experimental Investigation of Slanted Axial-flow pumping System,* Journal of Engineering Science and Technology Review, vol.6，no.2, pg.62-68;

[2]. Halima Hadziahmetovic, Nedim Hodzic, Damir Kahrimanovic, Ejub Dzaferovic, (2014) - *Computational fluid dynamics (CFD) based Erosion Prediction Model in Elbows,* Technical Gazette, vol.21, no.2, pg. 275-282;

结论

（1）本文中采用的数值计算方法，空化性能曲线与数值计算变化趋势一致，全空化范围内实测值小于数值计算值，对农业及流体泵类应用具有较好的指导意义。

（2）在靠近隔舌的叶片上，无论水泵是否出现空化现象，其中间流线上，压差系数最小。随着空化的发展，叶轮中间流线的压差系数明显增大，说明空化对叶片的载荷有重要影响。

（3）对于二次变曲率叶型离心泵，随着进口压力的降低，空泡首先出现在叶片进口处，然后沿流线向叶轮出口扩展，直至在叶片后弯部分的压力面出现大量空泡。

致谢

国家高技术研究发展计划（2012AA10A503），河南省科技攻关项目资助（142102210555）

参考文献

[1]. 杨帆, 刘超, (2013) - *斜式轴流泵系统的数值模拟和实验研究*,工程科学与技术杂志,第 6 卷,第 2 期, 62-68;

[2]. Halima Hadziahmetovic, Nedim Hodzic, Damir Kahrimanovic, Ejub Dzaferovic, (2014) -*基于计算流体动力学(CFD)的肘部流失模型预测,*科技公报,第 21 卷,第 2 期, 275-282;

[3]. Houlin Liu, Dongxi Liu,Yong Wang, (2012) - *Applicative Evaluation of Three Cavitating Models on Cavitating Flow Calculation in Centrifugal Pump,* Transactions of the CSAE, vol. 28, no. 16, pg.54-59;
[4]. Kunz R.F., Boger D.A., Stinebring D.R., (2000) - *A preconditioned Navier–Stokes method for two-phase flows with application to cavitation prediction*, Computers & Fluids, vol. 39, no.4, pg. 849-875.
[5]. Lei Tan, Shuliang Cao, Shaobo Gui, (2010) - *Experiment and Numerical Simulation of Cavitation Performance for Centrifugal Pump with Inlet Guide Vane,* Journal of Mechanical Engineering, vol.46, no.18, pg.177-182;
[6]. Weidong Cao, Xiaodi Zhang, Yi Gao, (2012) - *Cavitation Performance of the Low Specific-speed Centrifugal Pump with Radial Reflux Balance Hole,* Transactions of the Chinese Society for Agricultural Machinery, vol. 43, no 1, pg.37-41;
[7]. Yong Wang, Houlin Liu, Shouqi Yuan, (2012) - *Experimental Testing on Cavitation Vibration and Noise of Centrifugal Pumps under off-design Conditions,* Transactions of the CSAE, vol. 28, no.2, pg.35-38;
[8]. Wei Li, Weidong Shi, Bing Pei, (2013) - *Numerical Simulation and Improvement on Cavitation Performance of Engine Cooling Water Pump,* Transactions of CSICE. vol. 31, no.2, pg.165-170;
[9]. Wei Li, Weidong Shi, Hua Zhang, (2012) - *Cavitation Performance Prediction of Engine Cooling Water Pump based on CFD,* Journal of Drainage and Irrigation Machinery Engineering, vol. 30, no.2, pg.176-180;
[10]. Xianwu Luo, Yao Zhang, Junqi Peng, (2008) - *Effect of Impeller inlet Geometry on Centrifugal Pump Cavitation Performance,* J Tsinghua (Sci & Tech), vol. 48, no.5, pg.836-839;
[11]**.** Xingfan Guan, (1987) –*Theory and Design of Pump,* Beijing: China Machine Press;
[12]. Yongsheng Su, Yongsheng Wang, Xiangyang Duan, (2010) - *Cavitation Experimental Research on Centrifugal Pump,* Transactions of the Chinese Society for Agricultural Machinery, vol. 41, no 3, pg.77-80;
[13]. Yong Wang, Houlin Liu, Shouqi Yuan, (2011) -*CFD Simulation on Cavitation Characteristics in Centrifugal Pump,* Journal of Drainage and Irrigation Machinery Engineering, vol. 29, no.2, pg.99-103.

[3]. 刘厚林, 刘东喜, 王勇, 等.(2012) - *三种空化模型在离心泵空化流计算中的应用评价*, 农业工程学报, 第 28 卷, 第 16 期, 54-59;
[4]. Kunz R.F., Boger D.A., Stinebring D.R.,（2000）- *基于 Navier–Stokes 方程的两相流模型空化预测*,.计算流体， 第 29 卷, 第 8 期, 849-875;
[5]. 谭磊, 曹树良, 桂绍波, 等, (2012) - *带有前置导叶离心泵空化性能的试验及数值模拟*, 机械工程学报, 第 46 卷, 第 18 期, 77-80;
[6]. 曹卫东, 张晓娣, 高一, 等 (2012) - *径向回流平衡孔低比转数离心泵空化性能研究*, 农业机械学报, 第 43 卷, 第 1 期, 37-41;
[7]. 王勇, 刘厚林, 袁寿其, 等 (2012) - *离心泵非设计工况空化振动噪声的试验测试*, 农业工程学报, 第 28 卷, 第 2 期, 35-38;
[8]. 李伟,施卫东,裴冰,等 (2013) - *发动机冷却水泵空化特性的数值模拟与改进,* 内燃机学报, 第 31 卷, 第 2 期, 165-170;
[9]. 李伟, 施卫东, 张华,等.(2012)- *基于 CFD 的发动机冷却水泵汽蚀性能预测,* 排灌机械工程学报, 第 30 卷, 第 2 期, 176-180;
[10]. 罗先武, 张瑶, 彭俊奇,等.(2008) - *叶轮进口几何参数对离心泵空化性能的影响*, 清华大学学报(自然科学版), 第 48 卷, 第 5 期, 836-839;
[11]. 关醒凡.(1987) - *泵的理论与设计*,北京:机械工业出版社;
[12]. 苏永生, 王永生, 段向阳 (2010) - *离心泵空化试验研究,* 农业机械学报, 第 41 卷, 第 3 期, 77-80;
[13]. 王勇, 刘厚林, 袁寿其, 等 (2011) - *离心泵内部空化特性的 CFD 模拟*, 排灌机械工程学报, 第 29 卷, 第 2 期, 99-103.

MOIRÉ SUPPORTED STRESS DISTRIBUTION STUDY ON GEARS
/
APLICAÇÃO DA TÉCNICA DE MOIRÉ NO ESTUDO DA DISTRIBUIÇÃO DE CARGAS EM ENGRENAGENS

BSAE. Stud. Eng. Villa D.[1)], Prof. Ph.D. Eng. Gazzola J.[2)], Prof. Ph.D. Eng. Dal Fabbro I.M.[1)], Ph.D. Stud. Eng. Silva M.V.G. [1)],

[1)]Faculty of Agricultural Engineering, UNICAMP, Campinas, SP / Brazil; [2)]Department of Agricultural Engineering, UFS, Aracaju, SE / Brazil

Tel: +55 19 3521-1059; E-mail: inacio@feagri.unicamp.br

Abstract: *Gears are widely employed in farm machinery transmission units. However, the severe environment imposed to the machine operation generates special problems associated to maintenance, as well as to the expected time life. Machinery which works on field are exposed to excessive dust, moisture, heat, chemicals, uneven mechanical loading and quite frequently the manufacturer recommendations are not adequate or not even available. Based on that, the proposal of new methods for strain and stress distribution analysis on gears under different working conditions is considered necessary. This research paper introduces the application of moiré methods to replace the popular strain gage technique. The proposed method is included in the photomechanical techniques and is considered of easy as well as of low cost application. The moiré family of methods is based on the projection of optical grids onto the object under analysis, generating optical fringes which displace as the object is deformed under mechanical loads. In this research work the tests were carried under different working conditions, as (1) non lubricated clean gears, (2) clean and lubricated, (3) lubricated and contaminated with soil. The comparison of these three situations indicated the influence of soil contamination as well as of the lubrication. The conclusion emphasizes the application of the proposed method to gear transmission design as well as to maintenance.*

Key words*: gear design, gear maintenance, moiré methods, photoelastic moiré*

INTRODUCTION

Farm machinery works quite often in severe environments which are hazardous to the equipment time life as well as to the maintenance procedure and chronogram. The objective of this research work was to study the effects of lubrication and dirt on gears deformation and stress loading which directly affects time working life. The experimental procedure of this research includes the application of a moiré photoelastical technique, specifically the shadow moiré. Hertz contact stress theory assumes that the pressure exerted by spheres in contact follows an elliptical distribution [8,12]. Equations associated to that theory are important to numerical calculation, as well as, its use with finite elements to promote numerical simulations [3,10]. Numerical simulation shows that gear failure occurs due to certain kind of mechanical loading, as contact loading due normal stress and loading placed on teeth root [14]. Stress distribution on coupled gears is concentrated on regions of gears contact, on teeth root and stress concentration is distributed along specimen with some displacement in the same direction of gear rotation [15].

Resumo: *Elementos de transmissão são bastanteto aplicados a projetos de máquinas agrícolas e a engrenagem figura como um dos mais aplicados. Porém, o ambiente severo dos meios agrários exigem maiores cuidados no projeto de máquinas. Problemas como sujeira e ausência de lubrificação em engrenagens induzem a tensões que podem sair do comportamento esperado. Softwares de simulação computacional não são hábeis em determinar tais comportamentos devido à sua complexidade. Técnicas fotomecânicas analisam qualitativamente a distribuição de tensão em corpos indiferente de sua geometria em situações de carregamento adversas. Entre as técnicas fotomecânicas, destaca-se a técnica de moiré. Neste trabalho de pesquisa, objetiva-se analisar o comportamento mecânico de engrenagens sujeita a ação de contaminação por terra e por falta de lubrificação. Duas engrenagens de dente reto tiveram cargas aplicadas sob três situações: Limpa e sem lubrificação; Limpa e Lubrificada; Contaminada e sem lubrificação. Os dados da engrenagem limpa e sem lubrificação foram rebatidos com os resultados das outras duas situações. Os resultados mostraram a influência dos agentes contaminante e lubrificante sobre o comportamento mecânico de engrenagens. O trabalho é concluído com informações importantes para ser aplicados em projetos de transmissão por engrenagens.*

Palavras-chave: *Projeto de Máquinas Agrícolas; Engrenagens; Técnica de Moiré de Sombra*

INTRODUÇÃO

Máquinas agrícolas trabalhal frequentemente em ambientes severos ao qual são nocivos ao tempo de vida útil dos equipamentos, tão bem como, ao procedimento e cronograma de manutenção. O objetivo deste trabalho de pesquisa foi estudar os efeitos da lubrificação e da sujeira na distribuição de tensão e deformação em engrenagens ao qual afeta diretamente sua vida útil de trabalho. O procedimento experimental deste trabalho de pesquisa include a aplicação da técnica fotoelástica de moiré, especificadamente a técnica de moiré de sombra. A teoria de contato de Hertz assume que a pressão desenvolvida por esferas em contato apresenta uma distribuição elíptica [8,12]. As equações associada à teoria são importante para o cálculo numérico, tão bem como, seu uso com elementos finitos para promover a simulação numérica [3,10]. Simulação numérica mostra que a ruptura em engrenagens ocorre devido a certos tipos de carregamento mecânico, como carregamento de contato devido às tensões normais e carregamentos localizados no pé do dente [14]. A distribuição de tensão em engrenagens acopladas fica concentrada nas regiões de contato, na raiz do dente e a concentração de tensão está distribuída ao longo do corpo de prova com alguns deslocamentos na mesma direção de rotação da engrenagem [15].

The photoelasticity is a family of methods of experimental stress and strain analysis applied in evaluating, validating and developing of structural elements which is subjected to mechanical loadings. Photoelastic techniques permit determining strain and deformation at any point of interest on the structural element [6]. Stress direction and intensity are obtained from the information provided by the isocline and isochromatic fringes [13]. Isocline fringes inform regions which every main stresses exhibits the same direction, meanwhile the isochromatics inform regions where is able to obtain the angle between main stresses [17]. Photoelastic methods do not include destructive procedures and can be applied on structural members of any geometric configuration [1,4]. The *moiré* phenomenon is generated when screens of certain mesh density are superposed, producing waves like patterns or fringes, which move when its relative positions are displaced [7,11].

The selected method for this research work is named shadow *moiré*, which consists in generating an interference pattern with a grid before the object in study and its shade project onto the object [5,16]. *Moiré* interferometry gives support to similar photoelastic techniques, allowing similar applications as the conventional methods, presenting high precision and confidence as well. *Moiré* methods require low cost experimental setups and generate reliable results [2,9]. The objective of this research work is to carry on shadow *moiré* technique to determine stress distribution on coupled gears under compressive stress loading. Tests will be carried with clean gears, lubricated gears and lubricated dirt gears.

MATERIAL AND METHODS

The selected experimental setup to carry the shadow *moiré* tests in this research work included a SAMSUNG digital camera 7.1 mega pixels with remote control to avoid undesired movement, a white light source, a set of Ronchi grids of 0.2 mm period, a loading press, considered appropriate to carry Shadow *Moiré* tests, as recommended by [2]. Testing gears were coupled and diametrically loaded and the grid was placed in front of the specimen, before the light source and the digital camera, in an angular position as shown on Figure 01. Loaded and non-loaded specimen images were captured through the following procedure: (1) The Ronchi grid was projected onto the gears surface with no load and photographed to generate the image $I_1(x,y)$. (2) The grid was projected onto the gears under traction loads of 05 kgf, 10 kgf and 30 kgf, generating the images $I_2(x,y)$, $I_3(x,y)$ and $I_4(x,y)$ respectively. Image processing included the application of the software ImaeJ and Kilimanjaro. Image from load and non-load gears was captured and processing, including the creation of masks.

In this test, three different diametrical loads were applied on the coupled gears as 5 kgf, 10 kgf and 30 kgf. The 05 kgf and 10 kgf loads augmented the contact area between teeth, however the 30 kgf load rotated the gears from their original position besides of increasing the contact area.

A fotoelasticidade é uma família de métodos experimentais de análise de tensão e deformação específicas aplicadas para a avaliação, validação e desenvolvimento de elementos estruturais ao qual está sujeito a carregamentos mecânicos. Técnicas fotoelásticas permitem determinar tensão e deformação em qualquer ponto de interesse no elemento estrutural [6]. A direção e a intensidade das tensões são obtidas de informações providas da análise das franjas isóclinas e isocromáticas [13]. Franjas insóclinas informam regiões na qual todas as tensões principais exibem a mesma direção, enquanto que as franjas isocromáticas informam regiões onde é possível de se obter o ângulo entre as tensões principais [17]. Métodos fotoelásticos não incluem procedimentos destrutivos e podem ser aplicados em membros estruturais de qualquer configuração geométrica [1,4]. O fenômeno moiré é gerado quando duas telas de mesma densidade de malha são superpostas, produzindo ondas padrões ou franjas, ao qual movem-se quando sua posição relativa é deslocada [7,11].

O método selecionado para este trabalho de pesquisa é chamado de moiré de sombra, e consiste na geração e interferência das franjas padrões com uma grade posicionada antes do objeto em estudo e sua sombra projeta sob o objeto [5,16]. A interferometria moiré dá suporte a técnicas fotoelásticas similares, permitindo similar aplicação como os métodos convencionais, apresentando alta precisão e confiabilidade. O método *Moiré* requer equipamentos de baixo custo para o arranjo experimental e gera resultados confiáveis [2,9]. O objetivo deste trabalho de pesquisa foi desenvolver a técnica de moiré de sombra para determinar a distribuição de tensão e deformação em engrenagens acopladas sobtensão de compressão. Os ensaios foram feitos com engrenagens limpas, engrenagens lubrificadas e engrenagens lubrificadas e com presença de sujeiras.

MATERIAL E MÉTODOS

Os ensaios fotomecânicos foram levados a cabo no Laboratório de Óptica da Faculdade de Engenharia Agrícola da UNICAMP, localizado na cidade de Campinas/SP. Como corpo de prova selecionou-se duas engrenagens cilíndricas de dentes retos confeccionadas em material plástico. Uma mesa metálica foi utilizado para dar suporte aos corpos de prova. O arranjo experimental para o ensaio de carregamento ainda incluiu uma prensa hidráulica acoplada a sensores para determinar o módulo do carregamento. O ensaio fotomecânico de *moiré* incluiu uma grade Ronchi com período de 0,2 mm, um projetor multimídia da marca SONY e uma câmera digital da marca SAMSUNG de 6,1 Mega Pixels com controle remoto para a captura de imagens, prevenindo qualquer tipo de movimentação indesejável, como recomendado por [2]. O corpo de prova foi pintado de cor branca fosca para que as franjas padrões apresentassem maior contraste. A grade Ronchi foi posicionada frontalmente ao corpo de prova conforme está indicado na Figura 1 a qual ilustra o arranjo experimental utilizado para este trabalho de pesquisa.

Para este trabalho de pesquisa, três taxas de carga foram aplicadas no ensaio de carregamento (5, 10 e 30 kgf) e em três situações de trabalho diferentes, tais como, engrenagem limpa, lubrificada e lubrificada com sujeira.

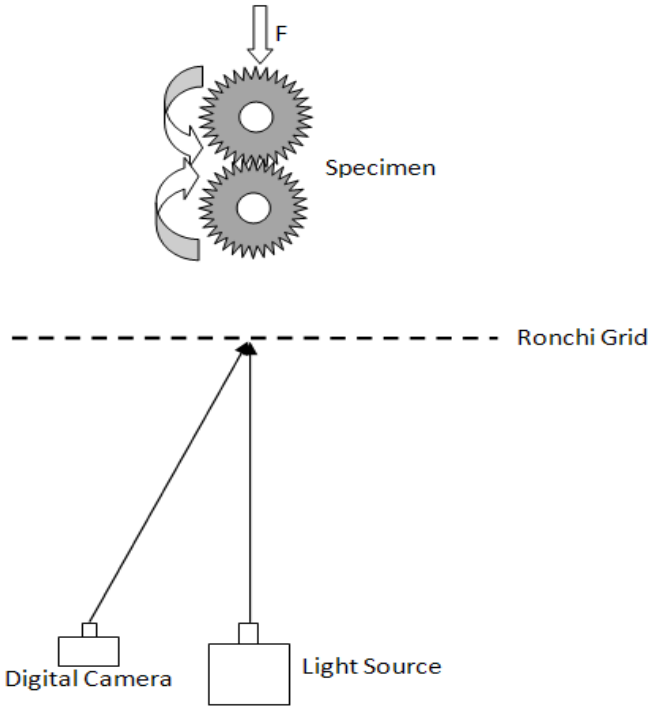

Fig. 1 – Shadow *moiré* setup selected to carry diametrical load on the coupled gears

RESULTS AND DISCUSSIONS.

Figures 2, 3 and 4 exhibits the resulting isodeformation maps as obtained through the shadow moiré method respectively for clean gears, lubricated gears and lubricated dirt gears.

RESULTADOS E DISCUSSÃO

As Figuras 2, 3 e 4 mostram os resultados do mapa de isodeformações, obtidos pela técnica de moiré de sombra para os casos de: engrenagem limpa, engrenagem lubrificada e engrenagem lubrificada com sujeira, respectivamente.

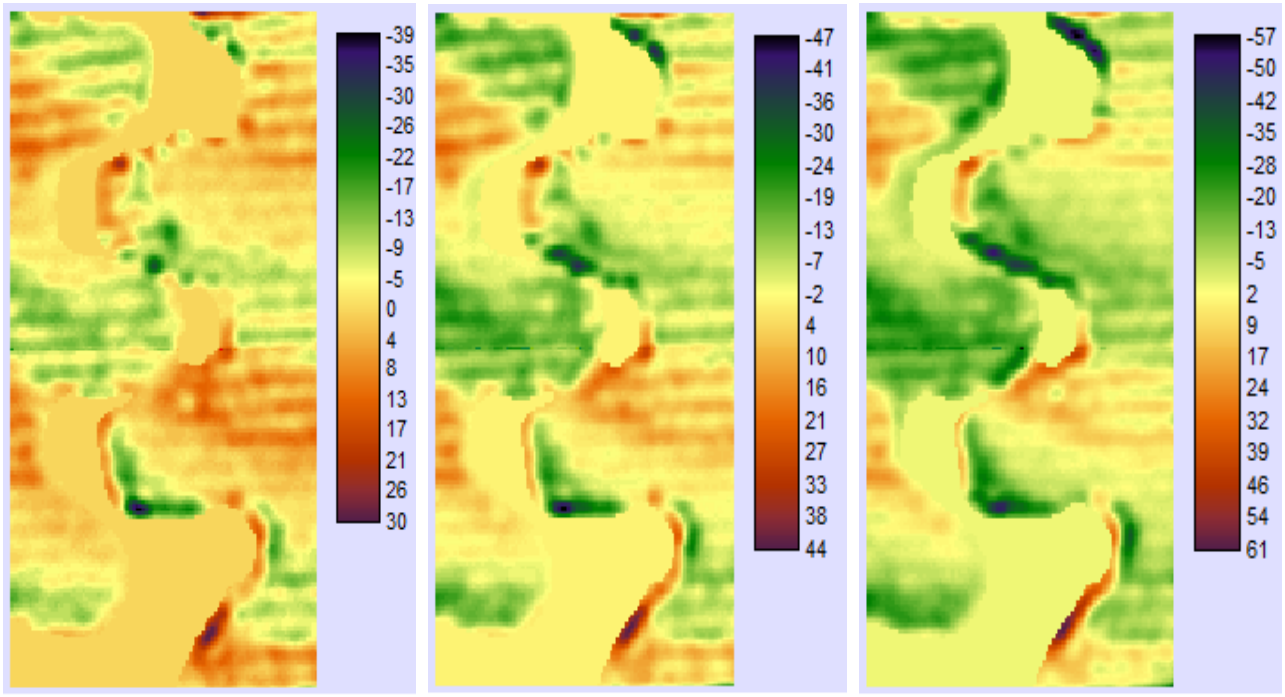

a) b) c)

Fig. 2 - Isodeformation maps of clean gears loaded with:
a) 05 kgf. b) 10 kgf. c) 30 kgf

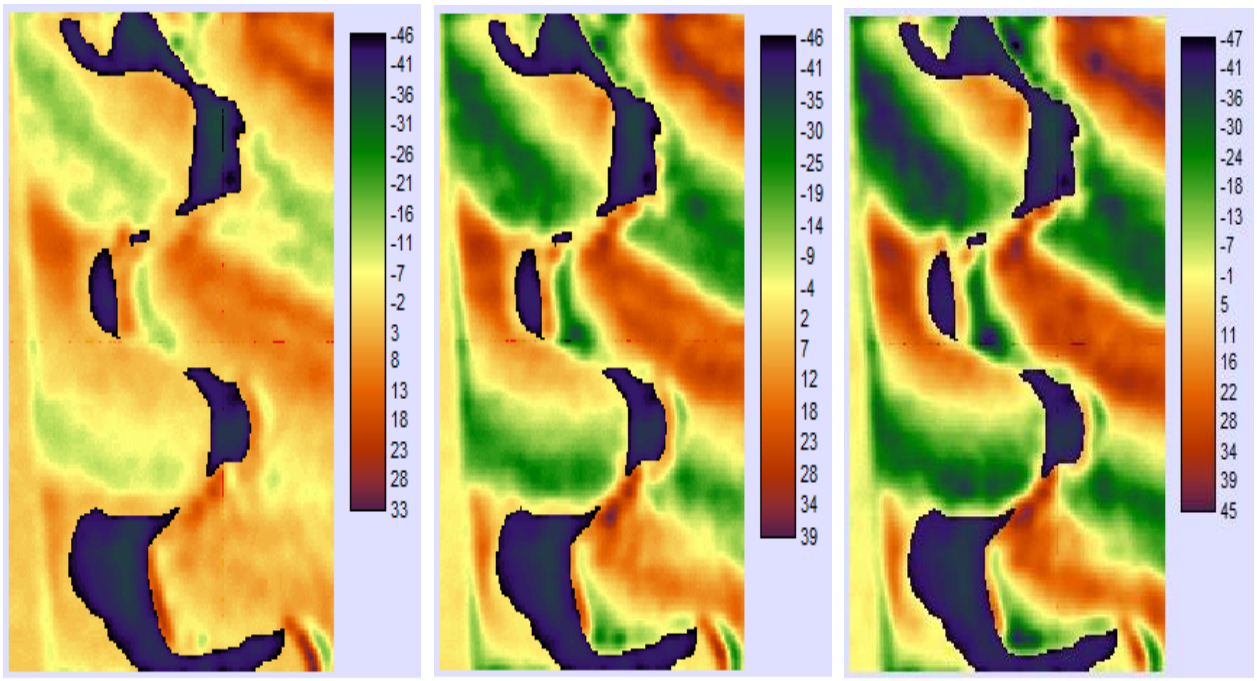

a) b) c)

Fig. 3 - Isodeformation maps of lubricated gears loaded with:
a) 5 kgf. b) 10 kgf. c) 15 kgf

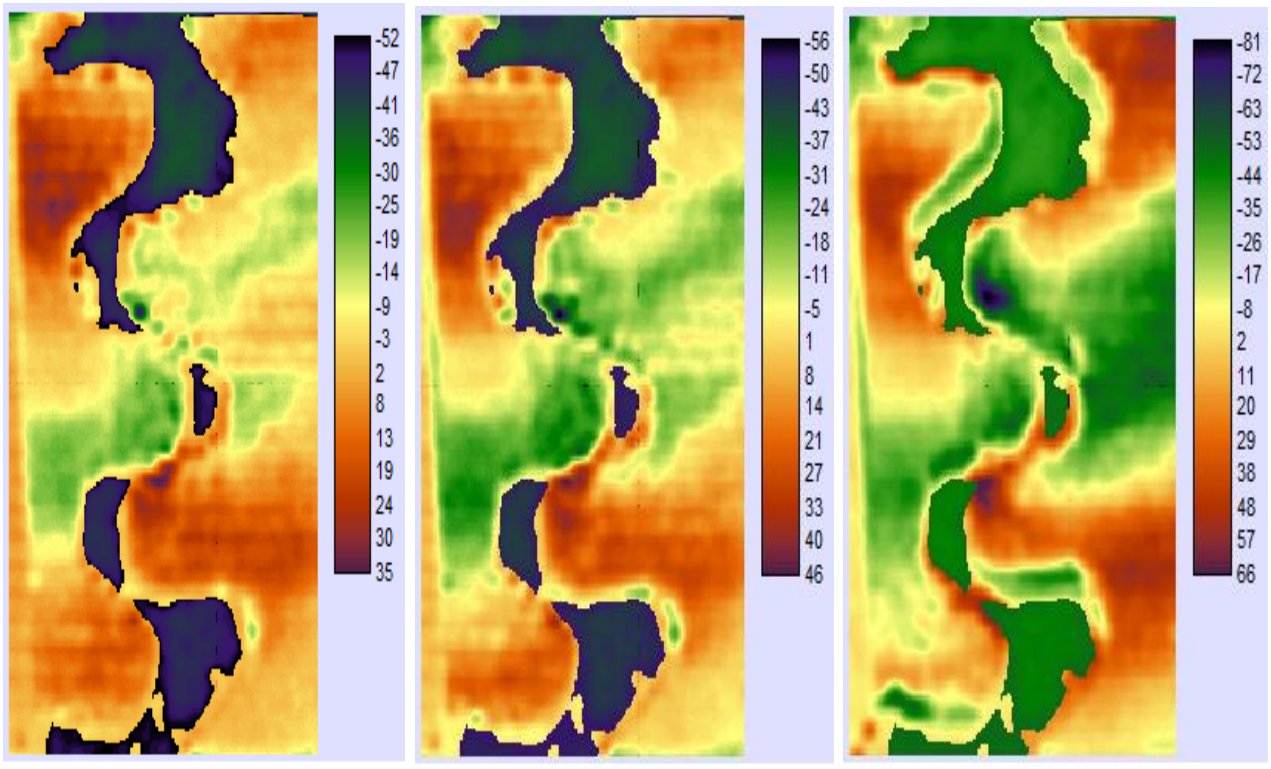

Fig. 4 - Isodeformation maps of lubricated dirt gears loaded with:
a) 5 kgf. b) 10 kgf. c) 30 kgf

Figures 5, 6 and 7 shows the isoclinics and isochromatic curves as obtained by the moiré method for respectively for clean gears, lubricated gears and lubricated dirt gears.

As Figuras 5, 6 e 7 mostram os resultados de franjas isocromáticas e isoclínicas, obtidos pela técnica de moiré de sombra para os casos de: engrenagem limpa, engrenagem lubrificada e engrenagem lubrificada com sujeira, respectivamente.

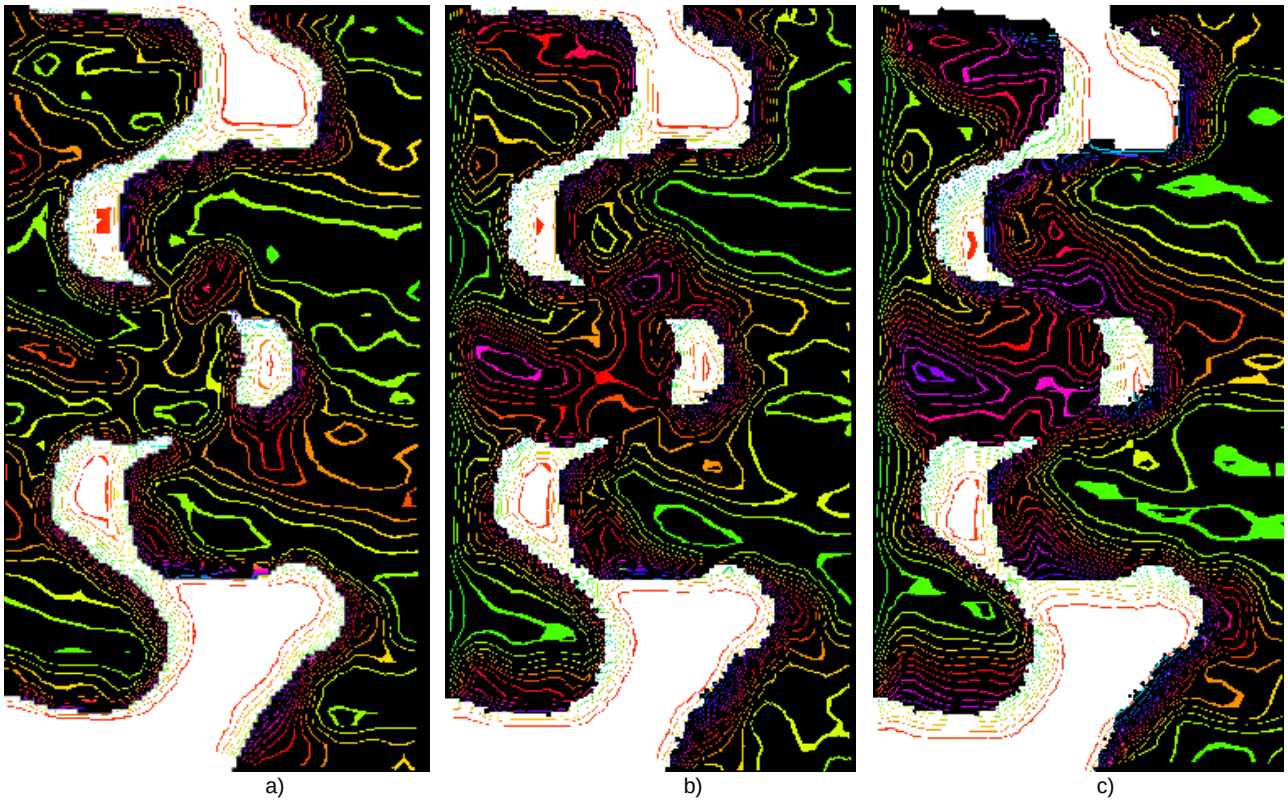

a) b) c)

Fig. 5 - Isoclinics and isochromatics curves for clean gears loaded with:
a) 5 kgf. b) 10 kgf. c) 30 kgf

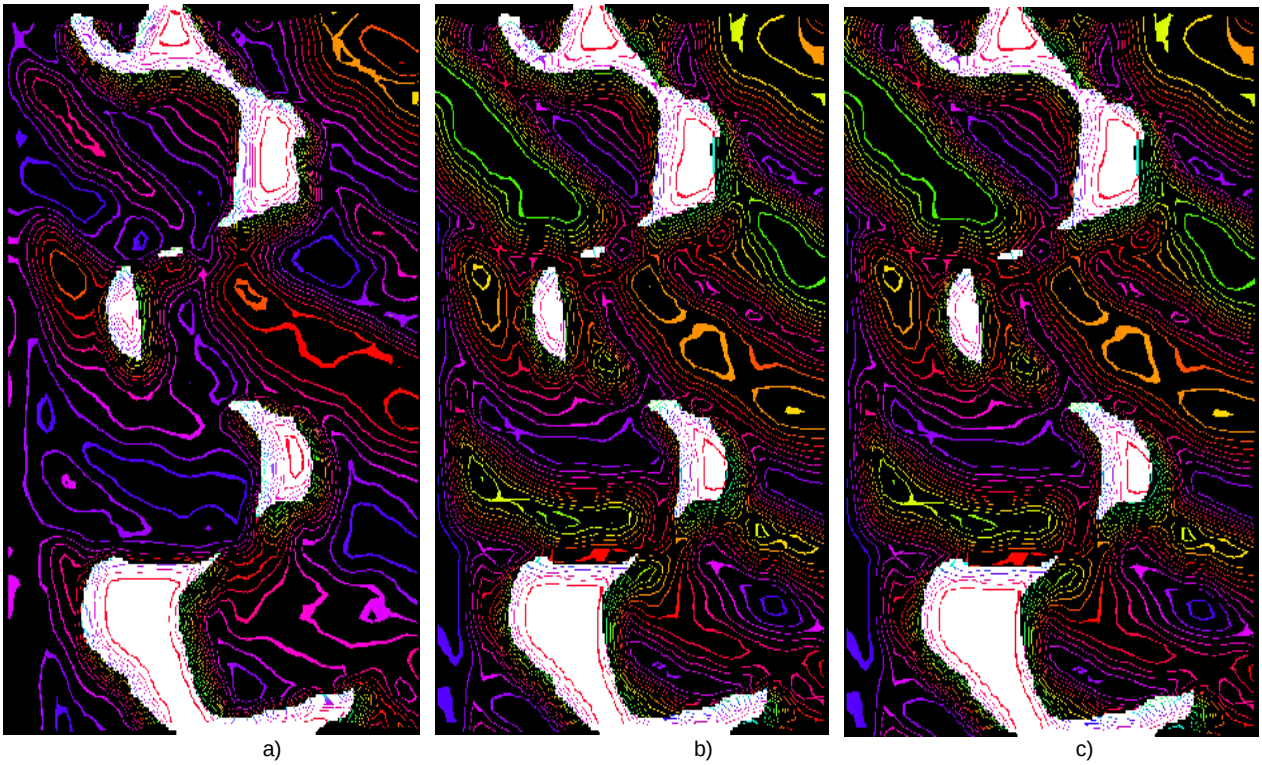

a) b) c)

Fig. 6 - Isoclinics and isochromatics curves for lubricated gears loaded with:
a) 5 kgf. b) 10 kgf. c) 30 kgf

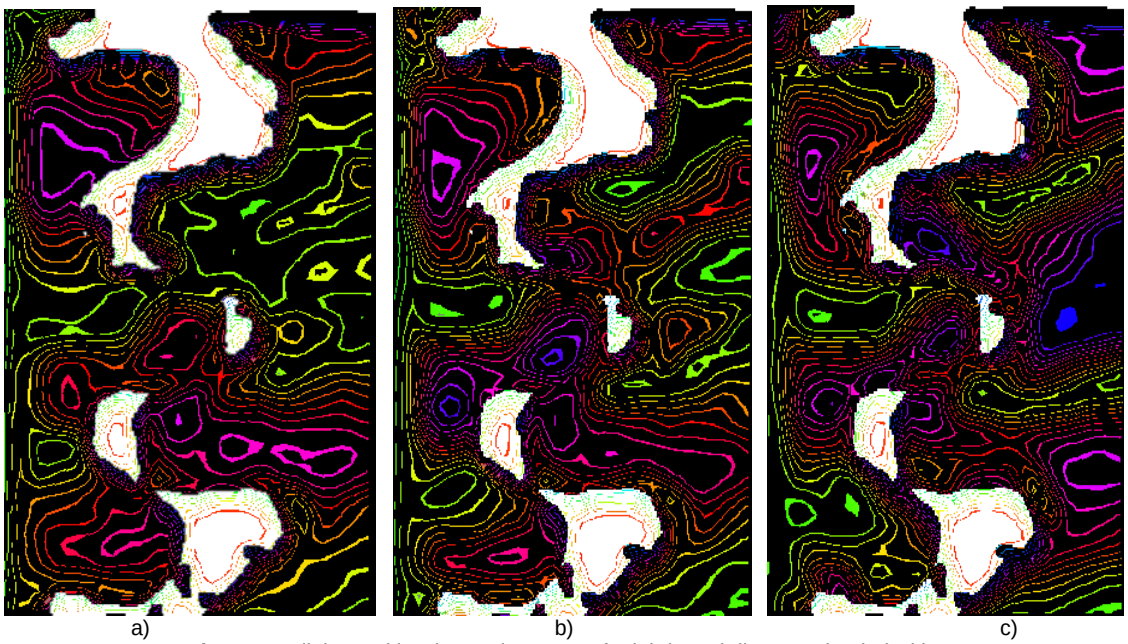

a) b) c)

Fig. 7 - Isoclinics and isochromatics curves for lubricated dirt gears loaded with:
a) 5 kgf. b) 10 kgf. c) 15 kgf

The differentiation of pattern fringes generaterd from deformed and non-deformed gears as shown on Figure 2, 3 and 4 produced a color scale associated to pixel color which varies according to the testing body deformation. The high the color variation, the high the body deformation, which can be verified in all the cases mentioned before. Color pixel variation starting with lubricated dirt gear which presented the highest pixel variation, the clean gear presenting average pixel variation meanwhile the lubricated gear presented the lowest pixel variation. Following, it is possible to state that dirt increases gear deformation, meanwhile lubrication minimizes deformation. Isochromatic lines presented on Figures 5, 6 and 7 when analyzed with the color scale indicate load and deformation concentration to be in close agreement despite the loading conditions, however certain discrepancies are also noted. Isochromatic fringes distribution indicates a clear association of stress with applied force. As loading increased isochromatic fringes spacing decreased, tending to occupy the whole observed area. Fringes distribution density indicates stress concentration. It was also noted that fringes concentrations were initially positioned at gears tooth top and bottom.

As soon as the loading increased, fringes concentration moved to tooth border, following, to gear central areas. Low material density areas, as tooth region, experienced high fringes concentration. The above referred discrepancies, as fringes slops, are associated to gears working conditions; clean gear presented the lowest fringe slop, followed by lubricated gear and finally by the lubricated dirty gear.

CONCLUSIONS

Based on what it has been exposed before, the following conclusions can be drawn. Lubricated gears presented the best load distribution, and the lowest

As figuras resultantes da diferenciação entre as franjas padrões do corpo de prova deformado e não deformado, apresentados nas Figuras 2, 3 e 4, obteve como resultado uma régua graduada relativa à intensidade das cores de pixel. A intensidade dos pixels pode ser relacionada de acordo com a deformação do objeto, i.e., quanto maior for a variação das cores de pixels, maior será a deformação relacionada à força aplicada. Analisando esta variação pixelar, percebe-se que, para todos os casos analisados, houve o aumento da intensidade do pixel à medida que o carregamento aplicado no corpo de prova foi ampliado. Também é notado que, de acordo com a variação dos pixels, a engrenagem com lubrificação apresentou menor variação que os outros casos. A engrenagem lubrificada e com sujeira apresentou o maior índice de variação pixelar, enquanto que a engrenagem limpa ficou com variação intermediária entre os casos. Logo, é possível afirmar que a lubrificação apresenta menores taxas de deformação que a engrenagem trabalhando sem lubrificação alguma e também é possível afirmar que a sujeira é um fator que aumenta consideravelmente a deformação do corpo de prova. Analisando as franjas isocromáticas da Figura 5, 6 e 7, e adotando a régua de cores obtidas pelo processamento da imagem, percebe-se que, comumente, independente da situação de carregamento a concentração de tensão e deformação apresenta situações de comum comportamento e outros de certa discrepância.

Analisando as franjas isocromáticas em termos de espaçamento, pode-se observar que as linhas isocromáticas ficam mais próximas umas das outras, ou seja, ocorre um aumento de tensão proporcional ao aumento da força aplicada. À medida que o carregamento foi ampliado, a distribuição de tensão foi tomando toda a área correspondente ao corpo de prova e seu distanciamento foi diminuindo. Esse aumento de densidade das linhas mostra a concentração de tensões no corpo de prova.

CONCLUSÕES

Pelo que foi exposto acima, pode-se concluir que engrenagens trabalham com melhor distribuição de tensão com lubrificação por ter uma menor variação da

deformation variation. In case of dirt penetration, stress concentration and stress intensity variation as well as deformation were shown to be higher, indicating decreasing element working life.

The results are considered very useful, since the working conditions of farm machinery are severe. In the case dirt material penetrated between gears, stress concentration and intensity variation were noted to be higher which implies in working life reduction.

REFERENCES

[1]. Cohen E. A., (2001) - *Stress Concentration Investigationof holes in Ortotropical Sheet appying the Reflection Fotoelasticity Method*, p.103, PhD. Thesis. University of São Paulo, São Paulo, Brazil;
[2] Dal Fabbro, I. M., Gazzola, J., Rabelo, G. F., Rodrigues, S., (2005) – *Mechanical Behavior of Sugarcane Stalks Under Diametrical Compression Assisted by a Moiré Technique*, In: Proceedings of ITAFE´05, pg. 234-236, ADANA, Turkey;
[3]. Doyle J.F., (2008) - *Hybrid Methods*, Springer handbook of Solid Mechanics, Ed. Sharpe, New York;
[4]. Gazzola J., Affonso E.A., Dal Fabbro I.M., (2013) - *Application of the Moiré Optical Technique in Determining the Deformation Map on Bodies under Axial Loading*, Journal Sinergia, São Paulo, pg. 211-216;
[5]. Gazzola J., Dal Fabbro I.M., Soriano J., Silva M.V.G., Rodrigues S., (2012) - *Photomechanical analysis of wooden testing bodies under flexural loading*, World Academy of Science, Engineering and Technology, v. 70, pg. 396-401;
[6]. Gazzola J., (2011) - *Application of the Moiré Technique in the Stress Distribution Study on Log Bundles Reduced Models and Cut Wooden Pieces*, Master Degree Dissertation. Faculty of Agricultural Engineering, State University of Campinas, SP, 151 p. Brazil;
[7]. Gomes S.T., (2009) - *Calibration of the Moiré Technique Applied to Mechanical Prototypes Profile*, Science and Agrotechnique, vol. 33, no. 2, Lavras Mar./Apr. 2009; http://dx.doi.org/10.1590/S1413-70542009000200033;
[8]. Koda F., (2009) - *Study of Contac Fatigue in Straight Teeths Cylindrical Gears*, Master Degree Thesis, Technological University of Paraná – UTFPR;
[9]. Kuninari F., Dal Fabbro I.M., Lino A.C.L., Almeida C., (2008) - *Moiré aided soil-tractor tire contact area and contact volume determination*, Journal of Agricultural Machinery Science, vol. 4, no. 1, p. 39-43;
[10]. Lei Z., Yun H., Yun D., Kang Y., (2007) - *Numerical analysis of phase-stepping interferometric photoelasticity for plane stress separation*, Optics and Laser in Engineering, vol.45, no.1, pg. 77-82;
[11]. Lino A.C.L., (2008) - *Application of the Phase Displacement Projection Moiré Method in Generating Plant Organs Digital Models*, PhD Thesis, Faculty of Agricultural Engineering, State University of Campinas, SP, 92 p., Brazil;
[12]. Maugis, D., (2000) – *Contact, adesion and rupture in elastic solids*. New York: Springler-Verlag;
[13]. Myiake, et al., (2004) *Experimental Stress Analysis applying Digital Processing of Reflection Fotoelastical Method*. In: Brazilian Society of Computational and Applied Mathematic, Ilha Solteira, v.1, p. 1427-1431;
[14]. Rodrigues L.E.M., (2008) - *Specialization Course on Total Productive Maintenace*, <http://www.ebah.com.br/content/ABAAAe5ocAJ/falhas-engrenagens>;
[15]. Santos A.A., (2002) - Notes on Machine Elements 2, Campinas, march,

deformação do corpo de prova, i.e., a lubrificação ajuda a conservar o elemento de máquina. Nos casos onde há a penetração de sujeira, o comportamento mecânico mostrou que a concentração de tensões e variação da intensidade de tensão e deformação foi maior, o que pode implicar seriamente na diminuição da vda útil do peça. Em projetos de engenharia agrícolas, estas informações são de crucial importância para o dimensionamento de engrenagens utilizados em máquinas, pois as condições de trabalho são de certa agressividade aos elementos mecânicos envolvidos.

REFERÊNCIAS

[1]. Cohen E. A., (2001) - *Investigação da Concentração de Tensões em Furos de Chapas Ortótropas usando o Método da Fotoelasticidade de Reflexão*, 103 p. Tese de Doutorado, Universidade de São Paulo, São Paulo, Brasil;
[2] Dal Fabbro, I. M., Gazzola, J., Rabelo, G. F., Rodrigues, S., (2005) – *Comportamento Mecânico das caules de cana de açúcar Sob diametral Compression Assistido por uma técnica de Moiré*, In: Anais da ITAFE´05, pg. 234-236, ADANA, Turkey;
[3]. Doyle J.F., (2008) - *Métodos híbridos*, Springer manual de Mecânica dos Sólidos, Ed. Sharpe, New York;
[4]. Gazzola J., Affonso E.A., Dal Fabbro I.M., (2013) – *Aplicação da Técnica Óptica de Moiré de Sombra na Determinação do Mapa de Deformações de Corpos Carregados Axialmente*, Revista Sinergia, São Paulo, 211-216;
[5]. Gazzola J., Dal Fabbro I.M., Soriano J., Silva M.V.G., Rodrigues S., (2012) - *Análise fotomecânica de organismos de ensaio de madeira sob o carregamento de flexão*, Academia Mundial da Ciência, Engenharia e Tecnologia, v. 70, pg. 396-401;
[6]. Gazzola J., (2011) - *Aplicação da técnica de Moiré no estudo de estresse Distribuição em modelos Log Bundles reduzidos e cortar pedaços de madeira*, Dissertação de Mestrado. Faculdade de Engenharia Agrícola, Universidade Estadual de Campinas, SP, 151 p., Brazil;
[7]. Gomes, S.T., (2009) - *Calibração da Técnica de Moiré aplicada a perfis de Protótipos Mecânicos, Ciência e Agrotecnologia*, Vol.33, no. 2, Lavras Mar./Abr. 2009; http://dx.doi.org/10.1590/S1413-70542009000200033;
[8]. Koda F., (2009) – *Estudo de Fadiga de Contato em engrenágens Cilíndricos Retos*, Tese de Doutorado, Universidade Tecnológica do Paraná – UTFPR;
[9]. Kuninari F., Dal Fabbro I.M., Lino A.C.L., Almeida C., (2008) - *Moiré iniciou a área de contato do pneu solo-trator e a determinação do volume em contato*, Revista da Maquinaria Agrícola Ciência, vol. 4, no. 1, p. 39-43;
[10]. Lei Z., Yun H., Yun D., Kang Y., (2007) - *Análise numérica de fotoelasticidade em passos em fase interferométrica para a separação em tensão nivelar*, Óptica e Laser em Engenharia, vol. 45, no. 1, p. 77-82;
[11]. Lino A.C.L., (2008) – *Aplicação do Método ao de Moiré de Deslocamento de Fase na Geração de Modelos Digitais de Órgãos de Plantas*, Tese de Doutorado, Faculdade de Engenharia Agrícola, Universidade Estadual de Campinas, Campinas, SP, 92 p., Brasil;
[12]. Maugis, D., (2000) - *Contacto, adesão e ruptura dos sólidos elásticos*. Nova York: Springler-Verlag;
[13]. Myiake, et al., (2004) - *Análise Experimental de Tensões Usando Processamento Digital de Imagens Fotoelásticas de Reflexão*. In: Sociedade Brasileira de Matemática Aplicada e Computacional, Ilha Solteira, v.1, p. 1427-1431;
[14]. Rodrigues L.E.M., (2008) – *Curso de Especialização em Manutenção Produtiva Total*. <http://www.ebah.com.br/content/ABAAAe5ocAJ/falhas-engrenagens>;
[15]. Santos A.A., (2002) - Notes de Elementos de Máquinas 2, Campinas, march,

http://www.fem.unicamp.br/~lafer/em618/, pdf/Apostila%20Engrenagens%204.pdf.
[16]. Sciammarella, C. A. (1982) - *The moiré method – A review*. Experimental Mechanics. v.44, n.8, p. 418-433;
[17]. Spinelli H.A., Silva F.A., (2003) - *Application of Photoelasticity on Structural Analysis of a Riveted Joint for Aeronautical Application*, Anais. Guaratinguetá.

http://www.fem.unicamp.br/~lafer/em618/, pdf/Apostila%20Engrenagens%204.pdf.
[16]. Sciammarella, C. A., (1982) - *O Método de Moiré.* Uma análise. Experimental Mechanics. v.44, n.8, p. 418-433;
[17]. Spinelli H.A., Silva F.A., (2003) - *Aplicação de fotoelasticidade sobre a Análise Estrutural de uma junta rebitada para Aplicação Aeronáutica*, Anais. Guaratinguetá.

INVESTIGATING A POWER TILLER HANDLE AND SEAT VIBRATION ON TRANSPORTATION MODE /
بررسی ارتعاش دسته و صندلی تراکتور دو چرخ در حالت حمل و نقل

MSc.Hossein Ahmadian[1)], Assoc. Prof. Seyed Reza Hassan-Beygi[2)], Assoc. Prof. Barat Ghobadian[3)]
[1)] Department of Agro-technology, College of Abouraihan, University of Tehran, Tehran / Iran
[2)]Dept. Agro-technology, College of Abouraihan, University of Tehran, Tehran / Iran.
[3)] Department of Mechanics of Agricultural Machinery Engineering, Tarbiat Modaress University, Tehran / Iran
Tel. +98 935 1894879; E-mail: ahmadian77@ut.ac.ir

Abstract: *In this paper, a power tiller vibration was investigated at handle position as well as seat position of a trailer pulled by the power tiller. The experiments were conducted at five levels of engine speed, four levels of transmission gear ratio during transportation, and in three directions. Then the weighted 1/3rd octave spectrum was calculated from the narrow band vibration acceleration signals. The amount of vibration damage on operator's body and allowable exposure limits were calculated based on ISO standards. The results showed that the vibration increased with increasing the engine speed for all the gear ratios and directions. The magnitude of vibration was the greatest at vertical direction in all the experiments. The vibration allowable exposure time was in the range of 2.32-5.7 years at the power tiller handle for the different engine speeds and gear ratios. The total equivalent vibration, A (8), at the trailer seat was in the range of 0.5 to 0.87 m/s^2 and it exceeded the allowable limits for the reduced comfort boundary, fatigue-decreased boundary and exposure limit for 8 hours/day. So, it is necessary to reduce the vibration transmitted to the operator's hand and body by designing and developing adequate insulating system.*

Keywords*: Vibration; operator; power tiller; 1/3rd octave; exposure limits*

INTRODUCTION

Applications of agricultural machines especially those machines that were guided entirely by hand, have caused many occupational safety and health problems for their operators. Operator of such equipment has been exposed to high levels of noise and vibration. Long time working with these machines can cause for movement disorders, damage to various organs of the human body including hearing loss, spine and gastrointestinal disorders and even neurological disorders. Continuous use of vibrating machinery can also cause various diseases affecting blood vessels, nerves, muscles and tissues attached to hands and arms. Dr. Maurice Raynaud (1862) initially recognized the symptoms of these diseases. Therefore, the disease was called Raynaud's phenomenon or white finger (1). Aside from these cases, the vibration reduces work efficiency and quality [4]. Economical features and user capabilities of power tillers in various conditions are factors encouraging the increasing use of the machine on farm applications and also for transporting agricultural products and human beings on rural roads [14; 5]. In transportation mode, the power tiller operator's is exposed to vibration transmitted to the hands through the power tiller handle, as well as vibration transmitted to the whole body through trailer seat. Single cylinder diesel engine of a power tiller does not promise a good balance. The forces acting on the piston during compression and power strokes are transmitted to crankshaft and engine block. Due to lack of vibration dampers between the engine and power tiller chassis, the engine forces are entered to the tractor chassis as shock and then through the chassis are transmitted to the power tiller handle as well as drawbar of a trailer mounted to it. The power tiller handle also acts

چکیده: در این تحقیق ارتعاش یک تراکتور دو چرخ در دو موقعیت دسته تراکتور و صندلی تریلر کششی آن بررسی شد. آزمایشها در پنج سطح سرعت موتور، چهار سطح نسبت دنده جعبه دنده و در سه جهت انجام شدند. سپس طیف وزندار شده باند 1/3 اکتاو از سیگنال های شتاب ارتعاش محاسبه شدند. میزان آسیب ناشی از ارتعاش بر روی کاربر و میزان حدود مجاز مواجهه بر مبنای استاندارد های ISO محاسبه گردید. نتایج نشان داد که ارتعاش با افزایش سرعت موتور در تمامی سطوح دنده و در تمتم جهات افزایش می یابد. مقدار ارتعاش در جهت عمودی در تمام آزماش ها بیشترین بود. زمان مجاز مواجهه با ارتعاش برای موقعیت دسته بین 2.32 تا 5.7 سال برای نسبت دنده ها و سرعت های مختلف موتور متغییر بود. مقدار ارتعش کلی معادل 8 ساعت A(8) برای صندلی در محدوده 0.5 تا 0.87 متر بر مجذور ثانیه بود و از حد مجاز راحتی، آسیب و حد مجاز رانندگی 8 ساعته فراتر بود. لازم و ضروری است که ارتعاش منتقل شده به دست و بدن کاربر بوسیله طراحی و توسعه سستم تعلیق مناسب انجام شود.

کلمات کلیدی: ارتعاش؛ کاربر؛ تراکتور دوچرخ؛ 1/3 اکتاو؛ حدود مجاز

مقدمه

کاربرد ماشین های کشاورزی بخصوص آن دسته که با دست هدایت می شوند باعث ایجاد مشکلات متعدد ایمنی و سلامت برای کاربرانشان شده اند. کاربران اینچنین وسایلی در معرض سطوح بالایی از ارتعاش و سروصدا قرار دارند. کار کردن طولانی مدت با این وسایل می تواند باعث بیماریهای حرکتی ، آسیب به ارگان های مختلف بدن انسان از جمله کاهش شنوایی، ستون فقرات و حی بیماریهای روانی گردد. استفاده مداوم از ماشین های مرتعش می تواند به بروز بیماریهای مختلفی از جمله رگهای خونی، اعصاب، عضلات و بافت های متصل به دست و بازو شود. دکتر موریس رینود (1862) اولین بار علائم چنین بیماریهایی را تشخیص داد. بنابراین این بیماری پدیده رینود یا انگشت سفید نامیده می شود (باربر 1992). علاوه براین موارد، ارتعاش بازده کاری و کیفیت آن را کاهش میدهد (گاگلیا و همکاران 2006). مزیت های اقتصادی و امکانات کاربری تراکتور دو چرخ در شرایط گوناگون باعث گسترش روز افزون استفاده از آن در کاربردهای مختلف از جمله حمل و نقل انسان و دام در جاده ها می باشد (سام و کاتیرول 2006؛ حسن بیگی و همکاران 2005). در حالت حمل ونقل کاربر تراکتور دوچرخ در معرض ازتعاشات منتقله به دست و از طریق دسته تراکتور و به بدن از طریق صندلی متصل به تراکتور قرار دارد.
موتور تک سیلندر دیزلی تراکتور دوچرخ دارای تعادل خوبی نیست. نیروی پیستون در مراحل احتراق و تراکم به میل لنگ و بلوک موتور منتقل می شوند. به علت نبود سیتم تعلیق بین موتور و شاسی تراکتور، نیروهای موتور به شاسی منتقل و از آنجا به دسته تزاکتور و همزمان به مالبند تریلر و صندلی آن منتقل می

like a cantilever beam so that one end is attached to the tractor chassis and free vibration of the other end is high [13]. In order to reduce the risks of working with such machines, the regulations have been developed by international organizations to limit working hours and duration of vibration exposure. The ISO standard No.2631 part 1 (1997) for whole body vibrations, ISO standard No.5349 parts 1 and 2 (2001) for hand-arm vibration, and ISO standard No. 8041 (2005) for vibration measuring instrumentation are the examples.

The results of pervious research work showed that farm machinery drivers suffer from higher back pain than the other agricultural workers [3]. [17] reported that the spinal movements caused by vibration were the main reason for these destructive injuries to the body, but the exact reasons have not been provided so far. In an investigation regarding the ergonomic conditions of an 8-HP power tiller, 200 farmers and 100 extension workers were studied. The study revealed that noise and vibration of the power tiller played an important role in damages experienced by them [10]. [11] measured vibration of a 7.5-kW power tiller seat. The results showed that the vibration acceleration increases with increasing forward speed of the power tiller. The vibration Root Mean Square (RMS) values on non-plowed farm were 2 to 2.5 times that of asphalt and dirt rural roads. These researchers recommended that the vibration exposure time for the power tiller operator's should be less than 2.5 hours per day. [12] determined the vibration acceleration envelope curves of a power tiller on transportation mode. The results showed that the maximum vibration amplitude values at operator's arm, wrist, chest, and head positions were occurred at 16Hz, 40Hz, 4Hz, and 5Hz, respectively. [15] assessed the vibrations of a 7.5-HP walking power tiller. Experiments were conducted at stationary condition and plowing operation. The vibration acceleration was measured on locations of chassis and handle of the power tiller as well as arm and chest of the driver. The results revealed that the vibration RMS values increased in all locations with increasing engine speed. It was observed that the dominant frequency of vibration in all locations were equal to engine speed (revolution per second). The vibration RMS values were decreased when transferring from the power tiller handle to the driver's chest. The research work conducted by [16] on power tillers with seat and without seat, showed that the greatest vibration RMS value was observed for the power tiller without seat (45 m/s^2), whereas it was 20 m/s^2 for the power tiller with seat. [2] investigated vibration of a power tiller in transportation mode on asphalt road as well as rotary tillage in dry and submerged farm. Experiments were carried out in three forward speed of 1.11, 1.71 and 2.31 m/s in transportation mode and forward speed of 0.3, 0.45 and 0.65 m/s in rotary tillage. The results showed that the RMS value of vibration in the vertical direction was greater than the other directions for all forward speeds on transportation and rotary tillage. Literature survey showed that there is limited published data concerning vibration characteristics of a 13-HP power tiller on transportation mode. In present study, vibration characteristics of a 13-HP power tiller is evaluated in transportation mode on asphalt rural road for various engine speeds and transmission gear ratios simultaneously at three perpendicular directions at the power tiller handle position as well as seat position of a trailer pulled by the power tiller.

MATERIAL AND METHOD

In this research work, vibration acceleration of a 13-HP power tiller (Mitsubishi CT-82) was measured at the

شود. دسته تراکتور دوچرخ همچنین به صورت یک تیر یک سر در گیر عمل کرده ویک سر آن به شاسی تراکتور متصل بوده و سر دیگر آن ارتعاشات شدیدی خواهد داشت (سالوخه و همکاران 1995). برای کاهش خطرات کار با اینچنین وسایلی سازمان های جهانی سازو کارهایی را درنظر گرفته اند تا ساعات کاری و دوره های در معرض ارتعاش را کاهش دهند. استاندارد ISO 2631 برای ارتعاشات کل بدن و استاندارد ISO 5349 برای ارتعاشات دست و بازو و استانداردر ISO 8041 برای دستگاههای اندازه گیری از این نمونه اند.

نتایج تحقیقات قبلی نشان میدهند، که کاربران ماشینهای کشاورزی از درد ستون فقرات بیشتر از دیگرا کارگران بخش کشاورزی احساس ناراحتی میکنند (فوتوسکا و همکاران 1998). ونگ وهمکاران (2004) دریافتند که حرکت ستون فقرات در اثر ارتعاش دلیل اصلی این اثرات مخرب بر بدن بوده ولی دلیل اصلی تا کنون توضیح داده نشده است. در تحقیقی که شرایط ارگونومیکی یک تراکتور دو چرخ 8 اسب بخار 200 کشاورز و 100 کارگر ماهر بررسی شدند. تحقیق آشکار کرد کهسر و صدا و ارتعاش نقش اساسی در آسیب وارده بر آنان داشت (کانگ و همکاران 1988). مهتا و همکاران (1997) ارتعاشات صندلی یک تراکتور دوچرخ را اندازه گرفتند. نتایج نشان داد که ارتعاشات با افزایش سرعت پیشروی تراکتور دوچرخ افزایش می یابد. میانگین ریشه مربعات ارتعاش (RMS) در زمین شخم نشده 2 تا 2.5 برابر آسفالت و شنی بود. این محققان توصیه کردند که زمان مجاز مواجهه باید کمتر از 2.5 ساعت در روز باشد. احمدیان و همکاران (2013) منحنی های همپوش شتاب ارتعاش تراکتور دوچرخ را در حالت حمل و نقل بررسی کردند. نتایج نشان داد که دامنه ماکزیمم ارتعاشات در موقعیت بازوف مچ، قفسه سینه و سر در 16، 40، 4، و 5 هرتز اتفاق می افتند. تقی زاده علی سرایی (2007) ارتعاش تراکتور دوچرخ پیاده را بررسی کرد. آزمایشها در حالت ایستایی و شخم انجام شدند. شتاب ارتعاش در موقعیت های شاسی و دسته تراکتور و بازو و قفسه سینه کاربر اندازه گیری شد. آزمایشها نشان داد که با افزایش سرعت موتور در تمام موقعیت ها مقدار RMS شتاب ارتعاش افزایش می یابد. مشاهده شد که فرکانس قالب در تمام موقعیت ها برابر با فرکانس دورانی موتور بود. مقادیر RMS ستاب ارتعاش از دسته تا قفسه سینه کاهش یافت. در یک تحقیق توسط تواری و همکاران (2004) بر روی تراکتور های دوچرخ با صندلی و بدون صندلی نشان داد که بیشترین مقدار ارتعاش برای حالت بدون صندلی (45 متر بر مجذور ثانیه) بود در حالی که 20 متر بر مجذور ثانیه برای تراکتور با صندلی بود. دوانگان و تواری (2009) ارتعاش تراکتور دوچرخ را در حالت حمل و نقل در جاده آسفالت و خاکورزی دوار در خاک خشک و زمین مستغرق را بررسی کردند. آزمایشها در سه سرعت 1.11، 1.71 و 2.31 متر بر ثانیه در حالت حمل و نقل و در سه سرعت 0.3، 0.45 و 0.65 متر بر ثانیه در حالت خاکورزی دوار انجام شد.

نتایج نشان داد که RMS شتاب ارتعاش در جهت عمودی در تمامی سرعت های پیشروی در حمل و نقل و خاکورزی دوار بیشترین مقدار را در مقایسه با دیگر جهات داشت. بررسی منابع نشان می دهد که اطلاعات منتشر شده زیادی در مورد بررسی ارتعاش تراکتور دوچرخ 13 اسب بخار وجود ندارد.

مواد و روش ها

در این تحقیق، شتاب ارتعاش یک تراکتور دوچرخ (Mitsubishi CT-82) در موقعیت دسته

right handle grip position as well as the seat position of a trailer attached with the drawbar and pulled by the power tiller. The power tiller specifications were given in Table 1. In order to simulate practical use of the power tiller at transportation conditions, load of 9000 N was placed inside the attached trailer.

تراکتور و صندلی تراکتور دوچرخ در حال کشش با تراکتور اندازه گیری شد.مشخصات تراکتور در جدول 1 داده شده است. برای اینکه شرایط عملی کار با تراکتور فراهم شود بار 9000نیوتن درون تریلر قرار داده شد.

Table 1

Specifications of the power tiller

Combustion system	Internal, diesel, Indirect injection
Stroke cycle	Four-stroke
Rated power	13-hp at 2200 rpm
Air intake system	Naturally aspirated
No. of cylinder	Single, vertical
Cooling system	Water cooled
Number of speeds	Six-forward, two-reverse
Type of clutch	Dry, multi-plates
Steering	Side brake system
Tire size (pneumatic)	152.4-305 mm

Experiments were conducted at five levels of engine speed (1400, 1600, 1800, 2000 and 2200 rpm), four levels of transmission gear ratio (2-light, 3-light, 2-heavy, and 3-heavy), and at the three perpendicular directions (lateral, longitudinal and vertical) on asphalt rural road. Number of three CTC-AC192 types of accelerometers was used to measure vibration of the power tiller at handle grip and the trailer seat positions. The accelerometers were screwed on a 2×2×2 cm^3 metallic cubic and the cubic glued at the power tiller right handle grip (Fig.1a) and the trailer seat (Fig.1b). The experiments were done while the operator was seated on the trailer seat and holding the handles to control the power tiller.

آزمایشها در 5 سطح سرعت موتور (1400ف 1600، 1800، 2000، و 2200 دور بر دقیقه)، 4 سطح نسبت دنده جعبه دنده (2-سبکف 3- سبک، 2- سنگین و 3 سنگین) و سه جهت عمود بر هم (جانبی، طولی و عمودی) روی جاده آسفالت انجام شدند. سه عدد شتاب سنج CTC-AC192 برای اندازه گیری ارتعاش بر روی دسته تراکتور و صندلی تریلر به کار رفت. شتاب سنج ها بر روی یک مکعب فلزی با ضلع 2 سانتی متر پیچ شده و مکعب با چسبیه دسته راست تراکتور(شکل 1 آ) و صندلی تریلر (شکل 1 ب) محکم شد. آزمایشها در حالی انجام شدند که کاربر بر روی صندلی نشسته بود و با دست تریلر را کنترل می کرد.

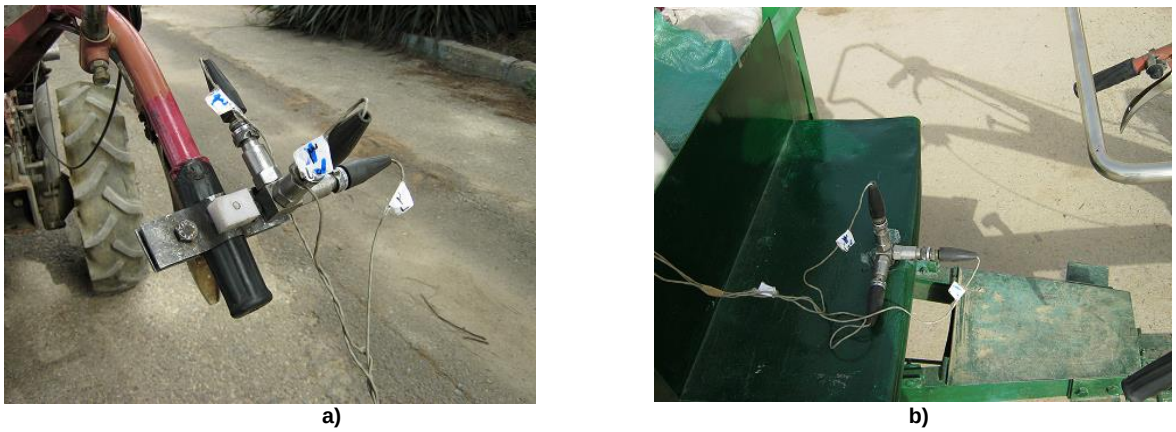

a) **b)**

Fig. 1 - Mounting accelerometers: (a) the power tiller handle grip and (b) the trailer seat

A 24-volt battery and an electronic circuit supplied the required power for this set up. Using an A/D converter, which was recognized and controlled by LABVIEW software program, the accelerometer analog output voltage was converted to digital ones with 40000 Hz sampling rate and recorded on lap-top computer hard disk. Fig.2 shows the instrumentation setup used in this study. The power tiller vibration assessment in time domain was carried out by the RMS values of vibration acceleration. The RMS was calculated by e.q. (1):

یک باتری 24 ولت و مداری الکترونیکی توان مورد نیاز دستگاه را فراهم می کرد. به وسیله یک A/D و نرم افزار LABVIEW ولتاژ آنالوگ خروجی حسگرها با سرعت نمونه برداریی 40000 نمونه در ثانیه به دیجیتال تبدیل شده و بر روی سخت افزار کامپیوتر ذخیره شدند. شکل 2 دستگاهه مورد استفاده در این تحقیق را نشان میدهد. بررسی شتاب ارتعاش در حوزه زمان با مقایسه مقادیر RMS ارتعاش انجام شد که با فرمول (1) محاسبه میشود:

$$a_{RMS} = \left[\frac{1}{T} \int_0^T a(t)^2 dt \right]^{1/2} \quad (1)$$

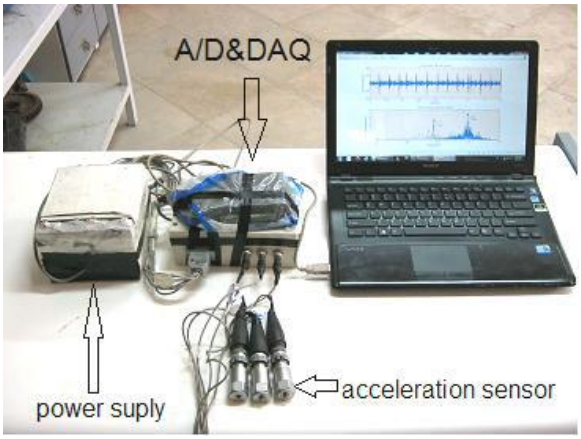

Fig. 2 - Vibration measurement and data acquisition set up

Where: a_{RMS} is root mean square of vibration acceleration (m/s^2), *a(t)* is measured vibration acceleration amplitude (m/s^2), and *T* is duration of measured vibration acceleration (s).

For a detailed investigation of the vibration signals and evaluation of operator health, it is necessary to do the analysis of the vibration signals in frequency domain. The recorded time domain digital signals were converted to frequency domain narrow band signals by fast Fourier transform (FFT) algorithm using MATLAB software program. To overcome the sudden changes and uncertainty of the narrow band signals, the narrow band frequency domain signals were converted to 1/3rd octave frequency band signals by a subroutine computer program. The 1/3rd octave frequency spectrum was weighed in order to calculate the allowable exposure limits and compare with standard values. Then the total weighted vibration acceleration RMS values in frequency domain calculated by Eq.(2):

در اینجا: a_{RMS} ریشه میانگین مربعات شتاب ارتعاش، a(t) دامنه شتاب ارتعاش (متر بر مجذور ثانیه) و T دوره زمانی اندازه گیری ارتعاش می باشد.

برای بررسی بیشتر سیگنالهای ارتعاش و اثرات آن بر کاربر لازم است تا تحلیل این سیگنالها در حوزه فرکانس صورت گیرد. سیگناهای حوزه زمتنی با الگوریتم تبدیل فوریه سریع به سیگنال باند باریک حوزه فرکانس و با نرم افزار MATLAB تبدیل شدند. برای فرار از تغیرات ناگهانی و عدم قطعیت سیگنالهای باند باریک این سیگنالها به سیگناهای باند 1/3 اکتاو تبدیل شدند. سپس این سیگنالها جهت محاسبه حدود مجاز مواجهه و مقایسه با مقادیر استاندارد وزن دار شدند. سپس شتاب وزندار شده کلی ارتعاش با استفاده از فرمول (2) محاسبه شد.

$$a_{RMS,T} = \left[\left(a_{RMS,X}\right)^2 + \left(a_{RMS,Y}\right)^2 + \left(a_{RMS,Z}\right)^2\right]^{1/2} \quad (2)$$

Where: $a_{RMS,T}$ is the root mean square of total weighted vibration acceleration (m/s^2), $a_{RMS,X}$ is the root mean square of weighted vibration acceleration in *X* direction (m/s^2), $a_{RMS,Y}$ is the root mean square of weighted vibration acceleration in *Y* direction (m/s^2), and $a_{RMS,Z}$ is the root mean square of weighted vibration acceleration in *Z* direction (m/s^2). The equivalent vibration acceleration for eight hours, *A(8)*, was calculated, using Eq.(3):

در اینجا $a_{RMS,T}$ ریشه میانگین مربعات شتاب کلی وزندار شده، و X, Y, Z هر یک از سه جهت می باشند. شتاب معادل ارتعاش برای 8 ساعت A(8) مطابق رابطه 3 محاسبه می گردد.:

$$A(8) = \left(a_{RMS,T}\right) \times \sqrt{\frac{t}{T(8)}} \quad (3)$$

Where: t is the time that the body expose to the vibration in a working day, *T(8)* is reference time (eight hours, s), *aRMS,T* is RMS of total weighted vibration acceleration (m/s^2) and *A(8)* is the equivalent vibration acceleration for eight hours working per day (m/s^2).

The amount of vibration damage on operator's body and the exposure limits were calculated in accordance with the ISO standard No.2631 (1997) by comparing the weighted 1/3rd octave acceleration signals with the ISO diagrams. The vibration exposure time for the operator's hand-arm was calculated using Eq.(4), accordance with the ISO standard No.5349 (2001).

در اینجا: t زمانی است که بدن در یک روز کاری در معرض ارتعاش قرار می گیرد، T(8) زمان مرجع برابر با 8 ساعت و $a_{RMS,T}$ ریشه میانگین مربعات شتاب کلی وزندار شده، شتاب معادل ارتعاش برای 8 ساعت A(8) می باشد.

میزان آسیب و حدود مجاز مواجهه کاربر با ارتعاش مطابق استاندارد ISO 2631 با مقایسه شتاب های وزندارشده باند 1/3 اکتاو با نمودار های استاندارد محاسبه شد. رای دست و بازوی کاربر مطابق با استاندارد ISO 5349 و فرمول (4) زمان مواجهه محاسبه شد.

$$\frac{D_y}{year} = 31.8\left(\frac{A(8)}{m/s^2}\right)^{-1.06} \quad (4)$$

where: D_y is time after which in 10% of operators exposed to the amount of hand-arm weighted vibration, *A(8)*, various diseases and disorders, and depreciation on their fingers may occur (year).

RESULTS AND DISCUSSION

1. The time domain vibration acceleration signals

The time domain vibration acceleration signals on vertical direction for the engine speed of 2200 rpm and 3-light gear ratio at the trailer seat and power tiller handle positions are shown in Fig.3a,b, respectively. As depicted from parts of this fig., the maximum peak amplitude at the trailer seat and tractor handle positions were ±10 m/s^2 and ±45 m/s^2, respectively. It is clear that reduction of vibration energy in transmission path from the power tiller engine to the trailer seat is more than that of the power tiller engine to the handle; therefore, the maximum peak amplitude at the seat position was lower than the handle position.

در اینجا D_y زمانی است که دز آن 10% از کاربران پس از 8 ساعت کار روزانه دچار آسیب در دست و انگشتان و علائم بیماری می شوند (بر حسب سال).

نتایج و بحث

1. سیگنالهای شتاب ارتعاش در حوزه زمان

سیگناهای شتاب ارتعاش در حوزه زمان در جهت عمودی و برای سرعت موتور 2200 دور ر دقیقه و در دنده 3-سبک در موقعی های دسته تراکتور و صندلی تریلر در شکل 3 نشان داده شده است. مطابق این شکل مقادیر قله برای صندلی و دسته به ترتیب برابر با 10± و 45± متر بر مجذور ثانیه است. واضح است که کاهش ارتعاش از موتور تا صندلی بیشتر از موتور تا دسته تراکتوز می باشد.

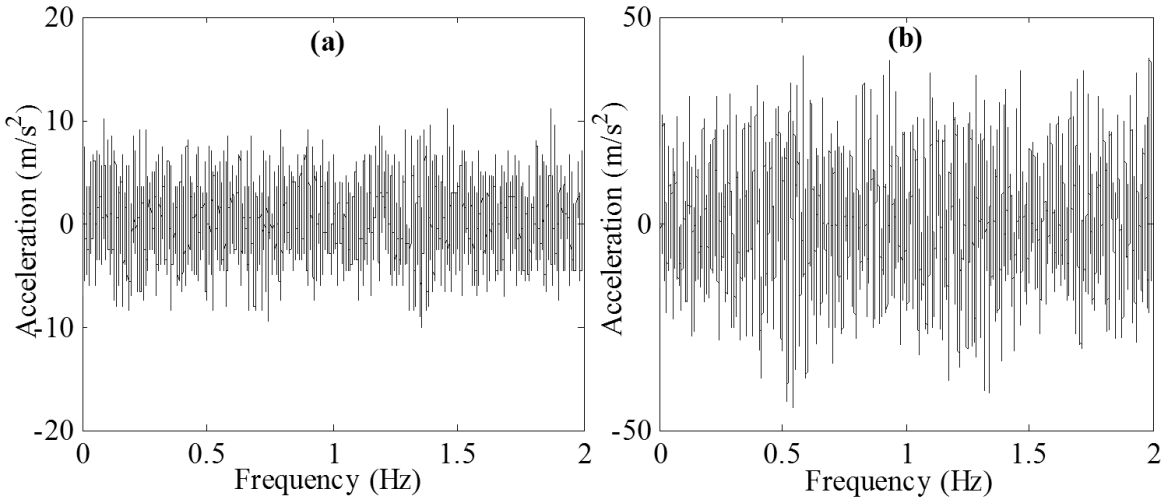

Fig. 3 - The time domain vibration acceleration signals on vertical direction for the engine speed of 2200 rpm and 3-light gear ratio at: (a) the trailer seat (b) the handle positions

Fig.4 shows the RMS values of total vibration acceleration (sum of the three x, y, and z directions) in time domain for the different engine speeds and gear ratios at the power tiller handle position. The total acceleration RMS values were in the range of 14-26 m/s^2 for the various engine speeds and gear ratios. The vibration RMS values increased for all the gear ratios when the engine speed is increased from 1400 to 2000 rpm. With increasing the engine speed, number of combustion strokes and the piston blows per the unit time were increased. Therefore, vibration at the base of the handle that was attached to the power tiller chassis is increased, consequently the vibration at the free end of the handle is also increased. This trend is confirmed by the other researchers for similar investigations [13; 14; 15]. However, the increasing trend is not observed at 2200 rpm engine speed because this speed is the rated engine speed. At this engine speed, the engine and its components are dynamically balanced. The maximum and minimum increases in vibration acceleration are observed for 2-light and 3- light gear ratios, respectively when the engine speed ranges from 1400 to 2200 rpm.

شکل 4 مقادی شتاب کلی ارتعاش را در حوزه زمان و برای نسبت دنده های مختلف و سرعت های متفاوت در دسته و صندلی نشان می دهد. مقادیر RMS کلی شتاب ارتعاش در محدوده 14-26 متر بر مجذور ثانیه و برای سرعتهای موتور و نسبت های دنده متفاوت می باشد. در تمام دنده ها هنگام افزایش سرعت موتور از 1400 تا 2000 میزان شتاب ارتعاش افزایش می یابد. با افزایش تعداد احتراق و تعداد ضربات پیستون در واحد زمان و سرعت موتور ارتعاش در شاسی افزایش یافته و سپس ارتعاش در سر آزاد دسته افزایش می یابد. ای روند در تحقیقات دیگر محققین نیز مشاهده شده است (سام و کاتیرول 2006، سالوخه و همکاران 1995، تقی زاده علی زاده سرائی 2007). اگرچه این روند برای دور 2200 مشاهده نشد و علت آن این است که این دور دور مشخصه موتور است. در این سرعت موتور موتور و اجزای متحرک آن دارای تعادل دینامیکی هستند. بیشینه و کمینه افزایش ارتعاش در دنده 2-سبک و 3-سبک مشاهده شد.

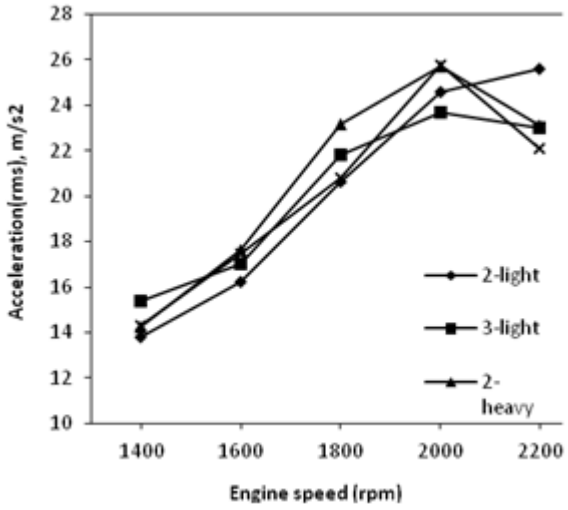

Fig. 4 - The effect of engine speed on the RMS values of total vibration acceleration for different gear ratios at the handle position

Variations of the total vibration acceleration RMS values versus the engine speed at the trailer seat position in time domain are shown in Fig.5 for the different engine speeds and gear ratios. The total acceleration RMS values were in the range of 2.8-4.8 m/s^2. With increasing engine speed, the vibration RMS values at the trailer seat position are increased for all the gear ratios. The reason for this increasing trend might be attributed to increasing number of combustion strokes and the piston blows per unit time. Of course, the vibration RMS increase at this position is lower than the handle position that could be as a result of dissipation of vibration energy and structural damping. The maximum and minimum increase in vibration acceleration is observed for 2-heavy and 3-heavy gear ratios, respectively when the engine speed is increased in range of 1400-2200 rpm. The variations of vibration acceleration in the different gear ratios for the engine speeds of 1400, 1600, 1800, 2000 and 2200 rpm were about 0.5, 0.7, 0.9, 1.1, and 1.3 m/s^2, respectively. The reason for these variations might be attributed to the trailer oscillations due to changing forward speeds or in other words, the effects of road unevenness.

Investigation of vibration signals in time domain revealed that the accelerations for the vertical direction were greater than the lateral and longitudinal directions, which could be attributed to vertical movement of piston within the diesel engine cylinder.

تغییرات ارتعاش در سرعت های مختلف موتور در موقعست صندلی در شکل 5 نشان داده شده است. مقادیرRMS شتاب ارتعاش در محدوده 2.8 تا 4.8 متر بر مجذور ثانیه متغیر است. با افزایش سرعت موتور در تمام دنده ها مقدار ارتعاش افزایش می یابد که علت آن می تواند افزایش تعداد مراحل احتراق در واحد زمان باشد. البته افزایش ارتعاش در موقعیت صندلی کمتر از افزایش آن برای دسته است که علت آن می تواند میرا شدن انرژی ارتعاش در اثر میرایی سازه ای باشد. بیشینه و کمینه شتاب ارتعاش در 2-سنگین و 3 سنگین مشاهده شد. تغییرات شتاب ارتعاش در دنده های مختلف و سرعت های موتور 1400، 1600، 1800، 2000 و 2200 دور بر دقیقه به ترتیب برابر با 0.5، 0.7، 0.9، 1.1 و 1.3 متر بر مجذور ثانیه بود. دلیل این تغییرات می تواند در اثر تغییرات سرعت پیشروی و ناهمواری های جاده باشد. بررسی سیگناهای ارتعاش در حوزه زمان آشکار کرد که در جهت عمودی ارتعاش بیشتر از جانبی و طولی بود که ممکن است در اثر حرکت عمودی پیستون در سیلندر باشد.

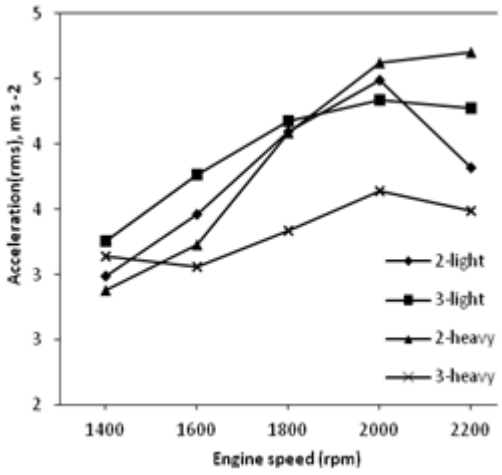

Fig. 5 - The effect of engine speed on the RMS values of total vibration acceleration for the different gear ratios at the trailer seat

2. The frequency domain vibration acceleration signals

Fig. 6 shows the narrow band frequency spectrum of vibration acceleration on vertical position for the trailer seat and power tiller handle positions at 2200 rpm engine speed and 3-light gear ratio. The maximum amplitude peaks at the trailer seat and handle positions reached to 1.5 m/s^2 and 10 m/s^2, respectively. Structural damping and reduction of vibration energy in transmission path might be responsible for peak amplitude reduction. At the handle position, the vibration acceleration amplitudes are damped strongly at frequencies greater than 200 Hz. The acceleration value at the handle position was very high in certain frequencies, which was due to free vibration of the power tiller handle. The power tiller handle acts as a cantilever beam with base excitation and free vibration at the end [13]. This phenomenon is also confirmed for a 7.5-HP power tiller vibration [15]. At the handle position, the maximum amplitude peak is occurred at 36.7 Hz which is related to rotational speed of the engine i.e. 2200 rpm. However, at the trailer seat position, the maximum amplitude peak is observed at 73.3 Hz which is related to two times of engine speed.

Due to un-smoothed nature of narrow band frequency spectra, comparing the data for different conditions is not so easy. Therefore, in order to explain the results and to calculate the vibration allowable exposure limits and compare with standard values, the smoother 1/3rd octave vibration frequency band is selected.

1. سیگنال های شتاب ارتعاش در حوزه فرکانس

شکل 6 طیف باند باریک شتاب ارتعاش را درجهت عمودی برای دسته تراکتور و صندلی تریلر و دور 2200 دور بردقیقه در دنده 3-سبک نشان می دهد. مقادیر قله به 1.5 و 10 متار بر مجذور ثانیه می رسد. میرایی سازه ای در مسیر انتقال ارتعاش می تواند علت این تفاوت باشد. در موقعیت دسته دامننه ارتعاش به شدت برای فرکانس های بالاتر از 200 هرتز به شدت کاهش می یابد.

مقدار شتاب ارتعاش در موقعیت دسته در فرکانس هایی خاص بسیار بالاست که در اثر ارتعاشات آزاد دسته تراکتور می باشد که همانند یک تیر یک سر در گیر عمل می کند (سالوخه وهمکاران 1995). این پدیده همچنین توسط تقی زاده علی سرائی (2007) تایید شد. در موقعیت دسته بیشینه قله در 36.7 هرتز اتفاق می افتد که مرتبط با سرعت دورانی 2200 دور بر دقیقه موتور است. اگرچه در موقعیت صندلی مقدار قله در 73.3 هرتز بود که دو بربر سرعت موتور است.

به علت ماهیت متغییر سیگنالهای باند باریک ارتعاش مقایسه بین طیف های دو حالت مختلف کار آسانی نیست. بنابراین برای برای محاسبه حدود مجاز مواجهه و مقایسه با مقادیر استاندارد از باند فرکانسی 1/3 اکتاو استفاده می شود.

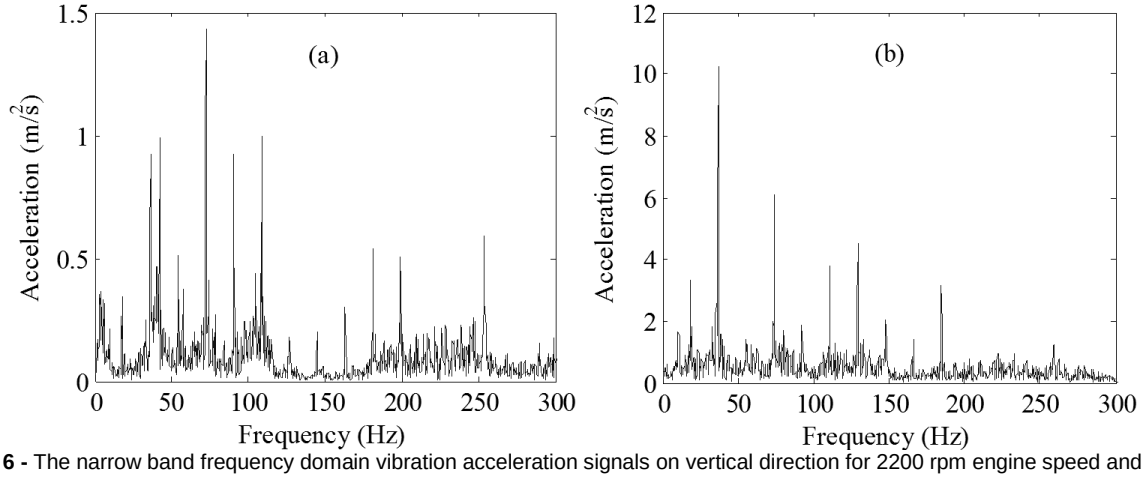

Fig. 6 - The narrow band frequency domain vibration acceleration signals on vertical direction for 2200 rpm engine speed and 3-light gear ratio at: (a) the trailer seat and (b) the handle positions

2.1. The 1/3rd octave spectrum of vibration acceleration at the tractor handle position

Fig.7 shows the effect of engine speed on 1/3rd octave total weighted vibration acceleration (sum of the three directions x, y and z) at the handle position for the different gear ratios. Different parts of this Fig. showed that at frequencies more than 100 Hz, the vibration acceleration was less than 1 m/s^2. However, at frequencies less than 100 Hz, the total weighted acceleration did not show uniform variations for the different engine speeds and gear ratios. As illustrated in Fig. 7, the vibration acceleration amplitude has some peaks at center frequencies of 12.5, 16, 20, 25, 31.5, and 40 Hz for the different gear ratios. The peaks observed at center frequency of 25, 31.5, and 40 Hz could be related to 1400 and 1600 rpm, 1800 to 2000 rpm, and 2200 rpm engine speed, respectively. The peaks at center frequencies of 12.5, 16 and 20 Hz could

1.2.طیف 1/3 اکتاو شتاب ارتعاش در موقعیت دسته تراکتور دوچرخ

شکل 7 اثرات سرعت دورانی موتور را بر شتاب کلی وزندار شده در موقعیت دسته نشان میدهد. قسمتهای مختلف این شکل نشان میدهد که برای فرکانسهای بالاتر از 100 هرتز شتاب وزندار شده دارای تغییرات زیادی در سرعتهای مختلف موتور و نسبت دنده های متفاوت نمی باشد. مطابق شکل 7 ارتعاش دارای قله هایی در 12.5، 16، 20، 25، 31.5، و 40 هرتز در دنده های مختلف می باشد. قله های مشاهده شده در مراکز فرکانسی 25 تا 31.5 هرتز و 40 هرتز می تواند مربوط به 1400 تا 1600 دور ردقیقه و 1800 تا 200 دور بر دقیقه باشند. قله های موجود در فرکانس های 12.5 و 16 هرتز و 20 هرتز می تواند مربوط به فزآیند احتراق و ارتعاشات

be related to the combustion process frequency and frequency of engine components including camshaft and injection pump, which had one half speed of the engine crankshaft. As depicted from this Fig., the greatest peak of vibration acceleration is observed in frequency of 31.5 Hz for all the gear ratios except 2-light. The maximum amplitude for 2-light gear ratio is observed at 40 Hz, which could be due to handle resonance. The maximum peak (11 m/s^2) at the frequency of 31.5 Hz is related to 2000 rpm engine speed and 3-heavy gear ratio. According to Fig. 7, the amplitude of total vibration acceleration in the frequency range of 10 to 80 Hz is greater than the allowable vibration exposure limit (2 m/s^2) for hand-arm. Investigation of [14] on a 7.5-HP power tiller at handle position and transportation mode with an empty trailer showed that the measured vibration was more than that of the hand-arm allowable vibration exposure limit.

2.2. The allowable exposure time for operator's hand-arm

The equivalent vibration acceleration for eight hours, A(8), at the power tiller handle position for the different gear ratios and engine speeds is shown in Fig. 8. The equivalent acceleration was increased with increasing the engine speed from 1400 to 2000 rpm for all the gear ratios at the handle position. The equivalent acceleration was reduced with further increase in the engine speed to 2200 rpm. The equivalent acceleration values in 2-heavy gear ratio at the engine speeds of 1600, 1800 and 2000 rpm are more than the other gear ratios. It seems that at the 2-heavy gear ratio, the vibration generated at the power tiller gearbox caused for resonance in the handle.

اجزای موتور مانند میل لنگ، پمپ انژکتور باشد که 1/2 سرعت موتور را دارد. مطابق این شکل بیشینه ارتعاش در فرکانشس 31.5 هرتز بود غیر از دنده 2-سبک. در این دنده مقدار بیشینه در فرکانس 40 هرتز رخ می دهد که ممکن است مربوط به رزونانس دسته باشد. مقدار قله (11 متر بر مجذور ثانیه) در فرکانس 31.5 هرتز و دور 200 دور بر دقیقه و دنده 3-سنگین رخ داده است.

مطابق شکل 7 مقدار دامنه ارتعاش در محدوده 10 تا 80 هرتز بزرگتر از حد مجاز ارتعاش (2 متر بر مجذور ثانیه) برای دست و بازو می باشد. در تحقیق سام و کاتیرول (2006) بر روی تراکتور دوچرخ 7.5 اسب بخار در دسته در حالت حمل و نقل تریلر خالی مشخص شد که ارتعاشات از حد مجاز بالاتر است.

2.2. زمان مجاز مواجهه برای دست و بازو

شتاب معادل ارتعاش 8 ساعته A(8) در موقعیت دسته برای نسبت دنده های مختلف و سرعت های موتور متفاوت در شکل 8 نشان داده شده است. شتاب معادل با افزایش 1400 تا 2000 دور بردقیقه و برای همه نسبت دنده ها افزایش بافت. ولی با افزایش بیشتر به 2200 دور بر دقیقه ارتعاش کاهش می یابد. شتاب معادل در دنده 2-سنگین و سرعت موتور 1600، 1800 و 2000 دور بر دقیقه بزرگتر از مقدار آن در سایر دنده ها بود. به نظر میرسد که در دنده 2-سنگین ارتعاش ایجاد شده در گیربکس باعث تشدید دسته تراکتور شده است.

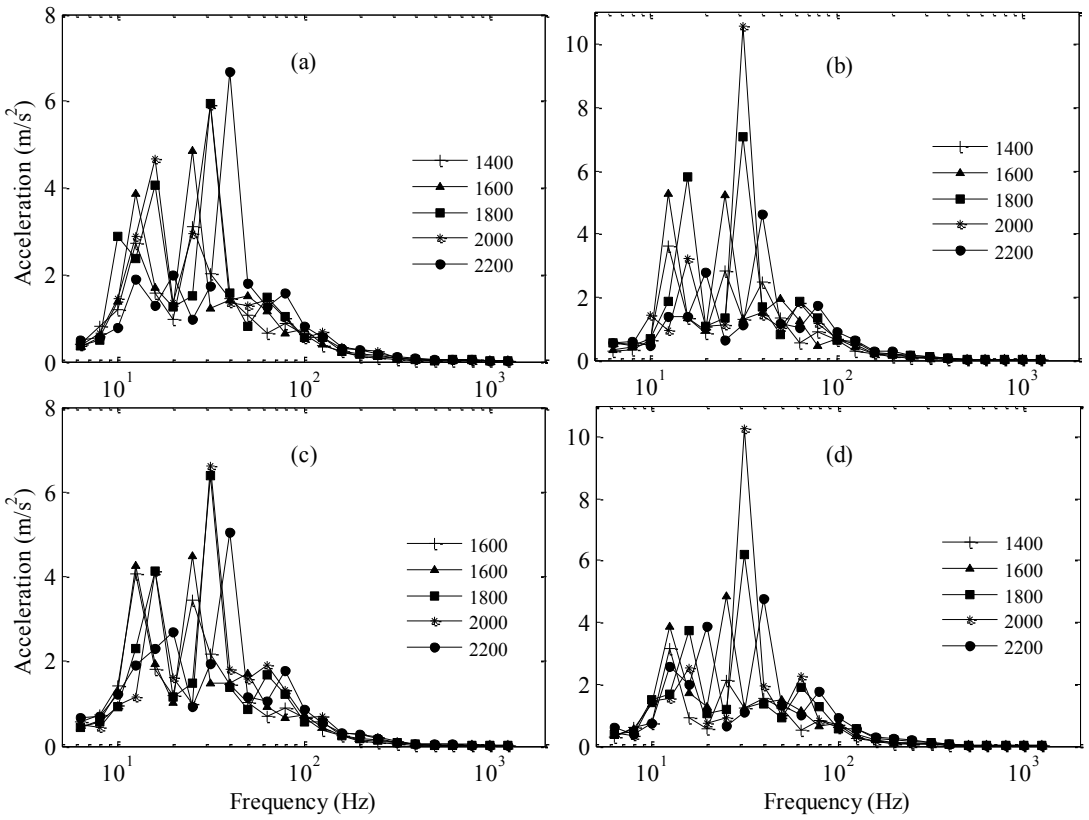

Fig. 7 - 1/3rd octave frequency band of total weighted acceleration for the different engine speeds at the handle position for gear ratios of: (a) 2-light, (b) 3-heavy, (c) 3-light, and (d) 2-heavy.

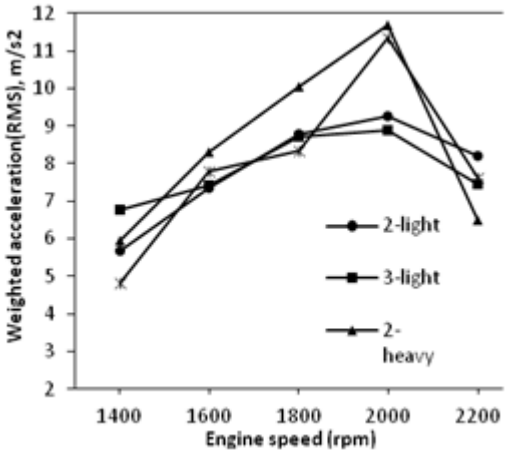

Fig. 8 - The effect of engine speed on the equivalent vibration acceleration, A(8), for the different gear ratios at the handle position

Fig. 9 shows the vibration allowable exposure time of the power tiller operator's hand-arm versus engine speed for the different gear ratios. The allowable exposure time was in range of 2.32 to 5.7 years for the different engine speeds and gear ratios. The allowable exposure time decreased for all the gear ratios when the engine speed was increased from 1400 to 2000 rpm. The allowable exposure time was increased at 2200 rpm engine speed for all the gear ratios, which could be related to more dynamic balance of the engine at the rated speed. The Fig. illustrated that after 2.32 years (at 2000 rpm engine speed and 2-heavy gear ratio) in 10% of the operators' exposed to the power tiller handle vibration the finger worn could be expected. It was reported that the vibration allowable exposure time of power tillers decreased with increasing the engine speed and travel speed. The allowable exposure time is reported in the range of 1.2 years for walking power tiller at tillage operation to 12 years for power tiller during pulling an empty trailer [14; 15; 16].

شکل 9 زمان مجاز مواجهه دست وبازو با ارتعاش دسته تراکتور دوچرخ را نشان می دهد. زمان نجاز مواجهه در محدوده 2.32 تا 5.7 سال برای نسبت دنده هه و سرعت های مختلف موتور می باشد. زمان مجاز مواجهه با افزایش سرعت موتور از 1400 تا 2000 دور بر دقیقه کاهش می یابد. برای تمتم نسبت دنده ها در 2200 دور بر دقیقه زمان مواجهه افزایش می یابد که میتواند در اثر تعادل بیشتر دینامیکی موتور و قطعات آن باشد. این شکل نشان می دهد که پس از 2.32 سال (در 2200 دور بر دقیقه و دنده 2-سنگین) در 10% از کاربران تراکتور دوچرخ بیماری دست و فرسودگی انگشتان میتواند رخ دهد. گزارش شده است که با افزایش دور موتور و سرعت پیشروی زمان مواجهه کاهش می یابد. زمان مواجهه برای تراکتور دوچرخ کنترل پیاده 1.2 سال تا 12 سال برای تراکتور دوچرخ در حال حمل و نقل تریلر خلی گزارش شد (سام و کاتیرول 2006، تقی زاده 2007، توای و همکاران 2004).

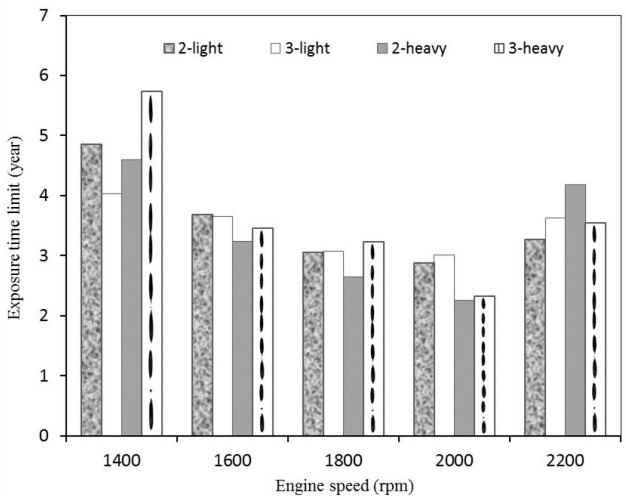

Fig. 9 - The effect of engine speed on the vibration allowable exposure time of the power tiller operator's hand-arm for the different gear ratios

2.3. The 1/3rd octave spectrum of vibration acceleration at the trailer seat position

The effect of engine speed on 1/3rd octave total weighted vibration acceleration (sum of the three directions x, y and z) at the trailer seat position for the different gear ratios is shown in Fig.10. Investigation of the 1/3rd octave spectra showed that the vibration amplitude was not considerable for frequencies more than 100 Hz for all the

3.2. طیف 1/3 اکتاو شتاب ارتعاش صندلی تریلر

اثرات سرعت موتور بر طیف 1/3 اکتاو شتاب وزندار شده ارتعاش صندلی تریلر برای دنده های مختلف در شکل 10 نشان داده شده است. بررسی طیف 1/3 اکتاو نشان می دهد که دامنه ارتعاش برای فرکانسهای بالاتر از 100 هرتز و

gear ratios and engine speeds. Meanwhile, the human body is sensitive to frequency range of 1 to 80 Hz (ISO 2631, 1997). Therefore, the Fig. 10 was drawn in the frequency range of 1 to 100 Hz. Different parts of Fig. 10 depicted that the total weighted vibration acceleration had some peaks at frequencies smaller than 10 Hz, which could be attributed to the ground effects. At frequencies smaller than 10 Hz, the investigations showed that the number of frequencies at which the vibration amplitude exceeded 0.2 m/s^2 for 3-light gear ratio were more than the other gear ratios (Fig. 10c), which could be attributed to more oscillation of the trailer seat due to faster forward speed of the trailer at this gear ratio.

در تمان دندهها و سرعت های موتور ناچیز است. در حالی که بدن انسان به فرکانس های 1 تا 80 هرتز بیشتر حساس است بنابراین شکل 10 از 1 تا 100 هرتز را نشان میدهد. مطابق این شکل ارتعاش دارای تعدادی قله در فرکانسهای کمتر از 10 هرتز است که می تواند ناشی از اثرات زمین باشد. در فرکانسهای زیر 10 هرتز تعداد فرکانشهای که ارتعاش در آنها از 0.2 متر بر مجذور ثانیه بیشتر است از دیگر دنده ها بیشتر است. که مربوط به افزایش سرعت پیشروی در این نسبت دنده باشد.

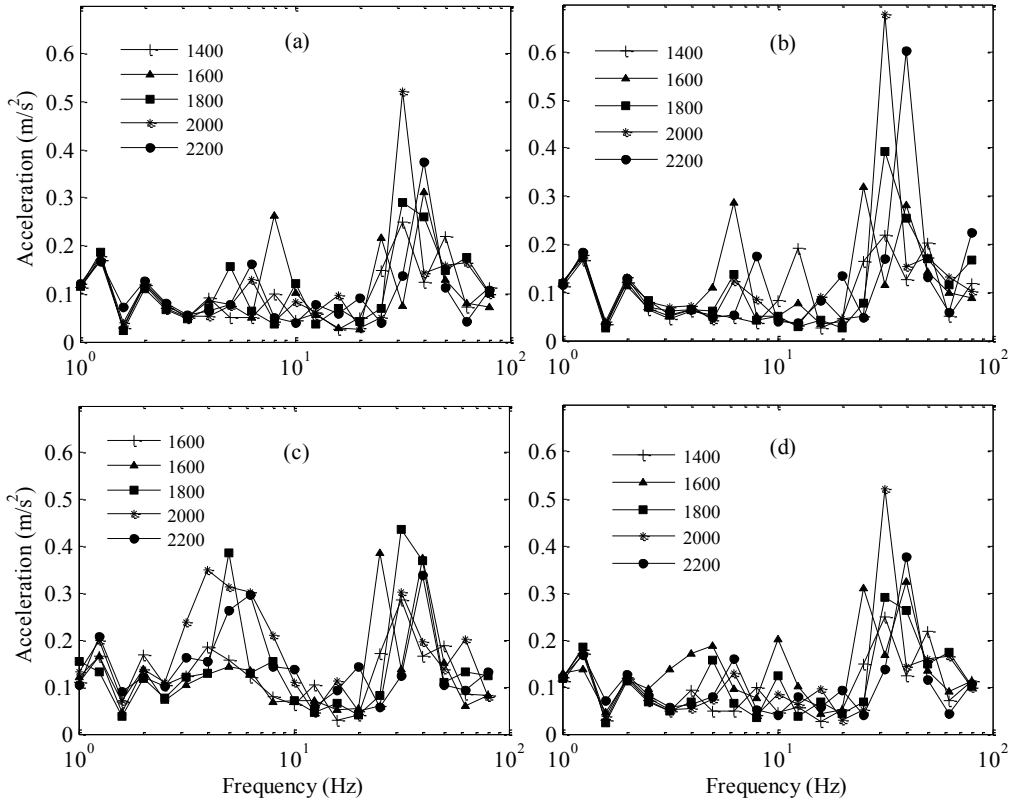

Fig. 10 - 1/3rd octave frequency band of total weighted acceleration for the different engine speeds at the trailer seat position for gear ratios of: (a) 3-heavy, (b) 2-heavy, (c) 3-light, and (d) 2-light

At frequencies greater than 20 Hz, the total weighted vibration acceleration had some peaks at center frequencies of 25, 31.5, and 40 Hz, that is attributed to the engine rotational speed. The maximum peak observed at center frequency of 31.5 Hz for all the gear ratios, which could be related to 1800 and 2000 rpm engine speeds. The maximum vibration amplitude is observed for 2-heavy gear ratio at frequency of 31.5 Hz with amplitude of 0.69 m/s^2 (Fig.10b). The vibration acceleration for frequency range of 25-40 Hz had amplitude greater than that of 0.3 m/s^2 for all the gear ratios, which was in the range of a little uncomfortable (ISO standard No. 2631, 1997). The vibration for 2-heavy gear ratio had amplitude greater than of 0.5 m/s^2 for frequency range of 25-40 Hz that was in the range of almost uncomfortable (ISO standard No.2631, 1997).

2.4.The allowable exposure time for operator's whole body

The total equivalent vibration acceleration for eight hours, A(8), at the trailer seat position for the different gear ratios and engine speeds is shown in Fig.11. The total equivalent vibration was in the range of 0.5 to 0.87

در فرکانس های بزرگتر از 20 هرتز شتاب کلی ارتعاش وزندار شده در فرکانس های 25، 31.5، 40 هرتز دارای قله است که مربوط به سرعت دورانی موتور است. بیشینه قله در فرکانس 31.5 هرتز در تمام دنده ها است که می تواند مربوط به سرعت موتور در 1800 و2000 دوربردقیقه باشد. بیشینه شتاب ارتعاش در دنده 2-سنگین و فرکانس 31.5 هرتز با دامنه 0.69 متر بر مجذور ثانیه مشاهده شد.

شتاب ارتعاش برای محدوده فرکانسی 25-40 هرتز بزرکتر از 0.3 متر بر مجذور ثانیه است که در محدوده کمی ناراحت (ISO standard No. 2631, 1997). دامنه ارتعاش در دند 2-سنگین بزرگتر از 0.5 متر بر ثانیه در محدوده 25-40 هرتز که در ناحیه ناراحت قرار دارد (ISO standard No. 2631, 1997).

4.2. زمان مجاز مواجهه کل بدن

شتاب معادل ارتعاش 8 ساعت برای موقعیت صندلی و دندها و سرعت های مختلف موتور در شکل 11 نشان داده شده است. مقدار شتاب معادل بین 0.5 تا 0.87 متر بر مجذور ثانیه است. شتاب معدل صندلی با افزایش سرعت موتور از

m/s^2. The seat equivalent acceleration is increased with increasing the engine speed from 1400 to 2000 rpm. The seat equivalent acceleration at 3-light gear ratio was the maximum value for all the engine speed levels except for 2200 rpm that could be caused by an increase in the power tiller forward speed. The variations of vibration acceleration in the different gear ratios at the engine speeds of 1400, 1600, 1800, 2000 and 2200 rpm were about 0.11, 0.13, 0.3, 0.2, and 0.25 m/s^2, respectively. The reason for these variations might be attributed to the trailer oscillations due to changing the forward speed, in other words the ground effect. The equivalent trailer seat acceleration, *A(8)*, is compared with the standard exposure limits for whole body vibration in Fig.12. As depicted in this fig., the weighted acceleration at the trailer seat exceeded the allowable limits for the reduced comfort boundary and fatigue-decreased boundary as well as it is about surpass the exposure limit for eight hours working per day. [14] have also reported that the allowable exposure time was eight hours for a power tiller pulling an empty trailer in transportation on asphalt rural road, and four hours in farm road.

1400 به 2000 افزایش می یابد. شتاب ارتعاش در دنده 3-سبک دارای مقدار بیشینه است که می تواند به علت افزایش سرعت پیشروی باشد. تغییرات شتاب معدل ارتعاش در دنده های مختلف و برای سرعت های موتور 1400، 1600، 1800، 2000، و 2200 به ترتیب برابر با 0.11، 0.13، 0.3، 0.2 و 0.25 متر بر مجذور ثانیه بود. دلیل این نوسانات می تواند مربوط به نوسانات تریلر در اثر تغییر سرعت پیشروی یا اثرات جاده باشد. در شکل 12 شتاب معدل صندلی تراکتور دوچرخ A(8) با حدود مجاز مواجهه کل بدن در استاندار مقایسه شده است.. مطابق این شکل شتاب وزندار شده معدل صندلی از حد مجاز کاهش راحتی و حد آسیب گذشته و تقریبا در حال گذشتن از حد مجاز رانندگی 8 ساعته است. سام وکاتیرول (2006) نیز گزارش کردند که تعداد ساعات مجاز کار با تراکتور دوچرخ در حال حمل تریلر خالی برابر با 8 ساعت در روز برای حملو نقل در جاده آسفالت و 4 ساعت برای جاده مزرعه ای است.

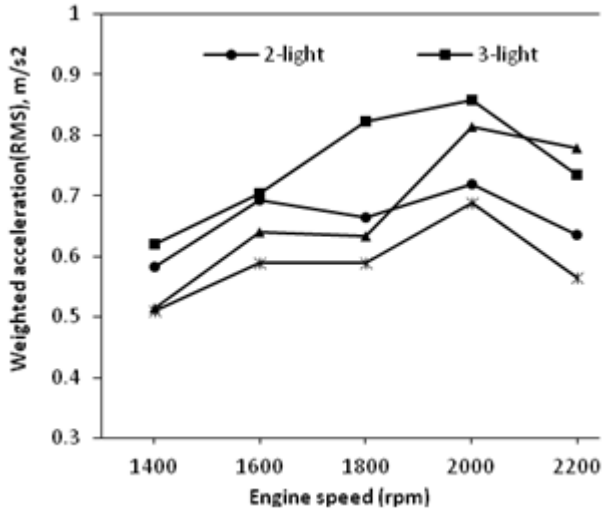

Fig. 11 - The effect of engine speed on the total equivalent acceleration, A(8), for the different gear ratios at the trailer seat position

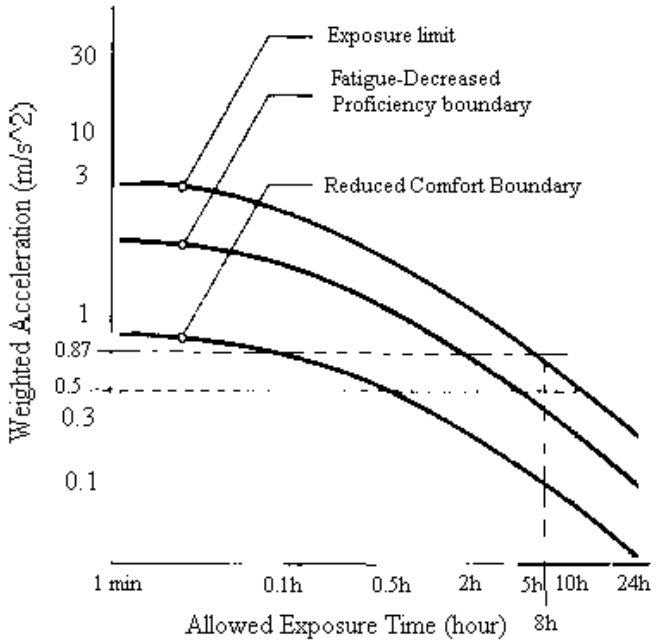

Fig. 12 - The equivalent acceleration for eight hours exposure to the trailer seat vibration, A(8), and its comparison with standard limits

Fig. 13 shows the maximum and minimum values of 1/3rd octave acceleration of the trailer seat position at the vertical direction for the different engine speeds and gear ratios which are compared to standard allowable driving time (ISO standard No. 2631, 1997) in the frequency range of 1 to 80 Hz. As shown in this Fig., the standard allowable driving time at frequency ranges of 4-6.3 Hz and 31.5-40 Hz was shorter than eight hours per day. The maximum acceleration was in frequency range of 31.5-40 Hz that could be related to the power tiller engine speed.

For the longitudinal direction, the vibration acceleration was less than standard eight hours limit at any frequency. Unlike the vertical direction, the vibration levels for the longitudinal direction was not considerable at frequencies related to the engine speed, which could be attributed to the placement of the engine related to chassis as well as existence of the trailer connection with drawbar and their effects on the damping of vibrations in this direction. The vibration acceleration in lateral direction was also less than standard eight hours limit and its value at all frequencies was less than 0.1 m/s^2. The allowable exposure time for the longitudinal and lateral directions is reported eight hours per day for 8-HP and 11-HP power tillers in different working conditions [14; 16; 2].

CONCLUSIONS

The conclusions drawn from this research work are as follows:

1. At the power tiller handle position, the vibration acceleration peaks were occurred in the frequency of the engine rotational speed.
2. The vibration acceleration increased with increasing engine speed throughout the experiments.
3. The vibration acceleration depends on measurement direction. The experimental results indicated that the maximum and minimum values belong to vertical and longitudinal directions, respectively.
4. The amplitude of total vibration acceleration at the power tiller handle position was greater than the allowable vibration exposure limit in the frequency range of 10-80 Hz.
5. The vibration acceleration at the trailer seat in the frequency ranges of 4-6.3 Hz and 31.5-40 Hz was more than the standard limit.
6. The vibration allowable exposure time for hand-arm of the power tiller operator's at eight hours working day were between 2.32 to 5.7 years for the different gear ratios and engine speeds.
7. The allowable exposure time in the heavy gears was greater than the lighter gears.
8. It is necessary to reduce the vibration transmitted to the user's hand and body by designing and developing adequate insulating systems or isolators.

ACKNOWLEDGMENT

The authors would like to express their appreciation to University of Tehran and National Bioenergy Research Center (NBERC) of Tarbiat Modaress University authorities for their full support to carry out this research work.

شکل 13 بیشینه و کمینه شتاب طیف 1/3 اکتاو صندلی تراکتور دوچرخ در جهت عمودی برای سرعت های موتور و نسبت دنده های مختلف و مقایسه آنها با حدود مجاز مواجهه استاندارد (ISO standard No. 2631, 1997) را در بازه فرکانسی 1 تا 80 هرتز نشان میدهد. مطابق این شکل زمان مواجهه مجاز در بازه فرکانسی 4-6.3 هرتز و 31.5 تا 40 هرتز کمتر از زمان مجاز رانندگی 8 ساعت در روز است. بیشینه شتاب در بازه فرکانسی 31.5 تا 40 هرتز و می تواند مربوط به موتور تراکتور باشد.

در جهت طولی شتاب ارتعاش در تمامی فرکانسها کمتر از مقدار مجاز برای 8 ساعت کار در روز بود. برخلاف جهت عمودی در جهت طولی مقدار ارتعاش در فرکانسهای مربوط به موتور زیادنبوده که می تواند به نحوه قرار گیری موتور نسبت به شاسی و وجود اتصال مالبند بین تریلر و تراکتور و اثر میرایی آن در این جهت باشد. شتاب ارتعاش در جهت جانبی نیز کمتر از حد استاندارد بوده و مقادیر آن در تمامی فرکانس ها کمتر از 0.1 متر بر مجذور ثانیه است. زمان مجاز مواجهه برای جهت های عمودی و طولی در تحقیقات دیگران و در شرایط کاری متفاوت 8 ساعت در روز برای یک تراکتور دوچرخ 11 اسب بخار آورده شده است (سام وکاتیرول 2006، تواری و دوانگان 2004).

نتیجه گیری

نتایج حاصله از این تحقیق به طور خلاصه عبارتند از:

1. در موقعیت دسته تراکتور قله شتاب ارتعاش در فرکانس های برابر با سرعت دورانی موتور رخ می دهند.
2. ارتعاش با افزایش سرعت موتور افزایش می یابد.
3. شتاب ارتعاش به جهت اندازه گیری وابسته است. مقادیر بیشینه و کمینه ارتعاش به ترتیب در جهت های عمودی و طولی بود.
4. مقدار دامنه ارتعاش در بازه 10 تا 80 هرتز برای دسته بیشتر از حد مجاز مواجهه بود.
5. شتاب ارتعاش در محدوده فرکانسی 4-6.3 و31.5-40 از حد استاندارد فرارتر بود.
6. حد مجاز مواجهه دست و بازو با ارتعاش تراکتور دوچرخ 8 ساعت در روز و بین 2.32 تا 5.7 سال برای نسبت دنده ها و سرعت های مختلف موتور بود.
7. زمان مجاز مواجهه در در دنده های سنگین بزرگتر از دنده های سبک بود.
8. لازم است که با طراحی و توسعه سیستم تعلیق مناسب ارتعاش تراکتور دوچرخ کاهش یابد

نویسندگان علاقه مندند مراتب تشکر خود ار از دانشگاه تهران و موسسه تحقیقات بیو انرژی دانشگاه تربیت مدرس جهت حمایت در انجام این تحقیق اعالم نمایند.

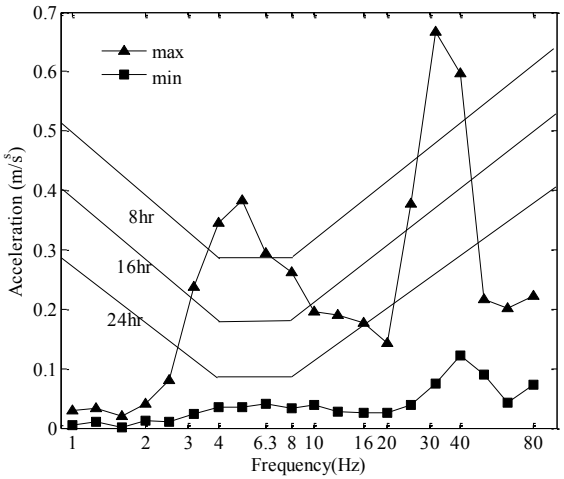

Fig. 13 - Comparing the maximum and minimum values of 1/3rd octave acceleration of the seat position at the vertical direction for the different engine speeds and gear ratios with standard allowable driving time

REFERENCES

[1]. Barber A., (1992) - *Handbook of Noise and Vibration Control.* Elsevier Advanced Technology Publication;

[2]. Dewangan K.N., Tewari V.K., (2009) - . Characteristics of hand transmitted vibration of a hand *tractor used in three operational modes*. International Journal of Industrial Ergonomics 39, 239-245;

[3]. Futatsuka M., Maeda S., Inaoka T., Nagano M., Shono M., Miyakita T., (1998) - *Whole body vibration and health effects in the agricultural machinery drivers.* Industrial Health 36,127-132;

[4]. Goglia V., Gospodaric Z., Filipovic D., Djukic I., (2006) - *Influence on operator's health of hand-transmitted vibrations from handles of a single-axle tractor*. Annals of Agricultural and Environmental Medicine 13, 33-38;

[5]. Hassan-Beygi S.R., Ghobadian B., (2005) - *Noise attenuation characteristics of different road surfaces during power tiller transport.* Agricultural Engineering International: the CIGRE Journal VII, Manuscript PM 04 009;

[6]. ISO 2631-1 (1997) - *Mechanical vibration and shock-Evaluation of human exposure to whole-body vibration. Part 1: General requirements.* International Standard Organization, Geneva;

[7]. ISO 5349-1(2001) - *Mechanical vibration - Measurement and evaluation of human exposure to hand-transmitted vibration. Part 1: General requirements*. International Standard Organization, Geneva;

[8]. ISO 5349-2 (2001) - *Mechanical vibration - Measurement and evaluation of human exposure to hand-transmitted vibration - Part 2: Practical guidance for measurement at the workplace.* ISO International standard.

[9]. ISO 8041 (2005) *Human response to vibration-Measuring instrumentation.* International Standard Organization, Geneva;

[10]. Kang C.II., Park N.J., Oh I.S., Lee Y.B., (1988) - *Study on the handling of power tiller in view of ergonomics*. Research Reports of the Rural Development Administration Agricultural Engineering and Farm Management 30, 67-71;

[11]. Mehta C.R., Tiwari P.S., Varshney A.C., (1997) - *Ride vibration on a 7.5 kW rotary power tiller*. Journal of Agricultural Engineering Research 66,169-176;

[12]. Ahmadian H., Hassan-Beygi S. R., Ghobadian B., (2013) *Power tiller vibration acceleration envelope curves on transportation mode.* Journal of Vibroengineering, September 2013, Vol.15, Issue 3;

مراجع

[1]. باربر آ. (1992)- هند بوک کنترل نویز و ارتعاش. انتشارات فنی الزیویر.

[2]. دوانگن ک. ن.، تواری و. ک.، (2009)- بررسی ارتعاشات تراکتور دوچرخ در سه وضعیت عملیاتی. ژورنال بین المللی ارگونومی صنعتی: 39، 239-245

[3]. فوتوسکا م.، مایدا س.، اینوکا ت.، ناگانو م.، شونو م. مایاکیتا ت.، (1998)- ارتعاشات وارد بر بدن و اثرات آن بر رانندگان ماشینهای کشاورزی. بهداشت صنعتی 36، 127-132.

[4]. گاگلیا و. گاسپاداریک ز. فیلیپوویک د. دیجوکیک ی.، (2006)- اثرات ارتعاشات منتقل شده به دست از دسته تراکتور دوچرخ بر کاربر. سالنامه پزکی در کشاورزی و محیط زیست: 13، 33-38.

[5]. حسن بیگی س. ر.، قبادیان ب.،(2005)- بررسی نویز تراکتور دوچرخ در حالت حمل و نقل در سطوح مختلف جاده. ژورنال بین المللی مهندسی کشاورزی، جلد 7 پ.م. 04009;

[6]. ISO 2631-1 (1997) - ارتعاشات مکانیکی و شوک انسان در معرض ارتعاش کل بدن. بخش اول: نیاز مندی های عمومی. سازمان بین المللی استاندارد، ژنو;

[7]. ISO 5349-1(2001) - ارتعاشات مکانیکی، اندازه گیری و بررسی انسان در معرض ارتعاشات دست وبازو. بخش اول: نیازمندی های عمومی. سازمان بین المللی استاندارد، ژنو;

[8]. ISO 5349-2(2001) - ارتعاشات مکانیکی، اندازه گیری و بررسی انسان در معرض ارتعاشات دست وبازو. بخش دوم: راهنمای اندازه گیری کاربردی در محل کار. سازمان بین المللی استاندارد، ژنو.

[9]. ISO 8041 (2005) - پاسخ انسان به ارتعاشات، دستگاههای اندازه گیری. سازمان بین المللی استاندارد، ژنو;

[10]. کانگ س. ل.، پارک ن. ج. آه ی. س.، لی ی.ب.(1988)- مطالعه کاربری تراکتور دوچرخ با رویکرد ارگونومیکی. گزارش تحقیق اداره توسعه مهندسی کشاورزی و مزرعه. 30، 67-71;

[11]. مهتا س. ر.، تواری پ. س.، وارشنف آ. س.، (1997)- ارتعاشات تراکتور دوچرخ 7.5ذ اسب بخار در حالت سوار. ژورنال تحقیق در مهدسی کشاورزی 66، 169-176;

[12]. احمدیان ح.، حسن بیگی س. ر.، قبادیان ب. (2013) منحنی های انولوپ ارتعاش تراکتور دوچرخ در حالت حمل ونقل. ژورنال ارتعاشات مهندسی، جلد 15، نسخه 3;

[13]. سالوخه و. م.، ماجومدر ب.، اسلام م. س. (1995)- بررسی ارتعاش تراکتور دوچرخ. ژورنالب ترامکانیک 32، 181-196;
[14]. سام ب.، کاتیرول ک.، (2006)- بررسی ارتعاش تراکتور دوچرخ سواره و پیاده. مهندسی بیوسیستم 95، 517-528;
[15]. تقی زاده علی سرائی آ. (2007)- بررسی تجربی ارتعاش یک تراکتور دوچرخ. دانشگاه تربیت مدرس، تهران، ایران;
[16]. تواری و. ک.، دوانگان ک. ن.، سوبراتا ک. (2004)- آسیب وارده بر کاربر از تراکتور دوچرخ در حال عملیات مزرعه. مهندسی بیوسیستم 89، 1-11;
[17]. وانگ و.، راخیا س. بویلیاب پ. ای.، (2004)- اثرات وضعیت نشستن بر پاسخ بیودینامیکی کاربران نشسته در ارتعاشات عمودی. ژورنال بین المللی ارگونومی صنعتی 34، 289-306.

[13]. Salokhe V.M., Majumder B., Islam M.S., (1995) - *Vibration characteristics of a power tiller*. Journal of Terramechanics 32, 181-196;
[14]. Sam B., Kathirvel K., (2006) - *Vibration characteristics of walking and riding type power tillers.* Biosystems Engineering 95, 517–528;
[15]. Taghizadeh-Alisaraei A., (2007) - *Experimental investigation of a power tiller vibration. MSc Thesis,* Dept. Mechanics of Agricultural Machinery Engineering. Tarbiat Modaress University, Tehran, Iran (In Persian);
[16]. Tewari V.K., Dewangan K.N., Subrata K., (2004) - *Operator's fatigue in field operation of hand tractors.* Biosystems Engineering 89, 1-11;
[17]. Wang W., Rakheja S., Boileaub P.E., (2004) - *Effects of sitting postures on biodynamic response of seated occupants under vertical vibration*. International Journal of Industrial Ergonomics 34, 289-306.

WRITING NORMS / *NORME DE REDACTARE*

Article Types

Three types of manuscripts may be submitted:

1. Regular articles: These should describe new and carefully confirmed findings, and experimental procedures should be given in sufficient detail for others to verify the work. The length of a full paper should be the minimum required to describe and interpret the work clearly (max. 8 pages);

2. Short Communications: A Short Communication is suitable for recording the results of complete small investigations or giving details of new models or hypotheses, innovative methods, techniques or apparatus. The style of main sections has not necessarily to be in accordance with that of full-length papers (max. 6 pages);

3. Reviews: Submissions of reviews and perspectives covering topics of current interest are welcome and encouraged (max. 8 pages).

Review Process

All manuscripts are reviewed by the 2 members of the Scientifically Review. Decisions will be made as rapidly as possible, and the journal strives to return reviewers' comments to authors in approx. 3 weeks. The editorial board will re-review manuscripts that are accepted pending revision.

NOTE: Submission of a manuscript implies: that the work described has not been published before (excepting as an abstract or as part of a published lecture, or thesis) that it is not under consideration for publication elsewhere.

1. REGULAR ARTICLES

- All portions of the manuscript must be typed *single-spaced, A4***,** top and bottom: 2 cm; left: 2 cm; right: 2 cm, font: **Arial,** size 9 pt, except the title which will be 11 pt. and explicit figures, which will be 8 pt.
- Text paper will be written in two equal columns of 8.3 cm, 0.4 cm space between them, except the title, authors and their affiliations, tables, figures, graphs and equations to be entered once.
- Text will be written in English in the left column, respectively in native language in the right column.
- The chapter titles are written Uppercase (eg: INTRODUCTION, MATERIAL AND METHODS), between chapters is left a space for 9 pt. At the beginning of each paragraph to leave a tab of 0.5 cm.
- The paper will be written in Word, "Justify" alignment;
- The paper should be transmitted by E-mail.
- There are allowed 2 papers by each first author.

The **Title** should be a brief phrase describing the contents of the paper. PAPER'S TITLE will be uppercase, Bold (the title in English language) and *Bold italic (the title in native language),* center, 11 pt. Under the paper's title, after an space (enter) 9 pt., write *authors' names* (eg: Vasilescu G.). (font: 9 pt., bold) and *affiliations*, the *name of the corresponding author* (next row), (9 pt., regular). Also be passed: the phone, fax and E-mail information, for the first author of paper's (font: 8 pt., italic).
Title should be short, specific and informative. Avoid long titles; a running title of no more than 100 characters is encouraged (without spaces).

The ***Abstract*** should be informative and completely self-explanatory, briefly present the topic, state the scope of the experiments, indicate significant data, and point out major findings and conclusions. The Abstract should be 100 to 300 words in length. Complete sentences, active verbs, and the third person should be used, and the abstract should be written in the past tense. Standard nomenclature should be used and abbreviations should be

Tipuri de Articole

Trei tipuri de manuscris pot fi trimise:

1. Articole obişnuite (normale): acestea trebuie să descrie cercetări noi şi confirmate, iar procedurile experimentale să fie descrise pentru a putea fi verificate in detaliu, fără a leza dreptul de proprietate intelectuală. Mărimea unei lucrări trebuie să cuprindă minimul necesar pentru a descrie şi interpreta în mod clar conţinutul (max.8 pagini);

2. Comunicări scurte: o comunicare scurtă este folosită pentru înregistrarea rezultatelor din investigaţii complete de dimensiuni reduse sau pentru a oferi detalii despre modele noi de ipoteze, metode inovative, tehnici sau infrastructuri. Tipul secţiunilor (capitolelor) principale nu trebuie să fie neapărat în concordanţă cu articolele normale (max. 6 pagini);

3. Sintezele: Prezentarea unor comentarii şi perspective acoperind subiecte de interes actual sunt binevenite şi încurajate (maxim 8 pagini).

Procesul de evaluare (recenzie)

Toate manuscrisele sunt evaluate de către 2 membri ai Comitetului Ştiinţific. Deciziile vor fi luate cât mai rapid posibil şi revista va returna comentariile evaluărilor înapoi la autori în aproximativ 3 săptămâni. Conducerea editorială va reevalua manuscrisele care sunt acceptate în vederea publicării în revistă.

Notă: Sunt acceptate numai lucrările care nu au mai fost publicate anterior. În cazul în care autorii trimit spre publicare lucrări ce conţin date, informaţii, capitole, etc., din alte lucrări publicate anterior şi nu se fac referiri la acestea în text, răspunderea aparţine acestora.

1. ARTICOLE OBIŞNUITE

- Toate capitolele manuscrisului trebuie să fie scrise *single-spaced, A4***,** sus şi jos: 2 cm; stânga: 2 cm; dreapta: 2 cm, font: **Arial,** mărime 9 pt, cu excepţia titlului care se scrie cu 11 pt. şi figurile explicite, care se scriu cu 8 pt.
- Textul lucrării va fi scris în două coloane egale de 8,3 cm, 0,4 cm spaţiul dintre ele, exceptând titlul, autorii şi afilierea acestora; tabelele, figurile şi ecuaţiile care nu se scriu pe coloane ci pe toată pagina (vezi modelul ataşat);
- Textul se va scrie în limba engleză în coloana din stânga, respectiv în limba maternă - coloana din dreapta.
- Titlurile capitolelor sunt scrise cu majuscule (ex: INTRODUCERE, MATERIAL ŞI METODE), între capitole se lasă un spaţiu de 9 pt. La începutul fiecărui paragraf se lasă un "tab" de 0.5 cm;
- Lucrarea va fi scrisă în Word, aliniere "Justify".
- Lucrarea trebuie trimisă prin e-mail.
- Sunt permise max. 2 lucrări ca prim autor.

Titlul trebuie să fie o frază scurtă care să descrie conţinutul lucrării. Acesta *va fi scris cu majuscule, centrat*, mărime: 11 pt., bolduit, (titlul in engleză) şi *bolduit italic (titlul în limba maternă)*. Sub titlul lucrării după un spaţiu de 9 pt., se scriu numele autorilor (ex: Vasilescu G.) (9 pt., bold), imediat sub numele autorilor se scrie: afilierea autorilor (9 pt., normal) iar pe următorul rând: telefonul, faxul, e-mailul corespunzător celui care a trimis lucrarea - primului autor (8 pt., italic).
Titlul trebuie să fie scurt, specific şi informativ. Evitaţi titlurile lungi, un titlu de sub 100 caractere este recomandat (fără spaţii).

Rezumatul trebuie să fie informativ şi uşor de înţeles; prezentaţi pe scurt topica, stadiul experimentelor, date semnificative, şi evidenţiaţi descoperirile majore şi concluziile. Rezumatul trebuie să cuprindă între 100 şi 300 cuvinte. Propoziţiile complete, verbele active, şi persoana a III-a trebuiesc folosite (rezumatul să fie scris la timpul trecut). Se va utiliza nomenclatura standard iar abrevierile trebuiesc evitate. Nu se vor utiliza citări de lucrări în

avoided. No literature should be cited (font: 9 pt., the title - *bold italic*; the text of abstract: *italic*).

Following the abstract, about 3 to 10 ***Keywords*** that will provide indexing references should be listed (font: 9, bold italic - the title and 9 pt., *italic* - the text).

A list of non-standard **Abbreviations** should be added. In general, non-standard abbreviations should be used only when the full term is very long and used often. Each abbreviation should be spelled out and introduced in parentheses the first time it is used in the text. Only recommended SI units should be used. Authors should use the Solidus presentation (mg/ml). Standard abbreviations (such as ATP and DNA) need not to be defined.

INTRODUCTION should provide a clear statement of the problem, the relevant literature on the subject, and the proposed approach or solution. It should be understandable to colleagues from a broad range of scientific subjects.

MATERIALS AND METHODS should be complete enough to allow experiments to be reproduced. However, only truly new procedures should be described in detail; previously published procedures should be cited, and important modifications of published procedures should be mentioned briefly. Capitalize trade names and include the manufacturer's name and address. Subheadings should be used. Methods in general use need not be described in detail.

RESULTS should be presented with clarity and precision. The results should be written in the past tense when describing findings in the authors' experiments. Results should be explained, but largely without referring to the literature. Discussion, speculation and detailed interpretation of data should not be included in the Results but should be put into the Conclusions section. Subheadings should be used.

CONCLUSIONS should interpret the findings in terms of the results obtained in this and in past studies on this topic. State the conclusions in a few sentences at the end of the paper. The Results and Discussion sections can include subheadings, and when appropriate, both sections can be combined.

Acknowledgments of people, grants, funds, etc. should be brief (if necessarily).

Tables should be kept to a minimum and be designed to be as simple as possible. Tables are to be typed single-spaced throughout, including headings and footnotes. Each table must be written on the entire width of the page, into the text where reference is made, the columns are broken - one column (see attached sample). Tables should be self-explanatory without reference to the text. The details of the methods used in the experiments should preferably be described in the legend instead of in the text. The same data should not be presented in both table and graph form or repeated in the text. Table's title will be centered bold (in English) and bold italic native language then separated by a slash. In the table, each row will be written in English (Arial, regular, size: 9 pt.) / *native language* (Arial, italic, 9 pt.). The table and its number is written right justified, bold - in English and bold italic - native language, separated by a slash (/).

Figure legends should be typed in numerical order. Graphics should be prepared using applications capable of generating high resolution JPEG before to introducing in the Microsoft Word manuscript file (Insert - From File -

"rezumat" (font: 9 pt., titlu - *bold italic*; textul rezumatului - *italic*).

Cuvinte cheie: ca urmare a rezumatului, între 3 şi 10 cuvinte cheie trebuiesc listate, aceste oferind referinţe de indexare (font: 9 pt., **bold italic** – titlul şi 9 pt., *italic* - textul).

Trebuie adăugată o listă de abrevieri specifice. În general, aceste abrevieri se folosesc atunci când termenul folosit este foarte lung şi des întâlnit în lucrare. Fiecare abreviere ar trebui introdusă în paranteză pentru prima dată când este folosită în text. Doar unităţi din SI trebuiesc folosite. Autorii trebuie să folosească prezentarea Solidus (mg/ml). Abrevierile standard (ca ATP sau ADN) nu trebuiesc definite.

INTRODUCEREA trebuie să ofere o expunere clară a problemei, esenţa relevantă a subiectului şi abordarea propusă sau soluţia. Aceasta trebuie să poată fi înţeleasă de către colegi din diferite domenii ştiinţifice.

MATERIALE ŞI METODE: trebuie să fie suficient de complete pentru a permite experimentelor să fie reproduse. Totuşi, numai metodele cu adevărat noi trebuie descrise în detaliu; metodele publicate anterior trebuie citate; modificările importante ale metodelor publicate trebuie menţionate pe scurt. Scrieţi cu majuscule denumirile comerciale şi includeţi numele şi adresa producătorilor. Subcapitolele trebuie utilizate. Metodele utilizate în general, nu trebuie descrise în detaliu.

REZULTATELE trebuie prezentate cu claritate şi precizie. Acestea trebuie scrise la timpul trecut, atunci când descriu constatările în experimentele autorilor. Rezultatele trebuie să fie explicite, dar în mare măsură, fără a se face referire la literatura de specialitate. Discuţiile, speculaţiile şi interpretarea detaliată a datelor nu trebuie să fie incluse în rezultate, ci trebuie incluse în capitolul Concluzii. Subcapitolele trebuie utilizate.

CONCLUZIILE trebuie să interpreteze constatările în ceea ce priveşte rezultatele obţinute în această lucrare şi în studiile anterioare pe această temă. Concluziile generale vor fi prezentate în câteva fraze la sfârşitul lucrării. Rezultatele şi discuţiile pot include subpoziţii, şi atunci când este cazul, ambele secţiuni pot fi combinate.

Mulţumirile către oameni, cei care au acordat burse, fonduri, etc., trebuie să fie scurte (dacă este necesar).

Tabelele trebuie menţinute la un nivel minim şi să fie proiectate pentru a fi cât mai simple posibil. Tabelele vor fi scrise la un rând, inclusiv titlurile şi notele de subsol. Fiecare tabel trebuie scris pe întreaga lăţime a paginii, între textul în care se face trimitere; coloanele sunt eliminate - o singură coloană (vezi ataşat modelul). Tabelele trebuie să fie auto-explicative, fără referire la text. Detaliile cu privire la metodele utilizate în experimente trebuie să fie, de preferinţă, descrise în legendă şi nu în text. Aceleaşi date nu trebuie prezentate atât în tabel cât şi sub formă grafică (decât dacă este absolut necesar) sau repetate în text. Titlul tabelului va fi scris centrat, bold (în engleză) şi bold italic (în limba maternă), separate de un slash (/). În tabel, fiecare rând va fi scris în limba engleză (9 pt., normal) / limba maternă (9 pt., italic). Tabelul şi numărul acestuia se scrie aliniat la dreapta, bold - în limba engleză şi bold italic în limba maternă, despărţite de un slash (/).

Figurile trebuie scrise în ordine numerică. Grafica trebuie realizată utilizând aplicaţii capabile să genereze JPEG de înaltă rezoluţie, înainte de a introduce în dosarul manuscris Microsoft Word (Insert - From File - ... JPEG).

...jpeg). Use Arabic numerals to designate figures and upper case letters for their parts (Figure 1). Begin each legend with a title and include sufficient description so that the figure is understandable without reading the text of the manuscript. Information given in legends should not be repeated in the text. Each figure must be inserted on the entire width of the page, into the text where reference is made, single columns (see attached sample). Leave a space between the figure and the text of figure, size: 3 pt., figure number is written in **Arial bold**, size: 8 pt., followed by what represent the figure or graph, written with Arial, regular, 8 pt. Left to write in English (regular), followed by a separating slash (/) and text in native language (*Arial italic*). Eg:

Fig 1 - Test stand / *Stand de testare* (size: 8 pt.)

The figures should be "*In line with text*" - Center, not "*Square*"; "*Tight*"; "*Behind text*" or "*In front of text*" (from "*Format picture*" - right mouse button on picture and then "*Layout*".

Folosiţi cifre arabe, pentru a desemna cifre şi litere majuscule pentru părţile lor (Figura 1). Începeţi fiecare legendă cu un titlu care să includă o descriere suficientă, astfel încât figura să poată fi înţeleasă, fără citirea textului din manuscris. Informaţiile furnizate în legende, nu trebuie repetate în text. Fiecare figură trebuie introdusă pe întreaga lăţime a paginii, în text, acolo unde se face referire, o singură coloană (vezi ataşat eşantion), centrat. Lăsaţi un spaţiu între figură şi textul figurii, mărimea: 3 pt.; numărul figurii va fi scris cu bold, 8 pct., centrat, urmat de ceea ce reprezintă figura sau graficul, scris cu 8 pt., normal. Prima dată se scrie textul în limba engleză (normal), urmat de un slash (/) apoi textul în limba maternă (italic).

Exemplu:

Fig. 1 - Test stand / *Stand de testare* (mărimea: 8 pt.)

Figurile introduse trebuie să fie "*In line with text*" - Center, nu "*Square*"; "*Tight*"; "*Behind text*" or "*In front of text*" (din "*Format picture*" - butonul dreapta mouse pe figură şi apoi "*Layout*").

Mathematics

Authors must provide instructions on how symbols and equations should be set. Equations should be numbered sequentially in the right-hand side and in parenthesis. They should be referred to in the text as Equation (4) or Eg. (4). Each equation must be written on the entire width of the page, into the text where reference is made, the columns are broken (see attached sample).

Formulele matematice, ecuaţiile: autorii trebuie să furnizeze instrucţiuni privind modul de simbolizare şi de ecuaţii stabilite şi utilizate. Ecuaţiile trebuie numerotate secvenţial, în partea dreaptă şi în paranteze. Ele trebuie menţionate în text ca ecuaţia (4) sau Ex. (4). Fiecare ecuaţie trebuie scrisă pe întreaga lăţime a paginii, în text, acolo unde se face referire, o singură coloană (vezi ataşat model).

REFERENCES: are made in the text; a reference identified by [1], [2], ... [n] is written in the order that was placed at the end of the work - alphabetically.

Example:

[1], [2], [3], ..., [n]

References should be listed at the end of the paper in alphabetical order. Articles in preparation or articles submitted for publication, unpublished observations, personal communications etc. should not be included in the reference list but should only be mentioned in the article text (e.g., A. Danciu, University of Bucharest, Romania, personal communication). Authors are fully responsible for the accuracy of the references.

REFERINŢELE: se fac în text; o referinţă identificată prin intermediul [1], [2], ...[n], se scrie în ordinea în care a fost trecută la sfârşitul lucrării - ordine alfabetică.

Exemplu:

[1], [2], [3], ..., [n]

Referinţele trebuie prezentate la sfârşitul lucrării în ordine alfabetică. Articole în curs de pregătire sau articole trimise spre publicare, observaţiile nepublicate, comunicările cu caracter personal, etc, nu trebuie incluse în lista de referinţă, dar pot fi menţionate în textul lucrării (exemplu, A. Danciu, Universitatea din Bucureşti, România, comunicare personală). Autorii sunt pe deplin responsabil pentru exactitatea referinţelor.

Examples:

Journal / Magazine:

[1]. Nicolescu M.A., (2007) - *Relevant characteristics of alternative liquid fuels aimed at Diesel engines exploitation in polycarburation duty*. INMATEH - Agricultural Engineering, vol. 27, no. 1/2009, ISSN 1583-1019, pg. 50-55;

[2]. Pirna I, Nicolescu M., Marin M., Voicea I., (2009) - *Alternative supply of agricultural tractors with raw oils*. INMATEH - Agricultural Engineering, vol. 29, no. 3/2009, ISSN 1583-1019, pg. 89-92.

Conference / Symposium:

[1]. Bungescu S, Stahli W, Biriş S, Vlăduţ V, Imbrea F, Petroman C., (2009) - *Cosmos programm used for the strength calculus of the nozzles from the sprayers,* Proceedings of the 35 International Symposium on Agricultural Engineering *"Actual Tasks on Agricultural Engineering",* Opatija - Croaţia, ISSN 1333-2651, pg. 177÷184.

Book:

[1]. Vlăduţ V., (2009) - *Studiul procesului de treier în aparatul cu flux axial*, Editura "Terra Nostra", ISBN 973-1888-26-8, Iasi - Romania.

Book Chapter:

[1]. Vlăduţ V., (2009) - Consideraţii şi ipoteze privind modelarea unui proces de treier şi separare. In: *Studiul procesului de treier în aparatul cu flux axial*, Editura "Terra Nostra", ISBN 973-1888-26-8, pg. 61-69, Iasi - Romania.

Exemple:

Jurnal / Revistă

[1]. Nicolescu M.A., (2007) - *Proprietăţile relevante ale combustibililor lichizi alternativi vizaţi pentru exploatarea motoarelor Diesel în regim policarburat*, INMATEH - Inginerie Agricolă, vol. 27, nr. 1 / 2009, ISSN 1583-1019, pg. 50-55;

[2]. Pirna I, Nicolescu M., Marin M., Voicea I., (2009) - *Alimentarea alternativă a tractoarelor agricole cu uleiuri vegetale crude,* INMATEH - Inginerie Agricolă, vol. 29, nr. 3 / 2009, ISSN 1583-1019, pg. 89-92.

Conferinţă / Simpozion

[1]. Bungescu S, Stahli W, Biriş S, Vlăduţ V, Imbrea F, Petroman C., (2009) - *Cosmos programm used for the strength calculus of the nozzles from the sprayers,* Proceedings of the 35 International Symposium on Agricultural Engineering *"Actual Tasks on Agricultural Engineering",* Opatija - Croaţia, ISSN 1333-2651, pag. 177÷184.

Carte

[1]. Vlăduţ V., (2009) - *Studiul procesului de treier în aparatul cu flux axial*, Editura "Terra Nostra", ISBN 973-1888-26-8, Iaşi - România.

Capitol din carte

[1]. Vlăduţ V., (2009) - Consideraţii şi ipoteze privind modelarea unui proces de treier şi separare. În: *Studiul procesului de treier în aparatul cu flux axial*, Editura "Terra Nostra", ISBN 973-1888-26-8, pg. 61-69, Iaşi - România.

Dissertation / Thesis:
[1]. Constantinescu A., (2010) - *Optimizarea agregatelor formate din tractoare de putere mare cu maşini agricole pentru pregătirea terenului în vederea însămânţării*. PhD dissertation, University of Transylvania Braşov, Romania.

Units, Abbreviations, Acronyms
- Units should be metric, generally SI, and expressed in standard abbreviated form.
- Acronyms may be acceptable, but must be defined at first usage.

2. SHORT COMMUNICATIONS
Short Communications are limited to a maximum of two figures and one table. They should present a complete study that is more limited in scope than is found in full-length papers. The items of manuscript preparation listed above apply to Short Communications with the following differences: (1) Abstracts are limited to 100 words; (2) instead of a separate Materials and Methods section, experimental procedures may be incorporated into Figure Legends and Table footnotes; (3) Results and Conclusions should be combined into a single section.

3. REVIEWS
Summaries, reviews and perspectives covering topics of current interest in the field, are encouraged and accepted for publication. Reviews should be concise (max. 8 pages). All the other conditions are similar with regular articles.

Disertaţii / Teze de doctorat
[1]. Constantinescu A., (2010) - *Optimizarea agregatelor formate din tractoare de putere mare cu maşini agricole pentru pregătirea terenului în vederea însămânţării*. Teză de doctorat, Universitatea Transilvania Braşov, România.

Unităţi, Abrevieri, Acronime
- unităţile metrice trebuie să fie, în general, SI, şi exprimate în formă prescurtată standard;
- acronimele pot fi acceptate, dar trebuie să fie definite la prima utilizare.

2. COMUNICĂRILE SCURTE
Comunicările scurte sunt limitate la maxim 2 figuri şi un tabel. Acestea trebuie să prezinte un studiu complet, care este mai limitat decât în cazul articolelor normale (de dimensiuni mai mari). Elementele de pregătire a articolelor normale (manuscriselor) enumerate mai sus se aplică şi la comunicările scurte, cu următoarele diferenţe: (1) Rezumatul este limitat la 100 cuvinte; (2) capitolele Materiale şi Metode, Procedurile experimentale pot fi scrise împreună, încorporând figurile şi tabelele; (3) Rezultatele şi Concluziile pot fi combinate într-o singură secţiune.

3. SINTEZELE
Sintezele, comentariile şi perspectivele acoperind subiecte de interes din domeniu sunt încurajate şi acceptate spre publicare. Sintezele trebuie să fie concise şi nu mai mari 8 pagini. Toate celelalte condiţii sunt similare cu cele de la articolele normale (obişnuite), enumerate mai sus.

Edited by: INMA Bucharest
6 Ion Ionescu de la Brad Blvd., sect. 1, Bucharest, ROMANIA
Tel: +4021.269.32.60; Fax: +4021.269.32.73
http://www.inmateh.eu